Copyright 2017. De Gruyter. All rights reserved. May not be reproduced in any form without permission from the publisher, except fair uses permitted under U.S. or applicable copyright law.

DE GRUYTER

Tiping Ding, Shaoyong Jiang,
Yanhe Li, Jianfei Gao, Bin Hu

GEOCHEMISTRY OF SILICON ISOTOPES

EBSCO Publishing : eBook Collection (EBSCOhost) - printed on 2/10/2023 8:05 PM via
AN: 1[illegible]12 ; Tiping Ding, Shaoyong Jiang, Yanhe Li, Jianfei Gao, Bin Hu.;
Geochemistry of Silicon Isotopes
Account: ns335141

Tiping Ding, Shaoyong Jiang, Yanhe Li, Jianfei Gao, and Bin Hu

Geochemistry of Silicon Isotopes

EBSCOhost - printed on 2/10/2023 8:05 PM via . All use subject to https://www.ebsco.com/terms-of-use

Also of Interest

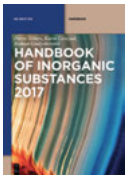

Handbook of Inorganic Substances 2017
Villars, Cenzual, Gladyshevskii, 2017
ISBN 978-3-11-044408-7, e-ISBN 978-3-11-044540-4

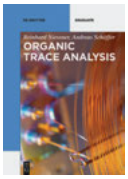

Organic Trace Analysis
Nießner, Schäfer, 2017
ISBN 978-3-11-044114-7, e-ISBN 978-3-11-044115-4

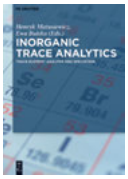

Inorganic Trace Analytics
Trace Element Analysis and Speciation
Matusiewicz, Bulska (Eds.), 2017
ISBN 978-3-11-037194-9, e-ISBN 978-3-11-036673-0

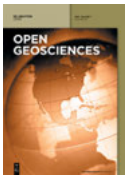

Open Geosciences
Formerly Central European Journal of Geosciences
Jankowski, Piotr (Editor-in-Chief)
ISSN 2391-5447

Geoscience Records
An Interdisciplinary Journal of Earth Sciences
ISSN 2299-6923

EBSCOhost - printed on 2/10/2023 8:05 PM via . All use subject to https://www.ebsco.com/terms-of-use

Tiping Ding, Shaoyong Jiang, Yanhe Li,
Jianfei Gao, and Bin Hu

Geochemistry of Silicon Isotopes

DE GRUYTER

EBSCOhost - printed on 2/10/2023 8:05 PM via . All use subject to https://www.ebsco.com/terms-of-use

Authors
Prof. Tiping Ding
Chinese Academy of Geological Science
Inst. of Mineral Resources
Baiwanzhuang Dajie 26
100037 Beijing
Xicheng District
China
tding@cags.ac.cn

Prof. Shaoyong Jiang
China University of Geosciences
Lumo Road 388
430074 Wuhan
Hongshang District
China
shyjiang@cug.edu.cn

Dr Yanhe Li
Chinese Academy of Geological Science
Inst. of Mineral Resources
Baiwanzhuang Dajie 26
100037 Beijing
Xicheng District
China
Lyh@cei.gov.cn

Dr Jianfei Gao
Chinese Academy of Geological Science
Inst. of Mineral Resources
Baiwanzhuang Dajie 26
100037 Beijing
Xicheng District
China
gao-780814@163.com

Dr Bin Hu
Chinese Academy of Geological Science
Inst. of Mineral Resources
Baiwanzhuang Dajie 26
100037 Beijing
Xicheng District
China
hubin@cags.ac.cn

ISBN 978-3-11-040242-1
e-ISBN (PDF) 978-3-11-040245-2
e-ISBN (EPUB) 978-3-11-040247-6

Library of Congress Cataloging-in-Publication Data
A CIP catalog record for this book has been applied for at the Library of Congress.

Bibliographic information published by the Deutsche Nationalbibliothek
The Deutsche Nationalbibliothek lists this publication in the Deutsche Nationalbibliografie; detailed bibliographic data are available on the Internet at http://dnb.dnb.de.

© 2018 Walter de Gruyter GmbH, Berlin/Boston
Typesetting: VTeX UAB, Lithuania
Printing and binding: CPI books GmbH, Leck
Cover image: Digital Vision/Photodisc/getty images
♾ Printed on acid-free paper
Printed in Germany

www.degruyter.com

EBSCOhost - printed on 2/10/2023 8:05 PM via . All use subject to https://www.ebsco.com/terms-of-use

Preface

Silicon is one of the major elements in the Earth that plays important role in various geological and biological processes. Silica and silicates comprise 87% of the weight of the Earth's crust. Besides, silicon is a major nutrition component for oceanic organs and appears as silica in diatoms, radiolarians and sponges. Silicon is also the major nutrition of a large number of terrestrial plants.

It is found that silicon consists of 4 isotopes, including stable isotope ^{28}Si, ^{29}Si and ^{30}Si and radioactive isotope ^{32}Si. As for other light elements, the natural variation of silicon isotopes has attracted the attention of isotope geochemists since the 1950s of the twentieth century. By the 1970s of the twentieth century, significant progress had been reached on the study of silicon isotope compositions in meteorite and lunar rocks, which shows a relatively large variation on silicon isotopes. However, due to the small variation range of silicon isotope compositions and limited precision of analytical methods, the studies on silicon isotope compositions of terrestrial samples are left behind. The first paper to describe the silicon isotope distribution in nature was published by Douthitt (1982). Soon after that, Ding et al. (1988a) improved the analytical method for silicon isotopes to satisfy the requirement of silicon isotope study on terrestrial samples. Then systematical investigations on the natural variation of silicon isotopes, the fractionation mechanisms of silicon isotopes and geological application of silicon isotopes on ore deposits were carried out by Ding and his cooperators, and a monograph entitled "*Silicon Isotope Geochemistry*" was published in 1996 (Ding et al., 1996), which made an important contribution in the development of this new branch of stable isotope geochemistry.

Since 1996, a large number of research groups have been involved in the studies of silicon isotope investigations and extensive progress has been achieved. The analytical method has been improved significantly. The MC-ICPMS method is established and the laser ablation IRMS and SIMS method are renovated. The thermodynamic silicon isotope fractionation and the kinetic biochemical silicon isotope fractionation have been carried out experimentally. Beside the results of the lithosphere, a large number of data on the samples from the hydrosphere and biosphere have been reported and a more systematical and meticulous picture on silicon isotope distribution in natural environments is delineated. The applications of silicon isotope study have been extended widely. Based on the new progress achieved in the recent two decades, this new book entitled "*Geochemistry of Silicon Isotopes*" is compiled to show readers the features of silicon isotope studies at the present stage.

https://doi.org/10.1515/9783110402452-201

EBSCOhost - printed on 2/10/2023 8:05 PM via . All use subject to https://www.ebsco.com/terms-of-use

EBSCOhost - printed on 2/10/2023 8:05 PM via . All use subject to https://www.ebsco.com/terms-of-use

Acknowledgements

The authors wish to express their deep thanks to the National Natural Science Foundation of China, the Ministry of Science and Technology of China, and the Ministry of Land and Resources of China for providing long term financial support for our research projects in related field.

Acknowledgements are given to G. R. Ma, L. H. Wu, G. Y. Shi, J. X. Zhou, T. R. Song, J. S. Wu, S. Y. Wu, D. F. Wan, S. H. Tian, Y. Zhao for their cooperation in studies of related projects.

We would like to thank H. Sakai, H. G. Thode, Q. L. Zhang, R. Gonfiantini, P. De Bievre, M. Palmer, S. Sheppard, J. Horita, K. Ziegler, for their critical comments and warm encouragements to our work related to this book.

We would like to thank the authors of all papers citied in this book for their excellent contributions to silicon isotope geochemistry.

Finally, we express our hearty thankfulness to the editors of this book for their excellent work in improving the quality of this book.

https://doi.org/10.1515/9783110402452-202

EBSCOhost - printed on 2/10/2023 8:05 PM via . All use subject to https://www.ebsco.com/terms-of-use

EBSCOhost - printed on 2/10/2023 8:05 PM via . All use subject to https://www.ebsco.com/terms-of-use

Contents

EBSCOhost - printed on 2/10/2023 8:05 PM via . All use subject to https://www.ebsco.com/terms-of-use

EBSCOhost - printed on 2/10/2023 8:05 PM via . All use subject to https://www.ebsco.com/terms-of-use

1 Introduction

Silicon isotope geochemistry is a relatively new branch of stable isotope geochemistry. It is applicable to the study of both terrestrial and cosmic environments. As with the stable isotope geochemistry of other elements, silicon isotope geochemistry comprises three main aspects: 1) the study of analytical methods for silicon isotope ratios; 2) the study on the mechanism of silicon isotope fractionation; and 3) the geological applications of silicon isotope studies. Before going into the details of these aspects, some background information of the geochemical characteristics of silicon will be presented, together with the history and the present status of silicon isotope studies.

1.1 Origin and characters of silicon and its isotopes

According to the theory of stellar nucleosynthesis, the elements in the stars were formed in the big-bang by a number of nuclear reactions. The proposed reactions (Burbidge and Burbidge, 1957; Cameron, 1959, 1973) includes 1) Cosmological nucleosynthesis; 2) Hydrogen burning; 3) Nova explosions; 4) Helium burning; 5) Carbon burning; 6) Oxygen burning; 7) Silicon burning; 8) Nuclear statistical equilibrium; 9) S-process; 10) P and R processes; 11) Cosmic ray spallation.

The major processes responsible to formation of silicon nuclei are oxygen burning (for ^{28}Si, ^{29}Si and ^{30}Si), and silicon burning (for ^{28}Si).

It is observed that the most abundant element in the solar system is hydrogen, which is followed by He, O, C, Ne, Fe, N and Si. Normalized to Si = 10^6, the abundance of H and He are 3.18×10^{10} and 2.21×10^9, respectively. The sum of H and He is accounted for more than 99% of the mass in the solar system, and Si makes 0.06% of the mass in the solar system.

1.2 A brief description of silicon geochemistry

Silicon has an atomic number of 14 and belongs to the third period and the fourth family of the periodic table. The silicon element was discovered in the nineteenth century. It is the most abundant element in the Earth after oxygen, and occupies a very important position in geochemistry. As a result, its chemical properties and geochemical characteristics have been studied in great detail.

1.2.1 Physicochemical properties of silicon

Through extensive and long term studies, a clear understanding has been obtained for the physicochemical properties of silicon. For simplicity, only those physicochemical properties that are most closely related to silicon geochemistry are listed in Table 1.1.

https://doi.org/10.1515/9783110402452-001

EBSCOhost - printed on 2/10/2023 8:05 PM via . All use subject to https://www.ebsco.com/terms-of-use

Table 1.1: Some basic physicochemical parameters of silicon.

Property	Parameter	Reference
atomic number	14	
atomic weight	28.0855	Barnes et al., 1975
atomic volume (cm^3/Gramatom)	12.1	Liu, 1984
atomic density (g/cm^3)	2.33	
electronic configuration	$3S^2 3P^2$	
melting point (°C)	1410	
boiling point (°C)	2355	
geochemical valence	$4^-, 4^+, (2^+)$	Rösler and Lange, 1973
electronegativity	1.9	Liu, 1984
atomic radius (nm)	0.1176	
covalent radius (nm)	0.1126	
ion radius (nm)	0.042 (4^+)	
(Six coordinated)	0.271 (4^-)	
ionization potential (eV)	8.149	
reducing potential (eV)	−1.2	
$SiF_6^{2-} \rightarrow Si^{4+} + 6F^-$		
ionic potential	9.5 (4^+)	

1.2.2 Silicon-bearing compounds in nature

So far, elemental silicon has not been found in nature yet, although silicon carbide and silicon nitride were discovered in carbonaceous chondrite, enstatite chondrite (Tang et al., 1988) and kimberlites (Hutcheon et al., 1994). The existence of compounds of silicon with nitrogen, boron and hydrogen in terrestrial samples has been proposed, but their presence is doubtful (Liu, 1984). Silicon fluoride may exist in natural samples, especially in volcanic and metasomatic products (Liu, 1984), but even if some of these exotic silicon compounds exist in nature, their abundance should be very low and of little significance in geochemical processes. The most important silicon-bearing compound is silicates, which constitute 75% of the earth's crust by weight. The second most abundant silicon-bearing compound is silica, SiO_2, which makes up 12% of the earth's crust. The observation that these two types of silicon-bearing compounds together account for 87% of the earth's crust by weight indicates how important silicon is in geochemical studies.

1.2.3 Crystal structure of silicates and silica

The basic unit of the crystal structure of silicates and silica is the silicon-oxygen tetrahedron. As the ionic radius of silicon is 0.042 nm and the ionic radius of oxygen is 0.132 nm, a cation of silicon can be enveloped by 4 anions of oxygen to form a stable

EBSCOhost - printed on 2/10/2023 8:05 PM via . All use subject to https://www.ebsco.com/terms-of-use

silicon-oxygen tetrahedron. These tetrahedra can be isolated from each other (e.g., forsterite) and linked by other cations (magnesium ions in the case of forsterite). However, more frequently the tetrahedra are polymerized by sharing one or more of their oxygen atoms. An oxygen atom shared by two silicon oxygen tetrahedra is formed an "oxygen bridge". Based upon the different styles of polymerization, silicates of different structures, such as inosilicate, cyclosilicate, phyllosilicate and tectosilicate, can be formed. Silicon-oxygen tetrahedra are also formed in silicate melt. Similarly, the polymerization of silicon-oxygen tetrahedra can also be observed in silicate melt.

1.2.4 The abundance and distribution of silicon in geological reservoirs

Silicon is the eighth most abundant element in cosmos. In the Earth, silicon is the second most abundant element, with an abundance of 27% by weight in the lithosphere. The distribution of silicon in various geological reservoirs is listed in Table 1.2.

Table 1.2: Distribution of silicon in various geological reservoirs.

Geological reservoirs	Content of silicon	Major forms of silicon bearing compounds	Reference
mantle	20.5–22.5%	nesosilicate and inosilicate: garnet peridotite, spinel peridotite, plagioclase peridotite	Macdonald (1983)
lower crust	25.1–27.8%	nesosilicate, inosilicate and tectosilicate: gabbro, amphibolite, magnesium granulite, eclogite and peridotite	
upper crust	27.7–30.9%	all kinds of silicate and silica: granitoid, basalts, intermediate and acidic rocks, volcanic rocks, argillites, siliceous rocks and metamorphic rocks	
ocean water	0.05×10^{-6}–5×10^{-6}	H_4SiO_4	Spencer (1983)
river water	2.0×10^{-6}–11×10^{-6}	H_4SiO_4	Aston (1983)
biosphere		SiO_2 in diatoms, radiolarian, sponges and equisetales	Spencer (1983)

1.3 The history of silicon isotope studies

Four isotopes of silicon exist in the natural environment: ^{28}Si, ^{29}Si, ^{30}Si and ^{32}Si. The first three isotopes are stable and the last one is radioactive. The relative abundances of ^{28}Si, ^{29}Si and ^{30}Si in the Earth are 92.23%, 4.67% and 3.10%, respectively (Barnes

EBSCOhost - printed on 2/10/2023 8:05 PM via . All use subject to https://www.ebsco.com/terms-of-use

et al., 1975). Variation in silicon isotope compositions has been found in terrestrial samples. As with the stable isotope compositions of other elements, silicon isotope compositions are expressed as δ values, i.e.,

$$\delta^{30}\mathrm{Si}(‰) = \frac{(^{30}\mathrm{Si}/^{28}\mathrm{Si})_{\mathrm{Sa}} - (^{30}\mathrm{Si}/^{28}\mathrm{Si})_{\mathrm{St}}}{(^{30}\mathrm{Si}/^{28}\mathrm{Si})_{\mathrm{St}}} \times 1000 \tag{1.1}$$

$$\delta^{29}\mathrm{Si}(‰) = \frac{(^{29}\mathrm{Si}/^{28}\mathrm{Si})_{\mathrm{Sa}} - (^{29}\mathrm{Si}/^{28}\mathrm{Si})_{\mathrm{St}}}{(^{29}\mathrm{Si}/^{28}\mathrm{Si})_{\mathrm{St}}} \times 1000 \tag{1.2}$$

where the subscript Sa means sample and St means standard.

By the 1920s, all three stable isotopes of silicon had been discovered. In 1924, Jaeger and Dijkstra tried to determine the silicon isotope ratios of natural samples by measuring their atomic weight. Six terrestrial samples of sand, analcime, leucite and chlorite as well as six samples of meteorites were analyzed, but no variation in silicon isotope compositions were detected in these samples. Reynolds and Verhoogen (1953) reported silicon isotope data on a variety of rocks and minerals by mass spectrometric analysis. The samples were pretreated chemically to convert their silicon to the form of $BaSiF_6$. The $BaSiF_6$ was then decomposed through heating to form SiF_4, which was introduced into the mass spectrometer for silicon isotope analysis. Fourteen samples of different rocks and minerals were analyzed. Using olivine from a peridotite in North Carolina, USA as a standard, they obtained δ^{30}Si variations from 1.0‰ to −2.1‰ for these samples. This research represents the first analysis of silicon isotope compositions by a mass spectrometer. Their SiF_4 method has been used by later researchers, although improvements have been made on the methods of SiF_4 preparation and on the instruments used in the analyses. However, the range of ^{30}Si enrichments in minerals observed in this study is basically the same as those obtained in later studies.

Grant (1954) published a paper dealing with the theoretical aspects of silicon isotope fractionation. Based on the crystal structure of silicate and the ground state vibrational frequency of SiO_4, he predicted silicon isotope fractionation would be less than 5‰ among different phases within igneous rocks. He also made some predictions about silicon isotope fractionations during weathering processes and precipitation of silica from solution. However, because of the lack of necessary basic data, his conclusions were not very precise, and some were contradicted by later observations. Nevertheless, his theoretical discussions provided an inspiration for subsequent studies of the geochemical fractionation of silicon isotopes.

In the same period, Allenby (1954) studied the silicon isotope ratio of various rocks and minerals. He also used SiF_4 gas for mass spectrometry analyses, but his method of SiF_4 preparation was much different from that of Reynolds and Verhoogen (1953). Silicon-bearing samples were reacted with HF in a vacuum metal system to produce SiF_4, which was purified and collected for silicon isotope analysis in the mass spectrometer. Twelve samples of rocks and minerals were analyzed and the results were reported as ^{28}Si/^{30}Si ratios. The lowest ^{28}Si/^{30}Si ratio, obtained from a silica sinter,

EBSCOhost - printed on 2/10/2023 8:05 PM via . All use subject to https://www.ebsco.com/terms-of-use

was 31.10, and the total δ^{30}Si variation was up to 14.1‰. However, the large variations he found in terrestrial samples were not supported by later analyses.

Preliminary studies of silicon isotope fractionation in natural samples continued in 1950s and 1960s, but the results of these early studies were inconsistent. No clear pattern of silicon isotope variation was found and the reliability of these early results was doubtful. It appeared that it would be rather difficult to make practical use of silicon isotope studies, so the field of silicon isotope study remained stagnant for a while.

As a result of the Apollo lunar landing program in the late 1960s and 1970s, lunar samples were brought back to the Earth and attracted wide interests among scientists working in different fields. Interest in the silicon isotope study of meteorites and lunar rocks was renewed and the silicon isotope compositions of these samples were investigated in detail using improved instruments and analytical methods.

Epstein and Taylor (1970) published the first paper on the variation of $^{30}Si/^{28}Si$ ratios in lunar rocks. Using their method of producing SiF_4 by reacting F_2+HF with samples, they were able to reach a precision of ±0.2‰ for silicon isotope analysis by a mass spectrometer. They found that the surface of lunar soil was enriched in ^{30}Si as well as ^{18}O, which provided strong evidence for the effect of bombardments of micrometeorites and cosmic particles on the isotope composition of lunar soils. Later, Yeh and Epstein (1978) also published their δ^{30}Si and δ^{29}Si results on meteorites.

In the same period, Clayton et al. (1978) had also studied the silicon isotope composition of lunar samples and meteorites using BrF_5 as a fluorination reagent to produce SiF_4. In addition to the effect of a meteorite impact on the silicon isotope composition of lunar soils, they also found large δ^{30}Si (up to 20‰) and δ^{29}Si (up to 10‰) variations between the chondrules and inclusions of meteorites.

On the basis of progress in silicon isotope studies on lunar samples and meteorites, Douthitt (1982) carried out a comprehensive study on silicon isotope variation in terrestrial samples, in which 132 new δ^{30}Si data were reported. In this study, the broad variations of the silicon isotope compositions in terrestrial samples were outlined, and the basic characteristics of the silicon isotope compositions of major terrestrial rock types, minerals and biogenic materials were documented. These results were encouraging. However, no practical geological applications of silicon isotope investigations were indicated in this study.

Ding et al. (1988a) renewed the study of silicon isotopes. First, the SiF_4 preparation method of Clayton et al. (1978) was revised, and the precision of silicon isotope analysis was improved (< ±0.1‰). Following this, the silicon isotope composition of a wide range of terrestrial samples was investigated. Up to 1996, more than 1,000 new silicon isotope data were obtained, and the silicon isotope systematics of terrestrial samples were outlined in more detail. As a result, several important applications of silicon isotope studies to geological problems have been proposed, which evoked wide interest in Si isotope geochemistry. In the meanwhile, de Bièvre and his colleagues have made progress in determining the absolute Si isotope ratio of some reference

EBSCOhost - printed on 2/10/2023 8:05 PM via . All use subject to https://www.ebsco.com/terms-of-use

materials and the molar mass of silicon (De Bièvre and Valkiers, 1994; De Bièvre et al., 1994).

In the 1980s and 1990s of the twentieth century, secondary ion mass spectrometry (SIMS) was used in silicon isotope analysis of meteorite samples (McKeegan et al., 1985; Zinner et al., 1987, 1989; Stone et al., 1991; Hoppe et al., 1993, 1995; Lugaro et al., 1999). These studies showed large variations of δ^{29}Si (up to 160‰) and δ^{30}Si (up to 110‰) in the SiC phase of meteorites. These large variations and their correlation provided important information concerning the cosmochemical processes responsible for the formation of SiC.

Since 1996, a large number of research groups have been involved in studies of silicon isotope investigations and extensive progress has been achieved. First, the analytical method has been improved significantly; especially, the MC-ICP-MS method has been used successfully for silicon isotope determination (De La Rocha, 2002; Cardinal et al., 2003, 2005; Georg et al., 2006a; Reynolds et al., 2006a, 2007; André et al., 2006; Engström et al., 2006; Opfergelt et al., 2006a; Van den Boorn et al., 2006). In the meanwhile, the laser ablation IRMS (De La Rocha et al., 1996; Gao and Ding, 2009) and SIMS methods (Knight et al., 2009; Marin-Carbonne et al., 2011; Heck et al., 2011; Chakrabarti et al., 2012) have been renovated. Second, besides the kinetic inorganic silicon isotope fractionation (Li et al., 1995a; Geilert et al., 2014a; Roerdink et al., 2015), the thermodynamic silicon isotope fractionation (Georg et al., 2007a; Shahar et al., 2009, 2011; Ziegler et al., 2010; Hin et al., 2014; Savage et al., 2009, 2011; Dupuis et al., 2015; Pollington et al., 2016) and the kinetic biochemical silicon isotope fractionation (De La Rocha et al., 1997; Opfergelt et al., 2006b; Ding et al., 2008b; Sun et al., 2008; Sutton et al., 2013) have been carried out systematically. Third, besides the results of the rocks and minerals, a large number of data from the samples on the hydrosphere and biosphere have been reported (De La Rocha et al., 1997, 1998, 2000; De La Rocha, 2003, 2006; De La Rocha et al., 2011; Varela et al., 2004; Milligan et al., 2004; Cardinal et al., 2005; Ding et al., 2004, 2005a, 2008a,b, 2011; Alleman et al., 2005; Reynolds et al., 2006b; Opfergelt and Delmelle, 2012; Opfergelt et al., 2006a,b, 2010, 2011a; Georg et al., 2007b, 2009a; Fripiat et al., 2011a; Hendry and Robinson, 2012; Hendry et al., 2010; Sun et al., 2013, 2014; Sutton et al., 2013; Panizzo et al., 2016) and more systematical and meticulous pictures on silicon isotope distribution in natural environments are presented. Fourth, the applications of silicon isotope study have been extended from rocks (Douthitt, 1982; Ding et al., 1996) and ore deposits (Jiang et al., 1992, 1993, 1994) to the global silicon cycle (Yool and Tyrrell, 2003; Ding et al., 2008a, 2011; Struyf et al., 2009; Bernard et al., 2010; Opfergelt and Delmelle, 2012; Frings et al., 2016), paleo-environmental variations of the ocean (Robert and Chaussidon, 2006; André et al., 2006; Steinhoefel et al., 2009; van den Boorn et al., 2007, 2010; Abraham et al., 2011; Marin-Carbonne et al., 2012, 2014; Geilert et al., 2014b; Stefurak et al., 2015) and biological processes (De La Rocha, 2003, 2006; De La Rocha et al., 1997, 1998, 2011; Varela et al., 2004; Milligan et al., 2004; Cardinal et al., 2005; Ding et al., 2005a, 2008a,b; Alleman et al., 2005; Reynolds et al., 2006b; Opfergelt et

EBSCOhost - printed on 2/10/2023 8:05 PM via . All use subject to https://www.ebsco.com/terms-of-use

al., 2006a, 2011a; Georg et al., 2007b, 2009b; Hendry and Robinson, 2012; Hendry et al., 2010; Sutton et al., 2013; Panizzo et al., 2016). As a result, the published papers on silicon isotope geochemistry have increased from tens articles before 1996 to thousands of articles by 2016.

EBSCOhost - printed on 2/10/2023 8:05 PM via . All use subject to https://www.ebsco.com/terms-of-use

EBSCOhost - printed on 2/10/2023 8:05 PM via . All use subject to https://www.ebsco.com/terms-of-use

2 Analytical methods of silicon isotope composition

The silicon isotope study started as early as in the 1950s of the twentieth century (Reynolds and Verhoogen, 1953; Allenby, 1954). However, significant progress has not been obtained until the 1970s of the twentieth century, when the mature silicon isotope analytical methods, used SiF_4 as the working gas in IRMS (isotope ratio mass spectrometer).

In the 1980s and 1990s of the twentieth century, the SiF_4 methods were modified and their analytical precisions were improved to be better than ±0.1‰ (Ding et al., 1988a, 1996; De La Rocha et al., 1996), which made these methods suitable to a silicon isotope study of the terrestrial samples.

In the early years of the twenty-first century, a new silicon analytical method using a multi-collector inductively coupled plasma mass spectrometer (MC-ICPMS) has been established (De La Rocha, 2002; Cardinal et al., 2003; Georg et al., 2006a; Chmeleff et al., 2008). This method does not require reaction of silica with a highly reactive gas (BrF_5 or F_2+HF) (De La Rocha, 2002; Georg et al., 2006a) and is much less time consuming (De La Rocha, 2002). After several steps of modification, the precision of the silicon isotope determination of this method has reached the same level as the SiF_4 method (Reynolds et al., 2006a). For these reasons, it has become the most popular method for silicon isotope analysis and has promoted the development of silicon isotope geochemical studies in various fields.

In the meantime, significant progress has been reached with the silicon isotope analytical method by using the secondary ion mass spectrometry (SIMS), which started to work with in situ Si isotope determination in the 1980s during the past century. Due to the relatively low precision of determination in the early stage, the application of this method was limited in the studies of meteorites, which show larger silicon isotope variation than those of terrestrial materials (McKeegan et al., 1985; Zinner et al., 1987, 1989; Stone et al., 1991; Hoppe et al., 1993, 1995; Lugaro et al., 1999). However, as significant improvement has been reached in the related instruments and methods in recent years, this method is now applied gradually to in situ silicon isotope determination of terrestrial materials, such as the quartz in a banded iron formation (BIF) and in chert beds (Marin-Carbonne et al., 2011; Chakrabarti et al., 2012; Heck et al., 2011).

Looking back into the history, there is no doubt that the establishment and improvement of the analytical method plays an important role in the development of the silicon isotope geochemistry. In this chapter, the present status, advantages and disadvantages of various silicon isotope analytical methods are discussed in detail.

https://doi.org/10.1515/9783110402452-002

EBSCOhost - printed on 2/10/2023 8:05 PM via . All use subject to https://www.ebsco.com/terms-of-use

2.1 Gas source isotope ratio mass spectrometric analysis of silicon isotopes

The silicon isotope analytical method by using the gas source isotope ratio mass spectrometer (IRMS) was firstly reported by Reynolds and Verhoogen (1953). Although there are a number of varieties, these methods have a common aspect in which samples of various types are transformed to SiF_4 before their silicon isotope compositions are determined in an IRMS. There are two major reasons for using SiF_4 as the gas for mass spectrometric analysis. Firstly, SiF_4 is relatively easy for preparation and is stable under laboratory conditions. Secondly, there is no need to make isotope corrections with SiF_4, as fluorine only has one stable isotope. There are three methods that have been used for SiF_4 preparation: a) the $BaSiF_6$ decomposition method (Reynolds and Verhoogen, 1953; De Bièvre and Valkiers, 1994; Valkiers et al., 2005); b) the direct fluorination method using F_2+HF (Epstein and Taylor, 1970) or BrF_5 (Clayton et al., 1978; Ding et al., 1988a; Ding, 2004) as fluorination reagents and c) the laser probe extraction method (De La Rocha et al., 1996). An introduction on the various methods and a brief discussion on the advantages and disadvantages of these methods are given in following subsections.

2.1.1 The methods of SiF_4 preparation for silicon isotope determination with IRMS

2.1.1.1 SiF_4 preparation by decomposition of $BaSiF_6$

This method consists of two basic steps (Reynolds and Verhoogen, 1953): a) converting the silicon in the sample to $BaSiF_6$, and b) decomposing $BaSiF_6$ to form SiF_4 for mass spectrometric analysis.

Firstly, the silicon in mineral samples is converted to SiO_2 through standard analytical procedures. Then 0.5 g of the SiO_2 is mixed with 2.5 g of sodium carbonate, and is fused in a 20 mL platinum crucible, yielding a clear melt. After cooling, the solidified melt is extracted as a pellet by pressing the crucible gently around the base. This pellet dissolves in 15 mL of water to give a clear solution, and then add 30 mL of concentrated perchloric acid into the solution and heating the solution on a hot plate (swirling constantly to avoid bumping) until copious dense fumes of perchloric acid have come off for ten minutes. When cooled, the solution solidifies to a gelatinous mass. It is taken up in 200 mL of water and brought to a boil. The precipitate of gelatinous silica is then filtered and transferred to a polyethylene beaker with 60 mL of water. Concentrated HF is added dropwise until the solution just clears reflecting total conversion of the silica gel to fluorosilicic acid, H_2SiF_6. About 20 mL of a solution containing 0.2 g of $BaCl_2 \cdot 2H_2O$ per mL is added to the clear solution. Under these conditions, $BaSiF_6$ precipitates while BaF_2 does not. To ensure complete precipitation of the silicon, the beaker is allowed to stand overnight before filtering and drying the $BaSiF_6$ at 110°C.

EBSCOhost - printed on 2/10/2023 8:05 PM via . All use subject to https://www.ebsco.com/terms-of-use

A series of analytical tests on the above procedure have been done to determine the chemical yield. A typical test consists of starting with an accurately weighed amount of silica, precipitating $BaSiF_6$ with a calibrated barium solution, weighing the precipitate, and extracting and weighing the unreacted barium in the filtrate as $BaSO_4$. Within the accuracy of these tests (±2%), the following observations are made:

a) $BaSiF_6$ is the correct formula of the barium chloride precipitate when the above procedure is adhered to strictly, i.e., occluded water and co-precipitated BaF_2 are not present in the final precipitate.
b) The yield of $BaSiF_6$ always exceeds 95% of the theoretical yield calculated from the amount of silica added at the start of the experiment.

This yield is sufficiently satisfactory for the method used in preparing samples for mass spectrometric analysis. The final step is to weigh out 150 mg of the dried precipitate into a short length of 10 mm Pyrex tubing, closed at one end. This tube is sealed to a 75 mL Pyrex sample bulb fitted with a stopcock. The bulb is evacuated with a diffusion pump for 12 hours or more, flaming gently from time to time in order to facilitate the removal of water vapor. Then with the stopcock closed, the $BaSiF_6$ is decomposed by heating the bottom of the 10 mm tube vigorously with an oxygen-gas flame until there is no further change visible in the solid material. The temperature of the glass is brought to such a point in this beating that the glass softens and begins to melt around the solid BaF_2 residue. Lastly, the lower half of the 10 mm tube is sealed with a torch from the rest of the sample bulb. This can remove the BaF_2 residue and prevent any recombination with the silicon that might be isotopic selective. Control experiments show that the percentage decomposition of the $BaSiF_6$ by this scheme is 90%. The SiF_4 obtained from the above steps is emplaced directly into the mass spectrometer for isotope analysis.

The procedures of this method are relatively common in wet chemistry. The equipment used in this method is simple and no elaborate techniques are needed. Correct and meticulous operation of this method yields reliable analytical results. However, there are problems with this method. Firstly, it needs relatively large amounts of the sample (in g level). Besides, the procedure is time consuming and requires great care to prevent silicon isotope fractionation, which can happen when thermal decomposition of $BaSiF_6$ is not complete. Furthermore, the produced SiF_4 may change its Si isotope composition by reacting with the glass during the high temperature decomposition of $BaSiF_6$. Due to these disadvantages, the $BaSiF_6$ method is rarely used in the routine analysis of silicon isotopes except in some special cases. For example, this method has been used at the Institute for Reference Material and Measurements (IRMM) to calibrate silicon isotope ratios of their silicon isotope reference materials and determine the molar mass (atomic weight) of silicon (De Bièvre and Valkiers, 1994; De Bièvre et al., 1994, 1995; Valkiers et al., 2005, 2011). In their studies, Cs_2SiF_6 was chosen as the form of silicon compound to prepare synthetic silicon isotope mixtures for calibration of absolute silicon isotope ratios. Then the Cs_2SiF_6 was converted to $BaSiF_6$, which

EBSCOhost - printed on 2/10/2023 8:05 PM via . All use subject to https://www.ebsco.com/terms-of-use

was loaded into an electro-polished stainless steel ampoule and decomposed to SiF_4 for mass spectrometry analyses. These modifications are very helpful to improve the precision of analysis.

2.1.1.2 SiF_4 preparation through direct fluorination

Different to the above mentioned $BaSiF_6$ method, the direct fluorination method does not need an intermediate step of $BaSiF_6$ preparation. Instead, the silicon-bearing rocks and minerals are reacted directly with a fluorinating reagent to produce SiF_4. The first reagent used to react with silicates and prepare SiF_4 for Si isotope analysis is HF (Allenby, 1954). However, due to the difficulty in handling and the unsatisfactory results, this reagent is no longer used. The most widely used reagents are F_2 + HF (Taylor and Epstein, 1962) and BrF_5 (Clayton and Mayeda, 1963).

The mixture of F_2 + HF was firstly used as the fluorination reagent to extract O_2 from silicate rocks for oxygen isotope analysis (Taylor and Epstein, 1962). This method was modified to prepare and collect SiF_4 for silicon isotope analyses of lunar samples and meteorites (Epstein and Taylor, 1970) and terrestrial samples (Douthitt, 1982). Similarly, the BrF_5 was also used at first in preparation of O_2 from silicates and oxides for oxygen isotope analyses (Clayton and Mayeda, 1963). As BrF_5 has a low vapor pressure (about 33 342 Pa) at room temperature, it is easily transferred and handled by evaporation and condensation in a metal vacuum system. Besides, BrF_5 is an active fluorination reagent, which can react with all kinds of silicates and oxides. In addition, the wastes and residues of the reaction process can be easily removed from the apparatus. For these reasons, the BrF_5 fluorination becomes the most popular method in preparing samples for oxygen isotope analyses of silicates and oxides. Later, this method has been modified by adding cryogenic parts (ethanol slush to –110°C and dry ice bath to –78°C) to collect and purify SiF_4 (Clayton et al., 1974) for silicon isotope determination of meteorites and lunar rocks (Molini-Velsko et al., 1986). After further modification, this method has become a conventional method for silicon isotope analysis of all kinds of terrestrial samples (Ding et al., 1988a, 1996; Ding, 2004).

A sample of the SiF_4 preparation line is illustrated in Figure 2.1, in which the silicon in silica and silicate samples is converted to SiF_4 through following reactions:

$$SiO_2 + 2BrF_5 = SiF_4 + 2BrF_3 + O_2 \tag{2.1}$$

$$KAlSi_3O_8 + 8BrF_5 = KF + AlF_3 + 3SiF_4 + 4O_2 + 8BrF_3 \tag{2.2}$$

For making reliable isotope ratio measurements with a gas isotope mass spectrometer, the gas sample prepared must reproducibly represent the isotopic composition of the original sample. For silicon isotope determination by using SiF_4, the key points are to guarantee 100% yield and to protect the sample from contamination by foreign silicon and other interfering impurities.

EBSCOhost - printed on 2/10/2023 8:05 PM via . All use subject to https://www.ebsco.com/terms-of-use

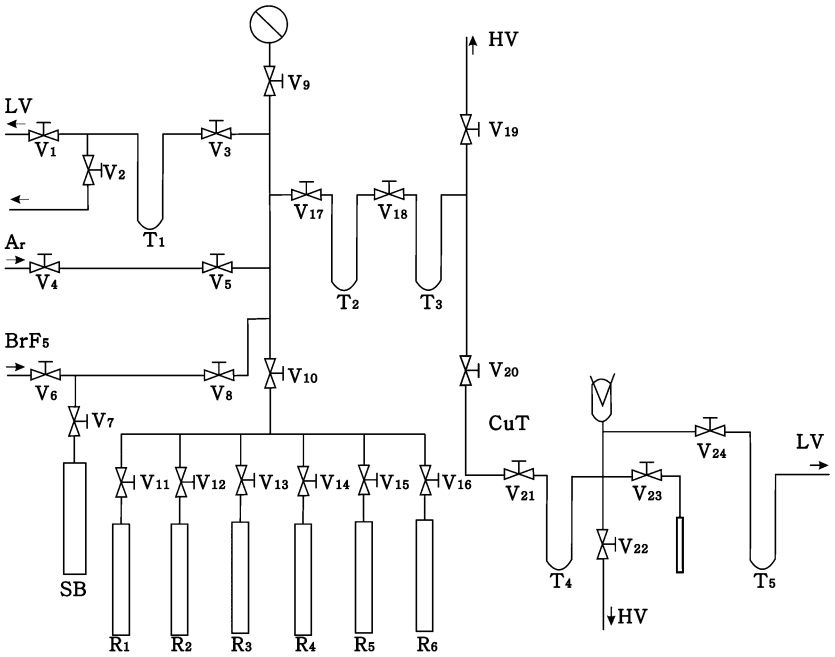

Figure 2.1: SiF_4 Sample preparation line (Ding, 2004). R_1–R_6: Reaction vessels; V_1–V_{24}: Whity valves; T_1–T_5: Cold traps; CuT: Copper tube containing Zn particles; SB: Storage vessel for BrF_5; ST: Sample tube; LV: Low vacuum; HV: High vacuum.

Normally, the BrF_5 reagent contains impurities of CF_4, SiF_4 and SF_6 (Figure 2.2) that will interfere with isotope determination of SiF_4 and need to be purified beforehand. The BrF_5 is purified through cryogenic vaporization and condensation at −78°C by using a bath of a dry ice-acetone mixture. At this temperature, BrF_5 remains in the solid phase, but the impurities, such as SiF_4, SF_6 and CF_4, are present in the vapor phase and can be pumped out.

The SiF_4 preparation method can be used for any sample containing silicon for isotopic analysis. However, different pre-treatment procedures are needed for different types of samples (Ding, 2004). For silica and high purity silicates of containing little or no C, S and B, no pre-treatment is needed. The sample can be fluorinated directly after grinding.

For samples containing significant contents (>1%) of S, C and B, chemical pre-treatment of the sample is necessary. When the impurities in the sample are carbonates or acid soluble sulphides, the HCl dissolution method is used. When the sample contains only graphite or organic carbon, high temperature oxidation and evaporation are used to remove the contaminants. When the sample contains boron compounds, sulphates or sulphides insoluble in HCl, wet chemical pre-treatment is required (Ding, 2004).

EBSCOhost - printed on 2/10/2023 8:05 PM via . All use subject to https://www.ebsco.com/terms-of-use

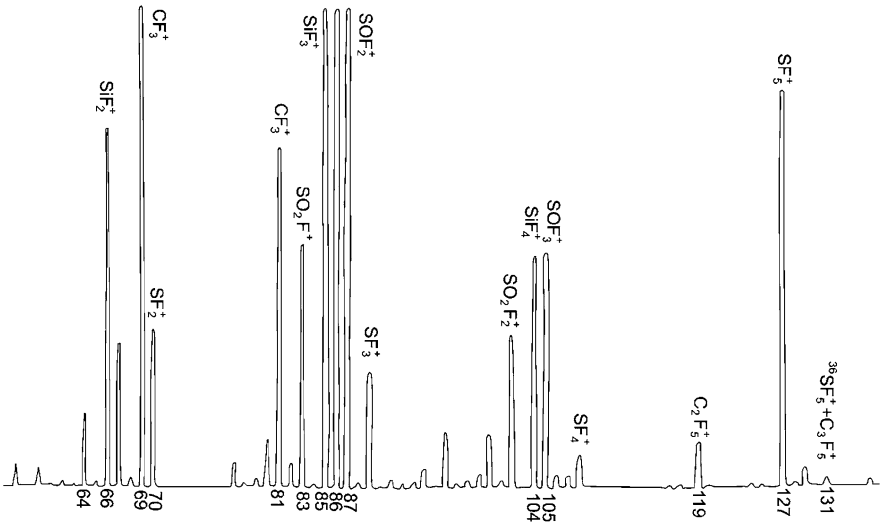

Figure 2.2: Mass-scanning diagram showing the impurities in the BrF_5 agent, which can be frozen by liquid N_2 but not by dry ice-acetone (Ding, 2004).

In the processes of SiF_4 extraction, three cycles of distillation and condensation at dry ice-acetone and liquid nitrogen temperatures are used for separating SiF_4 from O_2, N_2, BrF_5 and BrF_3. Through these processes, the SiF_4 obtained will contain no impurities of O_2 and N_2, but may contain trace amounts of BrF_5 and other active fluorine compounds. These impurities will react with the glass and grease of the sample tube to produce contaminants, such as SiF_4 and CF_4, which will interfere with the isotopic determination. For this reason, a new step for SiF_4 purification has been added. In this step, the primary purified SiF_4 is passed through a heated (50°C–60°C) Cu tube containing pure Zn particles, where BrF_5 and other active fluorine compounds (except SiF_4) react with Zn to form ZnF_2 and $ZnBr_2$. After purification (Figure 2.3), the SiF_4 is collected and ready for mass spectrometer analysis.

Compared with the $BaSiF_6$ method, the direct preparation method of SiF_4 reduces the sample size to the mg level, simplifies the operation procedure, increases the speed of sample preparation and improves the precision of the analyses. Hence, this method has become the routine method in preparation of SiF_4 for silicon isotope analysis.

2.1.1.3 Laser probe extraction method for SiF_4 preparation

The Laser probe extraction method for SiF_4 preparation was firstly reported in 1996 (De La Rocha et al., 1996). The sample preparation line is shown in Figure 2.4. It consists of two portions: a metal section for fluorination and a glass section for yield determination and sample collection.

Purified fluorine for sample reaction is generated inside the vacuum line by heating potassium hexafluonickelate at ~350°C. Purified silica samples containing 15–

EBSCOhost - printed on 2/10/2023 8:05 PM via . All use subject to https://www.ebsco.com/terms-of-use

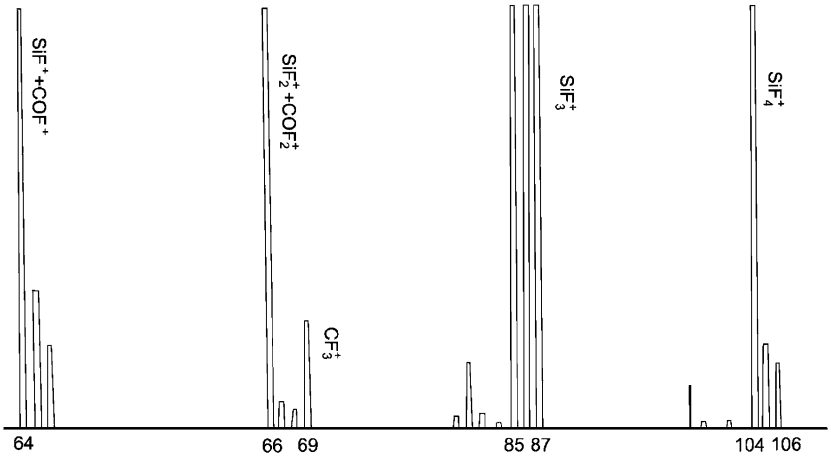

Figure 2.3: Mass-scanning diagram of purified SiF_4 gas (Ding, 2004).

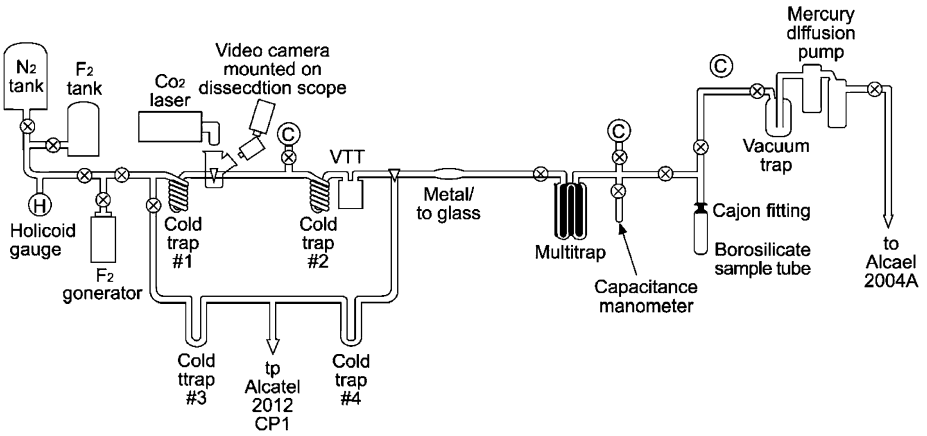

Figure 2.4: Schematic SiF_4 preparation line with a laser microprobe device (De La Rocha et al., 1996).

100 µmol of Si, are loaded into 0.5 cm deep wells drilled into a cylindrical nickel plate. Pieces of pure quartz can be fluorinated directly. The finely powdered silica purified through precipitation is melted under 1 atm of N_2 into lumps of glass before fluorination. The CO_2 laser is mounted on a motorized x–y translation stage and set to fire through a BaF_2 window on the top of the reaction chamber.

Samples are fluorinated under 0.1 atm of purified F_2 that has been passed through a liquid nitrogen trap. Silica samples react with F_2 upon being heated by the laser set to fire a continuous beam:

$$SiO_2 + 2F_2 \rightarrow SiF_4 + O_2 \tag{2.3}$$

EBSCOhost - printed on 2/10/2023 8:05 PM via . All use subject to https://www.ebsco.com/terms-of-use

Lasing of 1–3 mg samples takes approximately 10–20 min of continuous fluorination. When lasing has completed, the resulting SiF_4 is collected in a coil cooled to –195°C with liquid nitrogen. O_2 and F_2 are then pumped away through the coil. Any water present either in the silica or in the reaction chamber during fluorination will form HF, which may in turn form SiF_4 by etching the walls of the glass section of the line. For making separation, the SiF_4 (and any HF) is transferred from cold trap #2 into the variable-temperature trap, which has cooled at least –183°C with liquid nitrogen. The variable-temperature trap is then heated to –140°C, distilling SiF_4 while HF remains behind. Then the purified SiF_4 is collected for mass spectrometer analyses.

Another laser probe extraction method for SiF_4 preparation is established at the Institute of Mineral Resources (IMR) (Gao and Ding, 2009). Similar to the above mentioned method (De La Rocha et al., 1996), the CO_2 laser is used to fire through a BaF_2 window on the top of the reaction chamber to make the reaction. However, BrF_5 is used as the reagent to react with samples. The mineral grains of quartz, garnet and olivine, containing 5–20 μmol of Si, are loaded into 3 mm deep wells drilled into a cylindrical nickel plate. Lasing of 0.5–1 mg samples takes approximately 2–5 min of continuous fluorination.

2.1.2 Mass spectrometry analysis

The SiF_4 obtained from the above process is normally analyzed for its isotopic composition in a Nier-type gas mass spectrometer with multi-collector and dual inlet system, such as MAT-251 EM, MAT-252 and MAT-253. As mentioned above, silicon has 3 stable isotopes: ^{28}Si, ^{29}Si and ^{30}Si. Similar to the isotope compositions of other elements, the silicon isotope compositions are expressed as the δ values related to certain standard, i.e.,

$$\delta^{29}\mathrm{Si}(‰) = \left[\left(^{29}\mathrm{Si}/^{28}\mathrm{Si}\right)_{\mathrm{Sa}}/\left(^{29}\mathrm{Si}/^{28}\mathrm{Si}\right)_{\mathrm{St}} - 1\right] \times 10^3 \quad (2.4)$$

$$\delta^{30}\mathrm{Si}(‰) = \left[\left(^{30}\mathrm{Si}/^{28}\mathrm{Si}\right)_{\mathrm{Sa}}/\left(^{30}\mathrm{Si}/^{28}\mathrm{Si}\right)_{\mathrm{St}} - 1\right] \times 10^3 \quad (2.5)$$

where St indicates standard and Sa indicates sample. The most commonly used standard is NBS-28 (Clayton et al., 1978; Ding et al., 1988a, 1996; Ding, 2004; Molini-Velsko et al., 1986), although the sample of rose quartz was also used as the silicon isotope standard in some laboratories previously (Douthitt, 1982; Taylor and Epstein, 1973a).

The most abundant SiF_3^+ ions are normally used in silicon isotopic determination. Three collectors are simultaneously used to collect $^{28}SiF_3^+$, $^{29}SiF_3^+$ and $^{30}SiF_3^+$ at mass numbers of 85, 86 and 87. Dual inlet system allows rapid switching between sample gas and reference gas. The reproducibility of mass spectrometer measurement is better than ±0.01‰.

EBSCOhost - printed on 2/10/2023 8:05 PM via . All use subject to https://www.ebsco.com/terms-of-use

Besides, a specially modified MAT-271 type of gas isotope mass spectrometer is used in the IRMM to calibrate the silicon isotope ratios of the silicon isotope reference materials and determine molar mass of silicon (De Bièvre and Valkiers, 1994; De Bièvre et al., 1994, 1995; Valkiers et al., 2005, 2011). This mass spectrometer has a single molecular-flow inlet system and single collector. The $^{28}SiF_3^+$, $^{28}SiF_3^+$ and $^{30}SiF_3^+$ ions are measured by peak scanning.

2.2 Multi-collector inductively coupled plasma mass spectrometric (MC-ICPMS) analysis of silicon isotopes

The introduction of the inductively coupled plasma (ICP) in the 1970s of the twentieth century was a significant contribution to the field of multi-element trace analysis, because of its high detection power and rapid sample throughput without requiring extensive sample preparation. The application of multi-collector inductively coupled plasma mass spectrometry (MC-ICPMS) offered important advantages over the conventional methods, such as more time efficient, safer sample preparation techniques and higher sample throughput (De La Rocha, 2002). However, the use of MC-ICPMS has been associated with difficulties in accurately measuring ^{30}Si (De La Rocha, 2002; Cardinal et al., 2003), due to the presence and magnitude of the polyatomic interference consisting of $^{14}N^{16}O$ on the ^{30}Si isotope and also analytical difficulties originating from potential matrix effects during the isotopic analyses. However, as these analytical difficulties are overcome gradually, MC-ICPMS constitutes the most widely applied technique in recent years (De La Rocha, 2002; Cardinal et al., 2003, 2005; Georg et al., 2006a; Reynolds et al., 2006a, 2007; André et al., 2006; Engström et al., 2006; Opfergelt et al., 2006a; Van den Boorn et al., 2006).

2.2.1 Sample preparation

For making silicon isotope determination with MC-ICPMS, the sample needs to be converted to suitable forms for measurement. So far, there are three different forms to be used: H_2SiF_6 solution, H_4SiO_4 solution and original material of minerals and glass (for the laser ablation method).

2.2.1.1 Preparation of H_2SiF_6

The H_2SiF_6 solution was firstly used as the form for silicon isotope determination with MC-ICPMS in 2002 (De La Rocha, 2002). In this experiment, the silica samples and standards are dissolved in 0.25 M HF, with Si concentrations kept below 40 mM to avoid formation of the volatile SiF_4. The NBS-28 and other pure silica samples are used without further cleaning. The organics of diatom sediment and sponge spicules are

EBSCOhost - printed on 2/10/2023 8:05 PM via . All use subject to https://www.ebsco.com/terms-of-use

cleaned before dissolution. After dissolution in HF, samples are diluted to 10 ppm Si (in the form of H_2SiF_6) in a 0.12 M HCl solution. The method of extracting Si from plants includes three separate steps (Engström et al., 2006): a) removal of organic matter in a muffle furnace at 550°C; b) hydrofluoric acid dissolution of the residue; c) chemical purification based on anion-exchange chromatography. Since induced fractionation might be introduced during the sample dissolution if Si is lost as SiF_4 (g) (De La Rocha et al., 1996; Iler, 1979), the added amount of hydrofluoric acid must be carefully chosen.

2.2.1.2 Preparation of H_4SiO_4

In preparation of the H_4SiO_4 solution for silicon isotope determination, the silicate minerals and rocks need to be decomposed and dissolved first. To avoid the use of HF, an alkaline fusion is used to dissolve silicates instead of attacking them with HF. Through this way, solid silicate samples are transformed into an aqueous and HF-free solution, which can be processed as water samples (Georg et al., 2006a). For this purpose, a fusion procedure is deployed using a solid sodium hydroxide (NaOH) flux. It just forms NaCl and H_2O by neutralization with HCl (Georg et al., 2006a).

Fusion of 1–20 mg of the powdered silicate material and about 200 mg of the solid NaOH flux is carried out in Ag crucibles for 10 min at 730°C in a muffle furnace (Georg et al., 2006a). After slight cooling, the crucibles and fusion cake are dropped directly into 30 mL Teflon vials containing 20 mL MQ-e water, in which the fusion cake dissolves. An ultrasonic probe is used to agitate the water for a few minutes to aid dissolution. After 24 h, the crucible contents are washed through PTFE funnels into a weakly acidified solution with a molarity of 0.12 HCl. To ensure the fusion cake is completely transferred, the crucibles are rinsed several times with water. The ratio of flux to acid is approximately 3.1 mL of a 10 M HCl or 2.2 mL of a 14 M HNO_3 for 200 mg NaOH flux. Final solutions of 0.5 to 1.0 L are stored in pre-cleaned FEP bottles, with Si concentrations between 1 and 20 ppm.

2.2.1.3 Chromatographic separation of Si

The silicon in solutions of decomposed silicate and plants and acidified river water samples are all separated and purified by going through chemical processes.

One way to separate Si from an ambient ionic species is based on an anion-exchange process (Engström et al., 2006; Wickbold, 1959). To make Si exchangeable with the anion resin, it needs to be converted to the weak divalent acid H_2SiF_6 that dissociates to the exchangeable anionic species SiF_6^{2-}. The Si recovery is in excess of 97% and Si becomes effectively separated from the ambient ionic species. The disadvantage of this method is the requirement of using HF.

Another way is based on a cation-exchange process (Georg et al., 2006a). The prevailing species of dissolved Si in natural waters is essentially non-ionic monosilicic acid $Si(OH)_4$, which is in equilibrium with the anionic silicate species $H_3SiO_4^-$ for

EBSCOhost - printed on 2/10/2023 8:05 PM via . All use subject to https://www.ebsco.com/terms-of-use

the pH range from 2 to 8. Thus, cation-exchange columns will not retain either Si species. The Si separation and purification is achieved using the BioRad cation exchange resin DOWEX 50W-X12 (200–400 mesh) in H^+ form, filled to a 1.8 mL resin bed in BioRad columns (Georg et al., 2006a). The resin is cleaned before use by multiple rinsing with HCl and HNO_3 and MQ-e water. Before loading the sample on the resin, the eluting water is checked for a neutral pH to ensure complete removal of any acids. Since the prevailing Si species do not bind to the resin, the used elute is simply MQ-e water. The cation exchange resin effectively retains all the ambient cationic species. This chromatographic method allows relatively small amounts of the sample to be processed. The amount of Si used (Georg et al., 2006a) is approximately 80 times less than that used for the anion exchange approach (Engström et al., 2006). This procedure is used to process both fused solutions and acidified river water samples. Using this procedure, a set of river water samples can be completely processed through the columns within 4 h, including the pre-cleaning steps (Georg et al., 2006a).

2.2.1.4 Sample preparation of LA-MC-ICPMS analysis

For silicon isotope determination with laser ablation MC-ICPMS, the samples are mounted to a sample holder in the form of polished blocks, thin sections or as the original, unmodified material (Chmeleff et al., 2008).

Shahar et al. (2011) uses a 193 nm excimer as the tool of laser ablation, which operates with a pulse repetition rate of 2 to 5 Hz and UV fluence of ~22 J/cm^2. The cylindrical ablation pit diameters vary between 86 µm and 172 µm and are approximately 30–50 µm deep. Ablation products are flushed from the ablation cell in a flow of He gas and then mixed with Ar and N_2 gas before the introduction to the mass spectrometer. Accuracy of isotope ratios is found to be dependent on the distance of the torch from the sample cone of the mass spectrometer. This is a phenomenon that is widely understood as the result of changing the position within the plasma at which the sample is introduced (Pearson et al., 2008).

In another case, Chmeleff et al. (2008) uses an in-house built laser ablation system based on a 100 fs Ti-Sapphire regenerative amplifier system (Horn and von Blanckenburg, 2007). The output of the amplifier is 1.1 mJ/pulse at a wavelength of 785 nm. BBO (Barium-beta borate) crystals convert the fundamental wavelength into the UV range. The final output comprises two usable laser beams of different wavelengths with a pulse duration of about 200 fs: 196 nm with 0.03 mJ/pulse and 262 nm with 0.25 mJ/pulse. After frequency conversion, the laser beam is focused onto the sample material that is mounted to a sample holder as polished blocks, thin sections or as the original, unmodified material. The sample material together with the standards are placed in a 25 cm^3 cell made of Pyrex that has three gas inlets with a nozzle size of 0.5 mm and a gas outlet of 6 mm in diameter. That cell permits to minimize volume and maximize area to fit calibration standards together with a stan-

EBSCOhost - printed on 2/10/2023 8:05 PM via . All use subject to https://www.ebsco.com/terms-of-use

dard size thin section, which is essential when using the standard-sample bracketing technique. The spot location and visualization is carried out using a New Wave Femto XP stage/visualization system. The spot size can be varied from 50 µm to 2 µm. This system also allows fast spot location changes for the standard bracketing technique.

2.2.2 Silicon isotope determination by MC-ICPMS

As shown in Figure 2.5, the MC-ICPMS consists basically of 6 parts: (1) plasma region; (2) interface region and transfer optics; (3) electrostatic analyzer; (4) analyzer gate; (5) magnetic analyzer; (6) detector.

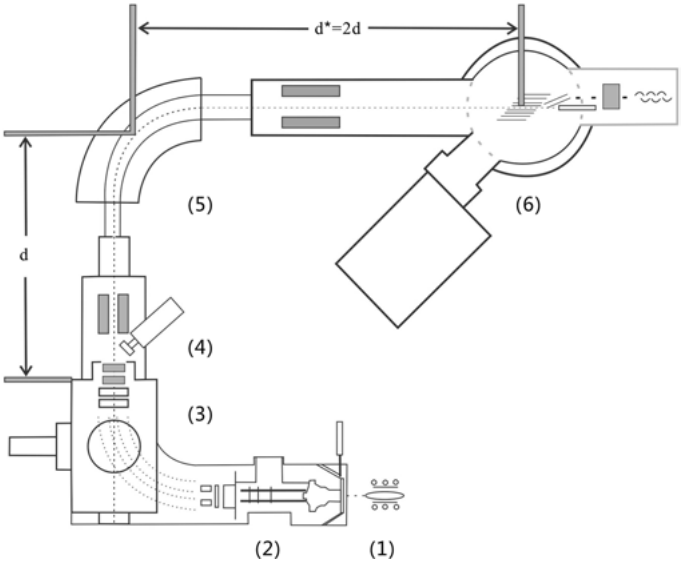

Figure 2.5: Schematic presentation of the high-resolution MC-ICP-MS Neptune; (1) plasma region; (2) interface region and transfer optics; (3) electrostatic analyzer; (4) analyzer gate; (5) magnetic analyzer; (6) detector.

As mentioned above, the major disadvantage of MC-ICPMS measurement of silicon isotopes during the early stage of the development of this method is the difficulties in accurately measuring ^{30}Si (De La Rocha, 2002; Cardinal et al., 2003), due to the presence of isobaric interferences formed within the ICP source. As the new instrument with high mass resolution power (MRP) appears, this analytical difficulty has been overcome (Figure 2.6).

EBSCOhost - printed on 2/10/2023 8:05 PM via . All use subject to https://www.ebsco.com/terms-of-use

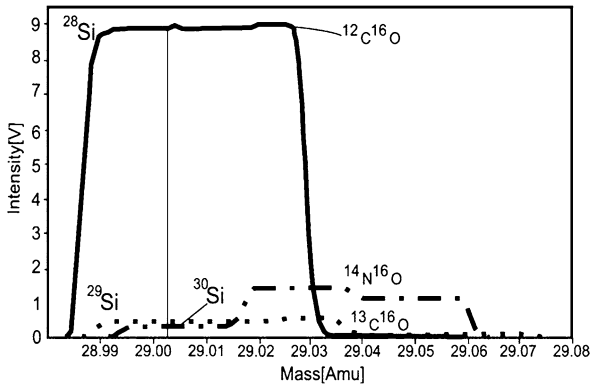

Figure 2.6: Mass scans of ^{28}Si, ^{29}Si and ^{30}Si showing that interferences are resolved for the three isotopes and that the interference-free plateaus are of sufficient width to allow for precise measurements. The sample used is IRMM-017 (pure Si), with a repetition rate of 25 Hz. After Chmeleff et al., 2008.

2.2.2.1 Analysis of H_2SiF_6

In the first practice of silicon isotope determination with MC-ICPMS (De La Rocha, 2002), the H_2SiF_6 solution is used as the form for silicon isotope determination and the measurement is carried out in an instrument manufactured by Nu Instruments Ltd. This mass spectrometer combines a double-focusing Nier–Johnson analyzer with variable dispersion ion optics, allowing the use of a fixed static array of Faraday collectors (Belshaw et al., 1998). RF power is set at 1 200 W, and samples are introduced through a HF-resistant PFA nebulizer, a HF-resistant, low-volume spray chamber and a ceramic and alumina fully demountable torch in order to avoid high silicon blanks associated with quartz nebulizers, spray chambers and torches. Desolvation of solutions containing Si and F results in the disappearance of silicon (most likely as SiF_4 gas) and is thus rejected as a method of sample introduction for Si analysis. Beams of masses 28, 29 and 30 are monitored on the innermost, axial and outermost Faraday collectors, respectively. Backgrounds for each sample are monitored using 0.12 M HCl solutions containing the same amount of HF as the sample in question. The measured backgrounds are then subtracted from the peak intensities of the sample. Instrumental mass fractionation is corrected for by standard-sample-standard bracketing. Isotope ratio variations are reported as δ^{29}Si or δ^{30}Si (De La Rocha, 2002).

2.2.2.2 Analysis of H_4SiO_4

At the present stage, the H_4SiO_4 solution is the major form for silicon isotope determination with MC-ICPMS (Georg et al., 2006a). The Nu Plasma 1700 and Neptune, which have high resolution capacity, are the most common instruments to be used. A mass resolution power (MRP) of 2 000 ($m/\Delta m$ at 10% peak valley) allows for a separation of the three Si^+ ion beams from all major polyatomic interferences, such as $^{12}C^{16}O^+$,

EBSCOhost - printed on 2/10/2023 8:05 PM via . All use subject to https://www.ebsco.com/terms-of-use

$^{14}N^{14}N^+$, $^{14}N^{15}N^+$, $^{14}N^{14}NH^+$ and $^{14}N^{16}O^+$. The unique high resolving power of the Nu Plasma 1700 and Neptune allows for the isolation of interferences to both the high and low mass sides of the Si^+ peak while maintaining flat-topped peaks. Furthermore, SiH^+ and Fe^{2+} interferences can be resolved. All three Si peaks are measured simultaneously in a static mode with Faraday collectors. The mass bias of the Nu Plasma 1700 is very stable with a drift in $^{30}Si/^{28}Si$ of standard solutions of < 1‰ over 60 h. It is corrected by standard-sample bracketing. External mass bias correction using Mg isotopes was proposed (Cardinal et al., 2003; Engström et al., 2006), but it has been later rejected due to the significant differential behavior of Si and Mg isotopes within the plasma (Georg et al., 2006a).

2.2.2.3 LA-MC-ICPMS determination of silicon isotopes

The Neptune MC-ICPMS (Weyer and Schwieters, 2003) is used more frequently (Chmeleff et al., 2008; Shahar et al., 2011) for measuring the silicon isotopic ratios of the laser ablation products of silicates and metals. Three Faraday collectors are spaced to collect $^{28}Si^+$, $^{29}Si^+$ and $^{30}Si^+$ simultaneously. Potential mass interference species ($^{12}C^{16}O^+$, $^{28}N_2^+$, $^{28}SiH^+$ and $^{14}N^{16}O^+$) are resolved by operating at a MRP of ~8 000. Corrections for instrumental mass bias are performed by sample-standard bracketing using San Carlos olivine (Shahar et al., 2011), IRMM017 and NBS28 (Chmeleff et al., 2008) as an in-house standard. Isotope analyses are corrected by subtracting a preceding on-peak background measurement.

Ablation products are flushed from the ablation cell in a flow of He gas and then mixed with Ar and N_2 gas before the introduction to the mass spectrometer. The addition of the nitrogen gas is essential to increase the sensitivity of the instrument. In the meanwhile, it also increases the background (especially $m/z = 28$). As the intensity of the three beams is large relative to the background and the background is stable, resulting from a steady flow of N_2, on-peak subtraction of the background is used for all measurements. By ablating a synthetic glass prepared with 1% ^{28}Si spike (Shahar and Young, 2007), the accuracy of isotope ratios is found to be dependent on the distance of the torch from the sample cone of the mass spectrometer. This phenomenon is explained as the result of changing the sample introduction position within the plasma (Pearson et al., 2008). As the torch moves away from the cones, the temperature of plasma decreases and the mass bias is changed. While this is not much of a problem for solutions, laser ablation is especially sensitive to the torch position. For example, in laser ablation runs, standard and sample do not have the same matrix composition and, therefore, standard sample bracketing does not compensate for the torch being in a less than optimal position. Accordingly, in order to ensure accuracy, the torch position is finely tuned several times each day using materials of a known isotopic composition. In practice, the optimal torch position is found to be stable for a day to several days. Precision of the LA-MC-ICPMS analyses is on the order of ±0.4‰ for $\delta^{30}Si$. NBS-28 and IRMM017 are mostly used as calibration samples in the Si isotope determination

EBSCOhost - printed on 2/10/2023 8:05 PM via . All use subject to https://www.ebsco.com/terms-of-use

with fs LA-MC-ICPMS (Chmeleff et al., 2008). Meanwhile, an in-house standard, such as the San Carlos olivine, is also used for calibrating the measurement results (Shahar et al., 2011). In the measurement made by using a fs LA-MC-ICPMS, signal intensities of standards and samples are matched using variable repetition rates of the laser so that any residual Si background level is cancelled out (Chmeleff et al., 2008). Since different matrices are investigated, such as the diopside composition glass or olivine, both of which contain less Si than the quartz that is used for standardization (NBS-28), repetition rates are increased accordingly. Typically, pure Si (IRMM-017) is measured with a repetition rate of 30 Hz, whereas quartz (NBS-28, SiO_2) is measured with a repetition rate of 80 Hz. For minerals like olivine, the repetition rate used is as high as 120 Hz. For diopside glass, the rate is usually 150 Hz.

In the determination process of using a fs LA-MC-ICPMS (Chmeleff et al., 2008), the instrument is optimized (gas flows and ion optics) on a daily basis in order to achieve the highest sensitivity and signal stability as well as the best peak shape of ^{28}Si. The stability and flatness of the isotope's plateaus are checked prior to the measurements. The plateau width on ^{29}Si and ^{30}Si are ~150 ppm. The instrument requires 2 h for stabilization after plasma ignition and laser tune-up.

The sample consumption per measurement is estimated to be $\sim 36 \times 10^3$ μm^3 for quartz and $\sim 67.5 \times 10^3$ μm^3 for materials with less Si (Chmeleff et al., 2008). The weight of the Si consumption in quartz can be calculated to be ~50 ng per sample (Chmeleff et al., 2008).

The reproducibility of the laser ablation methods is estimated to be ±0.24‰ (2std) for $\delta^{30}Si$, and ±0.15‰ (2std) for $\delta^{29}Si$ (Chmeleff et al., 2008).

2.3 Secondary ion mass spectrometry analyses

The secondary ion mass spectrometer (SIMS) was developed in the 1970s of the twentieth century (Andersen, 1970; Bakale et al., 1975; Giletti et al., 1978; Lee et al., 1977; Lovering, 1975; Yund and Anderson, 1974). Differing to IRMS, thermal ionization mass spectrometer (TIMS) and ICPMS, it measures secondary ions instead of the primary ions (Figure 2.7). In SIMS, secondary ions are produced by the ion bombardment on the surface of the sample to be analyzed. Firstly, the samples of the rock chips are cut from a drill core and hand samples with a water-cooled diamond saw, cleaned with distilled water and embedded in the epoxy plugs. Prior to SIMS analyses, all samples are carbon-coated and imaged with a scanning electron microscope (SEM) in backscattered electron (BSE) and secondary electron (SE) modes. After SIMS analyses, all SIMS pits and surrounding areas are imaged in BSE, SE to determine the accuracy in placement of the ion beam. Data from pits containing a mixture of minerals, large cracks or large cavities are rejected. Then the epoxy plugs with samples are put in a sample holder of the SIMS. Focusing of the bombarding ions into a fine beam allows in situ analysis of individual mineral phases.

EBSCOhost - printed on 2/10/2023 8:05 PM via . All use subject to https://www.ebsco.com/terms-of-use

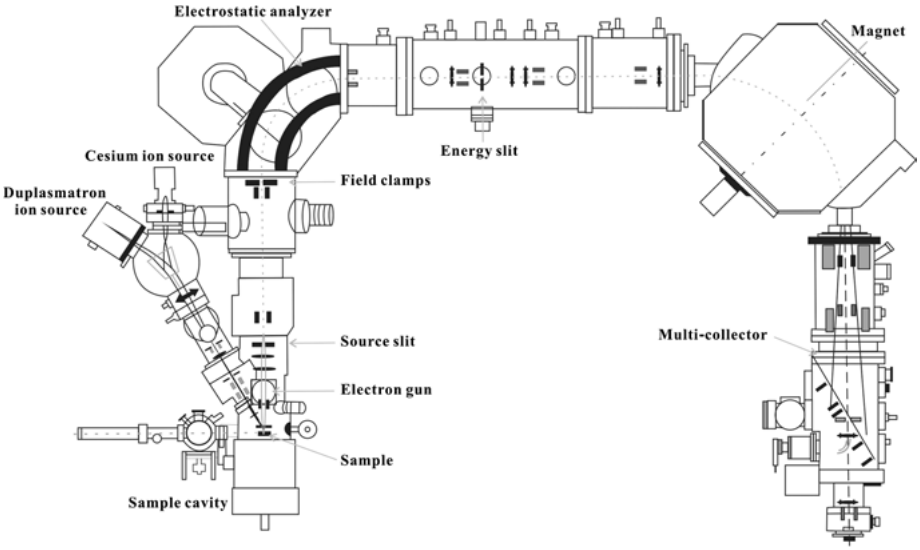

Figure 2.7: A schematic diagram of a secondary ion mass spectrometer. Modified from Kozdon et al. (2011).

The main advantages of the technique are high sensitivity, small sample size and measurement of elements that are difficult to analyze by other techniques. However, there are also problems with this technique, such as the interference of molecular ions with the atomic ions of interest, large variation of the ionization efficiencies of different elements and so-called matrix-effect.

Several types of SIMS, such as the IMS 3f, IMS 1270, IMS 1280, Nano-SIMS and the Sensitive High Mass Resolution Ion Microprobe (SHRIMP) have been applied to isotopic measurements on extra-terrestrial material and terrestrial rocks. The application includes U-Pb dating of individual zircons and the study of the distribution of Pb, S, H, C, O, Mg, Si isotopes in a number of minerals (Santosh et al., 2012; Kita et al., 2012; Girard et al., 2001; Russell et al., 2010; Kozdon et al., 2010; Arehart et al., 1993; Spetsius et al., 2009; Whitehouse et al., 2005). A schematic diagram of a SIMS is illustrated in Figure 2.7. The general aspects of isotopic measurement with SIMS have been described in detail (McKeegan et al., 1985; Clement and Compston, 1989).

SIMS was firstly used for silicon isotope determination in 1985 on individual interplanetary dust particles (McKeegan et al., 1985). In the 1980–1990s of the last century, SIMS was mainly used on silicon isotope determination of SiC from meteorites (Zinner et al., 1987, 1989; Stone et al., 1991; Hoppe et al., 1993, 1995; Lugaro et al., 1999). In this century, the SIMS method for silicon isotope determination has been used more frequently to terrestrial samples or laboratory experimental samples, such as the Precambrian chert (Marin-Carbonne et al., 2011; Chakrabarti et al., 2012), the quartz band in banded iron formation (BIF) (Heck et al., 2011), and the CAI-like vacuum evaporation residues (Knight et al., 2009).

EBSCOhost - printed on 2/10/2023 8:05 PM via . All use subject to https://www.ebsco.com/terms-of-use

Silicon isotopes can be measured as positive (McKeegan et al., 1985; Clayton et al., 1991) or negative ions (Zinner et al., 1987, 1989). The positive ions are generated by using the O^- primary beam and the negative ions are generated by using Cs^+ primary beam. It is found that negative secondary ions gave a higher ion yield and less instrumental mass fractionation than positive ones (Knight et al., 2009). Thus, the Cs^+ primary beam has been used more frequently recently, especially when silicon and oxygen isotopes of chert and quartz are determined simultaneously (Marin-Carbonne et al., 2011; Heck et al., 2011).

The characters of some secondary ion mass spectrometers are listed in Table 2.1. Now the commonly used instruments for silicon isotope determination are IMS 1270 and IMS 1280. The current of primary Cs^+ beam vary from 2.5–3.0 nA (Heck et al., 2011) to 8–30 nA (Marin-Carbonne et al., 2011). The diameter of the rastered field is normally 10–25 μm. The MRP used varies from 2 200 to 4 000 (Heck et al., 2011; Knight et al., 2009; Marin-Carbonne et al., 2011), depending on the required accompany analysis of isotopes other than Si. The analytical precisions can be reached are 0.30‰ for δ^{30}Si (2std) at the present stage (Heck et al., 2011).

Table 2.1: The characters of some secondary ion mass spectrometers.

Type of instrument	Sample	Primary beam	Current (nA)	Rastered diameter (μm)	MRP	Precision (‰) (2std)	Reference
IMS-3f	SiC	$^{16}O^-$	0.2–0.5	20	3 000–2 400	δ^{30}Si: < ±2	Stone et al. (1991)
IMS-3f	SiC	Cs^+	~0.1	20	~3 500	δ^{30}Si: ±4	Stone et al. (1991)
IMS 1270	cherts	Cs^+	8–30	25	~4 000	δ^{30}Si: ±0.6	Marin-Carbonne et al. (2011)
IMS-1280	BIF	Cs^+	2.5–3	10–15	2 200	δ^{30}Si: ±0.30	Heck et al. (2011)
IMS-1280	evaporation residues	Cs^+	5	10	2 200	δ^{29}Si: ±0.32 δ^{30}Si: ±0.52	Marin-Carbonne et al. (2011)

As for the LA-MC-ICPMS determination, proper correction on the "matrix effects" is very important to obtain accurate determination of the silicon isotope by using the SIMS method. It is known that for a number of elements, especially for silicon (Knight et al., 2009), the instrumental mass fractionation (IMF) varies as the chemical composition of sample changes. Such variations are often referred to as "matrix effects". The best way to make the proper correction on the "matrix effects" is to compare the data of the sample directly with that of the standard that has similar chemical composition. It has been found that there is no significant matrix effect between quartz and

EBSCOhost - printed on 2/10/2023 8:05 PM via . All use subject to https://www.ebsco.com/terms-of-use

chert (Marin-Carbonne et al., 2011), but the matrix effect in silicon isotope determination of the CAI-like vacuum evaporation residues is significant (Knight et al., 2009). In order to correct data of evaporation residues for matrix effects, a set of chemically and isotopically homogeneous glasses with bulk chemical compositions similar to those of the evaporation residues has been prepared and their silicon isotope compositions are calibrated. By examining the relationship between a number of compositional parameters and silicon isotope compositions, a proper correction on the matrix effects can be obtained.

2.4 Standards and reference materials for silicon isotope measurement

Generally, stable isotope compositions are expressed as the δ values related to a certain standard. Thus, preparation of related standards is critical to establish the basis and scales for isotope ratio measurements and obtain comparable results of isotope compositions. Two samples, i.e., NBS-28 and rose quartz, have been used as standards for silicon isotope compositions (Epstein and Taylor, 1970; Clayton et al., 1978; Douthitt, 1982; Ding et al., 1988a; De La Rocha et al., 1996; Ding, 2004). Besides, a number of other reference materials and in-house working standards have been proposed and used in various laboratories for different applications. The characters of some standards, reference material and in-house working standards for silicon isotopes are listed in Table 2.2.

NBS-28 is a sample of quartz sand distributed by the National Institute of Standards and Technology, USA (NIST) as an oxygen isotope reference material for silicates. It is used firstly in the laboratories of the Chicago University as silicon isotope reference material. Then this sample has been adopted in IMR and a number of other institutions as a standard of silicon isotope compositions. It is proven to be homogeneous in its silicon isotope compositions and is accepted as an international standard of silicon isotope compositions (Clayton et al., 1978; Ding et al., 1988a; De La Rocha et al., 1996; Ding, 2004; Chmeleff et al., 2008; Reynolds et al., 2007; Coplen et al., 2002).

Rose quartz is a quartz sample used in the California Institute of Technology as a reference material for oxygen and silicon isotopes. This sample has been measured in several laboratories, and its $\delta^{30}Si_{NBS\text{-}28}$ value (Table 2.2) is found to be slightly inhomogeneous (De La Rocha et al., 2000; Molini-Velsko et al., 1986; Georg et al., 2007a). IRMM 018 is a quartz sample distributed by IRMM. This sample has been measured by several laboratories with IRMS and ICPMS (Ding, 2004; Ding et al., 2005b; Chmeleff et al., 2008; De Bièvre et al., 1994; Reynolds et al., 2006a, 2007; Van den Boorn et al., 2006) and its silicon isotope composition has been found very inhomogeneous (Chmeleff et al., 2008; Reynolds et al., 2007). Besides, this sample has already been exhausted (Valkiers et al., 2005). IRMM 018a is another quartz sample distributed by

EBSCOhost - printed on 2/10/2023 8:05 PM via . All use subject to https://www.ebsco.com/terms-of-use

Table 2.2: The $\delta^{30}Si_{NBS\text{-}28}$ values of some reference materials and working standards for silicon isotopes

Sample No.	Type of sample	Origin of the sample	$\delta^{29}Si_{NBS\text{-}28}$ (‰) (2std)	$\delta^{30}Si_{NBS\text{-}28}$ (‰) (2std)	Reference
NBS-28	Quartz	NIST, USA	0	0	International standard
Rose Quartz	Quartz	Caltech, USA		−0.28(±0.2)	Molini-Velsko et al. (1986)
				−0.30(±0.2)	De La Rocha et al. (2000)
				−0.1(±0.1)	Georg et al. (2007a)
				0.26(±0.75)	Basile-Doelsch et al. (2005)
			0.05(±0.08)	0.10(±0.13)	Chmeleff et al. (2008)
IRMM-017	Si metal	IRMM, EU	−0.63	−1.28(±0.06)	Coplen et al. (2002)
			−0.72(±0.06)	−1.33(±0.06)	Ding et al. (2005b)
			−0.65(±0.14)	−1.25(±0.24)	Chmeleff et al. (2008)
IRMM-018	Quartz	IRMM, EU		0.0(±0.1)	Ding (2004)
			−0.03(±0.06)	−0.05(±0.06)	Ding et al. (2005b)
			0.79	1.58	De Bièvre et al. (1994)
			−0.83(±0.1)	−1.61(±0.14)	Reynolds et al. (2006a)
			−0.90(±0.1)	−1.75(±0.25)	Van den Boorn et al. (2006)
			−0.85(±0.14)	−1.62(±0.22)	Reynolds et al. (2007)
IRMM-018a	Quartz	IRMM, EU	0.08(±0.12)	−0.05(±0.16)	Valkiers et al. (2005)
SRM-990	Si metal	NIST, USA	0.30(±0.06)	0.58(±0.08)	Ding et al. (2005b)
GBW-04421	Quartz in Quartzite	IMR, CAGS		−0.02(±0.1)	Wan et al. (1997)
			−0.02(±0.08)	−0.04(±0.08)	Ding et al. (2005b)
GBW-04422	SiO_2 reagent	IMR, CAGS		−2.68(±0.1)	Wan et al. (1997)
			−1.36.(±0.08)	−2.65(±0.08)	Ding et al. (2005b)
Big Batch	SiO_2	Marine Science Institute, USCB, USA	−5.39(±0.3)	−10.52(±0.41)	Van den Boorn et al. (2006)
			−5.35(±0.3)	−10.48(±0.54)	Reynolds et al. (2007)
			−5.29(±0.82)		Cardinal et al. (2003)
Sponge needles	SiO_2	Atlantic Ocean	−1.10(±0.19)	−2.17(±0.32)	Chmeleff et al. (2008)
San Carlos Olivine	Olivine	Arizona, USA	−0.41(±0.11)	−0.81(±0.19)	Chmeleff et al. (2008)
JER-diopside glass	Diopside glass	Geoinstitute, Bayreuth, Germany		0.00(±0.09)	Chmeleff et al. (2008)
UWQ-1	quartz	Univ. of Wisconsin		−0.03(±0.08)	Heck et al. (2011)

IRMM to replace IRMM 018 (Valkiers et al., 2005). The silicon isotope composition of IRMM 018a is very close to that of NBS-28 (see Table 2.2).

GBW-04421 is a quartz sample separated from a Proterozoic quartzite, which has a silicon isotope composition similar to that of NBS-28 (see Table 2.2). GBW-04422 is a sample of SiO_2 chemical reagent, which has a silicon isotope composition much lower than that of NBS-28 (see Table 2.2). These two samples are prepared by IRM and have

EBSCOhost - printed on 2/10/2023 8:05 PM via . All use subject to https://www.ebsco.com/terms-of-use

been granted to be national standard materials for silicon isotope compositions in China (Wan et al., 1997; Ding, 2004; Ding et al., 2005b). Both of these two samples are homogeneous isotopically and have been used in China for more than 20 years.

IRMM-017 is a silicon metal sample distributed by IRMM, which has a silicon isotope composition slightly lighter than that of NBS-28. This sample has been used in several laboratories as silicon isotope reference material for silicon metal samples and is proven to be homogeneous isotopically (Ding et al., 2005b; Chmeleff et al., 2008; Coplen et al., 2002). SRM-990 is a silicon metal sample distributed by NIST, which has a silicon isotope composition slightly heavier than that of NBS-28. It is found that SRM-990 is homogeneous isotopically (Ding et al., 2005b; Coplen et al., 2002), and is suitable as a reference material for silicon metal samples.

Big Batch is a highly fractionated SiO_2 material prepared at the Marine Science Institute, University of California Santa Barbara. This sample has very light and homogeneous silicon isotope composition and can be used as a reference material to set the scale for silicon isotope calibration (Cardinal et al., 2003; Georg et al., 2006a; Chmeleff et al., 2008; Reynolds et al., 2007; Van den Boorn et al., 2006).

The samples of San Carlos Olivine (olivine mineral), JER-diopside glass (glass with diopside composition), UWQ-1(quartz) and Sponge needles (SiO_2) are all in-house working standards, which are prepared for making correction of the "matrix-effect" in silicon isotope determination with LA-MC-ICPMS and SIMS (Georg et al., 2006a; Heck et al., 2011).

According to the condition described above, significant progress has been achieved in preparation and calibration of silicon isotope standards and reference materials. However, there is still a long way to go before a proper set of silicon isotope reference materials is established. Firstly, a formal decision has to be made by the authoritative international organization on which material will be chosen as the international standard for silicon isotopes. Secondly, a set of reference materials on silicon isotope compositions need to be established to set the scale for silicon isotope measurement. Thirdly, a large number of working standards, including various minerals and glasses with different chemical compositions, needs to be prepared and their silicon isotope composition needs to be calibrated to satisfy the requirements of making in situ silicon isotope determination on materials with different chemical compositions by using LA-MC-ICPMS and SIMS.

Besides, calibration of "absolute" silicon isotope abundance ratios and revising atomic weights of silicon in the reference materials are also important tasks. The precise determination of "absolute" silicon isotope abundance ratios has very important significance to establish the basis and scales for silicon isotope determination.

Some research on this issue have been carried out in IRMM (Valkiers et al., 2005) and IMR (Ding et al., 2005b). The results are summarized in Table 2.3. It seems that there are some discrepancies between these results. More investigation has to be undertaken to solve these problems.

EBSCOhost - printed on 2/10/2023 8:05 PM via . All use subject to https://www.ebsco.com/terms-of-use

Table 2.3: The calibrated $^{29}Si/^{28}Si$ and $^{30}Si/^{28}Si$ ratios of several silicon isotope reference materials

Sample	$^{29}Si/^{28}Si$	$^{30}Si/^{28}Si$	Atomic weight of silicon	Reference
NBS-28	0.0507446 (26)	0.0341465 (15)	28.08653 (11)	Ding et al. (2005b)
	0.0508229 (20)	0.0335336 (20)	28.08553 (11)	Valkiers et al. (2005)
SRM-990	0.0507603 (30)	0.0341670 (21)	28.08658 (13)	Ding et al. (2005b)
IRMM-017	0.0507081 (30)	0.0341011 (18)	28.08642 (13)	Ding et al. (2005b)
	0.0507715 (66)	0.0334889 (78)	28.08541 (15)	De Bièvre et al. (1994)
IRMM-018	0.0507431 (30)	0.0341448 (18)	28.08653 (13)	Ding et al. (2005b)
	0.0508442 (48)	0.0335851 (66)	28.08564 (12)	De Bièvre et al. (1994)
IRMM-018a	0.0508272 (20)	0.0335320 (21)	28.08553 (11)	Valkiers et al. (2005)
GBW-04421	0.0507436 (33)	0.0341451 (21)	28.08653 (14)	Ding et al. (2005b)
GBW-04422	0.0506756 (33)	0.0340560 (21)	28.08632 (14)	Ding et al. (2005b)

The uncertainties (2std) are given in brackets. They apply to the last two digits.

2.5 Comparison of different methods on silicon isotope analyses

From the above description, we can see that there are three major types of silicon isotope analytical methods: IRMS, MC-ICPMS and SIMS. Each major type consists of several subtypes of analytical methods. The general characters and major applications of different methods are summarized in Table 2.4.

The IRMS determination method includes 4 subtypes of analytical methods: a) $BaSiF_6$ decomposition; b) reaction with (F_2+HF); c) reaction with BrF_5 and d) reaction with (F_2+HF) or BrF_5 under Laser heating.

The $BaSiF_6$ decomposition method needs relatively large amounts of the sample (in g level), and its chemical procedure is time consuming and requires great care to prevent silicon isotope fractionation. Thus, this method is rarely used in the routine analysis of silicon isotopes. At present, it is only used to make the determination of "absolute isotope ratios" and atomic weight of silicon (De Bièvre and Valkiers, 1994; Valkiers et al., 2005). However, some effort has been made to produce SiF_4 by using the acid decomposition of cesium hexafluosilicate and make the automated determination of silicon isotope compositions (Brzezinski et al., 2006).

The SiF_4 preparation method by reaction with (F_2+HF) needs also a relatively large sample and the precision of the method is not good enough (Epstein and Taylor, 1970; Douthitt, 1982). Thus, this method was only used in the 1970s and 1980s of the twentieth century. Since the 1990s of the twentieth century, no results obtained with this method have been reported.

The SiF_4 preparation method by reacting with BrF_5 can analyze a relatively small size of samples (containing about 2 mg of SiO_2) with high precision (±0.10‰, 2 std) (Ding, 2004; Ding et al., 2005b). All pure silica and silicate minerals can be fluorinated directly by BrF_5. All silicon-bearing materials (such as water samples, soils, plants, diatoms, radiolarian and sponge) can be converted by ordinary chemical processes to

EBSCOhost - printed on 2/10/2023 8:05 PM via . All use subject to https://www.ebsco.com/terms-of-use

Table 2.4: A comparison of Si isotope analytic methods

Type of the Instrument	Sample preparation	Minimum sample size (mol of Si)	Precision (2STD)	Major Application	Reference
IRM (MAT-251, MAT-252 and MAT-253)	SiF_4 preparation by $BaSiF_6$ decomposition	357	±0.30‰ for $\delta^{30}Si$	Determination of "absolute isotope ratios" and atomic weight of silicon	Reynolds and Verhoogen (1953), De Bièvre and Valkiers (1994), De Bièvre et al. (1994, 1995), Valkiers et al. (2005, 2011)
	SiF_4 preparation by reaction with (F_2+HF)	128	±0.6‰ for $\delta^{30}Si$	Silicon bearing minerals, rocks and soils	Epstein and Taylor (1970), Douthitt (1982)
	SiF_4 preparation by reaction with BrF_5	30	±0.10‰ for $\delta^{29}Si$, ±0.10‰ for $\delta^{30}Si$	a) silicon bearing minerals and rocks b) Si extracted from diatoms, soils waters, plants and silicate minerals c) determination of "absolute isotope ratios" and atomic weight of silicon	Coplen et al. (2002), Ding et al. (1988a, 2005b), Ding (2004)
	SiF_4 preparation by reaction with (F_2+HF) or BrF_5 under Laser heating	8	±0.10‰ for $\delta^{29}Si$, ±0.30‰ for $\delta^{30}Si$	a) silica and silicate minerals b) Si extracted from diatoms, soils, plants and waters	De La Rocha et al. (1996), Ding (2004)

EBSCOhost - printed on 2/10/2023 8:05 PM via . All use subject to https://www.ebsco.com/terms-of-use

Table 2.4: (Continued)

Type of the Instrument	Sample preparation	Minimum sample size (mol of Si)	Precision (2STD)	Major Application	Reference
MC-ICPMS (Nu Plasma 1700 and Neptune)	H_2SiF_6 solution	15	± 0.2% for $\delta^{29}Si$	Si extracted from diatoms and sponges	De La Rocha (2002)
	H_4SiO_4 solution	10	±0.10‰ for $\delta^{29}Si$, ±0.14‰ for $\delta^{30}Si$	Si extracted from diatoms, soils waters, plants and silicate minerals	Georg et al. (2006a), Reynolds et al. (2007)
	Laser ablation	0.0008	±0.15‰ for $\delta^{29}Si$, ±0.24‰ for $\delta^{30}Si$	a) in situ measurement of silica and silicate minerals b) Si extracted from diatoms, soils, plants and water	Chmeleff et al. (2008), Shahar et al. (2011)
SIMS (IMS-3f, IMS-1270 and IMS-1270)	Using O^- as primary ion	0.0001	±2‰ for $\delta^{30}Si$	In situ determination of SiC	Zinner et al. (1987, 1989), Stone et al. (1991), Hoppe et al. (1993, 1995), Lugaro et al. (1999)
	Using Cs^+ primary ion	0.0001	±0.32‰ for $\delta^{29}Si$, ±0.52‰ for $\delta^{30}Si$	In situ determination of quartz in BIF, chert and CAI-like vacuum evaporation residues	Marin-Carbonne et al. (2011), Heck et al. (2011), Knight et al. (2009)

EBSCOhost - printed on 2/10/2023 8:05 PM via . All use subject to https://www.ebsco.com/terms-of-use

SiO_2 first and then converted to SiF_4. So far, a large number of the silicon isotope data for rocks and minerals are obtained by using this method (Ding et al., 1988a, 1996; Song and Ding, 1990; Jiang et al., 1992, 1993, 1994). A large number of silicon isotope data for river water (Ding et al., 2004, 2011), plants (Ding et al., 2005a, 2008a,b) and radiolarian (Song and Ding, 1990; Wu et al., 1997) are also obtained by using this method. Due to the high accuracy of this method, it has been applied to the calibration of silicon isotope reference materials (Weyer and Schwieters, 2003; Ding, 2004) and to the determination of "absolute isotope ratios" and the atomic weight of silicon isotope standards (Ding et al., 2005b).

It was concerned that this method is not safe for using hazardous BrF_5 gas (De La Rocha, 2002; Georg et al., 2006a). However, this kind of problem is not a serious one, for the BrF_5 reagent and waste gas are all handled in the metal vacuum line and the amount of the BrF_5 reagent used for each sample is very small (about 300 mg for a SiO_2 sample of 10 mg) (Ding, 2004). On the other hand, it is true that this method is in some extent time consuming (Georg et al., 2006a). Thus, in some conditions, for example, to measure the silicon isotope composition of water solutions, this method may be replaced by using other more convenient methods. Nevertheless, this method is still the classical and conventional method for silicon isotope determination and will continue to play an important role in silicon isotope geochemical studies, especially in the analyses of rocks and minerals and in the calibration of silicon isotope reference materials and the determination of "absolute isotope ratios" and atomic weight of silicon isotope standards.

The method of the SiF_4 preparation by reaction with (F_2+HF) or BrF_5 under Laser heating is a newly established method for silicon isotope measurement. By using this method, a smaller sample (0.5 mg of garnet) than that of using convenient methods can be analyzed with good precision (±0.30‰ for δ^{30}Si, 2 std) (Gao and Ding, 2009). However, this method needs to be improved for analyzing even a smaller sample and making in situ determination of the silicon isotope variation within silicate minerals. If it is successful, it will be very helpful in preparing working standards for in situ silicon isotope determination and investigating silicon isotope fractionation between coexisting silicate minerals.

The MC-ICPMS method includes three subtype methods: a) H_2SiF_6 solution method; b) H_4SiO_4 solution method; and c) laser ablation method.

The H_2SiF_6 solution method was established in 2002 and used in the silicon isotope determination of Si extracted from diatoms and sponges (De La Rocha, 2002, 2003; De La Rocha and Bickle, 2005). However, this method is associated with some analytical difficulties. It is found that the presence of excess fluoride ions will impair the plasma ionization, and can lead to a loss of volatile SiF_4 during the sample introduction (Georg et al., 2006a). Furthermore, the use of HF requires special safety considerations and the need for special HF resistant sample introduction equipment (Georg et al., 2006a). Therefore, this method is not used very often at the present time.

EBSCOhost - printed on 2/10/2023 8:05 PM via . All use subject to https://www.ebsco.com/terms-of-use

The H_4SiO_4 solution method is the most commonly used method for the silicon isotope determination using MC-ICPMS. Using this method, a small sample with 1 mg silicate can be analyzed with the precision of ±0.14‰ (2 std) for δ^{30}Si determination. It has been used for the silicon isotope measurement of diatoms, soils, waters, plants and silicate minerals (Ziegler et al., 2005a,b; Georg et al., 2006a, 2009b; Reynolds et al., 2006b, 2007; Van den Boorn et al., 2006; Cardinal et al., 2010; Opfergelt et al., 2011b). This method has been even used to measure the isotopic purity of the ^{28}Si highly enriched silicon crystal that is specially prepared for the project of redetermination of the Avogadro constant (Pramann et al., 2011a,b). It has become one of conventional methods for silicon isotope determination; especially when doing the silicon isotope determination of natural water samples, this method is much faster and easier to be handled than the SiF_4 method. For analyzing samples of soils, plant, diatoms, sponges and radiolarian, the difference between the H_4SiO_4 solution method and the SiF_4 method becomes small, as both methods require samples to be purified through similar wet chemical processes. In contrast, in the analysis of separated silicate minerals and pure silicate rocks, the SiF_4 method is more convenient than the H_4SiO_4 solution method for no pre-treatment is needed for the former method.

The LA-MC-ICPMS method is a newly developed method for making in situ determination of silicon isotopes. The sample size for analysis can be as low as 50 ng (Chmeleff et al., 2008), and no chemical pre-treatment is needed for making analyses. The precision of analysis can reach to ±0.24‰ for δ^{30}Si (2 std) (Chmeleff et al., 2008). This method has been successfully applied to the in situ silicon isotope measurement of quartz and olivine minerals and glass samples. It will become a powerful method to study the silicon isotope fractionation between coexisting silicate minerals in various rocks and to investigate the silicon isotope variation in small bands of siliceous rocks or different layers in silicate minerals. These studies may provide us very important information on the forming conditions of the rocks and minerals and the paleenvironmental change of the Earth. Now the major task for developing this method is to overcome the so-called "matrix effect" by preparing a complete set of working standards that have chemical compositions similar to the materials to be studied, and calibrating their silicon isotope compositions.

The SIMS method includes two subtypes of methods: a) the method using O^- as the primary ion; and b) the method using Cs^+ primary ion.

By using O^- as the primary ion, the produced secondary ions are positive ones. This method was mainly applied at the silicon and carbon isotope determination of SiC in a meteorite (Zinner et al., 1987, 1989; Stone et al., 1991; Hoppe et al., 1993, 1995; Lugaro et al., 1999). The rastered diameter can be as small as 20 μm and sample size can be as small as 5 ng (Chmeleff et al., 2008; Zinner et al., 1987). The reported precision is ±2‰ for δ^{30}Si (2 std) (Zinner et al., 1987), which is sufficient for the study of the silicon isotope variation of SiC in a meteorite, which has a δ^{30}Si variation range of more than 100‰. However, due to the positive secondary ions giving a lower ion yield

EBSCOhost - printed on 2/10/2023 8:05 PM via . All use subject to https://www.ebsco.com/terms-of-use

and more instrumental mass fractionation than negative ones, this method is often replaced by the method of using Cs^+ as a primary beam (Knight et al., 2009).

When Cs^+ is used as a primary ion, the produced secondary ions are negative ones. As the negative secondary ions gave a higher ion yield and less instrumental mass fractionation than positive ones (Knight et al., 2009), the Cs^+ primary beam has been used more frequently recently, especially when silicon and oxygen isotopes of chert and quartz are determined simultaneously (Marin-Carbonne et al., 2011; Heck et al., 2011). Now this method has been used for the in situ determination of quartz in BIF, chert and CAI-like vacuum evaporation residues (Marin-Carbonne et al., 2011; Heck et al., 2011; Knight et al., 2009). The rastered diameter can be as small as 10 μm and sample size can be as small as 5 ng (Chmeleff et al., 2008; Zinner et al., 1987; Knight et al., 2009). The reported precision is ±0.32‰ for δ^{29}Si and ±0.52‰ for δ^{30}Si (2 std) (Zinner et al., 1987; Knight et al., 2009). There is no doubt that this method will be used more and more in the study of micro-scale silicon isotope variation in rocks and minerals and provide very important information on the genesis of rocks and minerals and the variation history of the Earth's environmental condition. As for the method of LA-MC-ICPMS, the major problem obstructing the further development of the SIMS method is the "matrix effect". For overcoming this problem, a complete set of working standards for the in situ determination of silicon isotopes should be prepared and their chemical and isotope compositions should be calibrated by the classical methods. These working standards should have chemical compositions similar to the materials to be studied, and their chemical and isotopic composition should be homogeneous enough.

EBSCOhost - printed on 2/10/2023 8:05 PM via . All use subject to https://www.ebsco.com/terms-of-use

3 Mechanisms of silicon isotope fractionation

In this chapter, we discuss the causes and mechanisms of silicon isotope fractionations, which provide the theoretical base for understanding the silicon isotope variation in nature. Similar to the isotopes of other elements, different Si isotope ratios occur between different silicon bearing compounds, different phases or different molecules, which are named as silicon isotope fractionations. The silicon isotope fractionation factor (α) is defined as the quotient between the silicon isotope ratio in matter A and that in matter B, i.e.,

$$\alpha = ({}^{*}\mathrm{Si}/{}^{28}\mathrm{Si})_{\mathrm{A}}/({}^{*}\mathrm{Si}/{}^{28}\mathrm{Si})_{\mathrm{B}} \tag{3.1}$$

where *Si can be referred to ^{29}Si or ^{30}Si.

There are two lines of factors controlling isotopic fractionation: the first is internal cause, i.e., the difference between the physical and chemical characteristics of different isotope species;the second is external cause, i.e., the variations in environmental conditions.

Isotopes of an element have the same number of protons, but a different number of neutrons, so their atomic masses are different from one another. For this reason, the different isotope species show different characters in various physical, chemical and biological processes, which cause isotope fractionations. In general, the degree of fractionation between two isotopic species is closely related to their relative mass differences $({}^{*}m - m)/m$; the larger the relative mass difference, the higher the degree of isotopic fractionation. The large fractionation between H and D is the most extreme example.

The relative mass difference between ^{30}Si and ^{28}Si is 1/14, which is equivalent to that between ^{15}N and ^{14}N, and even larger than that between ^{34}S and ^{32}S. Hence, the two silicon isotopes should have a large potential of isotopic fractionation.

However, the relative mass difference is just one factor affecting isotopic fractionation. It can play a role in isotopic fractionation only when favorable physical and chemical conditions are available, which are strongly dependent on the chemical characteristics of the element itself. Among these characters, the most important factors are whether the element can form compounds with different valences and whether their gas compounds exist in nature. In all silicon bearing compounds, silicon only shows a valence of +4. In the terrestrial environment, silicon always forms compounds with a Si–O bond and no gas compounds has been observed. Thus unlike other light elements, such as H, O, C, S and N, we do not see large silicon isotopic fractionation in the terrestrial samples. However, relatively large silicon isotope fractionation has been found in trace SiC mineral within meteorites, which might be formed from gas components.

It has been found that silicon isotope fractionation occurs in all kinds of extraterrestrial and terrestrial environments. Various types of silicon isotope fractionations

https://doi.org/10.1515/9783110402452-003

EBSCOhost - printed on 2/10/2023 8:05 PM via . All use subject to https://www.ebsco.com/terms-of-use

occurred in various physical, chemical and biological processes and have been studied by empirical investigation, experimental calibration and theoretical calculations. In general, the silicon isotope fractionation can be classified in two categories: i.e., the thermodynamic silicon isotope exchange fractionation and kinetic silicon isotope fractionation. In the following sections, we will discuss some major mechanisms of these two types of silicon isotope fractionation.

3.1 The thermodynamic silicon isotope exchange fractionation

Isotopic exchange reactions belong to an important class of stable isotope fractionation reactions. They include a number of processes with different mechanisms, but have the common characteristics of showing only the exchange of isotopes between different compounds, different phases or different molecules, but not chemical variations. In this section, the possibility and the scale of exchange equilibrium fractionation of silicon isotopes between different silicon-bearing compounds, phases and minerals will be discussed.

3.1.1 Types and structures of silicon-bearing compounds in nature

The existence of different types (composition and structures) of compounds is a prerequisite for isotopic exchange reactions, so the existence of different silicon bearing compounds is the basis of silicon isotope exchange reactions.

It was pointed out in Chapter 1 that there are only two important silicon-bearing compounds, i.e., the silicate and silica, even though silicon is very abundant in nature. They account for 87% of the Earth's crust by weight. The amounts of other silicon-bearing compounds, such as SiC, Si_3N_4 and Fe_3Si, are rather rare. The natural SiC, Si_3N_4 are found only in the meteorites and Fe_3Si is expected to occur in the core of the Earth.

The basic unit for silicates and silica is the Si–O tetrahedron. Because the ionic radii of silicon and oxygen are 0.042 nm and 0.132 nm, respectively, one cation of silicon can be enveloped by four anions of oxygen to form a stable Si–O tetrahedron. In the tetrahedron, Si and O are covalently bonded. Because of the similarity of the basic structure unit among different silicates and silica, a large isotopic exchange equilibrium fractionation of silicon isotopes is not expected between them.

Although the basic structures of silicates and silica are the same, the manner in which these basic units are connected can vary in different compounds. In some minerals, e.g., forsterite, the Si–O tetrahedra are isolated from each other, but connected through Mg cations, forming so-called nesosilicate (Figure 3.1a).

However, more often, the Si–O tetrahedra polymerize through one or more oxygen atoms to form silicates of different structure such as sorosilicate, cyclosilicate, inosili-

EBSCOhost - printed on 2/10/2023 8:05 PM via . All use subject to https://www.ebsco.com/terms-of-use

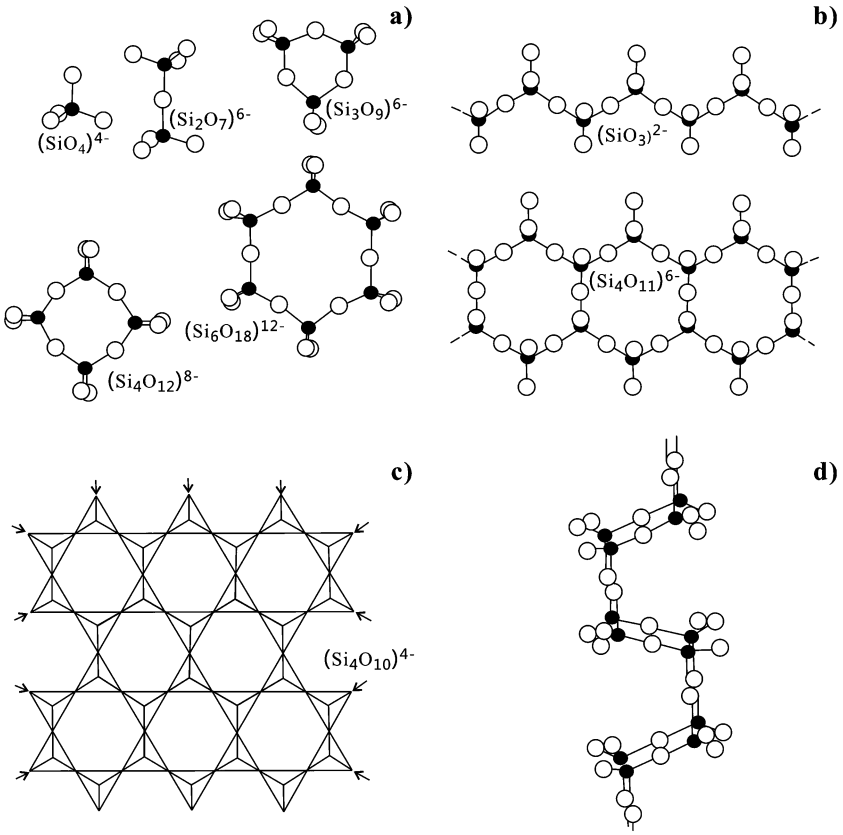

Figure 3.1: The structures of silicate crystals. a) Nesosilicate [$(SiO_4)^{4-}$], sorosilicate [$(Si_2O_7)^{6-}$], cyclosilicate (with Si:O=1:3); b) Inosilicate; c) Phyllosilicate; d) Tectosilicate.

cate, phyllosilicate and tectosilicate (Figure 3.1b, Figure 3.1c and Figure 3.1d). In these polymerized silicates, the oxygen atom shared by two Si–O tetrahedron is called an "oxygen bridge". The appearance of "oxygen bridges" causes variations in the vibrational frequency of the Si–O tetrahedron structure; the higher the fraction of "oxygen bridges" or degree of polymerization, the larger the vibrational frequency of the inner tetrahedron will be. According to the statistical mechanics, this kind of variation of vibrational frequency will cause silicon isotopic fractionation between silicate minerals and molecules with different degrees of polymerization.

However, the effects of polymerization on inner vibrational frequency are restricted, hence silicon isotope fractionation between different silicon bearing minerals is also limited.

Now, let us consider the case of silicate melt. According to the theory of crystallography, the basic difference between a melt and a crystal is the degree of order and the mobility of ions. At the temperature of crystallization, a crystal with a higher de-

EBSCOhost - printed on 2/10/2023 8:05 PM via . All use subject to https://www.ebsco.com/terms-of-use

gree of order is formed, in which the mobility of ions decreases. During melting, a melt with a low degree of order is formed, in which the mobility of ions increases. However, for silicate, the change of entropy during melting is small, so the difference in the degree of order between the melt and crystal is not large, hence changes in the partition coefficient and other coefficient of the molecules are also small (Zachariasen, 1932). Within the structure of silicate melt, metallic cations can move freely, but the anions of Si–O tetrahedra will polymerize with each other through oxygen bridges to form various kinds of networks similar to silicate crystal (Figure 3.2).

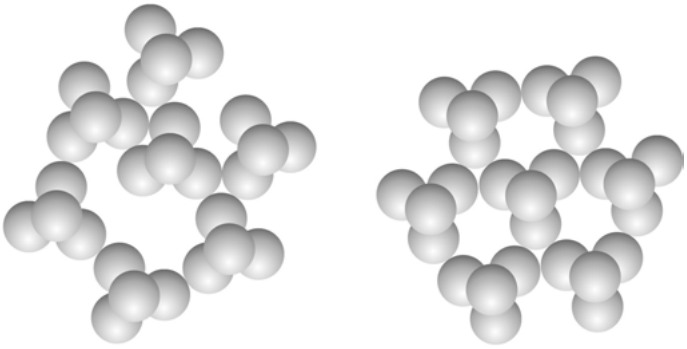

Figure 3.2: A comparison between the inner structure of silicate melts (left) and that of crystals (right).

However, in case those cations have a strong polarization ability, such as in the case of alkaline metal ions, the polymerization of the melt will be obstructed, which will favor the formation of individual ion species of SiO_4^{4-}. In this case, the activities of the highly polymerized Si–O anions will also increase. Under certain conditions, a melt with a high SiO_4^{4-} concentration will separate to form a melt with a high degree of polymerization, leading to differentiation between orthosilicates and metasilicates, forming a mafic magma and felsic magma.

In addition to silicates and silica, other silicon-bearing compounds, such as SiC, have been discovered in nature, especially in meteorites. If a silicate phase coexists with a SiC phase, large silicon isotope fractionation would be expected. However, so far, no study of this case has yet been made. Nevertheless, significant silicon isotope variations have been found in the SiC and Si_3N_4 phase of meteorites, which may indicate that a large degree of isotopic fractionation has happened between SiC and another silicon-bearing gas component. The possible presence of compounds of silicon with B and H has been predicted, but their existence has not been proven so far (Liu, 1984).

EBSCOhost - printed on 2/10/2023 8:05 PM via . All use subject to https://www.ebsco.com/terms-of-use

3.1.2 Thermodynamic silicon isotope fractionation between different silicon-bearing compounds

3.1.2.1 The general formula of isotopic exchange reaction

The general formula of isotopic exchange reaction is

$$aA + bB^* = aA^* + bB \tag{3.2}$$

where A and B represents two types of silicon-bearing compounds with different structures. The compound with the subscript* contains ^{30}Si or ^{29}Si, and the compounds without a subscript* contains ^{28}Si. Besides, a and b refer to the number of atoms involved in the exchange reaction.

Under certain conditions, when the isotope exchange reaction reaches equilibrium, the compound A and compound B will have different $^{30}Si/^{28}Si$ (or $^{29}Si/^{28}Si$) ratios. To reflect the degree of isotopic fractionation, a term of the isotopic fractionation factor (α) is introduced, which is defined as

$$\alpha_{A-B} = R_A/R_B \tag{3.3}$$

where R refers to the $^{30}Si/^{28}Si$ (or $^{29}Si/^{28}Si$) ratio, and the subscripts A and B refer to different types of silicon-bearing compounds.

According to statistical mechanics,

$$\alpha = \frac{Q_{A^*}/Q_A}{Q_{B^*}/Q_B} \tag{3.4}$$

where Q is the partition coefficient, and Q_{A^*}/Q_A is the reduced ratio of the partition coefficient.

For polyatomic molecules, the following equation is applicable:

$$\frac{Q_{A^*}}{Q_A} = \frac{\sigma_A}{\sigma_{A^*}} \prod_k \left(\frac{m_{kA^*}}{m_{kA}}\right)^{\frac{3}{2}} \prod_i \frac{u_{iA^*}}{u_{iA}} \cdot \frac{e^{-\frac{u_{iA^*}}{2}}}{e^{-\frac{u_{iA}}{2}}} \cdot \frac{1-e^{-u_{iA}}}{1-e^{-u_{iA^*}}} \tag{3.5}$$

where σ represents the degree of symmetry, m indicates the atomic mass of the isotopic species, k shows the number of atoms exchanged and U_i indicates the energy of molecule at i state.

When the above parameters of A, B, A* and B* are known, we can estimate the isotopic fractionation between the two compounds by calculating their ratio of partition coefficients.

3.1.2.2 Some theoretical calculation results for thermodynamic silicon isotope fractionation

Grant (1954) was the first to publish some calculated results on silicon isotope fractionation for quartz–topaz and orthosilicate-metasilicate. He stated that quartz can contain 6‰ and 5‰ more ^{30}Si than topaz at the temperature of 300°C and 380°C, respectively. In the meanwhile, he concluded that the silicon-rich phase (metasilicate) can have 4‰ and 2‰ more ^{30}Si than the silicon-poor phase (orthosilicate) at 1 000°C and

EBSCOhost - printed on 2/10/2023 8:05 PM via . All use subject to https://www.ebsco.com/terms-of-use

1 500°C, respectively. In quantitative terms, the results of Grant's calculations have not been confirmed by practical results, hence either some unknown factors had not been considered in Grant's calculation, or some parameters used in his calculation were not accurate. This is due to the complexity of the composition and structure of silicate.

To solve this problem, the density functional theory (DFT) has been introduced successfully into the field of isotopic fractionation investigation in last two decades. Theoretical approaches mostly consist in applying statistical thermodynamics to calculate the equilibrium constants of isotope exchange reactions from the rotational and vibrational energy levels of the reactants and products. The energy levels can be determined experimentally, i.e., from spectroscopic measurements, or theoretically from atomistic calculations, or more generally using a combination of both. However, spectroscopic data are usually lacking for isotopic species containing rare isotopes. Empirical rules and force-field models have thus been developed to extrapolate the spectroscopic constants of isotopic substituted molecules from those with the natural isotopic abundance (Rosenthal, 1935; Shaffer and Schuman, 1944; Richet et al., 1977; Zeebe, 2005). Alternatively, energy levels can be fully determined theoretically using empirical potentials or ab initio electronic structure calculations. In this last case, the energy levels are calculated using fundamental quantum mechanical theory.

For molecules in gas phase, theoretical calculations can reach a very good precision (Richet et al., 1977; Zeebe, 2005). For solids, an additional difficulty arises from the need to compute the complete vibrational density of state (VDOS) of pure and isotopic substituted compounds, whereas most of the vibrational spectroscopic experiments only provide a limited set of data. The most common approach is therefore to use a simplified model of the vibrational density of states, consisting of a Debye model for acoustic modes, optical continua for low-frequency optical modes and an Einstein model for high-frequency optical modes (Kawabe, 1978; Kieffer, 1982). Following Patel et al. (1991) and Dove et al. (1992), an alternative scheme was based on the computer modeling of crystal structures enabling a complete calculation of the VDOS. This calculation can also be done from first principles, within the framework of density functional perturbation theory (DFPT). Indeed, DFPT has proved to be accurate in determining harmonic phonon frequencies in crystalline solids for any wave vector (Baroni et al., 2001). DFPT has been successfully applied to the investigations of the vibrational spectroscopic properties of several minerals including quartz, zircon, kaolinite-group minerals, serpentine minerals and gibbsite (Gonze et al., 1994; Balan et al., 2001, 2002, 2006; Rignanese et al., 2001). The quality of the modeling of the IR and Raman spectra of these minerals indicate that accurate vibrational density of state, and thermodynamical functions, can be derived using DFPT.

Recently, this approach has been applied to isotopic fractionation between various isotopic systems of H (Reynard and Caracas, 2009; Méheut et al., 2010), O (Méheut et al., 2009, 2010; Blanchard et al., 2010; Javoy et al., 2012), C (Schauble et al., 2006), S (Otake et al., 2008; Balan et al., 2014; Liu et al., 2014a), B (Kowalski et al., 2013), Mg (Schauble, 2011; Huang et al., 2013; Pinilla et al., 2015; Wu et al., 2015a; Schott et al.,

EBSCOhost - printed on 2/10/2023 8:05 PM via . All use subject to https://www.ebsco.com/terms-of-use

2016), Ca (Feng et al., 2014), Li (Kowalski and Jahn, 2011), Fe (Ottonello and Zuccolini, 2008; Blanchard et al., 2009), Zn (Ducher et al., 2016), V (Wu et al., 2015b), Ge (Li and Liu, 2010), Se (Li and Liu, 2011) and Si (Méheut et al., 2007, 2009; Javoy et al., 2012; Méheut and Schauble, 2014; Huang et al., 2014; Wu et al., 2015a; He and Liu, 2015; Dupuis et al., 2015).

Méheut et al. (2007) used DFPT method first to calculate the silicon isotopic fractionation. They determined the isotopic fractionation of hydrogen, oxygen and silicon in the kaolinite, quartz, water system with a purely first-principles approach. In the meanwhile, they also calibrated isotopic fractionation between kaolinite/liquid-water and quartz/liquid-water by using the experimental gas/liquid-water fractionation. Good agreement between theory and experiment is obtained for mineral–water oxygen isotope fractionation, which indicates that this theoretical calculation approach can give reliable results on isotopic fractionation factors as a function of temperature. They obtained a fractionation factor of 1.6‰ for silicon isotope fractionation between quartz and kaolinite at 300 K.

Méheut et al. (2009) studied the structural control over equilibrium silicon and oxygen isotopic fractionation by using the same first-principles approach. The quartz, enstatite, forsterite, lizardite, kaolinite were chosen as examples of investigation, as they display various degrees of polymerization of silicate units. Good agreement between theory and experiment was found also in the case of oxygen. In the case of silicon, agreement and differences with previous estimates of equilibrium fractionation factors were discussed. The relationship between silicon and oxygen fractionation factors, silicate polymerization degree and chemical composition was studied and compared with previous semi-empirical models.

Méheut and Schauble (2014) made a further calculation on O and Si isotopic fractionation factors of phyllosilicates, albite and pyrope with first-principles methods based on density functional theory. Their results for O isotope fractionations agreed well with previous estimates for talc and albite, and their results for Si isotope fractionations qualitatively agreed with natural data. They found that Si isotope fractionation properties appeared to be correlated with stoichiometry for phyllosilicates and the effect of cation X on Si isotope fractionation increased with decreasing electronegativity of X. This could explain the enrichment in heavy silicon isotopes accompanying magmatic differentiation. This model provided a crystal chemical explanation for the correlation between Si isotope fractionation and Si–O distances. Based on this model, they suggested that attention should be given to chemical compositions in Si isotope studies.

Javoy et al. (2012) applied the first-principles methods to a few species of interest in cosmochemical problems: silicon monoxide and silicon monosulfide. They explored the isotopic composition of SiO and SiS during the genesis of silicon solid-solutions in chondritic Fe–Ni metal, a possible starting product for planetary cores. They obtained that at the time of E chondrites' formation the δ^{30}Si of the nebular gas, dominated by SiS, was ~ –6‰.

EBSCOhost - printed on 2/10/2023 8:05 PM via . All use subject to https://www.ebsco.com/terms-of-use

The equilibrium fractionations of Si isotopes are negligible among pyroxenes, olivine and pyrope, but are significant between olivine and its polymorphs (wadsleyite and ringwoodite). They found also that significant Si isotope fractionations existed between mantle minerals with different Si coordination numbers, such as Mg-perovskite (six coordinated) and olivine polymorphs (four coordinated) and that the $^{30}Si/^{28}Si$ ratio decreases in the order of olivine > pyroxenes > wadsleyite > majorite > ringwoodite > Mg-perovskite at equilibrium condition. They indicated also that significant Si isotope fractionation between mantle minerals might occur even at high pressure in a deep mantle and that Si isotope fractionation between silicate and metal could be a function of pressure. The Si isotopic fractionation factor obtained from low pressure experiments may not be applicable to Si isotope fraction during core formation which occurred at high pressure.

Wu et al. (2015a) calculated the Si isotopic fractionation that induced by phase transformation from olivine to wadsleyite, ringwoodite, bridgmanite and ferropericlase by the first-principle method. They found measurable Si isotope fractionations among these phases, even at the mantle's pressure–temperature conditions: wadsleyite and ringwoodite were depleted in heavy Si relative to olivine and bridgmanite was depleted in heavy Si among all phases. They found also that increasing pressure can slightly reduce the extent of Si isotope fractionation. They suggested that the Si isotope fractionation among Mg_2SiO_4 polymorphs might provide a promising way to "probe" the depth and temperature of origin of mantle xenoliths.

Dupuis et al. (2015) calculated the equilibrium fractionation factors for silicon isotopes of quartz, kaolinite, and dissolved silicic acid (H_4SiO_4 and $H_3SiO_4^-$) at 300 K by using first-principles methods. They found that at 300 K the $\Delta^{30}Si$ is $+2.1 \pm 0.2‰$ between quartz and H_4SiO_4, $+0.4 \pm 0.2‰$ between kaolinite and H_4SiO_4, and $-1.6 \pm 0.3‰$ between $H_3SiO_4^-$ and H_4SiO_4. These calculated solid-solution fractionations show important disagreement with natural observations in low-temperature systems, arguing against isotopic equilibration during silicon precipitation in these environments. On the other hand, the large fractionation associated with the de-protonation of silicic acid suggests the importance of speciation, and in particular pH, for the fractionation of silicon isotopes at a low temperature.

He and Liu (2015) calculated equilibrium Si isotope fractionation factors among orthosilicic acid (H_4SiO_4), quartz and the adsorption complexes of H_4SiO_4 on a Fe(III)-oxyhydroxide surface by using the full-electron wave-function quantum chemistry methods with a new cluster-model-based treatment. They found that under equilibrium conditions, heavy Si isotopes would be significantly enriched in quartz than in H_4SiO_4, which is in contrast to that observed in natural environments. To explain this discrepancy, they suggested that most silicon isotope fractionation between quartz and H_4SiO_4 was dominantly controlled by the kinetic isotope effect. However, they thought that their calculated equilibrium fractionation results might fit the quartz precipitated directly from a hydrothermal solution.

EBSCOhost - printed on 2/10/2023 8:05 PM via . All use subject to https://www.ebsco.com/terms-of-use

3.1.2.3 The thermodynamic Si isotope fractionation observed in natural environments and experimentally determination for some thermodynamic silicon isotope fractionation factors

In the early stage, much attention has been placed on empirical studies of silicon isotope fractionation between coexisting silicon-bearing minerals. For example, it has been found that in lunar rocks, the δ^{30}Si value of plagioclase is normally 0.2‰ higher than that of the pyroxene. In some granite rocks, the order of the ^{30}Si content from higher to lower is quartz → feldspar → muscovite → biotite, as predicted theoretically by Grant (1954). This order is also consistent with the order of ^{18}O enrichment. Other examples of silicon isotope fractionation between silicon bearing minerals include: the silicon isotope variation between albite, riebeckite and aegirine from Bayan Obo iron and rare earth ore deposit and the silicon isotope variation between quartz and tourmaline in the ore from the Ximeng tin deposit (Ding et al., 1996).

In recent years, more experimental investigations on silicon isotope fractionation have been carried out and important progress has been obtained in several fields.

Experimental determination of the Si isotope fractionation factor between liquid metal and liquid silicate

The cosmochemical and geophysical evidences indicate that elements lighter than iron and nickel must reside the Earth's core. Silicon has long been considered a possible light element in Earth's core. If differences in ^{30}Si/^{28}Si ratios between metal (core) and silicate (mantle and crust) can be quantified, silicon isotopes may be used to constrain the amount of this element in the core, and in so doing elucidate the conditions that attended Earth's differentiation (Georg et al., 2007a; Fitoussi et al., 2009).

Shahar et al. (2009) presented the first direct experimental evidence that silicon isotopes are not distributed uniformly between iron metal and rock when equilibrated at high temperatures. The silicon isotope ratios in iron–silicon alloy and silicate equilibrated at 1 GPa and 1800°C show that Si in silicate has higher ^{30}Si/^{28}Si than Si in metal, by at least 2.0‰. These findings provide an experimental foundation for using isotope ratios of silicon as an indicator of terrestrial planet formation processes. They imply that if Si isotope equilibrium existed during the segregation of the Earth's core-forming metal and silicate mantle, there should be an isotopic signature of Si in the core. The experimental results of Shahar et al. (2009), combined with previous measurements of Si isotope ratios in meteorites and rocks representing the bulk silicate Earth (BSE), suggest that the formation of the Earth's core imparted a high ^{30}Si/^{28}Si signature to BSE due to dissolution of ~6 wt.% Si into the early core.

Ziegler et al. (2010) investigated Si-isotope fractionation between metal and silicate in metal-rich enstatite meteorites as an analogue for Earth's differentiation. They found a 5 to 6‰ difference in the ^{30}Si/^{28}Si ratio between Si in metal and Si in silicate in the aubrites (enstatite achondrites) in Mount Egerton and Norton County. The meteorites are believed to have derived from enstatite chondrites by melting and thermal

EBSCOhost - printed on 2/10/2023 8:05 PM via . All use subject to https://www.ebsco.com/terms-of-use

metamorphism with final equilibration at 1 200 and 1 130±80 K, respectively. Using the measured silicate–metal Si-isotope fractionation in these rocks, they obtained a temperature dependence for fractionation of $\Delta^{30}Si_{silicate-metal} = 7.64(\pm0.47) \times 10^6/T^2$, in agreement with independent experimental and theoretical determinations. The measured silicate–metal fractionation suggests a ~0.8‰ difference in the $^{30}Si/^{28}Si$ ratio between Earth's core and mantle at P/T conditions relevant to core formation. These results, based on thermodynamic calculations for Si solubility in iron-rich metal and the measured Si isotope fractionation between silicate and metal, imply at least ~6 wt.% Si in the core (depending on the exact $\Delta^{30}Si_{BSE\text{-}chondrite}$ value). The Si isotope data also require that oxygen fugacity in the lower mantle increased during or after the process of core segregation by 1 to 2 log units.

Shahar et al. (2011) investigated the Si isotope fractionation between metal and silicate experimentally at 1 800, 2 000 and 2 200°C. They found that there was a significant silicon stable isotope fractionation at a high temperature between the metal and silicate in agreement with Shahar et al. (2009). Further, they found that this fractionation was insensitive to the structure and composition of the silicate as the fractionation between silicate melt and olivine is insignificant within the error of the analyses. The temperature-dependent silicon isotope fractionation is $\Delta^{30}Si_{silicate-metal} = 7.45(\pm0.41) \times 10^6/T^2$, and in excellent agreement with both theoretical calculations for olivine–Fe-rich metal (Georg et al., 2007a) and the observed fractionation between enstatite and Fe–Ni-rich metal in reduced enstatite meteorites (Ziegler et al., 2010).

Hin et al. (2014) present experimentally determined Si isotope fractionation factors between liquid metal and liquid silicate at 1 450°C and 1 750°C. They obtained that the temperature dependence of equilibrium Si isotope fractionation between metal and silicate can be described as $\Delta^{30}Si_{metal-silicate} = -4.42(\pm0.05) \times 10^6/T^2$, which is about 1.7 times smaller than previously proposed on the basis of experiments (Shahar et al., 2009, 2011). They doubted whether the average Si isotope fractionation factors of Shahar et al. (2009, 2011) represented equilibrium fractionation as Shahar et al. (2009, 2011) deduced an isotopic fractionation factor from heterogeneous Si isotope compositions in silicate and metal phases. However, Young et al. (2015) thought that the difference between the results of Shahar et al. (2009, 2011) and Ziegler et al. (2010) and that of Hin et al. (2014) was not unexplained, but might be related to open-system effects in longer experimental runs in the study of Hin et al. (2014) or the presence of abundant Sn in the metal phase in the lower-temperature runs in that study.

The fractionation factors of Georg et al. (2007a), Shahar et al. (2011, 2009), Ziegler et al. (2010) and Hin et al. (2014) are summarized in Table 3.1 and plotted in Figure 3.3.

Equilibrium Si isotope fractionation in magmatic processes

Douthitt (1982) and Ding et al. (1996) both showed that silica-rich (rhyolites, granites, dacites) lithologies have, on average, heavier Si isotope compositions than primitive (ultramafic and basaltic) material. There is also theoretical evidence to suggest that

EBSCOhost - printed on 2/10/2023 8:05 PM via . All use subject to https://www.ebsco.com/terms-of-use

Table 3.1: The Si isotope fractionation factors between mantle relevant silicates and Si-bearing Fe metal.

Formula	Method	Reference
$\Delta^{30}Si_{metal-silicate} = -(5.5 \sim 5.8) \times 10^6$	Theoretical calculation	Georg et al. (2007a) and Shahar et al. (2009)
$\Delta^{30}Si_{metal-silicate} = -7.45(\pm 0.41) \times 10^6/T^2$	Experimental calibration	Shahar et al. (2009, 2011)
$\Delta^{30}Si_{metal-silicate} = -7.64(\pm 0.47) \times 10^6/T^2$	Experimental calibration	Ziegler et al. (2010)
$\Delta^{30}Si_{metal-silicate} = -4.42(\pm 0.05) \times 10^6/T^2$	Experimental calibration	Hin et al. (2014)

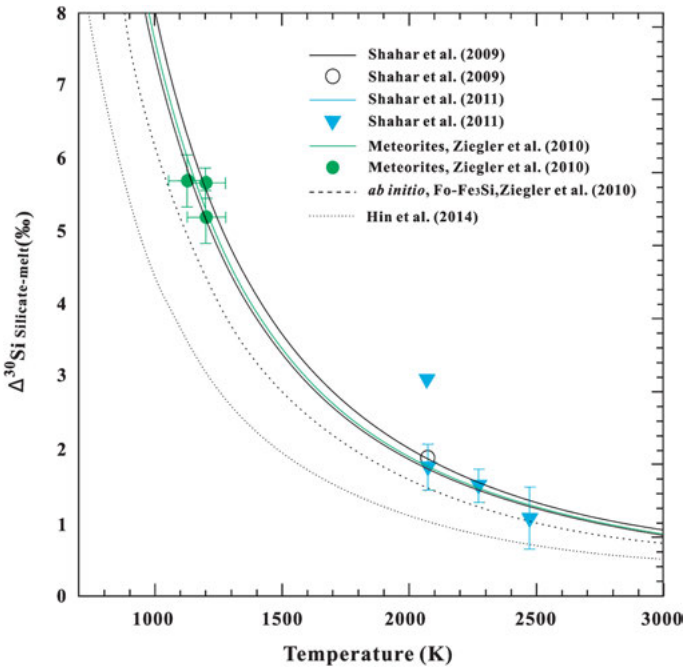

Figure 3.3: Summary of temperature-dependent Si isotope fractionations between mantle relevant silicates and Si-bearing Fe metal in the laboratory and in equilibrated meteorites (after Young et al. 2015). Data are from Shahar et al. (2009) in C capsules, Shahar et al. (2011) in C and MgO capsules and Ziegler et al. (2010) from the Mt. Egerton and Norton County meteorites. Also shown for comparison are experiments from Hin et al. (2014) and ab initio calculations for olivine–Fe_3Si (Georg et al., 2007a; Shahar et al., 2009).

resolvable equilibrium Si isotope fractionation occurs between co-existing mineral phases, suggesting that, e.g., fractional crystallization will affect bulk rock Si isotope compositions. Ding et al. (1996) had summarized the early results on silicon isotope equilibrium fractionation among various silicon bearing compounds, which pointed out that from nesosilicate → inosilicate → phyllosilicate → tectosilicate, the ^{30}Si content of mineral increases, in the same way as for that of ^{18}O. They suggested that the silicon isotopic fractionation between orthosilicate melts and metasilicate melts may

EBSCOhost - printed on 2/10/2023 8:05 PM via . All use subject to https://www.ebsco.com/terms-of-use

be of interest in the petrologic study of magmatic rocks, although the extent of silicon isotope exchange fractionation is small (less than 1.0‰ in general). The fact that the δ^{30}Si values of granites are normally higher than those of basalts may reflect the influence of this kind of fractionation.

Recently, more comprehensive investigation on equilibrium Si isotope fractionation in magmatic processes has been carried out.

Savage et al. (2011) investigated Si isotopic compositions of lavas from Hekla volcano, Iceland, which has formed in a region devoid of old, geochemically diverse crust. They show that Si isotopic composition varies linearly as a function of silica content, with more differentiated rocks possessing heavier isotopic compositions (Figure 3.4). Data for samples from the Afar Rift Zone, as well as various igneous USGS standards are collinear with the Hekla trend, providing evidence of a fundamental relationship between magmatic differentiation and Si isotopes (Figure 3.5). The effect of fractionation has been tested by studying cumulates from the Skaergaard Complex, which show that olivine and pyroxene are isotopically light, and plagioclase heavy, relative to the Si isotopic composition of the Earth's mantle. Therefore, Si isotopes can be utilized to model the competing effects of mafic and felsic mineral fractionation

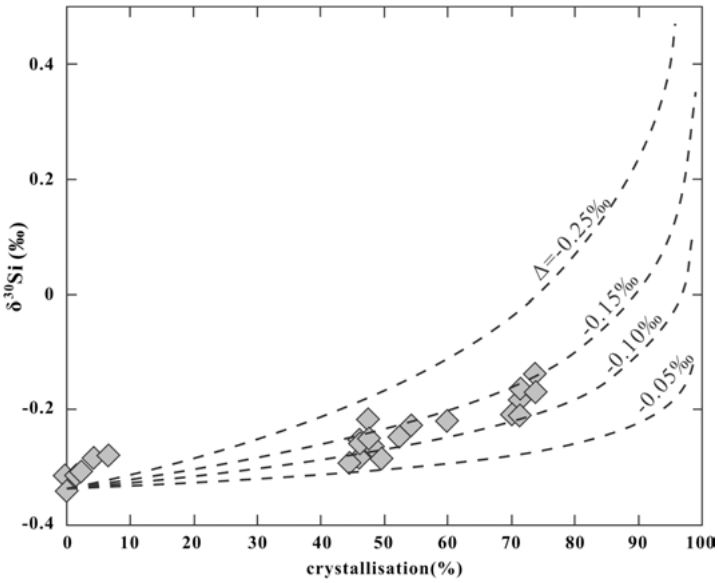

Figure 3.4: Rayleigh fractionation models of Si isotope evolution in a magma chamber, assuming a constant bulk fractionation factor between solid and melt. Curves are for different bulk fractionation factors (curve labels = $\Delta^{30}Si_{solid-melt} = 1000 \times \ln \alpha_{solid-melt}$). Sample HEK07-09 was used as the starting melt composition. The measured data are shown (grey diamonds), using Ba as a proxy for melt fraction and show that a bulk $\Delta^{30}Si_{solid-melt}$ value of −0.125‰ can describe the system at Hekla, and by inference, the igneous Si isotope system. Using K as a proxy for melt fraction yields a similar bulk $\Delta^{30}Si_{solid-melt}$ value. After Savage et al. (2011).

EBSCOhost - printed on 2/10/2023 8:05 PM via . All use subject to https://www.ebsco.com/terms-of-use

in evolving silicate liquids and cumulates. At an average SiO_2 content of ~60 wt.%, the predicted Δ^{30}Si value of the continental crust that should result from magmatic fractionation alone is −0.23 ± 0.05‰ (2 std), barely heavier than the mantle. This is, at most, a maximum estimate, as this does not take into account weathered material whose formation drives the products toward lighter Δ^{30}Si values. Mass balance calculations suggest that the removal of continental crust of this composition from the upper mantle will not affect the Si isotopic composition of the mantle.

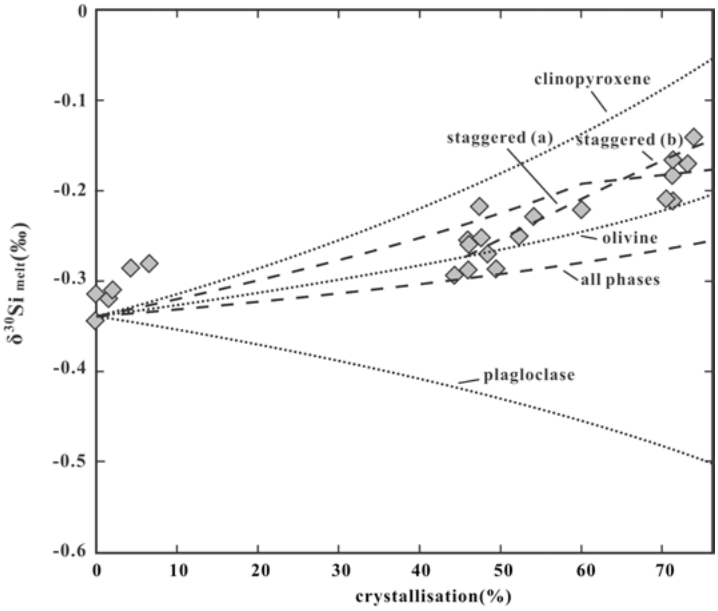

Figure 3.5: Models of the Si isotope evolution of a magma showing the effects of varying fractionating phases (olivine, clinopyroxene and plagioclase feldspar). The models assume Rayleigh fractionation and a constant isotopic fractionation factor between minerals and melt. Fractionation factors were calculated using data from Skaergaard mineral separates (Table 3.2), precipitating from a liquid whose original Si isotope composition was that of BSE (Savage et al., 2010) – each curve describes a different crystallization trend. Measured data (grey diamonds) plotted as in Figure 3.4. After Savage et al. (2011).

Savage et al. (2011) implicitly investigate the effect of magmatic differentiation on Si isotopes, principally using a set of samples taken from the volcano of Hekla. The δ^{30}Si values of the Hekla samples vary from −0.34‰ to −0.14‰ (Figure 3.6a), and define a wider range than that seen in mafic and ultramafic rocks. Crucially, the isotope data exhibit strong positive correlations with SiO_2 contents ($R^2 = 0.84$; Figure 3.6a).

1) The "igneous array" for silicon isotopes

For the relationship between the SiO_2 content and δ^{30}Si to be truly fundamental to the Si isotope system, it should be observable elsewhere. As well as the Hekla

EBSCOhost - printed on 2/10/2023 8:05 PM via . All use subject to https://www.ebsco.com/terms-of-use

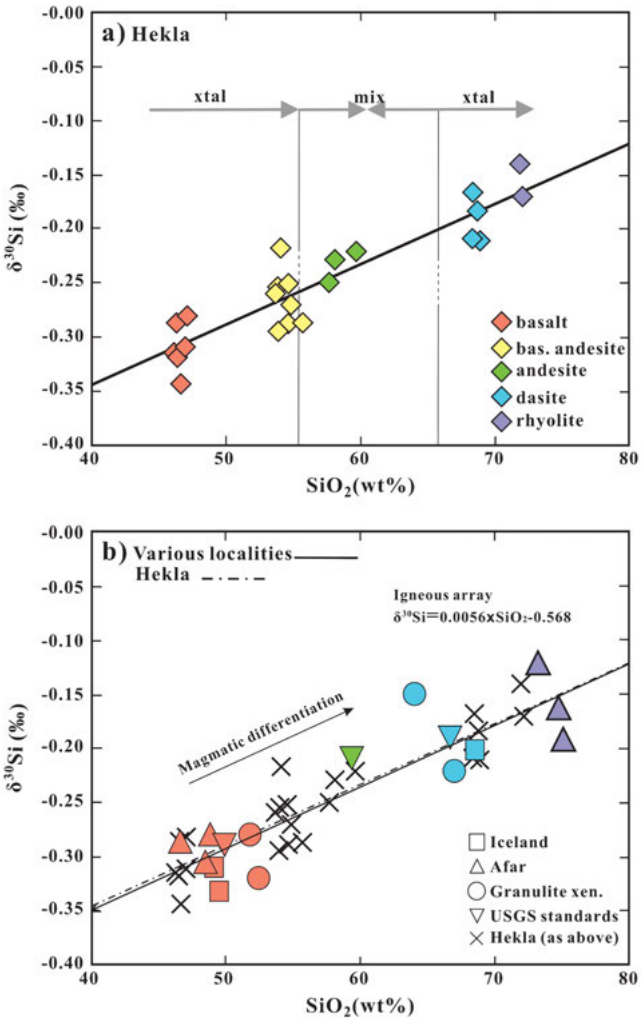

Figure 3.6: Silicon isotopic fractionation happened in process of magmatic differentiation. Figure 3.6a shows the sample data from Hekla volcano, Iceland, as a function of SiO_2 content and the apparent linear increase in $\delta^{30}Si$ over the range of differentiation, over both fractional crystallization and magma mixing regimes. Figure 3.6b shows other various "fresh" igneous samples, taken from various localities (lithology is shown as same as Figure 3.6a), which plot on the same array (solid line) as the Hekla data (dash line). This seemingly consistent behavior was termed the "igneous array" by Savage et al. (2011). Data taken from Savage et al. (2011, 2013a).

samples, Savage et al. (2011) analyzed a selection of igneous samples from elsewhere on Iceland, the Afar Rift zone in Ethiopia and the USGS standard collection. When plotted against SiO_2, all of these samples show an increase in the heavier Si isotopes as a function of increasing silica content. This is also true for a selection of granulite

EBSCOhost - printed on 2/10/2023 8:05 PM via . All use subject to https://www.ebsco.com/terms-of-use

Table 3.2: Silicon isotope fractionation factors between silicon bearing minerals and melts.

Mineral	$\Delta^{30}Si_{mineral\text{-}melt}$ (‰)		
	Savage et al. (2011)	**Georg (2006)**	**Savage et al. (2012)**
Mafic (Skaergaard layered intrusion)			
Orivine	−0.15		
Clinopyroxese	−0.21		
Plagioclase	0.11		
Felsic (Granites-SW England, Australia)			
Quart		0.04	0.05
Plagioclase			−0.05
Muscovite		0.01	−0.02
K-feldspar		0.02	0.06
Tourmaline			0.17
Biotite		−0.28	

faces xenoliths from the lower continental crust, whose protoliths were equilibrium melt assemblages (Savage et al., 2013a). More significantly, these data are all collinear with the Hekla samples (Figure 3.6b), i.e., they fall on the same array. Part of this phenomenon can be explained by the fact that the starting composition for all of these materials is that of BSE, which is homogeneous with respect to Si isotopes. Meanwhile, the observation that all the samples to exhibit essentially the same degree of the Si isotope fractionation away from the BSE, regardless of tectonic setting, is good evidence that such fractionation is a fundamental property of the Si isotope system. It appears then that the Si isotopes behave predictably during magmatic differentiation. As such, given a sample's silica content, its Si isotope composition can be estimated to a fairly accurate degree. This empirical formula, determined by Savage et al. (2011), was termed the "igneous array" for Si isotopes (Figure 3.6b), and is defined as such:

$$\delta^{30}\mathrm{Si}(‰) = 0.0056 \times \mathrm{SiO_2}(\mathrm{wt.\%}) - 0.567(\pm 0.05) \tag{3.6}$$

2) Intermineral Si isotope fractionation

Even though the Si–O bond frequency is most likely to be a major control over the Si isotope composition of various silicate phases, there must be some mass flux to generate isotopic fractionation. These processes, in igneous systems, are most likely to be either fractional crystallization during cooling, or partial melting (and restite formation). During crystallization, to first order, more mafic (less polymerized) phases will form first, and during melting the more felsic (more polymerized) phases will melt first. Table 3.2 provides a selection of mineral-melt Si isotope fractionation factors for both mafic (the Skaergaard layered intrusion, Greenland) and felsic (granites from SW England, Australia) lithologies. Both olivine and clinopyroxene are preferentially enriched in the lighter isotopes – fractional crystallization of one or both of these phases will drive the melt toward heavier isotopic compositions (following the trend seen on

EBSCOhost - printed on 2/10/2023 8:05 PM via . All use subject to https://www.ebsco.com/terms-of-use

Hekla and elsewhere in Figure 3.6) and leave isotopically light cumulate material. Conversely, partial melting of the same material will preferentially cause melting of the plagioclase and clinopyroxene, leaving an olivine rich restite (see Figure 3.5) again, and creates a melt that is preferentially enriched in the heavier isotopes relative to the solid. This simple description effectively describes the phenomena of the Si isotope fractionation during magmatic differentiation. The fractionation factors in Table 3.2 also illustrate that intermineral Si isotope fractionation is not completely controlled by the relative polymerization degree; although quartz seems always to be enriched in the heavier isotopes, and olivine in lighter isotopes, clinopyroxene is almost always lighter than coexisting olivine (Chakrabarti and Jacobsen, 2010; Georg et al., 2007a; Savage et al., 2011). As noted by Méheut et al. (2009), polymerization is not the only fundamental control over fractionation factor; both the v1 vibrational frequency (pulsation along the Si–O bond) and presence of other network-forming cations (such as Al) exert strong controls. As a result, their calculations predict that clinopyroxene should be isotopically lighter than olivine, as many researchers have measured. Such effects may also explain why, in Table 3.2, biotite is much lighter than muscovite, and tourmaline is much heavier than quartz. As far as the "igneous array" is concerned, this means that the predictable relationship between SiO_2 and $\delta^{30}Si$ will only hold where equilibrium melt assemblages are concerned. Cumulates, made up of mineral phases that are not in equilibrium, will not exhibit such a relationship. This fact was demonstrated by Savage et al. (2013a) who analyzed the Si isotope compositions of two suites of granulite facies (lower crustal) xenoliths from Queensland, Australia. The first suite, from McBride (Rudnick and Taylor, 1987) contains predominantly metaigneous rocks whose protoliths represent equilibrium melt derived material – these samples plot on the "igneous array" (Figure 3.6b and Figure 3.7a), as expected. Samples from the second suite, from Chudleigh (Rudnick et al., 1986) are all metaigneous rocks with cumulate protoliths. These samples have a similar range of Si isotope composition to the McBride suite, but do not exhibit a relationship with SiO_2 contents, or any other proxy for magmatic differentiation (Figure 3.7a). Instead, they show good relationships with mineralogical indices, for instance, Mg, Eu anomaly, normative diopside contents (Figure 3.7b), implying that the modal abundance of various mineral phases is the controlling factor on the Si isotope composition of the Chudleigh xenoliths. The negative relationship in Figure 3.7b also confirms the sense of isotopic fractionation between differing phases as described above: cumulates with more mafic phases have lighter Si isotope compositions than those with more felsic phases. A final point to make is that fractionation factors depend on the relative bond strengths of the various crystal phases as well as the coexisting melt. This means that specific phases will not have fixed mineral–melt fractionation factors. An example is plagioclase feldspar (Table 3.2). In mafic systems, it tends to have a positive $\Delta^{30}Si_{mineral-melt}$ value, whereas in felsic systems, it is enriched in the lighter isotopes.

Zambardi et al. (2014) studied the Si isotopic variations in a single well-characterized magmatic suite from Cedar Butte volcano (ID, USA), as well as a sill with progres-

EBSCOhost - printed on 2/10/2023 8:05 PM via . All use subject to https://www.ebsco.com/terms-of-use

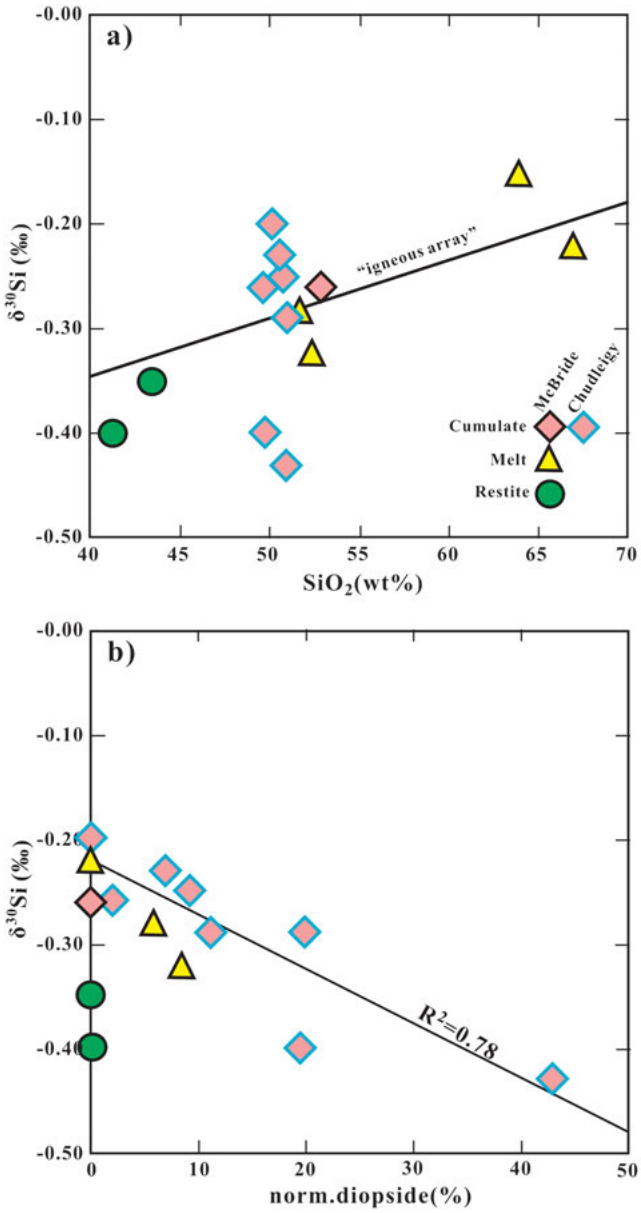

Figure 3.7: Silicon isotope variation in equilibrium melt assemblages compared to cumulate assemblages. The samples are all granulite facies xenoliths, analyzed by Savage et al. (2013a). In Figure 3.7a, samples that are representative of melts plot on the igneous array whereas cumulate samples do not. In Figure 3.7b, the same data are plotted against normative diopside content, and the cumulate samples show a good negative trend, indicating that the Si isotope composition of such samples is controlled by mineralogical abundances. After Savage et al. (2014).

EBSCOhost - printed on 2/10/2023 8:05 PM via . All use subject to https://www.ebsco.com/terms-of-use

sive compositional change within Finland granophyre (Duluth Complex, MN, USA). These isotopic systems show a significant enrichment in heavy isotopes in the more differentiated materials (Figure 3.8). In addition, the Finland granophyre sill shows a strong dependence between the isotopic composition and the sampling depth, suggesting the isotopic compositions follow a temperature gradient in which the cold part systematically enriches in heavy isotopes (Figure 3.9). They attribute this isotopic fractionation to a thermal migration process involving a top–down sill injection during which the isotopic distribution mostly follows a vertical temperature gradient.

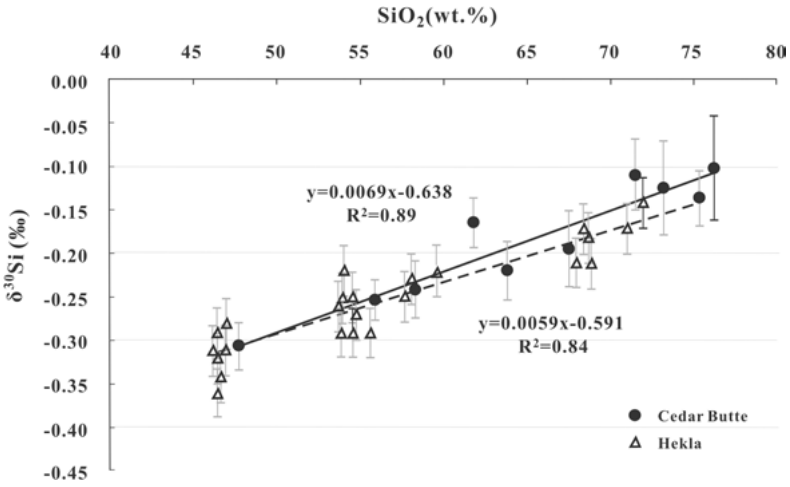

Figure 3.8: Silicon isotopic variations for volcanoes of Cedar Butte (Zambardi et al., 2014) and Hekla (Savage et al., 2011). The differentiation trend from CB clearly follows the igneous array defined in Savage et al. (2011).

Equilibrium Si isotope fractionation in hydrothermal processes

Quartz is a most common mineral that occurred in the products of hydrothermal processes, such as the gangue mineral of vein deposits, the silica sinter of hot spring and the silica band of banded iron formation and silcretes. The origin and forming process of quartz is an important issue in the study of the hydrothermal processes. The silicon isotope compositions of quartz have been investigated since the beginning of silicon isotope investigation, and more than thousands of data have been obtained. For interpretation of these data, the knowledge on the Si isotope fractionation factor between quartz and fluid is essential.

The experimental investigation on the Si isotope fractionation factor between quartz and fluid has been carried out by a number of research groups (Li et al., 1995a; Geilert et al., 2014a; Roerdink et al., 2015; Pollington et al., 2016).

EBSCOhost - printed on 2/10/2023 8:05 PM via . All use subject to https://www.ebsco.com/terms-of-use

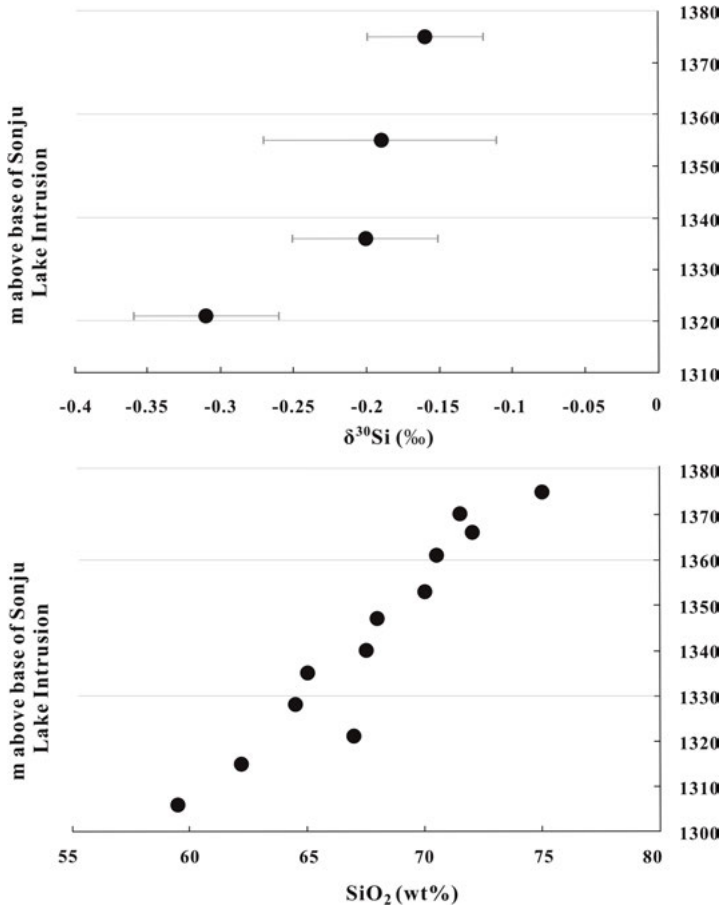

Figure 3.9: Isotopic signatures of Si as a function of the sample spatial position in the Finland Granophyre sill. The sill varies from high silica leucogranite (75 wt.% SiO_2) at its top to monzodiorite (59.5 wt.% SiO_2) at its base but has irregular SiO_2 variations within its middle. Si isotopic signatures show systematic changes with drill core depth/spatial position within the sill. Notably, they do not conform to previously defined trends of isotopic variation with SiO_2 (extent of differentiation). This observation implies that spatial position, perhaps indicative of a temperature gradient/thermal diffusion signature, better explains the isotopic signature than the differentiation index in this case. After Zambardi et al. (2014).

Li et al. (1995a) carried out an isotopic fractionation experiment on the precipitation of silica from the H_4SiO_4 solution. They found that rather than equilibrium fractionation, the major mechanism to control the silicon isotopic fractionation in this system is a kind of kinetic isotope fractionation.

Geilert et al. (2014a) performed seeded silica precipitation experiments using flow-through reactors in the temperature range of 10–60°C to quantify the silicon isotope fractionations when amorphous silica precipitates from a flowing aqueous

EBSCOhost - printed on 2/10/2023 8:05 PM via . All use subject to https://www.ebsco.com/terms-of-use

solution. They found that the effective Si isotope fractionation during precipitation from a solution was subject to changes in the saturation state, reactive surface area and flow regime. Therefore, they inferred that solid–fluid fractionation in natural surface environments was system dependent to a significant extent. They concluded that in their experiments the kinetic Si isotopic fractionation was dominated, which favored the lighter isotope in the solid reaction product at steady state and would tend to overprint any equilibrium fractionation.

Roerdink et al. (2015) studied experimentally the kinetic and equilibrium silicon isotope fractionation in the formation of non-biogenic chert deposits. They presented new constraints on the magnitudes of kinetic and equilibrium isotope effects during chemical precipitation of amorphous silica in batch-reactors. They suggest that silica deposition in the batch-reactors is kinetically-dominated at the start of the experiments but approaches a metastable equilibrium after ca. 400 hours.

Dupuis et al. (2015) calculated the equilibrium fractionation factors for silicon isotopes of quartz, kaolinite, and dissolved silicic acid at room temperature (300 K) by using first-principles methods. They found that quartz is more enriched in ^{30}Si than H_4SiO_4 by 2.1‰, which show significant disagreement with the observations in natural environment at low temperature where precipitated silica is enriched in lighter isotopes.

He and Liu (2015) calculated equilibrium Si isotope fractionation factors among orthosilicic acid (H_4SiO_4) and quartz by using the full-electron wave-function quantum chemistry methods with a new cluster-model-based treatment. Similarly, they found that heavy Si isotopes would be significantly enriched in quartz than in H_4SiO_4 solution.

Pollington et al. (2016) presented the measurements of silicon isotope ratios from experimentally precipitated quartz and estimate the equilibrium fractionation versus dissolved silica using SIMS to directly analyze experimental products. Quartz overgrowths up to 235 μm thick were precipitated in silica–H_2O–NaOH–NaCl fluids, at pH 12–13 and 250°C. At this temperature, $\Delta^{30}Si_{(Qtz-fluid)} = 0.55(\pm 0.10)‰$, yielding the relations $1\,000 \ln \alpha^{30}Si_{(Qtz-fluid)} = (0.15 \pm 0.03) \times 10^6/T^2$. The application of the experimental quartz growth results to observations from natural sandstone samples suggests that precipitation of quartz at low temperatures in nature is dominated by kinetic, rather than equilibrium, processes. These results agree well with recent calculations of silicon isotope fractionation (Figure 3.10), but are significantly different from previous experimental and empirical estimates.

The close agreement at 250°C between the experiments in Pollington et al. (2016) and recent calculations for H_4SiO_4 and $H_3SiO_4^-$ molecules (0.08‰ lower and 0.64‰ higher respectively than the current experiments) suggest that the values measured in Pollington et al. (2016) represent equilibrium fractionation between quartz and dissolved silica.

EBSCOhost - printed on 2/10/2023 8:05 PM via . All use subject to https://www.ebsco.com/terms-of-use

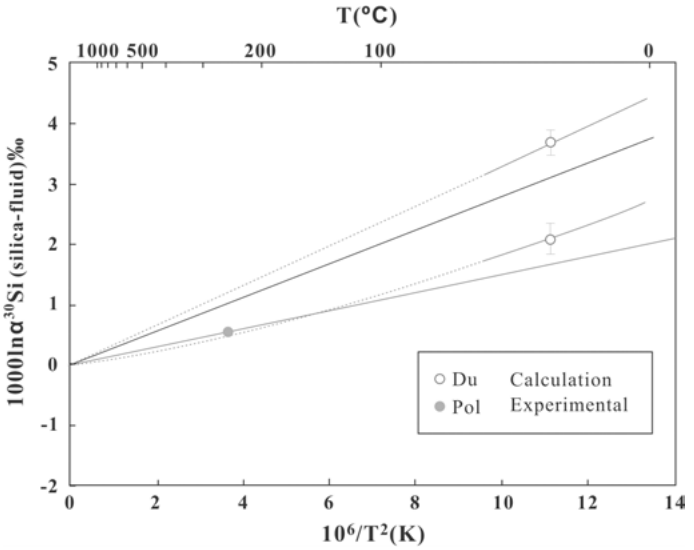

Figure 3.10: Estimations of silicon isotope equilibrium fractionation factors in silica–fluid (and quartz–fluid) system at low temperatures. Thick black line is fit through experimental data of Pollington et al. (2016) and 0‰ at infinite temperature. Open circles are calculations of Dupuis et al. (2015) based on phonon frequencies and represent $1\,000 \ln \alpha^{30}Si_{(Qtz-H_3SiO_4^-)} = 3.69$ and $1\,000 \ln \alpha^{30}Si_{(Qtz-H_4SiO_4)} = 2.09$; at the pH of experiments (≈12), the dominant species was $H_3SiO_4^-$, with minor $H_2SiO_4^{2-}$. Curves that pass through the open circles are temperature dependent fits calculated in Dupuis et al. (2015) for $1\,000 \ln \alpha^{30}Si_{(Qtz-H_3SiO_4^-)}$ and $1\,000 \ln \alpha^{30}Si_{(Qtz-H_4SiO_4)}$; curves are solid over the temperature range reported in the previous study (0–50°C) and dashed where extrapolated (50–1 000°C). Revised from Pollington et al. (2016).

3.2 Kinetic fractionation of silicon isotopes

Kinetic isotopic fractionation is an important type of isotopic fractionation, which is associated with incomplete and unidirectional processes like evaporation, dissociation reactions, biologically mediated reactions and diffusion. A kinetic isotope effect also occurs when the rate of a chemical reaction is sensitive to atomic mass at a particular position in one of the reacting species.

Kinetic fractionation is also important for silicon isotopes. Because compounds containing ^{30}Si, ^{29}Si and ^{28}Si have different molecular weights and vibration energies, they will show some differences in their rates of movement and reactions in various physical, chemical and biological processes, leading to kinetic fractionation of silicon isotopes. For example, in the process of preparation, extraction and mass analyses of SiF_4, silicon isotope fractionation can occur if the analysis is not performed correctly. Hence, measures must be adopted to avoid this kind of fractionation. However, because SiF_4 is rare in the nature, we will not pay too much attention to it here. In the discussion below, the kinetic fractionation of silicon isotopes observed in nature will be emphasized.

EBSCOhost - printed on 2/10/2023 8:05 PM via . All use subject to https://www.ebsco.com/terms-of-use

3.2.1 The generally characters of kinetic isotope fractionations

The theory of kinetic isotope fractionations has been discussed by Bigeleisen and Wolfsberg (1958), Melander (1960) and Melander and Saunders (1980). Knowledge of kinetic isotope effects is very important, because it can provide information about details of reaction pathways. Quantitatively, many observed deviations from simple equilibrium processes can be interpreted as the consequences of various isotopic components having different rates of reaction. Isotope measurements taken during unidirectional chemical reactions always show a preferential enrichment of the lighter isotope in the reaction products. The isotope fractionation introduced during the course of unidirectional reaction may be considered in terms of the difference on rate constants for the isotopic substances. Thus, for two competing isotopic reactions,

$$A_1 \rightarrow B_1, \quad \text{and} \quad A_2 \rightarrow B_2$$

The ratio of rate constants for the reaction of light and heavy isotope species k_1/k_2, as in the case of equilibrium constants, is expressed in terms of two partition function ratios, one for the two reactant isotopic species, and one for the two isotopic species of the activated complex or transition state, AX:

$$k_1/k_2 = [(Q^*_{(A2)}/Q^*_{(A1)})/(Q^*_{(AX2)}/Q^*_{(AX1)}] \times (\nu_1/\nu_2). \tag{3.7}$$

The factor ν_1/ν_2 in the expression is a mass term ratio for the two isotopic species. The determination of the ratio of rate constants is, therefore, principally the same as the determination of an equilibrium constant, although the calculations are not so precise because of the need for detailed knowledge of the transition state. The term *transition state* refers to the molecular configuration that is most difficult to attain along the path between the reactants and the products. This theory follows the concept that a chemical reaction proceeds from some initial state to a final configuration by a continuous change, and that there is some critical intermediate configuration called the activated species or transition state. There are a small number of activated molecules in equilibrium with the reacting species and the rate of reaction is controlled by the rate of decomposition of these activated species.

3.2.2 Several important kinetic Si isotope fractionation processes in natural environments

3.2.2.1 Silicon isotope fractionation in the evaporation and condensation processes of silicate

Reactions of solid and gas phases are important in the formation of the planet. Therefore, this kind of reaction is an important issue of scientific study. Tsuchiyama (1990)

EBSCOhost - printed on 2/10/2023 8:05 PM via . All use subject to https://www.ebsco.com/terms-of-use

and Uyeda and Tsuchiyama (1990) have made experimental studies on the silicon isotopic aspects of this reaction. In their studies, the experimental materials of pyroxene and olivine were placed in a vacuum furnace for evaporation and condensation experiments. The silicon isotopic compositions of residuals and condensates were analyzed with SIMS. The results show that at high temperature (>1 100°C), the condensate contains more ^{30}Si than the starting material. As the temperature decreases, the condensates become enriched in ^{28}Si. The condensates formed at 400°C had δ^{30}Si values which are 40‰ lower than those formed at a temperature of 1100°C. Uyeda et al. (1990) suggested that this variation could be explained by means of Rayleigh fractionation processes. The variation of silicon isotopic compositions found in meteorites and inclusions in meteorites can be interpreted in terms of this fractionation.

Volatility is the most important property that produced chemical differentiation among bodies in the solar system (Larimer, 1967; Larimer and Anders, 1967). At low temperatures, volatility brought about the distinction between the inner rocky planets and the outer gaseous planets. At higher temperatures, volatility was important in determining the compositions of the terrestrial planets. At very high temperatures, volatility was responsible for the formation of calcium-, aluminum-rich inclusions (CAIs) in carbonaceous chondrites, which play a key role in understanding early solar system processes (Grossman, 1972).

CAIs are <1 mm to >1 cm sized objects with mineralogy consistent with high condensation temperatures in a gas of solar composition (≥1 400 K at 10^{-3} atm, Grossman, 1972), and consist primarily of oxides and silicates of aluminum, calcium and magnesium with minor titanium. Relative to ferromagnesian chondrules and to bulk chondrites, the bulk compositions of CAIs are enriched in aluminum, calcium and titanium, and also in refractory trace elements; they are depleted in volatile elements such as sodium and iron. CAIs range in shape from highly irregular to nearly spherical. Different types of CAIs have been found in meteorites (Grossman, 1980; Macpherson et al., 1988).

There are two hypotheses for the origin of CAIs: either as early condensates from the cooling solar nebula (Grossman, 1972; Boynton, 1975; Davis and Grossman, 1979) or as evaporation residues of preexisting material (Kurat, 1970; Tanaka and Masuda, 1973; Chou et al., 1976; Notsu et al., 1978; Nagasawa and Onuma, 1979; Hashimoto et al., 1979; Lee et al., 1979, 1980; Hashimoto, 1983; Niederer and Papanastassiou, 1984; Clayton et al., 1988; Davis et al., 1990; Ireland et al., 1992). A recent model suggests that CAIs formed as condensates, but were modified by evaporation (Grossman et al., 2000).

Although the origin of CAIs in meteorites is still a disputed issue, evaporation is clearly an important process in the formation of some CAIs in the early solar nebula.

Stable isotope fractionation measurements can be used to distinguish between evaporation and condensation processes. Isotopic fractionation between a gas and a condensed phase is generally small if the two phases are in equilibrium with each other at high temperatures. In contrast, heavy-isotope enrichment, up to a few %/amu

EBSCOhost - printed on 2/10/2023 8:05 PM via . All use subject to https://www.ebsco.com/terms-of-use

in magnesium, silicon, oxygen, titanium and calcium can result from the kinetic effect between vapor and liquids or solids due to non-equilibrium evaporation of the precursor material (Davis et al., 1990, 1995).

Molini-Velsko et al. (1987) reported silicon isotope analysis of evaporation residues of one basalt and two carbonaceous chondrites produced by heating in a solar furnace. They found that the residues were enriched in the heavy isotopes of silicon by about +1.1 to +1.8‰/amu after 80% evaporation of the original sample. Davis et al. (1990) studied forsterite residues evaporated from the melt under vacuum and showed that the isotopic compositions of the residues are significantly enriched in the heavy isotopes of silicon and that the degree of evaporation and the isotopic compositions follow the Rayleigh law. Uyeda et al. (1991) used a Rayleigh law to explain isotopic fractionation in both the residue and the condensates by evaporating forsterite in the solid state under vacuum.

Wang et al. (2001) investigated the chemical and isotopic evolution during the evaporation process based on a synthetic material of solar elemental ratios of iron, magnesium, silicon, titanium, calcium and aluminum oxides doped with REE, evaporated in a vacuum furnace at 1 800 and 2 000°C for different durations. These oxides comprise more than 95 mol.% of the condensable solar material in the inner planetary region of the primordial solar nebula. Vacuum evaporation eliminates the complicated interaction between the gas and condensed phase and manifests the intrinsic nature of the evaporation of compound materials. Kinetic isotopic fractionation of silicon follows the Rayleigh distillation law during the laboratory evaporation of synthetic solar composition material. This implies that the residue is well mixed during the evaporation process and that the evaporation kinetic processes (both chemical and isotopic) are surface reaction-controlled. The isotopic mass fractionation factors are lower than those predicted from theoretical calculations by using the square root of mass ratios of likely evaporating species. Thus, the surface reaction is more complicated than decomposition into single gas species of each element.

Figure 3.11 illustrates the relationship between the isotopic ratio R in the residue relative to its starting ratio R_0 and the fraction (f) of its elemental abundance remaining for magnesium, oxygen and silicon. A linear relationship between $1\,000\ln(R/R_0)$ and $-\ln(f)$ is expected if evaporation follows the Rayleigh fractionation law: $R/R_0 = f^{(1/\alpha-1)}$, where, α is the gas-melt isotopic fractionation factor. The fact that the isotopic fractionations from the experiments reported here follow a Rayleigh distillation law indicates that the residual melt was isotopically homogeneous during the evaporation process. If diffusion is the main transport mechanism within the residues, the diffusion rates of magnesium, oxygen and silicon in the melt must be quite fast. Strictly speaking, the non-dimensionalized sizes, W [where W is defined as wv/D, with w = sample size, v = evaporation rate and D = diffusion coefficient (Wang et al., 1999)], of evaporation experiments should be less than 0.2. Evidence for Rayleigh behavior of the solar composition melt suggests that values of W are not very different from those of the forsterite melt.

EBSCOhost - printed on 2/10/2023 8:05 PM via . All use subject to https://www.ebsco.com/terms-of-use

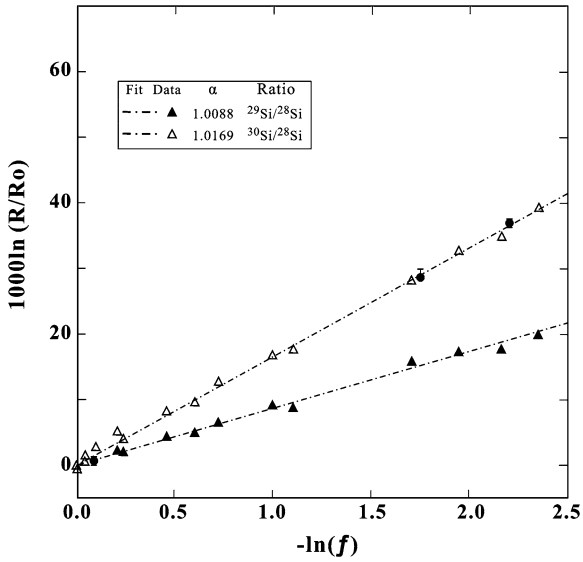

Figure 3.11: The silicon isotopic compositions of evaporation residues plot along straight lines in this diagram, as expected for a system that follows a Rayleigh relationship. R is the isotope ratio in the residue, R_0 is the isotope ratio in the starting material and f is the fraction of the element remaining in the residue. After Wang et al. (2001).

The slopes of the fitted lines in Figure 3.11 can be used to derive the fractionation factor α between the residual melt and the evaporating gas for $^{30}Si/^{28}Si$ [slope = $1000(1 - 1/\alpha)$]. The results are shown in the legend in Figure 3.11. The kinetic isotopic fractionation factors from other evaporation experiments and theoretical calculations are also listed in Table 3.3 for comparison.

Table 3.3: Melt/gas isotopic fractionation factors (α) during the evaporation process.

Starting material	$^{30}Si/^{28}Si$	Reference
Solar melt	1.0169 ± 0.0000	Davis et al. (1990)
Mg_2SiO_4	1.0142 ± 0.0004	Davis et al. (1990)
Theoretical	1.0225 (SiO)	Wang et al. (1999)
Theoretical	1.0165 (SiO_2)	Wang et al. (1994)

Isotopic fractionation factor α is defined as $R_{condensed}/R_{gas}$ at any moment during the evaporation process.

Mendybaev et al. (2013) conducted a series of experiments to test the proposition that the mass-fractionation effects of Si isotopic system in Fractionation and Unidentified Nuclear (FUN) CAIs (calcium-, aluminum-rich inclusions) were the result of evaporation of at least partially molten precursors. In their experiments, two magnesium-

EBSCOhost - printed on 2/10/2023 8:05 PM via . All use subject to https://www.ebsco.com/terms-of-use

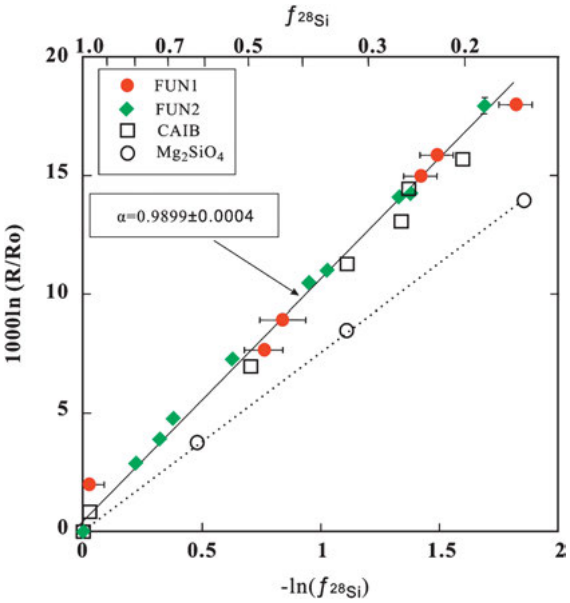

Figure 3.12: Rayleigh plot of the Si isotopic fractionation of the FUN1 and FUN2 evaporation residues as a function of the amount of ^{28}Si remaining in the residue. The silicon isotopic composition of all FUN1 and FUN2 residues plot along a single line fit by $\alpha_{29,28} = 0.9899 \pm 0.0004$, which is the same as 0.9899 ± 0.0004 obtained for residues of a Type B CAI-like melt by Knight et al. (2009). The data for molten Mg_2SiO_4 evaporated at 1900°C plot along a line with slope $\alpha_{29,28} = 0.9925 \pm 0.0001$ (Davis et al., 1990). The reason why molten Mg_2SiO_4 is characterized by different silicon fractionation factor than other compositions studied remains unclear. After Mendybaev et al. (2013).

and silicon-rich melts (FUN1 with 53.4 wt.% MgO and 41.3% SiO_2, and FUN2 with 32.7% MgO and 38.7% SiO_2, and Al_2O_3 and CaO in solar proportions) were evaporated into vacuum at 1900°C for various lengths of time. The chemical and isotopic compositions of the evaporation residues were measured and compared to two of the most highly mass-fractionated FUN CAIs, Vigarano 1623-5 and Allende C1.

The ^{29}Si/^{28}Si fractionation factor $\alpha_{29,28} = 0.9899 \pm 0.0004$ was found to fit the data from the entire set of residues. Simple linear correlation was found for δ^{29}Si as a function of the fraction of silicon remaining in the residues (Figure 3.12).

3.2.2.2 Silicon isotopic fractionation caused by meteorite impact on rocks in lunar surface

Epstein and Taylor (1971, 1973) studied the silicon isotope composition of lunar rocks and soils. Their data indicate that during meteorite impact on lunar rocks to form lunar soils, kinetic fractionation of silicon isotopes can occur, leading to ^{30}Si enrichment in lunar soils. This process can cause δ^{30}Si variations as large as 30‰. Detailed conditions will be described in Chapter 4.

EBSCOhost - printed on 2/10/2023 8:05 PM via . All use subject to https://www.ebsco.com/terms-of-use

3.2.2.3 Kinetic fractionation of silicon isotopes in the process of precipitation of SiO_2 from a solution

The kinetic silicon isotopic fractionation is found important in a large number of the biotic and abiotic processes of SiO_2 precipitation from a solution.

Based on the fact that the sponge spicules, opal sinter and clay minerals are always enriched in ^{28}Si relative to the solution, Douthitt (1982) suggested the existence of this kinetic fractionation and inferred that the $\alpha^{30}Si_{opal-solution}$ is 0.9963–0.996. Since then, quite a number of empirical and experimental studies on this kind of kinetic Si isotope fractionation have been carried out.

The kinetic silicon isotopic fractionation in abiotic processes of SiO_2 precipitation from a solution

The experimental investigation on the Si isotope fractionation factor between quartz and fluid has been carried out by a number of research groups (Li et al., 1995a; Geilert et al., 2014a; Roerdink et al., 2015; Pollington et al., 2016).

Li et al. (1995a) carried out an isotopic fractionation experiment on the precipitation of silica from a H_4SiO_4 solution. The steps used in their experiment were a reaction of Na_4SiO_4 with HCl to form a H_4SiO_4 solution, followed by H_4SiO_4 polymerization to form a SiO_2 precipitate. They found that the major mechanism to control the silicon isotopic fractionation in this system is a kind of kinetic isotope fractionation. The α values obtained in the experiments are from 0.9990 to 0.9996 (Figure 3.13).

Geilert et al. (2014a) performed seeded silica precipitation experiments using flow-through reactors in the temperature range of 10–60°C to quantify the silicon isotope fractionations when amorphous silica precipitates from a flowing aqueous solution. Their experiments were designed to simulate silica deposition induced by a temperature drop, with particular relevance for near surface hydrothermal systems associated with steep temperature gradients. Monitored differences in $^{30}Si/^{28}Si$ and $^{29}Si/^{28}Si$ ratios between input and output solutions showed a systematic sequence in behavior. Before the reaction system reached steady state, the observed isotope shifts were influenced by dissolution of the seed material, the saturation state of the solution and the specific surface area of the seeds. After reaching steady state, the selective incorporation of silicon isotopes by the solid phase exhibited an explicit temperature dependency: the lighter isotopes were preferentially incorporated, and apparent fractionation magnitudes increased with decreasing temperature. Calculated magnitudes of silicon isotope fractionations between precipitated and dissolved silica ($\Delta^{30}Si = \delta^{30}Si_{precipitate\ (calculated)} - \delta^{30}Si_{input\ solution}$) were −2.1‰ at 10°C, −1.2‰ at 20°C, −1.0‰ at 30°C, −0.5‰ at 40°C, 0.1‰ at 50°C and 0.2‰ at 60°C. Thus, the fractionation was nearly insignificant at temperatures higher than 50°C. They found also that the effective Si isotope fractionation during precipitation from a solution

EBSCOhost - printed on 2/10/2023 8:05 PM via . All use subject to https://www.ebsco.com/terms-of-use

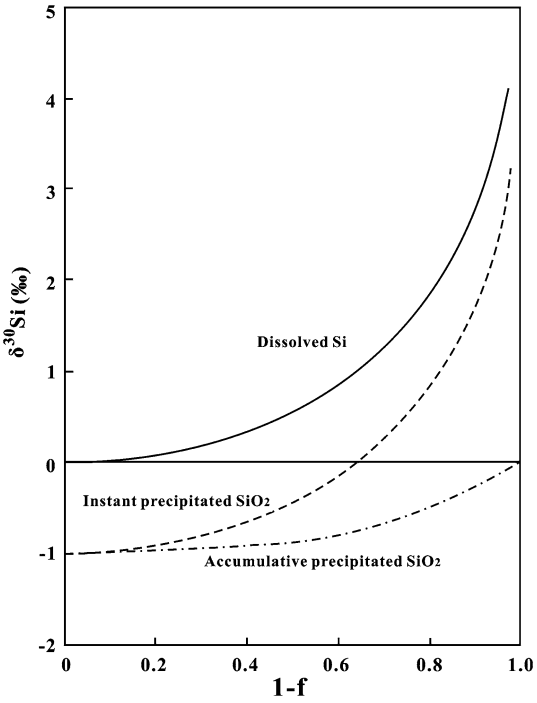

Figure 3.13: A plot showing silicon isotope fractionation during SiO_2 precipitation from a water solution in a Rayleigh process, where f is the fraction of remaining dissolved Si in a water solution and $1 - f$ is the fraction of accumulated precipitated SiO_2. The $\delta^{30}Si$ of the starting water solution is assumed to be 0‰ and the Si isotope fractionation factor between the SiO_2 precipitate and water solution (α_{Pre-WS}) is 0.999.

was subject to changes in the saturation state, reactive surface area and flow regime. Therefore, they inferred that solid–fluid fractionation in natural surface environments was system dependent to a significant extent.

They concluded that in their experiments the kinetic Si isotopic fractionation was dominated, which favored the lighter isotope in the solid reaction product at steady state and would tend to overprint any equilibrium fractionation.

Roerdink et al. (2015) studied experimentally the kinetic and equilibrium silicon isotope fractionation in the formation of non-biogenic chert deposits. They presented new constraints on the magnitudes of kinetic and equilibrium isotope effects during chemical precipitation of amorphous silica in batch-reactors at low temperature (10–35°C) and near-neutral pH (7.5–8.5), as an analogue for non-biogenic chert formation (Figure 3.14). The instantaneous fractionation factors [$\alpha_{inst} = (\delta^{30}Si_{ppt} + 1000)/(\delta^{30}Si_{TD} + 1000)$], derived from $\delta^{30}Si$ of the total dissolved silica (Si_{TD}) and mass balance computations, decrease with progressive precipitation and reduced reaction rates. This suggests that silica deposition in the batch-reactors is kinetically-

EBSCOhost - printed on 2/10/2023 8:05 PM via . All use subject to https://www.ebsco.com/terms-of-use

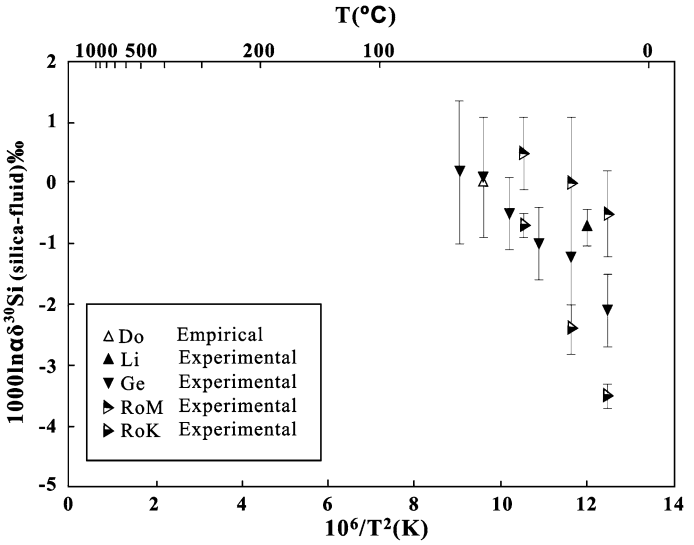

Figure 3.14: Experimental results of kinetic silicon isotope fractionation factors in the silica–fluid and quartz–fluid systems at low temperatures. The abbreviations are: Do = Douthitt (1982); Du = Dupuis et al. (2015); Li = Li et al. (1995a); Ge = Geilert et al. (2014a); RoM = metastable values from Roerdink et al. (2015); RoK = kinetic values from Roerdink et al. (2015). After Pollington et al. (2016).

dominated at the start of the experiments but approaches a metastable equilibrium after ca. 400 hours. Modeled kinetic fractionation factors range from 0.9965 at 10°C, to 0.9976 at 20°C and 0.9993 at 35°C and pH 8.5, whereas equilibrium isotope effects are smaller and range from 0.9995 at 10°C, to 1.000 at 20°C and 1.0005 at 35°C. Their results suggest that large isotope effects are only expressed in natural systems where dissolved and precipitated silica are not equilibrated, implying that the kinetic conditions of non-biogenic silica precipitation provide important constraints on silicon isotope ratios of siliceous rocks, with particular relevance for those preserved in the Archean chert record.

The kinetic Si isotope fractionation factor between precipitates and dissolved silica in fluids ($\Delta^{30}Si_{prec\text{-}diss}$) is still not well constrained in the literature. Large discrepancies exist between laboratory experiments and studies of natural samples (Li et al., 1995a; Delstanche et al., 2009; van den Boorn et al., 2010; Chakrabarti et al., 2012; Geilert et al., 2014a). Basile-Doelsch et al. (2005) used an average $\Delta^{30}Si_{prec\text{-}diss}$ value of –1.5‰ in their pedogenic and groundwater silcrete studies. Other values of –2.3‰ (van den Boorn et al., 2010), –2.0 and –3.0‰ (Chakrabarti et al., 2012) have also been used in the literature for kinetic fractionation of Si isotopes between solids and fluids. Recent theoretical work by Dupuis et al. (2015) suggested that $\Delta^{30}Si_{prec\text{-}diss}$ value at 27°C is +2.1‰ for equilibrium reactions, which is far from kinetic fractionation values.

EBSCOhost - printed on 2/10/2023 8:05 PM via . All use subject to https://www.ebsco.com/terms-of-use

The kinetic silicon isotopic fractionation in biological processes

Silica has been found to exist in a number of biological materials, such as the silica shells or skeletons in diatoms, radiolarian and sponges, and as phytoliths in plants of rice, bamboo, wheat, maize, banana, tomato, cucumber and equiseta. Large variations in δ^{30}Si values have been found in various kinds of organisms. It is found that in natural environments, when silicic acid is taken by biological species from water solution (sea water, surface water and pore water), the light silicon isotope (^{28}Si) always move into the biological bodies preferentially. When silica precipitates from silicon-bearing solution in plants, the light silicon isotope (^{28}Si) also precipitates preferentially.

To understand the silicon isotopic fractionation in biological processes, a number of experimental studies have been carried out.

1) The kinetic silicon isotopic fractionation in growth of marine diatoms from seawater

De La Rocha et al. (1997) studied the silicon isotope fractionation by marine diatoms the first time. They brought up three species of marine diatoms, *Skeletonema costatum*,*Thalassiosira weissflogii and Thalassiosira* sp. in batch culture and used the δ^{30}Si value of the diatom silica and that of the initial silicic acid in the culture medium to compute a fractionation factor (α). They found that the values of α for the three species were nearly identical, averaging 0.9989±0.0004, which corresponds to the production of diatom silica with a δ^{30}Si value that is 1.1‰ more negative than that of the dissolved silicon utilized for growth. Besides, they found also that the fractionation factor did not vary with temperature and the consequent change in growth rate. They simulated the silicon isotope fractionation during opal precipitation by diatoms as shown in Figure 3.15.

Later, Sutton et al. (2013) studied silicon isotope fractionation by seven species of polar and sub-polar marine diatoms grown in semi-continuous unialgal cultures under optimal irradiance and temperature for each diatom strain. They found that in the process of SiO_2 precipitation from seawater by diatoms the Si isotope fractionation factor was species-dependent. The greatest difference of the Si isotope composition between diatom and seawater ($\Delta^{30}Si_{diatom\text{-}SW}$) was observed in two species from the Southern Ocean, *Fragilariopsis kerguelensis* (−0.54‰, average for two strains) and *Chaetoceros brevis* (−2.09‰). The $\Delta^{30}Si_{diatom\text{-}SW}$ for the other species, both polar and sub-polar, ranged from −0.72‰ to −1.21‰. The two remaining polar diatoms had $\Delta^{30}Si_{diatom\text{-}SW}$ values of −0.74(±0.05)‰ for *Thalassiosira antarctica*, and −1.21(±0.04)‰ for *Thalassiosira nordenskioeldii*, while the sub-polar species had $\Delta^{30}Si_{diatom\text{-}SW}$ values of −0.72(±0.04)‰ for *Thalassiosira weissflogii*, −0.88(±0.06)‰ for *Thalassiosira pseudonana* (CCCM58), −0.97(±0.14)‰ for *Thalassiosira pseudonana* (CCMP1014) and −1.15(±0.03)‰ for *Porosira glacialis*. The range in $\Delta^{30}Si_{diatom\text{-}SW}$ for the diatoms evaluated in this study may be large enough to significantly impact the Si isotope composition measured in diatom opal ($\delta^{30}Si_{BSi}$) from marine sediments and

EBSCOhost - printed on 2/10/2023 8:05 PM via . All use subject to https://www.ebsco.com/terms-of-use

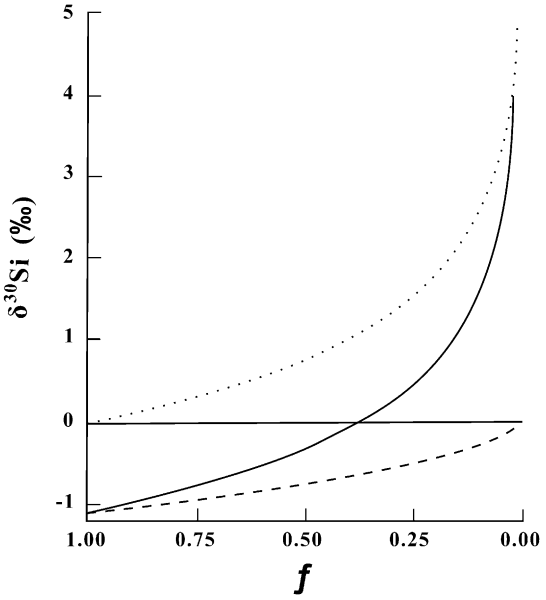

Figure 3.15: Simulation of silicon isotope fractionation during opal precipitation by diatoms. Curves depict changes in the δ^{30}Si of dissolved silicon (dotted line), biogenic silica produced at each instant during the depletion of dissolved silicon (solid line), and accumulating biogenic silica (dashed line). Rayleigh equations used were $R_{DSi} = R_o f^{(\alpha-1)}$, $R_{BSi} = \alpha R_0 f^{(\alpha-1)}$ and $R_{acc} = R_0(1 - f^{\alpha})/(1 - f)$, where $R = {}^{30}Si/{}^{28}Si$, $\alpha = 0.9989$, and f was the fraction of dissolved silicon remaining in solution. After De La Rocha et al. (1997).

its subsequent interpretation. They suggested that future work should assess phytoplankton taxonomic composition when using $\delta^{30}Si_{BSi}$ as a proxy for Si utilization.

2) The kinetic silicon isotopic fractionation between rice plants and nutrient solution

Ding et al. (2008b) studied the silicon isotope fractionation between a rice plant and nutrient solution experimentally. In their experiments, rice plants were grown to maturity with the hydroponic culture in a naturally-lit glasshouse. The nutrient solution was sampled for 14 times during the whole rice growth period. The rice plants were collected at various growth stages and different parts of the plants were sampled separately. The silica contents of the samples were determined by the gravimetric method and the silicon isotope compositions were measured using the SiF_4 method.

In the growth process, the silicon content in the nutrient solution decreased gradually from 16 mM at starting stage to 0.1~0.2 mM at harvest and the amount of silica in single rice plant increased gradually from 0.00013 g at start to 4.329 g at harvest. Within the rice plant, the SiO_2 fraction in roots reduced continuously from 0.23 at the seedling stage, through 0.12 at the tiller stage, 0.05 at the jointing stage, 0.023 at the heading stage, to 0.009 at the maturity stage. Accordingly, the fraction of SiO_2 in aerial parts increased from 0.77, through 0.88, 0.95, 0.977, to 0.991 for the same stages. The

EBSCOhost - printed on 2/10/2023 8:05 PM via . All use subject to https://www.ebsco.com/terms-of-use

silicon content in roots decreased from the jointing stage, through the heading stage, to the maturity stage, parallel to the decrease of silicon content in the nutrient solution. At the maturity stage, the silicon content increased from roots, through stem and leaves, to husks, but decreased drastically from husks to grains. These observations show that transpiration and evaporation may play an important role in silica transportation and precipitation within rice plants.

It was observed that the δ^{30}Si of the nutrient solution increased gradually from −0.1‰ at start to 1.5‰ at harvest, and the δ^{30}Si of silicon absorbed by bulk rice plant increased gradually from −1.72‰ at start to −0.08‰ at harvest, reflecting the effect of the kinetic silicon isotope fractionation during silicon absorption by rice plants from nutrient solutions (Figure 3.16). The calculated silicon isotope fractionation factor between the silicon instantaneously absorbed by rice roots and the silicon in nutrient solution vary from 0.9983 at start to 0.9995 at harvest. In the maturity stage, the δ^{30}Si value of rice organs decreased from −1.33‰ in roots to −1.98‰ in the stem, and then increased through −0.16‰ in the leaves and 1.24‰ in the husks, to 2.21‰ in the grains. This trend is similar to those observed in the field grown rice (Ding et al., 2005a) and bamboo (Ding et al., 2008a).

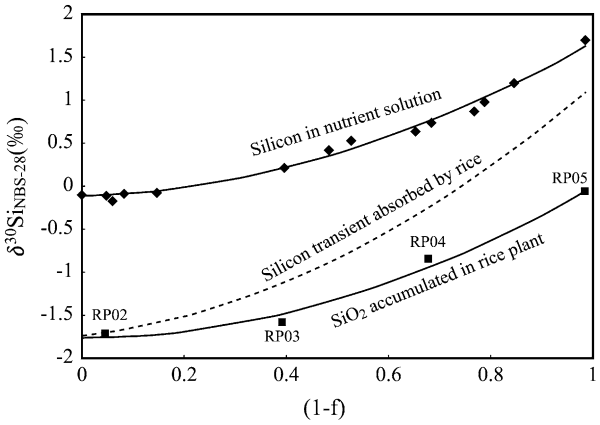

Figure 3.16: The δ^{30}Si variation curves for the silicon in the nutrient solution and Si accumulated in rice plant, as functions of $(1 - f)$. The δ^{30}Si of calculated Si transient absorbed by rice is also plotted. f = fraction of silicon remaining in nutrient solution. P02–P05: the samples of different stages. Revised from Ding et al. (2008b).

These quantitative data provide us a solid base for understanding the mechanisms of silicon absorption, transportation and precipitation in rice plants and the role of rice growth in the continental Si cycle.

Sun et al. (2008) studied the silicon isotope composition and Si distribution among different organs of rice plants collected at maturity stage. It was observed that there was a consistent increasing trend from lower to upper tissues (stem < leaf < husk

EBSCOhost - printed on 2/10/2023 8:05 PM via . All use subject to https://www.ebsco.com/terms-of-use

< grain). The range of δ^{30}Si variation among rice plant tissues was quite large (from −2.7‰ to 2.3‰). The trend and scale of δ^{30}Si variation observed in the experiment were similar to those observed in field grown rice (Ding et al., 2005a), reflecting kinetic isotope effects during Si deposition in the rice plant. They indicate that the isotope fractionation during Si deposition in the rice plant could be a Rayleigh-like process.

3) Silicon isotopic fractionation by banana grown in a continuous nutrient flow device

Opfergelt et al. (2006b) reported a study on silicon isotopic fractionation by banana grown in a continuous nutrient flow device. Banana plantlets were grown in hydroponics at variable Si supplies (0.08, 0.42, 0.83 and 1.66 mM Si). The $\Delta^{29}Si_{banana\text{-}DSi}$ between bulk banana plantlets and source solution is −0.40(±0.11)‰. This confirms that plants fractionate Si isotopes by depleting the source solution in ^{28}Si. The intra-plant Δ^{29}Si between roots and shoots amounts to −0.21(±0.08)‰. Si isotopic compositions of the various plant parts indicate that heavy isotopes discrimination occurs at three levels in the plant (at the root epidermis, for xylem loading and for xylem unloading). At each step, preferential crossing of light isotopes leaves a heavier solution.

3.2.2.4 Kinetic silicon isotope fractionation in adsorption and desorption of aqueous monosilicic acid on iron oxide

Monosilicic acid can be withdrawn from soil solution through its sorption onto aluminum and iron oxides (Beckwith and Reeve, 1963; Jones and Handreck, 1963; Mckeague and Cline, 1963). Delstanche et al. (2009) studied experimentally the silicon isotope fractionation in this process by using a system of H_4SiO_4 adsorption onto synthesized ferrihydrite and goethite. They found that the remaining solution was systematically enriched in ^{30}Si, reaching maximum δ^{30}Si values of 1.4‰ for ferrihydrite and 1.0‰ for goethite. Based on these results, they suggested that the sorption of H_4SiO_4 onto synthetic iron oxides produced a similar Si isotopic fractionation to that observed for Si uptake by plants and diatoms.

3.2.2.5 Kinetic silicon isotope fractionation when clay minerals precipitate from soil solution

Ziegler et al. (2005a) studied the silicon isotope fractionation when clay minerals precipitate from a soil solution in weathering processes. They observed experimentally that the δ^{30}Si value of a soil solution increases by about 1.5‰ when clay minerals precipitate at 25°C, but only by 1.0‰ when allophone precipitates at 90°C (Ziegler et al., 2005a).

EBSCOhost - printed on 2/10/2023 8:05 PM via . All use subject to https://www.ebsco.com/terms-of-use

EBSCOhost - printed on 2/10/2023 8:05 PM via . All use subject to https://www.ebsco.com/terms-of-use

4 Distribution of silicon isotopes in nature

Studies of the distribution of silicon isotopes in nature is one of the important issues in silicon isotope geochemistry, as it provides the foundation for geological applications of silicon isotopes. The study on the distribution of silicon isotopes in nature was started in the middle of the twentieth century. Quite a number of data on silicon isotope compositions of extraterrestrial materials were reported in the 1970s–1980s of the twentieth century. During 1980s–1990s of the last century, the study on silicon isotope compositions of terrestrial materials was carried out systematically, and a large amount of data have been obtained. Based on these results, a monograph entitled "Silicon Isotope Geochemistry" was published in 1996, in which the basic characteristics of silicon isotope distribution in nature were delineated in principle. Since then, especially in this new century, comprehensive studies on silicon isotope compositions have been undertaken on various types of natural materials, and tremendous data have been gathered. For providing a solid background for silicon isotope application, the silicon isotope distributions in various fields are summarized below (Figure 4.1).

4.1 Silicon isotope compositions of extraterrestrial materials

The silicon isotope compositions of extraterrestrial materials, such as meteorites and lunar samples, have been investigated since the 1950s of the twentieth century, and a wealth of data of them has been accumulated.

4.1.1 Meteorite

The silicon isotope compositions attracted the attention of geochemical researchers for two major reasons. Firstly, the silicon isotopic compositions of meteorites may represent the average values of the planetary system. Secondly, silicon in meteorites may preserve primary distinctive isotopic features from the time when the solar system was formed.

Analytical results for silicon isotopes in meteorites were firstly published by Reynolds and Verhoogen (1953). They analyzed the composition of silicon isotopes from the Melrose meteorite, and obtained a δ^{30}Si value of –1.0‰ relative to that of olivine from a dunite in North Carolina, USA. Since then, there has been more detailed study with analyses made by gas isotope mass spectrometry method, the SIMS method and the MC-ICPMS method. The analyzed materials include bulk samples of various chondrites and achondrites, CAIs and grains of SiC and graphite.

https://doi.org/10.1515/9783110402452-004

EBSCOhost - printed on 2/10/2023 8:05 PM via . All use subject to https://www.ebsco.com/terms-of-use

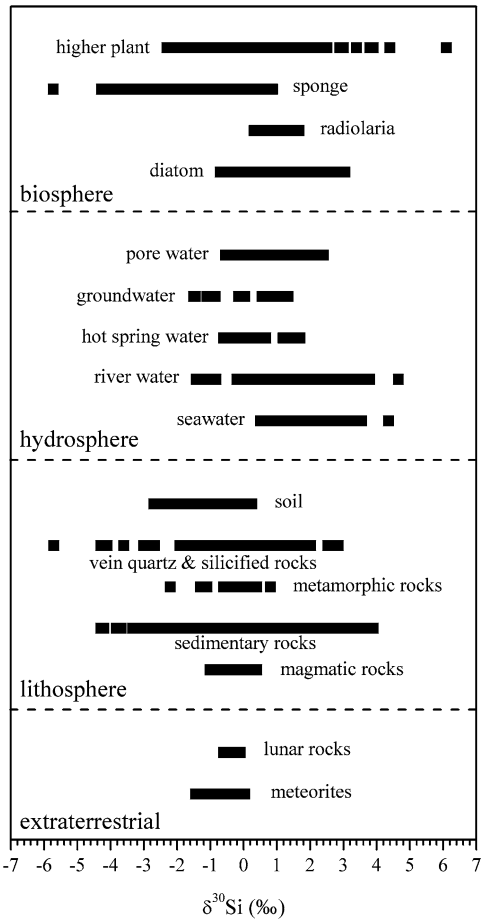

Figure 4.1: The silicon isotope distribution in various geological reservoirs. See other diagrams in this chapter for detailed references.

4.1.1.1 Silicon isotope compositions of bulk samples of meteorites

The silicon isotope compositions of bulk samples of meteorites were analyzed by Molini-Velsko et al. (1986), Grossman et al. (2008) with the SiF_4 method and by Georg et al. (2007a), Fitoussi et al. (2009), Savage et al. (2010), Zambardi and Poitrasson (2011), Armytage et al. (2011, 2012), Fitoussi and Bourdon (2012), Pringle et al. (2013), Savage and Moynier (2013), Zambardi et al. (2013), Savage et al. (2014) and Dauphas et al. (2015) with the MC-ICPMS method.

It can be seen from Figure 4.1 and Figure 4.2 that the δ^{30}Si values of bulk meteorites vary from –1.4‰ to 0. 0‰, with an average value of –0.5‰.

Considering the silicon isotope distribution in various meteorites separately, the δ^{30}Si values of different types of chondrites and achondrites are compared in Figure 4.3. The δ^{30}Si values of ordinary chondrites vary in a range from –0.8‰ to –0.1‰, with an average of –0.5‰. The δ^{30}Si values of achondrites vary in a range from –1.0‰ to –0.2‰, with an average of –0.5‰. The δ^{30}Si values of carbonaceous chondrites

EBSCOhost - printed on 2/10/2023 8:05 PM via . All use subject to https://www.ebsco.com/terms-of-use

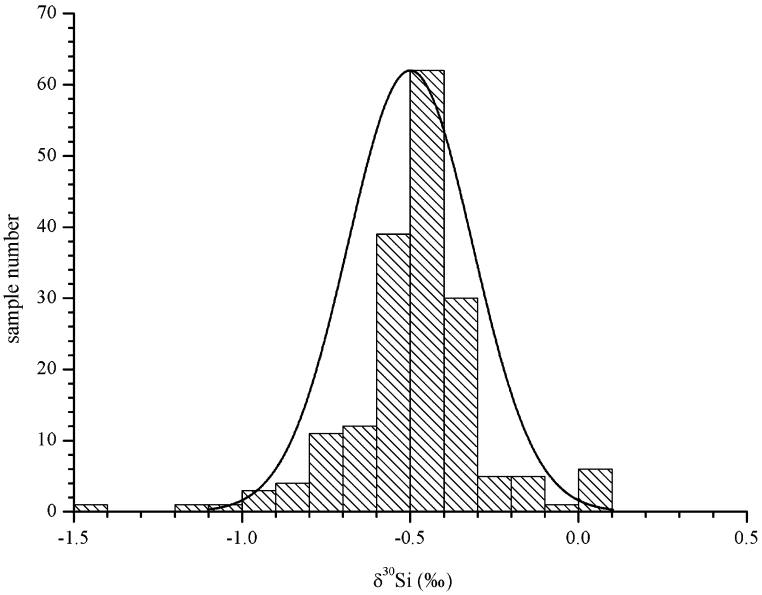

Figure 4.2: The histogram of δ^{30}Si values for all samples of bulk meteorites. Date are taken from Molini-Velsko et al. (1986), Grossman et al. (2008), Georg et al. (2007a), Fitoussi et al. (2009), Savage et al. (2010), Zambardi and Poitrasson (2011), Armytage et al. (2011, 2012), Fitoussi and Bourdon (2012), Pringle et al. (2013), Savage and Moynier (2013), Zambardi et al. (2013), Savage et al. (2014) and Dauphas et al. (2015).

vary in a range from –1.1‰ to 0.0‰, with an average of –0.5‰. These three types of meteorites show similar distribution, although the variation range for ordinary chondrites is a little smaller than those of other two types. However, the δ^{30}Si values of enstatite chondrites vary in a range from –1.4‰ to –0.4‰, with an average of –0.7‰, which is relatively lower than those of three other types of meteorites.

To understand the difference between enstatite chondrite with other types of meteorites, Ziegler et al. (2010), Savage and Moynier (2013), Zambardi et al. (2013) and Armytage et al. (2011) investigated the chemical and Si isotopic characteristics of enstatite chondrite in detail. It is known that enstatite chondrites contain significant (on the order of ~2 wt.%), and variable proportions of Si dissolved in the metal phases (Krot et al., 2007) and the δ^{30}Si value of Si in the metal phase is relatively lower than that in the silicate phase (Ziegler et al., 2010). Savage and Moynier (2013), Zambardi et al. (2013) and Armytage et al. (2011) analyzed the silicon isotope compositions of EH chondrite (high density enstatite chondrite) and EL chondrite (low density enstatite chondrite) separately. They found that the EH chondrite with relatively high Fe content shows δ^{30}Si values slightly lower than those of the EL chondrite with relatively low Fe content (Figure 4.4A). It seems that the δ^{30}Si values of the EL chondrite are more consistent to those of the ordinary chondrites, carbonaceous chondrites and achondrites.

EBSCOhost - printed on 2/10/2023 8:05 PM via . All use subject to https://www.ebsco.com/terms-of-use

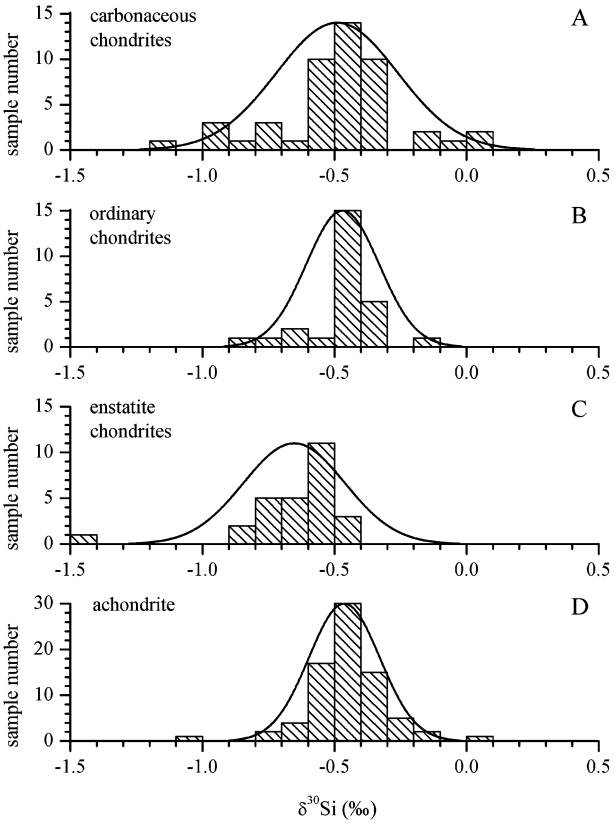

Figure 4.3: δ^{30}Si values of bulk samples of major types of meteorites. A: Carbonaceous chondrites; B: Ordinary chondrites; C: Enstatite chondrites; D: Achondrites. The data are from Molini-Velsko et al. (1986), Georg et al. (2007a), Fitoussi et al. (2009), Savage et al. (2010), Zambardi and Poitrasson (2011), Armytage et al. (2011, 2012), Fitoussi and Bourdon (2012), Pringle et al. (2013), Savage and Moynier (2013), Zambardi et al. (2013), Savage et al. (2014) and Dauphas et al. (2015).

The silicon isotope composition of different types of achondrites are shown in Figure 4.5. The δ^{30}Si values of aubrites vary in a range from −0.4‰ to −1.0‰, with an average of −0.6‰. The δ^{30}Si values of HED vary in a narrow range from −0.2‰ to −0.5‰, with an average of −0.4‰. The δ^{30}Si values of Martian meteorites vary in a narrow range from −0.3‰ to −0.8‰, with an average of −0.5‰. The δ^{30}Si values of ureilites vary in a narrow range from −0.2‰ to −0.6‰, with an average of −0.4‰. The Si isotope compositions of aubrites are slightly lighter than those of other achondrites.

Savage and Moynier (2013) made a comparison study on aubrites and enstatite chondrites. They point out that the Si isotope composition of aubrites are slightly lighter than the silicate phases of both EH and EL chondrites, which suggests that the post-accretion parent body differentiation processes have affected the Si isotope composition of the aubrites.

EBSCOhost - printed on 2/10/2023 8:05 PM via . All use subject to https://www.ebsco.com/terms-of-use

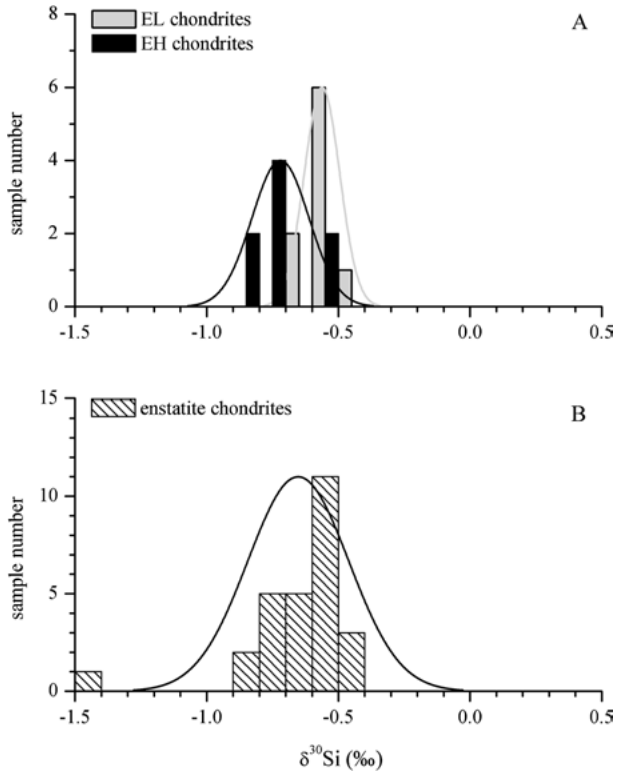

Figure 4.4: δ^{30}Si values of enstatite chondrites. A: Bulk samples of EL and EH enstatite chondrites. B: Bulk samples of enstatite chondrites. Date are taken from Savage and Moynier (2013), Zambardi et al. (2013) and Armytage et al. (2011).

For quite a number of meteorite samples, both of δ^{29}Si and δ^{30}Si values have been analyzed. A correlation plot of δ^{29}Si and δ^{30}Si for carbonaceous chondrites, ordinary chondrites, enstatite chondrites and achondrites is shown in Figure 4.6.

4.1.1.2 Silicon isotope compositions of CAIs in the chondritic meteorites

The refractory calcium-aluminum-rich inclusions (CAIs) in chondritic meteorites are the oldest dated solids in the solar system (Amelin et al., 2002; Bouvier and Wadhwa, 2010; Conley et al., 2012). CAIs are <1 mm to >1 cm sized objects, which range in shape from highly irregular to nearly spherical. Different types of CAIs have been found in meteorites (Grossman, 1980; Macpherson et al., 1988).

CAIs consist of primarily minerals of oxides and silicates of aluminum, calcium and magnesium with minor titanium. Compared to ferromagnesian chondrules and to bulk chondrites, the bulk CAIs are enriched in aluminum, calcium and titanium, and also in refractory trace elements such as the rare earth elements (REEs), scandium, strontium, yttrium, zirconium, niobium, barium, hafnium, tantalum, thorium,

EBSCOhost - printed on 2/10/2023 8:05 PM via . All use subject to https://www.ebsco.com/terms-of-use

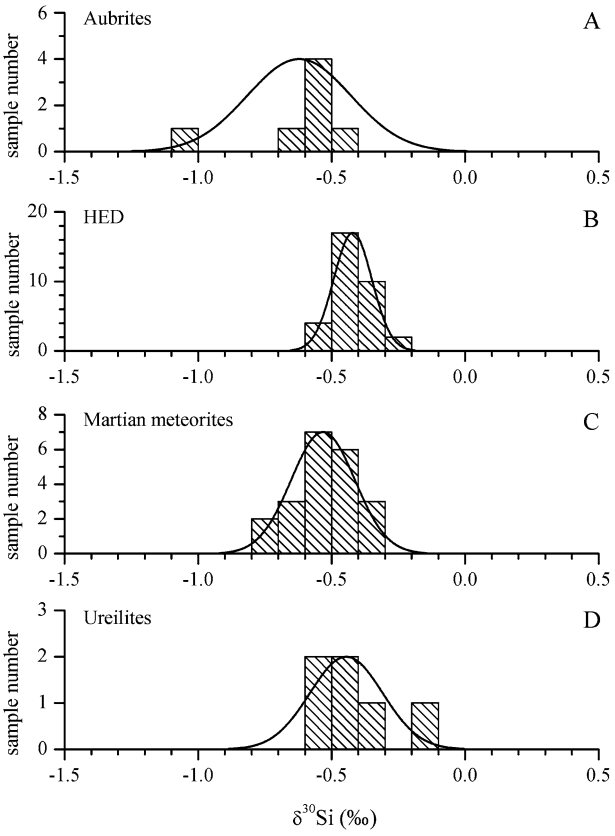

Figure 4.5: δ^{30}Si values of different types of Achondrites. A: Aubrites; B: HED; C: Martian meteorites; D: Ureilites. Data are from Molini-Velsko et al. (1986), Armytage et al. (2011), Fitoussi et al. (2009), Pringle et al. (2013).

uranium and refractory siderophile elements. In the meanwhile, CAIs are depleted in volatile elements such as sodium and iron.

The early observations show that: 1) CAIs are the oldest solids formed in the solar system and preserved today; 2) CAIs provide a record of nucleosynthetic processes (supernova events) that occurred before the formation of the solar system and 3) CAIs record early solar system conditions. Information on the genesis of CAIs should place constraints on conditions and processes that prevailed during the formation and earliest evolution of the solar nebula.

The silicon isotope compositions of CAIs from Allende, Efremovka, Leoville and Vigarano CV3 chondrites have been analyzed by a number of research groups (Clayton and Mayeda, 1984; Davis et al., 1991; Shahar and Young, 2007; Grossman et al., 2008; Williams et al., 2017). A plot of δ^{29}Si–δ^{30}Si relationship is shown in Figure 4.7. It can be seen that all of these CAIs have positive δ^{29}Si and δ^{30}Si values.

EBSCOhost - printed on 2/10/2023 8:05 PM via . All use subject to https://www.ebsco.com/terms-of-use

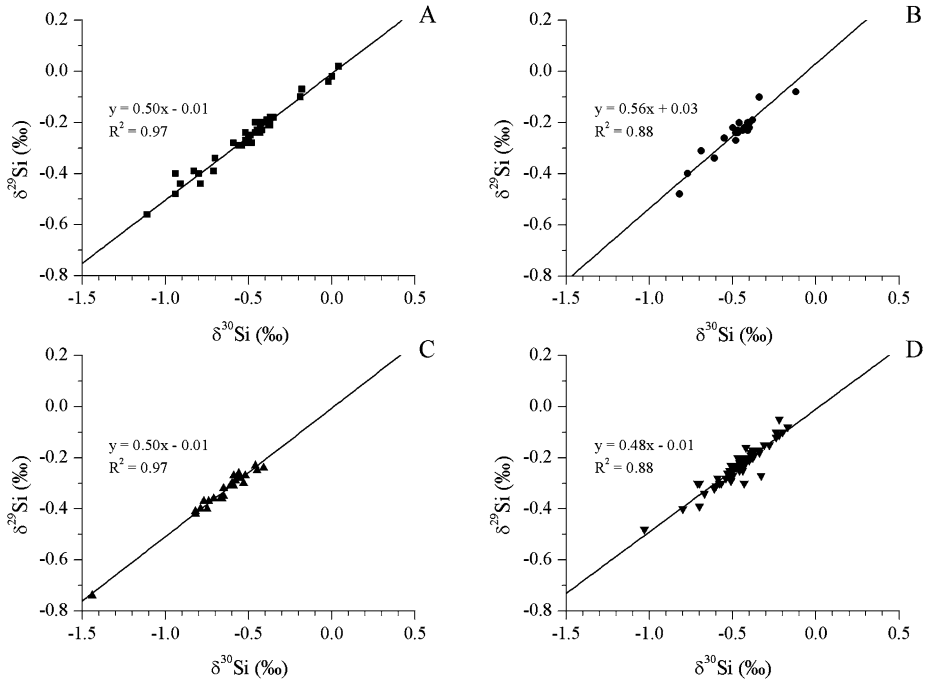

Figure 4.6: A plot showing correlation between δ^{29}Si and δ^{30}Si in major types of meteorites. A: Carbonaceous chondrites; B: Ordinary chondrites; C: Enstatite chondrites; D: Achondrites. Data are from Molini-Velsko et al. (1986), Dauphas et al. (2015), Fitoussi et al. (2009), Armytage et al. (2011), Savage and Moynier (2013), Chakrabarti and Jacobsen (2010), Pringle et al. (2013).

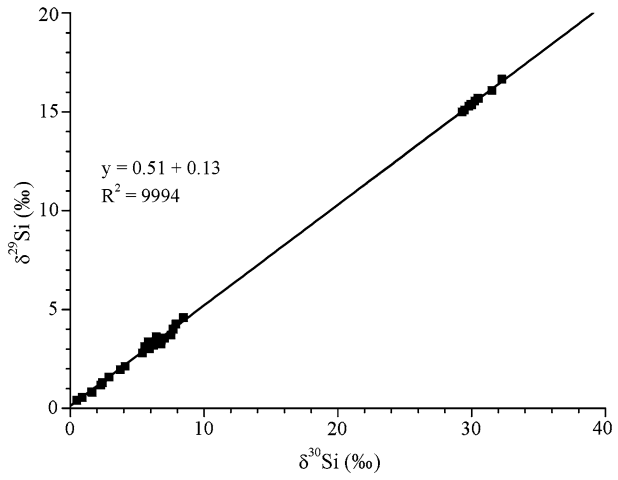

Figure 4.7: A plot showing δ^{29}Si vs. δ^{30}Si relationship for CAIs. Data are from Shahar and Young (2007), Williams et al. (2017) and Grossman et al. (2008).

EBSCOhost - printed on 2/10/2023 8:05 PM via . All use subject to https://www.ebsco.com/terms-of-use

The δ^{29}Si values of CAIs vary in a range from 0.4 to 16.7‰, with an average of 6.4‰, and δ^{30}Si values of CAIs vary in a range from 0.5 to 32.3‰, with an average of 12.3‰. Besides, in a δ^{29}Si–δ^{30}Si correlation diagram (Figure 4.7), all data fall in a linear line with a slope of 0.51, indicating CAIs has experienced a mass-dependent Si isotope fractionation.

There are two hypotheses for the origin of CAIs: either as early condensates from the cooling solar nebula (Grossman, 1972; Boynton, 1975; Davis and Grossman, 1979) or as evaporation residues of preexisting material (Kurat, 1970; Tanaka and Masuda, 1973; Chou et al., 1976; Notsu et al., 1978; Nagasawa and Onuma, 1979; Hashimoto et al., 1979; Lee et al., 1979, 1980; Hashimoto, 1983; Niederer and Papanastassiou, 1984; Clayton et al., 1988; Davis et al., 1990; Ireland et al., 1992). To check these two hypotheses, a series of experimental studies have been carried out using silicon isotopes. Detailed descriptions are given in Chapter 3.

4.1.1.3 Silicon isotope compositions of SiC and Si in graphite from carbonaceous chondrite

Elemental and isotopic abundances of the galaxy change with time. When stars reach the later stages of their lives, their nucleosynthetic products are expelled into space as gas and dust. Stars with masses less than 8 $M_\odot$ become asymptotic giant branch (AGB) stars and lose significant material as stellar wind during the thermally-pulsing AGB phase. Stars with masses $\geqslant$ 8 $M_\odot$ become core-collapse supernovae and the nucleosynthetic products in these stars are distributed into space through explosion. Gas and dust expelled from these stars are eventually incorporated into molecular clouds. Our solar system, located at 8.5 kpc from the center of the galaxy, formed from such a molecular cloud ~4.6 billion years ago. The parent molecular cloud of the solar system was believed to have been completely homogenized during the solar system formation (Cameron, 1962). This idea of an isotopically uniform solar system was reinforced by analyses of meteorites in the 1950s and 1960s, which showed uniform isotopic ratios (e.g., Podosek, 1978).

However, when Black and Pepin (1969) analyzed Ne in primitive meteorites by step-wise heating, they found a new ^{22}Ne-rich component, which later was named Ne-E (Black, 1972). The lowest ^{20}Ne/^{22}Ne ratio of 3.4 (compared to air value of 9.8) observed in their experiment is difficult to be explained by processes occurred in the solar system. Thus, a nucleosynthetic origin was proposed (Clayton, 1975).

After a long term investigation, it has been found that all carriers of these anomalous noble gas components are carbonaceous and fairly resistant to chemicals. So far, the presolar grains identified to date include diamond, SiC, graphite, oxides, silicon nitride (Si_3N_4) and silicates. Analyses of presolar grains have provided a wealth of information about nucleosynthesis in stars, mixing in stellar ejecta, and galactic chemical evolution.

EBSCOhost - printed on 2/10/2023 8:05 PM via . All use subject to https://www.ebsco.com/terms-of-use

Since the SIMS studies made by Zinner et al. (1987) and Tang et al. (1988) on silicon carbide in meteorites, and their discovery of extra-large anomalies of silicon isotope compositions, there have been more detailed studies of this subject (Zinner et al., 1989; Stone et al., 1991; Hoppe et al., 1993, 1996a; Alexander, 1993; Huss et al., 1997). As a result of these studies, there is clear evidence of mass-independent isotopic fractionation in silicon carbide (Figure 4.8 and Figure 4.9).

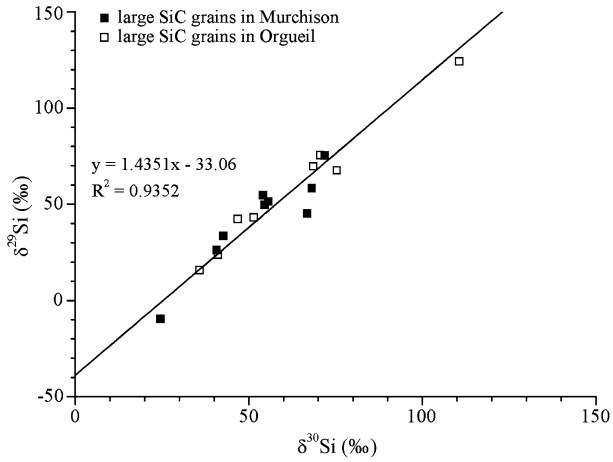

Figure 4.8: The δ^{29}Si vs. δ^{30}Si relationship of coarse platy SiC from Murchison and Orgueil meteorites. Data are taken from Stone et al. (1991), Hoppe et al. (1993), Zinner et al. (1989), Alexander (1993), Huss et al. (1997).

The Si isotope compositions of coarse platy SiC from the Orgueil and Murchison meteorites are shown in Figure 4.8 (Stone et al., 1991; Hoppe et al., 1993; Zinner et al., 1989; Alexander, 1993; Huss et al., 1997). The data of these samples vary in an area from 24.6‰ to 110.7‰ for δ^{30}Si and from –9.6‰ to 124.2‰ for δ^{29}Si, which is much broader than those of the silicate and CAIs in meteorites. The δ^{29}Si vs. δ^{30}Si relationship of coarse platy SiC from the Orgueil and Murchison meteorites (Figure 4.8) indicates that data fit well with a line of $\delta^{29}\text{Si} = 1.4351\delta^{30}\text{Si} - 33.06$, which has a slope much larger than the slope (around 0.515) of the mass-dependent line. This shows that the silicon isotopic compositions of the coarse platy SiC are affected by mass-independent isotopic fractionation. Stone et al. (1991) suggested that the above phenomenon may indicate disproportionate mixing of silicon components with different silicon isotope compositions. These observations suggested that there was either gas phase heterogeneity where the grains formed or gas-grain isotopic exchange post-dating their formation.

Isotopic compositions of some fine-grained SiC from the Orgueil and Murchison meteorites are shown in Figure 4.9 (Hoppe et al., 1996b; Huss et al., 1997). The data

EBSCOhost - printed on 2/10/2023 8:05 PM via . All use subject to https://www.ebsco.com/terms-of-use

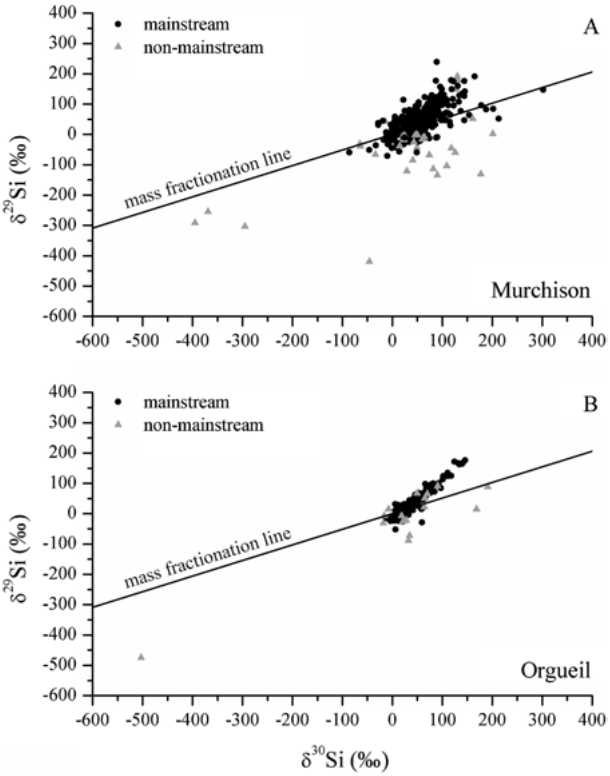

Figure 4.9: The δ^{29}Si vs. δ^{30}Si relationship of small grains of SiC from Murchison and Orgueil meteorites. Data are from Hoppe et al. (1996b) and Huss et al. (1997).

of these samples are scattered over a broader area (from −395‰ to 302‰ for δ^{30}Si and from −419‰ to 239‰ for δ^{29}Si) than those of the coarse-grained SiC. It can be observed that, in addition to the "mainstream" grains with silicon isotopic compositions similar to those of the coarse platy SiC, there are other "non-mainstream" grains with different isotopic compositions within fine-grained SiC. Comparing to the "mainstream" grains, one type of "non-mainstream" grains shows much lower δ^{30}Si and δ^{29}Si values, but another type of "non-mainstream" grains shows only lower δ^{30}Si values.

It is suggested that the large grains of SiC and "mainstream" small grains of SiC may belong to AGB star origin (Hoppe et al., 1996b). However, the stellar origin of "non-mainstream" small grains of SiC is still uncertain.

Amari et al. (1990) isolated the first presolar graphite grains from the Murchison CM2 meteorite by identifying the grains to be carriers of the exotic noble gas component Ne-E(L) (almost pure ^{22}Ne). Subsequently, extensive isotopic studies were carried out on the Murchison density fractions (Amari et al., 1990, 1995a, 2012; Hoppe et al., 1995; Zinner et al., 1995; Travaglio et al., 1999). All isotopically identified preso-

EBSCOhost - printed on 2/10/2023 8:05 PM via . All use subject to https://www.ebsco.com/terms-of-use

lar graphite grains in Murchison are spherical, with diameters >1 μm (ranging up to ~20 μm). Structural and isotopic properties of Murchison presolar graphite vary with density (Amari et al., 1995b; Hoppe et al., 1995). More recently, graphite grains were isolated from the Orgueil CI chondrite (Jadhav et al., 2006). Similar spherical grains were identified and studied in different density fractions of Orgueil (Jadhav et al., 2006, 2008). In general, graphite grains from Orgueil appear to be rather similar to those from Murchison, both morphologically and in their isotopic properties.

The Si isotope compositions of graphite from the Orgueil and Murchison meteorites are shown in Figure 4.10 (Jadhav et al., 2013 and Amari et al., 2014). The data of these samples are scattered over an even more broad area (from −660‰ to 916‰ for δ^{30}Si and from −451‰ to 1 341‰ for δ^{29}Si) than those of the fine-grained SiC.

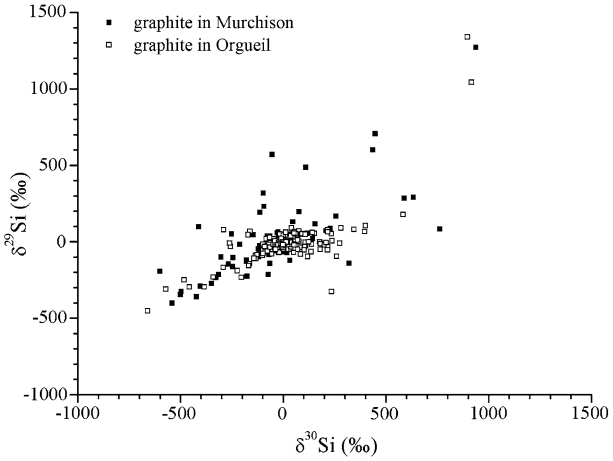

Figure 4.10: The δ^{29}Si vs. δ^{30}Si relationship of Si in graphite from Murchison and Orgueil meteorites. Data are from Jadhav et al. (2013) and Amari et al. (2014).

It has been found that the Si isotopic properties are dependent on density: low-density grains contain ^{28}Si excesses, while the majority of high-density grains are generally enriched in ^{29}Si and ^{30}Si (Jadhav et al., 2013). The ^{28}Si excesses in low-density grains may indicate an origin from supernovae. In order to explain the isotopic ratios measured in these grains, Jadhav et al. (2013) present mixing scenarios between different layers of supernovae and discuss the limitations of various theoretical models. In their model, ^{30}Si in high-density grains indicates an origin in AGB stars with low metallicities. Most low-density graphite grains originate from supernovae while high-density graphite grains have multiple stellar sources: low-metallicity and born-again AGB stars, Type II supernovae and possibly, J-type stars.

EBSCOhost - printed on 2/10/2023 8:05 PM via . All use subject to https://www.ebsco.com/terms-of-use

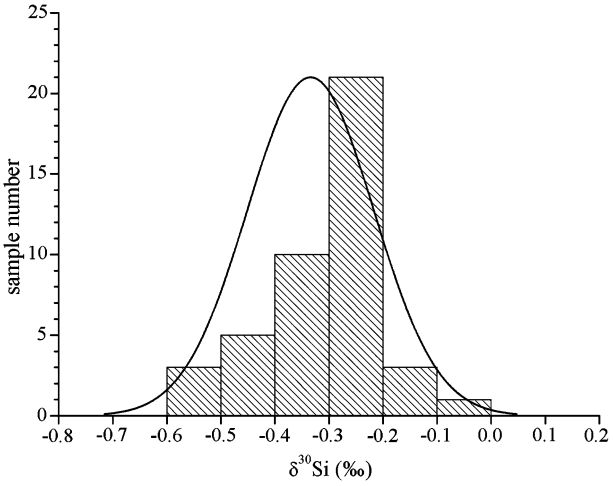

Figure 4.11: A histogram of δ^{30}Si values of lunar rocks. Data are from Epstein and Taylor (1971), Taylor and Epstein (1973a), Armytage et al. (2012), Zambardi et al. (2013), Savage et al. (2014) and Poitrasson and Zambardi (2015).

4.1.2 Tectite

So far, only two measurements of the silicon isotopic composition of tectites have been made. One sample taken from northern Thailand has a δ^{30}Si value of −0.3‰. The other sample from Hainan Island, China, gave a δ^{30}Si value of 0‰. These results are in accord with the hypothesis that tectites are formed through the impact of meteorites (Ding et al., 1996).

4.1.3 Lunar samples

Detailed studies of the silicon isotopic compositions of lunar rocks and soils have been made by Epstein and Taylor (1970, 1971, 1973). Since then, not much study has been undertaken on this aspect. Only recently, a few investigations on silicon isotope compositions of lunar rocks have been renewed to study the Moon's formation and the early history of the Earth (Armytage et al., 2012; Savage et al., 2014; Poitrasson and Zambardi, 2015) and the silicon isotope variations in the inner solar system (Zambardi et al., 2013).

A combination of available δ^{30}Si values of lunar rocks are shown in Figure 4.11. From available data, it can be found that the δ^{30}Si values of lunar rocks and glasses vary in a narrow range from −0.1‰ to −0.6‰, with an average of −0.3‰.

To study the relation between moon and meteorites, a diagram for the comparison between δ^{30}Si values of lunar rocks with those of different types of meteorites is plotted in Figure 4.12. It seems that the variation range of δ^{30}Si values of lunar rocks is

EBSCOhost - printed on 2/10/2023 8:05 PM via . All use subject to https://www.ebsco.com/terms-of-use

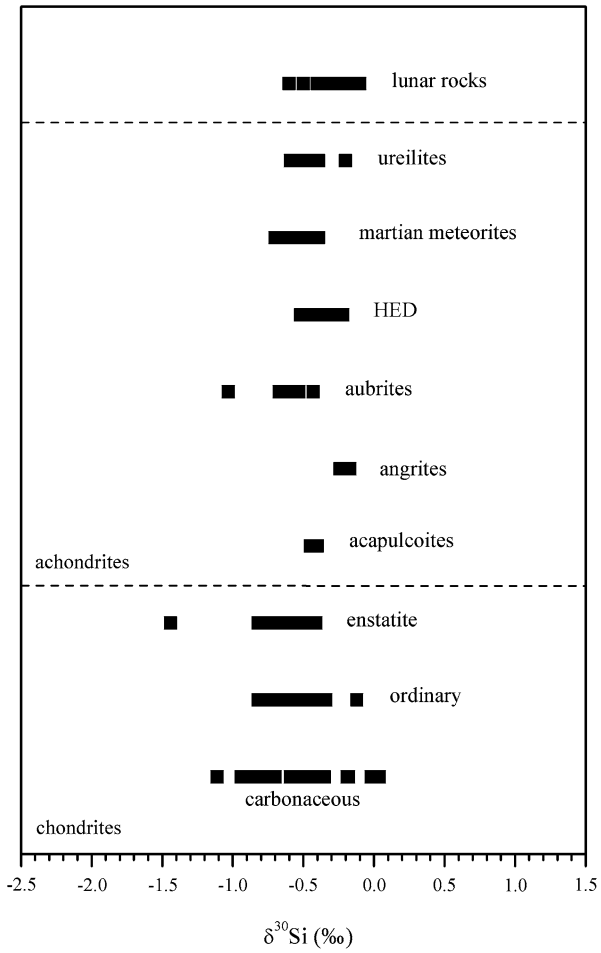

Figure 4.12: A comparison between δ^{30}Si values of lunar rocks with those of different types of meteorites. Data of lunar rocks are from Epstein and Taylor (1971), Taylor and Epstein (1973a), Armytage et al. (2012), Zambardi et al. (2013), Savage et al. (2014) and Poitrasson and Zambardi (2015).

similar to those of the majority types of meteorites, especially the ordinary chondrite, ureilites and HED. However, in comparison with enstatite chondrite and aubrites, the lunar rocks have relatively higher δ^{30}Si values. This is because that, as discussed in above subsection, some of enstatite chondrite and aubrites contain a fraction of metallic phase, which contains Si with lower δ^{30}Si values.

In Chapter 3, we have discussed the silicon isotope fractionation in terrestrial planet formation processes. During the segregation of the Earth's core and mantle, Si isotope equilibrium fractionation occurs between metal phase (dominated in the core) and silicate phase (in the mantle). The formation of the Earth's core imparted a high ^{30}Si/^{28}Si signature to BSE due to dissolution of ~6 wt.% Si into the early core.

EBSCOhost - printed on 2/10/2023 8:05 PM via . All use subject to https://www.ebsco.com/terms-of-use

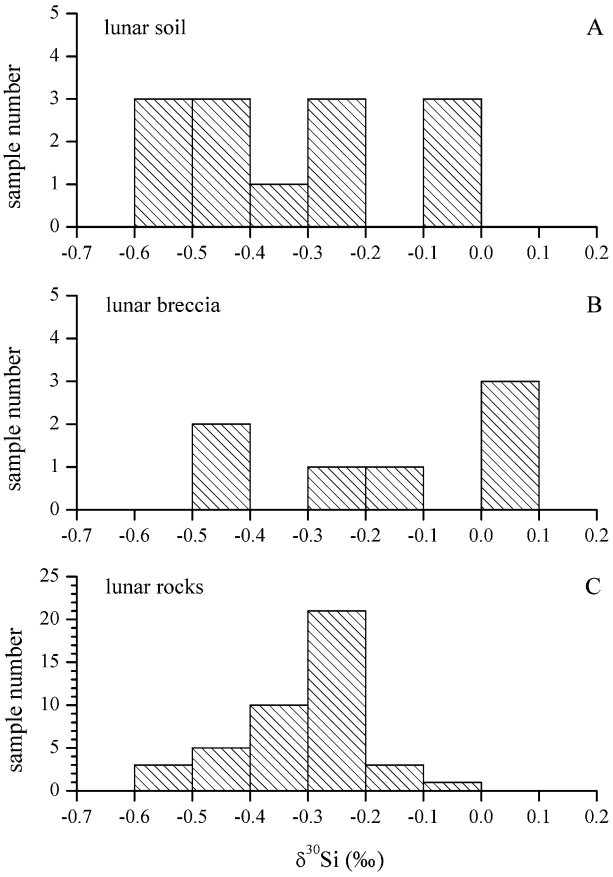

Figure 4.13: Comparison of silicon isotope compositions between lunar rocks with breccia and soils. A: the δ^{30}Si values of lunar soil; B: the δ^{30}Si values of lunar breccia; C: the δ^{30}Si values of lunar rocks. Data are from Epstein and Taylor (1971), Taylor and Epstein (1973a,b), Armytage et al. (2012), Zambardi et al. (2013), Savage et al. (2014) and Poitrasson and Zambardi (2015).

Similar to the BSE, the Si isotope compositions of the lunar rocks may represent those of the segregated silicate phase.

The δ^{30}Si values of lunar soils, breccia and rocks are compared in Figure 4.13. It can be seen that the δ^{30}Si values of lunar breccia vary from 0.0‰ to −0.5‰, averaging −0.2‰, which is slightly higher than the mean value (−0.3‰) of the bulk rock samples. Epstein and Taylor (1971) had suggested that there is an increase trend of δ^{30}Si values from lunar rocks to lunar breccia and soils, reflecting silicon isotope fractionation caused by preferential loss of ^{28}Si from the crushed lunar rocks due to bombardment by micrometeorites and cosmic particles on the lunar surface. However, this trend is not supported by the available data of lunar soils. The δ^{30}Si values of the lunar soils vary from −0.1‰ to −0.6‰, averaging −0.4‰, slightly lower than the δ^{30}Si values of the lunar breccia.

EBSCOhost - printed on 2/10/2023 8:05 PM via . All use subject to https://www.ebsco.com/terms-of-use

4.2 Silicon isotope distribution in lithosphere

As the most important accommodation of silicon in the Earth, the lithosphere is the first Earth's sphere to be studied for silicon isotope distributions (Reynolds and Verhoogen, 1953; Allenby, 1954; Douthitt, 1982; Ding et al., 1988a). By now, various Si reservoirs in the lithosphere, including magmatic rocks, sedimentary rocks, metamorphic rocks, hydrothermal veins and ore deposits and soils have been investigated comprehensively.

4.2.1 Magmatic rocks

From the early stages of silicon isotope geochemistry, attention has been given to the study of silicon isotope compositions of magmatic rocks. The silicon isotope standard adopted by Reynolds and Verhoogen (1953) was an olivine from a dunite rock body in North Carolina. Among the 14 data reported by them, four were minerals from igneous rocks. Among the 11 data reported by Allenby (1954), three were from igneous samples. Later, Douthitt (1982) made a more detailed study of the silicon isotopic composition of basalts and granites. Since 1988, Ding and his coworkers have made a detailed study of the silicon isotopic composition of igneous rocks from various parts of the world. Ding et al. (1996) summarized the early results on silicon isotope compositions of various igneous rocks in their monograph entitled "Silicon Isotope Geochemistry". In the twenty-first century, the studies on silicon isotope compositions of magmatic rocks are more connected to the issues of the silicon isotope composition of the bulk silicate earth (Georg et al., 2007a; Fitoussi et al., 2009; Savage et al., 2010; Chakrabarti and Jacobsen, 2010; Armytage et al., 2011; Pringle et al., 2016), the behaviour of Si isotopes during magmatic differentiation (Savage et al., 2011, 2013b; Chakrabarti and Jacobsen, 2010; Georg et al., 2007a) and the formation and composition of continental crust (Savage et al., 2012, 2014; Zambardi and Poitrasson, 2011).

4.2.1.1 The δ^{30}Si values of all kinds of magmatic rocks

By now, more than 400 δ^{30}Si data are available for bulk samples of magmatic rocks, which are shown in Figure 4.14. It can be seen that the δ^{30}Si values of bulk samples of magmatic rocks vary in a narrow range from –1.0‰ to 0.4‰, with an average of –0.2‰ and a peak value at –0.3‰.

4.2.1.2 Silicon isotope composition of the bulk silicate earth

Over 90% of Earth's Si is in the mantle. All of the Si present in oceanic and continental crust is derived also from the mantle. Thus, the knowledge on average Si isotope composition of the BSE is important for establishing a global terrestrial baseline.

EBSCOhost - printed on 2/10/2023 8:05 PM via . All use subject to https://www.ebsco.com/terms-of-use

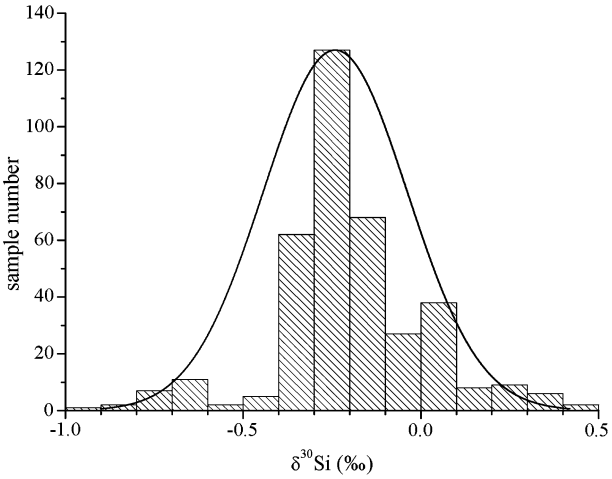

Figure 4.14: The δ^{30}Si values of all kinds of magmatic rocks. Data are from Savage et al. (2010, 2012), Zambardi et al. (2014), André et al. (2006), Zhou et al. (2007), Liu et al. (2015), Poitrasson and Zambardi (2015), Wang et al. (2015), Fitoussi et al. (2009), Armytage et al. (2011), Zhao et al. (2014), Pringle et al. (2016), Chemtob et al. (2015), Georg et al. (2007a).

The first estimation on Si isotope composition of the BSE was made by Douthitt (1982), who calculated an average δ^{30}Si value of −0.4 ± 0.3‰ (2std) by using predominantly island arc basalt (IAB) data from the Marianas. This was reappraised by Ding et al. (1996) who gave a lighter estimate of −0.61 ± 0.55‰. Then Ziegler et al. (2005a) proposed a δ^{30}Si of −0.5 ± 0.3‰ (2std) of BSE based on un-weathered basaltic flow from Hawaii.

In the new century, a number of new estimations are obtained by using MC-ICPMS analysis. Georg et al. (2007a) reported a $\delta^{30}Si_{BSE}$ estimate of −0.38 ± 0.13‰, Fitoussi et al. (2009) proposed a heavier $\delta^{30}Si_{BSE}$ value of −0.29 ± 0.06‰. Savage et al. (2010) provided a set of group data averages as $\delta^{30}Si_{ultramafic}$ = −0.33 ± 0.08‰, $\delta^{30}Si_{MORB}$ = −0.27 ± 0.06‰ and $\delta^{30}Si_{IAB}$ = −0.28 ± 0.06‰ (2std). All of these averages are similar, implying that there currently is no resolvable Si isotopic difference between ultramafic rocks and basaltic lavas; as such, no significant fractionation occurs during mantle melting. These and subsequent Si isotope studies have provided two groups of $\delta^{30}Si_{BSE}$, one close to −0.4‰ (Chakrabarti and Jacobsen, 2010; Georg et al., 2007a), the other nearer −0.3‰ (Armytage et al., 2011; Fitoussi et al., 2009; Savage et al., 2010; Zambardi et al., 2013). One explanation for the disparity might be the choice of samples. However, there is another possibility that the analytical issues are biasing the data of these two studies. Nevertheless, all the estimates are within error.

Savage et al. (2014) combined the data for whole rock ultramafic or basaltic samples from the studies of Abraham et al. (2008), Armytage et al. (2011, 2012), Fitoussi et al. (2009), Savage et al. (2010, 2011, 2013a), Savage and Moynier (2013) and Zambardi et al. (2013) to derive a new estimate for $\delta^{30}Si_{BSE}$. The calculated new $\delta^{30}Si_{BSE}$

EBSCOhost - printed on 2/10/2023 8:05 PM via . All use subject to https://www.ebsco.com/terms-of-use

is −0.29 ± 0.07‰ (2std), which is identical to that of Armytage et al. (2011), Fitoussi et al. (2009), Savage et al. (2010) and Zambardi et al. (2013), but with slightly improved precision.

4.2.1.3 Silicon isotopes and Earth's core formation

The origin and earliest history of the Earth are major issues of isotope geochemistry. Silicon isotope measurements have proved to be immensely valuable in both these fields. It is known that the density of the outer core is too low for it to be made only of an iron–nickel alloy; some other lighter element(s) must also be present and silicon has long been considered a possible light element in the Earth's core.

In the first section of this chapter, it has been indicated that the average δ^{30}Si values of bulk samples of ordinary chondrites, achondrites, carbonaceous chondrites and enstatite chondrites are −0.5‰, −0.4‰, −0.4‰ and −0.6‰, respectively. The calculated total average δ^{30}Si value of bulk meteorites is −0.5‰, which is nearly 0.2‰ lower than the estimated δ^{30}Si value (−0.29‰, Savage et al., 2014) of BSE (Figure 4.15).

This offset between the silicon isotopic composition of BSE and all meteorites has been proposed first by Georg et al. (2007a), but subsequent studies have not all agreed about the exact composition of meteorites and the magnitude of the difference relative to the BSE. However, most research groups agree that enstatite chondrites have the lightest δ^{30}Si of all the chondrites (Fitoussi and Bourdon, 2012; Savage and Moynier, 2013) and there is some δ^{30}Si difference between the BSE and meteorites (Armytage et al., 2011; Fitoussi et al., 2009; Georg et al., 2007a; Zambardi et al., 2013).

Georg et al. (2007a) and Fitoussi et al. (2009) proposed an explanation for the δ^{30}Si difference between the BSE and meteorites, in which the isotopically light Si is partitioned into the core. This interpretation has been reinforced by a number of experimental investigation on silicon isotope fractionation between iron metal and rock when equilibrated at high temperatures (Shahar et al., 2009, 2011; Hin et al., 2014) and the study on Si isotope fractionation between metal and silicate in metal-rich enstatite meteorites as an analogue for Earth's differentiation (Ziegler et al., 2010) (see Chapter 3). The available $\Delta^{30}Si_{metal-silicate}$ are listed in the Table 3.1 and shown in Figure 3.3.

According to this conception, the Si concentration in the core can be estimated from the $\Delta^{30}Si_{BSE\text{-}meteorite}$ value and the parameters (T and P) during core segregation. Based on published estimates for $\Delta^{30}Si_{BSE\text{-}meteorite}$, Savage et al. (2014) estimate that the core contains between ~10 and 5.4 wt.% Si, with their new estimate for $\Delta^{30}Si_{BSE\text{-}meteorite}$ (0.17‰) corresponding to a Si concentration in the core of 6.2 wt.%, which is in accord to geophysical estimates (e.g., Anderson and Isaak, 2002) and experimental estimates (Corgne et al., 2008; Wade and Wood, 2005).

EBSCOhost - printed on 2/10/2023 8:05 PM via . All use subject to https://www.ebsco.com/terms-of-use

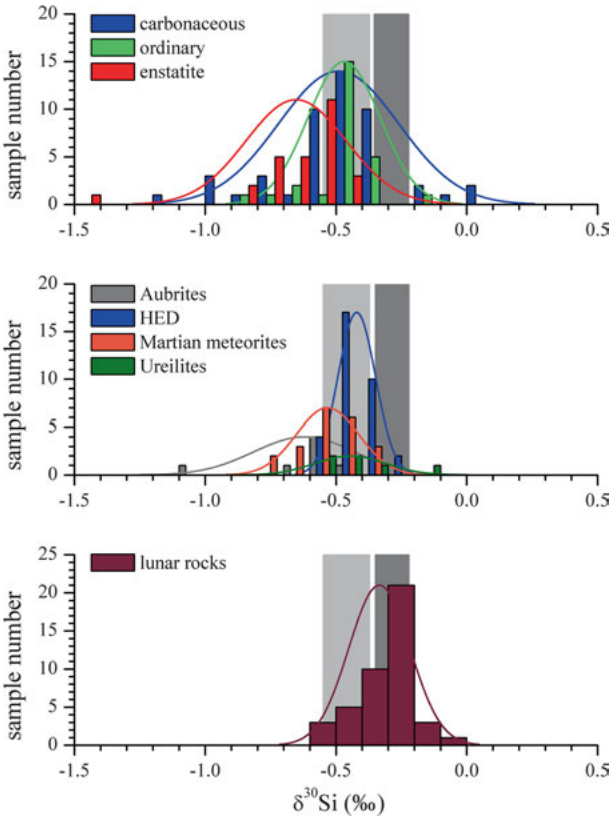

Figure 4.15: The comparison among the silicon isotope compositions of BSE, meteorites and lunar rocks, revised from Savage et al. (2014). The estimate of average composition (2std) of meteorites are shown in light gray box, and that of the BSE in dark gray box (Armytage et al., 2011; Fitoussi et al., 2009; Savage et al., 2010; Zambardi et al., 2013). Data are from Epstein and Taylor (1971), Taylor and Epstein (1973a), Molini-Velsko et al. (1986), Georg et al. (2007a), Fitoussi et al. (2009), Savage et al. (2010, 2014), Armytage et al. (2011, 2012), Zambardi and Poitrasson (2011), Fitoussi and Bourdon (2012), Pringle et al. (2013), Savage and Moynier (2013), Zambardi et al. (2013), Dauphas et al. (2015) and Poitrasson and Zambardi (2015).

4.2.1.4 A comparison between δ^{30}Si values of volcanic rocks and those of intrusive rocks

A comparison between δ^{30}Si values of volcanic rocks and those of intrusive rocks is shown in Figure 4.16. The δ^{30}Si values of volcanic rocks vary in a range from –0.8‰ to 0.2‰, with an average of –0.3‰ and a peak value at –0.3‰. The δ^{30}Si values of intrusive rocks vary in a range from –1.0‰ to 0.4‰, with an average of –0.2‰ and a peak value at –0.3‰ also. Comparing to volcanic rocks, the intrusive rocks show slightly larger variation range of δ^{30}Si values, reflecting more effect of country rock assimilation on the intrusive rocks. Besides, comparing to volcanic rocks, the sample

EBSCOhost - printed on 2/10/2023 8:05 PM via . All use subject to https://www.ebsco.com/terms-of-use

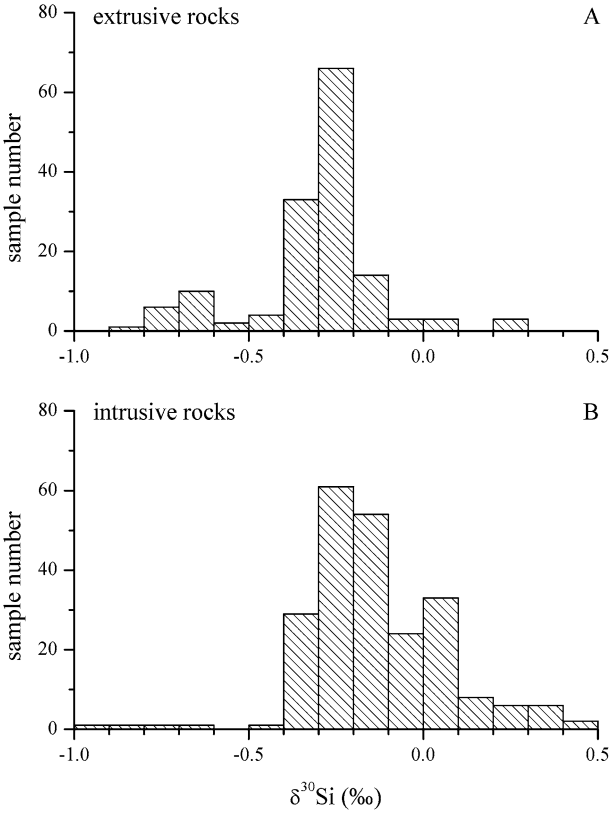

Figure 4.16: A comparison between δ^{30}Si values of volcanic rocks and those of intrusive rocks. A: Volcanic; B: Intrusive. Data are from Poitrasson and Zambardi (2015), Savage et al. (2010, 2012), Zambardi et al. (2014), André et al. (2006), Armytage et al. (2011, 2012), Zhou et al. (2007), Liu et al. (2015), Wang et al. (2015), Fitoussi et al. (2009), Zhao et al. (2014), Pringle et al. (2016), Chemtob et al. (2015), Georg et al. (2007a).

fraction at low δ^{30}Si side is much smaller and the sample fraction at high δ^{30}Si side is significantly larger, which is consistent with that the intrusive rocks are dominated by sialic rocks (especially granite), and the volcanic rocks are dominated by mafic rocks (especially basalts).

4.2.1.5 Comparison of the δ^{30}Si values of different types of magmatic rocks

The δ^{30}Si values of different types of intrusive magmatic rocks are shown in Figure 4.17. The δ^{30}Si values of ultramafic intrusive rocks vary in a range from −0.7‰ to 0.4‰, with an average of −0.3‰, but 90% of them are limited in a much narrow range of −0.4‰ ~ −0.2‰. The δ^{30}Si values of mafic intrusive rocks vary in a range from −0.9‰ to 0.3‰, with an average of −0.2‰ and a peak value at −0.3‰. The δ^{30}Si values of intermediate intrusive rocks vary in a range from −0.3‰ to 0.2‰, with

EBSCOhost - printed on 2/10/2023 8:05 PM via . All use subject to https://www.ebsco.com/terms-of-use

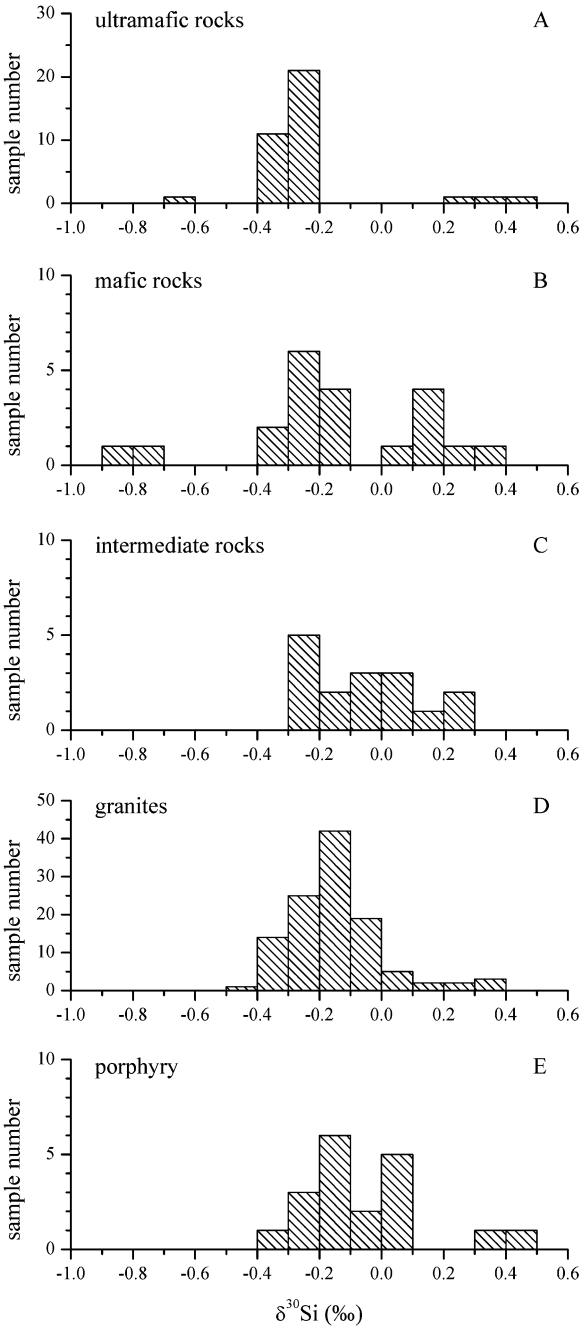

Figure 4.17: The δ^{30}Si values of different types of intrusive magmatic rocks. A: Ultramafic rocks; B: Mafic rocks; C: Intermediate rocks; D: Granitic rocks; E: Porphyry rocks. Data are taken from Poitrasson and Zambardi (2015), Savage et al. (2012), Zambardi et al. (2014), André et al. (2006), Armytage et al. (2011, 2012), Zhou et al. (2007), Liu et al. (2015) and Wang et al. (2015).

EBSCOhost - printed on 2/10/2023 8:05 PM via . All use subject to https://www.ebsco.com/terms-of-use

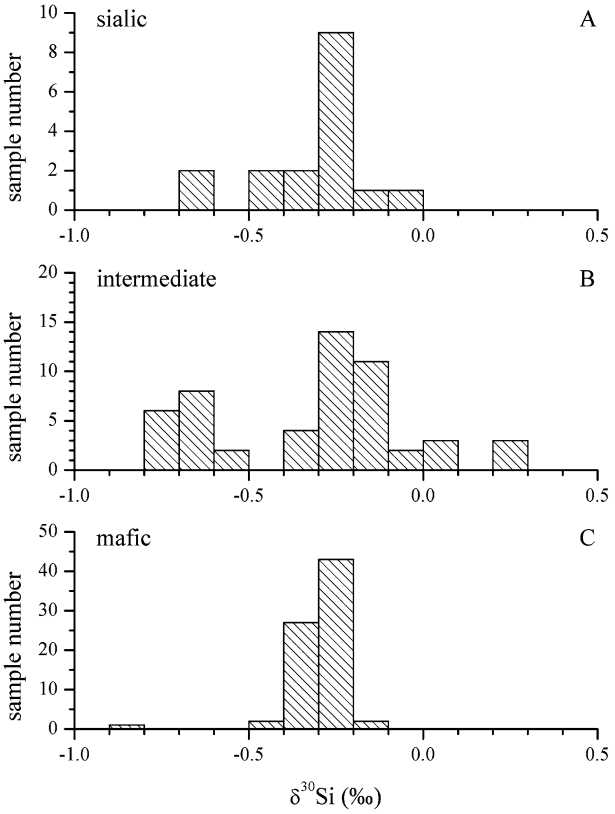

Figure 4.18: The δ^{30}Si distributions in different types of volcanic rocks. A: Sialic volcanic rocks; B: Intermediate volcanic rocks; C: Mafic volcanic rocks. Data are from Fitoussi et al. (2009), Zhao et al. (2014), Savage et al. (2010), Pringle et al. (2016), Poitrasson and Zambardi (2015), Armytage et al. (2011), Chemtob et al. (2015) and Georg et al. (2007a).

an average of −0.1‰ and a peak value at −0.3‰. The δ^{30}Si values of granitic rocks vary in a range from −0.5‰ to 0.3‰, with an average of −0.2‰ and a peak value at −0.2‰. The δ^{30}Si values of porphyry rocks vary in a range from −0.3‰ to 0.4‰, with an average of −0.1‰ and a peak value at −0.2‰. As pointed out in early studies (Douthitt, 1982; Ding et al., 1996), there is a trend of δ^{30}Si increase from ultramafic rocks to mafic rocks, intermediate rocks and acidic rocks.

The δ^{30}Si values of different types of volcanic rocks are shown in Figure 4.18. The δ^{30}Si values of sialic volcanic rocks vary in a range from −0.7‰ to −0.1‰, with an average of −0.4‰ and a peak at −0.3‰. The δ^{30}Si values of intermediate volcanic rocks vary in a range from −0.8‰ to 0.2‰, with an average of −0.3‰ and a peak value at −0.3‰. The δ^{30}Si values of mafic volcanic rocks, except for one sample with δ^{30}Si value of −0.8‰, vary in a range from −0.4‰ to −0.1‰, with an average of −0.3‰ and a peak value at −0.3‰.

EBSCOhost - printed on 2/10/2023 8:05 PM via . All use subject to https://www.ebsco.com/terms-of-use

4.2.1.6 The Si isotope variations during magmatic differentiation

As mentioned in Chapter 3, Douthitt (1982) first pointed out that silica-rich rocks have heavier Si isotope compositions than mafic and ultramafic rocks. Ding et al. (1996) summarized the early results on silicon isotope equilibrium fractionation among various silicate minerals, which pointed out that ^{30}Si contents of minerals increase from nesosilicate through inosilicate, phyllosilicate, to tectosilicate.

Recently, more comprehensive investigation on equilibrium Si isotope fractionation in magmatic processes has been carried out.

Savage et al. (2011) investigated Si isotopic compositions of lavas from the Hekla volcano, Iceland, samples from the Afar Rift Zone and various igneous USGS standards, and found out that Si isotopic composition varies linearly as a function of silica content, with more differentiated rocks possessing heavier isotopic compositions (Figure 3.6). Therefore, Si isotopes can be utilized to model the competing effects of mafic and felsic mineral fractionation in evolving silicate liquids and cumulates. This empirical relationship between silica content and the δ^{30}Si of igneous rocks was termed the "igneous array" for Si isotopes (Savage et al., 2011).

4.2.1.7 The δ^{30}Si distributions in different types of granites

The δ^{30}Si distributions in different types of granites are summarized by Savage et al. (2014) and available results are illustrated in Figure 4.19. The δ^{30}Si values of I-type granite vary in a narrow range from −0.25‰ to −0.10‰, the δ^{30}Si values of A-type granite vary in a narrow range from −0.20‰ to −0.10‰ and the δ^{30}Si values of aluminous and peralkaline granites vary in a narrow range from −0.20‰ to −0.05‰. All these granites show the silicon isotopic characters of mantle derived granites. In contrast, the δ^{30}Si values of S-type granite vary in a relatively wide range from −0.45‰ to −0.10‰ and the δ^{30}Si values of peraluminous and leucogranite vary in a narrow but more negative range from −0.25‰ to −0.40‰, reflecting the effect of assimilation of weathering materials from the crust.

Granites make up over half of the mass of the continental crust (Wedepohl, 1995), but are too Si-rich to be in equilibrium with the mantle (Rudnick, 1995). Formation of much of the continental crust cannot, therefore, be a result of simple mantle melting. Beside the process of mantle melting, a number of other processes, including fractional crystallization, partial melting of pre-existing mafic crust and sediment anatexis can all affect the genesis of granite. In particular, the anatexis of sedimentary lithologies should make the Si isotope compositions deviated from the Si isotope "igneous array". This is because weathering tends to enrich secondary minerals in the lighter Si isotopes relative to igneous material (Opfergelt et al., 2012; Ziegler et al., 2005a,b). Hence, partial melting of pelitic sediment, or contamination of mantle-derived melt by such material, should result in the formation of a crust, which has a lighter Si isotope composition than purely "igneous" (e.g., I-type granites and rhyolites) material. In this way, Si isotopes have the potential to differentiate between

EBSCOhost - printed on 2/10/2023 8:05 PM via . All use subject to https://www.ebsco.com/terms-of-use

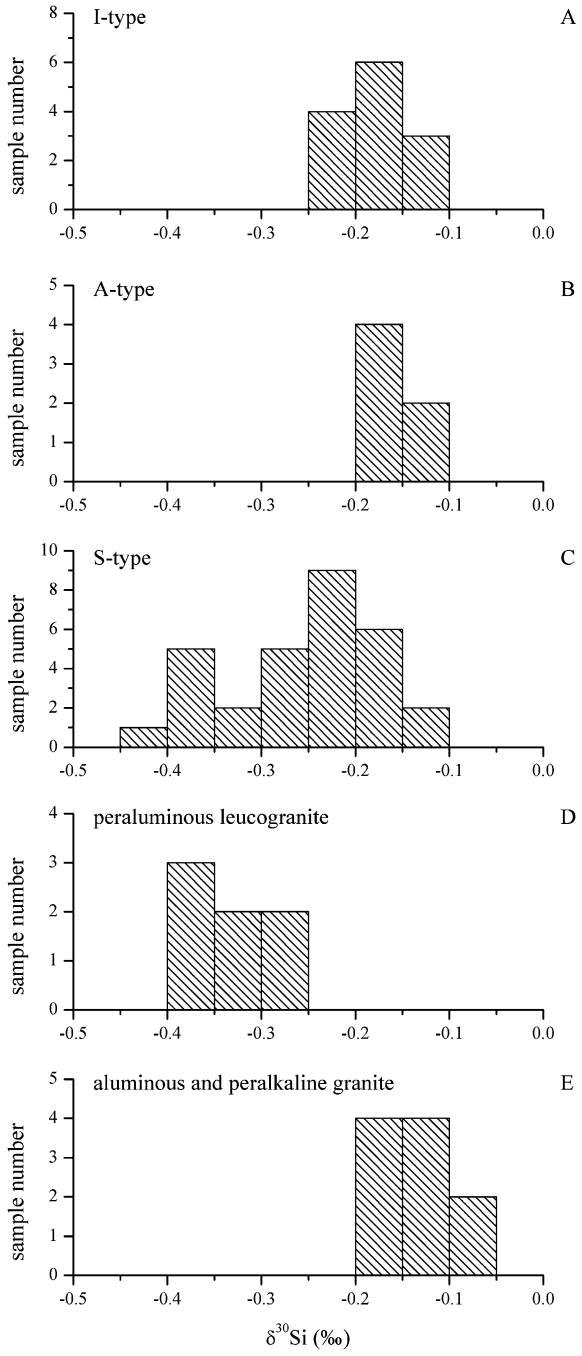

Figure 4.19: The δ^{30}Si distributions in different types of granites. A: I type of granite; B: A type of granite; C: S type of granite; D: Peraluminous and leucogranite; E: Aluminous and peralkaline granite. Data from Savage et al. (2012) and Poitrasson and Zambardi (2015).

EBSCOhost - printed on 2/10/2023 8:05 PM via . All use subject to https://www.ebsco.com/terms-of-use

granites that have sedimentary or igneous affinities, thus allowing us to identify mantle-derived, and hence "new" volumes of continental crust.

Douthitt (1982) is the first to test this hypothesis by analyzing a selection of I-type and S-type granites from the Lachlan Fold Belt, Australia. However, no systematic variations between the two granite types were noted. Subsequent work using MC-ICPMS further investigated this field, found the S-type samples analyzed displayed a resolvable lighter isotopic composition than the I-type, but the data were not formally published.

Savage et al. (2012) analyzed a broad selection of I-, S- and A-type samples, as well granitic hypabyssal lithologies from Australia and England. The data from Savage et al. (2012) define a broader range compared to other high-Si igneous rocks, such as rhyolites and dacites. In particular, the S-type granite samples define the broadest range of data and have, on average, the lightest Si isotope composition (Figure 4.19C). This deviation away from the predicted "igneous" value can be seen on a plot of δ^{30}Si vs. SiO_2 against the "igneous array" (Figure 4.20). Whereas both I- and A-type granites plot on or around the array, all but one of the S-type granites plot below the array, many to much more negative values than would be predicted in the absence of a sedimentary component. However, a caveat with the hypothesis that Si isotopes will differentiate between granite affinities is that the sedimentary material from which the granites are formed is isotopically distinct from that of igneous material (Savage et al., 2014).

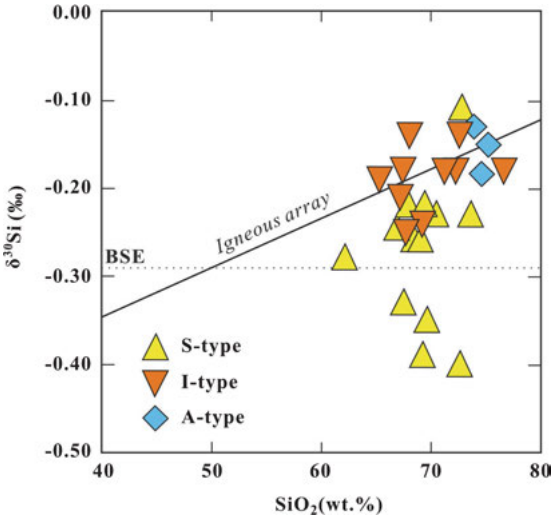

Figure 4.20: Correlation between δ^{30}Si and SiO_2 contents for different types of granite. Data are taken from Savage et al. (2012). I-type and A-type granites plot on the "igneous array" indicating an igneous protolith for these samples. The S-type samples have more scattered and light δ^{30}Si values, implying that these samples are derived from protoliths with lighter and more variable Si isotope compositions.

EBSCOhost - printed on 2/10/2023 8:05 PM via . All use subject to https://www.ebsco.com/terms-of-use

4.2.2 Sedimentary rocks

Sedimentary rocks are important reservoirs of silicon. Silicon is an important component of clastic rocks, clay stones and organic sedimentary rocks. Therefore, the silicon isotope compositions of sedimentary rocks have great significance in the study of silicon isotope geochemistry.

Reynolds and Verhoogen (1953), Allenby (1954) and Douthitt (1982) analyzed the silicon isotope composition of some sedimentary rocks and minerals. Ding et al. (1996) made the systematic silicon isotopic investigation on all kinds of clastic rocks, clay stones, chemical precipitates and organic sediments. Based on these data, the silicon isotope systematics have been outlined, and new evidence has been collected regarding the origin of various sedimentary rocks.

In this century, more comprehensive investigation has been made on silicon isotope distributions in sedimentary rocks. Significant progress has been achieved especially on BIFs, chert rocks and clays.

4.2.2.1 The δ^{30}Si values of all kinds of sedimentary rocks

There are more than 1,100 silicon isotope data available for the sedimentary rocks. Their δ^{30}Si values range from –4.3‰ to 3.9‰ (Figure 4.1 and Figure 4.21), much wider than that (–1.0‰ ~ 0.5‰) of magmatic rocks (Figure 4.1 and Figure 4.14). The highest frequency of δ^{30}Si value of sedimentary rocks appears at –0.2‰ (Figure 4.21), which is only 0.1‰ higher than that of magmatic rocks (Figure 4.14). These Si isotope characters indicate that the sedimentary rocks have experienced much more complicated and significant silicon isotope fractionation processes than those of magmatic rocks, but the ultimate source of sedimentary rocks are closely related to the magmatic rocks.

The δ^{30}Si distributions of the major sedimentary rocks are illustrated in Figure 4.22. Significant variations of δ^{30}Si are observed among different types of sedimentary rocks and within the same type of rocks.

4.2.2.2 Silicon isotope compositions of clastic sedimentary rocks

The available silicon isotopic compositions for sandstone, siltstone and shale are illustrated in Figure 4.23, in comparison with those of granites.

Silicon isotope compositions of sandstone

The δ^{30}Si values of sandstone vary in a relative narrow range from –0.5‰ to 0.5‰, with an average of –0.1‰ and a peak at –0.1‰, which is similar to that (–0.1‰) of granites (Ding et al., 1996). These characters indicate that the material in sandstone is the physical weathering products of granites.

EBSCOhost - printed on 2/10/2023 8:05 PM via . All use subject to https://www.ebsco.com/terms-of-use

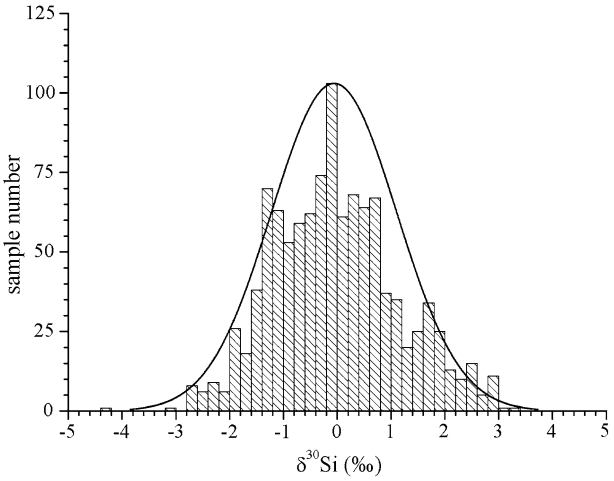

Figure 4.21: A histogram of silicon isotope compositions of sedimentary rocks. Data are from Wu et al. (2000), Geilert et al. (2014b, 2015), Cockerton et al. (2013), Pogge von Strandmann et al. (2014), Zhou et al. (2007), Frings et al. (2014c), Opfergelt et al. (2010), Cornelis et al. (2010), Liu et al. (1998, 2005, 2007, 2015), Wang et al. (2015), Abraham et al. (2011), Savage et al. (2013a), Ziegler et al. (2005b), Chemtob et al. (2015), Tatzel et al. (2015), van den Boorn et al. (2007, 2010), Pan et al. (2001), Steinhoefel et al. (2009, 2010), Chakrabarti et al. (2012), Peng et al. (2000), Fan et al. (2004), Gao et al. (2017), Song and Ding (1990), Ding et al. (1996, 2017), Robert and Chaussidon (2006), André et al. (2006), Marin-Carbonne et al. (2012, 2014), Stefurak et al. (2015), Zhao et al. (2014), Hu et al. (2013), Jiang et al. (1993), Heck et al. (2011), Hou et al. (2014), Li et al. (2014a).

Silicon isotope compositions of siltstone

The δ^{30}Si values of siltstone vary in a range from –0.6‰ to 0.7‰, slightly wider than that of sandstone. The average δ^{30}Si value of siltstone is –0.1‰. These characters indicate that the material in siltstone is still the physical weathering products of granites, but more chemical weathering products (clays) are involved.

Silicon isotope compositions of shale

The δ^{30}Si values of shale vary in a range from –0.8‰ to 1.3‰, much wider than those of sandstone and siltstone. The average δ^{30}Si value of shale is –0.2‰. These characters imply that the material in shale is dominated by the physical weathering products of granites, but a significant fraction of chemical weathering products (clays) are involved.

4.2.2.3 Silicon isotope compositions of clays

Silicon isotopic analysis has been made of clays from China, USA and Italy (Ding et al., 1988a; Xu and Huang, 1996; Ziegler et al., 2005a,b). The results of the analyses are shown in Figure 4.24.

EBSCOhost - printed on 2/10/2023 8:05 PM via . All use subject to https://www.ebsco.com/terms-of-use

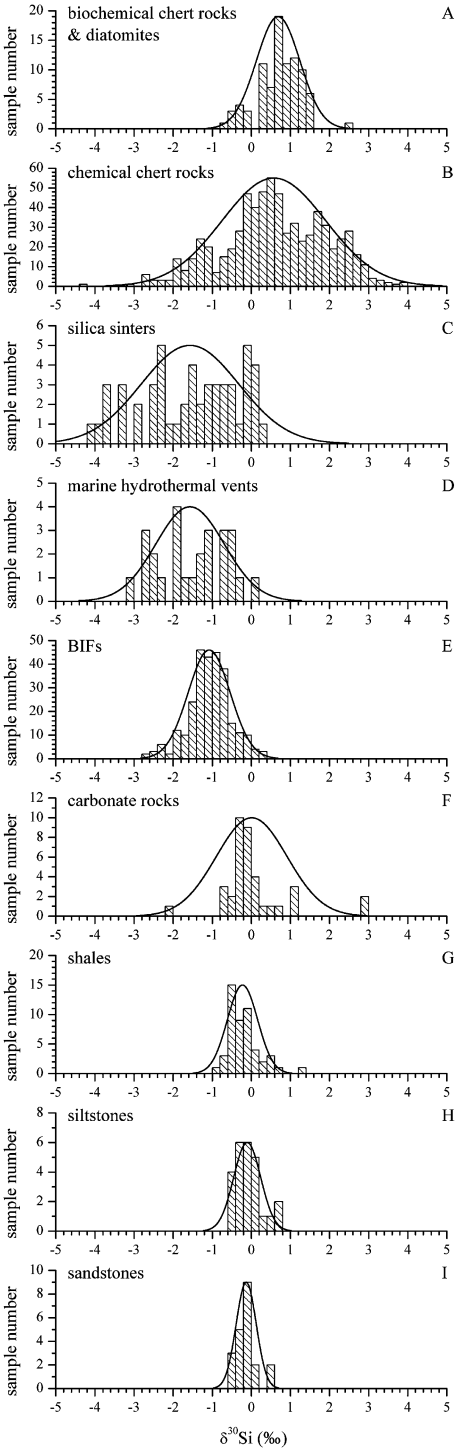

Figure 4.22: The histograms of δ^{30}Si values of various sedimentary rocks. A: Biochemical chert; B: Chemical chert; C: Silica sinter; D: Marine hydrothermal vent; E: BIF; F: Carbonate rocks; G: Shale; H: Siltstones; I: Sandstone. See references in Figure 4.21.

EBSCOhost - printed on 2/10/2023 8:05 PM via . All use subject to https://www.ebsco.com/terms-of-use

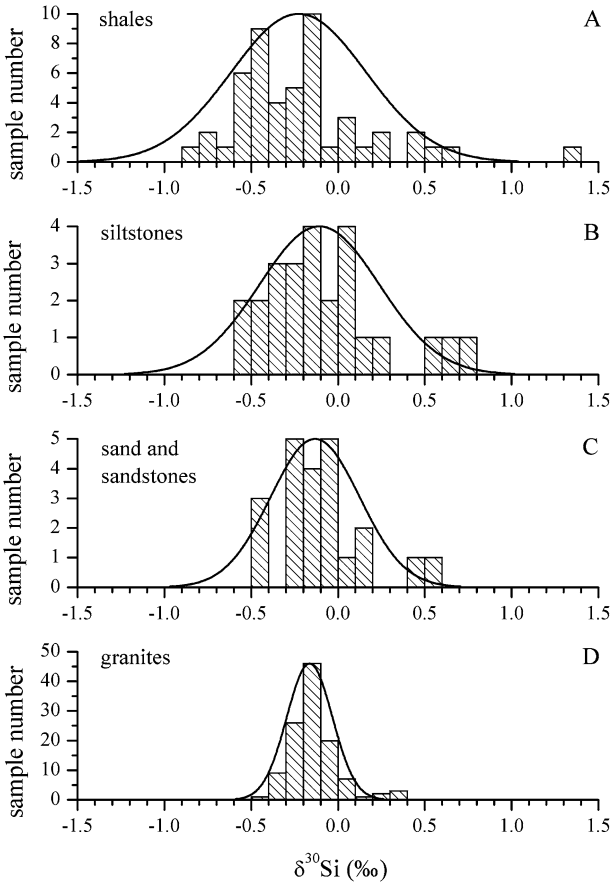

Figure 4.23: Comparison of δ^{30}Si values of clastic rocks (sandstone, siltstone and shale) with those granites. A: Shale; B: Siltstone; C: Sandstone and D: Granites. Data taken from Zhou et al. (2007), Frings et al. (2014c), Opfergelt et al. (2010), Cornelis et al. (2010), Liu et al. (1998, 2005, 2007, 2015), Wang et al. (2015), Abraham et al. (2011), Savage et al. (2012, 2013b), Ziegler et al. (2005b), Pogge von Strandmann et al. (2014), Poitrasson and Zambardi (2015).

The δ^{30}Si values of the clays range from –2.5‰ to 0.8‰, with two peaks at –2.1‰ and 0.1‰, respectively (Figure 4.24). The δ^{30}Si values of the kaolinite, montmorillonite and chlorite are illustrated in Figure 4.25, respectively. The δ^{30}Si values of the kaolinite range from –2.5‰ to 0.1‰, with two peaks at –2.1‰ and 0.1‰, respectively (Figure 4.25A). The kaolinite of different origins shows distinct silicon isotope compositions. The kaolinites formed by hydrothermal alteration have δ^{30}Si values varying from –0.2‰ to 0.1‰, with a peak of –0.2‰, which is approximately the same as that of granite (Ding et al., 1996). It indicates that during the formation of these kaolinites there was no apparent Si isotopic fractionation. The kaolinite formed through low temperature weathering have δ^{30}Si values varying from –1.0‰ to –2.5‰, with a peak

EBSCOhost - printed on 2/10/2023 8:05 PM via . All use subject to https://www.ebsco.com/terms-of-use

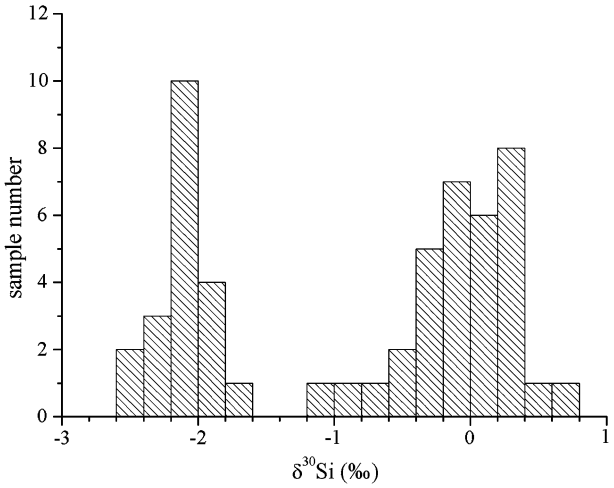

Figure 4.24: δ^{30}Si distribution of clays. Data taken from Ding et al. (1988a), Xu and Huang (1996), Liu et al. (1998) and Ziegler et al. (2005a).

at −2.1‰, showing that these kaolinites had apparently been subject to Si isotopic fractionation during weathering of its source rocks (granite and basalts). The kaolinites formed through sedimentation have δ^{30}Si values varying from −1.2‰ to −0.1‰, which are between those of hydrothermal kaolinites and weathering kaolinites. These intermediate silicon isotopic compositions may reflect a mixture of kaolinites with different origins (Ding et al., 1996).

There are only four data for silicon isotope compositions of chlorite (Figure 4.25B). These chlorites are all hydrothermal origin and their δ^{30}Si values range from −0.6‰ to 0.6‰.

The montmorillonite from the volcanic region of the Zhejiang Province, China, show δ^{30}Si values ranging from −0.3‰ to 0.5‰ (Figure 4.25C). They have a hydrothermal alteration origin (Xu and Huang, 1996).

4.2.2.4 Silicon isotope compositions of chemical precipitate rocks

Siliceous chemical precipitates include chert rocks, BIF (banded iron formation), siliceous sinters and sub-marine hydrothermal siliceous sediments. Although the volumes of these rocks are not large, they have great significance in various aspects of geology and mineral exploration, and so, they have drawn a lot of attention from geologists. The results of analyses of these rocks are shown in Figure 4.22 (A, B, C, D).

Silicon isotope compositions of chert rocks

Chert is a sedimentary rock composed mainly of microcrystalline quartz. It occurs in sedimentary strata from the early Archean to the present. Its chemical and isotopic

EBSCOhost - printed on 2/10/2023 8:05 PM via . All use subject to https://www.ebsco.com/terms-of-use

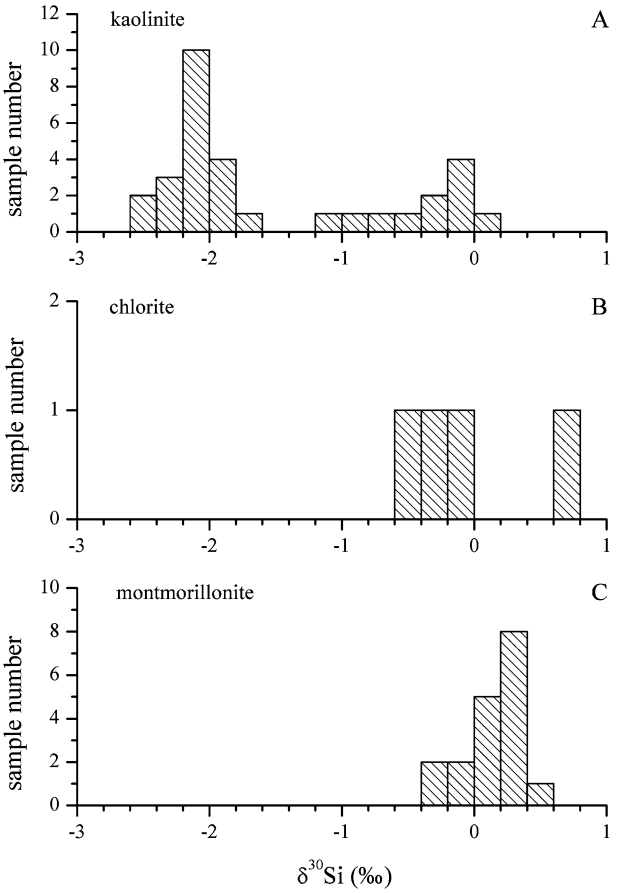

Figure 4.25: δ^{30}Si distributions of different clay minerals. Data are from Ding et al. (1988a), Xu and Huang (1996) and Ziegler et al. (2005a,b). A: kaolinite; B: chlorite; C: montmorillonite.

characteristics have been widely investigated to study the conditions of its formation. Recently, Si isotopes in chert have been used as an important tracer of environmental conditions in the global ocean (Song and Ding, 1990; Ding et al., 1996, 2017; Robert and Chaussidon, 2006; André et al., 2006; van den Boorn et al., 2007, 2010; Abraham et al., 2011; Marin-Carbonne et al., 2012, 2014; Chakrabarti et al., 2012; Geilert et al., 2014b; Stefurak et al., 2015; Tatzel et al., 2015).

The δ^{30}Si values of chert rocks vary in a wide range from –4.3‰ to 3.9‰ (Figure 4.22A and Figure 4.26), reflecting significant variation of silicon contribution of various source reservoirs and in precipitation processes. In general, the δ^{30}Si values of chert rocks have an average of ~0.6‰, which is significantly higher than those of magmatic and clastic sedimentary rocks, reflecting that their major Si source of oceanic water is enriched in ^{30}Si in most cases.

EBSCOhost - printed on 2/10/2023 8:05 PM via . All use subject to https://www.ebsco.com/terms-of-use

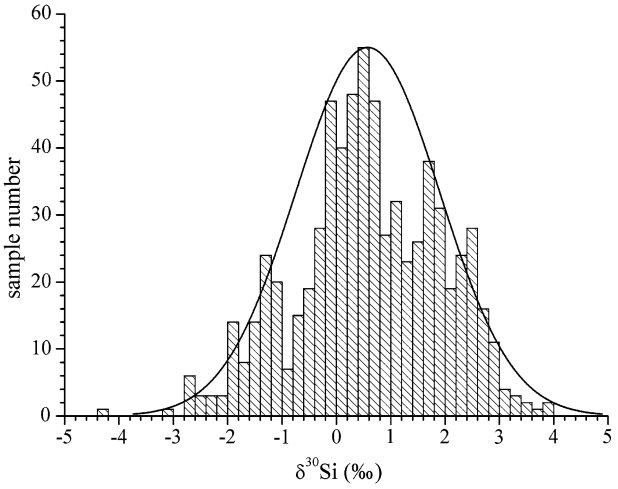

Figure 4.26: δ^{30}Si distributions of chert rocks. Data are from Song and Ding (1990), Ding et al. (1996, 2017), Robert and Chaussidon (2006), André et al. (2006), van den Boorn et al. (2007, 2010), Abraham et al. (2011), Marin-Carbonne et al. (2012, 2014), Chakrabarti et al. (2012), Geilert et al. (2014b), Stefurak et al. (2015), Tatzel et al. (2015), Zhang et al. (2014), Hu et al. (2013), Chemtob et al. (2015), Pan et al. (2001), Steinhoefel et al. (2009), Peng et al. (2000), Liu et al. (2007), Fan et al. (2004), Gao et al. (2017).

Song and Ding (1990) suggested distinguishing sedimentary facies of chert with silicon isotope compositions. Ding et al. (1996) indicated that different genetic types of cherts have different silicon isotope characters. They discussed variations in silicon content and silicon isotope composition in marine water according to the data from chert formed in shallow marine environments. According to the silicon isotope variation of chert, Robert and Chaussidon (2006) developed a temperature-evolution curve for the Precambrian ocean. It has been suggested that Precambrian cherts have much higher δ^{30}Si values than Phanerozoic cherts and that the former show a generally increasing trend from 3.5 to 0.85 Ga, thus reflecting a decrease in seawater temperature. However, these statements have been challenged because cherts can have various origins and their isotopic compositions might have been reset by metamorphic fluid circulation. Thus, different types of cherts need to be considered separately because their isotope composition might record various distinct processes. In addition, the factors that affect silicon isotope composition of chert have been investigated in detail. It was found that peritidal cherts are enriched in ^{30}Si, but that basinal cherts, which are associated with banded iron formations (BIF), are depleted in ^{30}Si; this difference is attributed to Si having been derived from hydrothermal sources in the BIFs. Detailed description on historic variation of silicon isotope compositions of chert and its implication on oceanic environmental conditions will be provided in the next chapter.

EBSCOhost - printed on 2/10/2023 8:05 PM via . All use subject to https://www.ebsco.com/terms-of-use

Silicon isotope compositions of silica in BIF

The banded iron formation (BIF) is a major type of iron deposits, which was formed in the Precambrian era, especially in late Archean and early Proterozoic. It is an important source of iron in the world, and is of great significance in the study on the early history of tectonic evolution in the Earth and environmental variation in the ocean. There are various hypotheses for the origin of BIF. Some geologists consider them to be the products of normal sedimentation, others regard them as products of volcanic exhalation, and biogenic activity may be a key factor in their formation.

Now there are three main types of BIF that are recognized according to their geotectonic settings:

1) Algoma-type banded iron formations that stratigraphically linked, or interlayered with, submarine-emplaced volcanic rocks in convergent margin settings of Archean and Paleo-Proterozoic granite–greenstone belts (Gross, 1980). The important examples of these types of deposits include the Archean Yilgarn- and Pilbara-type deposits.
2) Lake Superior-type banded iron formations (Gross, 1980) that developed in passive-margin Proterozoic sedimentary rock successions. These deposits contain some of the largest known BIF-hosted iron accumulations, such as the Hamersley in Australia and the Transvaal in South Africa.
3) Rapitan–Urucum-type BIFs that constrained to Neoproterozoic strata (715 to 580 Ma) in sedimentary successions that are interpreted to be mostly glaciogenic events (Hoffman et al., 1998). Representative deposits include Urucum in Brazil and Rapitan in Canada.

Jiang et al. (1993) made the first detailed silicon isotope study on silica from the BIF, by using the Gongchangling iron mine in Liaoning Province, China, as an example, to interpret the genesis of the BIF deposits. Ding et al. (1996) combined these data with some δ^{30}Si data for BIF samples collected from the Hebei province, China, and from the BIF mines near Lake Superior, USA, to trace the oceanic environmental variation in the Precambrian period. In recent decades, more investigations on silicon isotope compositions of BIF have been carried out, which are generally focused on tracing the temporal environmental variation of the global ocean in the Precambrian era (Robert and Chaussidon, 2006; André et al., 2006; van den Boorn et al., 2007, 2010; Abraham et al., 2011; Marin-Carbonne et al., 2012, 2014; Chakrabarti et al., 2012; Steinhoefel et al., 2009, 2010; Geilert et al., 2014b; Stefurak et al., 2015; Tatzel et al., 2015; Heck et al., 2011), although there are still some studies that mainly consider the genesis of the ore deposits (Hou et al., 2014; Li et al., 2014a).

The available δ^{30}Si values of silica from BIF are shown in Figure 4.27. It can be seen that the δ^{30}Si values of silica from BIF vary in a range from –2.8‰ to 0.3‰, with an average value of –1.1‰ and a peak value at –1.1‰, which are significantly lower than that of marine basalts.

EBSCOhost - printed on 2/10/2023 8:05 PM via . All use subject to https://www.ebsco.com/terms-of-use

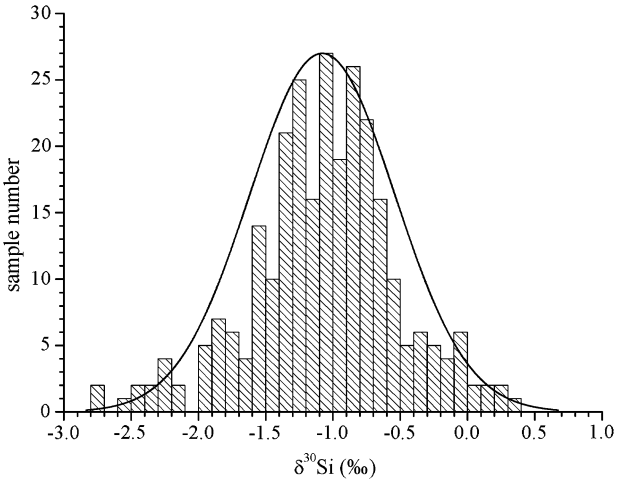

Figure 4.27: δ^{30}Si distributions of BIFs. Data are from Jiang et al. (1993), Ding et al. (1996), Robert and Chaussidon (2006), André et al. (2006), van den Boorn et al. (2007, 2010), Abraham et al. (2011), Marin-Carbonne et al. (2012, 2014), Chakrabarti et al. (2012), Steinhoefel et al. (2009, 2010), Geilert et al. (2014b), Stefurak et al. (2015), Tatzel et al. (2015), Heck et al. (2011), Hou et al. (2014), Li et al. (2014a).

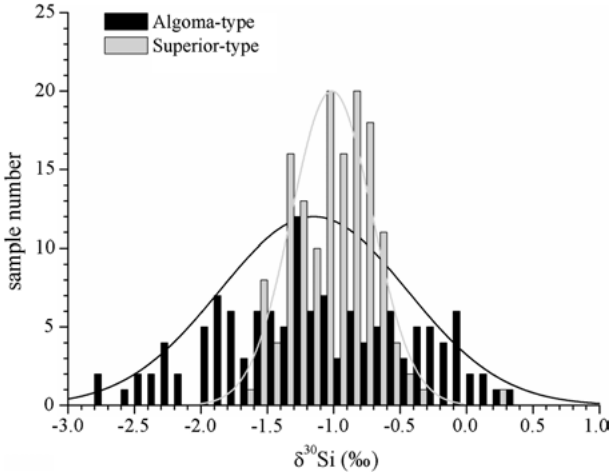

Figure 4.28: A comparison of δ^{30}Si distributions of the Algoma-type and Superior-type BIFs. Data are from Jiang et al. (1993), Ding et al. (1996), Robert and Chaussidon (2006), André et al. (2006), van den Boorn et al. (2007, 2010), Abraham et al. (2011), Marin-Carbonne et al. (2012, 2014), Chakrabarti et al. (2012), Steinhoefel et al. (2009, 2010), Geilert et al. (2014b), Stefurak et al. (2015), Tatzel et al. (2015), Heck et al. (2011), Hou et al. (2014), Li et al. (2014a).

A comparison of δ^{30}Si distributions of Algoma-type and Superior-type BIFs is illustrated in Figure 4.28. The δ^{30}Si values of the Algoma-type BIFs vary in a range from

EBSCOhost - printed on 2/10/2023 8:05 PM via . All use subject to https://www.ebsco.com/terms-of-use

–2.8‰ to 0.3‰, with an average of –1.2‰ and a peak at –1.2‰. The δ^{30}Si values of superior-type BIFs vary in a range from –1.7‰ to 0.2‰, with an average of –1.0‰ and a peak at –1.0‰.

On the basis of the silicon isotope data and the background of geology and geochemistry, it was suggested that the formation of BIF was linked to a process of volcanic exhalation, and their silicon was mainly derived from contemporary seawater (Jiang et al., 1993; Ding et al., 1996; Li et al., 2014a). In the late Archean and early Proterozoic periods, the silicon content of marine water remained in its saturated concentration at a given temperature, which is much higher than that in the modern ocean. During periodic volcanic eruptions, the pH value of the seawater would have varied frequently, leading to variations in solubility of silica and resulting in the formation of alternate ferruginous and siliceous bands. In this case, apparent kinetic isotope fractionation may be caused by the slow precipitation of the small fraction of the dissolved silicon from seawater, leading the formation of siliceous bands with negative δ^{30}Si values.

The difference in the Si isotope distributions between Algoma-type BIF and Superior-type BIF may reflect the variation of their forming conditions. The Algoma-type BIF is interlayered with submarine-emplaced volcanic rocks in convergent margin settings, indicating its formation experienced directly the effect of submarine hydrothermal activities. Their forming conditions, such as T, pH and Eh, are very unstable, causing that this type of BIF shows a wider δ^{30}Si range and with slightly lower average δ^{30}Si value than those of the Superior-type BIF. In contrast, the Superior-type BIF is developed in passive-margin Proterozoic sedimentary rock successions, indicating that its formation experienced indirectly and less intensive influence from submarine hydrothermal activities. Thus, the forming conditions of Superior-type BIF are relatively more stable than those for Algoma-type BIF, causing the Superior-type BIF to show a narrow δ^{30}Si range and with slightly higher average δ^{30}Si value than those of the Algoma-type BIF.

Silicon isotope compositions of silica sinter

Silica sinters are siliceous precipitates, composed mainly of opal, that are formed by hot springs at their vent sites. The size of siliceous precipitate is generally small when they are formed in a continental environment. Nevertheless, they are an important substance for the understanding of the geothermal process, particularly because of their close relationship with gold and cesium mineralization.

The available δ^{30}Si values of the silica sinter vary in a wide range from –4.2‰ to 0.2‰, with an average of –2.0‰. It is found that large variations in δ^{30}Si values may occur even within a single geothermal field. For example, the δ^{30}Si values of silica sinters from the Steamboat spring in Nevada vary from 0.1 to –1.2‰, those from Yellowstone National Park in Wyoming, USA, from –0.7‰ to –1.9‰ and those from the Tengchong geothermal field in Yunnan Province, China, range from –0.6‰ to 0.2‰.

EBSCOhost - printed on 2/10/2023 8:05 PM via . All use subject to https://www.ebsco.com/terms-of-use

Generally speaking, the δ^{30}Si values of silica sinters are negative, due to kinetic Si isotope fractionation when silica precipitates from hydrothermal solution. This kind of silicon isotope fractionation is discussed in more detail in Chapter 3.

The silicon isotope systematics of silica sinters is dependent on variations in the isotopic compositions of the source rocks, the precipitation environment and other conditions in the various geothermal fields. An understanding of these features can provide a framework for the study of ancient geothermal systems.

Silicon isotope compositions of submarine hydrothermal vent

The submarine hydrothermal systems on mid-ocean ridges and back-arc basins can provide important evidence for deciphering the modern process of mineralization. Unfortunately, there are few data on silicon isotope compositions of siliceous precipitates formed by these hydrothermal systems. By now, the only data on silicon isotope compositions of submarine hydrothermal systems are still that obtained from siliceous precipitates collected from sea-floor chimneys from the Mariana Trench and Okinawa Trough reported by Ding et al. (1996) and Wu et al. (2000) (Figure 4.22).

The available δ^{30}Si values of submarine hydrothermal systems vary in a wide range from −3.1‰ to 0‰, with an average of −1.5‰. The highest δ^{30}Si value of 0‰ is similar to the upper limit of the value for the Mariana Island-arc basalts, and the lowest δ^{30}Si value of −3.1‰ is slightly higher than that (−4.2‰) of the continental geothermal silica sinter.

In order to clarify the relationship between the silicon isotope compositions of the siliceous precipitates and their formation conditions, the relationship between temperature at sampling sites and δ^{30}Si values is studied (Ding et al., 1996). It is observed in the Mariana Trench that:

a) Black siliceous precipitates from sampling sites with temperature higher than 100°C show the highest δ^{30}Si values (−0.4‰ to −0.6‰), which are close to that of the local basalts;
b) Siliceous precipitates from sampling sites with temperatures lower than 100°C have more variable silicon isotope compositions, with their δ^{30}Si values varying from −0.6‰ to −3.1‰, and show no clear relationship with their color and temperature.

The silicon isotope compositions of the hydrothermal precipitates may reflect the origin of the silicon and their mode of formation. From their mode of occurrence, it is apparent that the silicon was mainly derived from the sea-floor basalts. This hypothesis is supported by the fact that the maximum δ^{30}Si values were obtained from the siliceous precipitates close or in proximity to the basalts. Silicon isotope fractionation will not be significant in the process of silicon dissolution. However, silicon isotope fractionation between precipitating silica and silicon remaining in solution may occur during precipitation (Chapter 3). This is a case of kinetic fractionation, with the

EBSCOhost - printed on 2/10/2023 8:05 PM via . All use subject to https://www.ebsco.com/terms-of-use

extent of fractionation depending on the rate, fraction and temperature of precipitation. Silica that precipitate from the solution rapidly and more or less completely have a silicon isotope composition similar to that of the silicon in solution prior to its precipitation, i.e., similar to that of the source rocks. This is the case for the black precipitates which formed at higher temperatures and show relatively high δ^{30}Si values. Precipitates may be subject to greater degrees of silicon isotope fractionation when precipitation of silica takes place slowly and less completely at lower temperature. The silica precipitates often have lower δ^{30}Si values due to this kinetic fractionation. In case of multistage dissolution and precipitation, there may be a multistage of silicon isotope fractionation, leading to the silica precipitates with large negative δ^{30}Si values. This is seen in the silicon isotope compositions of light-colored silica precipitates that are formed at lower temperature within the chimneys in the Mariana back arc basin.

In addition, several samples of silica precipitate from a hydrothermal chimney for the Okinawa Trough were analyzed for their silicon isotope compositions (Figure 4.22). Their δ^{30}Si values of 0‰ to −2.8‰ also reflect the effects of kinetic isotopic fractionation.

4.2.2.5 Biogenic siliceous precipitates

Almost all organisms contain some quantity of silicon. For some organisms, the silicon appears as opal in its basic structures. The silicon-rich organisms include diatoms, sponges and radiolarian and higher plants, such as tracheophyta (equisetum sp.), rice, wheat, banana, bamboo and tomato. Silicon isotope distributions on all these species will be discussed in the following section. It is known that the biogenic siliceous precipitates are responsible to form some type of chert rocks, such as diatom earth and radiolarian siliceous rocks.

So far, it is known that siliceous organisms are present since late Precambrian and throughout the Phanerozoic and include siliceous sponges (late Proterozoic to present; marine only) (Li et al., 1988), radiolarian (Middle Ordovician to present; marine only), and diatoms (Jurassic to present, most marine) (Platt et al., 1980). However, some researchers have reported the presence in thin sections of Precambrian chert of oval or spherical masses or "shells" of quartz and have inferred that they are recrystallized radiolarian tests (LaBerge, 1973). Cloud (1976), in an exhaustive analysis of geochemical and paleontological data, concludes that siliceous-shelled organisms have been possible since at least 1.3 Ga ago and perhaps as far back as 2 Ga ago. Recently, Ding et al. (2017) reported that a peak range in δ^{30}Si was observed in the cherts of 1.325–1.355 Ga, indicating a drastic reduction in Si content caused by a rapid increase in biological activity in the ocean prior to 1.355 Ga.

The available δ^{30}Si values of diatomite and radiolarian chert rocks are shown in Figure 4.29. A number of radiolarian chert from Cambrian to Jurassic strata was studied for their silicon isotope composition (Figure 4.30). The available data show that

EBSCOhost - printed on 2/10/2023 8:05 PM via . All use subject to https://www.ebsco.com/terms-of-use

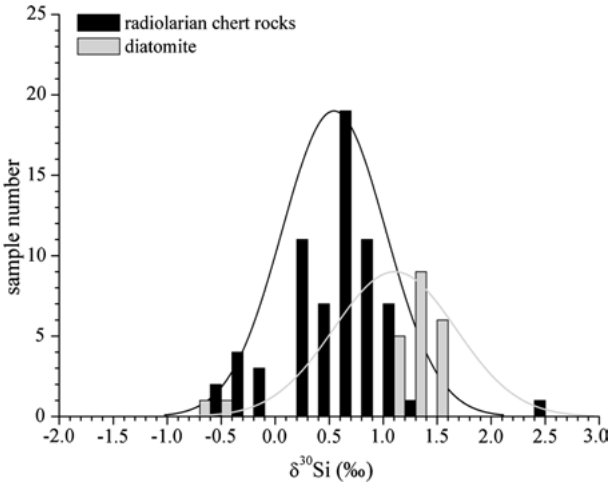

Figure 4.29: δ^{30}Si distributions of biogenic chert rocks. Data are from Song and Ding (1990), Ding et al. (1996, 2017), Cockerton et al. (2013).

radiolarian siliceous rocks have δ^{30}Si values ranging from –0.6‰ to 0.8‰. Song and Ding (1990) showed that the silicon isotope compositions of these rocks are related to their forming conditions. The abyssal radiolarian siliceous rocks often yield relatively low δ^{30}Si values, whereas the shallow-sea and/or bathyal ones give relatively high δ^{30}Si values.

4.2.3 Metamorphic rocks

Metamorphic rocks are a major reservoir of silicon, but as yet, few analyses of silicon isotopes has been made on metamorphic rocks. The metamorphic rocks analyzed include slates, schist, quartzite, hornfels, skarns, granulites, leucogranulites, migmatites, gneisses and plagioclase amphibolites. Below, the silicon isotope data obtained so far for various metamorphic rocks are introduced.

The available silicon isotope data of metamorphic rocks are shown in Figure 4.31. Their δ^{30}Si values vary in a range from –2.2‰ to 0.8‰, with an average of –0.2‰, which is similar to that (–0.3‰) of magmatic and that (–0.2‰) of sedimentary rocks. The Si isotope variation ranges of various metamorphic rocks are illustrated in Figure 4.32.

4.2.3.1 The silicon isotope compositions of slate and schist

The results of silicon isotopic compositions of slate and schist are shown in Figure 4.32.

19 samples of slates were analyzed for their silicon isotope compositions. Their δ^{30}Si values vary in a range from –0.6‰ to 0.2‰, with an average of –0.3‰. All these

EBSCOhost - printed on 2/10/2023 8:05 PM via . All use subject to https://www.ebsco.com/terms-of-use

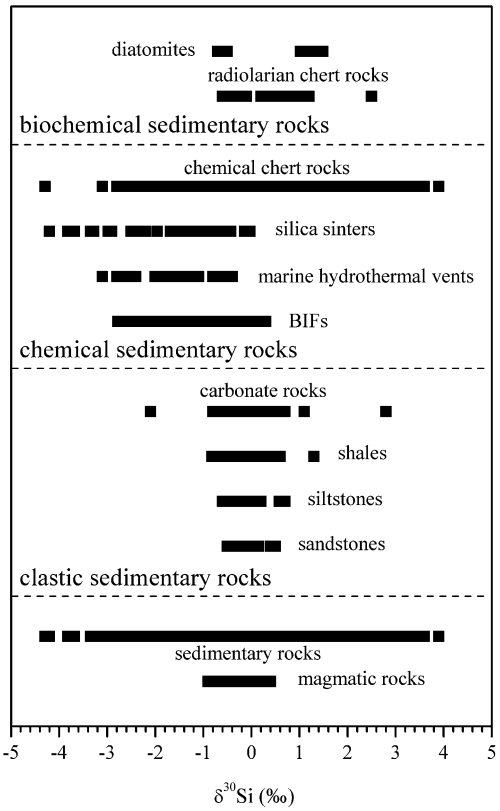

Figure 4.30: The δ^{30}Si ranges of all kinds of sedimentary rocks (references are listed in Figure 4.21). For comparison, the δ^{30}Si range of magmatic rocks is also shown (references are listed in Figure 4.14).

data fall in the area of the silicon isotopic compositions of clay stones. Four samples of phylite show δ^{30}Si values range from –0.4‰ to 0.0‰, with an average of –0.2‰. 22 samples of schist show δ^{30}Si values range from –2.2‰ to 0.8‰, with an average of –0.3‰.

The above data show that the silicon isotopic compositions of rocks can still be preserved during metamorphism to form slate and schist. Hence, their protoliths can be identified though the study of their silicon isotopic compositions.

4.2.3.2 The silicon isotope compositions of amphibolite

Twelve samples of amphibolite show δ^{30}Si values range from –0.6‰ to 0.4‰, with an average of –0.2‰. All these data fall in the area of the intermediate-basic volcanic rocks, indicating that the isotopic compositions were not subject to significant modification during metamorphism of the original rocks.

EBSCOhost - printed on 2/10/2023 8:05 PM via . All use subject to https://www.ebsco.com/terms-of-use

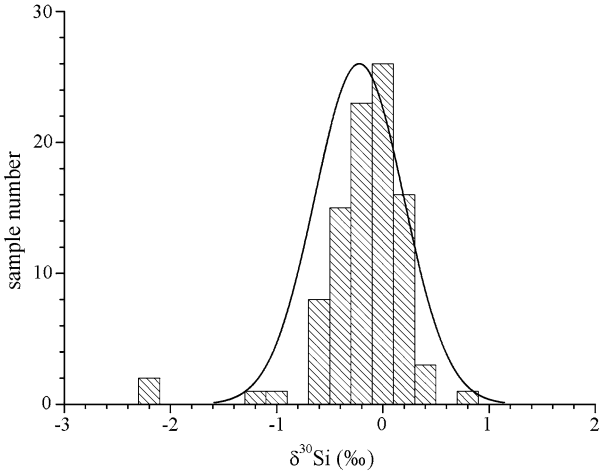

Figure 4.31: The general Si isotope distribution of metamorphic rocks. Data are from Ding et al. (1996), Abraham et al. (2011), André et al. (2006), Liu et al. (1998, 2005, 2015), Savage et al. (2013b).

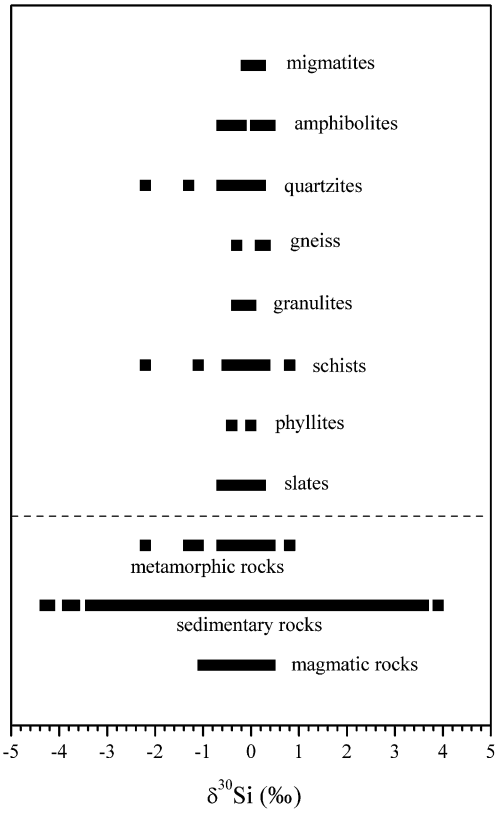

Figure 4.32: The Si isotope variation ranges of various metamorphic rocks. Data are from Ding et al. (1996), Abraham et al. (2011), André et al. (2006), Liu et al. (1998, 2005, 2015) and Savage et al. (2013b). For comparison, the ranges of magmatic and sedimentary rocks are also shown.

EBSCOhost - printed on 2/10/2023 8:05 PM via . All use subject to https://www.ebsco.com/terms-of-use

4.2.3.3 The silicon isotope compositions of granulite, migmatite and gneiss

Four samples of granulite show δ^{30}Si values range from −0.3‰ to 0.0‰, with an average of −0.2‰, which is similar to that of intermediate-acidic igneous rocks.

Three samples of migmatite show δ^{30}Si values range from −0.1‰ to 0.2‰, with an average of 0.0‰, which are similar to that of granitoid. Three samples of gneiss show δ^{30}Si values range from −0.3‰ to 0.3‰, with an average of 0.1‰, which is similar to that of granite. These data show that the δ^{30}Si values remain unchanged during the metamorphism of forming the granulite, gneiss and migmatite.

4.2.3.4 The silicon isotope compositions of quartzite

Twenty-four samples of quartzite show δ^{30}Si values range from −2.2‰ to 0.2‰, with an average of −0.2‰. Within these samples, two samples of magnetite quartzite show δ^{30}Si values of −2.2‰ to −1.3‰, reflecting their protoliths of BIF origin. In contrast, other 22 samples show δ^{30}Si values range from −0.6‰ to 0.2‰, indicating their protoliths of sandstone origin.

4.2.3.5 The silicon isotope compositions of hornfels

Three samples of hornfels show δ^{30}Si value from −0.4‰ to 0.1‰, with an average of −0.2‰, similar to those of their protoliths.

4.2.3.6 Silicon isotope fractionation of coexisting minerals in metamorphic rocks

Great attention has been given to silicon isotope fractionation between coexisting minerals in the study of silicon isotope compositions of metamorphic rocks.

1) Mica and quartz from quartz–sericite schist
   Silicon isotope compositions have been determined in ten pairs of coexisting quartz and mica, from quartz–sericite schists from the Hemlo gold mine, Ontario, Canada. It was found that five quartz minerals of the ten pairs of samples exhibit higher δ^{30}Si values than those of mica; and there are also three pairs of minerals where the mica exhibits higher δ^{30}Si values than the quartz. These data show that the silicon isotopic equilibrium does not always exist between mica and quartz in the quartz–sericite schists.
2) Garnet and biotite from garnet-biotite schist
   Garnet and biotite from garnet-biotite schist from the Qingchengzi mining area, Liaoning Province, were analyzed for their silicon isotope compositions. It is found that the δ^{30}Si values of the biotite are about 0.6‰ higher than those of the garnet.

EBSCOhost - printed on 2/10/2023 8:05 PM via . All use subject to https://www.ebsco.com/terms-of-use

4.2.4 Vein quartz and silicified rocks

4.2.4.1 Silicon isotope compositions of vein quartz

The total mass of vein quartz is not large in the lithosphere, but they are widespread in natural environment and are closely related to mineralization. Hence, a great deal of attention has been drawn to the study of silicon isotopic compositions of vein quartz. Reynolds and Verhoogen (1953), Allenby (1954) and Douthitt (1982) have all reported results of their studies on the isotopic composition of silicon from various vein quartz occurrences. A large number of quartz have been determined by Ding et al. (1996).

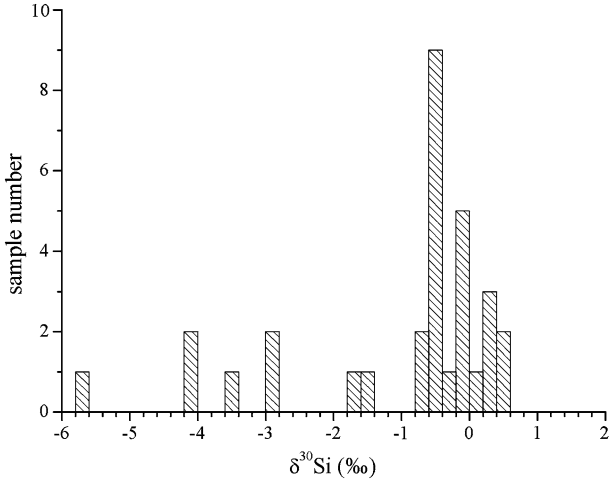

Figure 4.33: The Si isotope compositions of vein quartz. Data are from Ding et al. (1996), Basile-Doelsch et al. (2005) and Liu et al. (1998).

The available δ^{30}Si values of vein quartz are shown in Figure 4.33. It is found that the silicon isotope compositions of the vein quartz vary in a range from –5.7‰ to 0.5‰, with an average of –1.1‰. Most of the δ^{30}Si values obtained are in range from –0.9‰ to 0.5‰, indicating that silicon in the vein quartz has multiple sources, and may be subject to the influence of silicon isotope fractionation during its precipitation.

The δ^{30}Si values of most analyzed vein quartz show a normal distribution pattern, with a peak at –0.2‰, similar to the mean of δ^{30}Si values of crustal rocks. This is compatible with the observation that the majority of the vein quartz occurrences are related to granite, sandstone and felsic metamorphic rocks.

4.2.4.2 Silicon isotope compositions of silicified rocks

The silicon isotope compositions of some silicified rocks related to fissure structures have been analyzed, and the results are illustrated in Figure 4.34. The silicified rocks

EBSCOhost - printed on 2/10/2023 8:05 PM via . All use subject to https://www.ebsco.com/terms-of-use

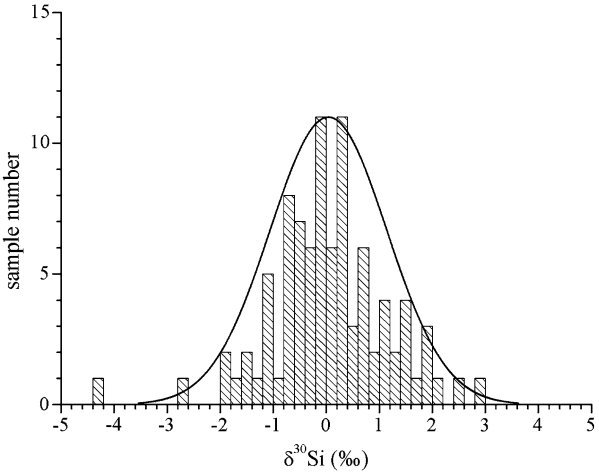

Figure 4.34: The Si isotope compositions of silicified rocks. Data are from Ding et al. (1996), Chakrabarti et al. (2012).

analyzed have δ^{30}Si values in range from −4.4‰ to 3.0‰, with an average of 0.0‰. Again, the silicon isotopic compositions imply multiple sources of silicon.

4.3 Silicon isotope compositions of soils

Soil has been considered as an individual ecosystem in the Earth and is an important component of the so called "critical zone" of the Earth. Soil continually undergoes development by way of numerous physical, chemical and biological processes, which include weathering with associated erosion. Soil is a mixture of minerals, organic matter, gases, liquids and countless organisms that together support life on Earth.

Soil profile development is dependent on the processes that form soils from their parent materials, the type of parent material and the factors that control soil formation. Parent materials are classified according to how they came to be deposited: 1) Residual materials are mineral materials that have weathered in place from primary bedrock; 2) Transported materials are those that have been deposited by water, wind, ice or gravity; 3) Cumulose material is organic matter that has grown and accumulates in place.

All factors that affect the growth and development of soils would have influence on the silicon isotope compositions. Thus, silicon isotope study of soils may provide some information for tracing these processes and factors. The silicon isotope investigation on soils may provide us some basic knowledge on mechanisms in plant growth. By now, no special and systematic investigation on silicon isotope distributions of soils has been conducted. The available silicon isotope data of soils were mostly byproducts in the studies of plant growth, river systems and the Loess Plateau.

EBSCOhost - printed on 2/10/2023 8:05 PM via . All use subject to https://www.ebsco.com/terms-of-use

The available δ^{30}Si values of soils vary in a range from –2.7‰ to 0.3‰, with an average of –0.5‰ and a peak value at –0.1‰ (Figure 4.35).

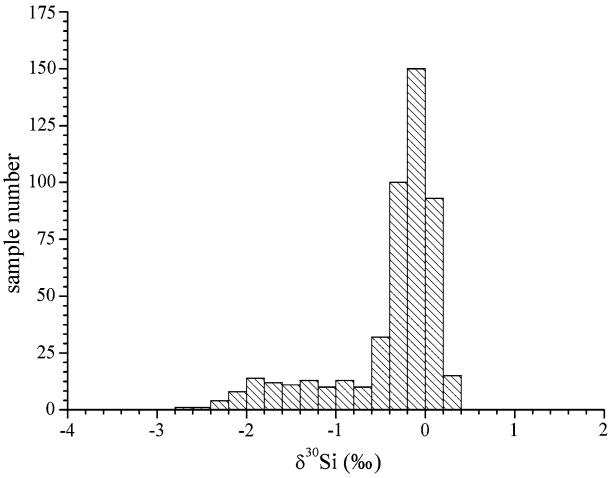

Figure 4.35: The silicon isotope distribution of bulk soils. Data are taken from Pogge von Strandmann et al. (2012), Cornelis et al. (2010), Opfergelt et al. (2010, 2011b), Pokrovsky et al. (2013), Savage et al. (2013a), Bern et al. (2010), Frings et al. (2014a), Ziegler et al. (2005a,b), Ding et al. (2005a, 2008a, 2014, 2016).

The δ^{30}Si values of different types of soils are shown in Figure 4.36. The δ^{30}Si values of sand vary in a range from –0.3‰ to 0.2‰, with an average of –0.1‰. The δ^{30}Si values of loess vary in a range from –0.3‰ to –0.2‰, with an average of –0.2‰. The δ^{30}Si values of suspended particulate matter (SPM) vary in a range from –1.1‰ to 0.3‰, with an average of –0.2‰. All of these three types of soils dominated by transported materials show generally same silicon isotope distribution similar to that of clastic sedimentary rocks. The δ^{30}Si values of residual soils vary in a range from –2.7‰ to 0.1‰, with an average of –1.4‰, reflecting the effect of significant amount of clay minerals in them.

4.4 Hydrosphere

Silicon is an important element in the Earth's hydrosphere. It occurs in various water reservoirs, such as seawater, river water, ground water, pore water and hot spring water, in the form of silicic acid (H_4SiO_4). These water reservoirs play important roles in a global Si cycle, ore formation and biological production. The silicon isotope compositions of various reservoirs in hydrosphere have been investigated intensively. The available results are summarized in Figure 4.37.

EBSCOhost - printed on 2/10/2023 8:05 PM via . All use subject to https://www.ebsco.com/terms-of-use

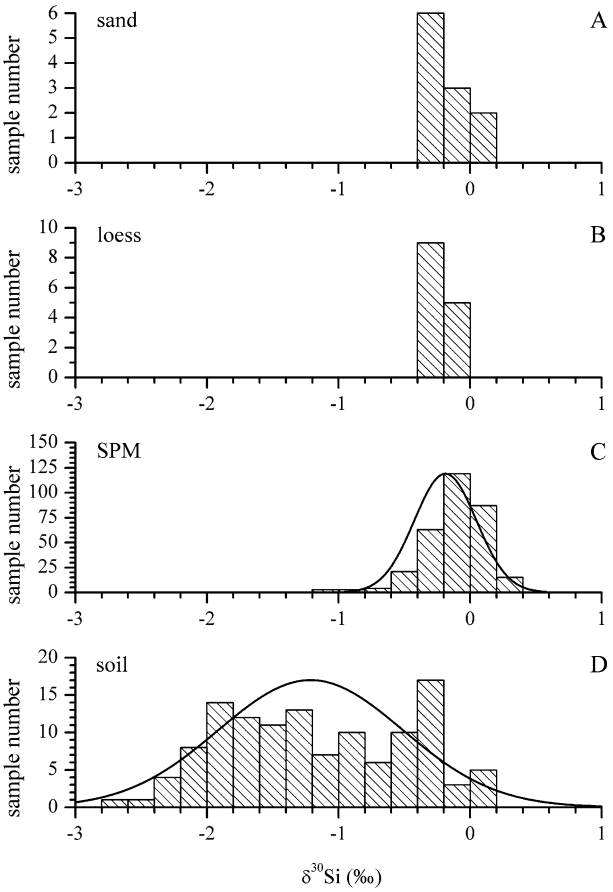

Figure 4.36: The δ^{30}Si values of different types of soils. Data are from Pogge von Strandmann et al. (2012), Cornelis et al. (2010), Opfergelt et al. (2010, 2011b), Pokrovsky et al. (2013), Savage et al. (2013a), Bern et al. (2010), Frings et al. (2014c), Ziegler et al. (2005a,b), Ding et al. (2005a, 2008a, 2014, 2016).

4.4.1 The silicon isotope composition of the seawater

The ocean is the most important silicon reservoir in the Earth's hydrosphere. It acts as a major sink of silicon supplied from continent by river and ground water input, Aeolian dust deposition and by seafloor weathering and hydrothermal process. The average dissolved silicon (DSi) concentration of the modern ocean is ~70 μM (Figure 4.38), which is lower by almost two orders of magnitude than its solubility in seawater. This severe unsaturation is mainly resulted from intensive biogeochemical absorption (see Chapter 5 for details). The silicon in seawater provides an important silicon source for specific marine organisms such as diatom, radiolarian and sponge. Among them, diatoms make 40% of oceanic primary productivity. The silicon isotope composition

EBSCOhost - printed on 2/10/2023 8:05 PM via . All use subject to https://www.ebsco.com/terms-of-use

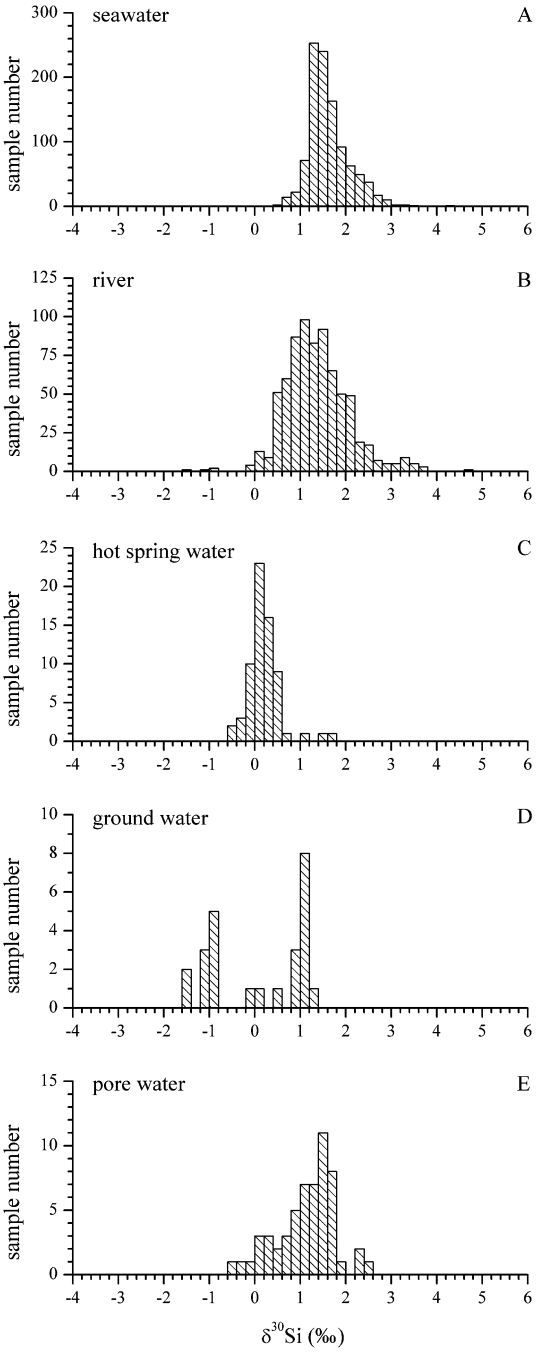

Figure 4.37: The δ^{30}Si values of different types of water. Data are from Geilert et al. (2015), Pogge von Strandmann et al. (2012, 2014), Ehlert et al. (2012, 2016a), White et al. (2012), Frings et al. (2014b, 2015), Ding et al. (2004, 2008b, 2011, 2014, 2016), Georg et al. (2006b, 2007b, 2009a,b), Opfergelt et al. (2009, 2011a, 2013), Engström et al. (2010), Hughes et al. (2012, 2013), Pokrovsky et al. (2013), Delvaux et al. (2013), Ziegler et al. (2005a,b), Fontorbe et al. (2013), Cockerton et al. (2013), De La Rocha et al. (2000, 2011), Cardinal et al. (2005), Reynolds et al. (2006b), Beucher et al. (2008, 2011), Fripiat et al. (2011a,b), de Souza et al. (2012a,b), Cao et al. (2012), Grasse et al. (2013), Singh et al. (2015).

EBSCOhost - printed on 2/10/2023 8:05 PM via . All use subject to https://www.ebsco.com/terms-of-use

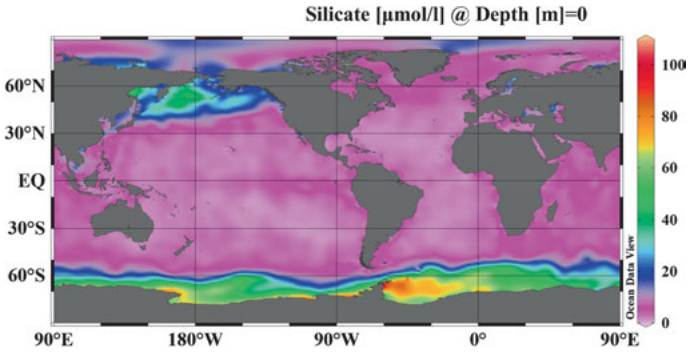

Figure 4.38: The DSi distribution of surface water in Global Ocean. Data are from Garcia et al. (2009).

of seawater was firstly reported by De La Rocha et al. (2000). Since then, the silicon isotope composition of oceanic water has been studied extensively (De La Rocha et al., 2000; Cardinal et al., 2005; Reynolds et al., 2006b; Beucher et al., 2008, 2011; De La Rocha et al., 2011; Fripiat et al., 2011a,b; de Souza et al., 2012a,b; Ehlert et al., 2012; Cao et al., 2012; Grasse et al., 2013; Singh et al., 2015).

The δ^{30}Si values of seawater vary in a range from 0.5‰ to 4.4‰, with an average of 1.6‰ (Figure 4.37A). The overall δ^{30}Si is higher than other reservoirs because: first, the major source of the oceanic silicon is river input, which has an average δ^{30}Si of 1.4‰; second, the silicon isotopic fractionation between diatoms and seawater causes further increase in the δ^{30}Si of seawater. Besides, the large δ^{30}Si variation range is another feature of seawater, which is caused by the variation of diatom productivity and dissolution of exported biogenic silica.

The vertical distribution of δ^{30}Si shows an obvious trend anti-correlated to water depth from the surface to the ocean's abyss (Figure 4.39). In the surface mixed layer, e.g., the upper 50 m in the water column, the silicon isotopic composition is relatively homogeneous with elevated δ^{30}Si values averaged at 2.1‰, due to mixing and biological uptake of lighter silicon isotopes. Within the euphotic zone (typically ~200 m in open ocean) where photosynthesis of phytoplankton takes place, an anti-correlation between δ^{30}Si and DSi concentration can be observed through the Pacific, the Atlantic and the Southern Ocean (De La Rocha et al., 2000; Reynolds et al., 2006b; de Souza et al., 2012a; Grasse et al., 2013). This may also explain the apparent anti-correlation between the δ^{30}Si and depth. In the deep ocean (>1000 m), where there is no strong vertical mixing; however, the δ^{30}Si is also homogeneous but with much lower δ^{30}Si values averaged at 1.2‰. This is because the Si in the deep ocean comes mainly from recycled biogenic silica (de Souza et al., 2014). Recent studies also show that the δ^{30}Si distribution in deep ocean is also influenced by relative contribution from different water masses (de Souza et al., 2014 and the reference therein).

In summary, the silicon isotope composition of seawater is closely related to the marine silicon cycle. See Chapter 5 for details.

EBSCOhost - printed on 2/10/2023 8:05 PM via . All use subject to https://www.ebsco.com/terms-of-use

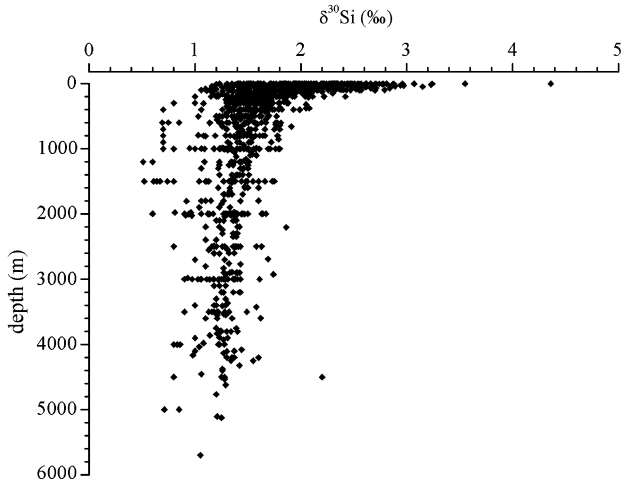

Figure 4.39: Vertical δ^{30}Si distribution of global seawater (De La Rocha et al., 2000; Cardinal et al., 2005; Reynolds et al., 2006b; Beucher et al., 2008, 2011; De La Rocha et al., 2011; Fripiat et al., 2011a,b; de Souza et al., 2012a,b; Ehlert et al., 2012; Cao et al., 2012; Grasse et al., 2013; Singh et al., 2015).

4.4.2 The silicon isotope composition of the river water

Rivers are the link between continents and the oceans. It carries large amount of substances, in the form of dissolved matter and suspended particulate matters (SPM) from continents to the ocean. As a major provider of dissolved silicon to the ocean (Tréguer et al., 1995), rivers play a significant role in the Si cycle of the hydrosphere, which is an important part of the surface environments of the Earth. To understand the global silicon cycle, it is therefore necessary to characterize silicon isotope variations and the average $\delta^{30}Si_{DSi}$ values of important terrestrial river systems.

A primary result on δ^{30}Si values of a few riverine samples was reported firstly by De La Rocha et al. (2000). A systematic investigation on silicon isotope compositions of the Yangtze River was done by Ding et al. (2004). Since then, a number of river systems in the world, such as the Yellow River (Ding et al., 2011, 2016), the Kalix River (Engström et al., 2010), Icelandic rivers (Georg et al., 2007b), Swiss rivers (Georg et al., 2006b), the rivers in the Congo Basin (Cardinal et al., 2010), the Nile River (Cockerton et al., 2013); Central Siberian rivers (Pokrovsky et al., 2013); and the Amazon River (Hughes et al., 2013) have been studied for their silicon isotope distributions.

The available silicon isotope data are shown in Figure 4.37B. The total δ^{30}Si values of river water vary in a range from –1.4‰ to 4.7‰, with an average of 1.4‰. The DSi and $\delta^{30}Si_{DSi}$ values of several important river systems in the world are listed in Table 4.1 and plotted in Figure 4.40.

EBSCOhost - printed on 2/10/2023 8:05 PM via . All use subject to https://www.ebsco.com/terms-of-use

Table 4.1: DSi and $\delta^{30}Si_{DSi}$ values of several river systems in the world

River	DSi (μM)			$\delta^{30}Si_{DSi}$ (‰)			Reference
	Max	Min	Average	Max	Min	Average	
Yangtze River	251	34	98.7	3.7	0.5	1.63	Ding et al. (2004, 2014)
Yellow River	323	16	143	2.9	0.4	1.34	Ding et al. (2011, 2016)
Kalix River	162	37	85.0	1.5	0.7	1.02	Engström et al. (2010)
Iceland Rivers	286	71	162.0	1.5	−0.1	0.63	Georg et al. (2007b)
Swiss Rivers	79	46	61.9	1.2	0.6	0.84	Georg et al. (2006b)
Congo River	236	136	207.4	1.2	0.8	0.98	Cardinal et al. (2010)
Nile River	673	39	206.7	4.7	0.5	2.00	Cockerton et al. (2013)
Siberian Rivers	352	52	164	2.7	0.6	1.62	Pokrovsky et al. (2013)
Amazon River	245	52	141	2.3	0	0.98	Hughes et al. (2013)

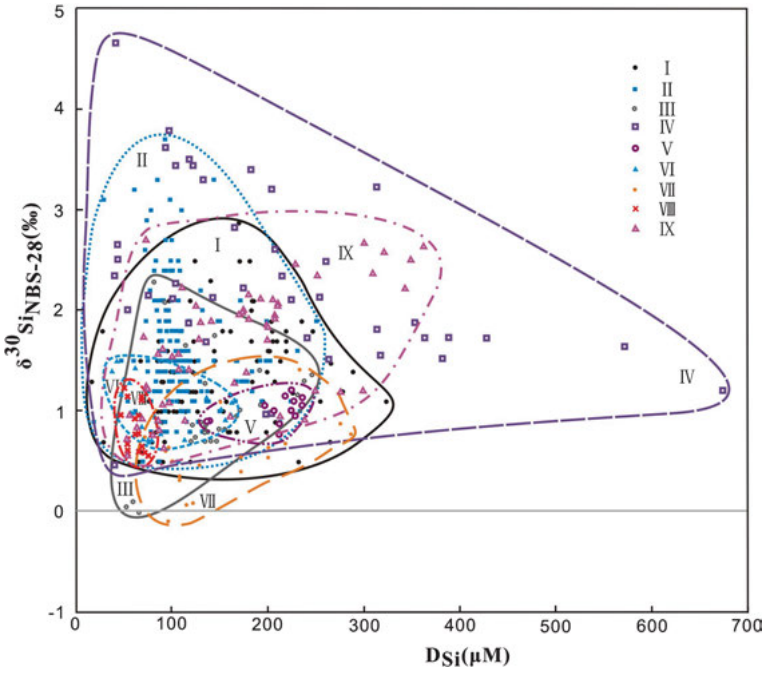

Figure 4.40: $\delta^{30}Si_{DSi}$–DSi relation for water samples from several river systems of the world. I – Yellow River (after Ding et al., 2011, 2016); II – Yangtze River (after Ding et al., 2004, 2014); III – Amazon River (after Hughes et al., 2013); IV – Nile River (after Cockerton et al., 2013); V – Congo River (after Cardinal et al., 2010); VI – Kalix River (after Engström et al., 2010); VII – Iceland rivers (after Georg et al., 2007b); VIII – Swiss rivers (after Georg et al., 2006b); and IX – Central Siberian rivers (after Pokrovsky et al., 2013).

It has been found that the silicon isotope composition in each river system show always spatial and temporal variations, reflecting affections of a number of processes

EBSCOhost - printed on 2/10/2023 8:05 PM via . All use subject to https://www.ebsco.com/terms-of-use

and factors, such as 1) The weathering process of silicate rocks; 2) Growth of phytoliths in plants; 3) Evaporation of water from the river system and addition of meteoric water into the river system; 4) Dissolution of phytoliths in soil; 5) Growth of fresh water diatom; 6) Adsorption and desorption of aqueous monosilicic acid on iron oxide; 7) Precipitation of silcretes and formation of clays coatings in aquifers; 8) Human activities.

Among these rivers, the average $\delta^{30}Si_{DSi}$ (2.02‰) of the Nile River is the highest, which is mainly attributed to the growth of aquatic organisms (diatoms and macrophytes) in the lakes and river of the Nile River basin (Cockerton et al., 2013).

The average $\delta^{30}Si_{DSi}$ (1.63‰) of the Yangtze River is the second highest at this stage, while it has an intermediate DSi value. Due to the relatively warm and humid climate, physical and chemical weathering and biological activity are intensive in this region. The dissolved silicon produced by weathering of silicate rocks plays a very important role in controlling the DSi and $\delta^{30}Si_{DSi}$ of the river. It was also suggested that the growth of rice and grass had a significant influence on DSi and $\delta^{30}Si_{DSi}$ of the river (Ding et al., 2004, 2014).

The average $\delta^{30}Si_{DSi}$ (1.62‰) of the central Siberian rivers is also quite high and significant variations of $\delta^{30}Si_{DSi}$ (0.6~2.72‰) and DSi (52~352 μM) are observed in these rivers (Pokrovsky et al., 2013). They are linked to specific features of Siberian rivers within the permafrost zone.

In contrast, the average $\delta^{30}Si_{DSi}$ values of the Iceland (0.63‰) and the Swiss rivers (0.84‰) are much lower. Both areas have very low average annual temperatures and feature less chemical weathering and low biological activity, which may be the reasons for the low $\delta^{30}Si_{DSi}$ values of these rivers.

The average $\delta^{30}Si_{DSi}$ value of the Kalix River is 1.02‰, slightly higher compared to the Icelandic and Swiss rivers, but much lower than the Yangtze River. According to Engström et al. (2010), the DSi and $\delta^{30}Si_{DSi}$ values of the Kalix River are mainly controlled by the weathering of silicate minerals, Si absorption by the boreal forest trees, dissolution of biogenic silica in the soil and Si uptake by fresh water diatoms in lakes.

The Congo River is situated in tropical Central Africa. Its main branch and largest tributaries have an average $\delta^{30}Si_{DSi}$ value of 0.98‰; while small tributaries have an average $\delta^{30}Si_{DSi}$ value of 0.02‰ (Cardinal et al., 2010). It was proposed that there are two different weathering regimes in the central Congo Basin (Cardinal et al., 2010): One is the regime of rain forests, wooded grassland and savanna, where newly formed clays remain stable and light Si isotopes are sequestered into clay minerals; the other regime is characterized by swamps, where clays are dissolved by the action of organic matter, resulting in the delivery of light Si isotopes to rivers.

The Amazon River is also situated in tropical area and has an average $\delta^{30}Si_{DSi}$ value of 0.98‰ (Hughes et al., 2013). The clear relation between $\delta^{30}Si$ signatures and Si mobility in the Amazon Basin can be observed and may be used as a good proxy for Si mobility and thereby for clay formation.

EBSCOhost - printed on 2/10/2023 8:05 PM via . All use subject to https://www.ebsco.com/terms-of-use

The average $\delta^{30}Si_{DSi}$ value of the Yellow River (1.34‰) is significantly lower than those of the Nile River, the Yangtze River and the Siberian Rivers, but higher than those of other rivers. This condition is consistent with differences in the intensity of chemical weathering and biological activity.

From the above comparison, it is clear that changes in the weathering intensity and biological activity in the catchment areas can significantly influence the DSi and $\delta^{30}Si_{DSi}$ values of global river systems. As a result, the DSi and $\delta^{30}Si_{DSi}$ of river water will be different from river to river, place to place and time to time, corresponding to the differences in climate, chemical weathering intensity and biological activity.

According to the available data, the $\delta^{30}Si_{DSi}$ values of global rivers display a large range from –1.4‰ to 4.7‰. However, there are a number of large rivers, such as the Mississippi River and the Zambezi River that have not yet been analyzed for their Si isotopic compositions. It is expected that even larger $\delta^{30}Si_{DSi}$ variations may be observed when more rivers are investigated. Therefore, further studies should be carried out to determine the variability of $\delta^{30}Si$ values in global rivers and gain a better understanding of the global Si isotope budget.

4.4.3 The silicon isotope composition of ground water

The ground water is also an important reservoir of Si in the hydrosphere. However, so far the studies on silicon isotope compositions are still rare. Georg et al. (2009a,b) reported the silicon isotope compositions of ground water in the Navajo Sandstone aquifer, Black Mesa, Arizona, USA, and in the Great Artesian Basin in Australia. Pogge von Strandmann et al. (2014) reported the silicon isotope compositions of groundwater from the Bengal Basin.

The available $\delta^{30}Si$ values of ground water vary in a range from –1.5‰ to 1.3‰, with an average of 0.1‰ (Figure 4.37D).

The positive $\delta^{30}Si$ values are often found in the shallow aquifer and lower $\delta^{30}Si$ values are found normally in deep samples (Georg et al., 2009a,b; Pogge von Strandmann et al., 2014). Besides, the $\delta^{30}Si$ reduction is also found along the flow path (Georg et al., 2009a,b). It is suggested that the chemistries of Si in groundwater are influenced by the dissolution of primary phases, the formation of secondary minerals and the reaction of solid phases with dissolved constituents, while isotopic variations are generated by uptake into clays, which preferentially incorporate the light isotopes (Georg et al., 2009a,b).

These data indicate that groundwater is isotopically distinct from riverine values. Thus, the relative contribution and silicon isotope composition of groundwater derived Si fluxes should be considered when estimating the continental input into the ocean.

EBSCOhost - printed on 2/10/2023 8:05 PM via . All use subject to https://www.ebsco.com/terms-of-use

4.4.4 The silicon isotope composition of the pore water

The pore water is a chain of silicon global cycle. The silicon content and silicon isotope composition in pore water are affected by the weathering processes of local rocks, by formation of secondary minerals in soil horizon, by absorption of plants and by dissolution of biogenic silica in soil materials. The silicon in pore water is the source of silicon in ground water and river water. Due to a large number of processes and factors that are involved in development of pore water, their silicon contents and silicon isotope compositions should vary in a large range and in a complicated manner. However, by now only a few papers have reported the data on silicon contents and silicon isotope compositions of pore water (Pogge von Strandmann et al., 2012; Ehlert et al., 2016b; White et al., 2012; Frings et al., 2014c; Ding et al., 2008a).

The available data of silicon isotope compositions of pore water are shown in Figure 4.37E. It is observed that the δ^{30}Si values of pore water vary in a range from –0.5‰ to 2.2‰, with an average of 1.0‰ (Figure 4.37E).

Pogge von Strandmann et al. (2012) present silicon isotope composition of pore waters from Histic Andosol in southwest Iceland. The δ^{30}Si values (–0.91‰ ~ –0.53‰) of the soils are lower than that (–0.29‰) of basalt, whereas the δ^{30}Si values (0.13‰ ~ 1.03‰) of pore waters are higher than that of basalt. The δ^{30}Si values of soil show a clear evolution between un-weathered basalt and the secondary minerals. Dissolved Si isotopes also respond to chemical weathering processes, and show that higher δ^{30}Si corresponds to higher cation fluxes and higher secondary mineral formation.

Ehlert et al. (2016b) analyzed the silicon isotope compositions in pore waters of sediment cores from the Peruvian margin upwelling region with distinctly different biogenic opal content. The δ^{30}Si values of pore water vary in a range from 1.1‰ to 1.9‰, with the highest values occurring in the uppermost part close to the sediment–water interface. These values are of the same order or higher than the δ^{30}Si (0.3‰ ~ 1.2‰) of the biogenic opal extracted from the same sediments and those (1.1‰ ~ 1.5‰) of the overlying bottom waters. Combining with the observation that the dissolved silicon concentration in the pore water is well below biogenic opal saturation, these observations are consistent with the formation of authigenic alumino-silicates from the dissolving biogenic opal.

White et al. (2012) studied the δ^{30}Si values of Santa Cruz biomass and pore water. They found that the average deep pore waters are slightly enriched in heavier Si than in granitic rocks, indicating probable fractionation during plagioclase weathering to kaolinite. Shallow pore waters exhibit greater variability, with the average larger than the deep pore waters.

Frings et al. (2014c) present δ^{30}Si data from pore waters together with surface waters, biogenic silica (BSi), clays, sand and vegetation from the Okavango Delta, Botswana, which is a freshwater sub-tropical, flood-pulse wetland. From the data, they made an estimation on the silicon isotope fractionation associated with BSi dissolution.

EBSCOhost - printed on 2/10/2023 8:05 PM via . All use subject to https://www.ebsco.com/terms-of-use

Ding et al. (2008a) reported the silicon isotope compositions of the soil and pore waters from several bamboo growth fields. The δ^{30}Si values of the bulk soils vary from −0.6‰ to −0.2‰, whereas the δ^{30}Si values of pore water in soils vary from 0.4‰ to 2.4‰, with an average of 1.16‰. The differences of δ^{30}Si values between bulk soil and pore water may be caused by several processes. Firstly, during the weathering processes of silicate rocks, silicon isotope fractionation occurs between produced secondary clay minerals and dissolved silicon in solution (Ding et al., 1996; Ziegler et al., 2005a,b). Compared to the initial silicate rock, the produced secondary clay minerals are always depleted in ^{30}Si and the silicon dissolved in pore water is enriched in ^{30}Si. Furthermore, the preferential absorption of light isotopes by plants will raise the δ^{30}Si value of pore water further (Ding et al., 2004). Secondly, the phytoliths in soils of bamboo growth field should mainly come from the leaves of bamboo, which are also enriched in ^{30}Si.

In general, the studies on silicon isotope compositions are still rare. More investigation on this aspect should be undertaken in the future.

4.4.5 The silicon isotope composition of the hot spring water

The hot spring water is also a silicon reservoir in hydrosphere, although the scale is rather small. Early study on silicon isotope compositions of hot spring water aimed to get some basic knowledge on hydrothermal solution related ore formation (Ding et al., 1996). Recently, the researchers are more interested of using hot springs as a natural experimental system to study silicon isotope fractionation when SiO_2 precipitation from hydrothermal solution, which is important in tracing the environmental variation in ancient oceans (Geilert et al., 2015). The available silicon isotope data of hot spring water are shown in Figure 4.37C. Their δ^{30}Si values vary in a range from −0.6‰ to 1.7‰, with an average of 0.2‰ (Figure 4.37C).

Geilert et al. (2015) investigated the silicon isotope compositions of dissolved silicon and silica sinter in the Geysir geothermal area (Iceland) to explore the extent and controls of silicon isotope fractionation in hot spring systems. The δ^{30}Si values of dissolved silica measured in the spring water and sampling sites along outflowing streams, covering a temperature range of 20 ~ 100°C, were relatively constant around +0.2‰, whereas the δ^{30}Si signatures of associated opaline sinters from the streambeds were between −0.1‰ and −4.0‰, becoming progressively more negative in the downstream parts of the aprons.

Compared to the data reported for Icelandic basalts, the δ^{30}Si values of the fluids and sinter deposits are higher and lower, respectively. The resulting values for apparent solid–water isotope fractionation ($\Delta^{30}Si_{solid-water}$) changed with a decreasing temperature from ca. −0.7‰ at ~80 °C to −3.7‰ at ~20 °C, locally down to −4.4‰. This temperature relationship was reproducible in each of the investigated hot spring

EBSCOhost - printed on 2/10/2023 8:05 PM via . All use subject to https://www.ebsco.com/terms-of-use

systems and is qualitatively consistent with recent findings in laboratory experiments on kinetic fractionation for a flowing fluid (see Chapter 3).

However, the apparent fractionation magnitudes observed in the field are ca. −2‰ more negative, and thus significantly larger. They infer that solid–water silicon isotope fractionation during deposition of amorphous silica from a flowing fluid correlates inversely with temperature, but is essentially a function of the precipitation rate, such that the fractionation factor decreases with an increasing rate. As an important corollary, the effective fractionation behavior during precipitation of silica from saturated solutions is a system-dependent feature, which should be taken into account when using silicon isotopes for paleo-environmental reconstructions.

4.5 Biosphere

Silicon isotope variation in biological processes is a frontier of biogeochemical study. Pioneering studies were done on silicon isotope composition of sponges (Douthitt, 1982; De La Rocha, 2003), diatoms (De La Rocha et al., 1997, 1998), radiolarians (Song and Ding, 1990; Ding et al., 1996; Wu et al., 1997) and higher plants, such as rice (Ding et al., 2005a), bamboo (Ding et al., 2008b), wheat (Hodson et al., 2008) and banana (Opfergelt et al., 2006a).

4.5.1 Silicon isotope composition of diatoms

Diatoms are the most important biogenic silica producers. They live both in seawater and freshwater environments. The diatoms in the sea contribute over 40% of the total primary biogenic production (Canfield et al., 2005).

Diatoms are the main driver of oceanic silicon cycle. Both the Si concentration and Si isotopic composition of modern seawater are mainly controlled by the production and dissolution of diatom derived biogenic silica (Tréguer and de La Rocha, 2013). Therefore, the silicon isotopic composition of diatom is considered to be a good proxy for silicic acid utilization and can be used in the studies of the silicon cycle in modern oceans and in the geological past since it was during the Cenozoic when diatoms begun to control the marine silicon cycle. The fresh water diatoms are also a factor affecting the continent Si cycle, although the effect is not so important as for plants and crops (Ding et al., 2004, 2011).

The silicon isotope data of diatoms are reported by a number of research groups (Doering et al., 2016; Chen et al., 2012; Sun et al., 2013; Swann et al., 2010; Sun et al., 2014; Cardinal et al., 2007; Ehlert et al., 2012; Fripiat et al., 2011a, 2012; Cao et al., 2012; Egan et al., 2012; De La Rocha et al., 1998), the available data are shown in Figure 4.41A. The δ^{30}Si values of diatoms vary in a range from −0.7‰ to 3.1‰, with an average of 1.0‰.

EBSCOhost - printed on 2/10/2023 8:05 PM via . All use subject to https://www.ebsco.com/terms-of-use

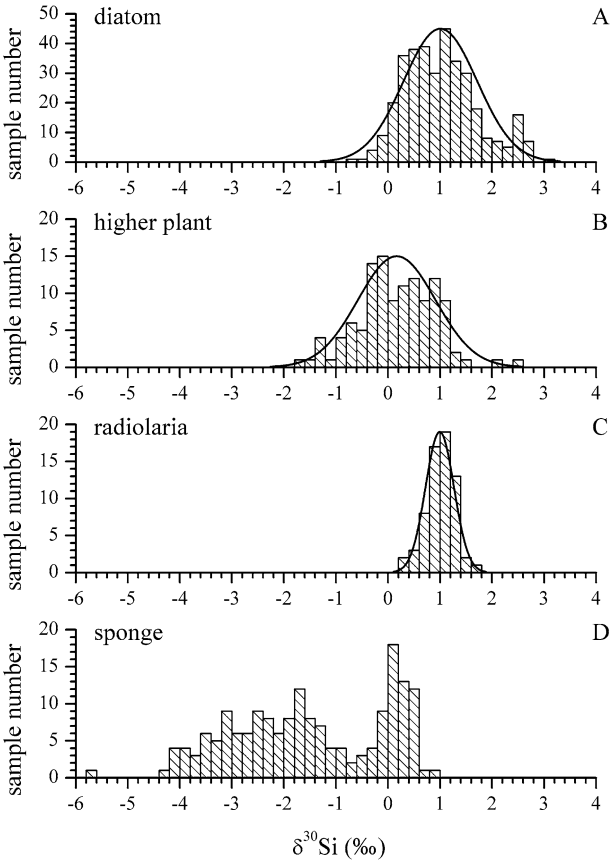

Figure 4.41: The δ^{30}Si values of different types of biological species. Data are from Fontorbe et al. (2016), Wille et al. (2010), Hendry and Robinson (2012), Hendry et al. (2010, 2016), Liu et al. (1998), Hughes et al. (2013), Hodson (2016), Leng et al. (2009), White et al. (2012), Frings et al. (2014a), Engström et al. (2008), Ehlert et al. (2012, 2016b), Ding et al. (2005a, 2008a), Doering et al. (2016), Chen et al. (2012), Sun et al. (2013), Swann et al. (2010), Sun et al. (2014), Cardinal et al. (2007), Fripiat et al. (2011a, 2012), Cao et al. (2012), Egan et al. (2012), Opfergelt et al. (2006a).

Cardinal et al. (2007) determined the silicon isotopic signatures of diatom from the Southern Ocean and compared them with the previously published data for dissolved silicic acid from the same locations. They found that the isotopic composition of diatoms is generally homogeneous in the mixed layer and does not exhibit a systematic isotopic fractionation linked to a size effect. $\delta^{29}Si_{BSi}$ are always lighter than the ambient dissolved silicic acid signatures ($\delta^{29}Si_{DSi}$), reflecting the preferential uptake of light isotopes by diatoms. A trend of lighter isotopic signatures southward is observed both in diatoms and seawater samples but the $\delta^{29}Si_{BSi}$ latitudinal gradient is much steeper.

EBSCOhost - printed on 2/10/2023 8:05 PM via . All use subject to https://www.ebsco.com/terms-of-use

Fripiat et al. (2011a) used silicon isotopic proxy to improve constraints on the Si-biogeochemical cycle, since it integrates over longer timescales in comparison with direct measurements and since the isotopic balance allows resolving the processes involved, i.e., uptake, dissolution, mixing.

Cao et al. (2012) presented the Si isotope data set from the northern South China Sea (NSCS) to examine sources and utilization of silicic acid. They found that surface $\delta^{30}Si_{Si(OH)_4}$ generally increased from values ~2.3‰ on the inner shelf to ~2.8‰ above the deep basin, suggesting an increasing utilization of dissolved $Si(OH)_4$ reflecting the transition from eutrophic to oligotrophic conditions. The $\delta^{30}Si_{BSi}$ values were systematically lower than the corresponding $\delta^{30}Si_{Si(OH)_4}$ in the euphotic zone (above 100 m) on the shelf and slope.

Egan et al. (2012) carried out a study to calibrate core top data with modern oceanographic conditions. They used a microfiltration technique to divide Southern Ocean core top silica into narrow size ranges, separating components such as radiolarian, sponge spicules and clay minerals from diatoms. In their study, a consistent size-$\delta^{30}Si$ pattern, related to the proportions of diatom and non-diatom components in a sample, has been demonstrated. This fact highlights the great potential for small amounts of non-diatom silica to significantly offset measured $\delta^{30}Si$ to lower values than diatom $\delta^{30}Si$. In order to create reliable down core records of diatom $\delta^{30}Si$, it is essential to eliminate such contamination by selecting the correct size fraction for analysis. In general, the 2–20 μm fraction has been found most appropriate for core tops in their study. When a pure diatom size fraction is selected, an extremely good correlation with surface water minimum annual silicic acid concentration is documented ($R^2 = 0.92$). In comparison, larger size fractions (~20–50 μm) exhibit a poorer correlation ($R^2 = 0.66$), again emphasizing the need for size targeted analyses.

Correlation with surface silicic acid concentration, and a good agreement between core top diatom $\delta^{30}Si$ and surface filtered diatom $\delta^{30}Si$, are highly supportive of the use of sedimentary diatom $\delta^{30}Si$ as a proxy for surface water silicic acid utilization and indicate no significant effect of dissolution or early diagenesis. The better correlation with minimum annual silicic acid reflects the fact that diatom $\delta^{30}Si$ records the seasonal extent of silicic acid utilization by diatoms, which should be kept in mind when interpreting diatom $\delta^{30}Si$ records. Core top diatom $\delta^{30}Si$ can be satisfactorily explained using a steady state or Rayleigh fractionation without the need to invoke a variable diatom fractionation factor.

The study of Sun et al. (2014) focuses on diatoms from high production areas in estuarine and coastal areas. They isolated two species of diatoms, *Thalassiosira baltica* and *Skeletonema marinoi*, from the brackish Baltic Sea and used them for laboratory investigations of Si isotope fractionation during diatom growth and the subsequent dissolution. Both species of diatoms give an identical Si isotope fractionation factor during growth of -1.50 ± 0.36‰ (2std) for $\Delta^{30}Si$, which falls in the range from −2.09‰ to −0.55‰ of published data. They also suggested a dissolution-induced

EBSCOhost - printed on 2/10/2023 8:05 PM via . All use subject to https://www.ebsco.com/terms-of-use

Si isotope fractionation factor of −0.86‰ at early stage of dissolution, but this effect was observed only in DSi and no significant Si isotope change was observed for BSi.

Doering et al. (2016) combined silicon isotope compositions of small mixed diatom species ($\delta^{30}Si_{BSi}$) and of large handpicked mono-generic (Coscinodiscus) diatom samples ($\delta^{30}Si_{Coscino}$) with diatom assemblages extracted from marine sediments in the Peruvian upwelling region to constrain present and past silicate utilization. They found that the $\delta^{30}Si_{Coscino}$ values record near complete Si utilization, as they are similar to the isotopic composition of the subsurface source waters feeding the upwelling. In contrast, the $\delta^{30}Si_{BSi}$ of small mixed diatom species increase southward along the shelf as well as towards the shore. They attribute highest $\delta^{30}Si_{BSi}$ values partly to transient iron limitation but primarily to the gradual increase of Si isotope fractionation within the seasonal diatom succession, which are mainly recorded by small diatom species during intense bloom events. In contrast, lower $\delta^{30}Si_{BSi}$ values are related to initial Si utilization during periods of weak upwelling, when low $Si(OH)_4$ concentrations do not permit intense blooms and small diatom species record substantially lower $\delta^{30}Si$ signatures. Thus, they propose that the intensity of the upwelling can be deduced from the offset between $\delta^{30}Si_{BSi}$ and $\delta^{30}Si_{Coscino}$ ($\Delta^{30}Si_{coscino-BSi}$), which is low for strong upwelling conditions and high for prevailing weak upwelling.

In Figure 4.42, the core top marine diatom $\delta^{30}Si$ (2–20 µm or 2–12 µm) compared to filtered diatom $\delta^{30}Si$ collected during in situ studies from the top 100 m of the water

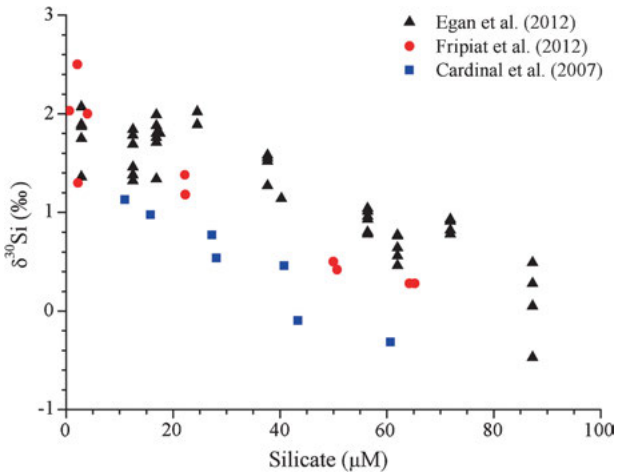

Figure 4.42: Core top diatom $\delta^{30}Si$ (2–20 µm or 2–12 µm) compared to filtered diatom $\delta^{30}Si$ collected during in situ studies from the top 100 m of the water column (Egan et al., 2012; Cardinal et al., 2007; Fripiat et al., 2012). Core top diatom $\delta^{30}Si$ is plotted against average annual silicic acid concentration, and the filtered diatom $\delta^{30}Si$ against the silicic acid concentration measured at the time of sampling. Core top diatom $\delta^{30}Si$ and filtered diatom $\delta^{30}Si$ are remarkably consistent, especially when they are from the same ocean basin.

EBSCOhost - printed on 2/10/2023 8:05 PM via . All use subject to https://www.ebsco.com/terms-of-use

column (Cardinal et al., 2007; Fripiat et al., 2012). Core top diatom $\delta^{30}Si$ is plotted against average annual silicic acid concentration, and the filtered diatom $\delta^{30}Si$ against the silicic acid concentration measured at the time of sampling. Core top diatom $\delta^{30}Si$ and filtered diatom $\delta^{30}Si$ are remarkably consistent, especially when they are from the same ocean basin.

Chen et al. (2012) measured the $\delta^{30}Si_{diatom}$ in the sediment core from Lake Huguangyan, a closed crater lake in China. The $\delta^{30}Si_{diatom}$ varies from −0.6‰ to 1.1‰, corresponding to a broad variation in contents of biogenic silica throughout the sediment core. They think $\delta^{30}Si_{diatom}$ is a reliable paleo-temperature proxy in Lake Huguangyan, for that a good correlation is observed between $\delta^{30}Si_{diatom}$ and available temperature records.

Sun et al. (2013) studied the Si isotope fractionation by following a massive nutrient limited diatom bloom in the Oder River, which is a eutrophied river draining the western half of Poland and entering the southern Baltic Sea. The rapid nutrient depletion and fast BSi increase observed during the spring bloom suggest a closed-system Rayleigh behavior for DSi and BSi in the river at certain time scales. A Si isotope fractionation ($\Delta^{30}Si_{DSi-BSi}$) of −1.6 ± 0.3‰ (2std) is found based on observations between April and June 2004. A very high $\delta^{30}Si$ value of 3.1‰ is obtained in BSi derived from diatoms, which is about 2 times higher than previously recorded $\delta^{30}Si$ in freshwater diatoms. The Rayleigh model used to predict the $\delta^{30}Si$ values of DSi suggests that the initial value before the start of the diatom bloom is close to +2‰, which is relatively higher than the previously reported values in other river water. This indicates that there is a biological control of the Si isotope compositions entering the river, probably caused by Si isotope fractionation during uptake of Si in phytoliths. Clearly, eutrophied rivers with enhanced diatom blooms deliver ^{30}Si-enriched DSi and BSi to the coastal ocean, which can be used to trace the biogeochemistry of DSi/BSi in estuaries.

4.5.2 Silicon isotope composition of radiolarian

Radiolarian is an important silicon bearing microorganism in marine environment. The chert rocks formed by radiolarian skeletons occur frequently in the sedimentary strata from Ordovician to present. The silicon isotope composition of these radiolarian chert rocks were studied by Douthitt (1982), Song and Ding (1990) and Ding et al. (1996). However, the silicon isotope investigation on modern radiolarian skeletons is very rare. Fontorbe et al. (2016) analyzed $\delta^{30}Si$ in radiolarian tests and sponge spicules from the Blake Nose Palae-oceanographic Transect (ODP Leg 171B) spanning the Palaeocene–Eocene (ca. 60–30 Ma). They found that the $\delta^{30}Si$ values of the radiolarian range from 0.3‰ to 1.7‰, with an average of 1.0‰ (Figure 4.41C). In the meanwhile, the $\delta^{30}Si$ values of the sponge range from −0.5‰ to 0.6‰.

EBSCOhost - printed on 2/10/2023 8:05 PM via . All use subject to https://www.ebsco.com/terms-of-use

By using an established relationship between ambient dissolved Si (DSi) concentrations and the magnitude of silicon isotope fractionation in siliceous sponges, they demonstrate that the Western North Atlantic was DSi depleted during the Palaeocene–Eocene throughout the water column. They think that their data can provide constraints on reconstructions of past-ocean circulation.

4.5.3 Silicon isotope composition of sponges

Sponge is the second abundant silicon bearing biological species after diatoms in the ocean. The chert rocks containing sponge skeletons are found in the sedimentary strata from late Precambrian to present (Li et al., 1988). However, there is no report on silicon isotope compositions on these chert rocks containing sponge skeletons. The silicon isotope studies of sponge are focused on the spicules of sponge collected from marine sediments (Wille et al., 2010; Hendry and Robinson, 2012; Hendry et al., 2010, 2016; Liu et al., 1998; Hughes et al., 2013). The available δ^{30}Si values of sponges vary in a range from −5.7‰ to 0.9‰, with an average of −1.5‰ (Figure 4.41D).

Wille et al. (2010) studied silicon isotope composition of deep-sea sponges from near Antarctica, sub-Antarctic waters (Tasmania Seamounts) and subtropical waters north of New Zealand. The δ^{30}Si values of these sponges vary widely from 0.9‰ to −3.4‰. They found that the δ^{30}Si values of sponge tend to decrease when the depth is increased. For example, δ^{30}Si varies of sponges from the Tasmania Seamounts varies from 0.9‰ to −3.1‰ when depth change from 100 m to 1 200 m. These changes in δ^{30}Si of sponges are inconsistent with a Rayleigh-type isotope fractionation model requiring constant δ^{30}Si fractionation between sponge and seawater. They conclude that overall Si isotope fractionation Δ^{30}Si ($\delta^{30}Si_{sponge} - \delta^{30}Si_{seawater}$) is influenced by seawater Si concentration, with more fractionated isotope values being associated with sponges collected from waters high in Si.

Hendry et al. (2010) report δ^{30}Si of modern deep-sea sponge spicules and show that they reflect seawater $Si(OH)_4$ concentration. They found that the silicon isotope fractionation between sponge and seawater shows a positive relationship with $Si(OH)_4$, which may be a growth rate effect.

Hendry and Robinson (2012) refined and widen the existing calibration by including a global distribution of modern sponges (Figure 4.43). On this base, they provide the first systematic calibration from spicules picked from core-top sediments that covers sites from different ocean basins. The observed relationship between $Si(OH)_4$ and δ^{30}Si in sponge spicules is the same in different ocean basins, between specimens that grew in different temperature and salinity conditions. Their core-top data agree well with the modern sponge calibration indicating there are no significant post-depositional effects or early diagenetic overprints. Thus, they believe the sponge δ^{30}Si can be used as a proxy for silicic acid concentrations in the past.

EBSCOhost - printed on 2/10/2023 8:05 PM via . All use subject to https://www.ebsco.com/terms-of-use

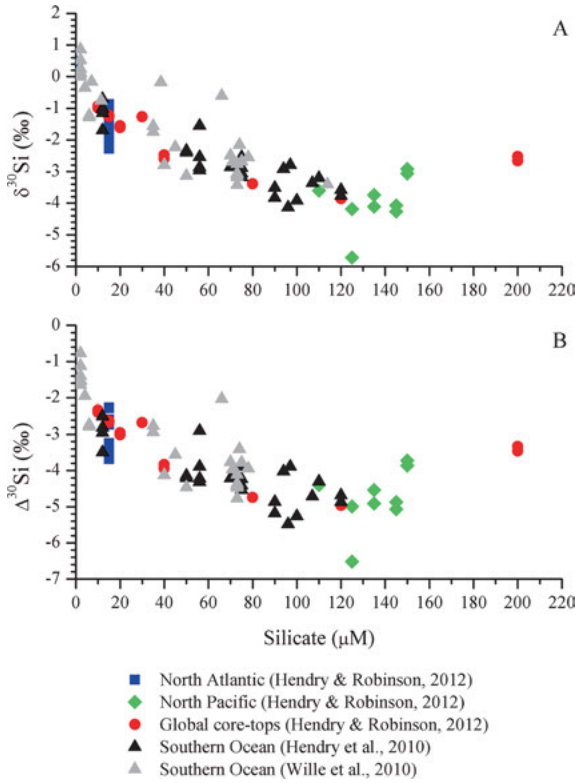

Figure 4.43: A: δ^{30}Si and B: Δ^{30}Si for all sponges from different ocean basins.

4.5.4 Silicon isotope composition of high plants

The role of silicon in plant growth had been overlooked for a long period, although silicon is present in plants in amounts equivalent to macronutrient elements, such as calcium, magnesium and phosphorus (Epstein, 1999). The contents and distribution patterns of silica in crops and grasses were found to be critical to their quality and production. Silica in plants contributes to the compression-resistance and rigidity of cell walls, which in turn improve light interception and drought resistance, and increase photosynthetic efficiency (Jones and Handreck, 1967). It strengthens the air canal, leading to more efficient oxygen supply to roots and limited loss of water by evapotranspiration (Sangster and Hodson, 1986; Sangster and Parry, 1981; Shui et al., 1995). It also increases the resistance to pathogens, blast, insects, mollusks and grazing by herbivores (Sangster and Hodson, 1986; Shui et al., 1995). These discoveries attracted much attention of researchers, and a large number of studies were carried out to investigate the effect of silicon on the growth condition of plant. The contents, forms and distribution patterns of silicon in a variety of plants, such as rice, sugar-

EBSCOhost - printed on 2/10/2023 8:05 PM via . All use subject to https://www.ebsco.com/terms-of-use

cane, sorghum, wheat, ryegrass, bamboo, tomato, cucumber, blueberry and banana were investigated. The role of plants on a global cycle of silicon also became another important issue of silicon biogeochemistry (Alexandre et al., 1997; Lux et al., 2003; Ding et al., 2005a; Desplanques et al., 2006; Fraysse et al., 2006a,b; Li et al., 2006; Opfergelt et al., 2006b). An emphasis has been placed on the widely distributed plants with high silicon content, such as rice, wheat and bamboo (Lux et al., 2003; Ding et al., 2005a, 2008a; Li et al., 2006; Hodson et al., 2008).

Silicon isotope variation in biological processes is a frontier of biogeochemical study. Extensive studies were done on silicon isotope composition of sponges (Douthitt, 1982; De La Rocha, 2003), diatoms (De La Rocha et al., 1997, 1998) and radiolarians (Song and Ding, 1990; Ding et al., 1996; Wu et al., 1997). Although the silicon isotope studies on terrestrial plants are still very limited, the preliminary results obtained on rice (Ding et al., 2005a), bamboo (Ding et al., 2008a), wheat (Hodson et al., 2008) and banana (Opfergelt et al., 2006a,b) are encouraging. Further studies on more types of plants may help us to understand the role of terrestrial plants in a global silicon cycle.

The available data for silicon isotope compositions are shown in Figure 4.41B (Hodson, 2016; Leng et al., 2009; White et al., 2012; Frings et al., 2014a; Engström et al., 2008; Ehlert et al., 2012, 2016b; Ding et al., 2005a, 2008b). The δ^{30}Si values of bulk samples and different parts of higher plants vary in a range from −2.3‰ to 6.1‰, with an average of 0.2‰.

4.5.4.1 Silicon isotope composition of rice plants

Ding et al. (2005a) studied the silicon isotope compositions of rice plants collected from the Zhejiang Province, China. They found that the SiO_2 contents in ignited rice plant samples increased generally from roots, through SL (stem and leaves), to husks. Large and systematic silicon isotope fractionation was observed among different organs of individual rice plants (Figure 4.44). Their δ^{30}Si values show a general increasing trend from roots and SL, through husks to grains, which can be explained by kinetic isotope fractionation in a Rayleigh process (see Chapter 5 for detailed discussion). A δ^{30}Si value of 6.1‰ was obtained in two samples of rice grains, which is much greater than the highest value (3.4‰) observed in terrestrial samples before.

It is inferred that monosilicic acid is the major silicon-bearing component taken up by rice roots. Passive uptake of silicon is important for rice and evapotranspiration may be the major mechanism for the transportation and precipitation of silicon in rice plants. It is suggested that silicon isotope study has a potential application in agriculture and biogeochemistry. See Chapter 5 for detailed discussion.

4.5.4.2 Silicon isotope composition of bamboo

Ding et al. (2008a) conducted a systematic investigation on silica contents and silicon isotope compositions of bamboos collected from seven locations in China. The root,

EBSCOhost - printed on 2/10/2023 8:05 PM via . All use subject to https://www.ebsco.com/terms-of-use

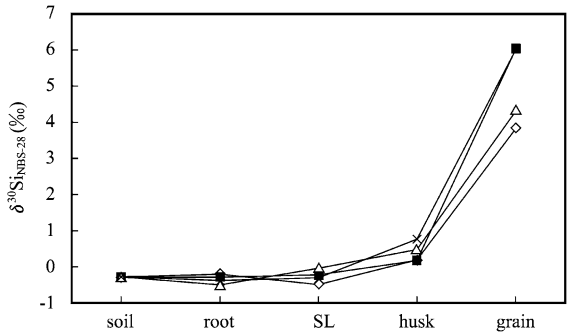

Figure 4.44: The δ^{30}Si values of different rice organs and soils. Diamonds, filled squares, triangles and crosses stand for different individual plants. Revised from Ding et al. (2005a).

stem, branch and leaves for each plant were sampled and their silica contents and silicon isotope compositions were determined. The silica contents and silicon isotope compositions of bulk and water soluble fraction of soils were also measured. The silica contents of studied bamboo organs vary from 0.30% to 9.95%. Within the bamboo plant, the silica contents show an increasing trend from stem, through the branch to the leaves. In bamboo roots, the silica is exclusively in the endodermis cells, but in the stem, branch and leaves, the silica is accumulated mainly in epidermal cells. The δ^{30}Si values of bamboos exhibit significant variation, from –2.3‰ to 1.8‰, and large and systematic silicon isotope fractionation was observed within each bamboo. The δ^{30}Si values decrease from roots to stem, but then increase from the stem, through the branch to the leaves. The ranges of δ^{30}Si values within each bamboo vary from 1.0‰ to 3.3‰. This kind of silicon isotope variation might be caused by isotope fractionation in a Rayleigh process when SiO_2 precipitated in the stem, branches and leaves gradually from plant fluid. Considering the distribution patterns of SiO_2 contents and δ^{30}Si values among different bamboo organs, evapotranspiration may be the driving force for an upward flow of a silicon-bearing fluid and silica precipitation. Passive silicon uptake and transportation may be important for bamboo, although the role of active uptake of silicic acid by roots may not be neglected. The samples with relatively high δ^{30}Si values all grew in soils showing high content of organic materials. In contrast, the samples with relatively low δ^{30}Si values all grew in soil showing a low content of organic materials. The silicon isotope composition of bamboo may reflect the local soil type and growth conditions. Besides, bamboos may play an important role in the global silicon cycle. See Chapter 5 for detailed discussion.

4.5.4.3 Silicon isotope composition of wheat

Hodson et al. (2008) studied mature wheat plants from one crop collected one week before harvest. The organs of culm, rachis, leaf sheaths, leaf blades and inflorescence bracts were separated and their silica contents were measured. The phytoliths isolated

EBSCOhost - printed on 2/10/2023 8:05 PM via . All use subject to https://www.ebsco.com/terms-of-use

from the individual organs were subsequently analyzed for δ^{29}Si and δ^{30}Si. The SiO_2 content was highest in the leaf sheaths and leaf blades and lower in the inflorescence bracts, culm and rachis. δ^{29}Si and δ^{30}Si were highly correlated, and both increased in the upper parts of the plant. They suggested that there are two routes for Si transport within the plant: 1) culm → leaf → sheath → leaf blade; and 2) culm → rachis → inflorescence → bracts. They found that heavier isotopes increased towards the end of both routes. See Chapter 5 for detailed discussion.

4.5.4.4 Silicon isotope composition of banana

Opfergelt et al. (2006b) studied the silicon isotopic fractionation between the different plant parts of banana. On mature banana from Cameroon, δ^{29}Si ranged from +0.13‰ in the petiole to +0.49‰ in the lamina, yielding to a 0.36‰ change towards heavier isotopic composition in the upper parts of the plant. This strongly accords with results obtained on in vitro banana plantlets cultivated in hydroponics, where the δ^{29}Si increase from pseudo-stems to lamina is 0.26‰. These preliminary results on in situ banana show a trend of intra-plant fractionation comparable with that of in vitro hydroponics banana plantlets and with previous data obtained on bamboo (Ding et al., 2003). See Chapter 5 for detailed discussion.

EBSCOhost - printed on 2/10/2023 8:05 PM via . All use subject to https://www.ebsco.com/terms-of-use

5 Several aspects of silicon isotope applications

By using the analytical methods described in Chapter 2, and on the basis of the knowledge on silicon isotope fractionation mechanisms discussed in Chapter 3 and silicon isotope distribution in various extraterrestrial and terrestrial reservoirs illustrated in Chapter 4, multidimensional investigations of silicon isotope applications have been carried out in various geological, geochemical and biochemical fields. In this chapter, the important progress obtained in four fields will be presented as the examples of silicon isotope applications. They are the studies on: 1) global silicon cycle; 2) environmental variation of ocean; 3) mechanisms of absorption, transportation and precipitation of silicon in plant growth processes; and 4) silicon sources and genesis of ore deposits.

5.1 Studies on global silicon cycle

The global Si cycle basically consists of two sub-cycles: 1) one relatively discrete sub-cycle on the continents; 2) another sub-cycle in the oceans (Figure 5.1). The transfer of Si between the two sub-cycles is essentially unidirectional, so the land-to-ocean Si flux is of interest both as an integrative function of the continental Si sub-cycle and as the chief input for the ocean Si sub-cycle.

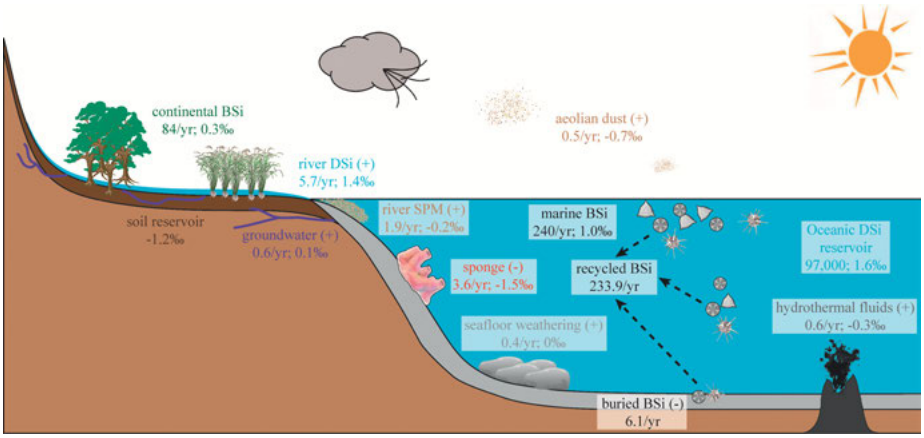

Figure 5.1: Schematic of modern global silicon cycle at steady-state. The fluxes (with "/yr") and reservoir size are shown in 10^{12} mol Si. Their associate silicon isotopic compositions are shown in permil (‰). Symbols (+) or (–) stand for inputs or outputs relative to the ocean. Dashed arrows indicate dissolution of marine biogenic silica. Flux data are compiled and reconsidered from published literatures (Tréguer et al., 1995; Canfield et al., 2005; Tréguer and de La Rocha, 2013; Frings et al., 2016), and δ^{30}Si values are from Chapter 4 of this book. See the text for details.

https://doi.org/10.1515/9783110402452-005

EBSCOhost - printed on 2/10/2023 8:05 PM via . All use subject to https://www.ebsco.com/terms-of-use

5.1.1 The continental Si sub-cycle

The key processes in the continental Si sub-cycle are illustrated in Figure 5.1. In this section, the discussion on this issue is based mainly on the systematic and detailed review done by Frings et al. (2016). This sub-cycle begins with the release of dissolved silicon (DSi) in weathering processes. A fraction of generated DSi may then be transferred directly to the fluvial system, via groundwater or soil water flow. The second fraction may be incorporated into, or adsorbed onto, secondary phases of variable stability. Finally, the third fraction may be utilized by vascular plants that take up DSi and subsequently precipitate it as biogenic silica (BSi) structures termed phytoliths (Carey and Fulweiler, 2012; Massey et al., 2006; Piperno, 2001). In the plant littering process, the BSi returns to the soil where it may dissolve, be stored or be structurally or chemically altered (Barão et al., 2014; Sommer et al., 2006). Ultimately, Si will be released into the fluvial system as both DSi and eroded particulate Si. BSi, altered BSi and pedogenic silicates are all un-crystalized and show similar solubility and reactivity. So they are commonly called 'amorphous silica' (ASi) (Saccone et al., 2007). The net result of continental Si cycling is that in many ecosystems, a soil–plant ASi pool develops that is orders of a magnitude larger than the annual release of DSi from primary minerals via weathering (Blecker et al., 2006; Clymans et al., 2011; Struyf et al., 2010). Thus, it is generally accepted that terrestrial soil–plant systems buffer the release of Si from the continents (Struyf and Conley, 2012), and that perhaps even a majority of river DSi passes through this buffer before export into the river system (Derry et al., 2005; Struyf et al., 2009). In the river system, both biotic and abiotic processes can further modify the Si flux (Bouwman et al., 2013; Conley and Malone, 1992; Frings et al., 2014a; Lauerwald et al., 2013; Milliman and Boyle, 1975; Weiss et al., 2015).

5.1.1.1 Silicon isotope variation in various steps of the continental sub-cycle

The silicon isotope compositions of various Si reservoirs in the continent are influenced by multiple processes, which vary according to place and time. The major processes are discussed below.

The weathering process of silicate rocks

In the weathering process, clay minerals and dissolved silicon are generated from silicate rocks and minerals (Tréguer et al., 1995). The dissolved silicon in soil water and groundwater is the major Si contributor to stream and river waters. Compared to the source rocks, the new-formed clay minerals tend to have lower δ^{30}Si (–2.6 ~ –0.2‰), while the dissolved silicon tends to have higher δ^{30}Si value (–0.3 ~ 2.1‰) (Ding et al., 1996, 2004; Ziegler et al., 2005a,b). The $\delta^{30}Si_{DSi}$ in the soil water is controlled by the type of source rock and the weathering conditions (Ziegler et al., 2005a,b).

Large δ^{30}Si variations were discovered among major rock types. The δ^{30}Si range is –1.0 ~ 0.4‰ for igneous rocks, –2.2 ~ 0.8‰ for metamorphic rocks, –0.5 ~ 0.5‰

EBSCOhost - printed on 2/10/2023 8:05 PM via . All use subject to https://www.ebsco.com/terms-of-use

for sandstone, −0.6 ~ 0.7‰ for siltstone, −0.8 ~ 1.3‰ for shale, −0.8 ~ 1.3‰ for clays, −4.3 ~ 3.9‰ for chert and −2.7 ~ 0.3‰ for soils (see Chapter 4 of this book). Some minor silica bearing rocks, such as quartz bands in BIFs, vein quartz, silica sinter in hot springs, cherty rocks in black smokers (Ding et al., 1996) and quartz in silcretes (Basile-Doelsch et al., 2005) show even larger variations in δ^{30}Si. It has been found that the δ^{30}Si values of soil water and small rivers are influenced by the rocks exposed in the drainage area. However, for large rivers, such as the Yangtze River, the Amazon River, the Nile River and the Congo River, a great variety of rocks occur in the drainage area, and the average δ^{30}Si of the source rocks might be similar to the crustal value. It means that the Si isotopic compositions of source rocks are unlikely to be responsible for any large differences in the $\delta^{30}Si_{DSi}$ values of the large rivers in the world.

Concerning the effect of weathering conditions, it is observed that the δ^{30}Si value of soil solution increases by about 1.5‰ when clay minerals precipitate at 25°C, but only by 1.0‰ when allophane precipitates at 90°C (Ziegler et al., 2005a). In a natural environment, the actual effect of the weathering temperature will not be so large, as differences in the weathering temperature are usually smaller than that used by Ziegler et al. (2005a).

It is also recognized that the δ^{30}Si values of soil solution depend on the degree of weathering. As soils develop and a greater fraction of Si resides in new-formed clay minerals, the δ^{30}Si values of the bulk soil change progressively towards more negative values and the δ^{30}Si values of soil solutions from older soils become less positive (Ziegler et al., 2005a). Furthermore, Cardinal et al. (2010) indicate that there are two types of weathering regimes in the Congo basin: one, where clays are formed and remain stable and has higher $\delta^{30}Si_{DSi}$ values (0.98 ± 0.15‰); the other, where clays are dissolved under the action of organic matter, exhibit the lowest $\delta^{30}Si_{DSi}$ values for running surface waters (0.02 ± 0.13‰).

The effect of weathering processes varies from place to place and from time to time. These variations are compared between two large drainage areas, the Yangtze River basin and the Yellow River basin, in China (Ding et al., 2014, 2016). The Yellow River basin is located north of the Yangtze River basin. In comparison to the Yangtze River basin, the climate in the Yellow River region is colder and drier (YRCC, 2007). The former features an annual average temperature of 16°C, an annual precipitation of 1 067 mm and an annual evaporation of 541 mm. In contrast, the latter is characterized by an annual average temperature of 12°C, an annual precipitation of 466 mm and an annual evaporation of 1 100 mm. Therefore, the natural chemical weathering intensity in the Yellow River region is lower compared to the Yangtze River basin.

Growth of phytoliths in plants

It is known that higher plants play an important role in the biogeochemical cycle of silicon (Tréguer et al., 1995; Alexandre et al., 1997; Conley, 2002; Raven, 2003; Ding et al., 2004, 2005a, 2008a,b; Derry et al., 2005; Ziegler et al., 2005a; Opfergelt et al.,

EBSCOhost - printed on 2/10/2023 8:05 PM via . All use subject to https://www.ebsco.com/terms-of-use

2006a,b). They take up silicon from the soil solution and transport and precipitate silica in their tissues. In this process, the DSi of the soil solution is significantly reduced and Si isotopic fractionation occurs between plants and soil solution. The Si isotope fractionation between plants and soil solution has been investigated for rice (Ding et al., 2005a, 2008b; Sun et al., 2008), wheat (Hodson et al., 2008), banana (Opfergelt et al., 2006a,b), bamboo plants (Ding et al., 2008a) and some trees (Engström et al., 2008). These studies show that plants preferentially take up light Si isotopes, and greater Si isotope fractionation occurs in plants with higher Si concentrations (Opfergelt et al., 2006a; Hodson et al., 2008). During these processes, the $\delta^{30}Si_{DSi}$ values of soil solutions are increased further. Thus, phytoliths growth in plants is an important process controlling the DSi and $\delta^{30}Si_{DSi}$ of soil water and river water. For example, it was suggested that the DSi and $\delta^{30}Si_{DSi}$ values of the Yangtze River are significantly influenced by the growth of rice and grass (Ding et al., 2004, 2008b, 2014), and the DSi and $\delta^{30}Si_{DSi}$ values of the Yellow River are influenced by growth of the wheat (Ding et al., 2011, 2016).

Evaporation of water from the river system and addition of meteoric water into the river system

Evaporation of water from the river system will increase the DSi of the river water, while addition of meteoric water to the river system will reduce the DSi of the river water. However, the $\delta^{30}Si_{DSi}$ of the river water will not change in these processes unless they are accompanied by precipitation or dissolution of Si-bearing minerals.

The effect of evaporation is especially significant in some drainage areas with a dry climate. For example, in the Yellow River basin, the annual precipitation is 466 mm, while the annual evaporation is 1100 mm. In its middle reaches, the annual precipitation is only 200~300 mm, but the annual evaporation is up to 2000 mm. Evaporation in the Yellow River region is thus very pronounced. This factor is exaggerated by the irrigation activities (Chen et al., 2006). The middle reaches are an important agricultural area of China, where the growth of wheat, corn, cotton and fruit trees relies chiefly on irrigation water from the Yellow River. After further evaporation in the farmland, the returned irrigation water is even more saline and characterized by a higher DSi value. This process provides a good explanation for the positive correlation that is observed between DSi and the total dissolved solids (TDS) (Ding et al., 2011).

Dissolution of phytoliths in soil

The phytoliths are returned to the soil during the plant littering process. Dissolution of phytoliths in the soil will provide some dissolved Si to the soil solution, which ultimately flows into the rivers and affects their DSi and $\delta^{30}Si_{DSi}$ (Farmer et al., 2005; Wickramasinghe and Rowell, 2006). The effect of dissolution of the phytoliths to DSi and $\delta^{30}Si_{DSi}$ in soil water and river water have been discussed for the Yangtze River

EBSCOhost - printed on 2/10/2023 8:05 PM via . All use subject to https://www.ebsco.com/terms-of-use

(Ding et al., 2014), Yellow River (Ding et al., 2011, 2016), Kalix River (Engström et al., 2010) and Siberian Rivers (Pokrovsky et al., 2013).

Growth of fresh water diatom

Fresh water diatoms are widely distributed in creeks, rivers and especially in lakes and reservoirs (Alleman et al., 2005; Mackay, 2007; Swann et al., 2010). Diatom growth is one of the major processes affecting the silicon cycle in the riverine system. The effect of diatom growth on the δ^{30}Si value of fresh water was studied in Lake Tanganyika by Alleman et al. (2005). From their δ^{29}Si values, the average δ^{30}Si values can be calculated to be 1.7‰ for surface water, 1.2‰ for deep water and 0.5‰ for epilimnion biogenic opal. Similar to the processes observed in the oceans, the growth of fresh water diatoms can reduce the DSi of lake and river waters and raise the $\delta^{30}Si_{DSi}$ values.

The very high $\delta^{30}Si_{DSi}$ value found in the Nile River is mainly attributed to the growth of aquatic organisms (diatoms and macrophytes) in the lakes and river of the Nile River basin (Cockerton et al., 2013). Low DSi concentrations and correspondingly enriched Si isotope values are found in the headwater lakes and in the main Nile where depletion of Si by aquatic organisms is thought to be most important (Cockerton et al., 2013). Then extensive downstream enrichment of Si isotopes and depletion of DSi are observed during both wet and dry seasons in the Nile River, reflecting active biochemical Si cycling (Cockerton et al., 2013). Similar effects are also observed in some lakes and reservoirs of the Yellow River system, although the influence is rather limited (Ding et al., 2016).

Adsorption and desorption of aqueous monosilicic acid on iron oxide

Monosilicic acid can be withdrawn from the soil solution through its sorption onto aluminum and iron oxides (Beckwith and Reeve, 1963; Jones and Handreck, 1963; Mckeague and Cline, 1963). Delstanche et al. (2009) studied experimentally the silicon isotope fractionation in this process by using a system of H_4SiO_4 adsorption onto synthesized ferrihydrite and goethite. They found that the remaining solution was systematically enriched in ^{30}Si, reaching maximum δ^{30}Si values of 1.4‰ for ferrihydrite and 1.0‰ for goethite. Based on these results, they suggested that the sorption of H_4SiO_4 onto synthetic iron oxides produced a similar Si isotopic fractionation to that observed for Si uptake by plants and diatoms.

The effect of H_4SiO_4 adsorption on the fractionation of Si isotopes in a natural system was studied by Opfergelt et al. (2009) in two weathering sequences of basaltic ash soils in Cameroon. They found that adsorption of H_4SiO_4 by the iron oxide minerals of soils left a solution depleted in light Si isotopes, confirming the results obtained with synthetic iron oxides. The solutions were systematically enriched in ^{30}Si, reaching maximum δ^{30}Si values of between 0.16‰ and 0.95‰ after 72 h of contact time. The enrichment of the solution in heavy isotopes increased with an increasing degree

EBSCOhost - printed on 2/10/2023 8:05 PM via . All use subject to https://www.ebsco.com/terms-of-use

of soil weathering, higher iron oxide content and larger proportions of short range ordered iron oxide (such as hydrous iron oxide). However, the Si isotopic composition of the solution was also partly influenced by the Si release, possibly through mineral dissolution and Si desorption from oxide surfaces. Opfergelt et al. (2009) also investigated the Si isotope compositions of rivers in the studied area. They found that in natural environments, H_4SiO_4 adsorption onto soil iron oxides has some impact on the Si isotopic compositions of the soil solution exported to streams.

The effect of H_4SiO_4 adsorption on the Si isotope variation in the Yangtze River system and Yellow River system are also discussed by Ding et al. (2011, 2014, 2016). It is reported that iron oxides are present in all SPM samples collected in these two river systems. The average contents of iron oxides in SPM are 8.01% and 4.61% for the Yangtze River and Yellow River, respectively. These indicate that iron oxides are commonly present in the soils of both two areas. Besides, it was previously reported that the loess soils had an average Fe_2O_3 content of 4.18% (Wen et al., 1996). Thus, H_4SiO_4 adsorption onto iron oxides should have an impact on the DSi and $\delta^{30}Si_{DSi}$ values of the soil solutions, as well as the stream and river waters of the Yangtze River basin and the Yellow River basin.

Precipitation of silcretes and formation of clays coatings in aquifers

The precipitation of silcretes (Basile-Doelsch et al., 2005) and the formation of clay coatings in aquifers (Georg et al., 2009b) will reduce the DSi of soil water and groundwater and generate higher $\delta^{30}Si_{DSi}$ values. This will ultimately affect the DSi and $\delta^{30}Si_{DSi}$ of the river water. Such processes might also play a role in the aquifers of the other large river systems, but this has not yet been investigated.

Human activities

Human activities, including agricultural, industrial and domestic water uses, can have an important impact on the DSi and $\delta^{30}Si$ values of river systems. While the effects of agriculture were already discussed above, the impacts of industrial and domestic water uses are likely to be complicated and they have not yet been investigated in detail.

5.1.1.2 Present-day continent inputs of DSi to the global ocean

The most important continent sources of DSi to the global ocean are supplied by the continental fluvial system. Chiefly, these sources are: 1) DSi in rivers, 2) DSi in groundwater and 3) the dissolution of river SPM. DSi derived from these sources must first pass through many fluvial 'filters', including wetlands, lakes, floodplains, estuaries and the coastal zone before reaching the open ocean. Besides, the dissolution of Aeolian dust also provides some DSi to the global ocean. In this section, the magnitude and isotopic compositions of these inputs to the ocean based on Frings et al. (2016) are presented (summarized in Table 5.1).

EBSCOhost - printed on 2/10/2023 8:05 PM via . All use subject to https://www.ebsco.com/terms-of-use

Table 5.1: Summary of the modern day inputs of DSi to the global ocean, together with estimates of their Si isotope composition (based on Frings et al., 2016).

Flux	DSi (10^{12} mol Si yr^{-1})		δ^{30}Si (‰)		Level of understanding
River DSi	6.3	±0.4	1.3	±0.7	OK
Estuarine removal	−0.6		0.1		Poor
Net River DSi input	5.7		1.4		
Dissolution of SPM	1.9	±1.0	−0.2	±0.3	Poor
Groundwater DSi	0.6	±0.5	0.1	±0.9	Poor
Dissolution of dust	0.5	±0.2	−0.7	±0.4	Poor
Hydrothermal fluids	0.6	±0.4	−0.3	±0.2	Poor
Low temperature alteration of oceanic crust	0.4	±0.3	0.0	±0.5	Poor
Sum	9.7	±1.3	0.7	±0.2	Poor

River DSi flux

As a major provider of dissolved silicon to the ocean (Tréguer et al., 1995), rivers play a significant role in the global Si cycle. Thus the DSi contents and silicon isotope compositions of terrestrial river systems has attracted wide attention recently. By now, a number of important river systems, such as the Yangtze River (Ding et al., 2004, 2014), the Yellow River (Ding et al., 2011, 2016), the Kalix River (Engström et al., 2010), Icelandic rivers (Georg et al., 2007b), Swiss rivers (Georg et al., 2006b), the rivers in the Congo Basin (Cardinal et al., 2010), the Nile River (Cockerton et al., 2013), Central Siberian rivers (Pokrovsky et al., 2013) and the Amazon River (Hughes et al., 2013) have been investigated for their DSi and $\delta^{30}Si_{DSi}$ characteristics, which are summarized in Table 4.1 and illustrated in Figure 4.40. The DSi and $\delta^{30}Si_{DSi}$ characteristics vary from one system to another due to change of relative importance of various processes occurred in different river systems.

Among these rivers, the average $\delta^{30}Si_{DSi}$ (2.02‰) of the Nile River is the highest, which is mainly attributed to the growth of aquatic organisms (diatoms and macrophytes) in the lakes and river of the Nile River basin (Cockerton et al., 2013). In the headwater lakes in the main Nile, the low DSi and high $\delta^{30}Si_{DSi}$ values were observed, which is considered to be the fact of freshwater diatoms and other aquatic organisms; in downstream of the river, significant depletion of DSi and increased $\delta^{30}Si_{DSi}$ values were found during both wet and dry seasons, reflecting also the biological activity (Cockerton et al., 2013). The heavy isotope ^{30}Si is enriched in surface waters during the dry season due to a reduction in mobilization of dissolved Si from the catchment relative to aquatic demand (Cockerton et al., 2013). Besides, localized anthropogenic impacts on the isotope composition of surface waters are identifiable with respect to both the hydrological and Si cycles, especially during the dry season and along the main Nile where irrigation and retention of stored floodwaters behind large dams are most prevalent (Cockerton et al., 2013).

EBSCOhost - printed on 2/10/2023 8:05 PM via . All use subject to https://www.ebsco.com/terms-of-use

The average $\delta^{30}Si_{DSi}$ (1.63‰) of the Yangtze River is the second highest, with an intermediate DSi value. Due to the relatively warm and humid climate, physical and chemical weathering and biological activity are intensive and play a very important role in controlling the DSi and $\delta^{30}Si_{DSi}$ of the river. It was also suggested that the growth of rice and grass had a significant influence on DSi and $\delta^{30}Si_{DSi}$ of the river (Ding et al., 2004, 2014). As red soils are common in the drainage basin, the adsorption and desorption of aqueous monosilicic acid onto iron oxides may also be one of the major processes affecting DSi and $\delta^{30}Si_{DSi}$ values of the Yangtze. Furthermore, growth of fresh water diatoms may also play a minor role in this aspect.

The average $\delta^{30}Si_{DSi}$ (1.62‰) of the central Siberian rivers is also quite high and significant variations of $\delta^{30}Si_{DSi}$ (0.6~2.72‰) and DSi (52~352 μM) are observed in these rivers (Pokrovsky et al., 2013). They are linked to specific features of Siberian rivers within the permafrost zone such as 1) high concentrations of suspended silicate matter during the spring flood, driving the congruent dissolution of clay minerals and river water enrichment in light Si isotopes; 2) the progressive increase of the soil active layer depth during summer accompanied by secondary mineral precipitation in surface layers and plant uptake of Si, leading to river water enrichment in heavy isotopes and finally 3) the impact of the permafrost-hosted deep underground waters during winter, when the porous fluid enrichment in heavy isotope occurs under a very high mineral/water ratio accompanied by secondary mineral precipitation in deep permafrost waters.

The average $\delta^{30}Si_{DSi}$ value of the Yellow River (1.34‰) is significantly lower than those of the Nile River, the Yangtze River and the Siberian Rivers, but higher than those of other rivers. This condition is consistent with differences in the intensity of chemical weathering and biological activity. The Yellow River catchment is an important agricultural area of China that features more intense chemical weathering and biological activity than the areas of the Swiss rivers, the Iceland Rivers and the Kalix River. However, due to colder weather and lower precipitation, the chemical and biological activities in the Yellow River basin are less intensive than in the Yangtze River region.

In contrast to above rivers, the average $\delta^{30}Si_{DSi}$ values of the Iceland (0.63‰) and the Swiss rivers (0.84‰) are much lower. The Swiss rivers are located in a high mountainous area (Georg et al., 2006b), while the Iceland rivers are located at high latitude area (Georg et al., 2007b). Both areas have very low average annual temperatures and feature less chemical weathering and low biological activity, which may be the reasons for the low $\delta^{30}Si_{DSi}$ values of these rivers.

The average $\delta^{30}Si_{DSi}$ value of the Kalix River is 1.02‰, slightly higher compared to the Icelandic and Swiss rivers, but much lower than the Yangtze River. The Kalix River catchment is situated in the boreal forest area of northern Sweden with a subarctic (boreal) climate and ice cover until May. According to Engström et al. (2010), the DSi and $\delta^{30}Si_{DSi}$ values of the Kalix River are mainly controlled by the weathering of silicate minerals, Si absorption by the boreal forest trees, dissolution of biogenic

EBSCOhost - printed on 2/10/2023 8:05 PM via . All use subject to https://www.ebsco.com/terms-of-use

silica in the soil and Si uptake by fresh water diatoms in lakes. Chemical weathering and biological activity in the Kalix River area are slightly stronger than those in the Swiss and Icelandic rivers, but much weaker than that in the Yangtze River catchment.

The Congo River is situated in tropical Central Africa. Its main branch and largest tributaries have an average $\delta^{30}Si_{DSi}$ value of 0.98‰; while small tributaries have an average $\delta^{30}Si_{DSi}$ value of 0.02‰ (Cardinal et al., 2010). As mentioned in Chapter 4, there are two different weathering regimes in the central Congo Basin (Cardinal et al., 2010): One is the regime of rain forests, wooded grassland and savanna, where newly formed clays that enriched in light Si isotopes remain stable; The other regime is characterized by swamps, where clays are dissolved by the action of organic matter, resulting in the delivery of light Si isotopes to rivers. The $\delta^{30}Si_{DSi}$ values of each regime are primarily controlled by silicate weathering intensity and the distribution of $\delta^{30}Si_{DSi}$ values in the Congo River therefore results mainly from mixing of water from two types of weathering regimes (Cardinal et al., 2010). Therefore, in a low relief and flooded area, organic acids may play a significant role in controlling weathering processes. It was concluded that the changes in the weathering intensity or extent of wetlands would lead to changes in the isotopic signal of Si delivered to the ocean (Cardinal et al., 2010).

The Amazon River is also situated in tropical area, whose $\delta^{30}Si_{DSi}$ was proposed to be influenced by three main factors, with an average of 0.98‰ (Hughes et al., 2013). The first is the formation of 2:1 clays, which probably cause a fractionation factor of −2.05‰. The second factor is the fractionation model followed in the different basins. The Rio Solimões clearly follows a Rayleigh fractionation model, while the Rio Madeira seems to follow a batch equilibrium model. The cause of this difference could be linked to the different mineralogy in this basin. The third factor is the fraction of dissolved Si incorporated in newly formed minerals. The clear relation between $\delta^{30}Si$ signatures and Si mobility in the Amazon Basin can be observed and may be used as a good proxy for Si mobility and thereby for clay formation. Compared to these factors, the effect of direct biological impact seems not so significant. All of these conditions may be the reasons that the Amazon River shows significantly lower $\delta^{30}Si_{DSi}$ values than those of the Nile River, the Yangtze River and the Siberian Rivers.

From the above comparison, it is clear that changes in the climate, weathering intensity and biological activity in the catchment areas can significantly influence the temporal and spatial distribution of DSi and $\delta^{30}Si_{DSi}$ values of individual river systems and the concentration and silicon isotopic composition of dissolved Si exported to the ocean. At this stage, the $\delta^{30}Si_{DSi}$ values of global rivers display a large range from −1.4‰ to 4.7‰, with an average of 1.4‰. More information on other large rivers may improve our understanding on the contribution of river system to the global Si cycle and Si isotope budget.

EBSCOhost - printed on 2/10/2023 8:05 PM via . All use subject to https://www.ebsco.com/terms-of-use

Magnitude of river DSi flux

Based on the discussion above, the modern river DSi flux is reasonably well constrained. Average river water DSi concentrations are ~160 μM (9.5 mg /L SiO_2) (Dürr et al., 2011b). Using nutrient model with a stepwise multiple linear approach, Beusen et al. (2009) predicts a DSi fluxes of 6.33×10^{12} mol yr^{-1} to the coastal ocean. A similar estimate (6.18×10^{12} mol yr^{-1}) was obtained by Dürr et al. (2011b). The data of Beusen et al. (2009) was accepted by Frings et al. (2016) and listed in Table 5.1.

$\delta^{30}Si_{DSi}$ of river flux

So far, more than 700 data of silicon isotope compositions of dissolve silicon in river water are reported (Figure 4.37B). The $\delta^{30}Si_{DSi}$ values vary from −1.4‰ to 4.7‰, with a mean of 1.35‰ and a standard deviation of 0.69‰. It is seen that seasonal and longitudinal variability of $\delta^{30}Si_{DSi}$ in river is typically large, on the order of 1.0‰. There are generally trends that: 1) $\delta^{30}Si_{DSi}$ in the river is higher than the minerals from which it ultimately derives; 2) $\delta^{30}Si_{DSi}$ in river decreases with increasing discharge; 3) There is no global relationship between $\delta^{30}Si_{DSi}$ and DSi concentrations; 4) Individual sampling stations tend to show seasonal variability of ca. 0.5‰ to 1.0‰ with lower values corresponding to high-discharge periods; 5) River $\delta^{30}Si_{DSi}$ tends to increase downstream (Figure 5.2).

The role of estuaries in modulating river Si fluxes

The estimates of sediment and DSi delivery via rivers to the ocean are based on the sampling of the river freshwater end-member, often a considerable distance upstream of its entrance to the ocean. It is acknowledged that storage of sediment fluxes between gauging stations and the end of the freshwater end-member may cause global sediment delivery to be overestimated (Allison et al., 1998; Milliman and Farnsworth, 2011). A similar problem exists with DSi as the river passes through the salinity gradient and across a continental shelf to reach the open ocean. Estuarine and other coastal environments are often highly productive. If this production removes Si and permanently stores it in estuarine or deltaic sediments, then the amount of DSi entering the global ocean will correspondingly decrease. Removal of DSi will be manifested as non-conservative mixing between the freshwater and saline end-members (Bien et al., 1958), and can occur biologically (Conley and Malone, 1992) and abiotically (Chou and Wollast, 2006). It has been reported that diatom blooms in the mixing zone may consume up to 50% of riverine DSi in the Amazon River (DeMaster, 2002) and almost 100% in the Scheldt (Chou and Wollast, 2006), although most of this will be regenerated. Using published transects along salinity gradients, DeMaster (2002) inferred 0.6×10^{12} mol Si yr^{-1} for estuarine Si removal based on the degree of non-conservative mixing (Table 5.1). The global estuarine surface area is ~1.1×10^6 km^2 (Dürr et al., 2011a), implying a sedimentation rate of ~33 g SiO_2 km^{-2} yr^{-1}, close to lake sedimentation rates (Frings et al., 2014a), and lower than the few estuarine BSi accumulation

EBSCOhost - printed on 2/10/2023 8:05 PM via . All use subject to https://www.ebsco.com/terms-of-use

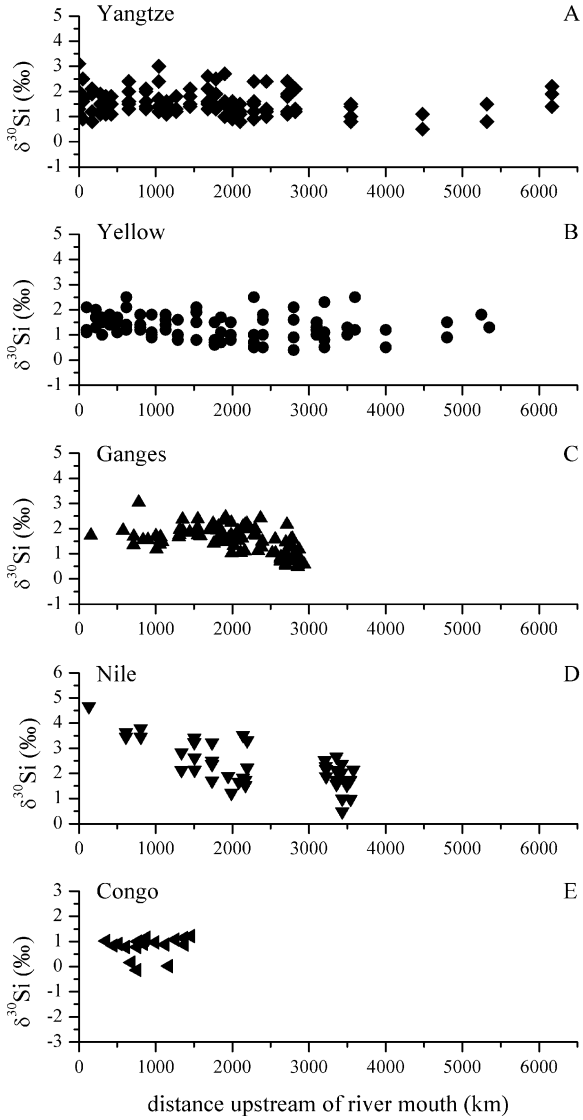

Figure 5.2: Longitudinal change in δ^{30}Si of river DSi. A: Yangtze (Ding et al., 2014); B: Yellow (Ding et al., 2016); C: Ganges (Fontorbe et al., 2013; Frings et al., 2015); D: Nile (Cockerton et al., 2013) and E: Congo (Cardinal et al., 2010).

rates found in the literature (60~500 g SiO_2 km^{-2} yr^{-1}) (Colman and Bratton, 2003; Qin et al., 2012; Carbonnel et al., 2013).

Isotopic effect of estuarine Si removal

DeMaster (2002) estimated that ~10% of river DSi is sequestered within estuaries today as biogenic silica. If this is associated with a typical fractionation of –1.1‰ (De La

EBSCOhost - printed on 2/10/2023 8:05 PM via . All use subject to https://www.ebsco.com/terms-of-use

Rocha et al., 1997), then the δ^{30}Si of river DSi entering the ocean is shifted towards a higher value by ~0.11‰ due to the presence of an estuarine filter, assuming no fractionation associated with reverse weathering. There is little work available to test this conclusion, and the available studies are equivocal. In the Tana River, Kenya, DSi mixes conservatively along the salinity gradient so there is no Si isotope fractionation (Hughes et al., 2012). In the Lena River delta, DSi is removed along the salinity gradient, but counter to expectations δ^{30}Si also decreases (Engström, 2009), interpreted as mixing with an unidentified ^{30}Si deplete water mass. Conversely, in the Elbe River estuary (Weiss et al., 2015) and the tidal freshwater section of the Scheldt river (Delvaux et al., 2013), DSi concentrations are depleted – presumably by biological activity – and δ^{30}Si of the residual DSi increases as expected, at least during the times of the year in which silicifying organisms grow.

Dissolution of river suspended particulate matter

Magnitude of DSi flux from dissolution of river particulate matter

River suspended particulate matter (SPM) is predominantly silicate material (Viers et al., 2009), some of which will dissolve in the ocean. Conventionally, river SPM is assumed to dissolve sufficiently slowly that it does not contribute to biological cycling. However, it need be only sparingly reactive to have a large effect (Oelkers et al., 2011; Jeandel and Oelkers, 2015), and recent work suggests that dissolution, desorption or ion-exchange of river SPM in estuaries and the coastal zone is indeed large enough to be a substantial component of ocean elemental or isotope budgets (Gislason et al., 2006; Jeandel et al., 2011; Jones et al., 2014; Oelkers et al., 2011). Estimates of the magnitude of the total river particulate flux cluster around $14\sim20 \times 10^9$ t yr^{-1} (e.g., Milliman and Meade, 1983; Syvitski et al., 2005) with a recent estimate being 19×10^9 t yr^{-1} (Milliman and Farnsworth, 2011). How much of this SPM will dissolve in the ocean? Insight can be gained by considering the amount of BSi carried by rivers, or by simple experimental approaches exploring the interaction of river sediment and seawater.

1) River transport of biogenic silica

Conley (1997) quantified the BSi material carried by rivers at $1.05 \pm 0.20 \times 10^{12}$ mol yr^{-1}, based on a simple extrapolation of surface water samples from a small dataset of 11 rivers. However, with a growing awareness that the conventional measurement protocols (weak alkali leaches, e.g., DeMaster, 1981) do not target BSi per se, but rather a range of non-crystalline siliceous phases, the term 'amorphous silica' (ASi) is now more prevalent (Barão et al., 2014, 2015), although some fraction of river SPM can indeed be 'true' BSi (Cary et al., 2005; Meunier et al., 2011). Dissolution rates of ASi are greater, by around a factor of 5, in the higher pH and electrolyte concentrations of seawater relative to freshwater ((Loucaides et al., 2008, 2012). As a result, the ASi fraction is assumed to dissolve rapidly along the salinity gradient, an assumption generally borne out in studies of estuarine particulate matter (Carbonnel et al., 2013; Lehtimäki et al., 2013; Pastuszak et al., 2008). Frings et al. (2014b) showed that in

EBSCOhost - printed on 2/10/2023 8:05 PM via . All use subject to https://www.ebsco.com/terms-of-use

the Ganges basin, the Si extracted by a conventional weak alkali leaching protocol (DeMaster, 1981) is a relatively consistent fraction (mean $\pm\sigma = 1.2 \pm 0.78\%$) of the total sediment load. Extending the calibration dataset to include 415 paired and globally distributed ASi-SPM measurements, Frings (2014) estimated that ~0.6% of global river SPM is 'ASi'. Taking a total SPM flux of 19×10^9 t, this implies that 1.9×10^{12} mol yr^{-1} ASi is carried by rivers.

2) Experimental approaches

Experimental work to investigate the interaction of river sediment and seawater has mostly used riverbed material from basaltic islands (e.g., Jones et al., 2012a,b; Pearce et al., 2013; Oelkers et al., 2011), though Jones et al. (2012b) also used material from the Amazon, Mississippi and Orange rivers. Over the full course of these experiments, only about 0.005 to 0.01% of the Si in the sediment was solubilized. However, given the high solid:solution ratios (ca. 1:3), a near-equilibrium concentration was quickly obtained, impeding further dissolution. Focusing on basaltic glass, Morin et al. (2015) confirmed Si dissolution rates increase as a function of salinity. Their experiments were conducted at 90°C, and based on an extrapolation to 16°C and assumptions about the quantity of sediment deriving from volcanic islands, they argue $2\sim8 \times 10^{12}$ mol Si yr^{-1} is released from basaltic glass dissolution alone, broadly equivalent to the river DSi flux. The young, basaltic sediment used in these studies is known to have high dissolution rates (Dupré et al., 2003) but is unlikely to be representative of global river SPM. These problems hamper extrapolation of the results to a global scale – further field or lab-based approaches in granitic or meta-sedimentary terrains are required. Nevertheless, they demonstrate the potential importance of dissolution of terrigenous material, which is reinforced by a mass-balance of the Mediterranean Si cycle that invokes dissolution of 1% of river SPM to close the budget (Jeandel and Oelkers, 2015).

Given that the ASi content of river SPM is of a very similar order of magnitude, this suggests the two approaches at least partially target the same Si. The relevant questions then become: 1) To what extent do the measurement protocols for river ASi reflect the behavior of river sediment in seawater? 2) To what extent do the extraction protocols target amorphous silica? and 3) To what extent is there a discrete ASi pool? These questions require further research. For the time being, we assume that the protocols developed for BSi analysis (e.g., DeMaster, 1981) fortuitously capture the amount of all Si likely to dissolve in seawater – both amorphous and lithogenic – and, therefore, take a flux of 1.9×10^{12} mol yr^{-1} as the input of DSi to the ocean from terrigenous sediment dissolution, which may need revising upwards if the results of Morin et al. (2015) can be confirmed.

δ^{30}Si of DSi flux from dissolution of river particulate matter

The δ^{30}Si of bulk SPM has been measured only in the Yellow (Ding et al., 2011, 2016) and the Yangtze rivers (Ding et al., 2004, 2014). The spatial and temporal variations

EBSCOhost - printed on 2/10/2023 8:05 PM via . All use subject to https://www.ebsco.com/terms-of-use

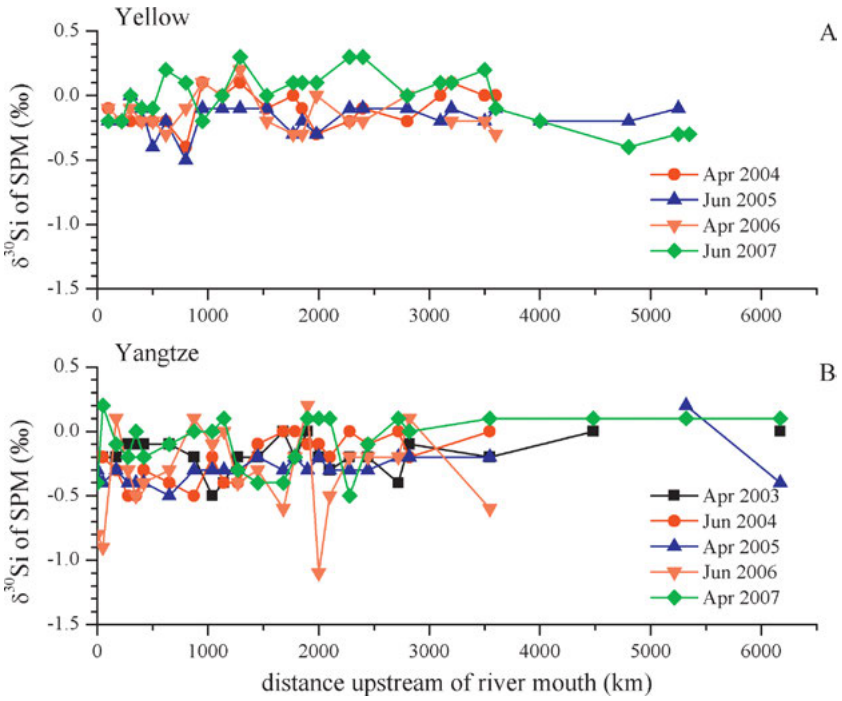

Figure 5.3: Longitudinal and temporal variations of $\delta^{30}Si_{SPM}$ in the Yangtze River and Yellow River. A: Yellow River (Ding et al., 2016); B: Yangtze River (Ding et al., 2014).

of $\delta^{30}Si_{SPM}$ values in these two rivers are shown in Figure 5.3. Both systems have low $\delta^{30}Si_{SPM}$, but the mean value (−0.02‰) of the Yellow River is about 0.3‰ higher than that (−0.34‰) of the Yangtze River. From upper stream to downstream, there is a general decrease trend of $\delta^{30}Si_{SPM}$ in both rivers. Besides, the samples collected in the dry season (April of 2004 and 2006) show generally lower $\delta^{30}Si_{SPM}$ values than those collected in wet season (July of 2003, 2005 and 2007). These variations seem to be related to the clay/sand ratio in the SPM (Ding et al., 2014, 2016). The $\delta^{30}Si$ of ASi has never been directly assessed in river sediment, although we can extrapolate from terrestrial ecosystem studies that these phases, whether formed biogenically (e.g., diatoms, phytoliths) or inorganically (e.g., poorly crystalline aluminosilicates), should tend towards even lower $\delta^{30}Si$. At this stage, we may take the mean of the Yellow and Yangtze Rivers of −0.18 ± 0.25‰ as a representative of the Si isotopic composition of terrigenous sediment.

Submarine groundwater discharge (SGD)

Magnitude of DSi flux from submarine groundwater discharge

It has long been recognized that the discharge of water from groundwater directly into the ocean may be a significant term ecologically, chemically and volumetrically (Jo-

EBSCOhost - printed on 2/10/2023 8:05 PM via . All use subject to https://www.ebsco.com/terms-of-use

hannes, 1980). Even if the flow rates are low, integrated over the entire length of a shoreline and combined with the generally higher solute concentrations in groundwater, SGD fluxes can be important (Moore, 1996). The patchy and variable nature of this water flux has made it difficult to quantify (Burnett et al., 2006). Nevertheless, significant regional inputs of DSi from SGD have been demonstrated in, e.g., the Mediterranean (Rodellas et al., 2015; Weinstein et al., 2011), the Bay of Bengal (Georg et al., 2009a) and from volcanic islands (Schopka and Derry, 2012).

The only global estimates of the SGD contribution to the ocean Si budget are 0.4 and 0.6×10^{12} mol DSi yr^{-1} to the oceans, or approximately 6~10% of the river DSi flux (Laruelle et al., 2009; Tréguer and de La Rocha, 2013). These are based on the product of a total SGD of 2 000 km^3 yr^{-1} (Slomp and Van Cappellen, 2004) and an arbitrarily assigned groundwater DSi concentration of 200 or 340 µM. Building on this approach, we note that estimates of the volume of SGD (Slomp and Van Cappellen, 2004; Knee and Paytan, 2011; Burnett et al., 2006; Taniguchi et al., 2002) range from 0.1 to 10% of the global river flux (approximately 37×10^3 km^3 yr^{-1}; Dai and Trenberth, 2002). These estimates are commonly based on global water budgets, with SGD being the residual of the other terms, such that the propagated uncertainty is of the same order of magnitude as the flux itself. Nonetheless, a consensus seems to be developing for a total flux of approximately 5% of river discharge, i.e., 1850 km^3 yr^{-1}, which we retain as the total SGD water flux with an uncertainty of ±50%.

Concerning the 'mean' groundwater DSi concentration, no systematic survey of global groundwater geochemistry is available. Based on the data of 1785 European bottled waters (Birke et al., 2010) and the database maintained by the USGS, Frings et al. (2016) suggested a total SGD DSi flux of $(0.65 \pm 0.54) \times 10^{12}$ mol yr^{-1} or about 10% of the river DSi flux, which is very close to the value suggested by Tréguer and de La Rocha (2013). We therefore retain the value of 0.6×10^{12} mol Si yr^{-1} as the SGD flux.

δ^{30}Si of DSi flux from submarine groundwater discharge

The range of δ^{30}Si reported for groundwater DSi is large and spans from −0.15‰ to +1.34‰ at various depths in the Bengal Basin (Georg et al., 2009a), from +0.35‰ to +1.01‰ for Icelandic springs (Opfergelt et al., 2011a), from −1.42 to +0.56‰ along a 100 km flowpath in a sandstone aquifer in Arizona (Georg et al., 2009b) and from −1.50 to −0.85‰ in the Great Artesian Basin, Australia (Pogge von Strandmann et al., 2014). Isolated values of +0.3‰, +0.5‰ and +0.7‰ have also been reported in Hawaiian systems (Ziegler et al., 2005a,b), and up to +2.07‰ in a Siberian permafrost landscape (Pokrovsky et al., 2013). Unsurprisingly, given the diversity of systems and processes, there is no relationship between groundwater DSi concentration and δ^{30}Si. We take the mean of the 25 published values of +0.12‰, with a range of ±1.0‰, as representing the δ^{30}Si of groundwater DSi inputs to the ocean.

EBSCOhost - printed on 2/10/2023 8:05 PM via . All use subject to https://www.ebsco.com/terms-of-use

DSi inputs from dissolution of atmospheric dust

Magnitude of DSi flux from dissolution of aeolian dust

All global Si budgets to date (Laruelle et al., 2009; Tréguer et al., 1995; Tréguer and de La Rocha, 2013) take a value of 0.5×10^{12} mol Si yr^{-1}. Somewhere between 500 and 5000×10^{12} g dust yr^{-1} is currently entrained into the atmosphere (Engelstaedter et al., 2006), of which 134 to 910×10^{12} g yr^{-1} is deposited in the oceans (Duce et al., 1991; Jickells et al., 2005). This is mostly in the form of wet deposition, i.e., scavenged by precipitation, although gravitational ('dry') settling of larger particles may be important in nearshore environments (Prospero and Arimoto, 2008). If the composition of the upper continental crust (Rudnick and Gao, 2003) reflects the composition of mineral dust (67% of SiO_2), somewhere between 1.5 and 10.2×10^{12} mol Si yr^{-1} is deposited on the ocean surface.

Anywhere between < 1% to more than 10% may potentially dissolve (Guerzoni et al., 1999; Tegen and Kohfeld, 2006), and a single value is hard to prescribe given regional differences in source composition, particle size, etc. Estimate (0.5×10^{12} mol yr^{-1}) made by Tréguer and de La Rocha (2013) is probably an upper bound. Clearly, the two key terms in this derivation (dust deposition rates and Si solubility) need much better quantification.

δ^{30}Si of DSi flux from dissolution of Aeolian dust

In the absence of direct measurements, there are two means of identifying the silicon isotope composition of Aeolian dust. The mean of published bulk soil δ^{30}Si determinations (Figure 4.36), equal to -1.21 ± 0.70‰ ($n = 122$), may suffice if soils can be considered broadly representative of the sources of dust to the ocean. Alternatively, the Pleistocene loess samples analyzed by Savage et al. (2013a) provide a mean of -0.22 ± 0.07‰ ($n = 14$), and a similar value of −0.2‰ provided plausible results in an endmember analysis of Si sources in the glacial east Philippines Sea (Xiong et al., 2015). However, loess deposits tend to be towards the larger end of the dust size spectrum (Muhs, 2013), while the long-range transport particles that enter the marine realm may be smaller clays that tend towards lower δ^{30}Si values. We therefore take a value intermediate between soils and loess of −0.65‰, but suggest that it should be empirically determined in future.

5.1.1.3 Potential for variability in continent-ocean Si fluxes

Impact of glacial climate on land-to-ocean Si fluxes

Impact of glacial climate on the river DSi flux and δ^{30}Si

The river DSi flux is the single largest input to the ocean, but inferring potential variability on glacial–interglacial (G–IG) timescales is difficult, partly because the parameters controlling DSi fluxes are not well understood and are probably compensatory to some degree (Kump and Alley, 1994). It is known that the flux, and its associated

EBSCOhost - printed on 2/10/2023 8:05 PM via . All use subject to https://www.ebsco.com/terms-of-use

δ^{30}Si, can vary in two ways (Frings et al., 2016): 1) via changes in the silicate weathering rate and the weathering style; 2) via changes in continental Si cycling, particularly the presence and efficiency of continental Si sinks (Billen et al., 1991; Meybeck and Vörösmarty, 2005). We know that first-order controls on silicate-weathering rates include temperature, water availability and lithology, plus the tectonic parameters that affect the exposure of new material (West et al., 2005). These parameters control the degree of soil development, physical erosion rates, catchment hydrology and ecosystem structure, which may be more direct determinants of silicate weathering rates. However, in practice, this makes it rather difficult to predict the change of silicate-weathering rates over G–IG cycles.

Based on the modelling of river DSi fluxes using lithology-specific runoff-Si flux relationships (Jones et al., 2002; Gibbs and Kump, 1994; Munhoven, 2002), Frings et al. (2016) assumed that the river DSi flux has been relatively invariant (±20%) since the last glacial maximum (LGM). They demonstrated that a decrease in Si fluxes resulting from lower continental precipitation was largely balanced by increased fluxes from newly-exposed continental shelf.

However, the $\delta^{30}Si_{DSi}$ of the river might be more variable. River $\delta^{30}Si_{DSi}$ primarily reflects weathering congruency, so if this could be inferred or reconstructed it can constrain the magnitude of any change in river $\delta^{30}Si_{DSi}$. Qualitatively, we suggest that the river DSi at the LGM likely had a lower associated δ^{30}Si. Mechanistically, lower glacial river δ^{30}Si may result from 1) reduced catchment fluid and/or sediment residence times, 2) lower temperatures acting to lower rates of secondary mineral formation via a reduction in the rate constants of precipitation or 3) the greater relative formation of 2:1 clays over 1:1 clays, which tends to be associated with a smaller magnitude of fractionation (Opfergelt and Delmelle, 2012). Altogether, these can act to reduce the total magnitude of clay formation (increase weathering congruency) and, therefore, reduce the expression of Si isotope fractionation during glacials. Thus, Frings et al. (2016) suggested a conservative reduction of 0.2 ± 0.25‰ of river DSi at the LGM relative to today.

Impact of glacial climate on the dust flux and δ^{30}Si

Marine and terrestrial sediments and ice-cores from both poles consistently show increased dust accumulation rates over the LGM (Muhs, 2013). Glacial dust fluxes have received attention for their potentially important role as a source of nutrients (particularly Fe or Si) to regions of the oceans where (siliceous) primary production is currently limited by lack of these nutrients (Harrison, 2000; Jickells et al., 2005; Martin, 1990). Due to expanded dust production areas, greater entrainment capabilities (drier soils and higher winds) and greater transport capacity due to less efficient washout (Muhs, 2013; Tegen and Kohfeld, 2006), total dust input to the glacial ocean was 2~10 times higher than modern deposition rates. Frings et al. (2016) assume that even if loci

EBSCOhost - printed on 2/10/2023 8:05 PM via . All use subject to https://www.ebsco.com/terms-of-use

of dust production are variable, the solubility and mean isotopic composition (i.e., -0.67 ± 0.45; Table 5.1) of the dust as estimated above are invariant.

Impact of glacial climate on the river sediment flux and δ^{30}Si

The boundary conditions that control river sediment export (e.g., temperature, precipitation, glacial activity and basin area) change over glacial cycles. Some larger rivers have sediment deliveries buffered by their alluvial plains on timescales as long as quaternary glacial cycles (Métivier and Gaudemer, 1999), although this does not apply to all large rivers (Clift and Giosan, 2014). Glaciers and ice-sheets produce large amounts of finely ground glacial flour, but the extent to which this contributes to enhanced sediment fluxes rather than providing for a potential post-glacial pulse (Vance et al., 2009) is unclear. Overall, Frings et al. (2016) consider that the net sediment load carried by rivers at the LGM was between 1 and 2 × modern (preindustrial) values. They make a simplifying assumption that the percentage of this sediment liable to dissolve was a constant fraction, and assume no post-glacial sediment pulses or lags, and that it had a constant δ^{30}Si.

Impact of continental ice-sheets on land-to-ocean Si fluxes

Subglacial and periglacial silicate weathering is different in style to subaerial weathering. Analysis of subglacial streams shows that silicate weathering tends to be more congruent, as evidenced by high Ge/Si (approaching the Ge/Si ratio of bedrock) and elemental stoichiometries (Tranter, 2005), and tends to be driven by acidity not sourced from atmospheric carbon (Anderson, 2005; Wadham et al., 2010). The few investigations of $\delta^{30}Si_{DSi}$ in glaciated catchments (Georg et al., 2007b; Opfergelt et al., 2013) show that these tend to be low δ^{30}Si rivers that approach the parent material isotopic composition. Therefore, a world with increased sub- or peri-glacial solute generation could perhaps be expected to introduce low $\delta^{30}Si_{DSi}$. Opfergelt et al. (2013) found a difference in δ^{30}Si of 0.8‰ between glaciated and non-glaciated catchments in Iceland and estimated a net decrease in river δ^{30}Si of 0.12‰ due to the presence of the high-latitude ice sheets, mountain ice-caps and valley glaciers.

Impact of lowered sea-level on land-to-ocean Si fluxes

At the LGM, global eustatic sea levels were approximately 130 m lower as a result of water storage in the polar ice caps (Lambeck et al., 2014). This may affect the inputs to the global ocean and ocean Si cycling in at least three ways: 1) a reduction in the 'fluvial filtering' of land to ocean fluxes, 2) the exposure of new land surface to subaerial weathering and remobilization of 'old' BSi, with an associated reduction in the area of continental shelf available for neritic BSi sedimentation and 3) alteration to groundwater flow dynamics.

EBSCOhost - printed on 2/10/2023 8:05 PM via . All use subject to https://www.ebsco.com/terms-of-use

Reduction in the 'fluvial filtering' of land to ocean fluxes

The base level of a river system is the lowest level to which it can be subaerially eroded, usually at sea level. In response to a sea-level change and, therefore, a channel shortening or lengthening, a river network can aggrade or incise to adjust towards a new equilibrium profile, although the nature of the adjustment depends on shelf and channel gradients, sediment supply, stream power, etc. Frings et al. (2016) speculate that water/sediment interaction times in alluvial plains were lower at the LGM because of the lowered base-level. In this condition, the secondary mineral formation will be reduced, with a correspondingly lower exported δ^{30}Si, which could cause the mean river $\delta^{30}Si_{DSi}$ to decrease by up to 0.2‰.

Lakes also act as biogeochemical reactors, converting some fraction of inflowing DSi into BSi and burying it in their sediments (Frings et al., 2014a; Harrison et al., 2012). This retention must shift δ^{30}Si of the residual DSi higher (Frings et al., 2014a; Hughes et al., 2012). During glacial periods, there were fewer lakes, causing less DSi retention and smaller fractionation. These may constitute a further lowering of fluvial δ^{30}Si by ca. 0.1‰ in glacial periods (Frings et al., 2016).

Estuaries provide a final example of how a less efficient fluvial filter may have altered river Si fluxes on millennial timescales. During the LGM when river discharge into the ocean was mostly direct (Kennett, 1982), a near cessation of estuarine Si filtering could conceivably lower the net δ^{30}Si of river DSi entering the open ocean by ~0.1‰ (Frings et al., 2016).

Exposure of continental shelf

BSi accumulation rates on continental shelves are high (~1.8×10^{12} mol yr^{-1}) because of high production rates and higher preservation efficiencies (DeMaster, 2002). This means that there are massive pools of BSi that could potentially become available to subaerial weathering during sea level lowstands. The δ^{30}Si of this is unknown, but it could alter the mean δ^{30}Si of river DSi by ±0.1‰ (Frings et al., 2016).

Potential modification of submarine groundwater discharge at the LGM

A lowering of base level both allows for greater freshwater storage in continental aquifers (Adkins et al., 2002) and increases the hydraulic gradient, which may be expected to increase the glacial submarine groundwater discharge (SGD) flux relative to today. Assuming a glacial SGD increase is counterbalanced by a decrease in river runoff of the same magnitude, Frings et al. (2016) estimated that the δ^{30}Si of SGD is held constant.

Impact of altered vegetation zonation on land-to-ocean Si fluxes

At the LGM, there was a general equatorward contraction in the zonation of vegetation communities towards lower altitudes and latitudes, and an expansion of grasslands

EBSCOhost - printed on 2/10/2023 8:05 PM via . All use subject to https://www.ebsco.com/terms-of-use

at both low and high latitudes (Harrison and Prentice, 2003). However, it is unclear to what extent there are systematic differences in silicate weathering rates beneath various biomes. The ratio of export of fractionated material to initial solubilization from bedrock is a key control on the silicon isotope composition of river water (Bouchez et al., 2013). If a larger fraction of the total Si exported is detrital biogenic opal or other secondary (alumino)silicates, then the degree of fractionation relative to bedrock of the residual DSi should be more pronounced. Vegetation and its associated fungal and bacterial communities are key players in soil/clay formation; it is likely that some biomes are more efficient at producing secondary solids than others. And some ecosystems may export more Si as biogenic Si. Besides, vegetation zonation may alter land-to-ocean Si fluxes through transient changes in the size of the ecosystem Si pool. There is the potential for a transient increase or decrease in river DSi fluxes and/or associated changes in δ^{30}Si as the pool aggrades or depletes. However, the impact of altered vegetation zonation on land-to-ocean Si fluxes cannot be evaluated clearly at this stage. It can be considered in combination with an impact of glacial climate on the river DSi flux and δ^{30}Si.

Synthesis of potential changes

A summary made by Frings et al. (2016) of these mechanisms for change, together with estimates of their impact on the Si flux magnitude and isotope composition, is presented in Table 5.2 and graphically in Figure 5.4. Overall, the total inputs of DSi to the ocean have declined slightly from the LGM to today, and that the weighted δ^{30}Si

Table 5.2: Summary of plausible changes to the magnitude and/or Si isotopic composition of dissolved Si inputs to the ocean, for the LGM relative to today. After Frings et al. (2016).

Altered flux	Mechanism for alteration	Change in associated DSi flux	Change in associated δ^{30}Si (‰)
River DSi	Altered weathering regimes	± 20%	−0.45 to +0.05
	Subglacial weathering		−0.15 to 0
	Lesser lake Si retention		−0.10 to 0
	Less alluvial plain interaction		−0.10 to +0.1
	Remobilization of continental shelf BSi deposits		−0.10 to 0
	Reduced estuarine filter	0~10%	−0.10 to 0
	Net:	−20 to +30%	−1.00 to +0.05
Dust	Greater dust generation; less efficient continental rainout	2~10 ×	Constant
River SPM	Increased glacial flour production, less vegetation stabilization	1~2 ×	Constant
SGD	Greater groundwater flow due to greater hydraulic head	1~2 ×	Constant

EBSCOhost - printed on 2/10/2023 8:05 PM via . All use subject to https://www.ebsco.com/terms-of-use

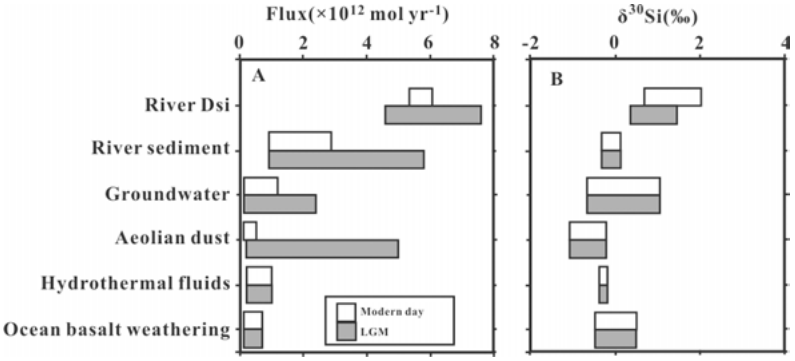

Figure 5.4: A visual depiction of potential changes in the magnitudes (A) and δ^{30}Si (B) of DSi fluxes to the ocean between modern day and LGM. The figure emphasizes that the most likely mechanism of altering the glacial ocean Si cycle is via a change in the relative importance of the individual fluxes, rather than via a change in their δ^{30}Si. After Frings et al. (2016).

of these inputs may have been up to 1‰ lower at the LGM, larger than the changes envisaged by previous work (Opfergelt et al., 2013; Georg et al., 2009a).

5.1.2 The oceanic Si sub-cycle

Silicon is a key nutrient element in the ocean. It is crucial to marine living organisms including mainly diatoms and siliceous sponges, and can be utilized by many others such as radiolarians, silicoflagellates, etc. Over the last few decades, we have realized that the marine silicon cycle is strongly linked to the carbon and nitrogen cycles, and thus the marine primary productivity, biological pump, and hence the global climate change (Tréguer et al., 1995; Ragueneau et al., 2006; Sarmiento et al., 2007). Since then, the silicon isotopic composition of seawater and silicon isotope signals preserved in sedimentary records (such as fossil diatoms, radiolarians and sponge spicules retrieved from marine sediment cores) has been considered to be a powerful tool to understand the marine silicon cycle in the present and in the geological past.

Dissolved silicon (DSi), which exists in the form of orthosilicic acid [$Si(OH)_4$], is the dominant inventory of Si in the ocean. Generally, DSi concentration is much lower in the surface ocean (~10 μM on average at ocean's surface) than in the deep ocean (~100 μM on average at 2 000 m). In the surface water, oceanic DSi concentration varies drastically, from <2 μM in most part of open ocean, to ~50 μM or even higher in the high nutrient-low chlorophyll (HNLC) regions, e.g., the Southern Ocean and the North Pacific (Garcia et al., 2009). Such vertical and horizontal distribution patterns are resulted mainly from the biological utilization. Marine diatoms are very competitive phytoplankton which contribute 20~25% of the global primary production, ~45% of the marine primary production and ~90% of biogenic silica production (Yool and Tyrrell, 2003; Canfield et al., 2005), due to their "boom and bust" ecological strategy

EBSCOhost - printed on 2/10/2023 8:05 PM via . All use subject to https://www.ebsco.com/terms-of-use

and probably their utilization of silicon. They are the main drivers of marine silicon cycle (Tréguer and de La Rocha, 2013), taking up DSi from the surface water within the euphotic zone, forming their opaline cell walls (frustules), transporting Si in the form of biogenic silica (opal) to the ocean's interior, and returning to DSi while being dissolved, or leaving the ocean as being buried in marine sediment. The biogeochemical flux of Si derived from diatom production is greater than the sum of any other input by at least an order of magnitudes, causing extensive silica unsaturation in the modern ocean. The near-exhausted DSi inventory is largely balanced by the dissolution of biogenic opal occurring at all depth from the surface mixed layer to the deep ocean and sediment-water interface, with most of the gross production recycled within the water column. The rest of the small portion of biogenic silica is preserved in marine sediments. The net export of biogenic silica are compensated mainly by river input and other input sources such as Aeolian dust, groundwater inputs, hydrothermal fluid and seafloor weathering (Tréguer and de La Rocha, 2013; Poitrasson, 2017).

5.1.2.1 Present-day input of DSi to the global ocean

Summary of continental input sources

As discussed in the Section 5.1.1 and listed in Table 5.1, the continental input fluxes, i.e., river DSi, river SPM, groundwater, Aeolian dust and related buffering effect of continental biogenic silica are in total 8.7×10^{12} mol Si yr^{-1}, making up about 90% of the gross silicon input to the ocean. Among these input sources, the river DSi input (5.7×10^{12} mol Si yr^{-1}) accounts for ~60%. An important feature of these processes is that the continental Si inputs are essentially unidirectional fluxes (Frings et al., 2016).

Non-continental input sources

Besides the continental sources, there are two rather minor but not least important non-continental or marine sourced DSi inputs, the marine hydrothermal processes and seafloor (basalt) weathering. Although they are probably less important than the riverine input and biogeochemical processes in modern context, they have the potential to affect local Si budget and isotopic composition in the ocean. More importantly, their magnitude and significance were much greater in the Earth's early history and they were the key component of the silicon cycle in the Archean and Proterozoic ocean (e.g., Ding et al., 2017; see Section 5.2). These two input sources involve water–rock reactions occurring at both high (>300°C) and low temperatures (<80°C). The definitions of fluids sourced from these two processes are somehow ambiguous. Here, we retain the identification of these two sources by the original literatures.

Magnitude and δ^{30}Si of DSi flux from marine hydrothermal processes

The marine hydrothermal process was once much more extensive than the present in the geological past when massive banded iron formations (BIFs) with iron-rich layers

EBSCOhost - printed on 2/10/2023 8:05 PM via . All use subject to https://www.ebsco.com/terms-of-use

and alternate silicon-rich layers deposited. The hydrothermal inputs were divided into two types: the axis hydrothermal systems with high temperature (>300°C), mobilizing silicon from the silicate melt, and the off-axis ridge flank systems where temperature is lower (<80°C) and clay minerals precipitate from the fluids (Tréguer and de La Rocha, 2013).

The estimate of DSi input from marine hydrothermal processes was initially made by the Ge/Si ratio method, which yielded a hydrothermal Si flux of $(0.2 \pm 0.1) \times 10^{12}$ mol Si yr^{-1} (Mortlock et al., 1993; Tréguer et al., 1995). However, this method underestimated the Si flux because it overlooked the non-opaline germanium sinks in the ocean and was biased from estimates derived from heat budget based water fluxes of $0.43\sim0.66 \times 10^{12}$ mol Si yr^{-1} and 0.65×10^{12} mol Si yr^{-1} (for axial only; Elderfield and Schultz, 1996; Wheat and McManus, 2005), although the latter ones themselves were also complicated by uncertainties of the average temperature of water flux off the axis of the mid-ocean ridges. The difficulties in constraining the off-axis water flux resulted in large errors in the estimation of off-axis DSi component. For example, Wheat and McManus (2005) concluded such flux alone could be as large as 10% of the total Si influx to the ocean (0.85×10^{12} mol Si yr^{-1}), while another study suggested values at least an order of magnitude lower (Tréguer and de La Rocha, 2013). Tréguer and de La Rocha (2013) reestimate the hydrothermal input and reported $(0.6 \pm 0.4) \times 10^{12}$ mol Si yr^{-1} for the axis plus ridge flank hydrothermal systems. This relatively new estimate included results from Ge/Si ratio corrected for non-opaline Ge sink and Ge isotope budget and we suggest this value as the best estimation of total hydrothermal input.

The study on the silicon isotopic composition of hydrothermal input is scarce. Currently, our knowledge of the δ^{30}Si of hydrothermal fluids comes from a single study. De La Rocha et al. (2000) reported the δ^{30}Si of two high temperature (255~355°C) hydrothermal fluid samples from the East Pacific Rise, both collected by the deep submergence vehicle *Alvin* (De La Rocha et al., 2000). The δ^{30}Si of sample with higher temperature and DSi is −0.4‰ and the other is −0.2‰, similar to the average of basaltic rocks (−0.3‰; see Chapter 4), consistent with the silicate melt origin of hydrothermal DSi and little isotopic fractionation accompanied at high temperature. Meanwhile, these δ^{30}Si values are higher than those of the hydrothermal vents (−1.5‰; see Chapter 4) by 1.2‰, consistent with the relatively large kinetic isotopic fractionation during precipitation. Although such small sample capacity excludes the possibility of any statistics, the results also suggest that the one with higher temperature, higher DSi and lower δ^{30}Si represent a sample that is closer to the primitive fluid composition.

Magnitude and δ^{30}Si of DSi flux from seafloor weathering

Seafloor weathering is the alteration or dissolution of mainly basalt in the oceanic crust or other terrigenous silicate-bearing sediments. It is a potential cause for the evolution of seawater elemental and isotopic compositions (e.g., Jaffres et al., 2007; Coggon et al., 2010; Grozeva et al., 2017). An early study by Tréguer et al. (1995) es-

EBSCOhost - printed on 2/10/2023 8:05 PM via . All use subject to https://www.ebsco.com/terms-of-use

timated that the annual silica flux through basalt weathering alone is $(0.4 \pm 0.3) \times 10^{12}$ mol Si yr^{-1}. A more recent review by Tréguer and de La Rocha (2013), after taking account for the dissolution of basalt and other terrigenous materials such as shale, clay and sand, updated the number into $(1.9 \pm 0.7) \times 10^{12}$ mol Si yr^{-1}, which is generally in agreement with the seafloor weathering flux calculated from the opal-poor regions using area extrapolation (Tréguer et al., 1995). However, as can be seen from the uncertainty given by those literatures, the flux of seafloor weathering still remains poorly constrained. After considering values estimated from various studies and reviews (Tréguer et al., 1995; Canfield et al., 2005; Tréguer and de La Rocha, 2013; Frings et al., 2016; Poitrasson, 2017), the input silica flux of the early version 0.4×10^{12} mol Si yr^{-1} is suggested.

The isotopic composition of silica flux from seafloor weathering is also poorly understood. The δ^{30}Si of basalt is on average −0.3‰ (see Chapter 4). On one hand, there is little silicon isotopic fractionation during most dissolution processes of minerals. On the other hand, the precipitation of secondary aluminosilicates occurred in altered seafloor basalts suggests that during the alteration there is probably associated isotopic fractionation (Frings et al., 2016). We here take the provisional estimate from Frings et al. (2016). As in their review, Frings et al. (2016) pointed out straightforward that the DSi fluxes derived from basalt in the oceanic crust are probably the most poorly understood among all rings in the chain of the global silicon cycle. More work needs to be done to precisely constrain the flux and isotopic composition of this input source.

5.1.2.2 Present-day output of BSi from the global ocean

Biogeochemical processes are the major components of marine silicon cycles (Tréguer and de La Rocha, 2013). The production of biogenic silica (BSi) with diatom and other origins and its transport, dissolution and recycling in the water column largely control the distribution of DSi, δ^{30}Si of seawater and the Si cycle of the ocean. Moreover, the BSi preserved in marine sediment provides important evidence for the Si cycle in the geological past. In the modern context, the most important output flux of silicon is the permanent burial of biogenic silica produced by diatoms. Contribution from radiolarians and silicoflagellates are likely much less, while siliceous sponge may act as a significant silica sink. Abiotic chemical precipitation is negligible in the modern ocean. However, as similar as the hydrothermal process and seafloor weathering, it is of great importance in the Precambrian ocean. Here, we will discuss the production and burial of diatom BSi and the biogeochemistry of siliceous sponge.

BSi production by diatoms

Magnitude of diatom BSi flux

Among all silica producers, diatoms are the most important organisms which contribute ~45% of the total oceanic primary production and over 90% of biogenic silica

EBSCOhost - printed on 2/10/2023 8:05 PM via . All use subject to https://www.ebsco.com/terms-of-use

production (Yool and Tyrrell, 2003; Canfield et al., 2005). According to an early estimation, the gross production of biogenic silica in the ocean is $(240 \pm 40) \times 10^{12}$ mol Si yr^{-1}, or $200\sim280 \times 10^{12}$ mol Si yr^{-1}, with the upper limit determined using global oceanic primary production, relative contribution of diatoms and a mean Si/C ratio, and the lower limit using a multi-compartment model (PANDORA) of nutrient, biological export of BSi and observed mean dissolution-to-production ratio of biogenic silica in the upper ocean (Nelson et al., 1995). Tréguer and de La Rocha (2013) recalculated biogenic silica production from coastal zones, open ocean and the Southern Ocean. In total, they found the sum of the oceanic BSi production obtained from the above three types of regions was totally 239×10^{12} mol Si yr^{-1} (136×10^{12} mol Si yr^{-1}, 23×10^{12} mol Si yr^{-1} and 80×10^{12} mol Si yr^{-1} for coastal zones, open ocean and Southern Ocean, respectively), almost identical to the early estimation. We therefore take 240×10^{12} mol Si yr^{-1} as the value of global BSi production.

Isotopic fractionation related to diatom production

The results from studies on silicon isotopic composition of diatoms have been presented in Chapter 4 of this book. In general, the δ^{30}Si of marine diatoms ranges from −0.7‰ to +3.1‰ with an average of +1.0‰. Compared to the δ^{30}Si of DSi in seawater where the diatoms grow, i.e., the upper 50 m or 100 m of water column, the δ^{30}Si of diatoms is lower by ~1.1‰ (Figure 5.5), which means that diatoms preferentially take up lighter silicon isotopes while they form their frustules. This simple, global statistic-

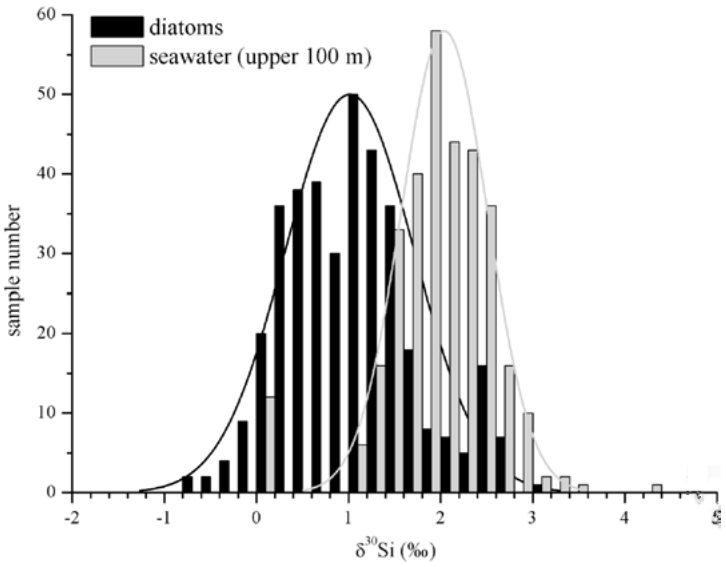

Figure 5.5: Comparison of diatom and surface seawater (upper 100 m) δ^{30}Si. See Figure 4.37 and Figure 4.41 for references.

EBSCOhost - printed on 2/10/2023 8:05 PM via . All use subject to https://www.ebsco.com/terms-of-use

based $\Delta^{30}Si_{diatom-SW}$ = −1.1‰ is identical to the results from the first silicon isotope study on diatoms cultured in laboratory by De La Rocha et al. (1997), and is within the range of some later culture experiments (−1.2 ~ −0.7‰ and −1.5‰; Sutton et al., 2013; Sun et al., 2014). Several field study at natural condition in the iron-depleted Southern Ocean suggest similar fractionation factors such as −0.9‰ ($\Delta^{29}Si_{diatom-SW}$ = −0.45‰) (Cardinal et al., 2005), −1.2‰ (Fripiat et al., 2011a) and −0.8 ~ −2.1‰ (Cardinal et al., 2007). It is also close to the values determined during the U. S. Southern Ocean Iron Fertilization Experiment (SOFeX) (−1.9 ~ −1.1‰; Varela et al., 2004) and the European Iron Fertilization EXperiment (EIFEX) (−1.36‰; Cavagna et al., 2011) with Fe supplied artificially to the Southern Ocean, which changed the normal condition of Fe limitation over primary productivity in the region. Data from other regions also support the $\Delta^{30}Si_{diatom-SW}$ of −1.1‰ (e.g., Beucher et al., 2008). According to the literature data shown above, the relatively consistent fractionation factors suggest that the diatom δ^{30}Si can be used as a proxy for silicic acid utilization in paleoceanographic studies.

Factors affect the diatom δ^{30}Si

There are other diatom-related factors that may affect the interpretation of diatom δ^{30}Si: the species-specific fractionation and the size effect. In an early study, De La Rocha et al. (2000) analyzed two species from genus *Thalassiosira* and one from genus *Skeletonema* and obtained almost identical fractionation factors for three species. Sun et al. (2014) also reported $\Delta^{30}Si_{diatom-SW}$ value for two species from these two genus which show larger BSi–DSi fractionation (−1.5‰) than the early study. Sutton et al. (2013) reported $\Delta^{30}Si_{diatom-SW}$ for various species from genus *Thalassiosira*, *Porosira*, *Fragilariopsis* and *Chaetoceros*, and suggest slightly different values for five species from *Thalassiosira* and *Porosira* (from −0.72‰ to −1.21‰) that are in general agreement to those proposed by De La Rocha et al. (2000), but also showed smaller negative $\Delta^{30}Si_{diatom-SW}$ value for *Fragilariopsis kerguelensis* (−0.54‰) and larger negative $\Delta^{30}Si_{diatom-SW}$ value for *Chaetoceros brevis* (−2.09‰). Besides, Doering et al. (2016) reported large and variable (0.2~1.0‰) discrepancies between δ^{30}Si of mixed species and large handpicked mono-generic *Coscinodiscus* at different sites in a Peruvian upwelling region, while the coretop and downcore variations of $\Delta^{30}Si_{Coscino-BSi}$ may attribute to the changes in strength of upwelling and different nutrient utilization strategy. In summary, the $\Delta^{30}Si_{diatom-SW}$ value for genus *Thalassiosira*, *Skeletonema*, *Porosira* are in agreement with each other.

The size fraction of diatoms could have potential influence on its δ^{30}Si. Cardinal et al. (2007) investigated modern diatoms in the Southern Ocean with size fractions >0.4 μm (bulk), 20~70 μm and >70 μm, and found no systematic difference between these three fractions. Similarly, Maier et al. (2013) cannot find distinguishable offset between size fractions 10~20 μm and >63 μm. However, Egan et al. (2012) found evidence in the coretops from the Southern Ocean that size fraction 2~20 μm is the most representative fraction for diatoms, while <2 μm might be contaminated by clay min-

EBSCOhost - printed on 2/10/2023 8:05 PM via . All use subject to https://www.ebsco.com/terms-of-use

erals and size fraction >50 μm might be with the presence of radiolarian or clastic materials (Egan et al., 2012). Therefore, Egan et al. (2012) suggested size fraction 2~20 μm to be the "correct" fraction, and indeed they found the best δ^{30}Si–DSi correlation from this fraction.

Although affected by the species-specific fractionation and size effect, clear correlation between silicon isotopic compositions of diatoms and silicic acid utilization are recorded by the literature cited above (see also Figure 4.42). If proper species and size fraction were chosen, the δ^{30}Si of diatoms is a reliable proxy for silicic acid utilization, which can be further interpreted as changes in the global silicon cycle, such as changes in silicic acid utilization, or silicon isotopic composition of seawater resulted from, e.g., physical circulation and continental input.

Impact of BSi production on the δ^{30}Si of seawater

The seawater δ^{30}Si is a good tracer for marine silicon cycle. As summarized in Chapter 4, the δ^{30}Si of seawater range from 0.5‰ to 4.4‰ with an average of 1.6‰. Generally, the biological pump causes Si depleted in surface water and enriched in deep water over all ocean basins, as similar as nitrate, phosphate and other nutrient elements. Diatoms preferentially incorporate lighter ^{28}Si rather than heavy isotopes during their silicification process, and leaving the residue, i.e., the seawater of euphotic zone, with enriched heavy isotopes. Therefore, the overall δ^{30}Si of surface water where the Si removal occurred is elevated by the diatom utilization, with δ^{30}Si values vary from ~1‰ to ~3‰. Although about half of the gross biogenic silica suffers dissolution within the surface mixed layer whilst there is a slight but measurable isotopic fractionation that may lower the δ^{30}Si of dissolved Si inventory during the opal dissolution (Demarest et al., 2009; Wetzel et al., 2014; see below), the strong utilization signal in the surface water cannot be easily overridden. The general vertical distribution of seawater δ^{30}Si is shown in Table 5.3. In surface water (e.g., the upper 50 m), the δ^{30}Si is higher

Table 5.3: General vertical distribution of seawater δ^{30}Si in the modern ocean. See Figure 4.39 for references.

Depth interval (m)	Averaged δ^{30}Si (‰)	*n*
≤10	2.1	119
10~20	2.1	18
20~50	2.1	53
50~100	1.9	118
100~200	1.7	127
200~1 000	1.5	299
1 000~2 000	1.3	123
2 000~3 000	1.3	95
3 000~4 000	1.2	57
4 000~5 000	1.3	27
>5 000	1.2	3

EBSCOhost - printed on 2/10/2023 8:05 PM via . All use subject to https://www.ebsco.com/terms-of-use

than that of the deep water (>1 000 m) by almost 1‰. It is also noteworthy that low δ^{30}Si values found at surface water (<2‰) are mainly from the Southern Ocean and the North Pacific which are known as HNLC regions, consistent with the relatively low primary productivity, and hence the weak Si utilization in these regions. In the ocean's interior, however, there is no diatom production, and the deep water δ^{30}Si (with an average of ~1.3‰) is dominated by the recycling of biogenic silica, causing lower δ^{30}Si in deep water than the surface water. In addition, isotopically light, non-continental input sources such as hydrothermal process and seafloor weathering also help lowering the δ^{30}Si of deep water in some regions.

Burial of diatom BSi

Tréguer and de La Rocha (2013) estimated that the net accumulation of exported BSi in the sediment is only 6.3×10^{12} mol Si yr^{-1} out of 240×10^{12} mol Si yr^{-1}, with 3.3×10^{12} mol Si yr^{-1}, $<1.04 \times 10^{12}$ mol Si yr^{-1} and $>2.0 \times 10^{12}$ mol Si yr^{-1} contribution from coastal zone, deep open ocean and the Southern Ocean, respectively. This revised new estimate is very close to the previous version of 6.1×10^{12} mol Si yr^{-1} (Tréguer et al., 1995). In Figure 5.1 assuming the marine silicon cycle at steady state, we retain the previous estimate. Overall, only 2.5% of the gross biogenic silica production are eventually buried and preserved in the sediment, while the major fraction (97.5%) is recycled within the water column.

Sponge as BSi output and DSi proxy

As a sink of marine dissolved silica, the role of siliceous sponge in marine silicon cycle has long been overlooked (e.g., Tréguer et al., 1995; Canfield et al., 2005). It is after several previously unrecognized or misrecognized input sources (such as groundwater and revised river inputs) being included into the calculation of gross silicon inputs that we have realized the imbalance might be attributed to the underestimated sponge utilization. Tréguer and de La Rocha (2013) estimated using published data that the gross Si uptake and DSi release from sponge are $(3.7 \pm 3.6) \times 10^{12}$ mol Si yr^{-1} and $(0.15 \pm 0.15) \times 10^{12}$ mol Si yr^{-1}, respectively. Therefore, the net biogenic silica export of siliceous sponge is $(3.6 \pm 3.7) \times 10^{12}$ mol Si yr^{-1}.

Sponges are among materials with most negative silicon isotopic composition (Douthitt, 1982). Unlike diatoms with relatively constant fractionation factor, the $\Delta^{30}Si_{sponge-SW}$ vary dramatically with the DSi concentration (Hendry et al., 2010; Wille et al., 2010; Hendry and Robinson, 2012), with smaller negative $\Delta^{30}Si_{diatom-SW}$ value higher than –1‰ at very low silicic acid concentration (<5 μM) and larger negative $\Delta^{30}Si_{diatom-SW}$ value lower than –5‰ at high concentration (>100 μM), which means that the silicon isotopes in sponges do not follow the Rayleigh fractionation (Hendry et al., 2010). Samples of living sponge and coretop spicules from different ocean basins confirmed a consistent relationship between sponge Δ^{30}Si and silicate concentration (see Figure 4.43), demonstrating that the δ^{30}Si of sponges can be used

EBSCOhost - printed on 2/10/2023 8:05 PM via . All use subject to https://www.ebsco.com/terms-of-use

as a proxy for silicic acid concentrations in the past ocean (Ellwood et al., 2010). Their benthic habitation further extend the application of sponge δ^{30}Si to the study of silicon cycle at any water depth (De La Rocha, 2003), rather than only surface water as for diatoms.

Turnover rate of oceanic DSi

Considering the size of the global oceanic DSi pool of ~97 000 × 10^{12} mol Si (Tréguer and de La Rocha, 2013) and the net export rate (or burial rate) of biogenic silica from diatoms and sponges [(6.1 + 3.6) × 10^{12} mol Si yr^{-1}], we can calculate the residence time or removal time (τ) for silicon in the ocean based on burial (τ_B) by working out their quotient, i.e., ~10 000 yr. We can also calculate the biological production based τ (τ_P) by taking the gross biological production [(240 + 3.6) × 10^{12} mol Si yr^{-1}] as denominator and get ~400 yr, which is ~25 times faster than the overall residence time. This means that silicon is recycled in the water column by 25 times on average before finally buried in the sediment while survived the dissolution at seawater–sediment interface and quit the marine silicon cycle. This number is lower than the 40 times estimated by Canfield et al. (2005) because the sponge output is ignored, which affect τ_B significantly while have almost no influence on τ_P.

5.1.2.3 The internal Si cycle of the ocean

As mentioned above, silicon in the ocean passes through many cycles of biological uptake and dissolution before being removed from the water column. The massive production or recycling fluxes are much greater than the sum of the input sources and output sinks by more than 20 times. This means that regarding only the flux, the internal Si cycle in the ocean is apparently the most important processes controlling the marine Si cycle compared to the input and output.

Dissolution and recycling of BSi

Magnitude of BSi dissolution and recycling

Because silica is severely unsaturated in the modern ocean, the biogenic silica produced by diatoms suffers from intense dissolution and is recycled at all depth, from the photic zone down to the seafloor. Tréguer and de La Rocha (2013) compiled silica dissolution to silica production ratio (D:P) of global ocean. They calculated production-weighted mean D:P of photic zone at 135 sites distributed in coastal zone, open ocean and the Southern Ocean and obtained a global mean annual D:P of 0.56, which means that ~56%, or 135 × 10^{12} mol Si yr^{-1} out of 240 × 10^{12} mol Si yr^{-1} is dissolved within the upper ~100 m of water column. The rest 44% (105 × 10^{12} mol Si yr^{-1}) is exported to the ocean's interior, although it does not mean this portion will be buried in the sediment nor will reach the seawater–sediment interface. Considering the flux of net buried BSi of 6.1 × 10^{12} mol Si yr^{-1}, 98.9 × 10^{12} mol Si yr^{-1} out of 105 × 10^{12} mol Si yr^{-1} of BSi

EBSCOhost - printed on 2/10/2023 8:05 PM via . All use subject to https://www.ebsco.com/terms-of-use

exported from the photic zone is dissolved in deep ocean and/or seawater–sediment interface.

Isotopic fractionation related to BSi dissolution

The silicon isotopic fractionation during biogenic silica dissolution has been studied by several groups. Demarest et al. (2009) first report that there was an isotopic fractionation during diatom dissolution with a $\Delta^{30}Si_{DSi-BSi} = -0.55‰$, which means preferential release of isotopically light silicon during dissolution. Sun et al. (2014) found even larger dissolution fractionation of −0.85‰ at early stage of dissolution, but concluded that this effect was observed only in DSi and no significant Si isotope change was observed for BSi, demonstrating that the amount of dissolution is very limited. This is also supported by a field study by Egan et al. (2012). Wetzel et al. (2014) also confirmed a little fractionation by dissolution experiment. In summary, although this fractionation is measureable, the $\delta^{30}Si$ of diatom appears to be robust against dissolution.

Physical controls on the marine Si cycle and Si isotopes in the deep ocean

The silicon isotopic composition of diatoms has been interpreted as a proxy for silicic acid utilization. However, paleoceanographic studies in recent two decades have observed in marine sediments that glacial–interglacial changes of $\delta^{30}Si$ in biogenic opal can be as large as ~1.0‰ or even greater (De La Rocha et al., 1998; Brzezinski et al., 2002; Beucher et al., 2007; Horn et al., 2011; Robinson et al., 2014). Similar but slightly smaller fluctuations (0.5~0.8‰) can also be found in sub-orbital (millennial) scale climate records such as Younger Dryas and Heinrich events (Pichevin et al., 2012; Maier et al., 2015). Considering the fractionation between diatom and seawater ($\Delta^{30}Si_{diatom-SW} = -1.1‰$), these records mean that a change in Si utilization from almost no usage to almost complete usage can barely cover such range if the diatom records are interpreted as fraction of utilized Si alone. Therefore, it is very likely that processes other than biological utilization may also influence the diatom $\delta^{30}Si$ record. Since the $\Delta^{30}Si_{diatom-SW}$ of diatom is relatively constant, the glacial–interglacial changes in diatom $\delta^{30}Si$ may be addressed to changes in $\delta^{30}Si$ of seawater, which may be further interpreted as changes in continental inputs or in ocean circulation regime. The former hypothesis has been discussed in Section 5.1.1 and we will discuss the latter one below using $\delta^{30}Si$ of deep water from various ocean basins (see Figure 5.6 for the distribution of stations and sections).

Horizontal distribution of $\delta^{30}Si$ in a global deep ocean (~2 000 m)

In the modern ocean, the influence of circulation on oceanic silicon cycle can be well illustrated by the silicon isotopic composition of deep water (Figure 5.7). From an interbasin view, the $\delta^{30}Si$ of deep ocean exhibit large gradient along the route of the merid-

EBSCOhost - printed on 2/10/2023 8:05 PM via . All use subject to https://www.ebsco.com/terms-of-use

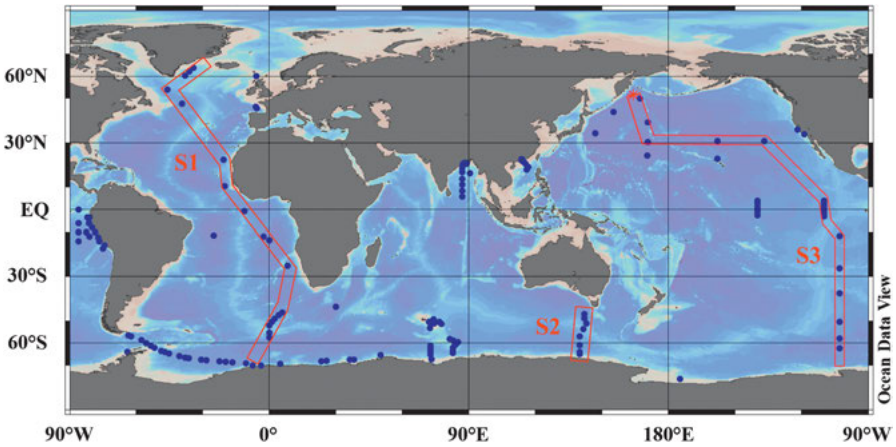

Figure 5.6: Station map of compiled seawater δ^{30}Si (data from De La Rocha et al., 2000; Cardinal et al., 2005; Reynolds et al., 2006b; Beucher et al., 2008, 2011; De La Rocha et al., 2011; Fripiat et al., 2011a,b; Cao et al., 2012; de Souza et al., 2012a,b; Ehlert et al., 2012; Grasse et al., 2013; Singh et al., 2015). Sections defined are shown in red frames. S1: North-South Atlantic Ocean; S2: Indian sector of Southern Ocean; S3: North-South Pacific Ocean.

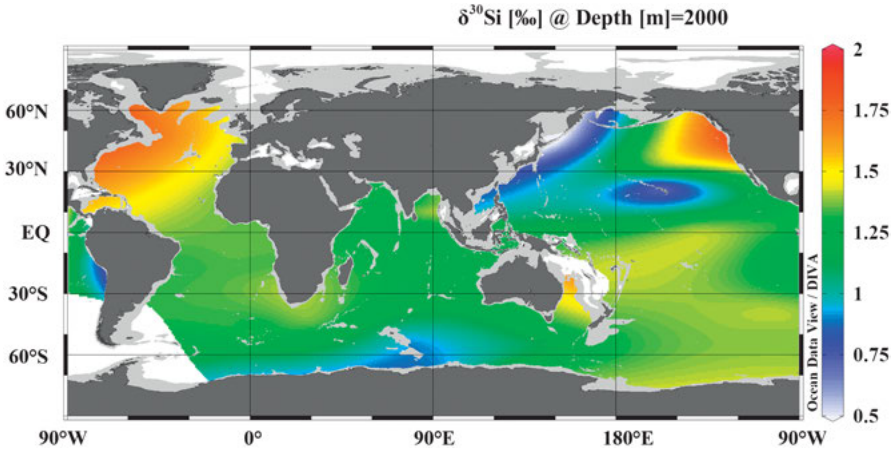

Figure 5.7: Global deep water δ^{30}Si distribution at 2 000 m. Data are from stations in Figure 5.6, and image is produced using DIVA gridding by Ocean Data View software.

ional overturning circulation (MOC) or the deep ocean conveyor belt (De La Rocha et al., 2000; de Souza et al., 2014). In the North Atlantic where there is strong deep water formation (i.e., the sinking of surface water due to loss of buoyancy), the δ^{30}Si of deep water (~2 000 m) is highest in the global deep ocean, ranging from +1.5~+1.8‰ (Figure 5.7; Figure 5.8A and B). The Southern Ocean bears a lower deep δ^{30}Si signal around 1.0~1.2‰, and the large meridional gradient (>0.6‰) in the Northern-Southern At-

EBSCOhost - printed on 2/10/2023 8:05 PM via . All use subject to https://www.ebsco.com/terms-of-use

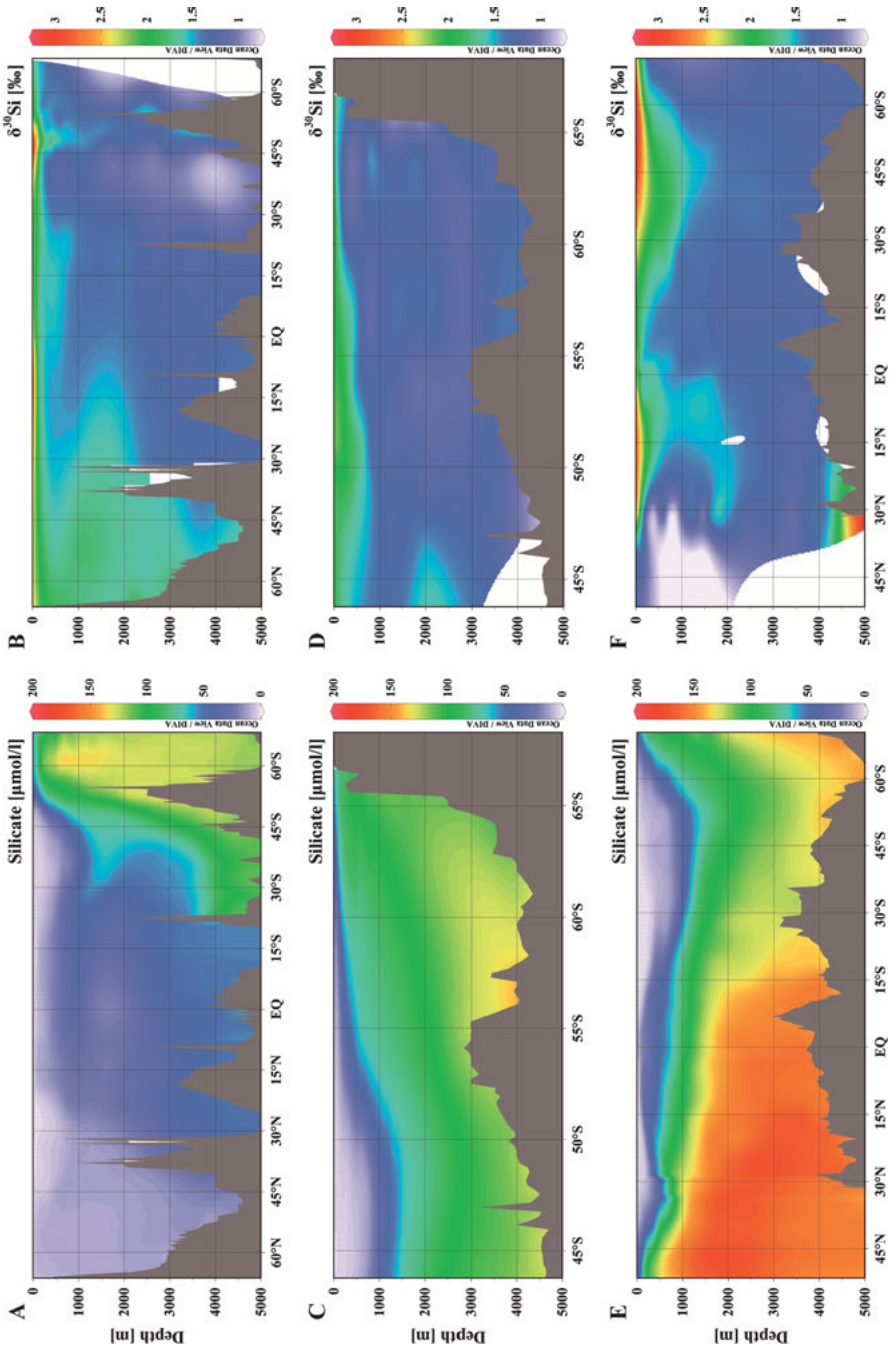

Figure 5.8: DSi (Silicate) concentration and δ^{30}Si of sections defined in Figure 5.6. A and B: S1; C and D: S2; E and F: S3. DSi data are from World Ocean Atlas 2009 (Garcia et al., 2009), and δ^{30}Si data are from stations in Figure 5.6. Images are produced using DIVA gridding by Ocean Data View software.

EBSCOhost - printed on 2/10/2023 8:05 PM via . All use subject to https://www.ebsco.com/terms-of-use

lantic Ocean (de Souza et al., 2012b) can be explained by the end-member mixing of the deep North Atlantic and the Southern Ocean. There are no significant zonal changes within the Southern Ocean probably due to strong mixing (Figure 5.7; Figure 5.8C and D), although a relatively small gradient is observed across the fronts near the sub-Antarctic region (Cardinal et al., 2005). From the Pacific sector of the Southern Ocean to the North Pacific which is the "end" of the MOC, the deep water δ^{30}Si decrease from ~1.2‰ to the global minimum ~0.5‰ (Figure 5.7; Figure 5.8E and F). An abnormally low value (0.6‰; De La Rocha et al., 2000) is observed near the Hawaiian Islands in the Central Pacific, where the region is characterized by hydrothermal basalt alteration (Santelli et al., 2008).

Circulation control and implications for marine Si cycle in glacial climate

As a nutrient element, the conservative behavior of silicon inferred from silicon isotope composition of deep water (Figures 5.7 and 5.8) is not expected. Since the first measurement of seawater δ^{30}Si (De La Rocha et al., 2000), the physical control on deep sea δ^{30}Si has been noted by various studies (e.g., Fripiat et al., 2011b; de Souza et al., 2012b). To further understand the controls on the deep δ^{30}Si, de Souza et al. (2014) applied the Modular Ocean Model 3.0 to estimate the relative contribution of preformed Si and regenerated Si (de Souza et al., 2014). The preformed Si is the Si and δ^{30}Si signal "generated" in the winter mixed layer and transported to the ocean's interior through deep water formation, and thus is conservative and controlled by physical circulation without biological cycling; while the regenerated Si is added to the deep ocean by opal dissolution, and is non-conservative. Model data showed that the preformed δ^{30}Si in the deep Atlantic Ocean is originated from the water mass mixing of North Atlantic Deep Water (NADW) and Antarctic Bottom Water (AABW). The former water mass is characterized by very high δ^{30}Si due to the sinking of Si-depleted surface water at the deep water formation site (as can be seen from Figure 5.8A and B), while the latter one by the HNLC characteristic and weak Si utilization (Figure 5.8C and D) due to iron limitation. Somewhat surprising, the regenerated component, however, is also controlled by circulation according to the model studies, because a dominant fraction of regenerated Si in regions north of 50°S is sourced from the northward spreading of deep water in the Southern Ocean by deep ocean circulation (de Souza et al., 2014; Holzer and Brzezinski, 2015).

These features are essential to interpret the glacial–interglacial variation of δ^{30}Si in marine sedimentary records, because the changes in the circulation regime during the glacial stage or deglaciation, e.g., the formation of Glacial North Atlantic Intermediate Water (GNAIW, shallower version of NADW during the glacial stage), the equatorward spreading of excess Si from the Southern Ocean by relatively shallow Subantarctic Mode Water (SAMW) and Antarctic Intermediate Water (AAIW), changes in stratification and related changes in surface nutrient supply from deep water, may be largely different (e.g., Brzezinski et al., 2002; Matsumoto et al., 2002; Meckler et

EBSCOhost - printed on 2/10/2023 8:05 PM via . All use subject to https://www.ebsco.com/terms-of-use

al., 2013; Robinson et al., 2014; Rousseau et al., 2016). These changes in physical circulation, especially the activities of NADW, AABW, SAMW and AAIW, together with enhanced Fe input in the Southern Ocean, could influence the content and distribution of the Si supply to the surface ocean, the physiology, ecology and biogeography of diatom and non-diatom phytoplankton (e.g., Brzezinski et al., 2002; Matsumoto et al., 2002), and hence the biogenic silica production with an extent from the southern high latitude to the equatorial regions (Griffiths et al., 2013; Hendry et al., 2016). Therefore, besides the biogeochemical cycle, ocean circulation is an alternative process that influences the silicon concentration, silicon isotopic composition and silicon cycle in the ocean.

5.2 Silicon isotope studies on environmental variation of ocean

The secular evolutions of the chemical and isotopic compositions and environmental conditions of the ocean are important issues in geological and geochemical studies. These issues are closely related to investigations of the development and evolution of lithosphere, atmosphere and biosphere of the Earth and attract the attention of researchers in various geochemical fields. Naturally, the secular evolution of the content and isotope composition of silicon dissolved in ocean water and their implications in the environmental variation of the ocean have become important topics since the beginning of the silicon isotope studies. Basically, the silicon isotope compositions of ancient seawater are speculated from the silicon isotope data of contemporaneous chert rocks.

As mentioned in Chapter 4, chert is a sedimentary rock composed mainly of microcrystalline quartz, which occurs in sedimentary strata from the early Archean to the present. Extensive investigations have been carried out on its chemical and isotopic characteristics to study its forming conditions and to trace the environmental variation in the global ocean (Song and Ding, 1990; Ding et al., 1996; Robert and Chaussidon, 2006; André et al., 2006; van den Boorn et al., 2007, 2010; Abraham et al., 2011; Marin-Carbonne et al., 2012, 2014; Chakrabarti et al., 2012; Geilert et al., 2014a,b; Stefurak et al., 2015; Steinhoefel et al., 2009, 2010; Oelze et al., 2015; Roerdink et al., 2015; Tatzel et al., 2015). Song and Ding (1990) suggested distinguishing sedimentary facies of chert with silicon isotope compositions. Ding et al. (1996) discussed variations in the silicon content and silicon isotope composition in marine water according to the data from chert formed in shallow marine environments. According to the silicon isotope variation of chert, Robert and Chaussidon (2006) developed a temperature-evolution curve for the Precambrian ocean. It has been suggested that Precambrian cherts have much higher δ^{30}Si values than Phanerozoic cherts and that the former show a generally increasing trend from 3.5 Ga to 0.85 Ga, thus reflecting a decrease in seawater temperature (Robert and Chaussidon, 2006). However, these statements have been challenged because cherts can have various origins and their isotopic com-

EBSCOhost - printed on 2/10/2023 8:05 PM via . All use subject to https://www.ebsco.com/terms-of-use

positions might have been reset by metamorphic fluid circulation (André et al., 2006; van den Boorn et al., 2007, 2010; Abraham et al., 2011; Marin-Carbonne et al., 2012, 2014). Thus, different types of cherts need to be considered separately (André et al., 2006; Marin-Carbonne et al., 2014; Chakrabarti et al., 2012; Geilert et al., 2014a; Stefurak et al., 2015) because their isotope composition might record various distinct processes (Steinhoefel et al., 2009, 2010; Geilert et al., 2014b; Oelze et al., 2015; Roerdink et al., 2015; Tatzel et al., 2015). In addition, the factors that affect silicon isotope composition of chert have been investigated in detail (Steinhoefel et al., 2009, 2010; Geilert et al., 2014b; Oelze et al., 2015; Roerdink et al., 2015; Tatzel et al., 2015). It was found that peritidal cherts are enriched in ^{30}Si, while basinal cherts, which are associated with banded iron formations (BIFs), are depleted in ^{30}Si. This difference is attributed to the changes in Si sources, as the major Si source for the peritidal cherts is the dissolved silica in the seawater while the major Si sources for BIFs is the hydrothermal fluids (Chakrabarti et al., 2012). Now, it is widely accepted that the formation of chert is a complicated process and that the Si isotope composition of chert is dependent on the relative contributions of various Si sources and the effects of different forming processes. It is known that the relative contributions of the various Si sources to the global ocean vary throughout geological history. Thus, specific types of chert might be representative for reconstructing the Si isotope composition of the ocean for different geological periods. For example, during the Archean period, sea-floor weathering and submarine hydrothermal fluids dominated the Si input to the ocean, and continent inputs were negligible; thus, the Si isotope compositions of chert in BIFs are likely the best approach for tracing the Si isotope compositions of the ocean. In contrast, in the Proterozoic and Phanerozoic periods, the Si input from the continent to the ocean became dominant, and the Si input from sea-floor weathering and submarine hydrothermal fluids became less prevalent; thus, peritidal chert may be more significant in tracing the Si isotope composition of the ocean.

5.2.1 Silicon content and silicon isotope composition of Archean ocean water and their implications to environmental variation

Silicon isotope compositions of cherts are an attractive tool for exploring the properties of Earth's ancient oceans (André et al., 2006). The silicon isotope compositions of seawater in the Archean ocean were basically speculated from the data of Archean chert. The chert rocks in Archean strata are divided into two genetic types, i.e., the C-chert (chemical precipitation of SiO_2) and S-chert (formed through silicification of precursor sediments or rocks). The schematic models of these two types of chert rocks are illustrated in Figure 5.9.

The chert rocks in BIFs are dominantly consistent of C-chert. The BIFs occur widely in Archean and Proterozoic strata all over the world and comprise an important iron ore resource in the world. The total amount of siliceous beds in BIFs is much

EBSCOhost - printed on 2/10/2023 8:05 PM via . All use subject to https://www.ebsco.com/terms-of-use

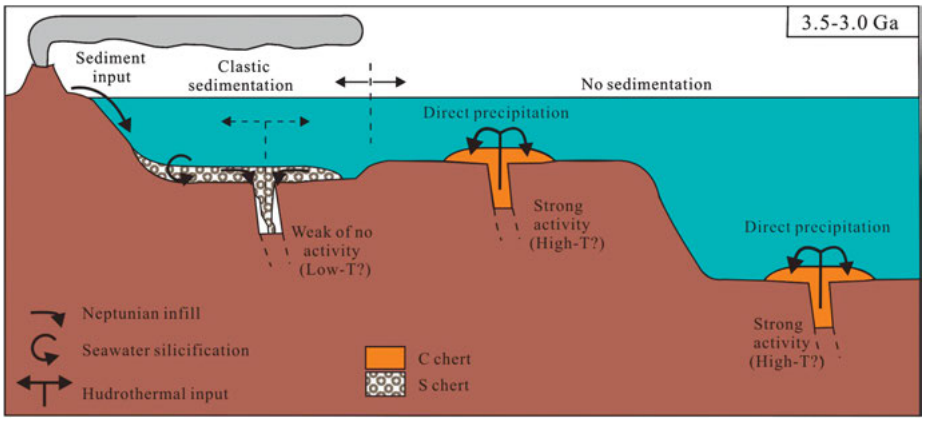

Figure 5.9: Schematic model of chert formation in the early Archean. S-chert was formed through silicification of precursory material by silica-saturated seawater in areas of active volcano-clastic sedimentation, which had relatively weak or no hydrothermal input. C-chert was formed through interaction between Si-rich fluids and seawater in sediment-starved environments. After van den Boorn et al. (2007).

larger than the total amount of siliceous beds during the Phanerozoic Eon. Based on the silicon isotopic data of chert bands in an Archean BIFs from the Gongchangling iron ore deposits, Liaoning, China, Jiang et al. (1993) provided the first estimation on silicon isotope compositions of seawater in the Archean ocean (Jiang et al., 1993). Then the silicon isotope compositions of the ocean water and the kinetic silicon isotopic fractionation factor between dissolved silicon and precipitated SiO_2 during BIF formation in Archean seawater were summarized by Ding et al. (1996). It was found that the granite and schist above and below the BIF have δ^{30}Si values from −0.6‰ to 0.2‰, consistent with those of granite and mafic volcanic rocks (Jiang et al., 1993; Ding et al., 1996). Thus, the dissolved silicon obtained by reaction between those rocks and seawater should have δ^{30}Si values of about −0.2‰. Besides, the quartz in the BIF has δ^{30}Si values ranging from −0.8‰ to −2.2‰, averaging −1.5‰, which is 1.3‰ lower than the δ^{30}Si value of contemporaneous oceanic water. The difference between quartz and seawater is consistent with the kinetic silicon isotopic fractionation factor between dissolved silicon and precipitated SiO_2 at Earth surface temperature, indicating that only a very small part of the silicon in the oceanic water was precipitated. The same phenomenon can be seen in similar rocks from northern Hebei, China, and Canada.

Since then, a number of investigations has been undertaken to trace the silicon content and silicon isotope composition of Archean ocean water and their implications to environmental variation (Robert and Chaussidon, 2006; van den Boorn et al., 2007, 2010; Steinhoefel et al., 2009; Heck et al., 2011; Marin-Carbonne et al., 2012, 2014; Geilert et al., 2014b; Zheng et al., 2016; Reddy et al., 2016).

EBSCOhost - printed on 2/10/2023 8:05 PM via . All use subject to https://www.ebsco.com/terms-of-use

Secular variations in the silicon isotope record of Precambrian cherts have been interpreted to indicate long-term ocean cooling (Robert and Chaussidon, 2006), whereas an alternative interpretation attributed this diversity to changing provenance of the silicon rather than seawater temperature (van den Boorn et al., 2007). Subsequent studies of various Precambrian cherts have provided growing evidence for the importance of provenance in creating isotope variability, and/or other subordinate controls (Steinhoefel et al., 2009; van den Boorn et al., 2010; Heck et al., 2011; Chakrabarti et al., 2012; Marin-Carbonne et al., 2012).

van den Boorn et al. (2010) investigated Si isotope systematics, in conjunction with geochemical and mineralogical data, in three well-characterized and approximately contemporaneous, ~3.5 Ga chert units from the Pilbara greenstone terrane (Western Australia; Figure 5.10). The Marble Bar Chert (~3.46 Ga) is composed dominantly by C-cherts. The Kitty's Gap Chert (~3.45 Ga) contains mainly S chert formed through replacement of volcanogenic sediments. The North Pole chert-barite unit (~3.49 Ga) is intermediate between above two end-member settings, and provides evidence for both mechanisms of chert formation (van den Boorn et al., 2007).

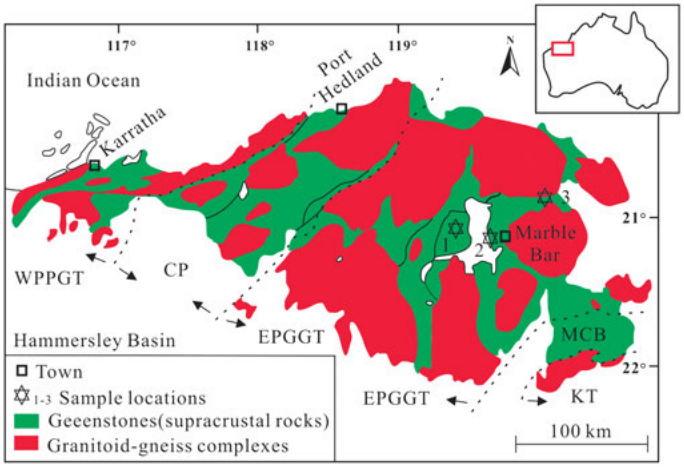

Figure 5.10: Simplified geological map (modified after Krapez and Eisenlohr, 1998) of the Pilbara terrane (North-western Australia). Sample locations are indicated with numbers: 1) North Pole; 2) Marble Bar; 3) Kitty's Gap.

It was found that the Si isotope compositions of chert rocks in these units vary in a large range from −2.4‰ to +1.3‰, which was induced by near-surface processes (Figure 5.11). Cherts that formed by chemical precipitation of silica show the largest δ^{30}Si spread from −2.4‰ to +0.6‰. Their silicon isotope systematics are explained by 1) mixing between hydrothermal fluids and seawater, and/or 2) fractionation of hydrothermal fluids by subsurface losses of silica due to conductive cooling (Figure 5.12).

EBSCOhost - printed on 2/10/2023 8:05 PM via . All use subject to https://www.ebsco.com/terms-of-use

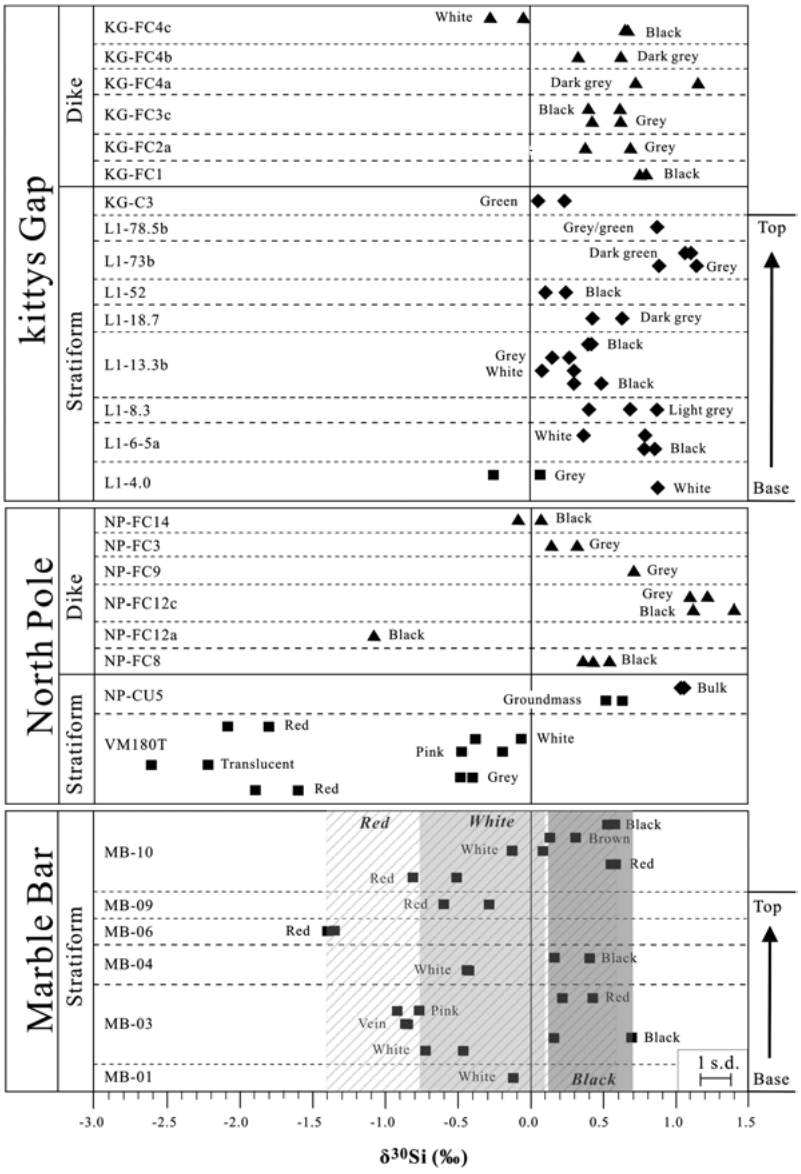

Figure 5.11: Silicon isotope variation in Early Archaean cherts from Marble Bar, North Pole and Kitty's Gap. Samples are indicated by codes and are separated by dotted lines. Squares: stratiform C-cherts; diamonds: stratiform S-cherts; triangles: dike cherts. Light and dark grey shades and hatched area indicate approximate ranges of white(/grey/pink), black(/brown) and red stratiform C-cherts in the Marble Bar Chert, respectively. After van den Boorn et al. (2010).

EBSCOhost - printed on 2/10/2023 8:05 PM via . All use subject to https://www.ebsco.com/terms-of-use

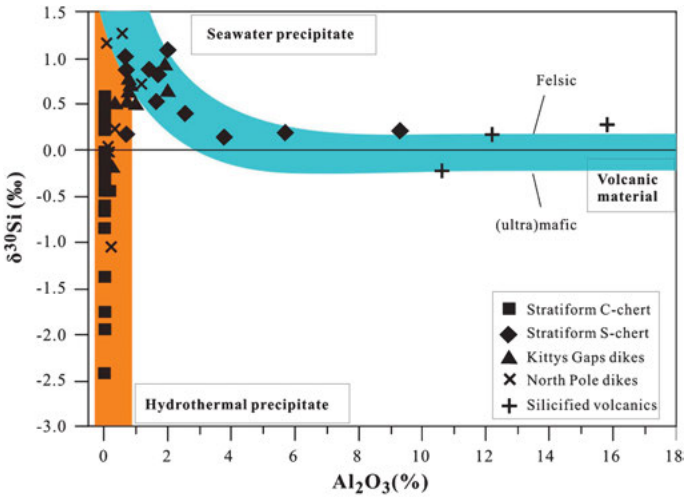

Figure 5.12: A plot showing relation between Al_2O_3 content and $\delta^{30}Si$ of chert samples. S-chert samples fall within the blue band that defines mixing between mafic or felsic volcanogenic sediments and seawater. Orange $\delta^{30}Si$ array represents mixing between hydrothermal fluids and seawater, or evolution of cooling hydrothermal fluids. After van den Boorn et al. (2010).

Rayleigh-type fractionation of hydrothermal fluids was largely controlled by temperature differences between these fluids and seawater. Lamina-scale Si isotope heterogeneity within individual chemical chert samples (up to 2.2‰) may reflect the dynamic nature of hydrothermal activity.

Silicified volcanogenic sediments exhibit a much more restricted range of positive $\delta^{30}Si$ (+0.1‰ to +1.1‰), which points to seawater as the dominant source of silica (Figure 5.12).

The proposed model for Si isotope variability in the Early Archean implies that chemical cherts with the most negative $\delta^{30}Si$ formed from pristine hydrothermal fluids, whereas silicified or chemical sediments with positive $\delta^{30}Si$ are closest to pure seawater deposits. Taking the most positive value of +1.3‰, and assuming that the Si isotope composition of seawater is governed by input of fractionated hydrothermal fluids, van den Boorn et al. (2010) infer that the temperature of ~3.5 Ga seawater was below ~55°C.

The silicon isotope compositions of C-chert layers in the similar age (3.33–3.55 Ga) chert formations of Barberton Greenstone Belt (South Africa) were reported by Abraham et al. (2011) and Geilert et al. (2014b). The silicon isotope compositions of quartz in oldest BIFs of ~3.8Ga in the Isua formation, south Greenland were reported by André et al. (2006) and Heck et al. (2011). Besides, the BIFs of Hamersley Group, Western Australia (~2.5 Ga) and Transvaal Group, South Africa (~2.5 Ga) were also studied for their silicon isotope compositions (Steinhoefel et al., 2010; Heck et al., 2011).

EBSCOhost - printed on 2/10/2023 8:05 PM via . All use subject to https://www.ebsco.com/terms-of-use

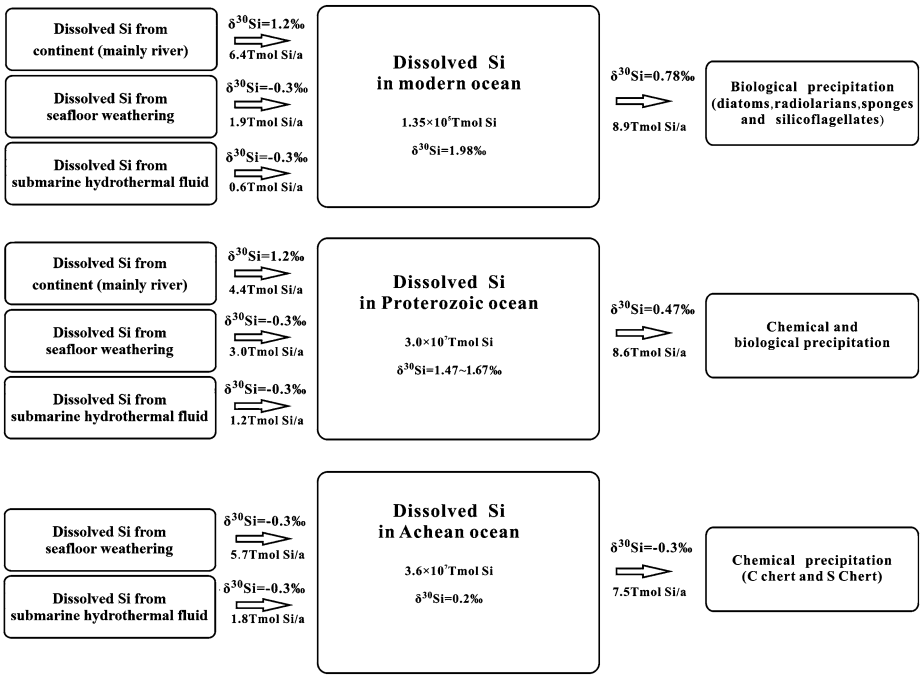

Figure 5.13: A schematic diagram showing Si cycles in the Archean (André et al., 2006; van den Boorn et al., 2007, 2010), Proterozoic and modern oceans (Tréguer and de La Rocha, 2013). Revised from Ding et al. (2017).

Based on the information obtained so far, Archean seawater was a water body with a relatively high temperature, low oxygen fugacity and weak alkalinity, in which biological activity was negligible. These estimations are consistent with those obtained from other geochemical and isotopic studies. As shown in Figure 5.13, during the Archean period, the input sources of dissolved Si to the ocean are submarine hydrothermal fluid and sea-floor weathering, and the output paths are chemical precipitation (to form C cherts) and silicification of the precursor sediments or rocks (to form S cherts) (André et al., 2006; van den Boorn et al., 2007, 2010). The Si concentration in ocean water remains in its saturated concentration at a given temperature, but the $\delta^{30}Si_{SW}$ ($\delta^{30}Si$ value of seawater) increases gradually due to Si isotope fractionation between dissolved Si and precipitated SiO_2. When a steady state is reached, $\delta^{30}Si_{Out}$ (the average $\delta^{30}Si$ value of all output Si) will be equivalent to $\delta^{30}Si_{In}$ (the average $\delta^{30}Si$ value of input Si), and $\delta^{30}Si_{SW}$ will be equal to ($\delta^{30}Si_{Out} - \Delta^{30}Si_{Out\text{-}SW}$), where $\Delta^{30}Si_{Out\text{-}SW}$ is the relative silicon isotope enrichment of the output Si to the ocean water ($\delta^{30}Si_{Out} - \delta^{30}Si_{SW}$). Because the average $\delta^{30}Si$ value of Si in the submarine hydrothermal fluid and Si from sea-floor weathering is ~−0.3‰ and $\Delta^{30}Si_{Out\text{-}SW}$ is ~−0.5‰ at a temperature of 40°C (Geilert et al., 2014a), the $\delta^{30}Si_{SW}$ value of that period is approximately 0.2‰.

EBSCOhost - printed on 2/10/2023 8:05 PM via . All use subject to https://www.ebsco.com/terms-of-use

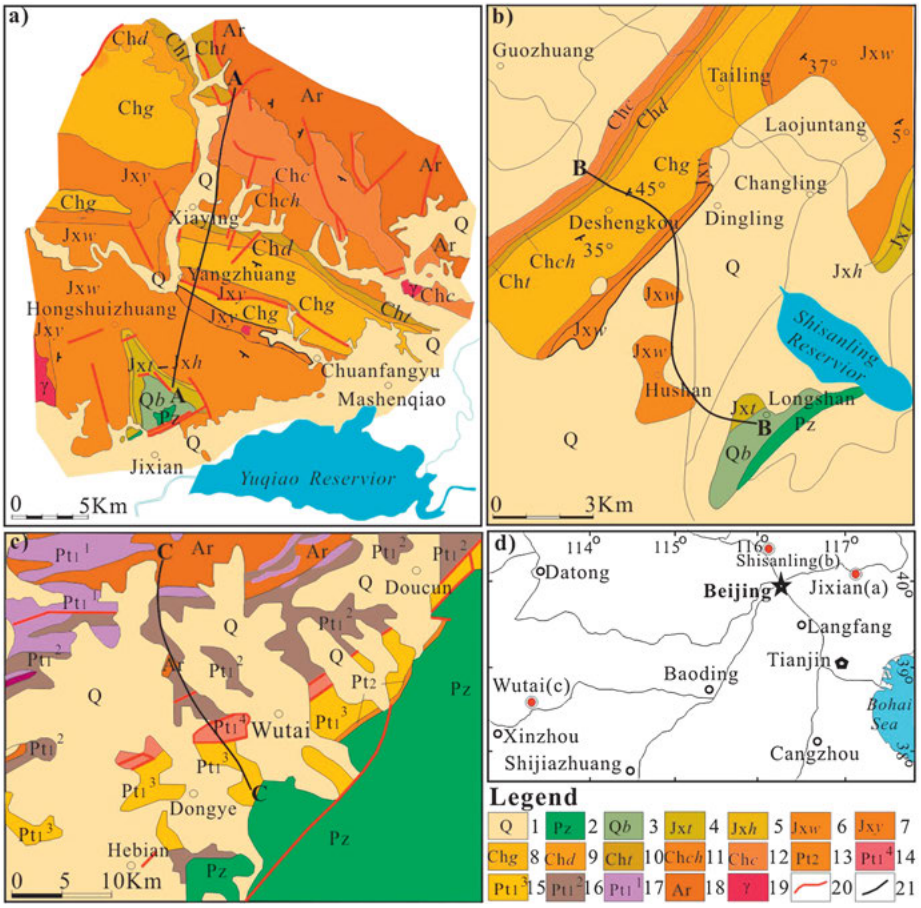

Figure 5.14: Schematic geological maps of sampling area (after Ding et al., 2017). a) Map of the Jixian area, Hebei province (Li et al., 2014b); b) Map of the Shisanlin area, Beijing (Zhang et al., 2002); c) Map of the Wutai area, Shanxi Province (Du et al., 2009); d) A sketch map showing the locations of sampling areas. The sampling areas of Jixian, Shisanlin and Wutai are indicated by red solid cycles in the map. 1 – Quaternary strata; 2 – Phanerozoic strata; 3 – Upper Proterozoic Qingbaikou System; 4 – Tieling Fm., Jixian system; 5 – Hongshuizhuang Fm., Jixian System; 6 – Wumishan Fm., Jixian System; 7 – Yangzhuang Fm., Jixian System; 8 – Gaoyuzhuang Fm., Changcheng System; 9 – Dahongyu Fm., Changcheng System; 10 – Tuanshanzi Fm., Changcheng System; 11 – Chuanlinggou Fm., Changcheng System; 12 – Changzougou Fm., Changcheng System; 13 – Middle Proterozoic strata; 14 – Sijizhuang Fm., Hutuo Group; 15 – Doucun Fm., Hutuo Group; 16 – Dongye Fm., Hutuo Group; 17 – Guojiazai Fm., Hutuo Group; 18 – later Archean Wutai strata; 19 – Granite; 20 – Fault; 21 – Sampling profiles in Jixian (Figure 5.14a, A–A), Shisanlin (Figure 5.14b, B–B) and Wutai (Figure 5.14c, C–C).

EBSCOhost - printed on 2/10/2023 8:05 PM via . All use subject to https://www.ebsco.com/terms-of-use

5.2.2 Silicon content and silicon isotope composition of Proterozoic ocean water and their implications to environmental variation

A number of papers have reported the δ^{30}Si values of cherts formed during the Proterozoic (Song and Ding, 1990; Ding et al., 1996; Robert and Chaussidon, 2006; Marin-Carbonne et al., 2012, 2014; Chakrabarti et al., 2012; Heck et al., 2011; Wang and Chen, 1996; Zhao et al., 2014; Hu et al., 2013; Ding et al., 2017). Among them, relatively more systematic results were presented by Chakrabarti et al. (2012) and Ding et al. (2017).

Chakrabarti et al. (2012) reported silicon isotopic compositions of 75 chert samples with ages ranging from ~2 600 Ma to 750 Ma. Their δ^{30}Si values range from −4.29‰ to +2.85‰. They explained this variability by 1) simple mixing of silica derived from continental (higher δ^{30}Si) and hydrothermal (lower δ^{30}Si) sources, 2) multiple mechanisms of silica precipitation and 3) Rayleigh-type fractionations within pore waters of individual basins. They found a ~3‰ variation in peritidal cherts from a single Neoproterozoic sedimentary basin (Spitsbergen) and explained it by Rayleigh-type fractionation during precipitation from silica-saturated pore waters. It was suggested that in some samples, post-dissolution and re-precipitation of silica could have added to this effect.

They also observed that peritidal cherts are enriched in the heavier silicon isotopes, whereas basinal cherts associated with banded iron formations (BIF) show lower δ^{30}Si values. This may indicate that the silicon in BIFs may be partly from hydrothermal sources. The δ^{30}Si difference between non-BIF and BIF cherts is consistent with the contrasting genesis of these deposits.

A clear pattern of secular variation was observed in their data. Low δ^{30}Si in Archean cherts is consistent with a dominant hydrothermal source of silica to the oceans at that time. They think that the monotonically increasing δ^{30}Si from 3.8 Ga to 1.5 Ga appears to reflect a general increase in continental versus hydrothermal sources of Si in seawater, as well as the preferential removal of lighter Si isotopes during silica precipitation in iron-associated cherts from silica-saturated seawater. The highest δ^{30}Si values were observed in 1.5 Ga peritidal cherts. However, the causes behind the reversal in trend towards lower δ^{30}Si in cherts younger than 1.5 Ga old are less clear.

Ding et al. (2017) collected a suite of samples of carbonate rocks containing chert bands and nodules from the early Proterozoic Hutuo Group (2.35–2.20 Ga) (Du et al., 2009) and the middle Proterozoic Changcheng and Jixian Systems (1.63–1.20 Ga) (Li et al., 2014b; Zhang et al., 2002) in Northern China (Figure 5.14). These cherts were selected because they showed good preservation of their original structure and composition (Figure 5.15 and Figure 5.16); i.e., no obvious effects of metamorphism or weathering were found in the selected samples. The Si and O isotopic compositions of the chert and the C and O isotopic compositions of dolomite were studied systematically.

Generally the chert consists of microscopic quartz grains ranging from 0.1 μm to a few μm in diameter. In some samples (e.g., JX-33), coarser quartz crystals of >10 μm

EBSCOhost - printed on 2/10/2023 8:05 PM via . All use subject to https://www.ebsco.com/terms-of-use

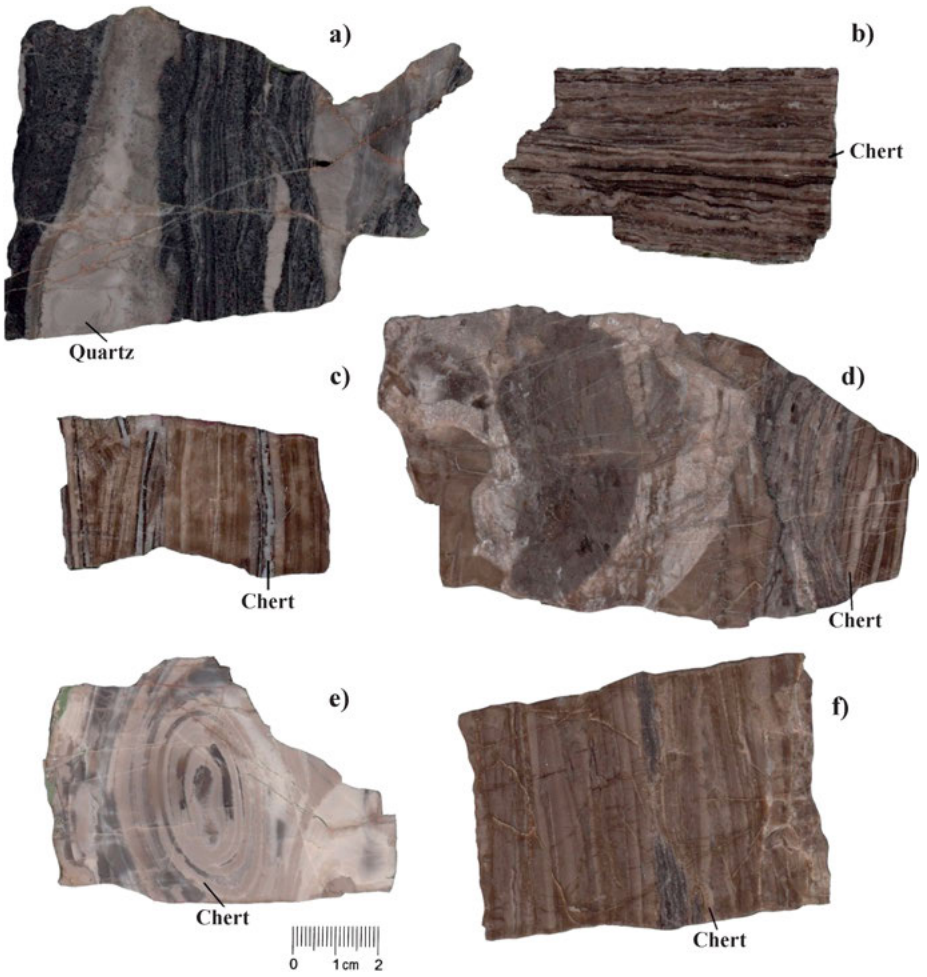

Figure 5.15: Photos of polished sections of sample specimens. a) JX-20; b) JX-26; c) JX-27; d) JX-33; e) JX-36; f) JX-40. The cherts commonly occur as fine bands, but quartz veins can be observed in some specimens (JX-20, JX-33 and JX-36). After Ding et al. (2017).

can be observed. The chert seems to have re-crystallized after the dolomite, indicating a diagenetic origin.

The Si and O isotope compositions of the cherts and the C and O isotope compositions of dolomites were measured and illustrated in Figure 5.17. The obtained $\delta^{13}C_{V\text{-}PDB}$ and $\delta^{18}O_{V\text{-}PDB}$ values of dolomites indicate their normal sedimentary origin in a shallow marine environment, but their $\delta^{18}O_{V\text{-}PDB}$ values had been influenced to some degree by diagenesis. The $\delta^{18}O_{V\text{-}SMOW}$ values of the chert samples also show that they were formed in a shallow marine environment but might have been slightly affected by diagenesis.

EBSCOhost - printed on 2/10/2023 8:05 PM via . All use subject to https://www.ebsco.com/terms-of-use

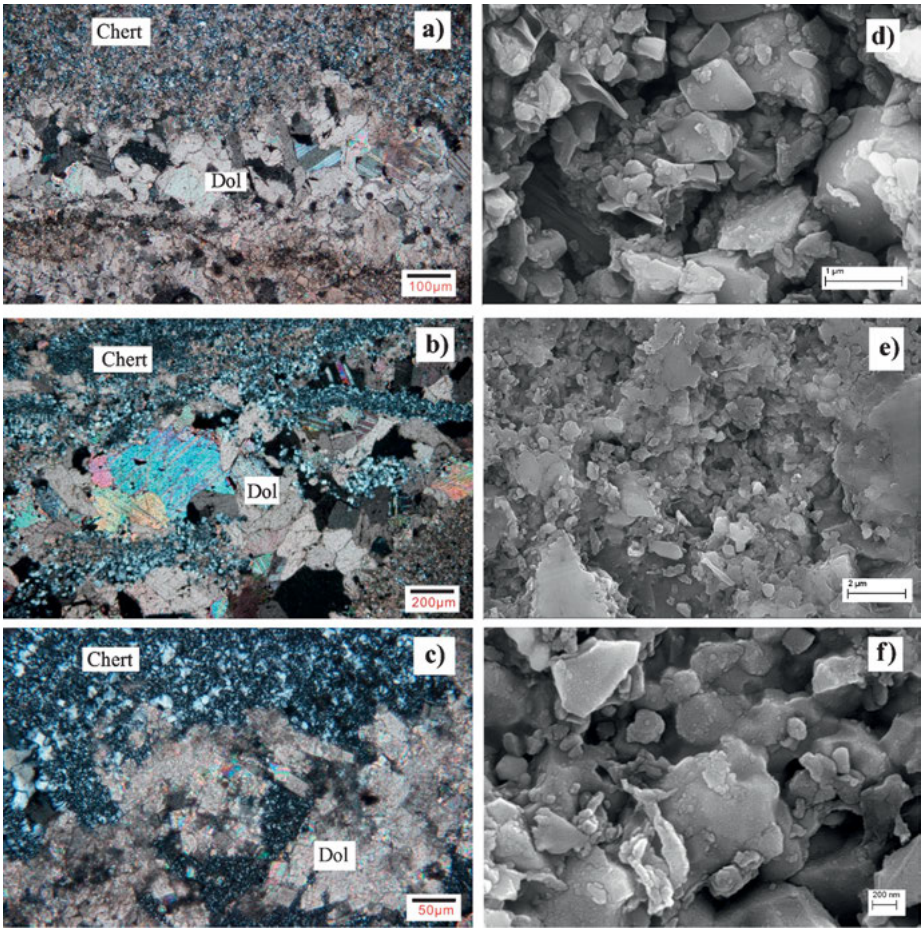

Figure 5.16: Microscopic and SEM photos of chert and dolomite. a), b) and c) are microscopic photos (crossed Nicols) of samples JX-26, JX-27 and JX-33, respectively; d), e) and f) are SEM images of samples JX-26, JX-27 and JX-27, respectively. After Ding et al. (2017).

The δ^{30}Si values of the cherts range from 0.1‰ to 3.9‰. Among them, the early Proterozoic cherts show lower δ^{30}Si values, ranging from 0.1‰ to 1.3‰, with an average of 0.75±0.43‰ (1std), compared to middle Proterozoic cherts ranging from 0.5‰ to 3.9‰, with an average of 2.22±0.74‰ (1std). Furthermore, a peak range in δ^{30}Si [2.2–3.9‰, averaging 3.12±0.56‰ (1std)] is observed in the cherts of 1.325–1.355 Ga. In addition, the δ^{30}Si variation of chert can also be observed on a millimetre scale. For example, 4 chert bands in sample JX-26 and 5 chert bands in sample JX-27 show δ^{30}Si variations of 2.3~3.9‰ and 3.1~3.6‰, respectively.

The increasing trend of δ^{30}Si from the early Proterozoic to middle Proterozoic is consistent with the trends reported by previous studies (Ding et al., 1996; Robert and

EBSCOhost - printed on 2/10/2023 8:05 PM via . All use subject to https://www.ebsco.com/terms-of-use

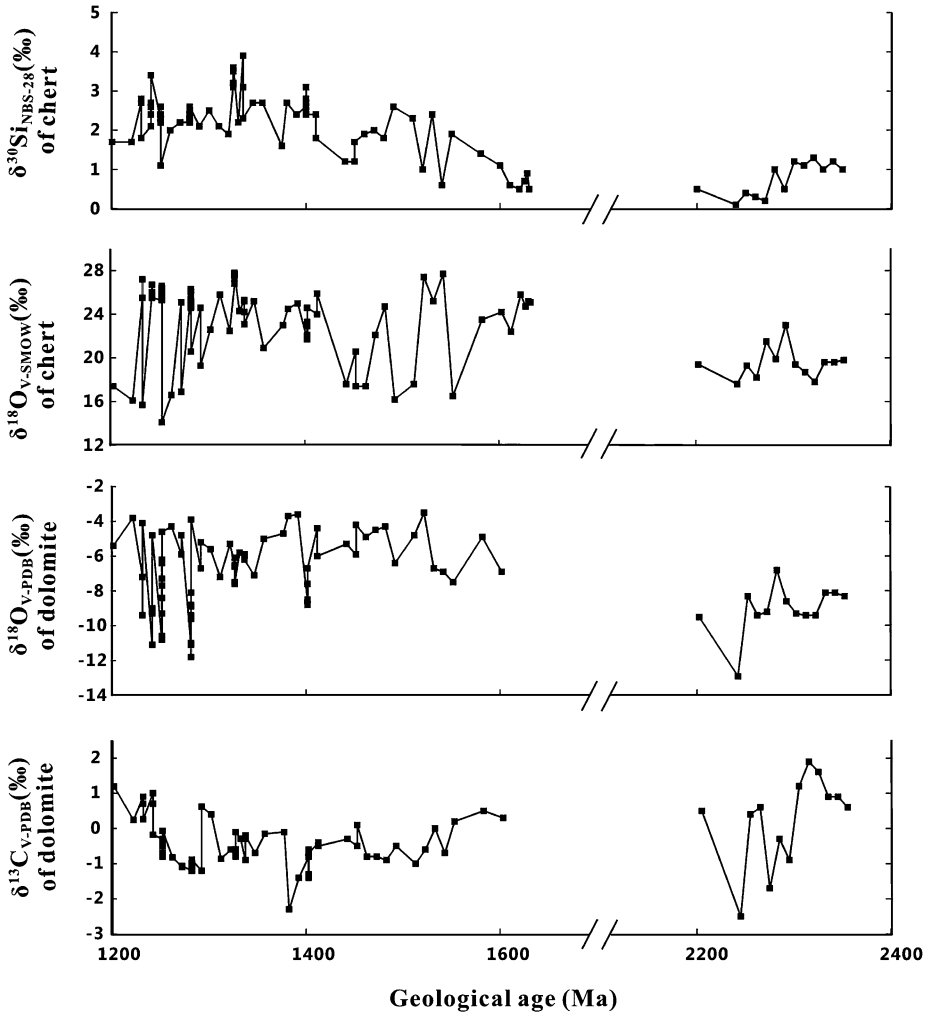

Figure 5.17: The temporal evolution of $\delta^{30}Si_{NBS\text{-}28}$ and $\delta^{18}O_{V\text{-}SMOW}$ values of chert and $\delta^{13}C_{V\text{-}PDB}$ and $\delta^{18}O_{V\text{-}PDB}$ values of dolomite for the samples collected in Ding et al. (2017). After Ding et al. (2017).

Chaussidon, 2006; van den Boorn et al., 2007, 2010; Abraham et al., 2011; Marin-Carbonne et al., 2012, 2014; Chakrabarti et al., 2012). Togerther, with the new data provided in Ding et al. (2017), the middle Proterozoic $\delta^{30}Si$ peak becomes a prominent feature in the Si isotope record of Precambrian cherts, which implies major environmental variations in the ancient ocean (Figure 5.17).

Combining data obtained using SiF_4 and MC-ICPMS methods, the $\delta^{30}Si$ variation trend from the early Archean to present is plotted for chert that formed in shallow marine environments (Figure 5.18). The upper limit of $\delta^{30}Si$ values of chert increases gradually from 0.8‰ at 3.50 Ga to 3.9‰ at 1.335 Ga and then decreases drastically to

EBSCOhost - printed on 2/10/2023 8:05 PM via . All use subject to https://www.ebsco.com/terms-of-use

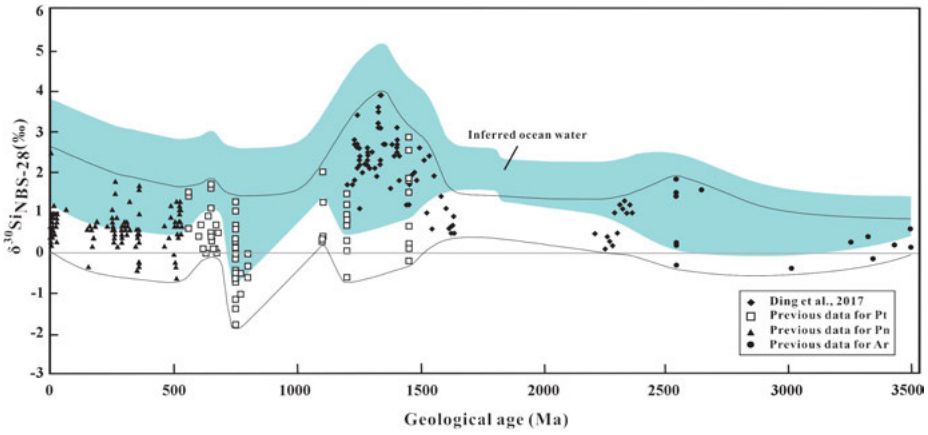

Figure 5.18: A plot showing δ^{30}Si variations of chert formed in a shallow marine environment, and inferred ocean water, from the late Archean to the present. Data for Archean chert are taken from Data for Proterozoic chert (Pt) are taken from Ding et al. (2017), Chakrabarti et al. (2012), Wang and Chen (1996), Zhao et al. (2014) and Hu et al. (2013). The data of Phanerozoic chert (Pn) are taken from Ding et al. (1996), Wang and Chen (1996), Shen et al. (2001), Xu et al. (1997), Xu (1998), Wu et al. (1997). Taking $\Delta^{30}Si_{Ch-SW}$ to be −0.5‰, −1.0‰ and −1.2‰ in the Archean, early Proterozoic and since the middle Proterozoic, respectively, $\delta^{30}Si_{SW}$ values are calculated from $\delta^{30}Si_{Ch}$.

2.0‰ at 1.104 Ga. After 1.104 Ga, the upper limit of δ^{30}Si values for chert fluctuates between 1.5‰ and 2.5‰.

Chert is normally formed by the recrystallization of a precipitated amorphous silica precursor in the diagenetic process. To test the possibility of using O and Si isotope compositions of chert to trace those of contemporary marine water, the relationship between the δ^{18}O and δ^{30}Si values of chert and those of the amorphous silica precursor are evaluated first.

It is known that the O isotope composition of silica would be reduced during diagenesis due to two factors. First, the chert nodular and band in the limestone are considered to form in the groundwater of mixed meteoric-marine coastal systems during diagenesis (Knauth, 1979). Due to the involvement of meteoric water, the O isotope composition of groundwater would be lighter than that of contemporary marine water, causing a reduction in the δ^{18}O value of chert to some extent. Second, as the diagenetic temperature is normally higher than that of marine water, the O isotope fractionation between silica and water at the diagenetic stage would be smaller than that in the precipitation stage, which would cause a δ^{18}O reduction in the chert. As shown by the microscopic and SEM examinations (Figure 5.16), the slight reduction in the δ^{18}O value of chert indicates that the studied cherts were formed in the diagenetic process and their δ^{18}O values cannot represent those of the amorphous silica precursor.

In contrast to the O isotope composition, the silicon isotope composition would not change during early diagenesis for following reasons: 1) Chert bands and nodules

EBSCOhost - printed on 2/10/2023 8:05 PM via . All use subject to https://www.ebsco.com/terms-of-use

are commonly confined in layers of sedimentary strata, which indicate that silica does not move over long distances during diagenesis. 2) The amorphous silica precursor is the dominant form of silica in dolomite rocks and the Si content in groundwater is rather limited. 3) δ^{30}Si variations at the millimetre scale or even the micrometre scale (Robert and Chaussidon, 2006; Marin-Carbonne et al., 2012; Steinhoefel et al., 2009, 2010; Heck et al., 2011; Marin et al., 2010) are preserved in cherts, which rules out the possibility of the large-scale mixing of silicon during diagenesis. Thus, the δ^{30}Si value of chert can be used as a representative of the amorphous silica precursor to trace the silicon isotope composition of contemporary seawater (van den Boorn et al., 2007).

In Figure 5.18, the inferred variation trend in $\delta^{30}Si_{SW}$ is shown. The $\delta^{30}Si_{SW}$ is calculated from the equation $\delta^{30}Si_{SW} = \delta^{30}Si_{Ch} - \Delta^{30}Si_{Ch\text{-}SW}$, where $\delta^{30}Si_{Ch}$ is the δ^{30}Si value of chert and $\Delta^{30}Si_{Ch\text{-}SW}$ is the relative Si isotope enrichment of chert to seawater. According to the theory of isotope fractionation, $\Delta^{30}Si_{Ch\text{-}SW}$ is temperature dependent. Thus, to determine a proper $\Delta^{30}Si_{Ch\text{-}SW}$ value, precipitation temperatures of the amorphous silica precursor of chert should be evaluated beforehand.

Based on the O isotope composition of chert, Robert and Chaussidon (2006) suggested the seawater temperatures were 70°C at 3.5 Ga and 35°C at 0.85 Ga. However, the inferred high Paleoarchean temperatures are controversial (Hren et al., 2009; Knauth and Lowe, 1978, 2003; Kasting et al., 2006; Walker and Lohmann, 1989), partly because δ^{18}O determinations of the Paleoarchean temperature rely on the assumption that δ^{18}O of the Archean ocean was similar to that of an ice-free modern ocean. However, it has been suggested by a number of researchers that the δ^{18}O value of the global ocean could have varied significantly over time (Knauth and Lowe, 1978, 2003; Kasting et al., 2006; Walker and Lohmann, 1989). Recently, Hren et al. (2009) studied the δ^{18}O and δD values of the 3.42 Ga Buck Reef chert rocks in South Africa and found that the chert with the highest δ^{18}O was formed in equilibrium with waters below 40°C. Blake et al. (2010) studied the oxygen isotope composition of phosphate in 3.2–3.5 Ga sediments of the Barberton Greenstone Belt and found that the phosphate with the highest δ^{18}O value was formed in seawater at a temperature range from 26°C to 35°C. According to these results, a temperature range of 35°C–40°C is more acceptable for the Archean ocean.

For the temperature of the Proterozoic ocean, fewer results have been reported. Based on the O isotope composition of chert, the temperatures in the Proterozoic ocean are estimated in the range of 35–60°C (Robert and Chaussidon, 2006). Assuming that diagenetic water has a δ^{18}O value of –10‰, and using the O isotope fractionation equation ($1000 \ln \alpha_{Dol\text{-}H2O} = 3.20 \times 10^6 T^{-2} - 2.0$) of Northrop and Clayton (1966), we obtained a diagenetic temperature range of 25~56°C (averaging 36±7°C) for dolomite in the early Proterozoic and a diagenetic temperature range of 12~50°C (averaging 26±9°C) for dolomite in the middle Proterozoic. Assuming the diagenetic water still has a δ^{18}O value of –10‰, and using the O isotope fractionation equation ($1000 \ln \alpha_{Chert\text{-}H2O} = 3.09 \times 10^6 T^{-2} - 3.29$) of Knauth and Epstein (1975), we obtained a diagenetic temperature range of 19~43°C (averaging 34±7°C) for chert in the early

EBSCOhost - printed on 2/10/2023 8:05 PM via . All use subject to https://www.ebsco.com/terms-of-use

Proterozoic and 1~63°C (averaging 17±15°C) for chert in the middle Proterozoic. The calculated average diagenetic temperature (34°C) for early Proterozoic chert is slightly lower than that (36°C) for early Proterozoic dolomite, and the calculated average diagenetic temperature (17°C) for middle Proterozoic chert is significantly lower than that (26°C) for middle Proterozoic dolomite. These observations may be caused by a difference between chert and dolomite during O isotope exchange process with diagenetic solution. The cherts are more resistant to O isotope exchange than dolomite in the diagenetic process. Thus, the calculated diagenetic temperature for dolomite may be more representative. Based on these considerations and assuming the diagenetic temperature is a little higher than the sedimentary temperature on the sea floor; we estimate the ocean temperature as 30°C in the early Proterozoic and 20°C in the middle Proterozoic.

Concerning $\Delta^{30}Si_{Ch\text{-}SW}$, there has been a number of investigations on Si isotope fractionation during abiotic silica precipitation (Geilert et al., 2014a; Oelze et al., 2015; Roerdink et al., 2015; Li et al., 1995a; Chen et al., 2016; Delstanche et al., 2009; Zheng et al., 2016). Early experimental studies on abiotic solid–fluid silicon isotope fractionation yielded $\Delta^{30}Si_{solid-fluid}$ values ranging from –2.0‰ to –1.0‰ (Li et al., 1995a; Delstanche et al., 2009). Geilert et al. (2014a) performed seeded silica precipitation experiments using flow-through reactors in the 10–60°C temperature range to quantify the silicon isotope fractionations during controlled precipitation of amorphous silica from a flowing aqueous solution. The obtained $\Delta^{30}Si_{Silica\text{-}solution}$ values were –2.1‰ at 10°C, –1.2‰ at 20°C, –1.0‰ at 30°C, –0.5‰ at 40°C, 0.1‰ at 50°C, and 0.2‰ at 60°C. These results can be used to calculate δ^{30}Si values of ocean water in different geological periods.

Assuming that the temperature of the ocean is 40°C, 30°C and 20°C in the Archean, early Proterozoic and since the middle Proterozoic, respectively, and $\Delta^{30}Si_{Ch\text{-}SW}$ are –0.5‰, –1.0‰ and –1.2‰ in the Archean, early Proterozoic and since the middle Proterozoic, respectively, δ^{30}Si values of ocean water are calculated from δ^{30}Si values of chert (Figure 5.18).

Figure 5.18 shows that the upper limit of inferred δ^{30}Si values in ocean water increases gradually from 1.3‰ at 3.53 Ga to 5.1‰ at 1.335 Ga and then decreases drastically to 3.2‰ at 1.104 Ga. After 1.104 Ga, the upper limit of inferred δ^{30}Si values in ocean water fluctuates between 2.7‰ and 3.7‰.

Ding et al. (2017) presented a conceptual model for the Si cycle of the Proterozoic ocean based on known and inferred boundary conditions (Figure 5.13). Similar to the conditions in the Archean ocean, submarine hydrothermal fluid and sea-floor weathering are still important input sources of dissolved Si to the Proterozoic ocean, but the amounts of these inputs decreased as the hydrothermal activity and ocean temperature decreased from their Archean to Proterozoic values. Further, the input of dissolved Si from the continents became significant as supercontinents appeared in the early Proterozoic. For the output of dissolved Si from the ocean in the Proterozoic

EBSCOhost - printed on 2/10/2023 8:05 PM via . All use subject to https://www.ebsco.com/terms-of-use

Eon, chemical precipitation was still a major pathway, but biological absorption may have also played a significant role (Li et al., 1988).

The Si concentration in ocean water remains in its saturated concentration at a given temperature (30°C for the early Proterozoic and 20°C for the middle and late Proterozoic). When a steady state is reached, $\delta^{30}Si_{Out}$ will be equivalent to $\delta^{30}Si_{In}$, and $\delta^{30}Si_{SW}$ will be equal to ($\delta^{30}Si_{Out} - \Delta^{30}Si_{Out\text{-}SW}$), where $\Delta^{30}Si_{Out\text{-}SW}$ is −1.0‰ for the early Proterozoic and −1.2‰ for the middle and late Proterozoic. The estimated $\delta^{30}Si_{SW}$ value of that period would be approximately 1.47~1.67‰ (Figure 5.13).

From the discussion above, extreme values of δ^{30}Si for chert and δ^{30}Si for seawater cannot be explained for an ocean at steady state conditions. Thus, this peak in δ^{30}Si indicates an extraordinary period at non-steady state suggesting a scenario at a transition stage.

From the Archean to present, there should be a transition period of the Si cycle in the ocean. In that period, the DSi in ocean water is reduced by approximately 2 orders of magnitude below that of the saturated concentration in seawater (Ding et al., 1996), and the $\delta^{30}Si_{SW}$ value first rises from ~0.2‰ to ~5.1‰ and then decreases to ~1.98‰. The rise of $\delta^{30}Si_{SW}$ is caused by Rayleigh fractionation when SiO_2 precipitates from ocean water (Figure 5.19). One mechanism that causes the DSi reduction in ocean water should be a decrease in ocean temperature. As the temperature decreases, the saturated Si concentration in ocean water would be reduced, causing additional SiO_2 precipitation. The saturated SiO_2 concentration in ocean water is ~263.5 mg/L, ~221.2 mg/L and ~178.9 mg/L at 40°C, 30°C and 20°C, respectively (Okamoto et al., 1957). When the temperature of seawater decreases from 40°C to 20°C, the fraction of dissolved Si remaining in the seawater (f) will be reduced to ~0.679. In the Rayleigh fractionation process, it will cause an increase of ~0.2‰ in $\delta^{30}Si_{SW}$. It seems that the decrease in seawater temperature alone cannot explain the significant increase in the $\delta^{30}Si_{SW}$ value, and other mechanisms should be considered. Another mechanism causing a DSi decrease in ocean water is the increase of Si absorption activities by biological species, which can reduce the DSi in ocean water two orders of magnitude lower than that of the saturated concentration. In the Rayleigh fractionation process, the combined effect of these two types of mechanisms can cause $\delta^{30}Si_{SW}$ to increase ~4.0‰ when f is reduced to 0.01. It is known that diatoms and radiolarians are Si-fixing organisms that were active in the Phanerozoic (Tréguer and de La Rocha, 2013); sponges were active in the Phanerozoic (Tréguer and de La Rocha, 2013) and the later Proterozoic (Li et al., 1988). Assuming their appearance is the start of a drastic decrease of DSi in ocean water, we should observe a $\delta^{30}Si_{SW}$ peak value in the later Proterozoic or early Phanerozoic. However, according to the data of Ding et al. (2017), the $\delta^{30}Si_{SW}$ peak appeared in the middle Proterozoic (1.325~1.355 Ga) instead, which indicates the drastic decrease in ocean water DSi happened prior to 1.355 Ga.

It is known that microbes were the dominant organism in the Precambrian. Stromatolites are found in early Archean strata from 3.5 Ga (Allwood et al., 2010) and are very well developed in Proterozoic strata (Du et al., 2009; Li et al., 2014b; Zhang et

EBSCOhost - printed on 2/10/2023 8:05 PM via . All use subject to https://www.ebsco.com/terms-of-use

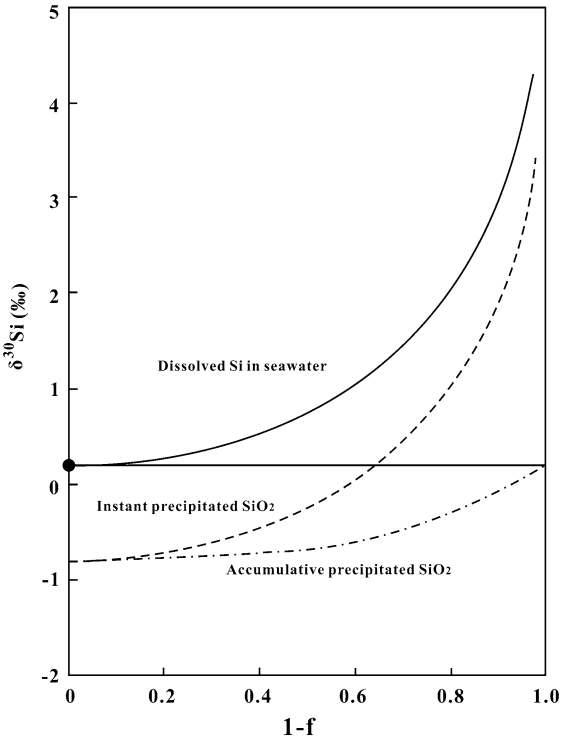

Figure 5.19: Plot showing silicon isotope fractionation during SiO_2 precipitation from ocean water in a Rayleigh process, where f is the fraction of remaining dissolved Si in ocean water and $1 - f$ is the fraction of accumulated precipitated SiO_2. The δ^{30}Si of the starting ocean water is assumed to be 0.2‰ (indicated by the filled circle) and the Si isotope fractionation factor between SiO_2 precipitate and ocean water ($\alpha_{Pre\text{-}SW}$) is 0.999. Revised from Li et al. (1995a).

al., 2002; Li et al., 1999; Chu et al., 2007; Wilson et al., 2010). REE and C, O, Nd isotope compositions have been used to study the formation conditions of stromatolite-bearing sediments, particularly the effect of biological activities (Li et al., 1999; Chu et al., 2007; Allwood et al., 2010; Wilson et al., 2010; Alexander et al., 2008). The early and middle Proterozoic chert-bearing dolomites investigated in Ding et al. (2017) are all rich in stromatolites, showing a close correlation between silica precipitation and biological activities. Moreover, macroscopic eukaryotic fossils were recently discovered in the 1.56 Ga Gaoyuzhuang formation in the Yanshan area of Northern China (Zhu et al., 2016). If some Proterozoic species are capable of absorbing or precipitating Si from ocean water, the Si content in the Proterozoic ocean water would be drastically reduced causing $\delta^{30}Si_{SW}$ to rise significantly. Thus, the high peak in $\delta^{30}Si_{SW}$ values in the middle Proterozoic ocean water may reflect a drastic reduction in Si content caused by a rapid increase in biological activity in the ocean. After that peak period, the DSi reduction rate in ocean water decreased gradually, and the $\delta^{30}Si_{SW}$ value decreases to a significantly lower value at steady state.

EBSCOhost - printed on 2/10/2023 8:05 PM via . All use subject to https://www.ebsco.com/terms-of-use

5.2.3 Silicon content and silicon isotope composition of Phanerozoic ocean water and their implications to environmental variation

The Si cycle in the modern ocean has been discussed in Section 5.1 of this chapter. A brief summary on silicon content and silicon isotope composition of Phanerozoic ocean water is given in Figure 5.13. The Si cycle in the modern and Phanerozoic ocean section are quite different with those of Archean and Proterozoic ocean (Tréguer and de La Rocha, 2013). First, dissolved Si from the continents (in rivers and groundwater) has become a dominant input source (6.4 Tmol Si/a) to ocean Si, and the Si input from submarine hydrothermal fluid (0.6 Tmol Si/a) and sea-floor weathering (1.9 Tmol Si/a) has become less significant (Tréguer and de La Rocha, 2013). $\delta^{30}Si_{in}$ is calculated as ~0.78‰ using the equation:

$$\delta^{30}Si_{in} = f_{Cont} \times \delta^{30}Si_{Cont} + f_{SFW} \times \delta^{30}Si_{SFW} + f_{SHF} \times \delta^{30}Si_{SHF} \quad (5.1)$$

In the equation, f represents the relative fraction of each Si source and the subscripts Cont, SFW and SHF indicate continent, sea-floor weathering and submarine hydrothermal fluid, respectively.

Second, the biological absorption of Si has become a dominant path for Si output from the ocean and Si contents in modern ocean water (0.05 mg/L~0.2 mg/L for shallow seawater and 0.3 mg/L~3.5 mg/L for deep seawater) are two orders of magnitude lower than those of the saturated concentration in seawater (Ding et al., 1996). At steady state, the amount and $\delta^{30}Si$ value of output Si from ocean water would be equal to those of input Si. Thus, $\delta^{30}Si_{Out}$ would also be ~0.78‰ at present.

The silicon isotope fractionations of diatoms-seawater and sponges-seawater have been experimentally studied. The determined $\Delta^{30}Si_{Diatom\text{-}SW}$ is commonly −1.0 ~ −1.1‰ (De La Rocha et al., 1997; Reynolds et al., 2006b; Sutton et al., 2013), but $\Delta^{30}Si_{Sponge\text{-}SW}$ varies from −1.1‰ to −3.7‰ (De La Rocha, 2003; Wille et al., 2010). Because diatoms are much more abundant in the ocean than sponges, we assume $\Delta^{30}Si_{Out\text{-}SW}$ in the modern ocean is ~−1.2‰. From the above estimation, the $\delta^{30}Si_{SW}$ value of the modern ocean can be calculated as ~1.98‰, which is very close to the value (1.9‰) of surface ocean water inferred previously (De La Rocha et al., 2000).

5.3 Studies on mechanisms of absorption, transportation and precipitation of silicon in plant growth processes

Silicon is present in plants with amounts equivalent to macronutrient elements, such as calcium, magnesium and phosphorus (Epstein, 1999). It has been observed that silicon is an important element for a large number of plants, such as rice, bamboo, spikemoss, horsetails, and a great number of other ferns, gymnosperms and angiosperms (Sangster and Hodson, 1986). The contents and distribution patterns of

EBSCOhost - printed on 2/10/2023 8:05 PM via . All use subject to https://www.ebsco.com/terms-of-use

silica in crops and grasses were proven to be critical to their quality and production. Silica is very helpful to increase the compression-resistance and rigidity of cell walls, and to improve light interception and drought resistance (Jones and Handreck, 1967). The present of Si strengthens the air canal, which provide more efficient oxygen supply to roots and reduce loss of water in evapo-transpiration processes. It can raise the capabilities to prevent pathogens, blast, insects, mollusks and grazing by herbivores (Sangster and Hodson, 1986; Shui et al., 1995). For these reasons, the role of silicon in plants have been studied by many investigators with different methods (Smithson, 1956; Takahashi and Okuda, 1962; Sangster, 1978; Sangster and Hodson, 1986; Jarvis, 1987; Sato et al., 1990; Sun et al., 1994; Hart, 1988; Hildebrand et al., 1997; Wang et al., 1998; Epstein, 1994, 1999; Cocker et al., 1998; Fu et al., 2000, 2001, 2002).

So far, amorphous silica (opal or silica gel) is the only silicon phase found in plants, which occurs on cell walls, in cell lumen and as extra-cellular deposits (Sangster and Parry, 1981). It is commonly accepted that Si enters plants as water-soluble $Si(OH)_4$ (Barber and Shone, 1966), which can be polymerized and precipitated as amorphous silica, frequently in close proximity to the transpiration conduit. However, there are different opinions on the issue of how roots take up and transport silicic acid. Active root uptake and transport of silicic acid were reported for rice, but passive diffusion was suggested for oats (Sangster and Hodson, 1986). Furthermore, Fu et al. (1998, 2000 and 2002) proposed that some plants could absorb silicate particles directly and selectively from the soil. This problem still remains to be solved. In addition, silicate-organic compounds were also considered as a form of silicon uptake and transportation. It was reported that some enzymes, silaffin and polyamine chains were capable of polymerizing silicic acid at neutral to acidic pHs (Mitzutani et al., 1998; Kröger et al., 2000; Pohnert, 2002). However, it is still unknown whether these compounds exist in plants.

In view of increasing applications of silicon isotope studies to biogeochemistry, its usefulness for the investigation of the mode and mechanism of silicon transport in plants was examined by several groups (Ding et al., 2005a, 2008a,b; Opfergelt et al., 2006a; Sun et al., 2008, 2016; Hodson et al., 2008). If sizeable silicon isotope variations exist in plants, they may provide direct and important information on their metabolic processes.

5.3.1 Silicon isotope studies on rice plants

Rice is a very abundant and important terrestrial plant, providing the major food supply to more than half of the world population. It also has large influence on the terrestrial environment and biogeochemical cycles of silica and other components. Thus, rice became the first plant to be studied for their silicon isotopic compositions (Ding et al., 2005a, 2008b; Sun et al., 2008, 2016).

EBSCOhost - printed on 2/10/2023 8:05 PM via . All use subject to https://www.ebsco.com/terms-of-use

5.3.1.1 Silicon isotope study on rice plants grown in rice field

For studying silicon isotope characters of rice plants, mature rice plants harvested from rice fields were investigated (Ding et al., 2005a). The studied 16 rice plants were collected in 2000 from paddy fields in four counties (Jiaxing, Pujiang, Fuyang and Shaoxing) of the Zhejiang province, China.

To investigate the silicon isotope variations among different kinds of rice, four types of rice plants were collected in each county: One (SX-9714) belongs to glutinous rice and three (C-97252, N-97-77 and XS-63CK) belong to round-grained non-glutinous rice.

Variations of SiO_2 in rice plants and paddy soils

The SiO_2 contents of paddy soils vary from 61.8% to 77.5%, averaging 66.6%. In dried plant samples, the SiO_2 contents of rice roots vary from 2.8% to 10.6%, averaging 6.0%; the SiO_2 contents of SL vary from 4.6% to 10.1%, averaging 7.6%; the SiO_2 contents of husks vary from 8.7% to 12.1%, averaging 10.6%; and the SiO_2 contents of grains vary from 0.017% to 0.053%, averaging 0.032% (Figure 5.20). The SiO_2 contents of SL are higher than those of roots in some cases, but lower in other cases. However, on average the SL is more enriched in SiO_2 than in the roots. On average, the husks are more enriched in SiO_2 than SL. The SiO_2 contents of grains are drastically reduced.

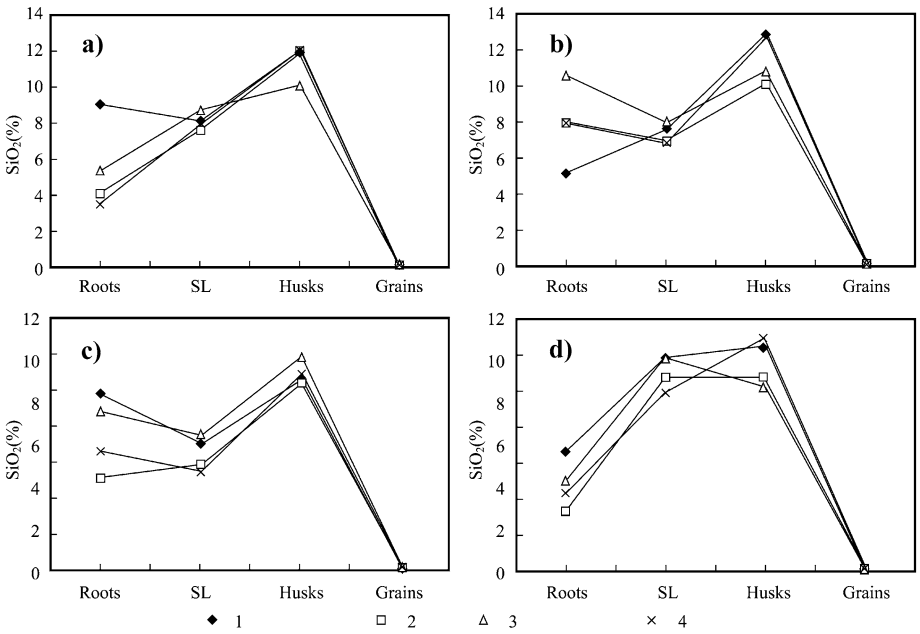

Figure 5.20: The SiO_2 contents of different rice organs in dried plants. After Ding et al. (2005a). a) Jiaxing; b) Pujiang; c) Fuyang; d) Shaoxing; 1: SX-9714; 2: C-97252; 3: N-97-77; 4: XS-63CK.

EBSCOhost - printed on 2/10/2023 8:05 PM via . All use subject to https://www.ebsco.com/terms-of-use

The highest SiO_2 content is observed in husks and lowest SiO_2 content is found in rice grains. It seems that SiO_2 is concentrated in the outer layers and higher positions within a rice plant. No systematic SiO_2 variations are observed between different types of rice.

Variations of silicon isotope composition in rice plants and paddy soils

The δ^{30}Si values of paddy soils vary from –0.4‰ to 0‰, averaging –0.25‰. The δ^{30}Si values of roots vary from –0.9‰ to 0.1‰, averaging –0.29‰. The δ^{30}Si values of SL vary from –0.5‰ to 0.4‰, averaging –0.16‰. The δ^{30}Si values of husks vary from 0.1‰ to 1.1‰, averaging 0.61‰. The δ^{30}Si values of rice grains vary from 1.0‰ to 6.1‰, averaging 2.98‰ (Figure 5.21). The δ^{30}Si value of 6.1‰, observed in the rice grains of samples JX-1 and JX-4, is much higher than the highest value (3.4‰) observed for terrestrial samples before (Ding et al., 1996). The δ^{30}Si values of different rice organs and paddy soils show significant variations from place to place and from plant to plant, reflecting differences in silicon sources, rice types and growth conditions (Figure 5.21). However, the most significant phenomenon is the large and systematic silicon isotope variations among different organs within individual rice plants. The average δ^{30}Si values are –0.25‰ for soils, –0.29‰ for roots, –0.16‰ for SL, 0.61‰ for husks and 2.98‰ for grains, showing an increase trend from roots and SL, through husks to grains (Figure 5.21).

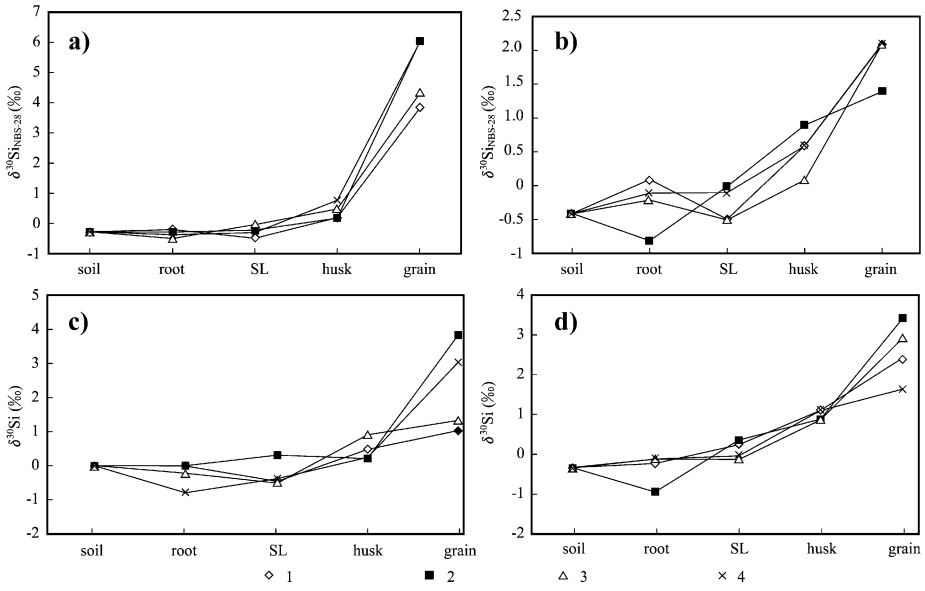

Figure 5.21: The δ^{30}Si values of different rice organs and soils. After Ding et al. (2005a). a) Jiaxing; b) Pujiang; c) Fuyang; d) Shaoxing; 1: SX-9714; 2: C-97252; 3: N-97-77; 4: XS-63CK.

EBSCOhost - printed on 2/10/2023 8:05 PM via . All use subject to https://www.ebsco.com/terms-of-use

Silicon isotope fractionation process during SiO_2 precipitation in rice plants

The $\delta^{30}Si$ values, along with the data of SiO_2 contents and the mass fractions of different rice organs, can be used to study silicon isotope fractionation process during SiO_2 precipitation in the rice plant. The average mass fractions of roots, SL, husks and grains are 5.9%, 45.5%, 8.3% and 40.4%, respectively. The average SiO_2 contents of roots, SL, husks and rice grains are 6.0%, 7.6%, 10.6% and 0.032%, respectively. Thus, the average fractions of SiO_2 in roots, SL, husks and grains are calculated to be 0.075, 0.735, 0.187 and 0.003, respectively. Then the $\delta^{30}Si$ value of bulk rice is calculated to be −0.02‰. Assuming that the silicon absorbed by rice is precipitated completely within the plant, this value should represent the initial $\delta^{30}Si$ value of the silicon-bearing solution in the rice plant.

Based on these data, a $\delta^{30}Si$ vs. $(1-f)$ diagram for studied rice is shown in Figure 5.22, where f is the fraction of dissolved silicon remaining in the rice plant. It is assumed that dissolved $Si(OH)_4$ in rice polymerizes and is precipitated gradually from roots, through SL and husks, to grains and that the initial $\delta^{30}Si$ value of the silicon-bearing solution in the rice plant is that of the total SiO_2 in the plants (−0.02‰). Fitting to a Rayleigh model yielded that the $\delta^{30}Si$ value of an initial SiO_2 precipitates in roots is about −0.44‰. The isotope fractionation factor, $\alpha^{30}Si_{Prec-DSi}$ is computed to be 0.99958. Because the polymerization process of $Si(OH)_4$ is a non-reversible process, and precipitated SiO_2 is unlikely to exchange silicon isotopes with $Si(OH)_4$ remained in a solution, the silicon isotope fractionation in a rice plant can be regarded as a kinetic isotope fractionation in a Rayleigh process. Figure 5.22 may be regarded as a model

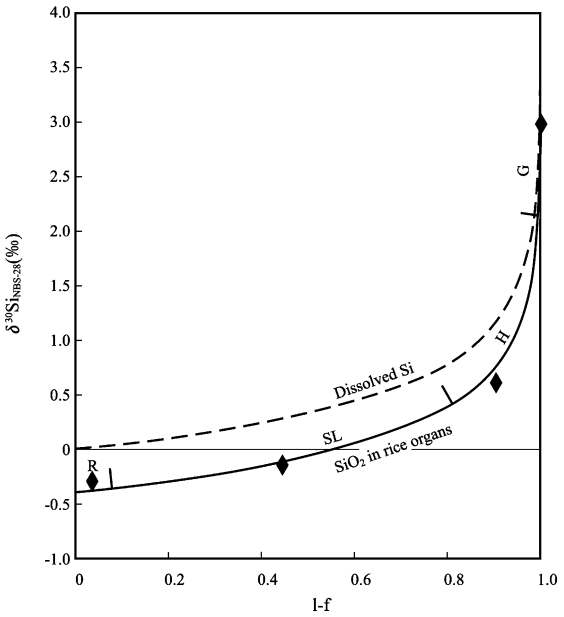

Figure 5.22: A plot showing the silicon isotope fractionation during SiO_2 precipitation in rice plants. After Ding et al. (2005a). R – roots, SL – stem and leaves, H – husks, G – grains. $\delta^{30}Si_{\sum Si} = -0.02‰$; f – fraction of dissolved silicon remained in the rice plant.

EBSCOhost - printed on 2/10/2023 8:05 PM via . All use subject to https://www.ebsco.com/terms-of-use

of silicon isotope fractionation in rice plants from the Zhejiang Province, China. During this process, the δ^{30}Si value of the dissolved silicon in plant water of rice increases gradually from −0.02‰ to 6.5‰ (at f value around 0.0001), and the δ^{30}Si value of the precipitated SiO_2 in rice plant increases simultaneously from −0.44‰ to 6.1‰ (at f value around 0.0001). This fractionation pattern is similar to those of Douthitt (1982), Li et al. (1995a), De La Rocha et al. (1997) for SiO_2 precipitation from solution in abiotic and biotic processes, although the magnitude of the fractionations are somewhat different.

Mechanisms of absorption, transportation and precipitation of Si in rice plants

Numerous investigations have been carried out on the behavior and the role of silicon in plants (Takahashi and Okuda, 1962; Sangster, 1978; Sangster and Hodson, 1986; Jarvis, 1987; Epstein, 1994, 1999; Cocker et al., 1998; Fu et al., 2000, 2001, 2002). However, there are still many controversies on the mechanism of absorption, transportation and precipitation of silicon in plants. It was suggested that Si enters plants as water-soluble $Si(OH)_4$ (Barber and Shone, 1966). However, Fu et al. (1998, 2000, 2002) proposed that some plants may absorb silicate particles directly and selectively from soil, then the soluble elements were leached from these silicate mineral particles and carried to the shoots as nutrients, leaving the residual silica particles in the cortex. Results obtained in this study lay some constraints on the issue of silicon uptake and transportation.

Firstly, the distribution of SiO_2 in various rice organs is considered. If the viewpoint of Fu et al. (1998, 2000, 2002) can apply to rice, the SiO_2 should be enriched in roots, but depleted in SL and husks. However, it is observed that, in all rice samples after ignition, the SiO_2 contents increase from roots to SL to husks (Figure 5.20), suggesting that water-soluble silicon is more likely the major silicon component absorbed by rice roots (Sangster and Hodson, 1986).

Secondly, the silicon isotope composition is considered. The average δ^{30}Si value of bulk rice is calculated to be −0.02‰, which is 0.23‰ higher than the average δ^{30}Si value (−0.25‰) of paddy soils. This relationship does not support the idea of absorbing silicate particles directly, because in that case, the δ^{30}Si values of the bulk rice plant should be equal to those of soils. In contrast, the idea of absorbing dissolved silicon from paddy water is more acceptable. It is known that during the weathering processes of silicate rocks, silicon isotope fractionation occurs between produced secondary clay minerals and dissolved silicon in solution. In comparison with the initial silicate rock, the former is always depleted in ^{30}Si (by about 1.5‰), and the latter is enriched in ^{30}Si (by about 0.75‰) (Ding et al., 1996; De La Rocha et al., 2000; Ziegler et al., 2005a,b). Therefore, the paddy water, which consists of irrigation and soil waters, normally has δ^{30}Si values higher than those of rocks and soils (Ding et al., 2004). The paddy water was not collected in 2000. However, three water samples were collected from the Qiantang River in 2002, which give an average δ^{30}Si value of 1.0‰ (Ding et

EBSCOhost - printed on 2/10/2023 8:05 PM via . All use subject to https://www.ebsco.com/terms-of-use

al., 2005a). Assuming the paddy water was dominated by irrigation water, the δ^{30}Si value of initial plant water in rice (−0.02‰) would be about 1.0‰ lower than that of the paddy water, suggesting that silicon isotope fractionation may occur when rice roots take up dissolved silicon from paddy water.

Besides, the high silica contents in the husks indicate the roles of transpiration and evaporation for silica precipitation in rice. Based on the variation patterns of SiO_2 contents and δ^{30}Si values among different rice organs (Figure 5.20 and Figure 5.21), it can be inferred that evapotranspiration is the driving force for an upward flow of a silicon-bearing solution and silica precipitation. Therefore, a passive mechanism of silica transport may be important for rice, although the role of active root uptake and transport of silicic acid cannot be ruled out completely.

5.3.1.2 The experimental studies on silicon isotope fractionation in growth process of rice plants

The experimental studies on silicon isotope fractionation in growth process of rice plants were carried out to get further information on the mechanism of Si accumulation in plants and biogeochemical Si cycle (Sun et al., 2008; Ding et al., 2008b).

The rice growth experiment was conducted in 2005 at the Zhejiang University. Rice (*Oryza sativa* L. cv. Zhenong 952) was grown to maturity with the hydroponic culture in a naturally lit glasshouse for three months. The detailed experimental processes were described in Sun et al. (2008) and Ding et al. (2008b).

The nutrient solution was sampled for 14 times in the rice grown process. The rice plants were sampled at various growth stages: i.e., the seedling stage (P01), the tiller stage (P02), the jointing stage (P03), the heading stage (P04) and maturity stage (P05). Different parts of the rice plants, such as roots, stem, leaves, husks and rice grains, were sampled separately. Besides some rice leaves in mature stage were cut in different parts: leaf sheath, leaf blade base, leaf blade middle and leaf blade top along the leaf axis.

The silicon content of the nutrient solution and the rice plant

The silicon content of the nutrient solution

The silicon content in the nutrient solution is shown in Figure 5.23. It was observed that in the rice growing process, the silicon content in the nutrient solution decreased gradually from 16 mM at start to 0.1~0.2 mM at harvest.

The silica contents and distribution in different organs of the rice plants

The SiO_2 contents (wt %) of different organs from the rice plants of various growth stages are plotted in Figure 5.24. Each represents the average value of 4 replicate samples.

EBSCOhost - printed on 2/10/2023 8:05 PM via . All use subject to https://www.ebsco.com/terms-of-use

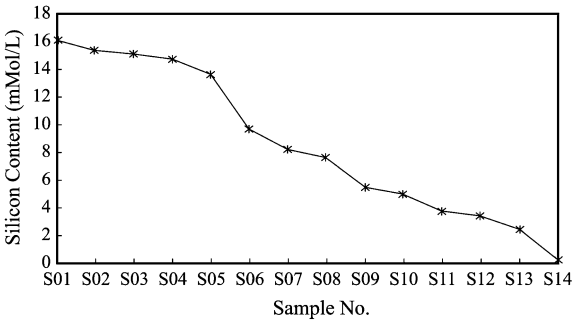

Figure 5.23: Variation of the silicon concentrations in samples of nutrient solution. After Ding et al. (2008b). The average values are plotted.

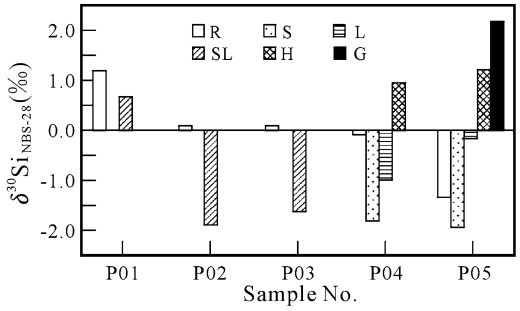

Figure 5.24: The silica contents in different organs of the rice plants from various growth stages. After Ding et al. (2008b). P01: seedling stage; P02: tiller stage; P03: jointing stage; P04: heading stage; P05: maturity stage. R – roots; S – stem; L – leaves; SL – stem plus leaves; H – husks; G – grains.

At the seedling stage (P01), the silica contents in roots (0.64%) and in SL (0.44%) were both very low and the silicon content in SL (stem plus leaves) was slightly lower than that in roots. At the tiller stage (P02), the silica contents in roots (3.55%) and SL (8.03%) were both higher than at the seedling stage and the silica content in SL became significantly higher than in roots. At the jointing stage (P03), the silica content in roots (3.67%) was slightly higher than at the tiller stage, but the silica content in SL (12.21%) became much higher than at the tiller stage. At the heading stage (P04), the silica content in roots (2.84%) became significantly lower than at the jointing stage. The silica content increased from roots, through stem (5.38%), to leaves (17.46%), but decreased from leaves to husks (12.05%). At the maturity stage (P05), the silica content in roots (1.43%) was much lower than at the heading stage, but the silica contents in stem (9.80%), leaves (19.97%) and husks (23.22%) were higher than at the heading stage. The silica content increased from roots, through stem and leaves, to husks, and then dropped drastically from husks to grains (0.11%), similar to the trend observed in rice plants from the paddy field (Ding et al., 2005a).

The amounts of silica in different organs of the rice plants were calculated from their SiO_2 contents and dry weights. From the amounts of silica in different organs of the rice plants, their SiO_2 fractions were also calculated. The results are shown in Figure 5.25. The SiO_2 fraction in roots decreased continuously from the seedling

EBSCOhost - printed on 2/10/2023 8:05 PM via . All use subject to https://www.ebsco.com/terms-of-use

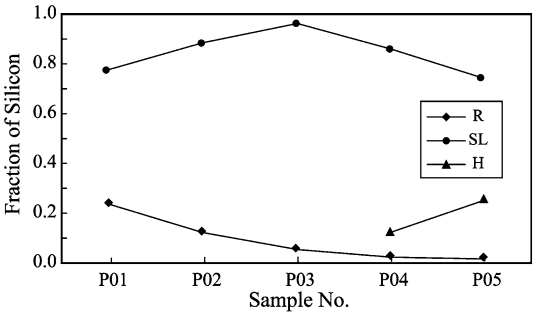

Figure 5.25: The fraction of silica for different organs of the rice plants from various growth stages. After Ding et al. (2008b). P01~P05: The sample numbers as in Figure 5.25. R – roots; SL – stem plus leaves; H – husks.

stage (0.23), through the tiller stage (0.12), jointing stage (0.05) and heading stage (0.023), to the maturity stage (0.009). Accordingly, the SiO_2 fraction in SL increased from the seedling stage (0.77), through the tiller stage (0.88), to the jointing stage (0.95). At the heading stage, the SiO_2 fraction in aerial parts (SL + husks) increased to 0.977. At the maturity stage, the SiO_2 fraction in aerial parts (SL + husks + grains) increased to 0.991. From the heading stage to the maturity stage, the SiO_2 fraction in husks increased from 0.119 to 0.249. All of these variations indicate that the silica intends to concentrate in the upper part of rice plant in its growing process.

The forms and distributions of silica in roots, stem, leaves and husks of the rice plant were examined by using an electron microprobe JXA-8800R (Figure 5.26). The backscatter electron image and X-ray mapping show that the silica in root is exclusively in endodermal cells (Figure 5.26a and Figure 5.26b), the silica in stem (Figure 5.26c and Figure 5.26d) and in husks (Figure 5.26g and Figure 5.26h) is accumulated mainly in epidermal cells, the silica in leaves is accumulated mainly in epidermal cells with the highest levels in specialized idioblasts (Figure 5.26e and Figure 5.26f). These distributions are similar to those observed by Kaufman et al. (1972) in rice and Lux et al. (2003) in bamboo.

The variation curves of silica contents in different rice organs and amounts of silica in bulk rice plants are plotted in Figure 5.27 as functions of $(1 - f)$, where f means the fraction of silicon left in the nutrient solution (including dissolved silicon and the amorphous silica gel). The silica content in SL and in husks and the amount of silica accumulated in bulk rice plant all show positive correlations with $(1 - f)$. In other words, the amount of accumulated silica in bulk rice plant and silica contents in SL and husks all increased gradually as the silicon concentration of the nutrient solution decreased.

Different correlation is observed between the silica content in roots and $(1 - f)$. The silica content in roots increased significantly from 0.44% to 3.55%, as $(1 - f)$ in-

EBSCOhost - printed on 2/10/2023 8:05 PM via . All use subject to https://www.ebsco.com/terms-of-use

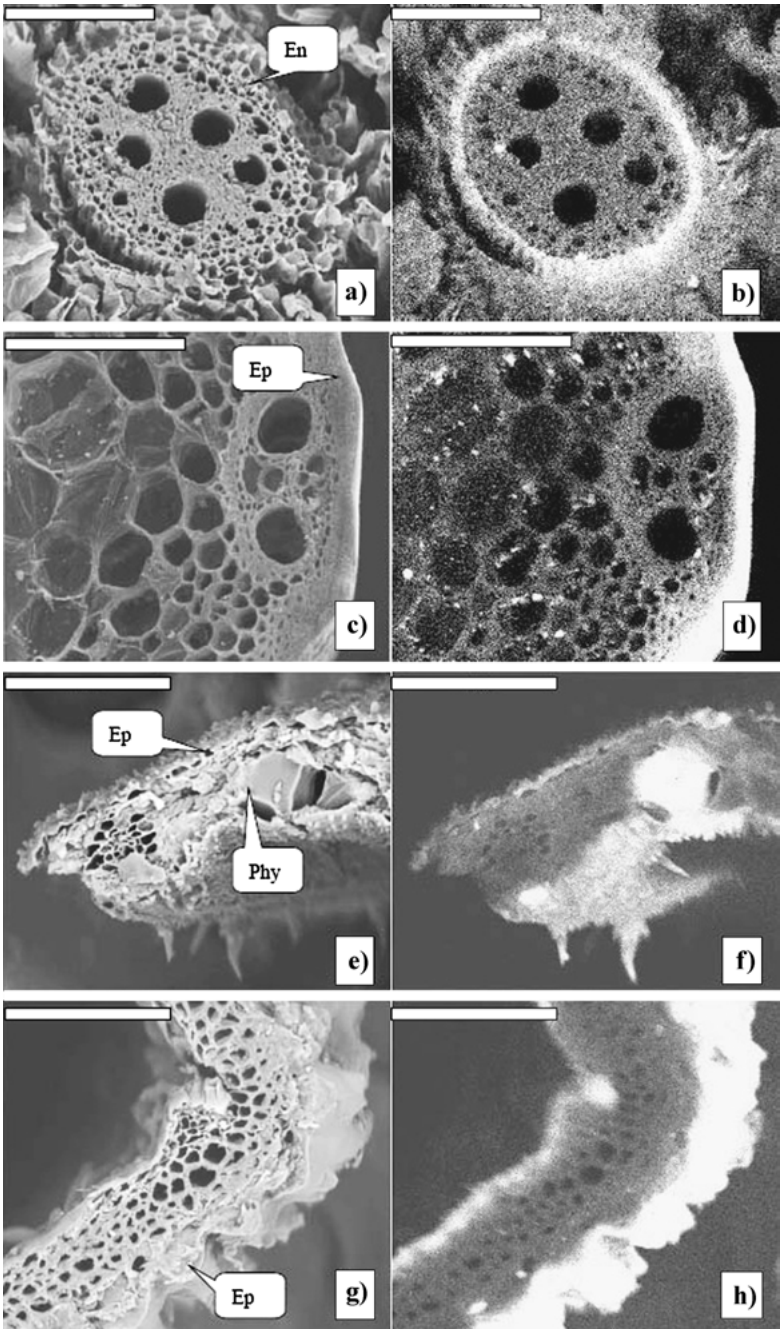

Figure 5.26: The electron micrographs for roots, stem, leave and husks of the rice plants. After Ding et al. (2008b). a), c), e), g) show electron backscattering images for root, stem, leaf and husk, respectively. b), d), f), h) show X-ray mappings of Si in root, stem, leaf and husk, respectively. Bars represent 100 μm. En – endodermis. Ep – epidermis. Phy – phytoliths.

EBSCOhost - printed on 2/10/2023 8:05 PM via . All use subject to https://www.ebsco.com/terms-of-use

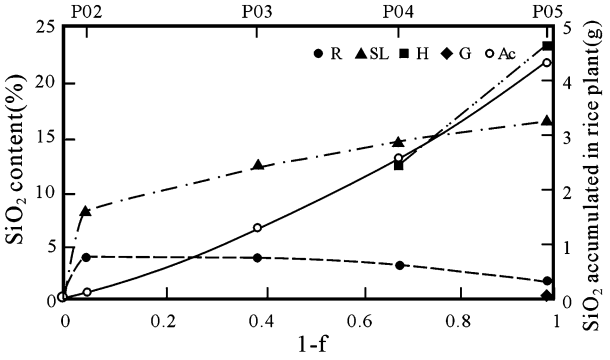

Figure 5.27: Variations of the silica content in different organs of the rice plant and the amount of silica in bulk rice plant as functions of $1-f$. After Ding et al. (2008b). f = fraction of silicon remaining in nutrient solution (including dissolved silicon and the amorphous silica gel). P02~P05: The samples of different stages; R – roots; SL – stem plus leaves; H – husks; G – grains; Ac – silica accumulated in bulk rice plant.

creased from 0 (the seedling stage) to 0.05 (the tiller stage), and then increased slightly to 3.67%, as $(1-f)$ increased to 0.4 (the jointing stage). However, the silica content in roots decreased from 3.67%, through 2.84%, to 1.43%, as $(1-f)$ increased from 0.4 (the jointing stage), through 0.69 (the heading stage) to 0.99 (the maturity stage). In other words, there was a positive correlation between silica content in the rice roots and the silicon content in the nutrient solution.

To understand this relation, we may recall the model of two silicon components for bamboo plant (Ding et al., 2008b). It was inferred that there were two silicon components in bamboo plant: one was the precipitated silica; the other was the dissolved silicon in plant fluid. The ratio of dissolved H_4SiO_4 to precipitated SiO_2 might be much higher in bamboo roots than in its stem, branch and leaves. As the silica distribution pattern in different organs of the rice plant (Figure 5.26) is similar to that observed in bamboo (Ding et al., 2008a), this model may be applicable to rice. In this condition, the silicon in rice roots might be dominated by dissolved H_4SiO_4 and the decrease of silicon content in rice roots from the jointing stage, through the heading stage, to the maturity stage might reflect mainly the decrease of silicon in the nutrient solution. The results obtained from the rice growth experiment in the open system (Sun et al., 2008) support also this correlation. The silica content in the rice roots of the maturity stage was 2.5 times higher (4.98%) for the open system (Sun et al., 2008) than that (1.43%) for the closed system, corresponding to that the silicon concentration of the nutrient solution at the maturity stage was much higher in the open system (3 mM) than that (0.17 mM) in the closed system. The increase of silica content in SL and husks may indicate that their silicon was dominated by the precipitated silica, which increased continuously in the rice growth process.

EBSCOhost - printed on 2/10/2023 8:05 PM via . All use subject to https://www.ebsco.com/terms-of-use

The silicon isotope composition of the nutrient solution and the rice plant

The silicon isotope composition of the nutrient solution

The silicon isotope compositions of the nutrient solution sampled at different time are plotted in Figure 5.28. The δ^{30}Si value of the nutrient solution increased gradually from –0.1‰ at the start to 1.5‰ at the harvest, reflecting the effect of preferential absorption of light silicon isotope by rice plants.

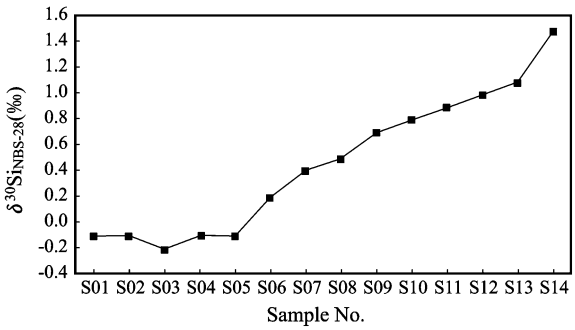

Figure 5.28: Variation of silicon isotope compositions of the nutrient solutions. The average values are plotted. After Ding et al. (2008b).

The silicon isotope composition of the rice plants

The silicon isotope compositions of different rice organs and bulk rice plants at various growth stages are plotted in Figure 5.29. At the seedling stage (P01), the δ^{30}Si values of SL and roots were 0.7‰ and 1.2‰, respectively. At the tiller stage (P02), the δ^{30}Si values of SL and roots were –1.9‰ and 0.05‰, respectively, both lower than those at the seedling stage, reflecting preferentially absorption of light silicon isotope from

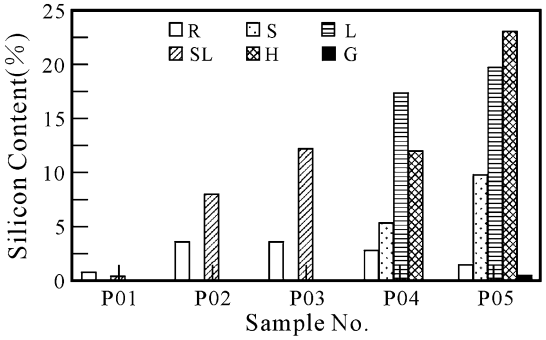

Figure 5.29: Silicon isotope compositions of different organs of the rice plants from various growth stages. After Ding et al. (2008b). P01~P05: The samples of different stages. R – roots; S – stem; L – leaves; SL – stem plus leaves; H – husks; G – grains.

EBSCOhost - printed on 2/10/2023 8:05 PM via . All use subject to https://www.ebsco.com/terms-of-use

the nutrient solution. The δ^{30}Si value of SL was much lower than that in the roots. At the jointing stage (P03), the situation was quite similar to the tiller stage, but the δ^{30}Si value of SL was slightly higher than that at the tiller stage. At the heading stage (P04), the δ^{30}Si value decreased from roots to stem, and then increased from stem, through leaves, to husks. At the maturity stage (P05), the δ^{30}Si value decreased from roots to stem, and then increased from stem, through leaves and husks, to grains. This trend is generally consistent with the trend observed in the field grown rice (Ding et al., 2005a). However, the picture presented in this study is more detailed as the δ^{30}Si values of stem and leaves have been determined separately.

The silicon isotope compositions of different rice organs in the rice plant collected at maturity stage (P05) are plotted in a cartoon (Figure 5.30) (Sun et al., 2008). It shows that the plant tissues display large variations in both Si isotope composition and Si contents. The Si content increases from grain to root to stem to leaf to husk, and the δ^{30}Si value increased from stem to root to leaf to husk to grain. From stem to leaf and husk, both δ^{30}Si value and SiO_2 content show trend of increase. Rice grain is the organ with highest δ^{30}Si value, but lowest SiO_2 content, indicating that its SiO_2 was the last small fraction precipitated from fluid in rice plant. The data of leaves show similar

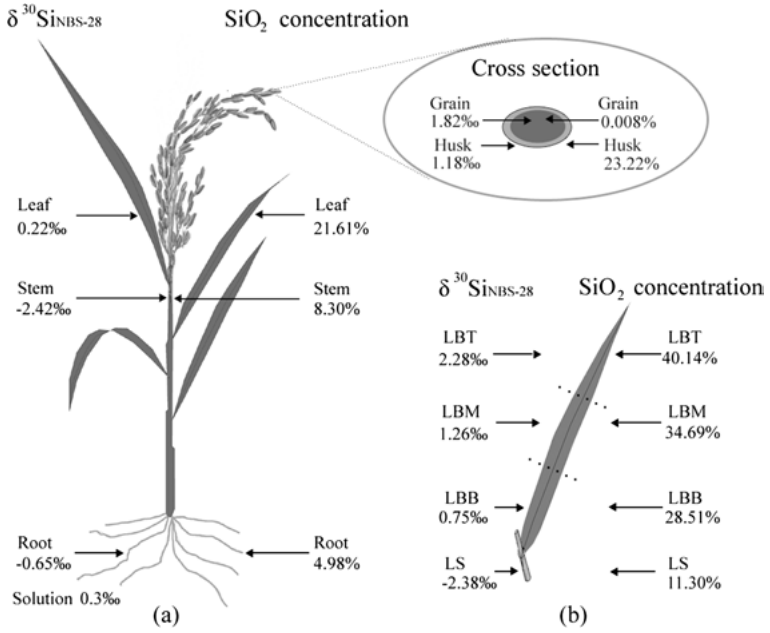

Figure 5.30: A cartoon picture showing δ^{30}Si values and SiO_2 contents of different rice organs in the rice plant collected at the maturity stage. After Sun et al. (2008). a) Mean δ^{30}Si values and SiO_2 contents of root, stem, leaf, husk and grain of rice plant, and mean δ^{30}Si value of nutrient solution. b) Mean δ^{30}Si values and SiO_2 contents of LS (leaf sheath), LBB (leaf blade base), LBM (leaf blade middle) and LBT (leaf blade top).

EBSCOhost - printed on 2/10/2023 8:05 PM via . All use subject to https://www.ebsco.com/terms-of-use

variation pattern that from lower part to upper part (from LS to LBB, LBM, LBT) the δ^{30}Si value and SiO_2 content both increase (Figure 5.30).

The δ^{30}Si values of the bulk rice plant at various growth stages were calculated from the δ^{30}Si values and Si fractions of different organs. The results are shown in Figure 5.31. It was found that at the seedling stage the δ^{30}Si value of bulk rice plant (0.85‰) was lower than that of the rice seeds (1.8‰), reflecting some contribution of silicon from the germination nutrient solution. At the tiller stage, the δ^{30}Si value of the bulk rice plant (−1.70‰) was much lower than that at the seedling stage, reflecting the preferential uptake of light silicon from the nutrient solution. At the jointing stage, the δ^{30}Si value of the bulk rice plant (−1.55‰) was slightly higher than that at the tiller stage, reflecting the raise of δ^{30}Si value of the nutrient solution. At the heading stage, the δ^{30}Si value of the bulk rice plant (−0.83‰) was significantly higher than at the jointing stage, reflecting the further raise of δ^{30}Si of the nutrient solution. At harvest, the δ^{30}Si value of the bulk rice plant (−0.08‰) was equivalent to the value of the starting nutrient solution, as the silicon fraction left in the nutrient solution became less than 0.01.

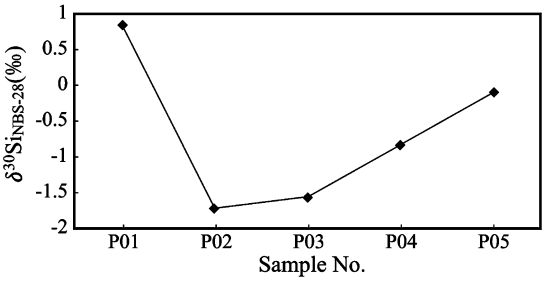

Figure 5.31: The δ^{30}Si values of bulk rice plants at various growth stages. After Ding et al. (2008b). P01–P05: The samples of different stages.

At the seedling, tiller and jointing stages, the δ^{30}Si values of roots were all higher than those of SL. At the heading and maturity stages, the δ^{30}Si values of roots were all higher than those of the stems. This kind of relation is similar to that observed in bamboo plants and may be explained with a model of two silicon components in plants (Ding et al., 2008a,b). From the seedling stage to the maturity stage, the δ^{30}Si values of roots show a trend of decrease, which may reflect the reducing of dissolved H_4SiO_4 to precipitated silica ratio in rice roots.

The δ^{30}Si variations of the silicon in the nutrient solution ($\delta^{30}Si_{NS}$) and the silicon absorbed by rice plant ($\delta^{30}Si_{Ab}$) as functions of $(1 - f)$

From the obtained data, a plot of δ^{30}Si variation curves for the silicon in the nutrient solution ($\delta^{30}Si_{NS}$) and the silicon absorbed by rice plant ($\delta^{30}Si_{Ab}$) as functions of $(1-f)$

EBSCOhost - printed on 2/10/2023 8:05 PM via . All use subject to https://www.ebsco.com/terms-of-use

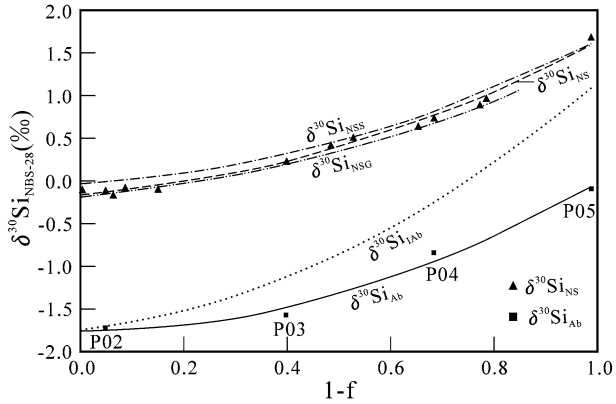

Figure 5.32: The δ^{30}Si variation curves for the silicon in the nutrient solution ($\delta^{30}Si_{NS}$) and the silicon absorbed by the rice plant ($\delta^{30}Si_{Ab}$) as functions of $(1-f)$. After Ding et al. (2008b). The calculated δ^{30}Si variation curves for dissolved Si in the nutrient solution ($\delta^{30}Si_{NSS}$), gel like silica in the nutrient solution ($\delta^{30}Si_{NSG}$) and silicon instantaneously absorbed by the rice plants ($\delta^{30}Si_{IAb}$) are also plotted. f = fraction of silicon remaining in nutrient solution. P02~P05: The samples of different stages.

is shown in Figure 5.32 (Ding et al., 2008b). In this plot, the $(1-f)$ values are calculated from the SiO_2 contents in a nutrient solution in different growth stages, the $\delta^{30}Si_{NS}$ values are measured from a nutrient solution in different growth stages. The $\delta^{30}Si_{Ab}$ values are calculated by using following equation:

$$\delta^{30}Si^{n}_{Ab} = (\delta^{30}Si^{n}_{BP} \times A^{n}_{BP} - \delta^{30}Si^{1}_{BP} \times A^{1}_{BP})/(A^{n}_{BP} - A^{1}_{BP}) \quad (5.2)$$

where A^{1}_{BP} represents the amount of silica in bulk rice plant at start (P01), A^{n}_{BP} represents the amount of silica in the bulk rice plant at stage n; $\delta^{30}Si^{1}_{BP}$ represents the δ^{30}Si value of silica in the bulk rice plant at start (P01), $\delta^{30}Si^{n}_{BP}$ represents the δ^{30}Si value of silica in the bulk rice plant at stage n. $\delta^{30}Si^{n}_{Ab}$ represents the δ^{30}Si value of silicon absorbed by rice plants by stage n.

Accordingly, the silicon isotope fractionation factors between instantaneously absorbed silicon by the rice plant and dissolved silicon in the nutrient solution, $\alpha_{IAb\text{-}NSS}$, vary in a range from 0.9983 to 0.9995.

This variation may reflect the changes of conditions in the rice growth process. It is well known that the isotope fractionation factor in the kinetic process is generally related to the temperature and rate of reaction. As their experiment was conducted in a naturally-lit glasshouse from May to August, the nutrient solution temperature increased as the monthly mean air temperature increased from ~16°C to ~30°C. Meanwhile, the absorption rate of silicon by the rice plant increased, as it grew up gradually. Considering above conditions, the decrease trend of silicon isotope fractionation between the nutrient solution and the silicon instantaneously absorbed by the rice plant is reasonable.

EBSCOhost - printed on 2/10/2023 8:05 PM via . All use subject to https://www.ebsco.com/terms-of-use

For comparison, the available data for silicon isotope fractionation factors between plants and growth solutions for rice, bamboo, banana and diatoms are listed in Table 5.4. It is noted that all plants absorb a preferentially light silicon isotope from growth solutions and the silicon isotope fractionation factors are very similar for all of these plants.

Table 5.4: The silicon isotope fractionation factors between rice, bamboo, banana and diatoms and growth solutions.

Plant	$\Delta^{30}Si_{Pl\text{-}Sol}$(‰)	$\alpha_{Pl\text{-}Sol}$	Reference	Note
Rice	−0.5 ~ −1.6	0.9995~0.9984	Ding et al., 2008b	From various growth stages
Bamboo	−0.8 ~ −1.4	0.9992~0.9986	Ding et al., 2008a	Obtained from 7 plants
Banana	−0.6 ~ −1.0	0.9994~0.9990	Opfergelt et al., 2006b	Calculated from $\delta^{29}Si_{Pl\text{-}Sol}$
Diatoms	−0.7 ~ −1.5	0.9993~0.9985	De La Rocha et al., 1997	Calculated from the data and standard deviations

Pl – Plant; Sol – Solution.

Implications for the mechanism of Si uptake by rice roots

How plants get silicon from their external environments is an important issue for agronomic, botanical, plant physiological and silicon biogeochemical studies. This issue consists of two aspects: a) What is the form of silicon absorbed by plant roots; and b) how roots uptake silicon from the external environment.

For the first aspect, it was suggested long time ago that Si enters plants as water-soluble H_4SiO_4 (Barber and Shone, 1966). This proposition was supported by laboratory and field studies carried out in recent years (Raven, 1983; Mitani and Ma, 2005; Ding et al., 2003, 2004, 2005a, 2008a,b; Opfergelt et al., 2006a,b). In contrast, Fu et al. (1998, 2000, 2002) proposed that some plants may absorb silicate particles directly and selectively from soils. However, this proposal was proven not applicable to rice (Ding et al., 2005a, 2008b) and bamboo (Ding et al., 2008a). The experimental studies of Sun et al. (2008) and Ding et al. (2008b) used a nutrient solution containing water-soluble H_4SiO_4, which provided a further evidence for uptake of water-soluble H_4SiO_4 by rice roots.

For the second aspect, two different opinions, i.e., active uptake and passive diffusion, have been raised. Active uptake was considered to play an important role in rice and wheat by a number of researchers (Ma et al., 2004; Tamai and Ma, 2003; Ma and Yamaji, 2006; Rains et al., 2006; Ma et al., 2007). It was suggested that Si uptake, mediated by a specific transporter, was much faster than that of water and was not affected by transpiration (Ma and Yamaji, 2006). Besides, the Lsi1 and Lsi2 genes, the specific transporters for active Si uptake and efflux, were recently discovered in rice (Ma et al., 2006, 2007).

EBSCOhost - printed on 2/10/2023 8:05 PM via . All use subject to https://www.ebsco.com/terms-of-use

However, the Lsi1 and Lsi2 genes are mainly expressed in roots, but not in SL (Ma et al., 2006, 2007), implying that they are not responsible for Si transportation and precipitation in SL. Besides, the silicon uptake system in higher plants was found to be different to that in diatoms, which required silicon as an essential element (Ma et al., 2006). Meanwhile, no silicon bearing organic compound has been identified in a higher plant so far (Knight and Kinrade, 2001). These conditions leave some room for other mechanisms. It was reported that the distribution of silica (Epstein, 1999; Raven, 2003; Motomura et al., 2004; Henriet et al., 2006) and δ^{30}Si value (Ding et al., 2005a, 2008b; Opfergelt et al., 2006b) in the stem and leaves of plants is markedly affected by the transpiration stream, indicating that passive mechanism may be important for transportation of silicon in stem and leaves of rice, bamboo and banana.

The experimental results obtained by Ding et al. (2008b) highlighted the role of passive mechanism on slicon uptake by plant roots. It was found that silicon isotope fractionation factors between plants and growth solutions were all similar in direction and extent for rice, bamboo, banana and diatoms, indicating that some common and basic mechanisms, other than genes, may play important role in the silicon uptake process for a wide range of plants. The passive uptake in the transpiration process may be regarded as a major candidate of these kinds of mechanisms. The patterns of silica distribution in roots (mainly in endodermal cells), SL and husks (mainly in epidermal cells) show also the effects of the transpiration process on silica precipitation in the rice plant. Besides, the close relation between the silicon content in the rice root and that in the nutrient solution implies also the important role of the passive mechanism on silicon uptake.

Recently, Sun et al. (2016) provided more experimental results on Si isotope compositions in the process of rice growth under different external silicon concentrations in hydroponic systems. It was still found that preferential precipitation of light silicon isotopes contributes to progressive isotope fractionation along the transpiration stream that moves from the uptake sites in roots to the transpiration termini in above ground parts. It was observed also at lower external silicon concentrations, heavy silicon isotopes entered plants more readily than light silicon isotopes. Conversely, at higher external silicon concentrations, light silicon isotopes entered plants more readily than heavy silicon isotopes.

A model for active and passive Si-uptake components co-existing in a plant was proposed and applied to maize, sunflower, bamboo and gourd (Motomura et al., 2004; Mitani and Ma, 2005; Liang et al., 2006; Ding et al., 2008a). Based on the evidence described above, this model might be also applicable to rice (Ding et al., 2008b).

5.3.2 Silicon isotope studies on bamboos

Bamboos have high silicon content and are widely distributed in sub-tropical and temperate zones, forming an important organic silicon pool (Li et al., 2006). They are sig-

EBSCOhost - printed on 2/10/2023 8:05 PM via . All use subject to https://www.ebsco.com/terms-of-use

nificant for landscape conservation (Christanty et al., 1997) and may play an important role in the silicon cycle. Bamboos are used widely as materials in the food industry, paper maker, building, handicraft and even medicine. They appear in numerous parks as ornamental plants. Thus, the contents, forms and distribution patterns of silica in bamboo were studied by many researchers (Ueda and Ueda, 1961; Takahashi et al., 1981; Lux et al., 2003; Li et al., 2006). The silicon isotopic method has been used to delineate the distribute pattern and ways for absorption, transportation and precipitation of silicon in bamboo plants and to understand the effect of silicon absorption by bamboos on the global silicon cycle (Ding et al., 2008a).

Seven bamboo plants and related soils were collected from seven locations in China. The roots, stem, branch and leaves for each plant were sampled and their silica contents and silicon isotope compositions were determined. The silica contents and silicon isotope compositions of bulk and water soluble fraction of soils were also measured. Based on the obtained data, the variation patterns of silica contents and silicon isotope compositions in different parts of bamboo plant were discussed and the silicon isotope fractionations in the processes of silicon absorption, transportation and precipitation in bamboo were delineated.

5.3.2.1 The silica content and distribution in bamboo

The silica contents in different organs of bamboos are shown in Figure 5.33 (Ding et al., 2008a). The silica contents in leaves vary from 8.12% to 9.95% with an average of 9.04%. The silica contents in branches vary from 1.21% to 2.04% with an average of 1.78%. The silica contents in stems vary from 0.30% to 0.45% with an average of 0.39%. The silica contents in roots vary from 0.58% to 1.00%, with an average of 0.79%. The silicon fractions of different organs of bamboos were calculated from their silica contents and biomass fractions. It was found that leaves contain more than 50% (from

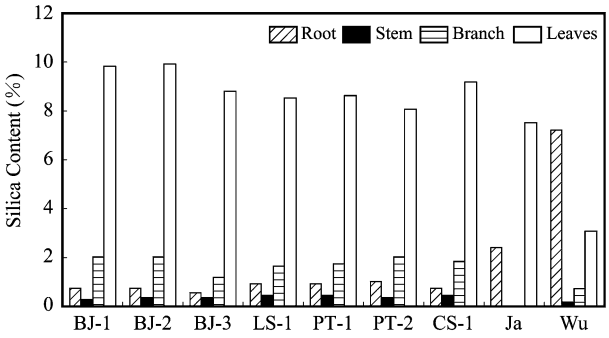

Figure 5.33: The silica contents in different parts of studied bamboos (after Ding et al., 2008a). BJ – Beijing; LS – Laoshan, Shandong; PT – Putuo, Zhejiang; CS – Changsha, Hunan. For comparison, the results of Lux et al. (2003) on Japanese bamboo (Ja) and Li et al. (2006) on Wuyishan bamboo (Wu) are also plotted.

EBSCOhost - printed on 2/10/2023 8:05 PM via . All use subject to https://www.ebsco.com/terms-of-use

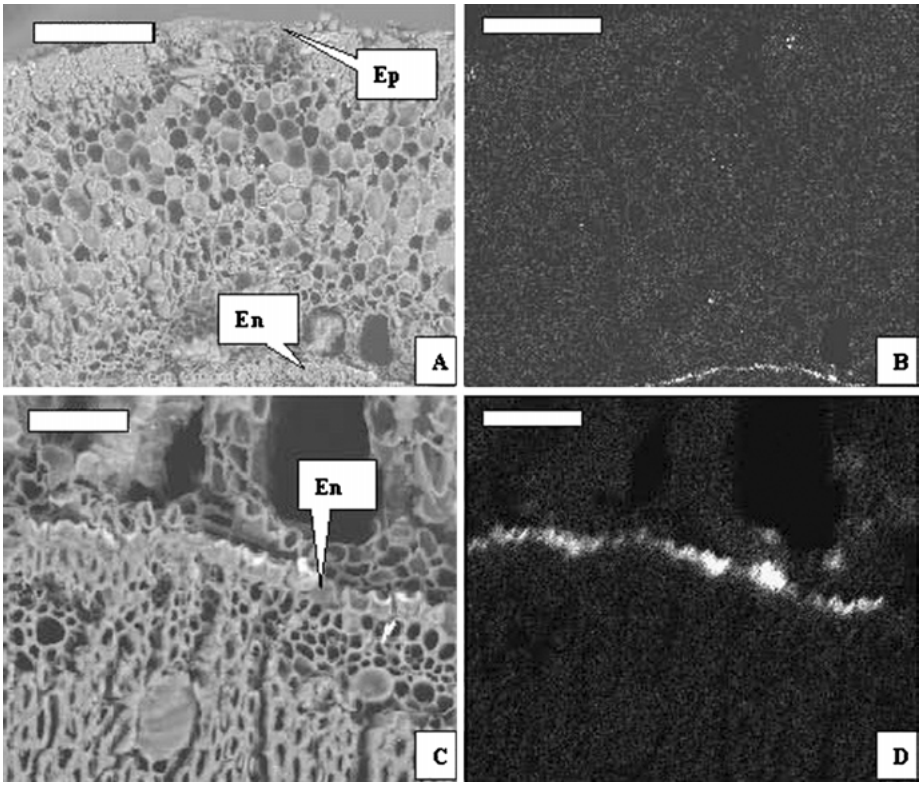

Figure 5.34: Electron micrographs of the root of bamboo BJ-3. Electron backscattering images (A and C) and X-ray mapping of Si show that Si is exclusively in endodermis cells (B and D). Bars represent 200 (A and B) and 50 μm (C and D). Ep – Epidermis; En – Endodermis. After Ding et al. (2008a).

52% to 66%) of silica in bamboo. The silica contents in bamboo were found to be related to their ages. For example, the samples of BJ-1, BJ-2 and BJ-3 belong to same species, grew in same climatic condition, and in same type of soil, but the older plants, BJ-1 and BJ-2 have higher silica content than the younger one, BJ-3.

As shown in Figure 5.33, in each studied bamboo the silica content of roots is always higher than that of the stem, but lower than those of the branch and leaves. The silica content increases from stem, through branch, to leaves consistently.

The forms and distributions of silica in roots, branch, stem and leaves of BJ-3 were examined by using an electron microprobe. Backscatter electron image and X-ray mapping show that the silica in root is exclusively in the endodermal cells (Figure 5.34B and D). The silica in bamboo leaves was found to be accumulated mainly in epidermal cells, with the highest levels in specialized idioblasts (Figure 5.35E and F). In the stem and branch of BJ-3 bamboo, silica was found mainly in their epidermal cells (Figure 5.35A to D).

EBSCOhost - printed on 2/10/2023 8:05 PM via . All use subject to https://www.ebsco.com/terms-of-use

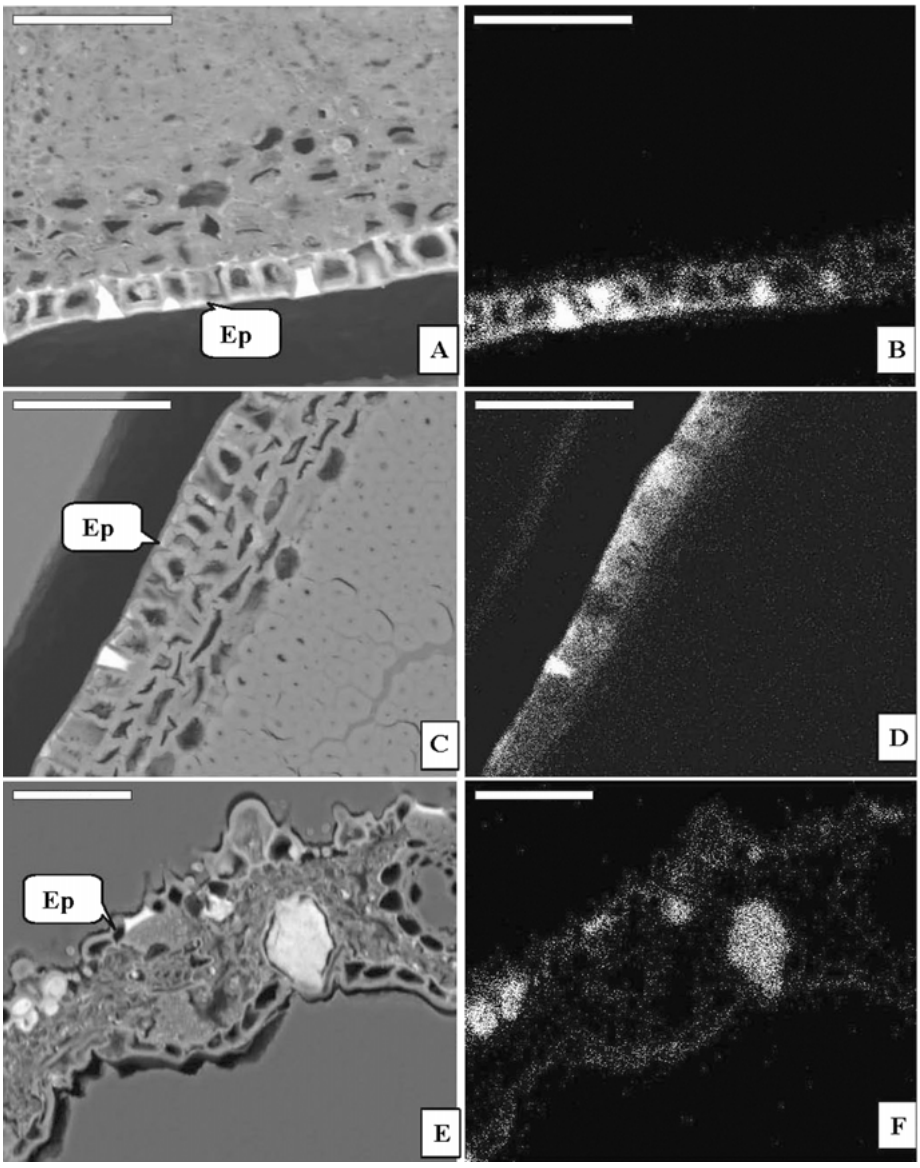

Figure 5.35: Electron micrographs of the stem (A, B), branch (C, D) and leaf (E, F) of bamboo BJ-3. Electron backscattering images (A, C) and X-ray mapping of Si (B, D) show that Si in the stem and branch is exclusively in epidermal cells. Electron backscattering image (E) and X-ray mapping of Si (F) show that Si in the leaf mainly in epidermal cells, with the highest levels in specialized idioblasts. Bars represent 50 µm. Ep – Epidermis. After Ding et al. (2008a).

EBSCOhost - printed on 2/10/2023 8:05 PM via . All use subject to https://www.ebsco.com/terms-of-use

5.3.2.2 δ^{30}Si values of bamboos

As shown in Figure 5.36, the whole variation range of δ^{30}Si values for the studied bamboos is up to 4.1‰, ranging from −2.3‰ to 1.8‰. In more detail, the δ^{30}Si values of leaves vary from −0.5‰ to 1.8‰, with an average of 0.80‰; the δ^{30}Si values of branches vary from −1.9‰ to 0.1‰, with an average of −1.06‰; the δ^{30}Si values of stems vary from −2.3‰ to −0.3‰, with an average of −1.40‰; the δ^{30}Si values of roots vary from −1.5‰ to 0.8‰, with an average of −0.29‰. This is remarkable compared to the total range of silicon isotope composition in terrestrial samples (7.0‰, Ding et al., 1996).

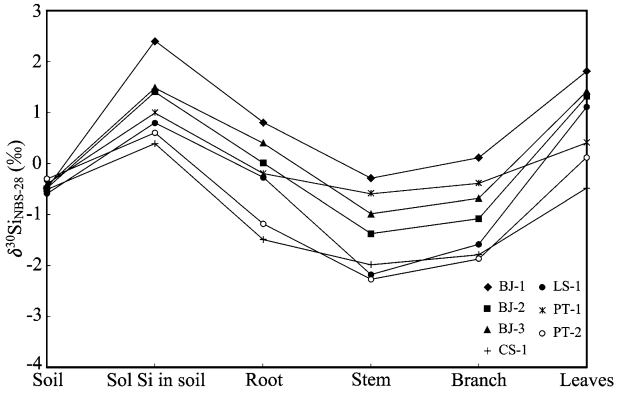

Figure 5.36: Silicon isotope compositions of studied bamboos. After Ding et al. (2008a).

In each bamboo plant, the δ^{30}Si value of stem is the lowest. There is a consistent trend of the δ^{30}Si increase from the stem, though branch, to leaves (Figure 5.36), similar to those observed in rice (Ding et al., 2005a, 2008b) and banana (Opfergelt et al., 2006a). It is noted that the δ^{30}Si values of roots are higher than those of stems and branches, but lower than those of leaves. The δ^{30}Si values of bulk bamboo were calculated from the SiO_2 fractions and δ^{30}Si values of different organs of bamboo.

5.3.2.3 SiO_2 contents and silicon isotope compositions of the soils

The silica contents of the bulk soils vary from 55.37% to 68.39%, with an average of 62.98%, whereas those of water soluble silica in studied soils vary from 0.011% to 0.025%, with an average of 0.016%.

The silicon isotope compositions of bulk soils and water soluble fractions are plotted in Figure 5.36. The silicon isotope compositions of the bulk soils vary from −0.6‰ to −0.2‰, falling in the range of suspended materials in the Yangtze River (Ding et al., 2004) and Yellow River (Gao et al., 2006) and shale rocks (Ding et al., 1996). This narrow range is in great contrast to the wide variation of δ^{30}Si values of bulk bamboo plants.

EBSCOhost - printed on 2/10/2023 8:05 PM via . All use subject to https://www.ebsco.com/terms-of-use

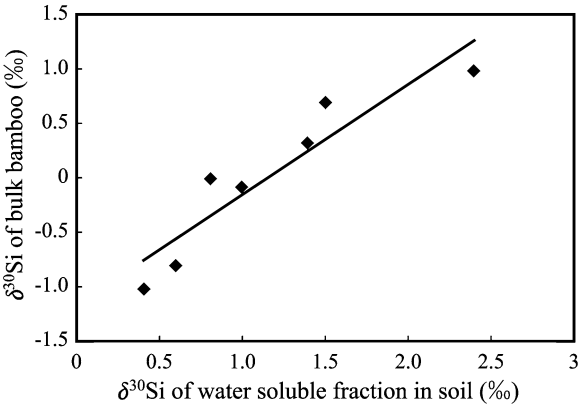

Figure 5.37: The relationship between the calculated δ^{30}Si values of bulk bamboo (y) and the δ^{30}Si values of water soluble fraction in soils (x). $y = 1.006x - 1.15$($R^2 = 0.8646$). After Ding et al. (2008a).

The silicon isotope compositions of water soluble fraction in studied soils vary from 0.4‰ to 2.4‰, with an average of 1.16‰, which is significantly higher than those of the bulk soils. The differences of δ^{30}Si values between bulk soil and water soluble fractions of soil may be caused by several processes. Firstly, during the weathering processes of silicate rocks, silicon isotope fractionation occurs between produced secondary clay minerals and dissolved silicon in solution (Ding et al., 1996; Ziegler et al., 2005a,b). Compared to the initial silicate rock, the produced secondary clay minerals are always depleted in ^{30}Si and the silicon dissolved in pore water is enriched in ^{30}Si. Furthermore, the preferential absorption of light isotopes by plants will raise the δ^{30}Si value of pore water further (Ding et al., 2004). Secondly, the phytoliths in soils of bamboo growth field should mainly come from the leaves of bamboo. When bamboos were collected, their stems and branches were moved out, but their leaves were usually left on soil surface. According to the results of this study, the leaves of bamboo tend to be enriched in ^{30}Si, so the phytoliths in soil should be also enriched in ^{30}Si.

A positive correlation can be seen between δ^{30}Si values of water soluble silica and contents of organic matter in soils (Ding et al., 2008a). However, no obvious relationship can be seen between the δ^{30}Si value and content of water soluble silica. A positive correlation is found between δ^{30}Si values of water soluble silicon in soils and those of bulk bamboos (Figure 5.37), indicating the silicon in bulk bamboo is closely related to the silicon in the water soluble fraction of soil. Thus, the dissolved silicon in pore water and phytoliths might be the direct source of silicon absorbed by bamboo roots (Farmer et al., 2005).

5.3.2.4 Implications for the mechanism of silicon absorption, transportation and precipitation in bamboo

Si uptake by bamboo root

The results obtained in this study lay some constraints on the issue of silicon uptake by roots of bamboo.

EBSCOhost - printed on 2/10/2023 8:05 PM via . All use subject to https://www.ebsco.com/terms-of-use

Firstly, the distribution of SiO_2 within the bamboo plant is considered. If the theory of Fu et al. (2000, 2001, 2002) can apply to bamboo, the SiO_2 should be enriched in the roots, but depleted in the stem, branch and leaves. However, it is observed in all studied bamboo plants that SiO_2 contents increase from the stem to branch and leaves (Figure 5.33). Although the SiO_2 content in the roots is slightly higher than in the stem, it is still much lower than in the branch and leaves. These observations suggest that direct absorption of silicate particles is not an important way for silicon uptake by bamboo roots. Instead, as suggested by Sangster and Hodson (1986), water-soluble silicon is more likely the major form for silicon absorption by bamboo roots.

Secondly, the silicon isotope composition is considered. As we know, there are generally three kinds of silicon bearing components in soils: a) silica and silicate minerals; b) dissolved silicon in pore solution; c) phytoliths (Sauer et al., 2006). The silicon in soil is dominated (more than 99%) by the silicon in silica and silicate minerals. If bamboo absorbs silicate particles directly from the soil, the silicon isotope composition of bulk bamboo should be the same or closely related to those of bulk soil. The δ^{30}Si values for bulk plants of studied bamboos vary in a wide range from –1.0‰ to 1.0‰ (Figure 5.37). In sharp contrast, the δ^{30}Si values of the bulk soils vary in a narrow range from –0.6‰ to –0.2‰ (Figure 5.36). Therefore, direct absorption of silicate particles cannot be applied to bamboo.

To examine the relations between silica in bamboos and dissolved silicon in pore solution and phytoliths in soils, the δ^{30}Si values of water soluble silicon in soils were determined and the results are plotted in Figure 5.36 and Figure 5.37. There is a positive correlation between the δ^{30}Si values of water soluble fractions in soils and those of bulk bamboos (Figure 5.37), indicating that the dissolved silicon in pore water and phytoliths in soil are the direct sources of silicon taken up by bamboo roots (Farmer et al., 2005). This correlation indicates also that a biochemical silicon isotope fractionation exists in process of silicon uptake by bamboo roots. Similar to the observation made on rice Ding et al. (2005a) and banana (Opfergelt et al., 2006b), the light silicon isotope is preferentially absorbed when the water soluble silicon is taken up by bamboo roots. Based on the difference between the average δ^{30}Si value of water soluble silicon in soil (1.16‰) and that of Si absorbed by bamboo (0.01‰), the silicon isotope fractionation factor is estimated to be 0.9988.

Another issue is how roots uptake water soluble silicon from soil. In general, there are two different opinions on this issue, i.e., the active uptake and passive diffusion. Some researchers suggest that Si uptake and transport in rice is an active process (Ma et al., 2002, 2004; Tamai and Ma, 2003; Ma and Yamaji, 2006). They think Si uptake, mediated by a specific transporter, is much faster than that of water and is not affected by transpiration. Furthermore, a gene (Lsi1) that is responsible for active Si uptake had recently been reported for rice (Ma et al., 2006). However, as described above, it was found that the content of the Si and δ^{30}Si value in bamboo, rice and banana are both higher at the terminal part of the transpiration stream than other locations of the plant

EBSCOhost - printed on 2/10/2023 8:05 PM via . All use subject to https://www.ebsco.com/terms-of-use

shoot, which strongly suggest that a passive mechanism of transportation may be important for bamboo, rice and banana (Ding et al., 2003, 2005a, 2008a,b; Opfergelt et al., 2006b). In the passive process, the supply of silicon in bamboo depends on the availability of $Si(OH)_4$ in soils of their growth area and the rates of water uptake and evaporation.

Transportation and precipitation of Si within bamboo plants

As described above, the amorphous silica (opal or silica gel) is the only form of silicon material found in plants and three types of silica deposits have been recognized in vascular plants (Sangster and Parry, 1981): 1) silica associated with cell walls; 2) silica filling the cell lumen; 3) the extracellular deposits. A variety of pathways may be inferred from the distribution pattern of silica deposits in various plant organs. It was suggested that silicon is transported subsequently from the roots, through the stem and branch, to the leaves. It can be polymerized and precipitated to form amorphous silica along the transpiration stream.

The results of Si contents and silicon isotope composition can place some constraint to the mechanisms of transportation and precipitation of Si within bamboo plants. As pointed out above, the silica content increases from the stem, through the branch, to the leaves in all studied bamboo plants (Figure 5.33). It is also observed that in aerial parts of bamboo, silica is always enriched in epidermal cells (Figure 5.35). In contrast, in roots, the underground part of bamboo, silica is enriched in endodermal cells (Figure 5.34). These phenomena indicate the important role of transpiration and evaporation for silica transportation and precipitation in the bamboo plant.

As demonstrated in the experimental results of Li et al. (1995a), the Si isotope composition of silica precipitated at the beginning can be 1.0‰ lower than that of the initial dissolved H_4SiO_4, but δ^{30}Si value of the last 10% of silica precipitates can be 2.0‰ higher than that of the initial dissolved $Si(OH)_4$. A similar model was used to explain the δ^{30}Si distribution pattern observed in the rice plant (Ding et al., 2005a). This kind of model might be also applied to silica precipitation in bamboo, for a similar δ^{30}Si distribution pattern is observed also in bamboo (Figure 5.36). However, this model alone cannot explain the whole picture of the silicon isotope variation in bamboo. If a simple SiO_2 precipitation controls the silicon isotope variation in bamboo, the δ^{30}Si value in root should be the lowest among all organs of the bamboo plant. However, in all studied bamboos, the δ^{30}Si values always decrease from root to stem (Figure 5.36).

Opfergelt et al. (2006b) had found that the silicon isotope composition in banana root was heavier than the rest of the plant. Based on this phenomenon, they inferred that comparing to the solution absorbed by roots from the external source, the solution transferred to the plant shoot was ^{30}Si depleted, and the solution residing in the root was ^{30}Si enriched. This postulation can explain the δ^{30}Si decrease from the roots to the stem of bamboo, but not the δ^{30}Si increase from the stem to the branch and

EBSCOhost - printed on 2/10/2023 8:05 PM via . All use subject to https://www.ebsco.com/terms-of-use

leaves. To solve this discrepancy, a model with two silicon components is proposed (Ding et al., 2008a). One is the accumulated silica precipitate in different organs of bamboo with the δ^{30}Si value lower than that of the solution entering them. The other is the silicon residing in plant fluid of different bamboo organs, which has δ^{30}Si value higher than that of entering solution. The δ^{30}Si value of a bamboo organ is determined by the δ^{30}Si values of these two components and their mass fractions (M_P and M_D), where subscripts P and D designate precipitated and dissolved phases. As an organ absorbing water and nutrition from soil, roots store a large amount of plant fluid. The content of plant fluid in roots is normally much higher than those in the aerial parts of bamboo plants. Therefore, the amount of silicon residing in fluid of roots should be also much larger than that in fluid of the aerial parts. Meanwhile, the content of accumulated silica precipitate in roots is lower than that in aerial parts of bamboo plants (Figure 5.34 and Figure 5.35). As a result, the ratio of dissolved H_4SiO_4 to precipitated SiO_2 (M_D/M_P) is much larger in the roots than in the aerial parts of bamboo. Thus, the δ^{30}Si value of total silicon in the roots would be more affected by the silicon residing in fluid, and the δ^{30}Si values of total silicon in aerial parts would be more dependent on the accumulated silica precipitate. This model can explain the trend of the δ^{30}Si decrease from the roots to the stem of bamboo, as well as the trend of the δ^{30}Si increase from the stem to the branch and leaves.

A diagram showing silicon isotope variation in bamboo during the process of SiO_2 precipitation from plant fluid is plotted in Figure 5.38. Assuming the silicon isotopic fractionation in bamboo is a Rayleigh process, the Si isotope variation curves of dissolved Si and precipitated Si are also drawn by fitting the data of starting fluid in bamboo and precipitated silica in the stem, branch and leaves of bamboo. In view of that, roots contained a significant amount of dissolved Si; its datum is left out in the fitting process.

The δ^{30}Si value of Si absorbed by bamboo (0.01‰), represented by the average δ^{30}Si value of bulk bamboos, is used as a starting value of fluid in bamboo. The average δ^{30}Si value (1.16‰) of water soluble Si in soil is also plotted. The data points of Si in roots (R), stem (S), branch (B) and leaves (L) are plotted according to their average δ^{30}Si values and SiO_2 fractions. It is assumed that the silica in roots, stem, branch and leaves precipitated when $(1 - f)$ varied from 0 to 0.07, from 0.07 to 0.24, from 0.24 to 0.42 and from 0.42 to 1.0, respectively. So their middle values of 0.035, 0.155, 0.33 and 0.71 are used to plot the point of the roots, stem, branch and leaves, respectively.

It is found that by using a fractionation factor of 0.9981 the obtained variation curves can fit the observed results best. Considering the relation between the observed δ^{30}Si values of bamboo organs and the average δ^{30}Si values of dissolved Si and precipitated Si in bamboo organs inferred from variation curves (Figure 5.38), the M_P/M_D ratios are estimated to be about 0.25 in roots, about 10 in stem, and >15 in branch and leaves. The M_P/M_D ratios in various organs of bamboo were not measured in this study, but the estimated results are consistent with the qualitative observation.

EBSCOhost - printed on 2/10/2023 8:05 PM via . All use subject to https://www.ebsco.com/terms-of-use

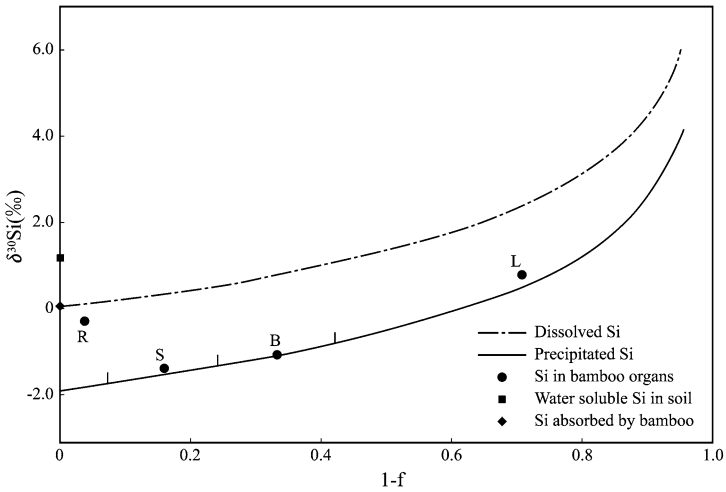

Figure 5.38: A plot showing silicon isotope variation in bamboo when SiO_2 precipitated from plant fluid. The δ^{30}Si value of Si absorbed by bamboo (0.01‰), represented by the average δ^{30}Si value of bulk bamboos, is used as a starting value of fluid in bamboo. The average δ^{30}Si value (1.16‰) of water soluble Si in soil is also plotted. The data points of Si in roots (R), stem (S), branch (B) and leaves (L) are plotted according to their average δ^{30}Si values and SiO_2 fractions. The Si isotope fractionation factor between dissolved Si and precipitated Si in bamboo ($\alpha_{pre-sol}$) is estimated to be 0.9981. The Si isotope fractionation factor between Si absorbed by bamboo and water soluble Si in soil (α_{bam-wa}) is estimated to be 0.9988. The data are from Ding et al. (2008a).

5.3.3 III. Silicon isotope studies on other plants

Besides rice and bamboos, a number of crop plants, such as wheat, banana, cucumber and maize, have been investigated also for their SiO_2 contents and silicon isotope compositions.

5.3.3.1 Silicon isotope study on the wheat plant

Wheat is a major food resource that is widely cultivated in the world. The silicon isotope compositions of phytoliths in wheat were also investigated (Hodson et al., 2008), which provided some more information on the distribution pattern of silicon in plants, although its emphasis was put on the utilization in palaeovegetation and palaeoenvironmental reconstruction.

Wheat plants were collected in July 2006 at Hill Farm, Warmington, UK. The plants were beyond the milk ripe stage, were very mature and were harvested in the following week. Six mature plants were used for phytolith and isotopic analysis. Wheat organs were separated as follows: culm, rachis, leaf sheaths, leaf blades and inflorescence bracts. A 'bulk' sample was a mixture of all organs to determine the values that would be obtained from whole plants.

EBSCOhost - printed on 2/10/2023 8:05 PM via . All use subject to https://www.ebsco.com/terms-of-use

SiO_2 content of the wheat organs and bulk wheat

The SiO_2 contents of wheat organs and bulk wheat are illustrated in Figure 5.39. The highest SiO_2 contents are obtained in the leaf sheaths (5.8%) and leaf blades (5.7%) and lower SiO_2 contents are observed in the inflorescence bracts (3.8%), culm (1.5%) and rachis (1.1%). There have been no previous measurements of the silica content of the rachis, but as this organ is of a similar anatomical structure to the culm, it is not surprising that it has a similar value.

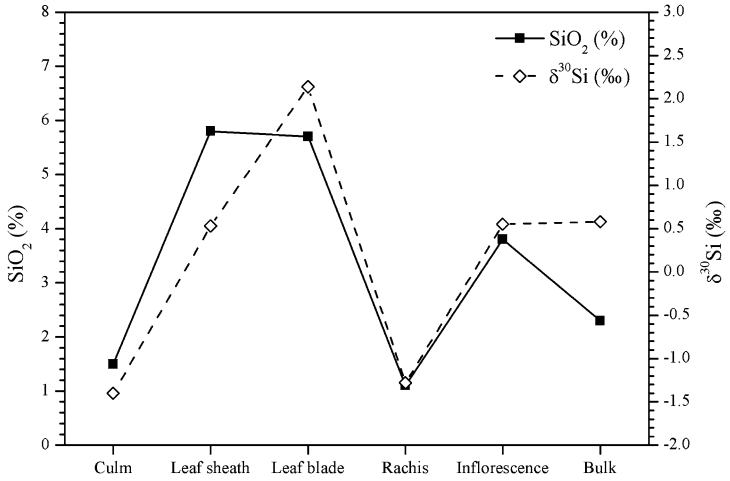

Figure 5.39: The SiO_2 contents and $\delta^{30}Si$ values of wheat organs and bulk wheat. Data are from Hodson et al. (2008).

Silicon isotopes compositions of the wheat organs and bulk wheat

The $\delta^{30}Si$ values of wheat organs and bulk wheat are shown also in Figure 5.39. Increasing trends can be observed from culm (–1.4‰) to leave sheath (0.53‰) and leaf blade (2.14‰), and from culm (–1.4‰) to rachis (–1.28‰) to inflorescence bracts (0.55‰). The highest $\delta^{30}Si$ value is found in the leaf blade (2.14‰). The bulk sample has $\delta^{30}Si$ value of 0.58‰.

Implication on silicon transport routes

It is apparent that there are two main routes for Si transport within the wheat plant, and that heavier isotopes increase towards the end of both routes: 1) culm → leaf sheath → leaf blade; and 2) culm → rachis → inflorescence bracts (Hodson et al., 2008). A similar pattern was reported by Ding et al. (2005a) on rice, which showed also the accumulation of heavy isotopes in the upper parts of the plant. Essentially, this would involve the lighter ^{28}Si isotope being more reactive, and thus more likely to be deposited in SiO_2. Thus, in wheat, proportionately more ^{28}Si isotope would be

EBSCOhost - printed on 2/10/2023 8:05 PM via . All use subject to https://www.ebsco.com/terms-of-use

deposited in the culm, and a greater proportion of ^{30}Si would continue in the transpiration stream to the leaf sheath. In the sheath, the same fractionation occurs, leading to an even greater concentration of heavier isotopes in the leaf blade. A similar process would explain the higher $\delta^{30}Si$ in the inflorescence bracts.

5.3.3.2 Silicon isotope study on the banana plant

Banana is an important economical and nutritive resource for many human communities in tropical areas and is also a Si-accumulator plant (Lahav and Reuveni, 1995). Opfergelt et al. (2006a) studied silicon isotopic fractionation between plant parts in the banana cropping system and compares these preliminary results with previous data obtained from hydroponics.

SiO_2 contents in different organs of the banana plant

Silica content in both natural and hydroponic plants vary in a range from 0.7% to 4%, with the highest value in the leaves (Figure 5.40). Moreover, SiO_2 contents of in situ banana leaves are higher than in hydroponics (4% vs. 3%, respectively). Although the latter were continuously supplied with a solution highly enriched in Si (47 mg/L), this slight difference must be related to the age of the plant (around 10 months in situ and 44 days in vitro) and to the soil conditions. Banana from Cameroon accumulated silicon during a longer time period and was grown in an Andosol rich in weatherable aluminosilicates (Delvaux, 1989). This general behavior is comparable to existing data on bamboo by Ding et al. (2003) who showed an increasing SiO_2 content (38% to 72%) from stem to branch and leaf, correlated to an increase of isotopic compositions in the plant.

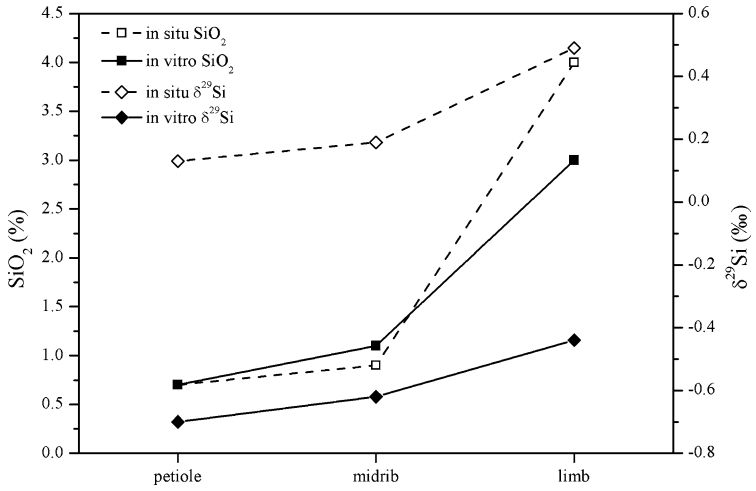

Figure 5.40: $\delta^{29}Si$ values (diamonds) and SiO_2 content (squares) in banana organs. In situ analyses are shown in open symbols and in vitro analyses are in filled symbols. After Opfergelt et al. (2006a).

EBSCOhost - printed on 2/10/2023 8:05 PM via . All use subject to https://www.ebsco.com/terms-of-use

Silicon isotope compositions of different organs of the banana plant

In banana from Cameroon (in situ), δ^{29}Si varied between +0.13‰ and +0.49‰ in petioles and lamina, respectively (Figure 5.40). This shows a trend of gradual δ^{29}Si increase of 0.36‰ from petioles to midribs and lamina. This trend towards heavier isotopic compositions in the upper parts of the plant is remarkably similar to the one observed on in vitro bananas, even if the δ^{29}Si change from pseudo-stems to leaves is slightly lower in hydroponics (0.26‰; Opfergelt et al., 2006a). Differences between silicon isotopic compositions in banana from Cameroon (+0.13‰ to +0.49‰) and hydroponics (–0.70‰ to –0.44‰) are attributed to different isotopic sources signatures. The hydroponic bananas were supplied by a H_4SiO_4 solution with an isotopic composition of –0.02‰ (Opfergelt et al., 2004). No isotopic data are yet available for the Si source in Cameroon but more positive isotopic signatures may be expected as usually observed in continental waters (De La Rocha et al., 2000; Ding et al., 2004).

5.3.3.3 Silicon isotope study on the cucumber plant

The distribution characteristics of silicon isotopes in cucumber, which is considered to be a representative of a more passive silicon uptake (Liang et al., 2006), were also studied in the laboratory for understanding the effects of different silicon concentrations in nutrient solutions on silicon absorption and utilization (Sun et al., 2016).

In the experimental investigation (Sun et al., 2016), the cucumber plant was grown hydroponically at different external silicon concentrations. The SiO_2 contents in various organs of individual cucumber plants were 0.21% to 0.89%, 0.24% to 1.11%, and 0.51% to 3.68% at 0.085 mM, 0.17 mM and 1.70 mM external silicon concentrations, respectively. The ranges of δ^{30}Si values in cucumber organs were –1.38‰ to 1.21‰, –1.33‰ to 1.26‰ and –1.62‰ to 1.40‰ at 0.085 mM, 0.17 mM and 1.70 mM external silicon concentrations, respectively. A general increasing trend in SiO_2 contents and δ^{30}Si values from lower to upper plant parts reflected the preferential incorporation of lighter silicon isotopes from transpired water to biogenic opal.

The data on δ^{30}Si values for the whole plants and nutrient solutions indicated that biologically mediated silicon isotope fractionation occurred during silicon uptake by roots. At lower external silicon concentrations, heavy silicon isotopes entered plants more readily than light silicon isotopes. Conversely, at higher external silicon concentrations, light silicon isotopes entered plants more readily than heavy silicon isotopes.

5.4 Studies on silicon source and genesis of ore deposits

Silicon isotopes have been applied in various types of ore deposits as a useful tool to trace the source of silicon and other related metals and to unravel the ore-forming conditions and ore genesis. In this section, we will summarize the application of silicon isotopes in the study of ore deposits, including banded ion formation (BIF), sed-

EBSCOhost - printed on 2/10/2023 8:05 PM via . All use subject to https://www.ebsco.com/terms-of-use

imentary exhalative submarine–hydrothermal Pb–Zn deposits (SEDEX), magmatic–hydrothermal Pb–Zn deposits, Sn deposits, W deposits and Au deposits.

5.4.1 Banded iron formation (BIF)

Banded iron formations (BIFs) are marine chemical sedimentary rocks that formed periodically throughout the Precambrian (mostly 3.8–1.8 Ga) and are usually characterized by alternating iron-rich (haematite, magnetite and siderite) and silica-rich (chert, jasper) layers with a thickness varying from micrometres to metres. Some of these types of iron deposits, such as those occurring in the Hamersley basin in western Australia, show laterally contiguous layers up to a hundred kilometers in distance (Trendall, 2002). The peak in BIF occurrence between 2.5 and 2.3 Ga appears to correlate with major changes in the Earth's history such as the rise of atmospheric oxygen and the change from anoxic to oxic conditions in the ocean (Canfield et al., 2005; Holland, 2006).

5.4.1.1 Silicon isotope variation in BIF

Jiang et al. (1993) was the first to carry out silicon isotope study on cherts of BIF. They studied the Archean banded iron formation in the Gongchangling iron deposit in Liaoning Province and found different silicon isotopic compositions for the host rocks and the iron ores, with the latter showing a large variation and negative δ^{30}Si values (Figure 5.41).

The Gongchangling iron deposit is located in the An-Ben area, Liaoning Province, which is one of the largest BIF-type iron deposits in China. The iron ores occur within metamorphic rocks of the Archean Anshan Group and this deposit has been considered as an Algoma-type BIF. In the Gongchangling iron deposit, a number of host rocks were analyzed for their silicon isotopic compositions, which show a generally small δ^{30}Si variation from −0.4‰ to +0.2‰. For example, the migmatitic granite samples show δ^{30}Si values of −0.3‰ to +0.2‰, and a quartz separate has a δ^{30}Si value of −0.1‰, which falls within the range of granitoid rocks worldwide. Plagioclase amphibolites from the upper ore-bearing zones show δ^{30}Si values from −0.6‰ to −0.2‰, falling within the variation range of mafic rocks worldwide. Amphibole schists from the lower ferruginous schist horizon show δ^{30}Si values of −0.1‰ to +0.1‰, which are slightly lower than those of plagioclase amphibolites. One micaceous quartzite from the upper leucogranulite layer has a δ^{30}Si value of −0.4‰, whereas one biotite granulite sample from the marker horizon K bed in the deposit has a δ^{30}Si value of −0.3‰. One quartz schist sample has δ^{30}Si value of 0‰, and one quartz separate from a micaceous quartzite has a δ^{30}Si value of +0.1‰. In contrast to the δ^{30}Si values of the host rocks, the quartz from the magnetite–quartzite ores both from the lower and upper ore zones show more negative δ^{30}Si values from −0.9‰ to −2.2‰ (Figure 5.41).

EBSCOhost - printed on 2/10/2023 8:05 PM via . All use subject to https://www.ebsco.com/terms-of-use

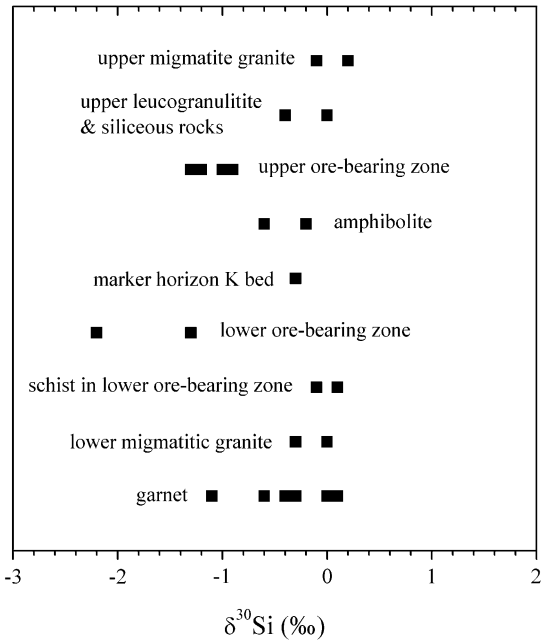

Figure 5.41: Diagram showing distribution of δ^{30}Si values for a variety of rocks and minerals in the Gongchangling iron deposit from Liaoning Province. Data are from Jiang et al. (1993).

Silicon isotope study of the BIFs from more than 20 iron deposits in Precambrian strata in North China Craton are also carried out (Li et al., 2010; Hou et al., 2014). All the BIF deposits regarding their ages and types show similar δ^{30}Si values from −2.0‰ to −0.3‰, with an average of −0.8‰. Oxygen isotopic compositions are also measured for the same samples; the results show that the quartz in BIF has high δ^{18}O value from 8.1‰ to 21.5‰. Both the silicon and oxygen isotopes are similar to those of seafloor black smokers, hot spring sinters and hydrothermal exhalatives.

André et al. (2006) reported significant Si isotope variations in ca. 3.8 Ga cherts and associated rocks from the Isua Greenstone belt, yielding a wide range δ^{30}Si of −2.8‰ to +0.7‰ with majority of them having negative values, providing insights into the Early Archean silicon cycle. van den Boorn et al. (2007) reported a large range (2.7‰) of silicon isotopic compositions from −1.6‰ to +1.1‰ of Early Archean (3.5–3.0 Ga) cherts from the Pilbara Craton, Australia. Samples from individual outcrops or even on the scale of laminae show the δ^{30}Si difference of 1.5‰ to 1.8‰.

5.4.1.2 Silicon isotopes as evidence for sea-floor hydrothermal origin of BIF

The origin of BIF has long been debated, and there is a growth number of evidence to support that the banded silicon-rich and iron-rich formations were precipitated from sea-floor hydrothermal fluids (Derry and Jacobsen, 1990; Bau and Dulski, 1996; Stein-

EBSCOhost - printed on 2/10/2023 8:05 PM via . All use subject to https://www.ebsco.com/terms-of-use

hoefel et al., 2009; Hou et al., 2014). They should be formed by chemical precipitation from turbulent seawater fed by submarine hydrothermal vents, instead of being deposited directly through a volcanic eruption like the surrounding host rocks.

The quartz from the magnetite–quartzite ores both from the lower and upper ore zones in the Gongchangling iron deposit show negative δ^{30}Si values from –0.9‰ to –2.2‰, which are similar to those values of siliceous precipitates from modern sea-floor hydrothermal vents and hot springs (Ding et al., 1996 and references therein), which led Jiang et al. (1993) to conclude that quartz from the iron ores were originally siliceous precipitates resulting from sea-floor hydrothermal activity. The inferred high concentration of silicon in the Archean ocean has been well supported by much evidence. For example, studies on the geochemistry and oxygen isotopes demonstrated that the temperature of the Archean seawater was in the range of 50–70°C. Apparently, at such high temperatures, the solubility of silica in seawater might reach up to $(10 - 110) \times 10^{-6}$ (Maliva et al., 2005). Initially, amorphous silica precipitates from the seawater and has been transformed later into chert with burial (Maliva et al., 2005).

Van den Boorn et al. (2007) analyzed cherts from the Early Archean Pilbara Craton and suggested that those cherts with negative δ^{30}Si values have a predominance of hydrothermal derived silica, in contrast to the positive δ^{30}Si cherts that may have derived from seawater or precursor volcaniclastic sediments. Steinhoefel et al. (2009) carried out both Si and Fe isotope analyses on Zimbabwean Archean BIFs using femtosecond LA-MC-ICPMS. They found that magnetite within the BIF was ^{56}Fe enriched, chert within the BIF was highly depleted in ^{30}Si and δ^{56}Fe and δ^{30}Si values varied consistently, indicative of precipitation from submarine hydrothermal fluids. The significant variations of δ^{30}Si from –1.0‰ to –2.6‰ in bulk layers suggested rapid precipitation of the silicate phases from hydrothermal-rich waters, and the changes of Fe and Si isotope signatures directly reflect the upwelling dynamics of hydrothermal-rich water, which govern the rates of Fe and Si precipitation and the development of layering (Steinhoefel et al., 2009). The combination of rare-earth-elements-and-yttrium patterns and relatively high δ^{30}Si (up to ca. +0.9‰) confirmed the marine origin of the cherts across the ~3.42 Ga in Buck Reef Chert (BRC) in the Barberton Greenstone Belt (South Africa). The observation that the δ^{30}Si of black chert bands show consistently higher values than co-existing translucent counterparts at the same stratigraphic level was interpreted as a primary feature acquired during deposition upon interaction between submarine discharging hydrothermal water and a stratified water body (Geilert et al., 2014b).

5.4.1.3 Possible models for formation of alternating iron- and silica-rich bands

Holland (1973) suggested that the layering in BIF was due to seasonal or decadal episodic hydrothermal pulsation and/or upwelling of anoxic, Fe-rich waters (roughly 0.02–0.5mM dissolved Fe(II)) into semi-restricted ocean basins already saturated with dissolved Si (Maliva et al., 2005).

EBSCOhost - printed on 2/10/2023 8:05 PM via . All use subject to https://www.ebsco.com/terms-of-use

Using silicon isotope evidence, Jiang et al. (1993) interpreted the alternating precipitation of silica-rich and iron-rich bands in BIF of the Gongchangling iron deposit in Liaoning Province, China. They suggested that each venting of hydrothermal fluids on to the sea floor brings reduced materials to the seawater to cause a more reduced and acidic condition which promote silica saturation and precipitation. In between the gaps of each venting, the ocean becomes more oxidized, and the change of pH and Eh would induce the oxidizing of Fe^{2+} into Fe^{3+} and precipitation of $Fe(OH)_3$. The periodic hydrothermal venting activity then causes the alternating bands in BIFs.

Later on, Ding et al. (1996) and Li et al. (2010) proposed a more detailed model for the alternating bands in BIF. Similarly, they both suggested the formation of the alternative silica-rich and iron-rich bands was related to the periodic venting of hydrothermal fluids on to the seawater. When the hydrothermal fluids vented and mixed with the seawater, colloidal precipitation of silica may occur immediately due to a quick drop of temperature which led to a saturation of silica in the seawater. The amounts of silica precipitated contain only a very small proportion due to the high Si concentrations in the seawater of Archean ocean, which caused the large silicon isotope fractionation with the precipitated silica having lighter Si-isotopes. This mixing process would also lead to an increase of the pH and Eh conditions in the seawater. As a result, some Fe^{2+} would be oxidized into Fe^{3+} to form $Fe(OH)_3$ precipitation. Due to the general low oxygen fugacity of the ocean, longer time may have been required to reach a more oxidized condition to cause Fe^{3+} precipitation.

Because the volume of seawater is much larger than that of the hydrothermal fluids discharged on the sea floor, variations in the pH value of the seawater would have been smaller, compared with that of the hydrothermal solutions. As a result, this would have led to slower precipitation of the silica. Consequently, the banded formations of $Fe(OH)_3$ and SiO_2 could have resulted from the different rate of precipitation of these two components. Following each discharge of hydrothermal fluids and their mixing with seawater, various chemical reactions would have caused the Si concentrations and pH values of the seawater to revert to their previous conditions, ready for the next cycle of precipitation. The high heat flow condition on the Archean sea floor led to far more frequent and much stronger volcanic and exhalative activities than those on the present sea floor, and thus created conditions favorable for the formation of those super large BIF deposits.

5.4.1.4 Did metamorphic overprinting alter the primary Si-isotopic signatures of BIF?

Jiang et al. (1993) analyzed a number of garnet from the Gongchangling iron deposit, and found a large δ^{30}Si variation (–1.1‰ to +0.1‰) for the garnet samples, which were thought to form during metamorphism. Two samples collected from the Mine NO.2 just above the Fe-6 iron ore bed have δ^{30}Si values of –1.1‰ and –0.4‰, which are similar to the quartz from magnetite ores and, therefore, their silicon sources may

EBSCOhost - printed on 2/10/2023 8:05 PM via . All use subject to https://www.ebsco.com/terms-of-use

derive from the banded iron-silica beds. Two samples from marker K in the sedimentary strata have δ^{30}Si values of 0.0 and +0.1‰, which are different from those of BIF, but similar to those host rocks of schists in the iron deposit. Therefore, the silicon to form these garnets may have directly derived from the host rocks. The δ^{30}Si values of the garnets also display a good correlation with the SiO_2 contents (Jiang et al., 1993).

The host rocks of the Gongchangling iron deposit have undergone a high grade of metamorphism, with the original granite being metamorphosed/migmatinized to migmatitic granite, and the original mafic–ultramafic volcanic rocks being metamorphosed to amphibolites or amphibole schists. From the δ^{30}Si of these metamorphic rocks, Jiang et al. (1993) found that they share similar values as their unmetamorphosed counterparts, for example, the migmatitic granites show a δ^{30}Si variation of −0.3‰ to +0.2‰, which are similar to those of granitoids (Ding et al., 1996); the δ^{30}Si of plagioclase amphibolites vary from −0.6‰ to −0.2‰, falling within those of mafic rocks on Earth (Ding et al., 1996). The δ^{30}Si of amphibole schists are from −0.1‰ to +0.1‰, slightly higher than those of plagioclase amphibolites, possibly indicate a mixing origin of terrigenous clastic rocks and the mafic rocks. It is therefore concluded that the metamorphic overprinting will not alter the primary silicon isotope signatures, which shed new light to use this tool to distinguish different protoliths of the metamorphic rocks.

André et al. (2006) also found that postdepositional alteration of Archean cherts, which possibly affected their original isotopic signatures such as oxygen isotopes (Knauth and Lowe, 2003), is not expected to have a significant effect on silicon isotope variations. The centimeter-scale variations of δ^{30}Si in a single chert specimen also indicate that this is the primary feature, not altered by the pervasive secondary modifications by circulating fluids (André et al., 2006).

5.4.2 Sediment-hosted submarine hydrothermal exhalative (SEDEX-type) deposits

5.4.2.1 Silicon isotope variations in SEDEX-type deposits

In this section, we summarize the silicon isotopic compositions of a number of important sediment-hosted submarine hydrothermal exhalative (SEDEX-type) deposits in the world.

Silicon isotopic compositions of the Sullivan Pb–Zn–Ag deposit

The Sullivan Pb–Zn–Ag ore body (British Columbia, Canada) is a classic example of a SEDEX-type deposit, and silicate minerals (tourmaline, albite, chlorite, biotite) associated with the formation and post-depositional evolution of the orebody occurring widespread throughout the deposit (Hamilton et al., 1982; Jiang et al., 1994). Hence a silicon isotope study of these minerals, together with host sedimentary rocks (Fig-

EBSCOhost - printed on 2/10/2023 8:05 PM via . All use subject to https://www.ebsco.com/terms-of-use

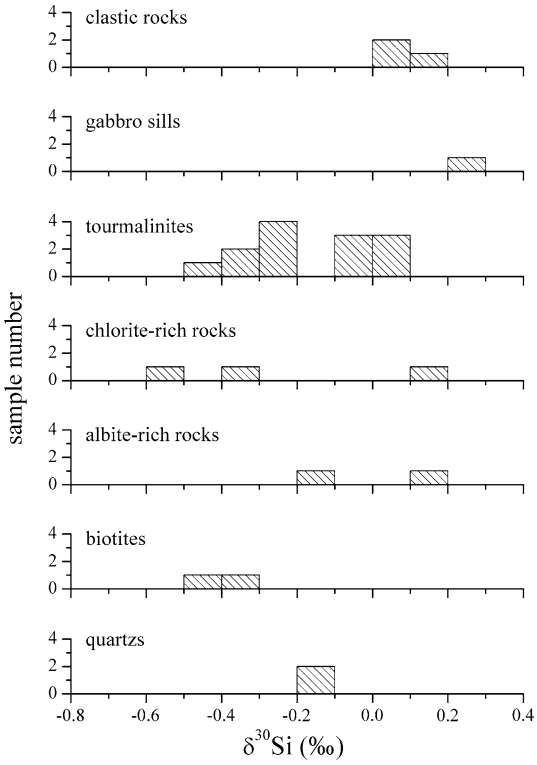

Figure 5.42: Diagram showing silicon isotope variation of selected rocks and minerals from the Sullivan deposit. After Jiang et al. (1994, 2000).

ure 5.42), was carried out, in order to trace the silicon source and the origin of the silicate minerals (Jiang et al., 1994, 2000).

Orebodies of the Sullivan deposit occur as lenses in the middle Proterozoic clastic rocks of the Aldridge Formation in concordance with the strata (Hamilton et al., 1982). In plain view, the orebody is approximately round with a diameter of 2 000 m. The maximal thickness of the orebody is 100 m. Tourmalinite is widespread in the deposit, in particular, in the footwall of the orebody, which shows a funnel shape crosscutting the sedimentary strata, covering an area of about $1\,500 \times 1\,000\ m^2$ and extending down for more than 450 m. Tourmalinite also occurs within the orebody and in the hanging wall, but it is much less abundant than the footwall. Locally, recrystallization of the tourmalinite can be seen in the vicinity of the albite–chlorite–pyrite altered rocks.

The hanging wall is composed of middle Aldridge sedimentary rocks with pyrite and some Pb–Zn sulfide beds intercalated within them. Above the vent complex, the hanging wall is altered to albite–chlorite rocks in association with pyrite and carbonates, extending up to 100 m thick. It is considered that the albitization was earlier, probably caused by an uprising flow of a brine rich in sodium, whereas the chloritization was slightly later, being formed through mixing of seawater rich in magnesium with a hydrothermal solution rich in silicon.

EBSCOhost - printed on 2/10/2023 8:05 PM via . All use subject to https://www.ebsco.com/terms-of-use

The clastic metasedimentary rocks of the lower Aldridge Formation that host the Pb–Zn orebody have the δ^{30}Si values of 0.0‰ to +0.1‰, similar to that obtained from other clastic sediments (Ding et al., 1988a; Jiang et al., 1992, 1993). One sample of gabbro shows a δ^{30}Si of +0.2‰, which is similar to the values of gabbros from the Panzhihua magmatic iron deposits in Sichuan Province, China (+0.1‰ to +0.3‰, Ding et al., 1996).

There are two types of tourmalinite occurrences in the Sullivan deposit (Slack, 1993; Slack et al., 2000). The first type is the funnel-like tourmalinite alteration pipe in the footwall, and the second type is represented by the stratiform tourmalinite and garnet-rich tourmalinite within the orebody and in the immediate footwall or hanging wall. Three samples from the deep footwall tourmalinites all give the same δ^{30}Si value of 0.0‰ and one sample from the shallow footwall tourmalinite gives a δ^{30}Si value of −0.3‰, whereas the second type of tourmalinites yield δ^{30}Si values of −0.1‰ to −0.5‰. Two samples of albite have δ^{30}Si values of +0.1‰ and −0.2‰, respectively. One garnet-rich sedimentary rock has a δ^{30}Si of 0.1‰. The biotite and chlorite-rich rock samples from alteration zones have δ^{30}Si values of −0.4‰ to −0.5‰ and −0.4‰ to −0.6‰, respectively, whereas two albite-rich rocks have δ^{30}Si values of +0.1‰ and −0.2‰. Two quartz samples from quartz–sulfide veins in the Sullivan deposit have δ^{30}Si values of −0.2‰.

Silicon isotopic compositions of the Devonian stratiform Pb–Zn deposits in the Qinling orogenic belt, northwestern China

A large number of stratiform Pb–Zn deposits occur in the Devonian sedimentary rocks in the Qinling orogenic belt. A lot of geological and geochemical work on this ore belt has been carried out (e.g., Zhang et al., 1988; Zhang, 1991; Xue, 1991). This metallogenic belt was developed in a Palaeozoic intercontinental or epicontinental rift basin between the North China Craton and the Yangtze Craton. Most of the Pb–Zn sulfide ores are hosted within the middle and upper Devonian rocks. Most of the orebodies show stratiform, stratiform-like or lenticular occurrence, and vein-type ores are also present in some of the deposits. The typical ore structures include massive, banded, brecciated, lumpy, disseminated, veinlet and stockwork. The major sulfide minerals include sphalerite, galena, pyrite, with only minor chalcopyrite. The gangue minerals are mainly quartz, calcite and ankerite with a minor amount of siderite, barite and fluorite. A characteristic suite of siliceous rocks and bedded rocks rich in albite, scapolite and barite is present among the host rocks, which give important indications concerning the ore genesis (Jiang et al., 1995). A number of geochemical and isotopic studies suggest that these deposits may have formed primarily through sea-floor hydrothermal exhalative sedimentation, and then they may have also undergone late hydrothermal alteration and metamorphic overprinting.

It is of great importance in the study of these ore deposits for a better understanding on how this suite of siliceous rock, albite, scapolite and barite-rich rock were

EBSCOhost - printed on 2/10/2023 8:05 PM via . All use subject to https://www.ebsco.com/terms-of-use

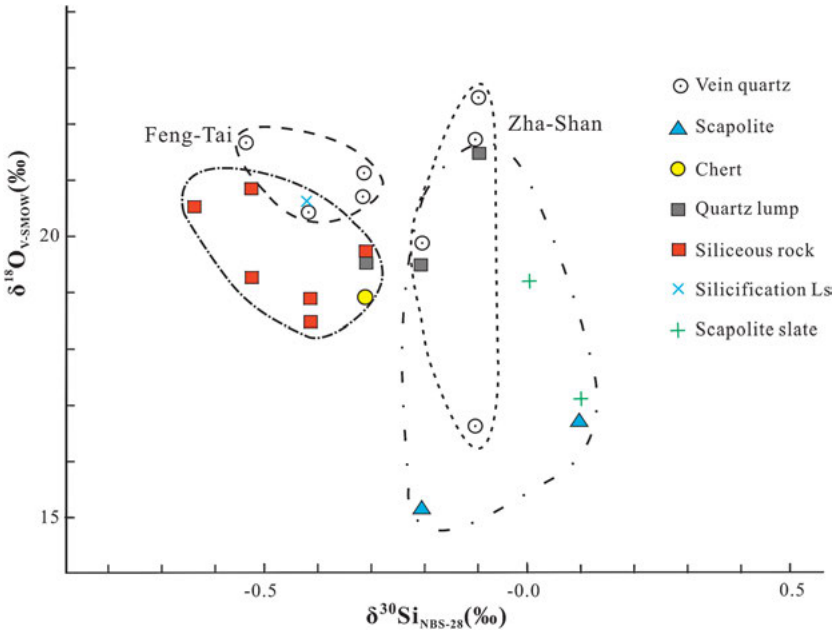

Figure 5.43: The $\delta^{18}O$ vs. $\delta^{30}Si$ diagram for rocks and minerals from the Devonian stratiform Pb–Zn deposits in the Qinling orogenic belt, northwestern China. After Ding et al. (1996).

formed. Hence, a silicon isotope study (Figure 5.43) has been carried out to provide a new constraint for the genesis of these rocks and the associated ore deposits (Li et al., 1995b; Xue et al., 1998).

Siliceous rocks are the major host rocks of the Devonian Pb–Zn deposits at Qinling. These rocks are stratiform, stratiform-like or lenticular, occurring in the transitional zone between limestones of the middle Devonian Gudaoling formation and phyllite of the upper Devonian Xinghongpu formation, conformable with the stratigraphical succession and they suffered simultaneous folding as the surrounding sedimentary rocks. The siliceous rocks are fine grained and compact, with a dark grey to grey-black colour and are mainly composed of microcrystalline quartz and with minor amounts of ankerite, siderite, sericite, chlorite and organic matter. Laminations are well developed in the siliceous rocks composed of organic and argillaceous laminae, quartz–ankerite and siderite laminae, and quartz–sulfide laminae. The siliceous rocks show a total $\delta^{30}Si$ variation from −0.6‰ to −0.3‰, while the $\delta^{18}O$ values vary from 18.6‰ to 21.0‰. These samples form a group with higher $\delta^{18}O$ and lower $\delta^{30}Si$ values in Figure 5.43.

Albitite rock is also a major host rock for the sulfide ore body in the Zha-Shan district at Qinling. This type of rock shows a grey, blue-grey and yellowish pink colour. The major constituent minerals include albite, quartz and ankerite with accessory tourmaline and apatite. The percentage of albite is commonly 40–60%. Some of the

EBSCOhost - printed on 2/10/2023 8:05 PM via . All use subject to https://www.ebsco.com/terms-of-use

albite are microcrystalline with a grain size of 0.01–0.1 mm, and most of the albite are aphanitic with grain size of 5–10 μm. The percentage of quartz is 30–40%, with similar grain size as those of aphanitic albite. Tourmaline is generally a minor mineral with an abundance of 3–5%, and may reach up to 10% locally. These rocks show banded or lamellar structures, and the thickness of individual laminae varies from 1 to 8 mm. The albitite rocks show a δ^{30}Si values of –0.4‰ to +0.2‰, with a δ^{18}O variation from 16.0‰ to 17.1‰.

The scapolite-bearing rocks are quite distinct and occur in the Yindongzi and Tongmugou deposits of the Zha-Shan district at Qinling. These rocks occur as interbedded layers within the ore-bearing rocks and in the immediately footwall of the ore body. The rocks are dark-grey or greyish white, and are composed of scapolite and biotite with minor amounts of chlorite, quartz, calcite, albite, siderite and dravitic tourmaline. The scapolite is mostly wernerite which is granular, tabular and subhedral in shape. The scapolitic rocks show δ^{30}Si values of –0.7‰ to +0.2‰, with a δ^{18}O variation from 15.1‰ to 20.0‰.

The quartz veins occur in the Feng-Tai district with a close association with siliceous rocks. The δ^{30}Si values of these vein quartz samples vary from –0.5‰ to –0.1‰, which are similar to those of surrounding siliceous rocks. Their δ^{18}O values vary from 20.6‰ to 22.6‰, slightly higher than those of siliceous rocks (19.4‰ to 21.0‰).

Silicon isotopic compositions of the Langshan Cu–Pb–Zn polymetallic mineral deposits, Inner Mongolia, NW China

The Langshan district (Inner Mongolia, NW China) is one of the most important Cu–Pb–Zn polymetallic mineral districts in northwestern China. A total of 12 important polymetallic ore deposits have been explored in this district. The five large scale deposits include the Hougeqi, Dongshengmiao, Tanyaokou and Jiashengpan (Ding and Jiang, 2000). The basement rocks in this district consist of the upper Archean Wulashan Group of granulite, migmatite, gneiss, quartzite and marble, and the lower Proterozoic Seertengshan Group of green schist and magnetite-bearing quartzite and the Erdaowa Group of chlorite schist, sericite schist, hornblende anorthosite and magnetite quartzite. The ore-bearing strata include the middle Proterozoic Zhaertai Group. Orebodies in the district are mainly bedded and lenticular. The major ore minerals include pyrite, pyrrhotite, chalcopyrite, sphalerite and galena, with some minor amounts of marcasite, aresenpyrite, cattierite, bornite and cobaltite. The gangue minerals include calcite, dolomite, siderite, quartz and chlorite. The metals of Cu, Pb, Zn show clear zonations in vertical and lateral direction both in the regional and deposit scales.

Ding and Jiang (2000) reported δ^{30}Si and δ^{18}O data for quartz and silicate minerals in rocks and ores from the Tanyaokou, Dongshengmiao and Jiashengpan ore deposits; the results are presented in Figure 5.44. Three samples of quartz from

EBSCOhost - printed on 2/10/2023 8:05 PM via . All use subject to https://www.ebsco.com/terms-of-use

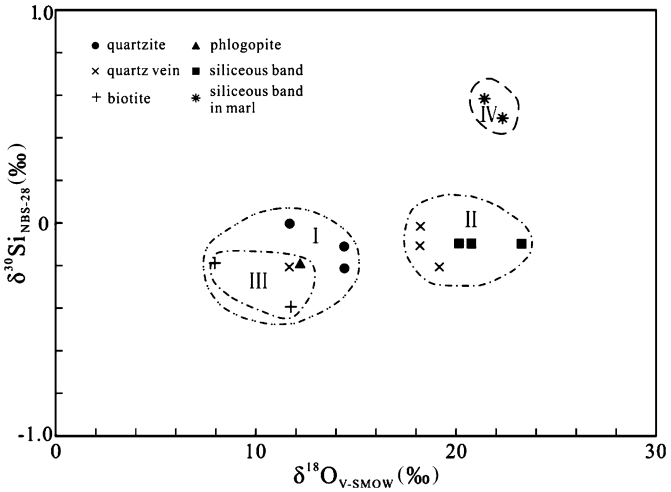

Figure 5.44: The relationship between δ^{30}Si and δ^{18}O values of quartz and silicate minerals from the Langshan ore district. I – Quartzite; II – Quartz vein and siliceous band; III – Biotite and phlogopite; IV – Siliceous band in marls. After Ding and Jiang (2000).

quartzites show δ^{18}O values of 11.5‰ to 14.2‰, and δ^{30}Si values of –0.2‰ to 0‰, indicating their protoliths of normal quartz sandstone. Six samples of chert bands and quartz lumps show δ^{18}O values of 17.2‰ to 21.2‰, and δ^{30}Si values of –0.2‰ to +0.8‰. Fourteen samples of vein quartz give δ^{18}O values of 11.5‰ to 23.1‰, and δ^{30}Si values of –0.2‰ to +0.5‰, which are close to their country rocks. These results may imply that these quartz veins might have formed with locally derived silica from country rocks during the hydrothermal processes under a low water/rock ratio.

Four biotite samples show δ^{18}O values of 7.8‰ to 12.7‰, two of them show δ^{30}Si values of –0.2‰ and –0.4‰. Two phlogopite samples give δ^{18}O values of 12.0‰ and 12.7‰, and δ^{30}Si values of –0.2‰ and –0.5‰. Two chlorite samples show δ^{18}O values of 5.4‰ and 4.2‰. In order to study the oxygen and silicon isotope fractionation among co-existing silicate minerals, quartz, biotite and phlogopite in one specimen (D-14) were analyzed both for the δ^{18}O and δ^{30}Si values. The δ^{18}O values for these three minerals are 18.0‰, 11.5‰ and 12.0‰, respectively, and a temperature of 437°C is calculated from oxygen isotope fractionation between quartz and biotite, which is significantly higher than the fluid inclusion temperature (347°C), and possibly indicating fully oxygen isotope equilibrium has not been reached during their formation. The co-existing quartz, biotite and phlogopite show δ^{30}Si values of 0‰, –0.4‰ and –0.2‰, which is in similar enrichment order as those of oxygen isotopes, but the fractionation of silicon isotopes is too small to be used to estimate the forming temperature of these minerals at this stage.

EBSCOhost - printed on 2/10/2023 8:05 PM via . All use subject to https://www.ebsco.com/terms-of-use

Silicon isotopic compositions of the bedded chert deposits below the Ni–Mo sulfide ore bed in the Ediacaran–Cambrian transition in South China

In the Yangtze platform, a succession of black rock series occurs including chert, phosphorite, Ni–Mo sulfide bed, barite and black shale (Jiang et al., 2003; Chen et al., 2009). A number of studies on the polymetallic Ni–Mo ores and barite deposits were carried out with two major contrasting genetic models proposed: one is the submarine exhalative hydrothermal origin model (Lott et al., 1999; Jiang et al., 2003; Chen et al., 2009) and the other is the seawater precipitation origin model (Mao et al., 2002). Similarly, the origin of these chert deposits at the Precambrian–Cambrian boundary has also been regarded as either hydrothermal (Li and Gao, 1996; Li, 1997) or marine (biogenic) origins (Guo et al., 2007; Chang et al., 2008).

Li et al. (1995c) was the first to report the δ^{30}Si values of the Precambrian–Cambrian strata in the Meishucun profile of the Yunnan Province. They found the interbedded volcanic ash has δ^{30}Si values of 0.0‰ to +0.1‰. Negative δ^{30}Si values (−2.1‰ to −0.2‰) are observed for siliceous materials in the siliceous dolomite and phosphorite just above the ash bed, which have been suggested as an indicator for hydrothermal input of Si (Li et al., 1995c). The negative δ^{30}Si values were also observed in other stratigraphic sections in South China, such as the Sancha and the Taojiang sections in Hunan Province (Wang and Chen, 1996; Jiang and Li, 2005).

Fan et al. (2013) sampled cherts from the Yinjiang section of northeast Guizhou Province and the Chuanyanping section of western Hunan Province, South China. Four intervals (I to IV) of chert are distinguished. The first interval chert samples with a thin-layer structure show positive Si isotopic compositions from +0.2‰ to +0.7‰ (Figure 5.45). The second interval chert samples, locating on the K-bentonite layer, yield negative δ^{30}Si value in the narrow range from −0.3‰ to −0.5‰. The δ^{30}Si values of the third interval cherts (+0.1‰ to +0.7‰) are consistent with those of the first interval cherts. The δ^{30}Si value achieves a peak of +1.2‰ in the fourth interval, which is similar to that of modern chemical sedimentary rocks (De La Rocha et al., 1997). The δ^{30}Si values of the K-bentonites (0‰ to +0.1‰) is close to modern felsic rocks (−0.1‰, Ding et al., 1996; −0.12‰, André et al., 2006). The δ^{30}Si value of black shales on the top of the fourth interval cherts is +1.0‰, similar to that of the fourth interval chert samples.

5.4.2.2 Silicon isotope fingerprinting of the sea-floor exhalative hydrothermal origin

It is suggested that the stratiform tourmalinite, especially spessartine- and sulfide-rich varieties within and immediately underlying the Sullivan deposit, are thought to have formed by syngenetic-exhalative processes coeval with local clastic sedimentation and formation of the bedded Pb–Zn–Ag ores (Slack et al., 2000).

This type of tourmalinite from the Sullivan deposit shows a δ^{30}Si range from −0.5‰ to −0.1‰. Similar δ^{30}Si values are obtained for one stratiform tourmalinite

EBSCOhost - printed on 2/10/2023 8:05 PM via . All use subject to https://www.ebsco.com/terms-of-use

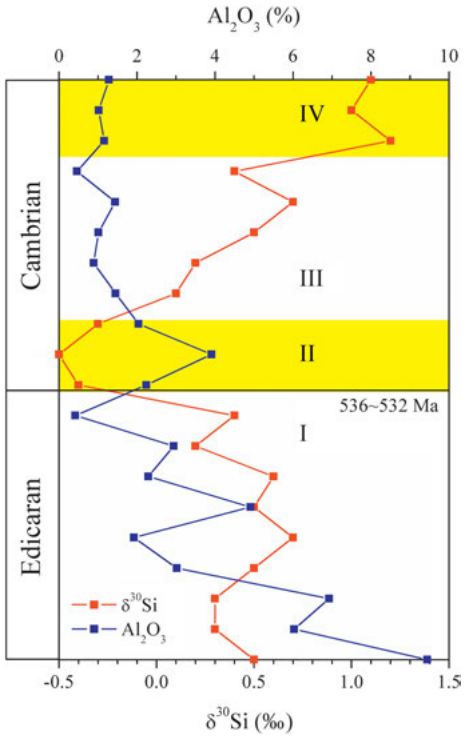

Figure 5.45: Variation of δ^{30}Si and Al_2O_3 concentrations of cherts in Precambrian–Cambrian intervals from the Chuanyanping section (Hunan Province) and the Yinjiang section (Guizhou Province). After Fan et al. (2013).

(Neg-2) from the Neg Lake prospect (δ^{30}Si = –0.3‰) and one spessartine-rich tourmalinite from the North Star hill (JS-93-48) just below the projected horizon of the North Star massive sulfide deposit (δ^{30}Si = –0.5‰). These δ^{30}Si values are different from the sedimentary rocks, but similar to those obtained from hydrothermal siliceous precipitates formed on the sea floor (Ding et al., 1988a, 1996). The silicon isotope data clearly support the hypothesis of their formation by means of syngenetic hydrothermal exhalation. It is most likely that the negative δ^{30}Si values of this type of tourmalinite (–0.5‰ to –0.1‰) result from various amounts of mixing of hydrothermal and detrital components, rather than reflecting a purely hydrothermal component like the banded iron formation we discussed above, because the chert or magnetite–quartz beds in the Precambrian banded iron formations, which probably contain little or no detrital silica, have more negative δ^{30}Si values (–2.2‰ to –0.9‰, Jiang et al., 1993) than those of the Sullivan stratiform tourmalinites.

Mn-rich (spessartine) garnet is regarded as an indicator mineral for exhalative hydrothermal activity. Spessartine garnet-rich tourmalinite is locally present in the shallow footwall of the Sullivan orebody, and their occurrence may indicate the former existence of a brine pool prior to exhalative Pb–Zn mineralization (Slack et al., 2000). It is suggested that these garnet-rich tourmalinites may have originated either from exhalative precipitation of the Mn-borate minerals jimboite and sussexite, which re-

EBSCOhost - printed on 2/10/2023 8:05 PM via . All use subject to https://www.ebsco.com/terms-of-use

acted with detrital clays and hydrothermal carbonates during diagenesis and/or metamorphism to form a tourmaline–spessartine assemblage, or from exhalative precipitation of boron and manganosiderite that similarly reacted with detrital clays to form spessartine-rich tourmalinites (Slack et al., 2000). Previously, it is thought that the Al in the spessartine garnet and tourmaline was provided by detrital clays (Slack et al., 2000). However, the silicon isotope data of the garnet-rich tourmalinite suggest a hydrothermal component for the Si, arguing against a wholly detrital source for the Si, and possibly for the Al also.

Ethier and Campbell (1977) proposed a hydrothermal colloid or gel origin for the tourmalinites at Sullivan. It is likely that hydrothermal colloids or gels were precursors to at least some tourmalinites associated with coticules or sulfide in the shallow footwall and hanging wall of the Sullivan deposit, including those that have negative δ^{30}Si values (−0.5‰ to −0.1‰); some of these tourmalinites also display a distinctive spheroidal texture that is consistent with a colloidal/gel origin (Slack et al., 2000).

The silicon isotope data (−0.6‰ to −0.3‰) of the siliceous rocks from the Devonian stratiform Pb–Zn deposits in the Qinling orogenic belt, northwestern China also suggest these rocks are of submarine hydrothermal exhalative in origin. In the Qinling area, the siliceous rocks are often closely related to limestone, indicating they should have formed in a shallow marine condition. The relatively high contents of ankerite and siderite, and Al, Ti, K and Na as well, support the idea that these rocks were formed through a chemical process of precipitation rather than a biochemical process like those of diatomaceous siliceous rocks. Moreover, no radiolaria and diatoms have been found, although organic matter is contained in the siliceous rocks. Hence, the contribution of siliceous organisms to the formation of these rocks is equivocal. The oxygen isotope data of the siliceous rocks also support their formation by chemical precipitation in a marine environment, with their δ^{18}O values from 18.6‰ to 21.0‰ which are higher than those of sandstone and lower than those of biogenic opaline rocks. Generally, only the δ^{18}O values of microcrystalline quartz precipitated from sea water under a higher temperature could fall in such an field as plotted in the diagram (Figure 5.43). Hence, the isotopic compositions of both silicon and oxygen can be used, with other geological and geochemical evidence, to constrain the submarine hydrothermal origin of the siliceous rocks at Qinling.

Silicon and oxygen isotopes, in combination with other geological and geochemical evidence, are also applied for those chert deposits and silicified dolomite and phosphorite in the Precambrian–Cambrian transitional interval in the Yangtze platform, South China, to demonstrate a submarine hydrothermal condition at that time (Wang and Chen, 1996; Jiang and Li, 2005; Fan et al., 2013). The temperature of the hydrothermal fluids present at Precambrian–Cambrian boundary are estimated from the homogenization temperature of fluid inclusions within quartz that crosscut the Ni–Mo polymetallic sulfide ore bed in the Lower Cambrian black shales (up to 260°C, Lott and Coveney, 1996), and from fluid inclusion measurements of the stratiform barite deposits from Guizhou Province (150 ~ 190°C, Yang et al., 2008). Using the δ^{18}O of

EBSCOhost - printed on 2/10/2023 8:05 PM via . All use subject to https://www.ebsco.com/terms-of-use

the cherts, Jiang and Li (2005) estimated that the temperature of the mixed fluid responsible for chert formation from seawater and hydrothermal fluid was 80 ~ 98°C. The oxygen isotopic composition of the cherts ($\delta^{18}O$ = 18.1 ~ 22.6‰) showed a hydrothermal characteristic ($\delta^{18}O$ = 20.7 ~ 23.0‰), rather than that of volcanogenetic cherts, which have lower $\delta^{18}O$ values of 1.9‰ to 9.2‰ and normal marine cherts that have higher $\delta^{18}O$ value of 25.6‰ (Jiang and Li, 2005). Significant enrichment in trace metals such as V, Mo, Zn, As and Ba and positive Eu anomaly also suggested that hydrothermal fluid played an important role in governing the geochemical characters of these cherts from the Precambrian–Cambrian intervals in South China (Jiang and Li, 2005).

Fan et al. (2013) also suggested that the submarine hydrothermal activity is an important process to explain the vast changes in the oceanic environment during the Precambrian–Cambrian interval when widespread bedded cherts and massive metallic ore deposits occurred together with the biological diversity. They adopted a mixing model to explain the formation of cherts with different sources of silicon and various isotopic compositions as those previously proposed by van den Boorn et al. (2007). As suggested by van den Boorn et al. (2007), the three end-members may have contributed to the $\delta^{30}Si$ variation of the cherts from Precambrian–Cambrian boundary in South China: 1) hydrothermal fluids, 2) silicon-rich seawater and 3) volcanic materials. Fan et al. (2013) found that most of the first interval chert samples are Al_2O_3-rich (>2.94%), whereas other chert samples are depleted in Al_2O_3 (<2.24%) (Figure 5.45). The Al_2O_3-rich endmember reflects primarily volcanic or clastic sedimentary materials with a $\delta^{30}Si$ value of ca. 0‰. The Al_2O_3-poor cherts are interpreted as chemical precipitation from mixtures of ^{30}Si-rich and ^{30}Si-poor fluid (van den Boorn et al., 2007, 2010). The negative $\delta^{30}Si$ values (–0.5‰ to –0.3‰) in the chert samples resemble the $\delta^{30}Si$ values of hydrothermal siliceous precipitates (–0.6‰ to –0.4‰, Ding et al., 1996; Coplen et al., 2002), which is also supported by the positive Eu anomalies, highly Ba level and unusual correlation between Ce/Ce^* and Pr/Pr^* (Fan et al., 2013).

5.4.2.3 Using silicon isotopes to distinguish various alteration types and protoliths

Widespread hydrothermal alteration occurs at many SEDEX-type deposits, for example, tourmaline, chlorite, albite, biotite, muscovite and carbonate alterations are present at Sullivan deposit, formed tourmalinite, chlorite-rich rocks and albitite, which have already lost their primary features of unaltered protoliths. Using silicon isotopes of these alteration rocks, it is possible to distinguish the types of alterations and their protoliths.

A funnel-like alteration zone of tourmalinite occurs in the footwall beneath the orebody at Sullivan deposit, which has been suggested as products of submarine hydrothermal alteration of clastic sediments of the Aldridge Formation (Slack et al., 2000). Textural evidence shows selective replacement of clay and/or feldspar in the matrix of siltstones and argillites by tourmaline, and the trace element distribution

EBSCOhost - printed on 2/10/2023 8:05 PM via . All use subject to https://www.ebsco.com/terms-of-use

patterns of this type tourmalinite are also similar to the unaltered Aldridge metasediments (Slack et al., 2000). During the metasomatic alteration of the argillite to form tourmalinite, addition of B, Mg and Mn and depletion of Na, K and Ca occurred; there was also a moderate amount of Fe introduced. The source of Al and Si in the tourmalinites is from in situ clastic sediments (Slack et al., 2000). This alteration model for the tourmalinite formation is supported by the study of silicon isotopic compositions. For instance, all three samples taken from the funnel-like altered zone of the tourmalinite show δ^{30}Si value of 0‰, which are consistent with the δ^{30}Si values (0‰ to +0.1‰) for samples of metasedimentary rocks in the mine area. It seems to indicate that these alteration rocks may have an inherited silicon isotope signature from their original sedimentary rocks.

Chlorite and albite alteration are also widespread in the Sullivan deposit, especially in the hanging wall of the Sullivan orebody. A body of albite–chlorite–pyrite altered rock extends from just below the orebody to 150 m stratigraphically above it at Sullivan. The chlorite-rich rocks locally contain substantial (10–20%) garnet and minor biotite. A sample of low-Mn garnet-bearing chlorite rock (397-1) from the hanging wall of the Sullivan orebody has a whole-rock δ^{30}Si value of +0.1‰. This value is distinct from those of the spessartine and sulfide-bearing tourmalinites of hydrothermal exhalative origin, but very similar to the δ^{30}Si values of the clastic metasedimentary host rocks, indicating that in this case the Si is derived from in situ clastic sediments and that this garnet-bearing chlorite rock is the product of alteration of normal Aldridge sediments.

It is suggested that the albite–chlorite–pyrite alteration in the hanging wall of the Sullivan orebody formed by hydrothermal overprinting of part of the hanging wall tourmalinite zone and by the alteration of adjacent Aldridge sediments (Turner and Leitch, 1992; Shaw, 1993). Two chlorite-rich rocks (4209-1 and 93SY-84-3) from the hanging wall albite–chlorite–pyrite alteration zone close to the main massive sulfide orebody have δ^{30}Si values of −0.6‰ and −0.4‰. Two possibilities exist for these negative δ^{30}Si values: one is the chlorites may have formed by the replacement of hydrothermal-exhalative tourmalinites; the second possible model is incorporation of hydrothermal silicon from fluids to form the albite–chlorite–pyrite altered rocks. If the former is correct, then this would indicate that precursor tourmalinites at the hanging wall also represent a boron-rich hydrothermal exhalative sediment as they do in the shallow footwall to the main sulfide orebody. This interpretation appears to be more likely than the second alternative, because the chlorite-rich rocks are depleted in SiO_2 compared to their possible precursors of tourmalinite or Aldridge quartzitic sediment (Shaw, 1993). The net loss of Si during chloritization mitigates against a significant incorporation of hydrothermal Si into chlorite during the replacement process. However, we cannot totally exclude the second possibility as the chlorite-rich rocks have slightly lower δ^{30}Si values (−0.6‰ to −0.4‰) than the hydrothermal exhalative tourmalinites (−0.5‰ to −0.1‰).

EBSCOhost - printed on 2/10/2023 8:05 PM via . All use subject to https://www.ebsco.com/terms-of-use

One albite-rich sample from the albite–chlorite–pyrite alteration zone (4209-2) has a δ^{30}Si value of +0.1‰ that possibly suggests this rock was altered from a protolith of normal Aldridge clastic sediments. Another albite-rich rock from the same alteration zone (JS-93-14A), but with relict tourmaline, has a negative δ^{30}Si value of −0.2‰. This slightly lower δ^{30}Si value may suggest that the original sediments contained a chemical-exhalative component. In this case, the δ^{30}Si value of the albite-rich rock may record mixing between exhalative hydrothermal Si and Si derived from clastic sediments.

The argillitic sediment, tourmalinite and albitite in the Sullivan deposit all show 65 ~ 68% SiO_2, thus tourmalization and albitization of the Aldridge argillites did not necessary involve a net loss of Si (Shaw, 1993; Slack et al., 2000). However, if the precursor rock was coarse-grained greywacke or quartzite that shows an average of 78% SiO_2, then a net loss of SiO_2 is needed during albitization. It appears that silicon isotopes may fractionate during hydrothermal alteration with loss of Si to a solution. Previous silicon isotope fractionation studies on precipitated silica and solution reveal that the siliceous precipitates are uniformly enriched in ^{28}Si (Douthitt, 1982; Li et al., 1995a; De La Rocha et al., 1997). However, the silicon isotope fractionation experiments were conducted at room temperature, which is in sharp contrast to the high temperatures (probably >200°C) for the hydrothermal alteration events at Sullivan (Jiang et al., 2000). During low temperature processes (e.g., chemical weathering) significant silicon isotope fractionation does occur (Douthitt, 1982; Ding et al., 1996). For example, clays can be formed from weathering of granites, and Ding et al. (1996) reported a lower δ^{30}Si value from −1.9‰ to −1.0‰ for this type of clay in contrast to the δ^{30}Si value of the granite (near zero). Ding et al. (1996) proposed that in this type of chemical weathering, dissolution of primary silicate minerals occurs to form clays with a loss of Si to the solution. If taking feldspar as an example, this process can be expressed by the following equation:

$$2KAlSi_3O_8 + 2H^+ + 9H_2O = Al_2Si_2O_5(OH)_4 + 2K^+ + 4H_4SiO_4 \quad (5.3)$$

The ^{28}Si-enriched clay minerals formed during weathering, imply a dissolved Si (i.e., H_4SiO_4 in the equation above) moved to the solution with ^{30}Si enriched. However, during high temperature processes, such as hydrothermal alteration of granite, the resultant clay minerals have nearly identical δ^{30}Si values (−0.1‰ to +0.1‰) to those of the granites (~0‰), reflecting a lack of silicon isotope fractionation during this alteration (Ding et al., 1996).

It is generally accepted that stable isotope fractionations are temperature-dependent such as oxygen and hydrothermal isotopes, but previous studies have shown that temperature-related fractionation of silicon isotopes is insignificant over the temperature range inferred for chlorite- and albite-related alteration at Sullivan (Jiang et al., 1993). Hence, it is most likely that the differences in δ^{30}Si values for the chlorite and albite altered rocks at Sullivan record their different protoliths.

EBSCOhost - printed on 2/10/2023 8:05 PM via . All use subject to https://www.ebsco.com/terms-of-use

In the Qinling Devonian stratiform Pb–Zn deposits, hydrothermal alteration produced albitite and scapolite. These rocks show a δ^{30}Si variation of –0.4‰ to +0.2‰, falling in the δ^{30}Si range of immediate-felsic volcanic rocks and sedimentary sandstones. The mineralogical and geochemical characteristics of these rocks exclude the possibility that the parent rocks of these altered rocks were sandstone. As a result, it is suggested that the protoliths of these rocks might be submarine volcanic rocks such as volcanic tuffs. The high δ^{18}O values (19.0‰ to 21.7‰) of these rocks may indicate an isotope exchange with seawater under medium to low temperatures.

From the discussion above, it can be seen that the silicon isotopic compositions of the altered rocks and minerals from various SEDEX-type deposits can reflect the character of their original rocks. Hence, it is possible to use the silicon isotope data to distinguish the protoliths of the alteration.

5.4.2.4 Does silicon isotope fractionate during metamorphic or hydrothermal overprinting in the SEDEX-type deposits?

A middle to upper greenschist grade regional metamorphism with T = 450°C and P = 3.8 kb occurred at Sullivan after the deposition of the sulfide ores (De Paoli and Pattison, 1995). Although in the above discussion we interpreted the different δ^{30}Si values in the hydrothermal alteration rocks and minerals to reflect their different Si sources and protoliths, we need to discuss if the δ^{30}Si variations may also relate to metamorphism of the deposit.

Taking the footwall funnel-like tourmalinite as an example, it is possible that Si in this type of tourmalinite also had a hydrothermal origin as those of stratiform tourmalinite, i.e., with negative δ^{30}Si values, but have been reset to its present range of δ^{30}Si values of near 0 during metamorphism. If this is the case, this would require the transport of large amounts of isotopically heavy silicon by very large amounts of metamorphically-derived fluids through the feeder zone. In this event, the less permeable massive sulfide orebody may have obstructed the flow of metamorphic fluids close to the orebody, thereby shielding hydrothermal silicate minerals (chlorite, albite, tourmaline) in and adjacent to the massive sulfide zone from metamorphic re-equilibration of silicon isotopes and allowing partial retention of originally negative δ^{30}Si values of hydrothermal signatures.

However, this model of metamorphic resetting of δ^{30}Si values at Sullivan footwall tourmalinite is very unlikely. First, there is no evidence for high water/rock ratios during metamorphism of the footwall that would be required to reset the silicon isotopic compositions. Second, oxygen and boron isotope values of tourmaline are not greatly altered by subsequent metamorphism due to its refractory nature (Taylor and Slack, 1984; Palmer and Slack, 1989; Jiang et al., 2000), and silicon is much less mobile than boron. Further evidence for the resistance of silicon isotopes to resetting during metamorphism comes from a silicon isotope study of the Gongchangling iron deposit in

EBSCOhost - printed on 2/10/2023 8:05 PM via . All use subject to https://www.ebsco.com/terms-of-use

Liaoning Province, China, which underwent high grade amphibolite to granulite facies metamorphism (Jiang et al., 1993), as we discussed in Section 5.4.1. Ding et al. (1996) reported that quartzite and metamorphic sandstone samples from other localities have δ^{30}Si values close to 0‰, identical to the values of their unmetamorphosed equivalents. Ding et al. (1996) also found that although metamorphic schists show a wide range of δ^{30}Si values (–1.1‰ to +0.4‰), they are well correlated values of the precursor rocks. For example, mica schists collected from the Ximeng area in Yunnan Province, China, which are metamorphosed argillaceous sediments, display δ^{30}Si values of –1.1‰ to –0.4‰, whereas amphibolite and biotite schists in the same area that represent metamorphosed mafic volcanic rocks have δ^{30}Si values of +0.2‰ to +0.4‰. Therefore, the utility of silicon isotopes is that they can identify hydrothermal, sedimentary and volcanic protoliths in metamorphic terranes (Jiang et al., 1993; Ding et al., 1996).

In conclusion, the resistance of silicon isotopes to metamorphic resetting arises because the great abundance of silica in most rocks requires a large-scale Si exchange to significantly alter original silicon isotope compositions. However, small quartz veins in a quartz-rich clastic host rock may be isotopically reset during metamorphism, where the amount of silicon of hydrothermal origin is very small compared to the silicon contained in detrital minerals of the metasedimentary host rock.

The silicon isotopic compositions of the quartz still show a relationship with their host rocks if the Si were derived locally from the host rocks, as the example in the Qinling Devonian SEDEX-type Pb–Zn deposit in northern-west China. At Qinling, the silicon isotopes of the quartz veins are similar to the country siliceous rocks. The δ^{18}O value of the vein quartz is slightly higher than that of the surrounding siliceous rocks. The reason for this phenomenon may be different in different locations. In the Feng-Tai district, for example, the δ^{18}O value of quartz vein is 1–2‰ higher than those of the country rocks. This may be caused by the oxygen exchange between the underlying carbonate rocks and the hydrothermal solution that formed the quartz veins. Because the $\delta^{18}O_{VSMOW}$ value of the Devonian marine carbonate is generally higher than 20‰, quartz precipitated from hydrothermal solutions in equilibrium with it must have a δ^{18}O value higher than 20‰. In the Zha-Shan district, the vein quartz has a δ^{18}O value higher than that of the bulk rock samples of the albititic and scapolitic rocks, but close to that of quartz separates from these rocks. This may indicate equilibration between the rocks and hydrothermal solutions that formed the vein quartz.

5.4.3 Hydrothermal Pb–Zn deposits

5.4.3.1 Silicon isotopic compositions of the Taolin Pb–Zn deposit, Hunan Province, China

Taolin Pb–Zn ore deposits (Hunan Province, China) is a typical hydrothermal Pb–Zn deposits in South China. Detailed studies have been made on the geological charac-

EBSCOhost - printed on 2/10/2023 8:05 PM via . All use subject to https://www.ebsco.com/terms-of-use

teristic, mineral association, fluid inclusions and isotope geochemistry (e.g., Ding and Rees, 1984; Ding et al., 1986). In order to trace the silicon source and the origin of this deposit, a study has been carried out on the silicon isotopes.

Both the granite, metamorphic rocks and the vein quartz from the Taolin deposit are analyzed for their silicon isotopic compositions (Figure 5.46). Two granite samples show δ^{30}Si values of –0.1‰ and +0.3‰, falling into the normal δ^{30}Si range of the granites worldwide. A chlorite schist from the host rock has a δ^{30}Si value of –0.1‰, and a hornfel sample has a δ^{30}Si value of –0.2‰. A quartzite and a slate from the host rock have identical value of –0.3‰. In general, the δ^{30}Si values of the metamorphic rocks are slightly lower than those of the granite. Eight quartz samples are analyzed. Two samples of barren quartz veins within the altered granite gave the same δ^{30}Si value of –0.3‰. Five quartz samples from the mineralization stage yielded δ^{30}Si values from –0.5‰ to –1.5‰, which are apparently lower than those of granites, host metamorphic rocks and the barren quartz.

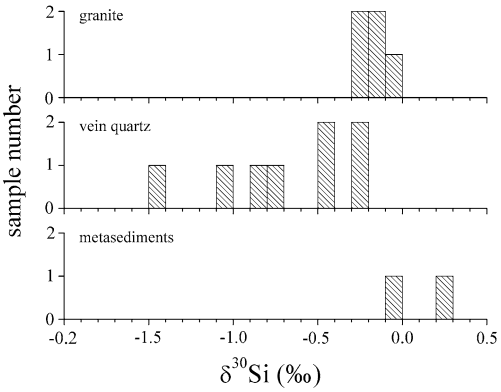

Figure 5.46: Histogram showing the silicon isotopic compositions of the vein quartz, granites and metasedimentary rocks from the Taolin Pb–Zn deposit. Data are from Ding et al. (1996).

5.4.3.2 Using silicon isotopes to constrain the mid- and low-temperature hydrothermal origin of the Taolin Pb–Zn deposit

In the Taolin Pb–Zn deposit, all the δ^{30}Si values (–0.3‰ to –1.5‰) for the ore-bearing and barren quartz veins are much lower than those of the granite and the host metasedimentary rocks (–0.1‰ to +0.3‰). Therefore, the source of silicon in the quartz veins may not derive from the granite nor the host metasedimentary rocks, because if this is the case, then they should have similar silicon isotope signatures. Moreover, the large age gap between the granitic magmatism and the mineralization also prevents a genetic link between them. Oxygen and hydrogen isotope data suggest dominantly meteoric water instead of magmatic water. If the silicon sourced

EBSCOhost - printed on 2/10/2023 8:05 PM via . All use subject to https://www.ebsco.com/terms-of-use

from the country rocks, then it would require a leaching process of silicon from the metasedimentary rocks and re-deposit in the veins. In this case, if the temperature of the hydrothermal fluids was high enough, the precipitated silica should show a δ^{30}Si value similar to that of the country rocks. Due to the limited number of analysis for host rocks, the possible existence of rocks with relatively low δ^{30}Si values cannot be excluded totally. Indeed a co-variation relationship between the quartz vein and the host rocks can be seen. For instance, the δ^{30}Si values of two barren quartz veins from the altered granites are –0.3‰, corresponding to the relatively higher δ^{30}Si values of the granites, whereas the δ^{30}Si values of the ore-bearing quartz veins from the metasedimentary rocks are in the range of –0.5‰ to –1.5‰, which correspond to the relatively lower δ^{30}Si values of the host rocks. This suggests that the surrounding host rocks may indeed have a contribution of silicon to the formation of vein quartz. However, the vein quartz and the host metasedimentary rocks show clearly different silicon isotopic compositions. Therefore, there must be either another source which supplied silicon with a lower δ^{30}Si value and/or a large fractionation of silicon isotopes must occur when the vein quartz was precipitated.

As discussed previously, the silicon isotope fractionation might happen between the precipitated SiO_2 and the silica remaining in the residual solutions at a suitable temperature and precipitation conditions. As a result, the precipitated silica could have a lower δ^{30}Si value than the primary solutions, and the SiO_2 remaining in a solution should have a higher δ^{30}Si value. This phenomenon has been observed in the siliceous precipitates of hot spring fields, the sea-floor black smokers and the Precambrian BIF. For instance, in the modern hot spring area of Tengchong County, Yunnan Province, the δ^{30}Si values of the subsurface quartz veins show a variation of –0.1‰ to –0.9‰, whereas the surface siliceous sinter has a δ^{30}Si value of –0.6‰ to +0.2‰. The spring water has a δ^{30}Si value of 0.0‰ to +0.4‰. The silicon isotopic compositions of vein quartz in the Taolin Pb–Zn deposit are similar to those in the Tengchong hot springs. Therefore, we suggest that the Taolin deposit may have also formed in a low-temperature epithermal hydrothermal system, but the epithermal systems are no longer in existence on the surface today. As a result, based on the silicon isotope data, we suggest the following model for the formation of Taolin Pb–Zn deposit. It is likely that hydrothermal activity existed for a long time after the granitic magmatism. Meteoric water was heated and circulated through the rocks. Silicon was leached from the surrounding metasedimentary rocks and the granites, and was then precipitated at the interface where the hydrothermal conditions were changing. Due to kinetic fractionation of silicon isotopes, the earlier precipitated SiO_2 would have δ^{30}Si values lower than the source rocks. Later on, the residual solutions with higher δ^{30}Si values but lower silica concentrations would have risen up and been diluted by ground water near the surface and subsurface. This model is also supported by results of lead and strontium isotopes in this deposit.

EBSCOhost - printed on 2/10/2023 8:05 PM via . All use subject to https://www.ebsco.com/terms-of-use

5.4.4 Sn deposits

5.4.4.1 Silicon isotope variations in Dachang Sn-polymetallic ore deposit

The Dachang Sn-polymetallic ore deposit in Guangxi Province of China is one of the largest Sn deposits in the world, and the second largest Sn producer in China (more than 10^6 tons of tin). There are various models proposed in order to explore the ore genesis of the deposit, and the major debates are focusing on whether the stratiform Sn–Pb–Zn orebodies are syn-sedimentary in origin or products of the Yanshannian magmatic–hydrothermal event (~100 Ma) (Chen et al., 1985, 1993; Ding et al., 1988b; Han and Hutchinson, 1990, 1991; Jiang et al., 1999).

Regionally, the occurrence of Devonian siliceous rocks in Guangxi is restricted by syngenetic faulting (Liu et al., 2014b). They are generally well developed in the subordinate depressed basin localized by intersecting faults, where their thickness may reach up to 100–120 m. Towards the margin of the basin, the siliceous rocks become thinner, with the thickness of marls and limestones increasing gradually. Siliceous rocks in D_3^1 are characterized by their massive structure. They are 60–70 m thick, greyish black, rich in carbonaceous materials and show regular flat-bedding. Major minerals include microcrystalline quartz, chalcedony, opal and small amounts of sericite and pyrite. The microcrystalline quartz makes up 85–90%. They are euhedral and/or subhedral, granular, with grain diameters varying from 0.01 to 0.02 mm, and showing mosaic texture. No interstitial material can be seen between the grains and a distinctive stylolite structure is clearly displayed.

Siliceous rocks in the thick-banded limestone (D_3^{2a}), thin-banded limestone (D_3^{2b}) and small lenticular limestone (D_3^{2c}) are characterized by ribbon banding, usually intercalated with cassiterite–sulfide and limestone bands. The bands are 0.1–2.0 cm thick in general. The minerals include microcrystalline quartz, chalcedony, opal and a significant amounts of other minerals such as sericite, calcite, tourmaline, K-feldspar, carboneceous matters and sulfides.

Song and Ding (1990) made the first silicon isotope analyses of these rocks. A more systematic study of silicon and oxygen isotopes on these siliceous rocks was followed by Yao and Ding (1994).

1) Barren siliceous rocks

   Thirteen barren siliceous rocks are analyzed for their δ^{30}Si and δ^{18}O values. Except for one sample (Dc9016-1) with a δ^{30}Si value of −0.2‰, all others show positive δ^{30}Si value of +0.2‰ to +0.8‰. Their δ^{18}O values are from 12.0‰ to 21.4‰. Siliceous rocks with such a high δ^{30}Si value could not be derived from protolith quartz sandstone, nor be precipitated directly through sea-floor hydrothermal exhalation. Their formation through silicification via magmatic–hydrothermal processes can also be excluded. Only shallow sea radiolarian siliceous rocks could have such δ^{30}Si characteristics (Song and Ding, 1990). In fact, a great quantity of radiolarian remains have been found in these siliceous rocks, thus providing direct evidence for their origin of biogenic precipitation.

EBSCOhost - printed on 2/10/2023 8:05 PM via . All use subject to https://www.ebsco.com/terms-of-use

2) Siliceous and sulfide bands in stratiform orebodies
Bands of siliceous rocks often appear along with cassiterite–sulfide ores occurring concordantly with sedimentary bedding. Ten samples of quartz separate and/or quartz–feldspar mixing from these rocks are analyzed for their silicon and oxygen isotopes. The δ^{30}Si values show a large variation from –0.6‰ to +0.6‰. Three samples with positive δ^{30}Si values may have similar biogenic origin as those littoral radiolarian siliceous rocks. The rest of samples may have more complicated origin as we will discuss later on.

The siliceous bands show a δ^{18}O variation from 13.2‰ to 15.9‰, whereas those of the mixed samples (quartz+feldspar+clay minerals) from the sulfide bands vary from 14.5‰ to 16.0‰. The difference in their ranges is rather small, and the total range of variation is also rather limited.

A number of veins are found in the Dachang ore deposit, including two major types; one is the small and short veins or veinlets that are "non-transgressive", being confined within certain stratigraphic horizons. They form the so-called concordant orebodies in combination with the banded ores, constituting important parts of the orebody No. 91 and No. 92. The other type of vein is the so-called "transgressive" type. They are large and cut through various sedimentary strata, such as the veins No. 1 and No. 38.

The two types of vein show different mineralogy. The first type of non-transgressive vein has a simple mineral assemblage, representing mainly pyrite, sphalerite, cassiterite, quartz and calcite. The second type of transgressive vein shows a more complicated mineral assemblage. Beside the former minerals, they also contain arsenopyrite, marcasite, stiblite, galena, jamesonite and other sulfasalts.

1) Non-transgressive veins
Quartz from ten samples of non-transgressive veins in different strata has been analyzed for their δ^{30}Si and δ^{18}O values. Their δ^{30}Si values vary from –0.2‰ to +0.5‰. Only one sample shows a negative value (–0.2‰), three samples show a value of 0 and six samples show positive values of +0.1‰ to +0.5‰. The δ^{30}Si values of samples from some non-transgressive veins are compared with those of samples from their adjacent siliceous rocks and bands (Figure 5.47). Of the six pairs, there are five with δ^{30}Si difference of 0.1‰ to 0.3‰, and only one pair has a difference of 0.6‰. This relationship suggests a close relationship in their silicon isotope compositions between the samples compared, which indicate an in-situ derivation of Si in the non-transgressive veins.
2) Transgressive veins
Two samples of transgressive veins are analyzed for their silicon and oxygen isotopic compositions. The δ^{30}Si values of quartz are –0.1‰ and +0.3‰, which are within the δ^{30}Si range of siliceous rocks at Dachang, but they are also close to those values of granite and diorite dikes at Dachang (–0.3‰ to –0.1‰). Therefore, only with these two data, it is difficult to discuss their origin. The two quartz

EBSCOhost - printed on 2/10/2023 8:05 PM via . All use subject to https://www.ebsco.com/terms-of-use

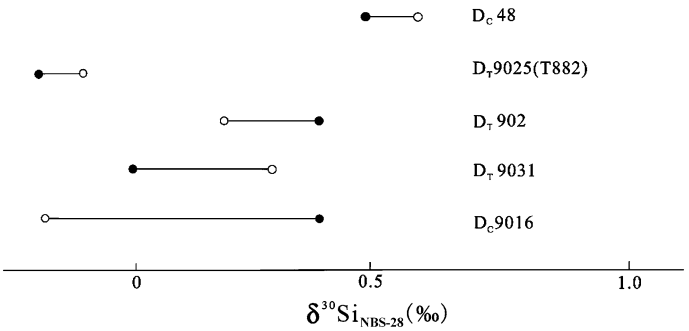

Figure 5.47: A comparison of δ^{30}Si value of non-transgressive veins with those of adjacent siliceous rocks and bands. The solid circles represent non-transgressive veins; the open circles represent siliceous rocks or bands. After Ding et al. (1996).

samples show δ^{18}O values of 18.2‰ and 24.0‰: one is similar and one is higher than those of non-transgressive veins.

5.4.4.2 Different origin of siliceous rocks from the Dachang Sn-polymetallic ore deposit

The origin for the siliceous rocks from the Dachang mining area is hotly debated, including two contrasting viewpoints of submarine hydrothermal exhalative precipitation origin and the normal sedimentary/biogenic origin. For example, Chen and Zeng (1989) considered them as hydrothermal sediments deposited in a starved basin. Xu and Wang (1987) found a large number of radiolarian fossils in the upper Devonian siliceous rocks from Dachang, and thus provided a plausible evidence for their biogenic origin.

A systematic survey on silicon and oxygen isotopes among siliceous rocks and bands at Dachang reveals two individual origins of siliceous rocks (Figure 5.48).

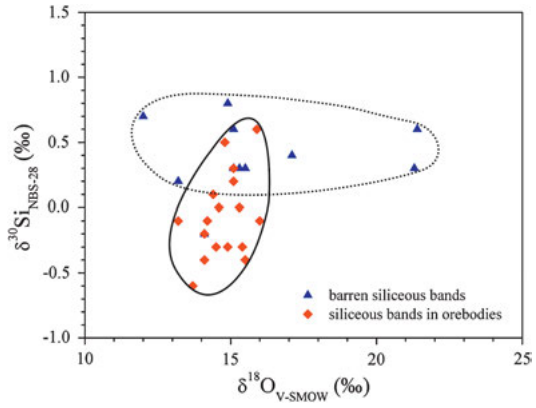

Figure 5.48: Distribution of δ^{30}Si–δ^{18}O among siliceous rocks in the Dachang deposit. Data are from Ding et al. (1996).

EBSCOhost - printed on 2/10/2023 8:05 PM via . All use subject to https://www.ebsco.com/terms-of-use

(i) Shallow radiolarian siliceous rocks without mineralization, which show positive δ^{30}Si (+0.2‰ to +0.8‰) and wide variation of δ^{18}O values (+12.0‰ to +21.4‰). These types of rocks formed thick sedimentary units and are widespread through the basin. Their silica was derived from seawater. The existence of a large amount of radiolarian in these rocks places direct evidence for the biogenic deposition origin.
(ii) The thin-laminated siliceous and K-feldspar rocks associated with cassiterite–sulfide ores with negative δ^{30}Si (i.e., −0.1‰ to −0.6‰) and uniform δ^{18}O values (i.e., +13.2‰ to +16.0‰).

It is possible that these rocks were formed through a process of magmatic–hydrothermal replacement of limestone strata. Silicon isotope analyses have been made on samples of granites and dioritic-porphyrite dykes in the mining area, and their δ^{30}Si values range from −0.1‰ to −0.3‰. If the magmatic–hydrothermal metasomatism took place, then the resulted silicification should have similar δ^{30}Si as those magmatic rocks. It is hard to explain the data from Dachang mining area, for example, in the sample D_T9024, the δ^{30}Si value of siliceous bands is +0.6‰, whereas quartz from the sulfide bands in the same specimen has a δ^{30}Si of −0.4‰. It is therefore unlikely for a magmatic–hydrothermal alteration origin to explain the silicon isotope difference in different bands in a single specimen. In addition, the well-developed bands could also hardly result from magmatic–hydrothermal replacement.

The negative δ^{30}Si values of siliceous rocks are characteristics for submarine hydrothermal exhalative origin as have been demonstrated in many locations worldwide. For example, in the Qinling area in the Shaanxi Province, sea-floor hydrothermal exhalations resulted in the formation of siliceous rocks with δ^{30}Si values of −0.3‰ to −0.5‰. Therefore, this explanation may also account for those samples within the siliceous and sulfide bands. This model is also in good agreement with the sulfur isotope data reported by Ding et al. (1988b).

In summary, the Si–O isotope data of siliceous rocks in the Dachang Sn-polymetallic ore deposit do not support a skarn or replacement-type origin (Chen et al., 1985; Fu et al., 1991) but are more compatible with a submarine hydrothermal exhalative origin (Han and Hutchinson, 1990, 1991).

5.4.5 W deposits

The Xihuashan tungsten deposit is a typical wolframite–quartz vein-type deposit which is located in the Dayu County, Jiangxi Province. In the mining area, the Yanshanian Xihuashan composite granite stock was emplaced into Cambrian and Neoproterozoic argillaceous–arenaceous rocks of lower degrees of metamorphism. Due to contact metamorphism of the country rocks caused by intrusion of the granite, hornfels facies and spotted slate occur within several hundreds of meters of contact zone.

EBSCOhost - printed on 2/10/2023 8:05 PM via . All use subject to https://www.ebsco.com/terms-of-use

There are six tungsten deposits occurring around the composite granitic stock. The most important is the Xihuashan wolframite deposit, and the second is the Dangping tungsten deposit. The Xihuashan deposit is located on the southwestern periphery of the stock. The deposit is composed of more than 600 wolframite-bearing quartz veins occurring on the top of the granitic stock. The veins are deeply dipping, and strike predominantly E-W, occasionally WNW or ENE. The veins are often parallel to each other, but sometimes, they may appear in form of an en echelon arrangement. The veins occur mainly in medium-grained biotite granite (γ_5^{2b}), rarely in porphyritic medium-grained biotite granite (γ_5^{2a}). The veins contain predominantly quartz, with minor amounts of other minerals such as K-feldspar, muscovite, calcite, dolomite, fluorite, topaz and beryl.

Silicon isotopic compositions of the granite, metamorphic rocks and quartz veins are analyzed, and the results are presented in Figure 5.49.

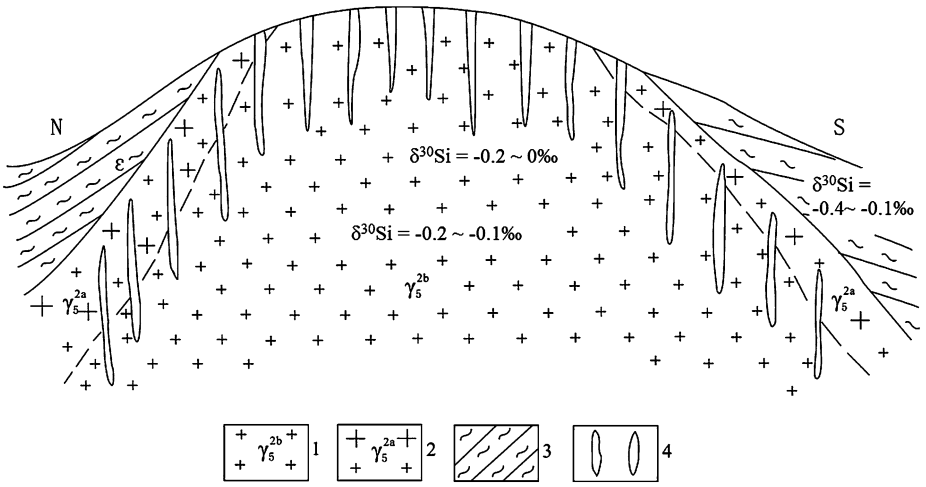

Figure 5.49: A schematic geologic section of the Xihuashan tungsten deposit with silicon isotope compositions of granite, host sedimentary rock and quartz vein. 1 – Median-grained biotite granite; 2 – Porphyritic median-grained biotite granite; 3 – Cambrian low-grade metamorphosed rocks (slate and siltstone); 4 – Wolframite-bearing quartz veins. After Ding et al. (1996).

The δ^{30}Si values of hornfels formed through metamorphism of Cambrian sedimentary rocks vary from −0.2‰ to −0.4‰. The biotite granites show a δ^{30}Si value of −0.1‰ to −0.2‰, which are also within the typical range of granite worldwide. The different minerals in granite show a δ^{30}Si decreasing trend from quartz, through feldspar, to mica, which conform to the regularity of silicon isotope fractionation under conditions of isotope exchange equilibrium. The quartz from the wolframite-bearing veins show a δ^{30}Si value of −0.2‰ to 0‰, which are similar to those of granite and the hornfels.

EBSCOhost - printed on 2/10/2023 8:05 PM via . All use subject to https://www.ebsco.com/terms-of-use

5.4.6 Au deposits

The Hemlo gold deposit in Ontario, Canada, is one of the most well-known giant gold deposits in the world. The ore-bearing rocks are metamorphosed intermediate-felsic volcanics and sedimentary rocks of the Archean Heron Bay Group. The orebodies in the Hemlo gold deposit occur at the contact zone between the crystalline tuffs and the metamorphosed sedimentary rocks. Near the orebody, the tuffs have suffered strong alteration, containing sericite, tourmaline, green chrome-bearing mica, barite and hematite. The mineralized rocks are represented by sericite schists, siliceous rocks and brecciated rocks.

The most common sulfide mineral is pyrite. Subordinate sulfide minerals include molybdenite, sphalerite, chalcopyrite and pyrrhotite. Minor sulfide minerals are stiblite, cinnabar, realgar, orpiment, boulangerite, jamesonite, bournonite, tetrahedrite and arsenopyrite, native antimony, arsenic and magnetite. The gangue minerals include quartz, barite, mica, feldspar, calcite, amphibole, chlorite, epidote, tremolite, silimanite, garnet, staurolite, rutile, tourmaline, sphene and graphite. Barite may occur either as disseminated or banded. The green mica contains vanadium, chromium and barium.

Ding and Thode (1991) carried out a detailed trace element geochemical study and found a good positive correlation between the contents of gold and those of molybdenum, antimony and arsenic (Figure 5.50). The $\delta^{18}O$ values of quartz and mica from the host rocks show a parallel trend of variation (Figure 5.50). The equilibrium temperatures calculated from oxygen isotope fractionation between quartz and magnetite are between 434–543°C, which are in good agreement with sulfur isotope temperatures of sulfide and barite (360–511°C), and are also consistent with high-grade metamorphism of amphibolite facies. This indicates that the isotope fractionation might have attained local equilibrium on a small scale during metamorphism, but still retains its original values on a large scale.

Thirteen samples of quartz and 11 samples of mica from 13 specimens are analyzed for their $\delta^{30}Si$ values, and the results are shown in Figure 5.50. Most of the data show a $\delta^{30}Si$ range from −0.3‰ to +0.2‰, which is close to the values of intermediate-felsic volcanics and clastic sediments. The majority of samples show a tendency of higher $\delta^{30}Si$ in quartz than in mica, although a few samples show the opposite. This relationship may suggest a general tendency towards isotopic equilibrium among coexisting minerals, but that complete equilibrium was not reached. It is interesting to note that the $\delta^{30}Si$ values are significantly higher in the samples with extremely high gold content (Figure 5.50). For example, samples HB2731, HB2743, HB2760 show $\delta^{30}Si$ values of +0.6‰, +0.5‰, +0.8‰, respectively, possibly reflecting specific conditions at the time of gold mineralization.

The rocks with high $\delta^{30}Si$ values often contain high Si content, indicating a strong silicification with Si addition into the rocks as compared with their overlying and underlying rocks. The Si may have two sources, one is in-situ from the host rocks

EBSCOhost - printed on 2/10/2023 8:05 PM via . All use subject to https://www.ebsco.com/terms-of-use

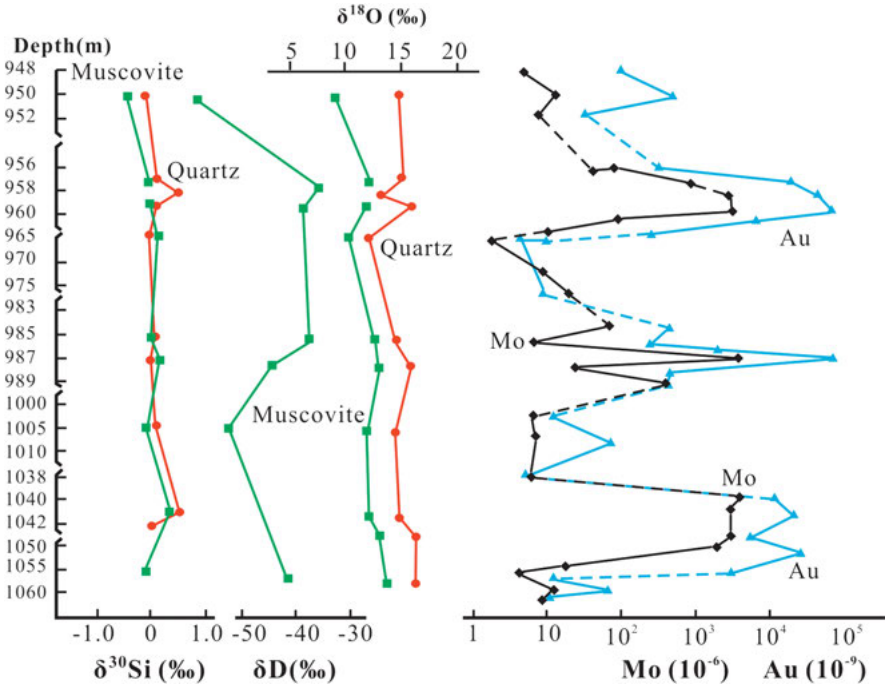

Figure 5.50: Diagram showing the variations of silicon, oxygen, hydrogen isotopes and the contents of Au, Mo, Sb, As along the depth in drill hole T220 in the Hemlo gold deposit. Revised from Ding et al. (1996).

of intermediate-felsic volcanics and sediments whose δ^{30}Si values are close to zero; the other source of Si may have an external origin whose δ^{30}Si values are >+0.8‰ or even higher. According to the available data, this Si may have come from two different sources: one is a remnant of dissolved Si in submarine hydrothermal water after its preliminary precipitation, while the other is dissolved Si in shallow seawater.

5.4.7 The Bayan Obo Nb-REE-Fe deposit, Inner Mongolian, China

5.4.7.1 Silicon isotope variation of the Bayan Obo deposit

The Bayan Obo Nb-REE-Fe deposit is a well-known giant deposit with the largest REE resource and the second largest niobium resource in the world, and also a large iron deposit in China. Although a great deal of geological and geochemical investigation has been carried out for this deposit, its origin is still in hot debate. The deposit is located in the northern margin of the North China Craton. The host rocks are the Mesoproterozoic Bayan Obo Group of mostly low grade metasedimentary rocks, which can be divided into nine units (H1 to H9). The H8 dolomite is the main host of the orebodies, and its origin is hotly debated. Some researchers consider it to be a mantle-derived

EBSCOhost - printed on 2/10/2023 8:05 PM via . All use subject to https://www.ebsco.com/terms-of-use

carbonatite (e.g., Bai and Yuan, 1985; Fan et al., 2016), while others suggest a sedimentary origin but with extensive hydrothermal metasomatism (e.g., Yang et al., 2009; Lai and Yang, 2013; Lai et al., 2016). The H8 dolomite occurs in both sides of the Kuangou Fault, but those in the north side are devoid of any mineralization.

There is also argument regarding the origin of the H9 potassic slate, which extend E-W for about 18 km and has maximum thickness near the main orebodies. Some consider it to be product of hydrothermal alteration (Institute of Geochemistry, 1988), while others think it is an intermediate-felsic volcanic tuff, which has gone through slight metamorphism (Bai et al., 1996) or potassic sedimentary-hydrothermal exhalite (Yuan et al., 1992).

Magmatic rocks outcropping in the mining area include gabbro and granitoids distributed in the eastern and southern parts of the mine. These magmatic rocks are intruded during the Hercynian (Ling et al., 2014).

The iron orebodies at Bayan Obo can be divided into three parts: i.e., the Main, East and West orebodies. The major iron ore minerals include dominantly magnetite and lesser hematite. The REE and Nb mineralization distributed more widespread and the entire H8 dolomite in southern part of the Kuangou Fault has been strongly mineralized. The major ore minerals include monazite, bastnaesite, huanghoite and various kinds of REE and Nb minerals.

Silicon and oxygen isotope analyses are obtained on a variety of siliceous rocks and minerals from the Bayan Obo mining area, and the results are presented in Figure 5.51 and Figure 5.52. In the H8 dolomite, trace amounts of quartz and biotite exist, and 5 samples of bulk dolomite rocks yield δ^{30}Si of −0.8‰ to −0.3‰, indicating the original substances of these siliceous minerals might be clay or tuffaceous. The H9 potassic slate is mainly composed of microcline. Due to the influence of late hydrothermal alteration, it often shows sodian-augitization, riebeckitization and bioti-

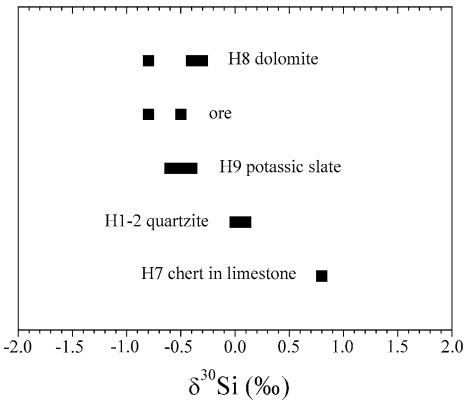

Figure 5.51: Comparison of δ^{30}Si values of rocks and ores from the Bayan Obo deposit. Revised from Ding et al. (1996).

EBSCOhost - printed on 2/10/2023 8:05 PM via . All use subject to https://www.ebsco.com/terms-of-use

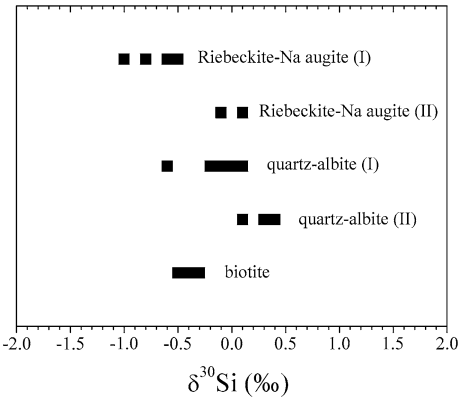

Figure 5.52: Comparison of δ^{30}Si values for different stages of mineralization in the Bayan Obo deposit. Revised from Ding et al. (1996).

tization. Occasionally, there are felsic and fluorite veins which cut across each other. The unaltered potassic slate exhibits δ^{30}Si values of –0.6‰ to –0.4‰, whereas the altered potassic slate exhibits δ^{30}Si values of –0.1‰ to 0‰. Therefore, it is likely those unaltered potassic slate might be derived from either volcanic tuffs or hydrothermal exhalative precipitates. The H1 quartz sandstone and H2 quartzite have δ^{30}Si values from 0‰ to +0.1‰, indicating a typical value for those clastic sediments. The chert band sample from the H7 limestone gave a δ^{30}Si value of +0.8‰, which is suggestive of shallow sea biochemical precipitates.

The Hercynian granitoids in the mining area show δ^{30}Si values from –0.2‰ to –0.1‰, which falls in the δ^{30}Si range of normal granites worldwide. The quartz, plagioclase, K-feldspar and biotite in a granite sample show δ^{30}Si values of +0.3‰, 0‰, –0.2‰ and –0.3‰, respectively. These data indicate an isotope equilibrium fractionation between different minerals in the granite. One diorite-gabbro sample shows a δ^{30}Si value of –0.4‰. The δ^{30}Si values of hornblendes from two gabbro-diorites are –0.4‰ and –0.3‰. An altered basic dike gave a δ^{30}Si value of +0.1‰.

In the iron ores, two massive magnetite ores show δ^{30}Si values of –0.8‰ and –0.5‰. One hematite ore shows a δ^{30}Si of –0.5‰. These data are similar to those data for H8 dolomite. One sample of secondary limonite shows a δ^{30}Si value of –1.8‰, possibly reflecting kinetic fractionation of silicon isotopes during precipitation in supergene conditions. Two sodian augite mineral samples from the Main and East orebodies have δ^{30}Si values of –1.0‰ and –0.8‰. A fine-grained sodian augite has a higher δ^{30}Si value of –0.1‰. The δ^{30}Si values of sodian augite from ores and veins are similar to each other, varying from –0.6 to –0.5‰. A sample of altered sodian augite near to the Dulahala carbonatite dike has a δ^{30}Si value of –0.1‰, and a riebeckite sample shows a δ^{30}Si value of +0.1‰, which are apparently different from those of the minerals from the Main and East orebodies.

EBSCOhost - printed on 2/10/2023 8:05 PM via . All use subject to https://www.ebsco.com/terms-of-use

Biotite samples from the hanging wall of the Main and East orebodies and the H9 potassic slate show δ^{30}Si values of −0.5‰ to −0.3‰. The albite and quartz from the later veins in the Main and East orebodies show δ^{30}Si values of −0.1‰ to +0.1‰ and −0.6‰ to −0.2‰, respectively. The δ^{30}Si values of the silicified veins from the alteration zone of the Dulahala carbonatite dike and the eastern contact zone carbonate veins range from +0.3‰ to +0.4‰, whereas a K-feldspar phenocryst from the altered rocks has a δ^{30}Si value of +0.1‰. The δ^{30}Si values of quartz and siliceous bands from the North Bayan Obo iron orebody in the north of the Kuangou Fault range from 0‰ to +0.1‰, whereas the δ^{30}Si values of the auriferous quartz veins from the Saiyinwusu gold deposit range from −0.5‰ to −0.2‰.

5.4.7.2 Source of Si in the ores deduced from the silicon isotope data

In order to examine the source of Si in the ores, a comparison of silicon isotopic composition of ores with those of a variety of rocks in the Bayan Obo mining area has been made (Figure 5.51). From this figure, it can be seen that the range of δ^{30}Si values for the ores is quite similar to that of H8 dolomite and H9 potassic slate, rather than those for clastic sediments (quartz sandstone and quartzite) and chert bands in limestone. They are also quite different to those of the Hercynian igneous rocks. It is therefore suggested that the ores and host rocks of H8 and H9 may share a similar Si source; it should not derive from the normal clastic sediments or the Hercynian magmatic–hydrothermal fluids. It is possible that the Si was introduced during seafloor hydrothermal exhalation.

A comparison of the silicon isotopic compositions of minerals in ores associated with the major mineralization with those of the later veins has been made in Figure 5.52. Results show that the δ^{30}Si values of minerals in ores from the major mineralization (I) are 0.5‰ to 1.0‰ lower than those of the equivalents from the later veins and alteration minerals (II), which indicate these two types of minerals should have different origin and they cannot be products of the same mineralization event. Therefore, the silicon isotope study also indicate that the Bayan Obo may have a multiple stage history of mineralization.

EBSCOhost - printed on 2/10/2023 8:05 PM via . All use subject to https://www.ebsco.com/terms-of-use

EBSCOhost - printed on 2/10/2023 8:05 PM via . All use subject to https://www.ebsco.com/terms-of-use

References

Abraham, K., Opfergelt, S., Fripiat, F., Cavagna, A. J., de Jong, J. T. M., Foley, S. F., Andre, L., Cardinal, D. (2008): δ^{30}Si and δ^{29}Si determinations on USGS BHVO-1 and BHVO-2 reference materials with a new configuration on a Nu plasma multicollector ICP-MS. Geostand. Geoanal. Res., 32, 193–202.

Abraham, K., Hofmann, A., Foley, S. F., Cardinal, D., Harris, C., Barth, M. G., André, L. (2011): Coupled silicon–oxygen isotope fractionation traces Archaean silicification. Earth Planet. Sci. Lett., 301(1–2), 222–230.

Adkins, J. F., McIntyre, K., Schrag, D. P. (2002): The salinity, temperature and δ^{18}O of the glacial deep ocean. Science, 298, 1769–1773.

Alexander, C. M. O. D. (1993): Presolar SiC in chondrites: how variable and how many sources? Geochim. Cosmochim. Acta, 57(12), 2869–2888.

Alexander, B. W., Bau, M., Andersson, P., Dulski, P. (2008): Continentally-derived solutes in shallow Archean seawater: rare earth element and Nd isotope evidence in iron formation from the 2.9 Ga Pongola Supergroup, South Africa. Geochim. Cosmochim. Acta, 72, 378–394.

Alexandre, A., Meaner, J. D., Colin, F., Koud, J. M. (1997): Plant impact on the biogeochemical cycle of silicon and related weathering processes. Geochim. Cosmochim. Acta, 61, 677–682.

Alleman, L. Y., Cardinal, D., Cocquyt, C., Plisnier, P. D., Descy, J. P., Kimirei, I., Sinyinza, D., André, L. (2005): Silicon isotopic fractionation in Lake Tanganyika and its main tributaries. J. Great Lakes Res., 31(4), 509–519.

Allenby, R. J. (1954): Determination of the isotopic ratios of silicon in rocks. Geochim. Cosmochim. Acta, 5(1), 40–48.

Allison, M., Kuehl, S., Martin, T., Hassan, A. (1998): Importance of flood-plain sedimentation for river sediment budgets and terrigenous input to the oceans: insights from the Brahmaputra–Jamuna river. Geology, 26, 175–178.

Allwood, A. C., Kamber, B. S., Walter, M. R., Burch, I. W., Kanik, I. (2010): Trace elements record depositional history of an early Archean stromatolitic carbonate platform. Chem. Geol., 270, 148–163.

Amari, S., Anders, E., Virag, A., Zinner, E. (1990): Interstellar graphite in meteorites. Nature, 345(6272), 238–240.

Amari, S., Hoppe, P., Zinner, E., Lewis, R. S. (1995a): Trace-element concentrations in single circumstellar silicon carbide grains from the Murchison meteorite. Meteoritics, 30(6), 679–693.

Amari, S., Zinner, E., Gallino, R. (2012): Presolar graphite from the Murchison meteorite: puzzles related to its origins. Annu. Meet. Meteorit. Soc., 44(7), 5322.

Amari, S., Zinner, E., Gallino, R. (2014): Abundances of presolar graphite and SiC from supernovae and AGB stars in the Murchison meteorite. AIP Conf. Proc., 1594(1), 307–312.

Amari, S., Zinner, E., Lewis, R. S. (1995b): Large ^{18}O excesses in circumstellar graphite grains from the Murchison meteorite: indication of a massive-star origin. Astrophys. J. Lett., 447(2), L147.

Amelin, Y., Grossman, L., Krot, A. N., Pestaj, T., Simon, S. B., Ulyanov, A. A. (2002): U-Pb age of refractory inclusions from the CV carbonaceous chondrites allende and efremovka. In Lunar and Planetary Science Conference.

Andersen, C. A. (1970): Analytic methods for the ion microprobe mass analyzer – II. Int. J. Mass Spectrom. Ion Phys., 3(6), 413–428.

Anderson, O. L., Isaak, D. G. (2002): Another look at the core density deficit of Earth's outer core. Phys. Earth Planet. Inter., 131(1), 19–27.

Anderson, S. P. (2005): Glaciers show direct linkage between erosion rate and chemical weathering fluxes. Geomorphology, 67, 147–157.

https://doi.org/10.1515/9783110402452-006

EBSCOhost - printed on 2/10/2023 8:05 PM via . All use subject to https://www.ebsco.com/terms-of-use

André, L., Cardinal, D., Alleman, L. Y., Moorbath, S. (2006): Silicon isotopes in ~3.8 Ga West Greenland rocks as clues to the Eoarchaean supracrustal Si cycle. Earth Planet. Sci. Lett., 245, 162–173.

Arehart, G. B., Eldridge, C. S., Chryssoulis, S. L., Kesler, S. E. (1993): Ion microprobe determination of sulfur isotope variations in iron sulfides from the Post/Betze sediment-hosted disseminated gold deposit, Nevada, USA. Geochim. Cosmochim. Acta, 57(7), 1505–1519.

Armytage, R., Georg, R., Savage, P., Williams, H., Halliday, A. (2011): Silicon isotopes in meteorites and planetary core formation. Geochim. Cosmochim. Acta, 75, 3662–3676.

Armytage, R. M. G., Georg, R. B., Williams, H. M., Halliday, A. N. (2012): Silicon isotopes in lunar rocks: implications for the Moon's formation and the early history of the Earth. Geochim. Cosmochim. Acta, 77, 504–514.

Aston, S. R. (1983): Silicon in igneous and metamorphic rocks. In S. R. Aston (Ed.) Silicon geochemistry and biogeochemistry.

Bai, G., Yuan, Z. X. (1985): Carbonatites and related mineral resources. In Bulletin of institute of mineral deposit, Chinese academy of geological sciences. Beijing: Geological Publishing House, pp. 18e34 (in Chinese).

Bai, G., Yuan, Z. X., Wu, C. Y., Zhang, Z. Q., Zheng, L. X. (1996): Demonstration on the geological features and genesis of the Bayan Obo Ore deposit. Beijing: Geological Publishing House (in Chinese with English abstract).

Bakale, D. K., Colby, B. N., Evans, C. A. (1975): High mass resolution ion microprobe mass spectrometry of complex matrices. Anal. Chem., 47(9), 1532–1537.

Balan, E., Saitta, A. M., Mauri, F., Calas, G. (2001): First-principles modeling of the infrared spectrum of kaolinite. Am. Mineral., 86(11–12), 1321–1330.

Balan, E., Saitta, A. M., Mauri, F., Lemaire, C., Guyot, F. (2002): First-principles calculation of the infrared spectrum of lizardite. Am. Mineral., 87(10), 1286–1290.

Balan, E., Lazzeri, M., Morin, G., Mauri, F. (2006): First-principles study of the OH-stretching modes of gibbsite. Am. Mineral., 91(1), 115–119.

Balan, E., Blanchard, M., Pinilla, C., Lazzeri, M. (2014): First-principles modeling of sulfate incorporation and $^{34}S/^{32}S$ isotopic fractionation in different calcium carbonates. Chem. Geol., 374, 84–91.

Barão, L., Clymans, W., Vandevenne, F., Meire, P., Conley, D. J., Struyf, E. (2014): Pedogenic and biogenic alkaline-extracted silicon distributions along a temperate land-use gradient. Eur. J. Soil Sci., 65, 693–705.

Barão, L., Vandevenne, F., Clymans, W., Frings, P., Ragueneau, O., Meire, P., Conley, D. J., Struyf, E. (2015): Alkaline-extractable silicon from land to ocean: a challenge for biogenic silicon determination. Limnol. Oceanogr., Methods, 13, 329–344.

Barber, D. A., Shone, G. T. (1966): The absorption of silica from aqueous solutions by plants. J. Exp. Bot., 17, 569–578.

Barnes, I. L., Moore, L. J., Machlan, L. A., Murphy, T. J., Shields, W. R. (1975): Absolute isotopic ratios and atomic weight of a reference sample of silicon. J. Res. Natl. Bur. Stand., 79A, 727–735.

Baroni, S., de Gironcoli, S., Corso, A. D. (2001): Phonons and related crystal properties from density-functional theory. Rev. Mod. Phys., 73, 515–562.

Basile-Doelsch, I., Meunier, J. D., Parron, C. (2005): Another continental pool in the terrestrial silicon cycle. Nature, 433, 399–402.

Bau, M., Dulski, P. (1996): Distribution of yttrium and rare earth elements in the Penge and Kuruman iron formations, Transvaal Supergroup, South Africa. Precambrian Res., 79, 37–55.

Beckwith, R. S., Reeve, R. (1963): Studies on soluble silica in soils. I. The sorption of silicic acid by soils and minerals. Aust. J. Soil Res., 1(2), 157–168.

EBSCOhost - printed on 2/10/2023 8:05 PM via . All use subject to https://www.ebsco.com/terms-of-use

Belshaw, N. S., Freedman, P. A., O'Nions, R. K., Frank, M., Guo, Y. (1998): A new variable dispersion double-focusing plasma mass spectrometer with performance illustrated for Pb isotopes. Int. J. Mass Spectrom., 181(1–3), 51–58.

Bern, C. R., Brzezinski, M. A., Beucher, C., Ziegler, K., Chadwick, O. A. (2010): Weathering, dust and biocycling effects on soil silicon isotope ratios. Geochim. Cosmochim. Acta, 74, 876–889.

Bernard, C. Y., Laruelle, G. G., Slomp, C. P., Heinze, C. (2010): Impact of changes in river fluxes of silica on the global marine silicon cycle: a model comparison. Biogeosciences, 7(2), 441–453.

Beucher, C. P., Brzezinski, M. A., Crosta, X. (2007): Silicic acid dynamics in the glacial sub-Antarctic: implications for the silicic acid leakage hypothesis. Glob. Biogeochem. Cycles 21(3).

Beucher, C. P., Brzezinski, M. A., Jones, J. L. (2008): Sources and biological fractionation of silicon isotopes in the eastern equatorial Pacific. Geochim. Cosmochim. Acta, 72(13), 3063–3073.

Beucher, C. P., Brzezinski, M. A., Jones, J. L. (2011): Mechanisms controlling silicon isotope distribution in the eastern equatorial Pacific. Geochim. Cosmochim. Acta, 75(15), 4286–4294.

Beusen, A. H. W., Bouwman, A. F., Dürr, H. H., Dekkers, A. L. M., Hartmann, J. (2009): Global patterns of dissolved silica export to the coastal zone: results from a spatially explicit global model. Glob. Biogeochem. Cycles, 23, GB0A02.

Bien, G., Contois, D., Thomas, W., (1958): The removal of soluble silica from fresh water entering the sea. Geochim. Cosmochim. Acta, 14, 35–54.

Bigeleisen, J., Wolfsberg, M. (1958): Theoretical and experimental aspects of isotope effects in chemical kinetics. Adv. Chem. Phys., 1, 15–76.

Billen, G., Lancelot, C., Meybeck, M., Mantoura, R., Martin, J.-M., Wollast, R. (1991): N, P and Si retention along the aquatic continuum from land to ocean. Ocean margin processes in global change (Vol. 1, pp. 19–44). John Wiley & Sons.

Birke, M., Reimann, C., Demetriades, A., Rauch, U., Lorenz, H., Harazim, B., Glatte, W. (2010): Determination of major and trace elements in European bottled mineral water – analytical methods. J. Geochem. Explor., 107, 217–226.

Black, D. C. (1972): On the origins of trapped helium, neon and argon isotopic variations in meteorites—II. Carbonaceous meteorites. Geochim. Cosmochim. Acta, 36(3), 377–394.

Black, D. C., Pepin, R. O. (1969): Trapped neon in meteorites- II. Earth Planet. Sci. Lett., 6(69), 395–-405.

Blake, R. E., Chang, S. J., Lepland, A. (2010): Phosphate oxygen isotopic evidence for a temperate and biologically active Archaean ocean. Nature, 464, 1029–1032.

Blanchard, M., Poitrasson, F., Meheut, M., Lazzeri, M., Mauri, F., Balan, E. (2009): Iron isotope fractionation between pyrite (FeS_2), hematite (Fe_2O_3) and siderite ($FeCO_3$): a first-principles density functional theory study. Geochim. Cosmochim. Acta, 73, 6565–6578.

Blanchard, M., Morin, G., Lazzeri, M., Balan, E. (2010): First-principles study of the structural and isotopic properties of Al- and OH-bearing hematite. Geochim. Cosmochim. Acta, 74(14), 3948–3962.

Blecker, S. W., McCulley, R. L., Chadwick, O. A., Kelly, E. F. (2006): Biologic cycling of silica across a grassland bioclimosequence. Glob. Biogeochem. Cycles, 20, GB3023.

Bouchez, J., von Blanckenburg, F., Schuessler, J. A. (2013): Modeling novel stable isotope ratios in the weathering zone. Am. J. Sci., 313, 267–308.

Bouvier, A., Wadhwa, M. (2010): The age of the Solar System redefined by the oldest Pb-Pb age of a meteoritic inclusion. Nat. Geosci., 3(9), 637–641.

Bouwman, A. F., Bierkens, M. F. P., Griffioen, J., Hefting, M. M., Middelburg, J. J., Middelkoop, H., Slomp, C. P. (2013): Nutrient dynamics, transfer and retention along the aquatic continuum from land to ocean: towards integration of ecological and biogeochemical models. Biogeosciences, 10, 1–22.

EBSCOhost - printed on 2/10/2023 8:05 PM via . All use subject to https://www.ebsco.com/terms-of-use

Boynton, W. V. (1975): Fractionation in the solar nebula: condensation of yttrium and the rare earth elements. Geochim. Cosmochim. Acta, 39(5), 569–584.

Brzezinski, M. A., Pride, C. J., Franck, V. M., Sigman, D. M., Sarmiento, J. L., Matsumoto, K., Gruber, N., Rau, G. H., Coale, K. H. (2002): A switch from $Si(OH)_4$ to NO_3^- depletion in the glacial Southern Ocean. Geophys. Res. Lett., 29.

Brzezinski, M. A., Jones, J. L., Beucher, C. P., Demarest, M. S., Berg, H. L. (2006): Automated determination of silicon isotope natural abundance by the acid decomposition of cesium hexafluosilicate. Anal. Chem., 78(17), 6109–6114.

Burbidge, E. M., Burbidge, G. R. (1957): Chemical composition of the BA II star HD 46407 and its bearing on element synthesis in stars. Astrophys. J., 126(2), 357.

Burnett, W. C., Aggarwal, P. K., Aureli, A., Bokuniewicz, H., Cable, J. E., Charette, M. A., Kontar, E., Krupa, S., Kulkarni, K. M., Loveless, A., Moore, W. S., Oberdorfer, J. A., Oliveira, J., Ozyurt, N., Povinec, P., Privitera, A. M. G., Rajar, R., Ramessur, R. T., Scholten, J., Stieglitz, T., Taniguchi, M., Turner, J. V. (2006): Quantifying submarine groundwater discharge in the coastal zone via multiple methods. Sci. Total Environ., 367, 498–543.

Cameron, A. (1959): Photobeta reactions in stellar interiors. Astrophys. J., 130(2), 452.

Cameron, A. G. W. (1962): The Formation of the Solar Nebula. In R. Jastrow, A. G. W. Cameron, (Eds.) Origin of the Solar System (pp. 339–342), New York: Academic Press.

Cameron, A. (1973): Porphyrius: the charioteer. Oxford: Clarendon Press.

Canfield, D. E., Erik, K., Bo, T. (2005): The silicon cycle. In Donald E. Canfield, E. Kristensen, B. Thamdrup (Eds.) Advances in marine biology, (Vol. 48, pp. 441–463). Academic Press.

Cao, Z., Frank, M., Dai, M., Grasse, P., Ehlert, C. (2012): Silicon isotope constraints on sources and utilization of silicic acid in the northern South China Sea. Geochim. Cosmochim. Acta, 97, 88–104.

Carbonnel, V., Vanderborght, J.-P., Lionard, M., Chou, L. (2013): Diatoms, silicic acid and biogenic silica dynamics along the salinity gradient of the Scheldt estuary (Belgium/The Netherlands). Biogeochemistry, 113, 657–682.

Cardinal, D., Alleman, L. Y., De Jong, J., Ziegler, K., Andre, L. (2003): Isotopic composition of silicon measured by multicollector plasma source mass spectrometry in dry plasma mode. J. Anal. At. Spectrom., 18(3), 213–218.

Cardinal, D., Alleman, L. Y., Dehairs, F., Savoye, N., Trull, T. W., André, L. (2005): Relevance of silicon isotopes to Si-nutrient utilization and Si-source assessment in Antarctic waters. Glob. Biogeochem. Cycles, 19, GB2007.

Cardinal, D., Savoye, N., Trull, T. W., Dehairs, F., Kopczynska, E. E., Fripiat, F., Tison, J.-L., André, L. (2007): Silicon isotopes in spring Southern Ocean diatoms: large zonal changes despite homogeneity among size fraction. Mar. Chem., 106(1–2), 46–62.

Cardinal, D., Gaillardet, J., Hughes, H. J., Opfergelt, S., André, L. (2010): Contrasting silicon isotope signatures in rivers from the Congo Basin and the specific behaviour of organic-rich waters. Geophys. Res. Lett., 37(12), 245–269.

Carey, J. C., Fulweiler, R. W. (2012): The terrestrial silica pump. PLoS ONE, 7, e52932.

Cary, L., Alexandre, A., Meunier, J. D., Boeglin, J. L., Braun, J. J. (2005): Contribution of phytoliths to the suspended load of biogenic silica in the Nyong basin rivers (Cameroon). Biogeochemistry, 74, 101–114.

Cavagna, A. J., Fripiat, F., Dehairs, F., Wolf-Gladrow, D., Cisewski, B., Savoye, N., Andrè, L., Cardinal, D. (2011): Silicon uptake and supply during a Southern Ocean iron fertilization experiment (EIFEX) tracked by Si isotopes. Limnol. Oceanogr., 56(1), 147–160.

Chakrabarti, R., Jacobsen, S. B. (2010): Silicon isotopes in the inner Solar System: implications for core formation, solar nebular processes and partial melting. Geochim. Cosmochim. Acta, 74(23), 6921–6933.

EBSCOhost - printed on 2/10/2023 8:05 PM via . All use subject to https://www.ebsco.com/terms-of-use

Chakrabarti, R., Knoll, A. H., Jacobsen, S. B., Fischer, W. W. (2012): Si isotope variability in Proterozoic cherts. Geochim. Cosmochim. Acta, 91, 187–201.
Chang, H. J., Chu, X. L., Feng, L. J. (2008): REE geochemistry of the Liuchapo chert in Anhua, Hunan. Geol. China, 35, 879–887 (in Chinese with English abstract).
Chemtob, S. M., Rossman, G. R., Young, E. D., Ziegler, K., Moynier, F., Eiler, J. M., Hurowitz, J. A. (2015): Silicon isotope systematics of acidic weathering of fresh basalts, Kilauea Volcano, Hawai'i. Geochim. Cosmochim. Acta, 169, 63–81.
Chen, D. Z., Wang, J. G., Qing, H. R., Yan, D. T., Li, R. W. (2009): Hydrothermal venting activities in the Early Cambrian South China: petrological, geochronological and stable isotopic constraints. Chem. Geol., 258, 168–181.
Chen, H. D., Zeng, Y. F. (1989): Depositional characteristics and genesis of Upper Devonian silicalites in Danchi basin, Guangxi. Minerals and Rocks, 9(4), 22–29.
Chen, J., Li, J., Tian, S., Kalugin, I., Darin, A., Xu, S. (2012): Silicon isotope composition of diatoms as a paleoenvironmental proxy in Lake Huguangyan, South China. J. Asian Earth Sci., 45, 268–274.
Chen, J. S., Wang, F. Y., He, D. W. (2006): Geochemistry of the Yellow River water. Earth Sci. Front., 13(1), 158–173.
Chen, X., Chafetz, H. S., Andreasen, R., Lapen, T. (2016): Silicon isotope compositions of euhedral authigenic quartz crystals: implications for abiotic fractionation at surface temperatures. Chem. Geol., 423, 61–73.
Chen, Y. C., Huang, M., Xu, C. (1985): Geological characteristics of the Dachang cassiterite sulphide deposits and metallogenetic series. Acta Geol. Sin., 59, 228–240 (in Chinese).
Chen, Y. C., Huang, M. Z., Xu, J., Hu, Y. Z., Tang, S. H., Li, Y. Q., Meng, L. K. (1993): Tin Deposits of Dachang. Beijing: Geological Publishing House (in Chinese with English abstract).
Chmeleff, J., Horn, I., Steinhoefel, G., von Blanckenburg, F. (2008): In situ determination of precise stable Si isotope ratios by UV-femtosecond laser ablation high-resolution multi-collector ICP-MS. Chem. Geol., 249, 155–166.
Chou, L., Wollast, R. (2006): Estuarine silicon dynamics. In D. Ittekkot, C. Unger, C. Humborg, N. Tac An (Eds.) The silicon cycle: human perturbations and impacts on aquatic systems. Scope. (pp. 93–120).
Chou, C. L., Baedecker, P. A., Wasson, J. T. (1976): Allende inclusions: volatile-element distribution and evidence for incomplete volatilization of presolar solids. Geochim. Cosmochim. Acta, 40(1), 85–94.
Christanty, L., Kimmins, J. P., Mailly, D. (1997): 'Without bamboo, the land dies': a conceptual model of the biogeochemical role of bamboo in an Indonesian agroforestry system. For. Ecol. Manag., 91(1), 83–91.
Chu, X. L., Zhang, T. G., Zhang, Q. R., Timothy, W., Lyons, T. W. (2007): Sulfur and carbon isotope records from 1700 to 800 Ma carbonates of the Jixian section, northern China: implications for secular isotope variations in Proterozoic seawater and relationships to global supercontinental events. Geochim. Cosmochim. Acta, 71, 4668–4692.
Clayton, R. N., Mayeda, T. K. (1963): The use of bromine pentafluoride in the extraction of oxygen from oxides and silicates for isotopic analysis. Geochim. Cosmochim. Acta, 27, 43–52.
Clayton, D. D. (1975): ^{22}Na, Ne–E, extinct radioactive anomalies and unsupported ^{40}Ar. Nature, 257(5521), 36–37.
Clayton, R. N., Mayeda, T. K., Hurd, J. M. (1974): Loss of oxygen, silicon, sulfur, and potassium from the lunar regolith. In Proceedings of the 5th lunar science conference (pp. 1801–1809).
Clayton, R. N., Mayeda, T. K., Epstein, S. (1978): Isotopic fractionation of silicon in Allende inclusions. In Lunar and planetary science conference proceedings.
Clayton, R. N., Mayeda, T. K. (1984): The oxygen isotope record in Murchison and other carbonaceous chondrites. Earth Planet. Sci. Lett., 67(2), 151–161.

EBSCOhost - printed on 2/10/2023 8:05 PM via . All use subject to https://www.ebsco.com/terms-of-use

Clayton, R. N., Hinton, R. W., Davis, A. M. (1988): Isotopic variations in the rock-forming elements in meteorites. Philos. Trans. R. Soc. Lond. Ser. A, Math. Phys. Sci., 325(1587), 483–501.

Clayton, D. D., Obradovich, M., Guha, M., Brown, L. E. (1991): Silicon and titanium isotopes in SiC from AGB stars (abstract). Lunar Planet. Sci., XXII, 221–222.

Clement, S. W., Compston, W. (1989): SIMS at high sensitivity and high mass resolution. In Proceeding of the 7th international conference on secondly ion mass-spectroscopy. J Wiley & Sons.

Clift, P., Giosan, L. (2014): Sediment fluxes and buffering in the post-glacial Indus Basin. Basin Res., 26, 369–386.

Cloud, P. (1976): Beginnings of biospheric evolution and their biogeochemical consequences. Paleobiology, 2(4), 351-387.

Clymans, W., Struyf, E., Govers, G., Vandevenne, F., Conley, D. J. (2011): Anthropogenic impact on biogenic Si pools in temperate soils. Biogeosciences, 8, 2281–2293.

Cocker, K. M., Evans, D. E., Hodson, M. J. (1998): The amelioration of aluminum toxicity by silicon in wheat (*Triticum aestivum* L.): malate exudation as evidence for an in planta mechanism. Planta, 204, 318–323.

Cockerton, H. E., Street-Perrott, F. A., Leng, M. J., Barker, P. A., Horstwood, M. S. A., Pashley, V. (2013): Stable-isotope (H, O, and Si) evidence for seasonal variations in hydrology and Si cycling from modern waters in the Nile Basin: implications for interpreting the Quaternary record. Quat. Sci. Rev., 66, 4–21.

Coggon, R. M., Teagle, D. A. H., Smith-Duque, C. E., Alt, J. C., Cooper, M. J. (2010): Reconstructing past seawater Mg/Ca and Sr/Ca from mid-ocean ridge flank calcium carbonate veins. Science, 327(5969), 1114–1117.

Colman, S. M., Bratton, J. F. (2003): Anthropogenically induced changes in sediment and biogenic silica fluxes in Chesapeake Bay. Geology, 31, 71–74.

Conley, D. J. (1997): Riverine contribution of biogenic silica to the oceanic silica budget. Limnol. Oceanogr., 42, 774–777.

Conley, D. J. (2002): Terrestrial ecosystems and the global biogeochemical silica cycle. Glob. Biogeochem. Cycles, 16, 1121.

Conley, D. J., Malone, T. C. (1992): The annual cycle of dissolved silicate in Chesapeake Bay: implications for the production and fate of phytoplankton biomass. Mar. Ecol. Prog. Ser., 81, 121–128.

Connelly, J. N., Bizzarro, M., Krot, A. N., Nordlund, Å., Wielandt, D., Ivanova, M. A. (2012): The absolute chronology and thermal processing of solids in the solar protoplanetary disk. Science, 338(6107), 651-655.

Coplen, T. B., Bohlke, J. K., De Bievre, P., Ding, T., Holden, N. E., Hopple, J. A., Krouse, H. R., Lamberty, A., Peiser, H. S., Revesz, K., Rieder, S. E., Rosman, K. J. R., Roth, E., Taylor, P. D. P., Vocke, R. D., Xiao, Y. K. (2002): Isotope-abundance variations of selected elements – (IUPAC technical report). Pure Appl. Chem., 74(10), 1987–2017.

Corgne, A., Keshav, S., Wood, B. J., McDonough, W. F., Fei, Y. (2008): Metal–silicate partitioning and constraints on core composition and oxygen fugacity during Earth accretion. Geochim. Cosmochim. Acta, 72(2), 574–589.

Cornelis, J. T., Delvaux, B., Cardinal, D., Andre, L., Ranger, J., Opfergelt, S. (2010): Tracing mechanisms controlling the release of dissolved silicon in forest soil solutions using Si isotopes and Ge/Si ratios. Geochim. Cosmochim. Acta, 74, 3913–3924.

Dai, A., Trenberth, K. E. (2002): Estimates of freshwater discharge from continents: latitudinal and seasonal variations. J. Hydrometeorol., 3, 660–687.

EBSCOhost - printed on 2/10/2023 8:05 PM via . All use subject to https://www.ebsco.com/terms-of-use

Dauphas, N., Poitrasson, F., Burkhardt, C., Kobayashi, H., Kurosawa, K. (2015): Planetary and meteoritic Mg/Si and variations inherited from solar nebula chemistry. Earth Planet. Sci. Lett., 427, 236–248.

Davis, A. M., Grossman, L. (1979): Condensation and fractionation of rare earths in the solar nebula. Geochim. Cosmochim. Acta, 43(10), 1611–1632.

Davis, A. M., Hashimoto, A., Clayton, R. N., Mayeda, T. K. (1990): Isotope mass fractionation during evaporation of Mg_2SiO_4. Nature, 347(6294), 655–658.

Davis, A. M., Macpherson, g. J., Clayton, R. N., Mayeda, T. K., Sylvester, P. J., Grossman, L., Hinton, R. W., Laughlin, J. R. (1991): Melt solidification and late-stage evaporation in the evolution of a FUN inclusion from the Vigarano C3V chondrite. Geochim. Cosmochim. Acta, 55(2), 621–637.

Davis, A. M., Hashimoto, A., Clayton, R. N., Mayeda, T. K. (1995): Isotopic and chemical fractionation during evaporation of $CaTiO_3$. Lunar Planet. Sci., 26, 317–318.

De Bièvre, P., Valkiers, S. (1994): Molar Mass Determinations for N A (Avogadro) Projects: Present Status and Potential for the Future. Metrologia, 31(3), 245–249.

De Bièvre, P., Valkiers, S., Pesier, H. S. (1994): New Values for Silicon Reference Materials, Certified for Isotope Abundance Ratios. J. Res. Natl. Inst. Stand. Technol., 99(2), 201–202.

De Bièvre, P., Lenaers, G., Murphy, T. J., Pieser, H. S., Valkiers, S. (1995): The chemical preparation and characterization of specimens for "absolute" measurements of the molar mass of an element, exemplified by silicon, for redeterminations of the Avogadro constant. Metrologia, 32, 103–110.

De La Rocha, C. L. (2002): Measurement of silicon stable isotope natural abundances via multicollector inductively coupled plasma mass spectrometry (MC-ICP-MS). Geochem. Geophys. Geosyst., 3(8), art. no. 1045.

De La Rocha, C. L. (2003): Silicon isotope fractionation by marine sponges and the reconstruction of the silicon isotope composition of ancient deep water. Geology, 31, 423–426.

De La Rocha, C. L. (2006): The biological pump. Oceans Mar. Geochem., 6, 83–112.

De La Rocha, C. L., Bickle, M. J. (2005): Sensitivity of silicon isotopes to whole-ocean changes in the silica cycle. Mar. Geol., 217, 267–282.

De La Rocha, C. L., Brzezinski, M. A., DeNiro, M. J. (1996): Purification, recovery, and laser-driven fluorination of silicon from dissolved and particulate silica for the measurement of natural stable isotope abundances. Anal. Chem., 68, 3746–3750.

De La Rocha, C. L., Brzezinski, M. A., DeNiro, M. J. (1997): Fractionation of silicon isotopes by marine diatoms during biogenic silica formation. Geochim. Cosmochim. Acta, 61(23), 5051–5056.

De La Rocha, C. L., Brzezinski, M. A., DeNiro, M. J., Shemesh, A. (1998): Silicon-isotope composition of diatoms as a indicator of past oceanic change. Nature, 395, 680–683.

De La Rocha, C. L., Brzezinski, M. A., DeNiro, M. J. (2000): A first look at the distribution of the stable isotopes of silicon in natural waters. Geochim. Cosmochim. Acta, 64(14), 2467–2477.

De La Rocha, C. L., Bescont, P., Croguennoc, A., Ponzevera, E. (2011): The silicon isotopic composition of surface waters in the Atlantic and Indian sectors of the Southern Ocean. Geochim. Cosmochim. Acta, 75(18), 5283–5295.

De Paoli, G. R., Pattison, D. R. M. (1995): Constraints on temperature–pressure conditions and fluid composition during metamorphism of the Sullivan orebody. Can. J. Earth Sci., 32(11), 1937–1949.

de Souza, G. F., Reynolds, B. C., Johnson, G. C., Bullister, J. L., Bourdon, B. (2012a): Silicon stable isotope distribution traces Southern Ocean export of Si to the eastern South Pacific thermocline. Biogeosciences, 9(11), 4199–4213.

de Souza, G. F., Reynolds, B. C., Rickli, J., Frank, M., Saito, M. A., Gerringa, L. J. A., Bourdon, B. (2012b). Southern Ocean control of silicon stable isotope distribution in the deep Atlantic Ocean. Glob. Biogeochem. Cycles, 26 (2).

EBSCOhost - printed on 2/10/2023 8:05 PM via . All use subject to https://www.ebsco.com/terms-of-use

de Souza, G. F., Slater, R. D., Dunne, J. P., Sarmiento, J. L. (2014): Deconvolving the controls on the deep ocean's silicon stable isotope distribution. Earth Planet. Sci. Lett., 398, 66–76.
Delstanche, S., Opfergelt, S., Cardinal, D., Elsass, F., André, L., Delvaux, B. (2009): Silicon isotopic fractionation during adsorption of aqueous monosilicic acid onto iron oxide. Geochim. Cosmochim. Acta, 73(4), 923–934.
Delvaux, B. (1989): Role of constituents of volcanic soils and their charge properties in the functioning of the banana agroecosystem in Cameroon. Fruits, 309–319.
Delvaux, C., Cardinal, D., Carbonnel, V., Chou, L., Hughes, H. J., André, L. (2013): Controls on riverine δ^{30}Si signatures in a temperate watershed under high anthropogenic pressure (Scheldt – Belgium). J. Mar. Syst., 128, 40–51.
Demarest, M. S., Brzezinski, M. A., Beucher, C. P. (2009): Fractionation of silicon isotopes during biogenic silica dissolution. Geochim. Cosmochim. Acta, 73(19), 5572–5583.
DeMaster, D. J. (1981): The supply and accumulation of silica in the marine-environment. Geochim. Cosmochim. Acta, 45, 1715–1732.
DeMaster, D. J. (2002): The accumulation and cycling of biogenic silica in the Southern Ocean: revisiting the marine silica budget. Deep-Sea Res., Part 2, Top. Stud. Oceanogr., 49, 3155–3167.
Derry, L. A., Jacobsen, S. B. (1990): The chemical evolution of Precambrian seawater: evidence from REEs in banded iron formation. Geochim. Cosmochim. Acta, 54, 2965–2977.
Derry, L. A., Kurtz, A. C., Ziegler, K., Chadwick, O. A. (2005): Biological control of terrestrial silica cycling and export fluxes to watersheds. Nature, 433, 728–731.
Desplanques, V., Cary, L., Mouret, J.-C., Trolard, F., Bourrié, G., Grauby, O., Meunier, J.-D. (2006): Silicon transfers in a rice field in Camargue (France). J. Geochem. Explor., 88(1–3), 190–193.
Ding, T. (2004): Analytical methods for silicon isotope determinations. In P. A. De Groot (Ed.) Handbook of stable isotope analytical techniques (Vol. 1, pp. 523–537) Elsevier.
Ding, T. P., Rees, C. E. (1984): The sulfur isotope systematics of the Taolin Pb-Zn ore deposit, China. Geochem. Cosmochim Acta., 48, 2381–2392.
Ding, T. P., Jiang, S. Y. (2000): Stable isotope study of the Langshan polymetallic mineral district, Inner Mongolia, China. Resour. Geol., 50, 25–38.
Ding, T. P., Thode, H. G. (1991): Stable isotope and trace element studies on the Hemolo gold deposit, Ontario, Canada. Bulletin Chinese Academy of Geol Sci., 24, 47–61.
Ding, T. P., Yonge, C., Schwarcz, H. P., Peng, Z. C. (1986): Oxygen, hydrogen, and lead isotope studies of the Taolin lead-zinc ore deposit, China. Econ. Geol., 81(2), 421–429.
Ding, T., Wan, D., Li, J., Jiang, S., Song, H., Li, Y., Liu, Z. (1988a): The analytic method of silicon isotopes and its geological application. Monogr. Ser. Miner. Depos., 7(4), 90–95 (in Chinese).
Ding, T. P., Peng, Z. C., Li, H., Li, Y. H. (1988b): Stable isotope study on several typical deposits in the South Range Area, China. Beijing: Beijing Publishing House on Science and Technology (in Chinese with English abstract).
Ding, T. P., Jiang, S. Y., Wan, D. F., Li, Y. H., Li, J., Liu, Z. (1996): Silicon isotope geochemistry. Beijing: Geological Publishing House.
Ding, T. P., Wan, D. F., Wang, C. Y., Zhang, F. (2003): Large and systematic silicon isotope fractionation discovered in single sticks of bamboo. Geochim. Cosmochim. Acta, 67, A79.
Ding, T. P., Wan, D., Wang, C., Zhang, F. (2004): Silicon isotope compositions of dissolved silicon and suspended matter in the Yangtze River, China. Geochim. Cosmochim. Acta, 68, 205–216.
Ding, T. P., Ma, G. R., Shui, M. X., Wan, D. F., Li, R. H. (2005a): Silicon isotope study on rice plants from the Zhejiang province, China. Chem. Geol., 218, 41–50.
Ding, T., Wan, D., Bai, R., Zhang, Z., Shen, Y., Meng, R. (2005b): Silicon isotope abundance ratios and atomic weights of NBS-28 and other reference materials. Geochim. Cosmochim. Acta, 69(23), 5487–5494.

EBSCOhost - printed on 2/10/2023 8:05 PM via . All use subject to https://www.ebsco.com/terms-of-use

Ding, T. P., Zhou, J. X., Wan, D. F., Chen, Z. Y., Wang, C. Y., Zhang, F. (2008a): Silicon isotope fractionation in bamboo and its significance to the biogeochemical cycle of silicon. Geochim. Cosmochim. Acta, 72(5), 1381–1395.

Ding, T. P., Tian, S. H., Sun, L., Wu, L. H., Zhou, J. X., Chen, Z. Y. (2008b). Silicon isotope fractionation between rice plants and nutrient solution and its significance to the study of the silicon cycle. Geochim. Cosmochim. Acta, 72(23), 5600–5615.

Ding, T. P., Gao, J. F., Tian, S. H., Wang, H. B., Li, M. (2011): Silicon isotopic composition of dissolved silicon and suspended particulate matter in the Yellow River, China, with implications for the global silicon cycle. Geochim. Cosmochim. Acta, 75(21), 6672–6689.

Ding, T., Gao, J., Tian, S., Shi, G., Chen, F., Wang, C., Luo, X., Han, D. (2014): Chemical and isotopic characteristics of the water and suspended particulate materials in the Yangtze river and their geological and environmental implications. Acta Geol. Sin. (Engl. Ed.), 88(1), 276–360.

Ding, T., Gao, J., Tian, S., Wang, H., Li, M., Wang, C., Luo, X., Han, D. (2016): Chemical and isotopic characteristics of the water and suspended particulate materials in the Yellow river and their geological and environmental implications. Acta Geol. Sin. (Engl. Ed.), 90(1), 285–351.

Ding, T. P., Gao, J. F., Tian, S. H., Fan, C. F., Zhao, Y., Wan, D. F., Zhou, J. X. (2017): The δ^{30}Si peak value discovered in middle Proterozoic chert and its implication for environmental variations in the ancient ocean. Sci. Rep., 7, 44000.

Doering, K., Ehlert, C., Grasse, P., Crosta, X., Fleury, S., Frank, M., Schneider, R. (2016): Differences between mono-generic and mixed diatom silicon isotope compositions trace present and past nutrient utilisation off Peru. Geochim. Cosmochim. Acta, 177, 30–47.

Douthitt, C. B. (1982): The geochemistry of the stable isotopes of silicon. Geochim. Cosmochim. Acta, 46, 1449–1458.

Dove, M. T., Winkler, B., Leslie, M., Harris, M. J., Salje, E. K. H. (1992): A new interatomic potential model for calcite – applications to lattice-dynamics studies, phase-transition, and isotope fractionation. Am. Mineral., 77, 244–250.

Du, L. L., Yang, C. H., Ren, L. D., Wan, Y. S., Wu, J. S. (2009): Petrology, geochemistry and petrogenesis of the metabasalts of the Hutuo Group, Wutai Mountains, Shanxi, China. Geol. Bull. China, 28(7), 867–876 (in Chinese with English abstract).

Duce, R. A., Liss, P. S., Merrill, J. T., Atlas, E. L., Buat-Menard, P., Hicks, B. B., Miller, J. M., Prospero, J. M., Arimoto, R., Church, T. M., Ellis, W., Galloway, J. N., Hansen, L. Jickells, T. D., Knap, A. H., Reinhardt, K. H., Schneider, B., Soudine, A., Tokos, J. J., Tsunogai, S., Wollast, R., Zhou, M. (1991): The atmospheric input of trace species to the world ocean. Glob. Biogeochem. Cycles, 5, 193–259.

Ducher, M., Blanchard, M., Balan, E. (2016): Equilibrium zinc isotope fractionation in Zn-bearing minerals from first-principles calculations. Chem. Geol., 443, 87–96.

Dupré, B., Dessert, C., Oliva, P., Goddéris, Y., Viers, J., François, L., Millot, R., Gaillardet, J. (2003): Rivers, chemical weathering and Earth's climate. C. R. Géosci., 335, 1141–1160.

Dupuis, R., Benoit, M., Nardin, E., Méheut, M. (2015): Fractionation of silicon isotopes in liquids: the importance of configurational disorder. Chem. Geol., 396, 239–254.

Dürr, H. H., Laruelle, G. G., van Kempen, C. M., Slomp, C. P., Meybeck, M., Middelkoop, H. (2011a). Worldwide typology of nearshore coastal systems: defining the estuarine filter of river inputs to the oceans. Estuar. Coast., 34, 441–458.

Dürr, H. H., Meybeck, M., Hartmann, J., Laruelle, G. G., Roubeix, V. (2011b): Global spatial distribution of natural riverine silica inputs to the coastal zone. Biogeosciences, 8, 597–620.

Egan, K. E., Rickaby, R. E. M., Leng, M. J., Hendry, K. R., Hermoso, M., Sloane, H. J., Bostock, H., Halliday, A. N. (2012): Diatom silicon isotopes as a proxy for silicic acid utilisation: a Southern Ocean core top calibration. Geochim. Cosmochim. Acta, 96, 174–192.

EBSCOhost - printed on 2/10/2023 8:05 PM via . All use subject to https://www.ebsco.com/terms-of-use

Ehlert, C., Grasse, P., Mollier-Vogel, E., Böschen, T., Franz, J., de Souza, G. F., Reynolds, B. C., Stramma, L., Frank, M. (2012): Factors controlling the silicon isotope distribution in waters and surface sediments of the Peruvian coastal upwelling. Geochim. Cosmochim. Acta, 99, 128–145.

Ehlert, C., Doering, K., Wallmann, K., Scholz, F., Sommer, S., Grasse, P., Geilert, S., Frank, M. (2016a): Stable silicon isotope signatures of marine pore waters – Biogenic opal dissolution versus authigenic clay mineral formation. Geochim. Cosmochim. Acta, 191, 102–117.

Ehlert, C., Reckhardt, A., Greskowiak, J., Liguori, B. T. P., Böning, P., Paffrath, R., Brumsack, H.-J., Pahnke, K. (2016b): Transformation of silicon in a sandy beach ecosystem: insights from stable silicon isotopes from fresh and saline groundwaters. Chem. Geol., 440, 207–218.

Elderfield, H., Schultz, A. (1996): Mid-ocean ridge hydrothermal fluxes and the chemical composition of the ocean. Annu. Rev. Earth Planet. Sci., 24(1), 191–224.

Ellwood, M. J., Wille, M., Maher, W. (2010): Glacial silicic acid concentrations in the Southern Ocean. Science, 330, 1088–1091.

Engelstaedter, S., Tegen, I., Washington, R. (2006): North African dust emissions and transport. Earth-Sci. Rev., 79, 73–100.

Engström, E. (2009): Fractionation of the stable silicon isotopes studied using MC-ICP-MS. department of chemical engineering and geosciences. Luleå: Luleå University of Technology.

Engström, E., Rodushkin, I., Baxter, D. C., Öhlander, B. (2006): Chromatographic purification for the determination of dissolved silicon isotopic compositions in natural waters by high-resolution multicollector inductively coupled plasma mass spectrometry. Anal. Chem., 78(1), 250–257.

Engström, E., Rodushkin, I., Ohlander, B., Ingri, J., Baxter, D. C. (2008): Silicon isotopic composition of boreal forest vegetation in northern Sweden. Chem. Geol., 257, 250–259.

Engström, E., Rodushkin, I., Ingri, J., Baxter, D. C., Ecke, F., Osterlund, H., Ohlander, B. (2010): Temporal isotopic variations of dissolved silicon in a pristine boreal river. Chem. Geol., 271, 142–152.

Epstein, E. (1994): The anomaly of silicon in plant biology. Proc. Natl. Acad. Sci. USA, 91, 11–17.

Epstein, E. (1999): Silicon. Annu. Rev. Plant Physiol. Plant Mol. Biol., 50, 641–664.

Epstein, S., Taylor, H. P. Jr. (1970): $^{18}O/^{16}O$, $^{30}Si/^{28}Si$, D/H, and $^{13}C/^{12}C$ studies of lunar rocks and minerals. Science, 167(3918), 533–535.

Epstein, S., Taylor, H. P. Jr. (1971): O^{18}/O^{16}, Si^{30}/Si^{28}, D/H and C^{13}/C^{12} ratios in lunar samples. In Proceedings of the 2nd lunar science conference.

Epstein, S., Taylor, H. P. Jr. (1973): The isotopic composition and concentration of water, hydrogen, and carbon in some Apollo 15 and 16 soils and in the Apollo 17 orange soil. Opt. Lett., 27(9), 45–46.

Ethier, V. G., Campbell, F. A. (1977): Tourmaline concentrations in Proterozoic sediments of the southern Cordillera of Canada and their economic significance. Can. J. Earth Sci., 14(14), 2348–2363.

Fan, D., Zhang, T., Ye, J., Pašava, J., Kribek, B., Dobes, P., Varrin, I., Zak, K. (2004): Geochemistry and origin of tin–polymetallic sulfide deposits hosted by the Devonian black shale series near Dachang, Guangxi, China. Ore Geol. Rev., 24(1), 103–120.

Fan, H., Wen, H., Zhu, X., Hu, R., Tian, S. (2013): Hydrothermal activity during Ediacaran–Cambrian transition: silicon isotopic evidence. Precambrian Res., 224, 23–35.

Fan, H. R., Yang, K. F., Hu, F. F., Liu, S., Wang, K. Y. (2016): The giant Bayan Obo REE-Nb-Fe deposit, China: Controversy and ore genesis. Geosci. Front., 7(3), 335–344.

Farmer, V. C., Delbos, E., Miller, J. D. (2005): The role of phytolith formation and dissolution in controlling concentrations of silica in soil solutions and streams. Geoderma, 127, 71–79.

EBSCOhost - printed on 2/10/2023 8:05 PM via . All use subject to https://www.ebsco.com/terms-of-use

Feng, C. Q., Qin, T., Huang, S. C., Wu, Z. Q., Huang, F. (2014): First-principles investigations of equilibrium calcium isotope fractionation between clinopyroxene and Ca-doped orthopyroxene. Geochim. Cosmochim. Acta, 143, 132–142.

Fitoussi, C., Bourdon, B. (2012): Silicon isotope evidence against an enstatite chondrite Earth. Science, 335, 1477–1480.

Fitoussi, C., Bourdon, B., Kleine, T., Oberli, F., Reynolds, B. C. (2009): Si isotope systematics of meteorites and terrestrial peridotites: implications for Mg/Si fractionation in the solar nebula and for Si in the Earth's core. Earth Planet. Sci. Lett., 287(1–2), 77–85.

Fontorbe, G., De La Rocha, C. L., Chapman, H. J., Bickle, M. J. (2013): The silicon isotopic composition of the Ganges and its tributaries. Earth Planet. Sci. Lett., 381, 21–30.

Fontorbe, G., Frings, P. J., De La Rocha, C. L., Hendry, K. R., Conley, D. (2016): A silicon depleted North Atlantic since the Palaeogene: evidence from sponge and radiolarian silicon isotopes. Earth Planet. Sci. Lett., 453, 67–77.

Fraysse, F., Pokrovsky, O. S., Schott, J., Meunier, J. D. (2006a): Surface properties, solubility and dissolution kinetics of bamboo phytoliths. Geochim. Cosmochim. Acta, 70(8), 1939–1951.

Fraysse, F., Cantais, F., Pokrovsky, O. S., Schott, J., Meunier, J. D. (2006b): Aqueous reactivity of phytoliths and plant litter: physico-chemical constraints on terrestrial biogeochemical cycle of silicon. J. Geochem. Explor., 88(1–3), 202–205.

Frings, P. J. (2014): Integrating fluvial processes into the global Si cycle. Department of geology. Lund: Lund University (161 pp.).

Frings, P., Clymans, W., Jeppesen, E., Lauridsen, T., Struyf, E., Conley, D. (2014a): Lack of steady-state in the global biogeochemical Si cycle: emerging evidence from lake Si sequestration. Biogeochemistry, 117, 255–277.

Frings, P. J., Clymans, W., Conley, D. J. (2014b): Amorphous silica transport in the Ganges Basin: implications for Si delivery to the oceans. Proc. Earth Planet. Sci., 10, 271–274.

Frings, P. J., De La Rocha, C., Struyf, E., van Pelt, D., Schoelynck, J., Hudson, M. M., Gondwe, M. J., Wolski, P., Mosimane, K., Gray, W., Schaller, J., Conley, D. J. (2014c): Tracing silicon cycling in the Okavango Delta, a sub-tropical flood-pulse wetland using silicon isotopes. Geochim. Cosmochim. Acta, 142, 132–148.

Frings, P. J., Clymans, W., Fontorbe, G., Gray, W., Chakrapani, G. J., Conley, D. J., De La Rocha, C. (2015): Silicate weathering in the Ganges alluvial plain. Earth Planet. Sci. Lett., 427, 136–148.

Frings, P. J., Clymans, W., Fontorbe, G., De La Rocha, C. L., Conley, D. J. (2016): The continental Si cycle and its impact on the ocean Si isotope budget. Chem. Geol., 425, 12–36.

Fripiat, F., Cavagna, A.-J., Savoye, N., Dehairs, F., André, L., Cardinal, D. (2011a): Isotopic constraints on the Si-biogeochemical cycle of the Antarctic Zone in the Kerguelen area (KEOPS). Mar. Chem., 123(1–4), 11–22.

Fripiat, F., Cavagna, A. J., Dehairs, F., Speich, S., André, L., Cardinal, D. (2011b): Silicon pool dynamics and biogenic silica export in the Southern Ocean inferred from Si-isotopes. Ocean Sci., 7(5), 533–547.

Fripiat, F., Cavagna, A.-J., Dehairs, F., de Brauwere, A., André, L., Cardinal, D. (2012): Processes controlling the Si-isotopic composition in the Southern Ocean and application for paleoceanography. Biogeosciences, 9(7), 2443–2457.

Fu, F. F., Akagi, T., Shinotsuka, K. (1998): Distribution pattern of rare earth elements in fern: implication for intake of fresh silicate particles by plants. Biol. Trace Elem. Res., 64, 13–26.

Fu, F. F., Akagi, T., Yabuki, S., Iwaki, M., Ogura, N. (2000): Distribution of rare earth elements in seaweed: implication for two different sources of rare earth elements and silicon in seaweed. J. Phycol., 36, 62–70.

EBSCOhost - printed on 2/10/2023 8:05 PM via . All use subject to https://www.ebsco.com/terms-of-use

Fu, F. F., Akagi, T., Yabuki, S., Iwaki, M. (2001): The variation of REE (rare earth elements) pattern in soil-grown plants: a new proxy for the source of rare earth elements and silicon in plants. Plant Soil, 235, 53–64.

Fu, F. F., Akagi, T., Yabuki, S. (2002): Origin of silica particles found in the cortex of Matteuccia roots. Soil Sci. Soc. Am. J., 66, 1265–1271.

Fu, M., Changkakoti, A., Krouse, H. R., Gray, J., Kwak, T. A. P. (1991): An oxygen, hydrogen, sulfur, and carbon isotope study of carbonate-replacement (skarn) tin deposits of the Dachang tin field, China. Econ. Geol., 86(8), 1683–1703.

Gao, J. F., Ding, T. P. (2009): Laser microprobe silicon isotope analysis method and geology applications. Geochim. Cosmochim. Acta, Suppl., 73, 413.

Gao, J., Ding, T., Tian, S. (2006): Silicon isotope compositions of dissolved silicon and suspended matter in the Yellow river, China. Geochim. Cosmochim. Acta, 70(18S), A192.

Gao, J., Yang, R., Chen, J., Zheng, L., Cheng, W., Wei, H. (2017): Multiple proxies indicating methane seepage as the origin of Devonian large barite deposit in Zhenning-Ziyun, Guizhou, SW China. Ore Geol. Rev., 80, 18–26.

Garcia, H. E., Locarnini, R. A., Boyer, T. P., Antonov, J. I., Zweng, M. M., Baranova, O. K., Johnson, D. R. (2009): World Ocean Atlas 2009, Volume 4: Nutrients (phosphate, nitrate, silicate). In S. Levitus (Ed.) NOAA Atlas NESDIS 71. Washington, D.C: U.S. Government Printing Office (398 p.).

Geilert, S., Vroon, P. Z., Roerdink, D. L., Van Cappellen, P., van Bergen, M. J. (2014a): Silicon isotope fractionation during abiotic silica precipitation at low temperatures: inferences from flow-through experiments. Geochim. Cosmochim. Acta, 142, 95–114.

Geilert, S., Vroon, P. Z., van Bergen, M. J. (2014b): Silicon isotopes and trace elements in chert record early Archean basin evolution. Chem. Geol., 386, 133–142.

Geilert, S., Vroon, P. Z., Keller, N. S., Gudbrandsson, S., Stefánsson, A., van Bergen, M. J. (2015): Silicon isotope fractionation during silica precipitation from hot-spring waters: evidence from the Geysir geothermal field, Iceland. Geochim. Cosmochim. Acta, 164, 403–427.

Georg, R. B. (2006). Geochemistry of stable silicon isotopes measured by High-Resolution Multi-Collector Inductively-Coupled Plasma Mass Spectrometry (HR-MC-ICP-MS). Switzerland: ETH Zurich.

Georg, R. B., Reynolds, B. C., Frank, M., Halliday, A. N. (2006b): Mechanisms controlling the silicon isotopic compositions of river waters. Earth Planet. Sci. Lett., 249, 290–306.

Georg, R. B., Reynolds, B. C., Frank, M., Halliday, A. N. (2006a): New sample preparation techniques for the determination of Si isotopic compositions using MC-ICPMS. Chem. Geol., 235, 95–104.

Georg, R. B., Halliday, A. N., Schauble, E. A., Reynolds, B. C. (2007a): Silicon in the Earth's core. Nature, 447, 1102–1106.

Georg, R. B., Reynolds, B. C., West, A. J., Burton, K. W., Halliday, A. N. (2007b): Silicon isotope variations accompanying basalt weathering in Iceland. Earth Planet. Sci. Lett., 261, 476–490.

Georg, R. B., West, A. J., Basu, A. R., Halliday, A. N. (2009a): Silicon fluxes and isotope composition of direct groundwater discharge into the Bay of Bengal and the effect on the global ocean silicon isotope budget. Earth Planet. Sci. Lett., 283, 67–74.

Georg, R. B., Zhu, C., Reynolds, B. C., Halliday, A. N. (2009b): Stable silicon isotopes of groundwater, feldspars, and clay coatings in the Navajo Sandstone aquifer, Black Mesa, Arizona, USA. Geochim. Cosmochim. Acta, 73, 2229–2241.

Gibbs, M. T., Kump, L. R. (1994): Global chemical erosion during the last glacial maximum and the present – sensitivity to changes in lithology and hydrology. Paleoceanography, 9, 529–543.

Giletti, B. J., Semet, M. P., Yund, R. A. (1978): Studies in diffusion – III. Oxygen in feldspars: an ion microprobe determination. Geochim. Cosmochim. Acta, 42(1), 45–57.

EBSCOhost - printed on 2/10/2023 8:05 PM via . All use subject to https://www.ebsco.com/terms-of-use

Girard, J.-P., Munz, I. A., Johansen, H., Hill, S., Canham, A. (2001): Conditions and timing of quartz cementation in Brent reservoirs, Hild Field, North Sea: constraints from fluid inclusions and SIMS oxygen isotope microanalysis. Chem. Geol., 176(1–4), 73–92.

Gislason, S. R., Oelkers, E. H., Snorrason, Á. (2006): Role of river-suspended material in the global carbon cycle. Geology, 34, 49–52.

Gonze, X., Charlier, J., Allan, D. C., Teter, M. P. (1994): Interatomic force constants from first principles: the case of alpha-quartz. Phys. Rev. B, Condens. Matter, 50(17), 13035–13038.

Grant, F. S. (1954): The geological significance of variations in the abundances of the isotopes of silicon in rocks. Geochim. Cosmochim. Acta, 5(5), 225–242.

Grasse, P., Ehlert, C., Frank, M. (2013): The influence of water mass mixing on the dissolved Si isotope composition in the Eastern Equatorial Pacific. Earth Planet. Sci. Lett., 380, 60–71.

Griffiths, J. D., Barker, S., Hendry, K. R., Thornalley, D. J. R., van de Flierdt, T., Hall, I. R., Anderson, R. F. (2013): Evidence of silicic acid leakage to the tropical Atlantic via Antarctic Intermediate Water during Marine Isotope Stage 4. Paleoceanography, 28(2), 307–318.

Gross, G. A. (1980): A classification of iron formations based on depositional environments. Can. Mineral., 18(1), 215–222.

Grossman, L. (1972): Condensation in the primitive solar nebula. Geochim. Cosmochim. Acta, 36(5), 597–619.

Grossman, L. (1980): Refractory inclusions in the Allende meteorite. Annu. Rev. Earth Planet. Sci., 8(1), 559–608.

Grossman, L., Ebel, D. S., Simon, S. B., Davis, A. M., Richter, F. M., Parsad, N. M. (2000): Major element chemical and isotopic compositions of refractory inclusions in C3 chondrites: the separate roles of condensation and evaporation. Geochim. Cosmochim. Acta, 64(16), 2879–2894.

Grossman, L., Simon, S. B., Rai, V. K., Thiemens, M. H., Hutcheon, I. D., Williams, R. W., Galy, A., Ding, T., Fedkin, A. V., Clayton, R. N., Mayeda, T. K. (2008): Primordial compositions of refractory inclusions. Geochim. Cosmochim. Acta, 72(12), 3001–3021.

Grozeva, N. G., Klein, F., Seewald, J. S., Sylva, S. P. (2017): Experimental study of carbonate formation in oceanic peridotite. Geochim. Cosmochim. Acta, 199, 264–286.

Guerzoni, S., Molinaroli, E., Rossini, P., Rampazzo, G., Quarantotto, G., De Falco, G., Cristini, S. (1999): Role of desert aerosol in metal fluxes in the Mediterranean area. Chemosphere, 39, 229–246.

Guo, Q. J., Shields, G. A., Liu, C. Q., Strauss, H., Zhu, M. Y., Pi, D. H., Goldberg, T., Yang, L. X. (2007): Trace element chemostratigraphy of two Ediacaran–Cambrian successions in South China: implications for organosedimentary metal enrichment and silicification in the early Cambrian. Palaeogeogr. Palaeoclimatol. Palaeoecol., 254, 194–216.

Hamilton, J. M., Bishop, D. T., Morris, H. C., Owens, O. E. (1982): Geology of the Sullivan orebody, Kimberley, B.C., Canada. Spec. Pap., Geol. Assoc. Can., 25, 597–665.

Han, F., Hutchinson, R. W. (1990): Evidence for exhalative origin of the Dachang tin-polymetallic sulfide deposits-their geological and geochemical characteristics. Monogr. Ser. Miner. Depos., 9, 309–324 (in Chinese).

Han, F., Hutchinson, R. W. (1991): Synthetic studies on the origin of the Dachang tin-polymetallic deposits and their metallogenetic model. Chinese Acad. Geol. Sci. Bull., 22, 61–80 (in Chinese).

Harrison, K. G. (2000): Role of increased marine silica input on paleo-pCO_2 levels. Paleoceanography, 15, 292–298.

Harrison, S. P., Prentice, C. I. (2003): Climate and CO_2 controls on global vegetation distribution at the last glacial maximum: analysis based on palaeovegetation data, biome modelling and palaeoclimate simulations. Glob. Change Biol., 9, 983–1004.

EBSCOhost - printed on 2/10/2023 8:05 PM via . All use subject to https://www.ebsco.com/terms-of-use

Harrison, J. A., Frings, P. J., Beusen, A. H. W., Conley, D. J., McCrackin, M. L. (2012): Global importance, patterns, and controls of dissolved silica retention in lakes and reservoirs. Glob. Biogeochem. Cycles, 26, GB2037.

Hart, D. M. (1988): The plant opal content in the vegetation and sediment of a swamp at Oxford Falls, New South Wales, Australia. Aust. Syst. Bot., 36, 159–170.

Hashimoto, A. (1983): Evaporation metamorphism in the early solar nebula. Evaporation experiments on the melt FeO–MgO–SiO_2–CaO–Al_2O_3 and chemical fractionations of primitive materials. Geochem. J., 17(3), 111–145.

Hashimoto, A., Kumazawa, M., Onuma, N. (1979): Evaporation metamorphism of primitive dust material in the early solar nebula. Earth Planet. Sci. Lett., 43(1), 13–21.

He, H. T., Liu, Y. (2015): Silicon isotope fractionation during the precipitation of quartz and the adsorption of $H_4SiO_{4(aq)}$ on Fe(III)-oxyhydroxide surfaces. Chin. J. Geochem., 34(4), 459–468.

Heck, P. R., Huberty, J. M., Kita, N. T., Ushikubo, T., Kozdon, R., Valley, J. W. (2011): SIMS analyses of silicon and oxygen isotope ratios for quartz from Archean and Paleoproterozoic banded iron formations. Geochim. Cosmochim. Acta, 75(20), 5879–5891.

Hendry, K. R., Robinson, L. F. (2012): The relationship between silicon isotope fractionation in sponges and silicic acid concentration: modern and core-top studies of biogenic opal. Geochim. Cosmochim. Acta, 81, 1–12.

Hendry, K. R., Georg, R. B., Rickaby, R. E. M., Robinson, L. F., Halliday, A. N. (2010): Deep ocean nutrients during the last glacial maximum deduced from sponge silicon isotopic compositions. Earth Planet. Sci. Lett., 292(3–4), 290–300.

Hendry, K. R., Gong, X., Knorr, G., Pike, J., Hall, I. R. (2016): Deglacial diatom production in the tropical North Atlantic driven by enhanced silicic acid supply. Earth Planet. Sci. Lett., 438, 122–129.

Henriet, C., Draye, X., Oppitz, I., Swennen, R., Delvaux, B. (2006): Effects, distribution and uptake of silicon in banana (*Musa* spp.) under controlled conditions. Plant Soil, 287(1–2), 359–374.

Hildebrand, M., Volcani, B. E., Gassmann, W., Schroeder, J. I. (1997): A gene family of silicon transporters. Nature, 385, 688–689.

Hin, R. C., Fitoussi, C., Schmidt, M. W., Bourdon, B. (2014): Experimental determination of the Si isotope fractionation factor between liquid metal and liquid silicate. Earth Planet. Sci. Lett., 387, 55–66.

Hodson, M. J. (2016): The development of phytoliths in plants and its influence on their chemistry and isotopic composition. Implications for palaeoecology and archaeology. J. Archaeol. Sci., 68, 62–69.

Hodson, M. J., Parker, A. G., Leng, M. J., Sloane, H. J. (2008): Silicon, oxygen and carbon isotope composition of wheat (*Triticum aestivum* L.) phytoliths: implications for palaeoecology and archaeology. J. Quat. Sci., 23, 331–339.

Hoffman, P. F., Kaufman, A. J., Halverson, G. P., Schrag, D. P. (1998): Neoproterozoic Snowball Earth. Science, 281(5381), 1342–1346.

Holland, H. D. (1973): The oceans: a possible source of iron in iron-formations. Econ. Geol., 68, 1169–1172.

Holland, H. D. (2006): The oxygenation of the atmosphere and oceans. Philos. Trans. R. Soc. Lond. B, Biol. Sci., 361(1470), 903–915.

Holzer, M., Brzezinski, M. A. (2015): Controls on the silicon isotope distribution in the ocean: new diagnostics from a data-constrained model. Glob. Biogeochem. Cycles, 29(3), 267–287.

Hoppe, P., Geiss, J., Bühler, F., Neuenschwander, J., Amari, S., Lewis, R. S. (1993): Fingerprints of carbon, nitrogen, and silicon isotopes in small interstellar SiC grains from the Murchison meteorite. Geochim. Cosmochim. Acta, 57(16), 4059–4068.

EBSCOhost - printed on 2/10/2023 8:05 PM via . All use subject to https://www.ebsco.com/terms-of-use

Hoppe, P., Amari, S., Zinner, E., Lewis, R. S. (1995): Isotopic compositions of C, N, O, Mg and Si, trace element abundances, and morphologies of single circumstellar graphite grains in four density fractions from the Murchison meteorite. Geochim. Cosmochim. Acta, 59(19), 4029–4056.

Hoppe, P., Strebel, R., Eberhardt, P., Amari, S., Lewis, R. S. (1996a): Type II Supernova Matter in a Silicon Carbide Grain from the Murchison Meteorite. Science, 272(5266), 1314–1316.

Hoppe, P., Strebel, R., Eberhardt, P., Amari, S., Lewis, R. S. (1996b): Small SiC grains and a nitride grain of circumstellar origin from the Murchison meteorite: Implications for stellar evolution and nucleosynthesis. Geochimica et Cosmochimica Acta, 60(5), 883–907.

Horn, I., von Blanckenburg, F. (2007): Investigation on elemental and isotopic fractionation during 196 nm femtosecond laser ablation multiple collector inductively coupled plasma mass spectrometry. Spectrochim. Acta, Part B, 62, 410–422.

Horn, M. G., Beucher, C. P., Robinson, R. S., Brzezinski, M. A. (2011): Southern ocean nitrogen and silicon dynamics during the last deglaciation. Earth Planet. Sci. Lett., 310(3), 334–339.

Hou, K. J., Li, Y. H., Gao, J. F., Liu, F., Qin, Y. (2014): Geochemistry and Si–O–Fe isotope constraints on the origin of banded iron formations of the Yuanjiacun Formation, Lvliang Group, Shanxi, China. Ore Geol. Rev., 57, 288–298.

Hren, M. T., Tice, M. M., Chamberlain, C. P. (2009): Oxygen and hydrogen isotope evidence for a temperate climate 3.42 billion years ago. Nature, 462, 205–208.

Hu, G. Y., Fan, C. F., Wan, D. F. Li Y. H., Chen, S. M. (2013): Geochemistry of bedded cherts in the cap carbonates in Three Gorges Region, Hubei Province, and its paleoenvironmental implications. Acta Geol. Sin., 87(9), 1469–1476 (in Chinese with English abstract).

Huang, F., Chen, L. J., Wu, Z. Q., Wang, W. (2013): First-principles calculations of equilibrium Mg isotope fractionations between garnet, clinopyroxene, orthopyroxene, and olivine: Implications for Mg isotope thermometry. Earth Planet. Sci. Lett., 367, 61–70.

Huang, F., Wu, Z. Q., Huang, S. C., Wu, F. (2014): First-principles calculations of equilibrium silicon isotope fractionation among mantle minerals. Geochim. Cosmochim. Acta, 140, 509–520.

Hughes, H. J., Bouillon, S., André, L., Cardinal, D. (2012): The effects of weathering variability and anthropogenic pressures upon silicon cycling in an intertropical watershed (Tana River, Kenya). Chem. Geol., 308–309, 18–25.

Hughes, H. J., Sondag, F., Santos, R. V., André, L., Cardinal, D. (2013): The riverine silicon isotope composition of the Amazon Basin. Geochim. Cosmochim. Acta, 121, 637–651.

Huss, G. R., Hutcheon, I. D., Wasserburg, G. J. (1997): Isotopic systematics of presolar silicon carbide from the Orgueil (CI) chondrite: Implications for solar system formation and stellar nucleosynthesis. Geochim. Cosmochim. Acta, 61(23), 5117–5148.

Hutcheon, I. D., Mathez, E. A., Fogel, R. A., Marshintsev, V. K. (1994): Carbon and nitrogen isotopic composition of Moissanite in Yakutian kimberlites. U.S.

Iler, R. K. (1979): The chemistry of silica. New York: Wiley.

Institute of Geochemistry, Chinese Academy of Sciences, (1988): The geochemistry of the Bayan Obo ore deposit. Beijing: Science Press.

Ireland, T. R., Zinner, E. K., Fahey, A. J., Esat, T. M. (1992): Evidence for distillation in the formation of HAL and related hibonite inclusions. Geochim. Cosmochim. Acta, 56(6), 2503–2520.

Jadhav, M., Amari, S., Marhas, K. K., Zinner, E., Maruoka, T., Gallino, R. (2008): New Stellar Sources for High-Density, Presolar Graphite Grains. Astrophys. J., 682(2), 1479.

Jadhav, M., Amari, S., Zinner, E., Maruoka, T. (2006): Isotopic analysis of presolar graphite grains from Orgueil. New Astron. Rev., 50(7), 591–595.

Jadhav, M., Pignatari, M., Herwig, F., Zinner, E., Gallino, R., Huss, G. R. (2013): Relics of ancient post-AGB stars in a primitive meteorite. Astrophys. J., 777(2), 134–142.

EBSCOhost - printed on 2/10/2023 8:05 PM via . All use subject to https://www.ebsco.com/terms-of-use

Jaffres, J. B. D., Shields, G. A., Wallmann, K. (2007): The oxygen isotope evolution of seawater: a critical review of a long-standing controversy and an improved geological water cycle model for the past 3.4 billion years. Earth-Sci. Rev., 83(1–2), 83–122.

Jarvis, S. C. (1987): The uptake and transport of silicon by perennial ryegrass and wheat. Plant Soil, 97, 429–437.

Javoy, M., Balan, E., Méheut, M., Blanchard, M., Lazzeri, M. (2012): First-principles investigation of equilibrium isotopic fractionation of O- and Si-isotopes between refractory solids and gases in the solar nebula. Earth Planet. Sci. Lett., 319–320, 118–127.

Jeandel, C., Oelkers, E. H. (2015): The influence of terrigenous particulate material dissolution on ocean chemistry and global element cycles. Chem. Geol., 395, 50–66.

Jeandel, C., Peucker-Ehrenbrink, B., Jones, M. T., Pearce, C. R., Oelkers, E. H., Godderis, Y., Lacan, F., Aumont, O., Arsouze, T. (2011): Ocean margins: the missing term in oceanic element budgets? EOS Trans. Am. Geophys. Union, 92.

Jiang, Y. H., Li, S. R. (2005): A study of the fluid environment of silicalite of transitional Precambrian-Cambrian age in Hunan and Guizhou provinces. Earth Sci. Front., 12, 622–629 (in Chinese with English abstract).

Jiang, S. Y., Ding, T. P., Wan, D. F. (1992): A study on silicon and oxygen isotope geochemistry of some lead–zinc ore deposits in China. Chin. Sci. Bull., 37 (12), 1022–1027.

Jiang, S. Y., Ding, T. P., Wan, D. F., Li, Y. H. (1993): Silicon isotopic compositions of Archean Banded Si–Fe Formation (BIF) in the Gongchangling ore deposit, Liaoning Province, China. Sci. China Ser. B, 36, 482–489.

Jiang, S. Y., Palmer, M. R., Ding, T. P. (1994): Silicon isotope geochemistry of the Sullivan Pb–Zn deposit, Canada: a preliminary study. Econ. Geol., 89, 1623–1629.

Jiang, S. Y., Palmer, M. R., Li, Y. H., Xue, C. J. (1995): Chemical compositions of tourmaline in the Yindongzi-Tongmugou Pb-Zn deposits, Qinling, China: Implications for hydrothermal ore-forming processes. Miner. Depos., 30(3), 225–234.

Jiang, S. Y., Han, F., Shen, J. Z., Palmer, M. R. (1999): Chemical and Rb–Sr, Sm–Nd isotopic systematics of tourmaline from the Dachang Sn-polymetallic ore deposit, Guangxi Province, P.R. China. Chem. Geol., 157(1), 49–67.

Jiang, S. Y., Palmer, M. R., Slack, J. F., Ding, T. P. Wan, D. F. (2000): Silicon isotope compositions of tourmalinites and selected silicate minerals from the Sullivan deposit and vicinity, and their significance to mineral exploration and ore genesis. In J. W. Lydon, T. Hoy, J. F. Slack, M. E. Knapp (Eds.) The geological environment of the Sullivan deposit, British Columbia. Geological association of Canada special publication (Vol. 1, pp. 782–790).

Jiang, S. Y., Yang, J. H., Ling, H. F., Feng, H. Z., Chen, Y. Q., Chen, J. H. (2003): Trace- and rare earth element geochemistry and Pb–Pb dating of black shales and intercalated Ni–Mo–PGE–Au sulfide ores in Lower Cambrian strata, Yangtze Platform, South China. Miner. Depos., 41, 453–468.

Jickells, T. D., An, Z. S., Andersen, K. K., Baker, A. R., Bergametti, G., Brooks, N., Cao, J. J., Boyd, P. W., Duce, R. A., Hunter, K. A., Kawahata, H., Kubilay, N. laRoche, J., Liss, P. S., Mahowald, N., Prospero, J. M., Ridgwell, A. J., Tegen, I., Torres, R. (2005): Global iron connections between desert dust, ocean biogeochemistry, and climate. Science, 308, 67–71.

Johannes, R. (1980): Ecological significance of the submarine discharge of groundwater. Mar. Ecol. Prog. Ser., 3, 365–373.

Jones, L. H. P., Handreck, K. A. (1963): Effects of iron and aluminium oxides on silica in solution in soils. Nature, 198(4883), 852–853.

Jones, L. H. P., Handreck, K. A. (1967): Silica in soil, plants and animals. Adv. Argon., 19, 107–149.

Jones, I. W., Munhoven, G., Tranter, M., Huybrechts, P., Sharp, M. J. (2002): Modelled glacial and non-glacial HCO_3^-, Si and Ge fluxes since the LGM: little potential for impact on atmospheric

EBSCOhost - printed on 2/10/2023 8:05 PM via . All use subject to https://www.ebsco.com/terms-of-use

CO_2 concentrations and a potential proxy of continental chemical erosion, the marine Ge/Si ratio. Glob. Planet. Change, 33, 139–153.

Jones, M. T., Pearce, C. R., Jeandel, C., Gislason, S. R., Eiriksdottir, E. S., Mavromatis, V., Oelkers, E. H. (2012a): Riverine particulate material dissolution as a significant flux of strontium to the oceans. Earth Planet. Sci. Lett., 355(356), 51–59.

Jones, M. T., Pearce, C. R., Oelkers, E. H. (2012b): An experimental study of the interaction of basaltic riverine particulate material and seawater. Geochim. Cosmochim. Acta, 77, 108–120.

Jones, M. T., Gislason, S. R., Burton, K. W., Pearce, C. R., Mavromatis, V., Pogge von Strandmann, P. A. E., Oelkers, E. H. (2014): Quantifying the impact of riverine particulate dissolution in seawater on ocean chemistry. Earth Planet. Sci. Lett., 395, 91–100.

Kasting, J. F., Howard, M. T., Wallmann, K., Veizer, J., Shields, G., Jaffrés, J. (2006): Paleoclimates, ocean depth, and the oxygen isotopic composition of seawater. Earth Planet. Sci. Lett., 252(1), 82–93.

Kaufman, P. B., Soni, S. L., LaCroix, J. D., Rosen, J. J., Bigelow, W. C. (1972): Electron-probe microanalysis of silicon in the epidermis of rice (*Oryza sativa* L.) internodes. Planta. (Berl.), 104, 10–17.

Kawabe, I. (1978): Calculation of oxygen isotope fractionation in quartz–water system with special reference to the low temperature fractionation. Geochim. Cosmochim. Acta, 42(6), 613–621.

Kennett, J. P. (1982): Marine geology. New Jersey: Prentice–Hall (752 pp.).

Kieffer, S. W. (1982): Thermodynamics and lattice vibrations of minerals: 5. Applications to phase equilibria, isotopic fractionation, and high-pressure thermodynamic properties. Rev. Geophys., 20(4), 827–849.

Kita, N. T., Ushikubo, T., Knight, K. B., Mendybaev, R. A., Davis, A. M., Richter, F. M., Fournelle, J. H. (2012): Internal ^{26}Al–^{26}Mg isotope systematics of a Type B CAI: remelting of refractory precursor solids. Geochim. Cosmochim. Acta, 86, 37–51.

Knauth, L. P. (1979): A model for the origin of chert in limestone. Geology, 7, 274–277.

Knauth, L. P., Epstein, S. (1975): Hydrogen and oxygen isotope ratios in silica from the JOIDES deep sea drilling project. Earth Planet. Sci. Lett., 25, 1–10.

Knauth, L. P., Lowe, D. R. (1978): Oxygen isotope geochemistry of cherts from the Onverwacht group (3.4 Ga), Transvaal, South Africa, with implications for secular variations in the isotopic compositions of cherts. Earth Planet. Sci. Lett., 41, 209–222.

Knauth, L. P., Lowe, D. R. (2003): High Archean climatic temperature inferred from oxygen isotope geochemistry of cherts in the 3.5 Ga Swaziland Supergroup, South Africa. Geol. Soc. Am. Bull., 115, 566–580.

Knee, K. L., Paytan, A. (2011): Submarine groundwater discharge: a source of nutrients, metals, and pollutants to the Coastal Ocean. In E. Wolanski, D. McLusky (Eds.) Treatise on estuarine and coastal science (pp. 205–233). Waltham: Academic Press.

Knight, C. T. G., Kinrade, S. D. (2001): A primer on the aqueous chemistry of silicon. In L. E. Datnoff, G. H. Snyder, G. H. Korndorfer (Eds.) Silicon in agriculture (pp. 57–84). The Netherlands: Elsevier.

Knight, K. B., Kita, N. T., Mendybaev, R. A., Richter, F. M., Davis, A. M., Valley, J. W. (2009): Silicon isotopic fractionation of CAI-like vacuum evaporation residues. Geochim. Cosmochim. Acta, 73(20), 6390–6401.

Kowalski, P. M., Jahn, S. (2011): Prediction of equilibrium Li isotope fractionation between minerals and aqueous solutions at high P and T: an efficient ab initio approach. Geochim. Cosmochim. Acta, 75(20), 6112–6123.

Kowalski, P. M., Wunder, B., Jahn, S. (2013): Ab initio prediction of equilibrium boron isotope fractionation between minerals and aqueous fluids at high P and T. Geochim. Cosmochim. Acta, 101, 285–301.

EBSCOhost - printed on 2/10/2023 8:05 PM via . All use subject to https://www.ebsco.com/terms-of-use

Kozdon, R., Kita, N. T., Huberty, J. M., Fournelle, J. H., Johnson, C. A., Valley, J. W. (2010): In situ sulfur isotope analysis of sulfide minerals by SIMS: precision and accuracy, with application to thermometry of ~3.5 Ga Pilbara cherts. Chem. Geol., 275(3–4), 243–253.

Kozdon, R., Kelly, D. C., Kita, N. T., Fournelle, J. H., Valley, J. W. (2011): Planktonic foraminiferal oxygen isotope analysis by ion microprobe technique suggests warm tropical sea surface temperatures during the Early Paleogene. Paleoceanography, 26(3), PA3206.

Kröger, N., Deutzmann, R., Bergsdort, C., Sumper, M. (2000): Species specific polyamines control silica morphology. Proc. Natl. Acad. Sci. USA, 97, 14133–14138.

Krapez, B., Eisenlohr, B. (1998): Tectonic settings of Archaean (3325-2775 Ma) crustal-supracrustal belts in the West Pilbara Block. Precambrian Res., 88(1), 173–205.

Krot, A. N., Yurimoto, H., Hutcheon, I. D., Chaussidon, M., MacPherson, G. J., Paque, J. (2007): Remelting of refractory inclusions in the chondrule-forming regions: Evidence from chondrule-bearing type C calcium-aluminum-rich inclusions from Allende. Meteorit. Planet. Sci., 42(7–8), 1197–1219.

Kump, L., Alley, R. B. (1994): Global chemical weathering on glacial time scales. In Material fluxes on the surface of the Earth (pp. 46–60).

Kurat, G. (1970): Zur genese der Ca–Al-reichen einschlüsse im chondriten von lancé. Earth Planet. Sci. Lett., 9(3), 225–231.

LaBerge, G. L. (1973): Possible Biological origin of precambrian iron-formations. Econ. Geol., 68(7), 1098–1109.

Lahav, E., Reuveni (1995): In vitro culture of bananas, in: Bananas and Plantains, London UK: Chapman & Hall. 147–178.

Lai, X., Yang, X. (2013): Geochemical characteristics of the Bayan Obo giant REE–Nb–Fe deposit: Constraints on its genesis. J. South Am. Earth Sci., 41, 99–112.

Lai, X., Yang, X., Liu, Y., Yan, Z. (2016): Genesis of the Bayan Obo Fe-REE-Nb deposit: evidence from Pb–Pb age and microanalysis of the H8 Formation in Inner Mongolia, North China Craton. J. Asian Earth Sci., 120, 87–99.

Lambeck, K., Rouby, H., Purcell, A., Sun, Y., Sambridge, M. (2014): Sea level and global ice volumes from the last glacial maximum to the Holocene. Proc. Natl. Acad. Sci., 111, 15296–15303.

Larimer, J. W. (1967): Chemical fractionations in meteorites – I. Condensation of the elements. Geochim. Cosmochim. Acta, 31(8), 1215–1238.

Larimer, J. W., Anders, E. (1967): Chemical fractionations in meteorites – II. Abundance patterns and their interpretation. Geochim. Cosmochim. Acta, 31(8), 1239–1270.

Laruelle, G. G., Roubeix, V., Sferratore, A., Brodherr, B., Ciuffa, D., Conley, D. J., Dürr, H. H., Garnier, J., Lancelot, C., Le Thi Phuong, Q., Meunier, J. D., Meybeck, M., Michalopoulos, P., Moriceau, B., Ní Longphuirt, S. Loucaides, S., Papush, L., Presti, M., Ragueneau, O., Regnier, P., Saccone, L., Slomp, C.P., Spiteri, C., Van Cappellen, P. (2009): Anthropogenic perturbations of the silicon cycle at the global scale: key role of the land-ocean transition. Glob. Biogeochem. Cycles, 23, GB4031.

Lauerwald, R., Hartmann, J., Moosdorf, N., Dürr, H. H., Kempe, S. (2013): Retention of dissolved silica within the fluvial system of the conterminous USA. Biogeochemistry, 112, 637–659.

Lee, T., Papanastassiou, D. A., Wasserburg, G. J. (1977): Aluminum-26 in the early solar system: fossil or fuel? Astrophys. J., 211, L107–L110.

Lee, T., Russell, W. A., Wasserburg, G. J. (1979): Ca isotopic anomalies and the lack of ^{26}Al in an unusual Allende inclusion. Astrophys. J., 228.

Lee, T., Mayeda, T. K., Clayton, R. N. (1980): Oxygen isotopic anomalies in Allende Inclusion Hal. Geophys. Res. Lett., 7(7), 493–496.

Lehtimäki, M., Tallberg, P., Siipola, V. (2013): Seasonal dynamics of amorphous silica in Vantaa River Estuary. Silicon, 5, 35–51.

EBSCOhost - printed on 2/10/2023 8:05 PM via . All use subject to https://www.ebsco.com/terms-of-use

Leng, M. J., Swann, G. E. A., Hodson, M. J., Tyler, J. J., Patwardhan, S. V., Sloane, H. J. (2009): The potential use of silicon isotope composition of biogenic silica as a proxy for environmental change. Silicon, 1(2), 65–77.

Li, Y. Y. (1997): The geological characteristics of seafloor exhalative sedimentary chert in the Lower Cambrian-black shales in Dayong-Cili area, Hunan Province. Acta Petrol. Sin., 13, 121–126 (in Chinese with English abstract).

Li, S. R., Gao, Z. M. (1996): Silicalites of hydrothermal origin in the Lower Cambrian black rock series of South China. Chin. J. Geochem., 15(2), 113–120.

Li, X. F., Liu, Y. (2010): First-principles study of Ge isotope fractionation during adsorption onto Fe(III)-oxyhydroxide surfaces. Chem. Geol., 278(1), 15–22.

Li, X. F., Liu, Y. (2011): Equilibrium Se isotope fractionation parameters: a first-principles study. Earth Planet. Sci. Lett., 304(1), 113–120.

Li, C. W., Chen, J. Y., Hua, T. E. (1988): Precambrian sponges with cellular structures. Science, 279, 879–882.

Li, Y., Hou, K., Wan, D., Zhang, Z., Yue, G. (2010): Formation mechanism of precambrian banded iron formation and atmosphere and ocean during early stage of the earth. Acta Geol. Sin., 84(9), 1359–1373 (in Chinese with English abstract).

Li, Y., Ding, T., Wan, D. (1995a): Experimental study of silicon isotope dynamic fractionation and its application in geology. Chin. J. Geochem., 14(3), 212–219.

Li, Y. H., Jiang, S. Y., Xue, C. J. (1995b): Silicon and oxygen isotope evidence for exhalative genesis of the Devonian Pb-Zn deposits in the Feng-Tai region, Qinling Mountains, China. Chin. Sci. Bull., 40, 87–88.

Li, Y. H., Wan, D. F., Jiang, S. Y. (1995c): Silicon isotope study on the Meishucun Precambrian–Cambrian boundary section, Yunnan. Geol. Rev., 41, 179–187 (in Chinese with English abstract).

Li, R. W., Chen, J. S., Zhang, S. K. (1999): Stable carbon and oxygen isotopic compositions of carbonates in middle Mesoproterozoic Wumishan Formation and sea-level change. Chin. Sci. Bull., 44, 2130–2136.

Li, Z., Lin, P., He, J., Yang, Z., Lin, Y. (2006): Silicon's organic pool and biological cycle in moso bamboo community of Wuyishan Biosphere Reserve. J. Zhejiang Univ. Sci. B, 7(11), 849–857.

Li, Y. H., Hou, K. J., Wan, D. F., Zhang, Z. J., Yue, G. L. (2014a): Precambrian banded iron formations in the North China Craton: Silicon and oxygen isotopes and genetic implications. Ore Geol. Rev., 57, 299–307.

Li, H. K., Su, W. B., Zhou, H. Y., Xiang, Z. Q., Tian, H., Yang, L. G., Huff, D. W., Ettensohn, R. F. (2014b): The first precise age constraints on the Jixian System of the Meso- to Neoproterozoic Standard Section of China: SHRIMP zircon U–Pb dating of bentonites from the Wumishan and Tieling formations in the Jixian Section, North China Craton. Acta Petrol. Sin., 30(10), 2999–3012.

Liang, Y. C., Hua, H., Zhu, Y. G., Zhang, J., Cheng, C., Römheld, V. (2006): Importance of plant species and external silicon concentration to active silicon uptake and transport. New Phytol., 172(1), 63–72.

Ling, M. X., Zhang, H., Li, H., Liu, Y. L., Liu, J., Li, L. Q., Li, C. Y., Yang, X. Y., Sun, W. D. (2014): The Permian–Triassic granitoids in Bayan Obo North China Craton: a geochemical and geochronological study. Lithos, 190–191, 430–439.

Liu, Y. J. (1984): Element geochemistry. Beijing: Science Press.

Liu, X., Ni, S., Lu, Q., Jin, J., Zhu, L. (1998): Silicon isotope geochemistry of micro-fine disseminated gold deposits in SW Guizhou and NW Guangxi China. Chin. J. Geochem., 17(3), 249–257.

EBSCOhost - printed on 2/10/2023 8:05 PM via . All use subject to https://www.ebsco.com/terms-of-use

Liu, X., Lu, Q., Long, X., Tao, Z., Song, X. (2005): Characteristics of isotope geochemistry of deep mantle constraints on metallization in alkali-enriched porphyry systems. In Eighth biennial SGA meeting, Beijing, China. Berlin, Heidelberg: Springer.

Liu, J., Zheng, M., Cook, N. J., Long, X., Denga, J., Zhai, Y. (2007): Geological and geochemical characteristics of the Sawaya'erdun gold deposit, southwestern Chinese Tianshan. Ore Geol. Rev., 32, 125–156.

Liu, S. Q., Li, Y. B., Tian, H. Q., Yang, J. L., Liu, J. M., Shi, Y. L. (2014a): First-principles study of sulfur isotope fractionation in sulfides. Eur. J. Mineral., 26(6), 203–208.

Liu, C. M., Qin, D. X., Yang, D. M. (2014b): A research on ore-bearing silica rocks in Changpo-Tongkeng mining area of Dachang Sn deposit in Guangxi. Mineral Resources and Geology, 28(3), 321–329.

Liu, J., Dai, H., Zhai, D., Wang, J., Wang, Y., Yang, L., Mao, G., Liu, X., Liao, Y., Yu, C., Li, Q. (2015): Geological and geochemical characteristics and formation mechanisms of the Zhaishang Carlin-like type gold deposit, western Qinling Mountains, China. Ore Geol. Rev., 64, 273–298.

Lott, D. A., Coveney, R. M. Jr. (1996): Fluid-inclusion evidence for the origins of organic rich Chinese nickel–molybdenum ores. In Abstracts of 30th IGC. Beijing (713 p.).

Lott, D. A., Conveney, R. M. Jr., Murowichick, J. B., Grauch, R. I. (1999): Sedimentary exhalative nickel–molybdenum ores in South China. Econ. Geol., 94, 1051–1066.

Loucaides, S., Van Cappellen, P., Behrends, T. (2008): Dissolution of biogenic silica from land to ocean: role of salinity and pH. Limnol. Oceanogr., 53, 1614–1621.

Loucaides, S., Cappellen, P., Roubeix, V., Moriceau, B., Ragueneau, O. (2012): Controls on the recycling and preservation of biogenic silica from biomineralization to burial. Silicon, 4, 7–22.

Lovering, J. F. (1975): Application of SIMS microanalysis techniques to trace element and isotopic studies in geochemistry and cosmochemistry. Natl. Bur. Stand. Spec. Publ., 427, 135–178.

Lugaro, M., Zinner, E., Gallino, R., Amari, S. (1999): Si isotopic ratios in mainstream presolar SiC grains revisited. Astrophys. J., 527, 369–394.

Lux, A., Luxova, M., Abe, J., Morita, S., Inanaga, S. (2003): Silicification of bamboo (*Phyllostachys heterocycla* Mitf.) root and leaf. Plant Soil, 255, 85–91.

Ma, J. F., Yamaji, N. (2006): Silicon uptake and accumulation in higher plants. Trends Plant Sci., 11(8), 392–397.

Ma, J. F., Tamai, K., Ichii, M., Wu, G. F. (2002): A rice mutant defective in Si uptake. Plant Physiol., 130(4), 2111–2117.

Ma, J. F., Mitaniet, N., Nagao, S., Konishi, S., Tamai, K., Iwashita, T., Yano, M. (2004): Characterization of the silicon uptake system and molecular mapping of the silicon transporter gene in rice. Plant Physiol., 136(2), 3284–3289.

Ma, J. F., Tamai, K., Yamaji, N., Mitani, N., Konishi, S., Katsuhara, M., Ishiguro, M., Murata, Y., Yano, M. (2006): A silicon transporter in rice. Nature, 440, 688–691.

Ma, J. F., Yamaji, N. Mitani, N., Tamai, K., Konishi, S., Fujiwara, T., Katsuhara, M., Yano, M. (2007): An efflux transporter of silicon in rice. Nature, 448, 209–212.

Macdonald, R. (1983): Silicon in igneous and metamorphic rocks. In S. R. Aston (Ed.) Silicon geochemistry and biogeochemistry. London: Pergamon Press Inc.

Mackay, A. W. (2007): The paleoclimatology of Lake Baikal: A diatom synthesis and prospectus. Earth-Sci. Rev., 82(3), 181–215.

Macpherson, G. J., Wark, D. A., Armstrong, J. T. (1988): Primitive material surviving in chondrites – refractory inclusions. Meteor. Early Sol. Syst., 746–807.

Maier, E., Chapligin, B., Abelmann, A., Gersonde, R., Esper, O., Ren, J., Friedrichsen, H., Meyer, H., Tiedemann, R. (2013): Combined oxygen and silicon isotope analysis of diatom silica from a deglacial subarctic Pacific record. J. Quat. Sci., 28(6), 571–581.

EBSCOhost - printed on 2/10/2023 8:05 PM via . All use subject to https://www.ebsco.com/terms-of-use

Maier, E., Méheust, M., Abelmann, A., Gersonde, R., Chapligin, B., Ren, J., Stein, R., Meyer, H., Tiedemann, R. (2015): Deglacial subarctic Pacific surface water hydrography and nutrient dynamics and links to North Atlantic climate variability and atmospheric CO_2. Paleoceanography, 30(7), 2014PA002763.

Maliva, R. G., Knoll, A. H., Simonson, B. M. (2005): Secular change in the Precambrian silica cycle: Insights from chert petrology. Geol. Soc. Am. Bull., 117, 835–845.

Mao, J. W., Lehmann, B., Du, A. D., Zhang, G. D., Ma, D. S. (2002): Re–Os dating of polymetallic Ni–Mo–PGE–Au mineralization in Lower Cambrian black shales of South China and its geologic significance. Econ. Geol., 97, 1051–1061.

Marin, J., Chaussidon, M., Robert, F. (2010): Microscale oxygen isotope variations in 1.9 Ga Gunflint cherts: assessments of diagenesis effects and implications for oceanic paleotemperature reconstructions. Geochim. Cosmochim. Acta, 74, 116–130.

Marin-Carbonne, J., Chaussidon, M., Boiron, M.-C., Robert, F. (2011): A combined in situ oxygen, silicon isotopic and fluid inclusion study of a chert sample from Onverwacht Group (3.35 Ga, South Africa): New constraints on fluid circulation. Chem. Geol., 286(3–4), 59–71.

Marin-Carbonne, J., Chaussidon, M., Robert, F. (2012): Micrometer-scale chemical and isotopic criteria (O and Si) on the origin and history of Precambrian cherts: Implications for paleo-temperature reconstructions. Geochim. Cosmochim. Acta, 92, 129–147.

Marin-Carbonne, J., Robert, F., Chaussidon, M. (2014): The silicon and oxygen isotope compositions of Precambrian cherts: a record of oceanic paleo-temperatures? Precambrian Res., 247, 223–234.

Martin, J. H. (1990): Glacial–interglacial CO_2 change: the iron hypothesis. Paleoceanography, 5, 1–13.

Massey, F. P., Ennos, A. R., Hartley, S. E. (2006): Silica in grasses as a defence against insect herbivores: contrasting effects on folivores and a phloem feeder. J. Anim. Ecol., 75, 595–603.

Matsumoto, K., Sarmiento, J. L., Brzezinski, M. A. (2002): Silicic acid leakage from the Southern Ocean: a possible explanation for glacial atmospheric pCO_2. Glob. Biogeochem. Cycles, 16(3), 5-1–5-23.

Mckeague, J. A., Cline, M. G. (1963): Silica in soil solution: II. The adsorption of monosilicic acid by soil and by other substance. Can. J. Soil Sci., 43(1), 83–96.

McKeegan, K. D., Walker, R. M., Zinner, E. (1985): Ion microprobe isotopic measurements of individual interplanetary dust particles. Geochim. Cosmochim. Acta, 49(9), 1971–1987.

Meckler, A. N., Sigman, D. M., Gibson, K. A., Francois, R., Martinez-Garcia, A., Jaccard, S. L., Rohl, U., Peterson, L. C., Tiedemann, R., Haug, G. H. (2013): Deglacial pulses of deep-ocean silicate into the subtropical North Atlantic Ocean. Nature, 495(7442), 495–498.

Méheut, M., Schauble, E. A. (2014): Silicon isotope fractionation in silicate minerals: insights from first-principles models of phyllosilicates, albite and pyrope. Geochim. Cosmochim. Acta, 134, 137–154.

Méheut, M., Lazzeri, M., Balan, E., Mauri, F. (2007): Equilibrium isotopic fractionation in the kaolinite, quartz, water system: prediction from first-principles density-functional theory. Geochim. Cosmochim. Acta, 71(13), 3170–3181.

Méheut, M., Lazzeri, M., Balan, E., Mauri, F. (2009): Structural control over equilibrium silicon and oxygen isotopic fractionation: a first-principles density-functional theory study. Chem. Geol., 258(1–2), 28–37.

Méheut, M., Lazzeri, M., Balan, E., Mauri, F. (2010): First-principles calculation of H/D isotopic fractionation between hydrous minerals and water. Geochim. Cosmochim. Acta, 74(14), 3874–3882.

Melander, L. (1960): Isotope effects on reaction rates. New York: Ronald Press Company.

EBSCOhost - printed on 2/10/2023 8:05 PM via . All use subject to https://www.ebsco.com/terms-of-use

Melander, L. C., Saunders, W. H. (1980): Reaction rates of isotopic molecules. Wiley.
Mendybaev, R. A., Richter, F. M., Georg, R. B., Janney, P. E., Spicuzza, M. J., Davis, A. M., Valley, J. W. (2013): Experimental evaporation of Mg- and Si-rich melts: implications for the origin and evolution of FUN CAIs. Geochim. Cosmochim. Acta, 123, 368–384.
Métivier, F., Gaudemer, Y. (1999): Stability of output fluxes of large rivers in South and East Asia during the last 2 million years: implications on floodplain processes. Basin Res., 11, 293–303.
Meunier, J.-D., Braun, J.-J., Riotte, J., Kumar, C., Sekhar, M. (2011): Importance of weathering and human perturbations on the riverine transport of Si. Appl. Geochem., 26, S360–S362 (Supplement).
Meybeck, M., Vörösmarty, C. (2005): Fluvial filtering of land-to-ocean fluxes: from natural Holocene variations to Anthropocene. C. R. Géosci. 337, 107–123.
Milligan, A. J., Varela, D. E., Brzezinski, M. A., Morel, F. (2004): Dynamics of siliconmetabolism and silicon isotopic discrimination in a marine diatom as a function of pCO_2. Limnol. Oceanogr., 49, 322–329.
Milliman, J. D., Boyle, E. (1975): Biological uptake of dissolved silica in the Amazon river estuary. Science, 189, 995–997.
Milliman, J. D., Farnsworth, K. L. (2011): River discharge to the coastal ocean: a global synthesis. Cambridge: Cambridge University Press.
Milliman, J. D., Meade, R. H. (1983): World-wide delivery of river sediment to the oceans. J. Geol., 91, 1–21.
Mitani, N., Ma, J. F. (2005): Uptake system of silicon in different plant species. J. Exp. Bot., 56, 1255–1261.
Mitzutani, A. J., Nagase, H., Fujiwara, N., Ogoshi, H. (1998): Silicic acid polymerization catalyzed by amines and polyamines. Bull. Chem. Soc. Jpn., 71, 2017–2022.
Molini-Velsko, C., Mayeda, T. K., Clayton, R. N. (1986): Isotopic composition of silicon in meteorites. Geochim. Cosmochim. Acta, 50(12), 2719–2726.
Molini-Velsko, C., Mayeda, T. K., Clayton, R. N. (1987): Silicon isotope systematics during distillation. In Lunar and planetary science conference, Lunar Planet. Sci.
Moore, W. S. (1996): Large groundwater inputs to coastal waters revealed by ^{226}Ra enrichments. Nature, 380, 612–614.
Morin, G. P., Vigier, N., Verney-Carron, A. (2015): Enhanced dissolution of basaltic glass in brackish waters: impact on biogeochemical cycles. Earth Planet. Sci. Lett., 417, 1–8.
Mortlock, R. A., Froelich, P. N., Feely, R. A., Massoth, G. J., Butterfield, D. A., Lupton, J. E. (1993): Silica and germanium in Pacific Ocean hydrothermal vents and plumes. Earth Planet. Sci. Lett., 119(3), 365–378.
Motomura, H., Fujii, T., Suzuki, M. (2004): Silica deposition in relation to ageing of leaf tissues in *Sasa veitchii* (Carriere) Rehder (Poaceae: Bambusoideae). Ann. Bot., 93(3), 235–248.
Muhs, D. R. (2013): The geologic records of dust in the Quaternary. Aeolian Res., 9, 3–48.
Munhoven, G. (2002): Glacial–interglacial changes of continental weathering: estimates of the related CO_2 and HCO_3^- flux variations and their uncertainties. Glob. Planet. Change, 33, 155–176.
Nagasawa, H., Onuma, N. (1979): High temperature heating of the Allende Meteorite II. Fractionation of the rare earth elements. In Lunar and planetary science conference.
Nelson, D. M., Tréguer, P., Brzezinski, M. A., Leynaert, A., Quéguiner, B. (1995): Production and dissolution of biogenic silica in the ocean: revised global estimates, comparison with regional data and relationship to biogenic sedimentation. Glob. Biogeochem. Cycles, 9(3), 359–372.
Niederer, F. R., Papanastassiou, D. A. (1984): Ca isotopes in refractory inclusions. Geochim. Cosmochim. Acta, 48(6), 1279–1293.

EBSCOhost - printed on 2/10/2023 8:05 PM via . All use subject to https://www.ebsco.com/terms-of-use

Northrop, D. A., Clayton, R. N. (1966): Oxygen isotope fractionation in systems containing dolomite. J. Geol., 74, 174–196.
Notsu, K., Onuma, N., Nishida, N., Nagasawa, H. (1978): High temperature heating of the Allende meteorite. Geochim. Cosmochim. Acta, 42(6), 903–907.
Oelkers, E. H., Gislason, S. R., Eiriksdottir, E. S., Jones, M., Pearce, C. R., Jeandel, C. (2011): The role of riverine particulate material on the global cycles of the elements. Appl. Geochem., 26, S365–S369 (Supplement).
Oelze, M., von Blanckenburg, F., Bouchez, J., Hoellen, D., Dietzel, M. (2015): The effect of Al on Si isotope fractionation investigated by silica precipitation experiments. Chem. Geol., 397, 94–105.
Okamoto, G., Okura, T., Oto, K. (1957): Properties of silica in water. Geochim. Cosmochim. Acta, 12, 123–131.
Opfergelt, S., Delmelle, P. (2012): Silicon isotopes and continental weathering processes: assessing controls on Si transfer to the ocean. C. R. Géosci., 344, 723–738.
Opfergelt, S., Cardinal, D., Henriet, C., Delvaux, B., André, L. (2004): Silicon Isotope Fractionation by Banana Under Continuous Nutrient and Silica Flux. In: AGU Fall Meeting. San Francisco: AGU.
Opfergelt, S., Cardinal, D., Henriet, C., André, L., Delvaux, B. (2006a). Silicon isotope fractionation between plant parts in banana: in situ vs. in vitro. J. Geochem. Explor., 88 (1–3 S), 224–227.
Opfergelt, S., Cardinal, D., Henriet, C., André, L., Delvaux, B. (2006b): Silicon isotopic fractionation by banana (*Musa* spp.) grown in a continuous nutrient flow device. Plant Soil, 285(1–2), 333–345.
Opfergelt, S., de Bournonville, G., Cardinal, D., André, L., Delstanche, S., Delvaux, B. (2009): Impact of soil weathering degree on silicon isotopic fractionation during adsorption onto iron oxides in basaltic ash soils, Cameroon. Geochim. Cosmochim. Acta, 73, 7226–7240.
Opfergelt, S., Cardinal, D., André, L., Delvigne, C., Bremond, L., Delvaux, B. (2010): Variations of δ^{30}Si and Ge/Si with weathering and biogenic input in tropical basaltic ash soils under monoculture. Geochim. Cosmochim. Acta, 74, 225–240.
Opfergelt, S., Eiriksdottir, E., Burton, K., Einarsson, A., Siebert, C., Gislason, S., Halliday, A. (2011a): Quantifying the impact of freshwater diatom productivity on silicon isotopes and silicon fluxes: Lake Myvatn, Iceland. Earth Planet. Sci. Lett., 305, 73–82.
Opfergelt, S., Georg, R. B., Burton, K. W., Guicharnaud, R., Siebert, C., Gislason, S. R., Halliday, A. N. (2011b): Silicon isotopes in allophane as a proxy for mineral formation in volcanic soils. Appl. Geochem., 26, S115–S118.
Opfergelt, S., Georg, R. B., Delvaux, B., Cabidoche, Y. M., Burton, K. W., Halliday, A. N. (2012): Silicon isotopes and the tracing of desilication in volcanic soil weathering sequences, Guadeloupe. Chem. Geol., 326–327, 113–122.
Opfergelt, S., Burton, K. W., Pogge von Strandmann, P. A. E., Gislason, S. R., Halliday, A. N. (2013): Riverine silicon isotope variations in glaciated basaltic terrains: implications for the Si delivery to the ocean over glacial–interglacial intervals. Earth Planet. Sci. Lett., 369–370, 211–219.
Otake, T., Lasaga, A. C., Ohmoto, H. (2008): Ab initio calculations for equilibrium fractionations in multiple sulfur isotope systems. Chem. Geol., 249(3), 357–376.
Ottonello, G., Zuccolini, M. V. (2008): The iron-isotope fractionation dictated by the carboxylic functional: an ab-initio investigation. Geochim. Cosmochim. Acta, 72(24), 5920–5934.
Palmer, M. R., Slack, J. F. (1989): Boron isotopic composition of tourmaline from massive sulfide deposits and tourmalinites. Contrib. Mineral. Petrol., 103(4), 434–451.
Pan, J., Zhang, Q., Ma, D., Li, C. (2001): Cherts from the Yangla copper deposit, western Yunnan Province: geochemical characteristics and relationship with massive sulfide mineralization. Sci. China, Ser. D: Earth Sci., 44(3), 237.

EBSCOhost - printed on 2/10/2023 8:05 PM via . All use subject to https://www.ebsco.com/terms-of-use

Panizzo, V. N., Swann, G. E. A., Mackay, A. W., Vologina, E., Sturm, M., Pashley, V., Horstwood, M. S. A. (2016): Insights into the transfer of silicon isotopes into the sediment record. Biogeosciences, 13, 147–157.

Pastuszak, M., Conley, D. J., Humborg, C., Witek, Z., Sitek, S. (2008): Silicon dynamics in the Oder estuary. Baltic Sea. J. Mar. Syst., 73, 250–262.

Patel, A., Price, G. D., Mendelssohn, M. J. (1991): A computer simulation approach to modelling the structure, thermodynamics and oxygen isotope equilibria of silicates. Phys. Chem. Miner., 17(8), 690–699.

Pearce, C. R., Jones, M. T., Oelkers, E. H., Pradoux, C., Jeandel, C. (2013): The effect of particulate dissolution on the neodymium (Nd) isotope and Rare Earth Element (REE) composition of seawater. Earth Planet. Sci. Lett., 369(370), 138–147.

Pearson, N. J., Griffin, W. L., O'Reilly, S. Y. (2008): Mass fractionation correction in laser ablation multiple-collector ICP-MS: implications for overlap corrections and precise and accurate in situ isotope ratio measurement. In P. Sylvester (Ed.) Laser ablation-ICP-MS in the Earth sciences: current practices and outstanding issues (pp. 93–116). Mineralogical Association of Canada.

Peng, J., Yi, H., Xia, W. (2000): Geochemical criteria of the Upper Sinian cherts of hydrothermal origin on the southeast continental margin of the Yangtze plate. Chin. J. Geochem., 19(3), 217.

Pichevin, L., Ganeshram, R. S., Reynolds, B. C., Prahl, F., Pedersen, T. F., Thunell, R., McClymont, E. L. (2012): Silicic acid biogeochemistry in the Gulf of California: insights from sedimentary Si isotopes. Paleoceanography, 27(2), PA2201.

Pinilla, C., Blanchard, M., Balan, E., Natarajan, S. K., Vuilleumier, R., Mauri, F. (2015): Equilibrium magnesium isotope fractionation between aqueous Mg^{2+} and carbonate minerals: insights from path integral molecular dynamics. Geochim. Cosmochim. Acta, 163, 126–139.

Piperno, D. R. (2001): Phytoliths. In J. P. Smol, H. J. B. Birks, W. M. Last (Eds.) Tracking environmental change using Lake Sediments Terrestrial, Algal and Siliceous indicators (pp. 235–252). London: Kluwer.

Platt, T., Gallegos, C. L., Harrison, W. G. (1980): Photoinhibition of photosynthesis in natural assemblages of marine phytoplankton. J. Mar. Res., 38, 687–701.

Podosek, F. A. (1978): Isotopic structure in Solar System materials. Ann. Rev. Astron. Astrophys., 16, 293–334.

Pogge von Strandmann, P. A. E., Opfergelt, S., Lai, Y.-J., Sigfússon, B., Gislason, S. R., Burton, K. W. (2012): Lithium, magnesium and silicon isotope behaviour accompanying weathering in a basaltic soil and pore water profile in Iceland. Earth Planet. Sci. Lett., 339–340, 11–23.

Pogge von Strandmann, P. A. E., Porcelli, D., James, R. H., van Calsteren, P., Schaefer, B., Cartwright, I., Reynolds, B. C., Burton, K. W. (2014): Chemical weathering processes in the Great Artesian Basin: evidence from lithium and silicon isotopes. Earth Planet. Sci. Lett., 406, 24–36.

Pohnert, G. (2002): Biomineralization in diatoms mediated through peptide- and polyamine assisted condensation of silica. Angew. Chem. Int. Ed., 41, 3167–3169.

Poitrasson, F. (2017): Silicon isotope geochemistry. Rev. Mineral. Geochem., 82(1), 289–344.

Poitrasson, F., Zambardi, T. (2015): An Earth–Moon silicon isotope model to track silicic magma origins. Geochim. Cosmochim. Acta, 167, 301–312.

Pokrovsky, O. S., Reynolds, B. C., Prokushkin, A. S., Schott, J., Viers, J. (2013): Silicon isotope variations in Central Siberian rivers during basalt weathering in permafrostdominated larch forests. Chem. Geol., 355, 103–116.

Pollington, A. D., Kozdon, R., Anovitz, L. M., Georg, R. B., Spicuzza, M. J., Valley, J. W. (2016): Experimental calibration of silicon and oxygen isotope fractionations between quartz and water at 250 °C by in situ microanalysis of experimental products and application to zoned low δ^{30}Si quartz overgrowths. Chem. Geol., 421(5), 127–142.

EBSCOhost - printed on 2/10/2023 8:05 PM via . All use subject to https://www.ebsco.com/terms-of-use

Pramann, A., Rienitz, O., Schiel, D., Güttler, B. (2011a): Novel concept for the mass spectrometric determination of absolute isotopic abundances with improved measurement uncertainty: part 2 – development of an experimental procedure for the determination of the molar mass of silicon using MC-ICP-MS. Int. J. Mass Spectrom., 299(2–3), 78–86.

Pramann, A., Rienitz, O., Schiel, D., Güttler, B., Valkiers, S. (2011b): Novel concept for the mass spectrometric determination of absolute isotopic abundances with improved measurement uncertainty: part 3 – molar mass of silicon highly enriched in ^{28}Si. Int. J. Mass Spectrom., 305(1), 58–68.

Pringle, E. A., Savage, P. S., Badro, J., Barrat, J.-A., Moynier, F. (2013): Redox state during core formation on asteroid 4-Vesta. Earth Planet. Sci. Lett., 373, 75–82.

Pringle, E. A., Moynier, F., Savage, P. S., Jackson, M. G., Moreira, M., Day, J. M. D. (2016): Silicon isotopes reveal recycled altered oceanic crust in the mantle sources of Ocean Island Basalts. Geochim. Cosmochim. Acta, 189, 282–295.

Prospero, J., Arimoto, R. (2008): Atmospheric transport and deposition of particulate material to the oceans. Encyclopedia of Ocean Sciences, 248–257.

Qin, Y.-C., Weng, H.-X., Jin, H., Chen, J., Tian, R.-X. (2012): Estimation of authigenic alteration of biogenic and reactive silica in Pearl River estuarine sediments using wet chemical digestion methods. Environ. Earth Sci., 65, 1855–1864.

Ragueneau, O., Schultes, S., Bidle, K., Claquin, P., Moriceau, B. (2006): Si and C interactions in the world ocean: importance of ecological processes and implications for the role of diatoms in the biological pump. Glob. Biogeochem. Cycles, 20 (4).

Rains, D. W., Epstein, E., Zasoski, R. J., Aslam, M. (2006): Active silicon uptake by wheat. Plant Soil, 280, 223–228.

Raven, J. A. (1983): The transport and function of silicon in plants. Biol. Rev. Camb. Philos. Soc., 58(2), 179–207.

Raven, J. A. (2003): Cycling silicon – the role of accumulation in plants – commentary. New Phytol., 158(3), 419–421.

Reddy, T. R., Zheng, X.-Y., Roden, E. E., Beard, B. L., Johnson, C. M. (2016): Silicon isotope fractionation during microbial reduction of Fe(III)–Si gels under Archean seawater conditions and implications for iron formation genesis. Geochim. Cosmochim. Acta, 190, 85–99.

Reynard, B., Caracas, R. (2009): D/H isotopic fractionation between brucite $Mg(OH)_2$ and water from first-principles vibrational modeling. Chem. Geol., 262(3), 159–168.

Reynolds, J. H., Verhoogen, J. (1953): Natural variations in the isotopic constitution of silicon. Geochim. Cosmochim. Acta, 3, 224–234.

Reynolds, B. C., Georg, R. B., Oberli, F., Wiechert, U., Halliday, A. N. (2006a): Re-assessment of silicon isotope reference materials using high-resolution multi-collector ICP-MS. J. Anal. At. Spectrom., 21(3), 266–269.

Reynolds, B. C., Frank, M., Halliday, A. N. (2006b): Silicon isotope fractionation during nutrient utilization in the North Pacific. Earth Planet. Sci. Lett., 244(1–2), 431–443.

Reynolds, B. C., Aggarwal, J., Andre, L., Baxter, D., Beucher, C., Brzezinski, M. A., Engström, E., Georg, R. B., Land, M., Leng, M. J., Opfergelt, S., Rodushkin, I., Sloane, H. J., van den Boorn, S. H. J. M., Vroon, P. Z. Cardinal, D., (2007): An inter-laboratory calibration of Si isotope reference materials. J. Anal. At. Spectrom., 22(5), 561–568.

Richet, P., Bottinga, Y., Javoy, M. (1977): A review of hydrogen, carbon, nitrogen, oxygen, sulphur, and chlorine stable isotope fractionation among gaseous molecules. Annu. Rev. Earth Planet. Sci., 5(5), 65–110.

Rignanese, G. M., Gonze, X., Pasquarello, A. (2001): First-principles study of structural, electronic, dynamical, and dielectric properties of zircon. Phys. Rev. B, 63(10), 385–392.

EBSCOhost - printed on 2/10/2023 8:05 PM via . All use subject to https://www.ebsco.com/terms-of-use

Robert, F., Chaussidon, M. (2006): A palaeotemperature curve for the Precambrian oceans based on silicon isotopes in cherts. Nature, 443(7114), 969–972.

Robinson, R. S., Brzezinski, M. A., Beucher, C. P., Horn, M. G. S., Bedsole, P. (2014): The changing roles of iron and vertical mixing in regulating nitrogen and silicon cycling in the Southern Ocean over the last glacial cycle. Paleoceanography, 29(12), 2014PA002686.

Rodellas, V., Garcia-Orellana, J., Masqué, P., Feldman, M., Weinstein, Y. (2015): Submarine groundwater discharge as a major source of nutrients to the Mediterranean Sea. Proc. Natl. Acad. Sci., 12(13), 3926–3930.

Roerdink, D. L., van den Boorn, S. H. J. M., Geilert, S., Vroon, P. Z. van Bergen, M. J. (2015): Experimental constraints on kinetic and equilibrium silicon isotope fractionation during the formation of non-biogenic chert deposits. Chem. Geol., 402, 40–51.

Rosenthal, J. E. (1935): Vibrations of symmetrical tetratomic molecules. Phys. Rev., 47(3), 235–237.

Rösler, H. J., Lange, H. (1973): Geochemical tables. Amsterdam, London, New York: Elsevier Publishing Company.

Rousseau, J., Ellwood, M. J., Bostock, H., Neil, H. (2016): Estimates of late Quaternary mode and intermediate water silicic acid concentration in the Pacific Southern Ocean. Earth Planet. Sci. Lett., 439, 101–108.

Rudnick, R. L. (1995): Making continental crust. Nature, 378(6557), 571–578.

Rudnick, R. L., Gao, S. (2003): 3.01 – composition of the continental crust. In H. D. Holland, K. K. Turekian (Eds.) Treatise on geochemistry (pp. 1–64). Oxford: Pergamon.

Rudnick, R. L., Taylor, S. R. (1987): The composition and petrogenesis of the lower crust: a xenolith study. J. Geophys. Res., Solid Earth, 92(B13), 13981–14005.

Rudnick, R. L., McDonough, W. F., McCulloch, M. T., Taylor, S. R. (1986): Lower crustal xenoliths from Queensland. Australia: evidence for deep crustal assimilation and fractionation of continental basalts. Geochim. Cosmochim. Acta, 50(6), 1099–1115.

Russell, S. D. J., Longstaffe, F. J., King, P. L., Larson, T. E. (2010): The oxygen-isotope composition of chondrules and isolated forsterite and olivine grains from the Tagish Lake carbonaceous chondrite. Geochim. Cosmochim. Acta, 74(8), 2484–2499.

Saccone, L., Conley, D. J., Koning, E., Sauer, D., Sommer, M., Kaczorek, D., Blecker, S. W., Kelly, E. F. (2007): Assessing the extraction and quantification of amorphous silica in soils of forest and grassland ecosystems. Eur. J. Soil Sci., 58, 1446–1459.

Sangster, A. G. (1978): Silicon in the roots of higher plants. Am. J. Bot., 65, 929–935.

Sangster, A. G., Hodson, M. J. (1986): Silica in Higher Plants, In D. Evered, M. O'Connor, (Eds.) Silicon Biochemistry (pp. 90–111) Chichester, UK: John Wiley & Sons, Ltd.

Sangster, A. G., Parry, D. W. (1981): Ultrastructure of silica deposits in higher plants. In T. L. Simpson, B. E. Vocani (Eds.) Silicon and siliceous structures in biological systems (pp. 385–407).

Santelli, C. M., Orcutt, B. N., Banning, E., Bach, W., Moyer, C. L., Sogin, M. L., Staudigel, H., Edwards, K. J. (2008): Abundance and diversity of microbial life in ocean crust. Nature, 453(7195), 653–656.

Santosh, M., Xiao, W. J., Tsunogae, T., Chetty, T. R. K., Yellappa, T. (2012): The Neoproterozoic subduction complex in southern India: SIMS zircon U–Pb ages and implications for Gondwana assembly. Precambrian Res., 192–195, 190–208.

Sarmiento, J. L., Simeon, J., Gnanadesikan, A., Gruber, N., Key, R. M., Schlitzer, R. (2007): Deep ocean biogeochemistry of silicic acid and nitrate. Glob. Biogeochem. Cycles, 21 (1).

Sato, Y., Fujiwara, H., Udatsu, T. (1990): Morphological differences in silica body derived from Motor cell of Indica and Japonica in rice. Jpn. J. Breed, 40, 495–504.

EBSCOhost - printed on 2/10/2023 8:05 PM via . All use subject to https://www.ebsco.com/terms-of-use

Sauer, D., Saccone, L., Conley, D. J., Herrmann, L., Sommer, M. (2006): Review of methodologies for extracting plant-available and amorphous Si from soils and aquatic sediments. Biogeochemistry, 80, 89–108.

Savage, P. S., Moynier, F. (2013): Silicon isotopic variation in enstatite meteorites: Clues to their origin and Earth-forming material. Earth Planet. Sci. Lett., 361, 487–496.

Savage, P. S., Georg, R. B., Williams, H. M., Halliday, A. N. (2009): Uniform silicon isotopes in the depleted mantle and no melt-induced fractionation. Geochim. Cosmochim. Acta, 73(13).

Savage, P. S., Georg, R. B., Armytage, R. M. G., Williams, H. M., Halliday, A. N. (2010): Silicon isotope homogeneity in the mantle. Earth Planet. Sci. Lett., 295(1–2), 139–146.

Savage, P. S., Georg, R. B., Williams, H. M., Burton, K. W., Halliday, A. N. (2011): Silicon isotope fractionation during magmatic differentiation. Geochim. Cosmochim. Acta, 75(20), 6124–6139.

Savage, P. S., Georg, R. B., Williams, H. M., Turner, S., Halliday, A. N., Chappell, B. W. (2012): The silicon isotope composition of granites. Geochim. Cosmochim. Acta, 92, 184–202.

Savage, P. S., Georg, R. B., Williams, H. M., Halliday, A. N. (2013a): The silicon isotope composition of the upper continental crust. Geochim. Cosmochim. Acta, 109, 384–399.

Savage, P. S., Georg, R. B., Williams, H. M., Halliday, A. N. (2013b): Silicon isotopes in granulite xenoliths: insights into isotopic fractionation during igneous processes and the composition of the deep continental crust. Earth Planet. Sci. Lett., 365, 221–231.

Savage, P. S., Armytage, R. M. G., Georg, R. B., Halliday, A. N. (2014): High temperature silicon isotope geochemistry. Lithos, 190–191, 500–519.

Schauble, E. A. (2011): First-principles estimates of equilibrium magnesium isotope fractionation in silicate, oxide, carbonate and hexaaquamagnesium(2+) crystals. Geochim. Cosmochim. Acta, 75(3), 844–869.

Schauble, E. A., Ghosh, P., Eiler, J. M. (2006): Preferential formation of ^{13}C–^{18}O bonds in carbonate minerals, estimated using first-principles lattice dynamics. Geochim. Cosmochim. Acta, 70(10), 2510–2529.

Schopka, H. H., Derry, L. A. (2012): Chemical weathering fluxes from volcanic islands and the importance of groundwater: the Hawaiian example. Earth Planet. Sci. Lett., 339, 67–78.

Schott, J., Mavromatis, V., Fujii, T., Pearce, C. R., Oelkers, E. H. (2016): The control of carbonate mineral Mg isotope composition by aqueous speciation: theoretical and experimental modeling. Chem. Geol., 445, 120–134.

Shaffer, W. H., Schuman, R. P. (1944): The infra-red spectra of bent XYZ molecules part I. Vibration-rotation energies. J. Chem. Phys., 12(12), 504–513.

Shahar, A., Young, E. D. (2007): Astrophysics of CAI formation as revealed by silicon isotope LA-MC-ICPMS of an igneous CAI. Earth Planet. Sci. Lett., 257(3–4), 497–510.

Shahar, A., Ziegler, K., Young, E. D., Ricolleau, A., Schauble, E. A., Fei, Y. W. (2009): Experimentally determined Si isotope fractionation between silicate and Fe metal and implications for Earth's core formation. Earth Planet. Sci. Lett., 288(1–2), 228–234.

Shahar, A., Hillgren, V. J., Young, E. D., Fei, Y. Y., Macris, C. A., Deng, L. W. (2011): High-temperature Si isotope fractionation between iron metal and silicate. Geochim. Cosmochim. Acta, 75(23), 7688–7697.

Shaw, D. R. (1993). Geochemistry of albite-chlorite-pyrite and chlorite-pyrrhotite alteration, Sullivan Zn–Pb deposit, British Columbia; Current Research, Part A. Geological Survey of Canada.

Shen, S. Y., Wei, Q. R., Cheng, H. L., Mo, X. X. (2001): Characteristics and geotectonic implications of two sorts of silicalites in Ailao Mountain Belt, "Three-River" Area. Acta Petrol. Mineral., 20(1), 42–46 (in Chinese with English abstract).

Shui, M., Du, X., Chen, D., Ye, C., Li, Q. (1995): Effect of soluble silicon fertilizer on rice resistance to blast. Acta Agriculturae Zhejiangensis, 7(4), 289–292.

EBSCOhost - printed on 2/10/2023 8:05 PM via . All use subject to https://www.ebsco.com/terms-of-use

Singh, S. P., Singh, S. K., Bhushan, R., Rai, V. K. (2015): Dissolved silicon and its isotopes in the water column of the Bay of Bengal: internal cycling versus lateral transport. Geochim. Cosmochim. Acta, 151, 172–191.

Slack, J. F. (1993): Models for tourmalinite fromation in the Middle Proterozoic belt and Purcell Supergroups (Rocky Mountains) and their exploration significance. Canada Geological Survey Paper, 93-1E, 33–40.

Slack, J. F., Shaw, D. R., Leitch, C. H. B., Turner, R. J. W. (2000): Tourmalinites and coticules from the Sullivan Pb-Zn-Ag deposit and vicinity, British Columbia: Geology, geochemistry, and genesis. In J. W. Lydon, J. F. Slack, T. Höy, M. E. Knapp (Eds.), The Geological Environment of the Sullivan Deposit, British Columbia. Geological Association of Canada, Mineral Deposits Division, Special Publication 1, (pp. 736–767).

Slomp, C. P., Van Cappellen, P. (2004): Nutrient inputs to the coastal ocean through submarine groundwater discharge: controls and potential impact. J. Hydrol., 295, 64–86.

Smithson, F. (1956): Silica particles in some British soil. J. Soil Sci, 7, 122–129.

Sommer, M., Kaczorek, D., Kuzyakov, Y., Breuer, J. (2006): Silicon pools and fluxes in soils and landscapes – a review. J. Plant Nutr. Soil Sci., 169, 310–329.

Song, T. R., Ding, T. P. (1990): A new probe on application of silicon isotopes composition (δ^{30}Si) in siliceous rocks to sedimentary facies analysis. Chin. Sci. Bull., 35, 761–766.

Spencer, C. P. (1983): Marine biogeochemistry of silicon. In S. R. Aston (Ed.) Silicon geochemistry and biogeochemistry. London: Pergamon Press Inc.

Spetsius, Z. V., Vries, D. F. W. D., Davies, G. R. (2009): Combined C isotope and geochemical evidence for a recycled origin for diamondiferous eclogite xenoliths from kimberlites of Yakutia. Lithos, 112(2), 1032–1042.

Stefurak, E. J. T., Fischer, W. W., Lowe, D. R. (2015): Texture-specific Si isotope variations in Barberton Greenstone Belt cherts record low temperature fractionations in early Archean seawater. Geochim. Cosmochim. Acta, 150, 26–52.

Steinhoefel, G., Horn, I., von Blanckenburg, F. (2009): Micro-scale tracing of Fe and Si isotope signatures in banded iron formation using femtosecond laser ablation. Geochim. Cosmochim. Acta, 73(18), 5343–5360.

Steinhoefel, G., von Blanckenburg, F., Horn, I., Konhause, K. O., Beukes, N. J., Gutzmer, J. (2010): Deciphering formation processes of banded iron formations from the Transvaal and the Hamersley successions by combined Si and Fe isotope analysis using UV femtosecond laser ablation. Geochim. Cosmochim. Acta, 74, 2677–2696.

Stone, J., Hutcheon, I. D. Epstein, S., Wasserburg, G. J. (1991): Silicon, carbon, and nitrogen isotopic studies of silicon carbide in carbonaceous and enstatite chondrites. In H. P. Taylor Jr., J. R. O'Neil, I. R. Kaplan (Eds.) Stable isotope geochemistry: a tribute to Samuel Epstein (Vol. 3). The geochemical society.

Struyf, E., Conley, D. J. (2012): Emerging understanding of the ecosystem silica filter. Biogeochemistry, 107, 9–18.

Struyf, E., Smis, A., Van Damme, S., Meire, P., Conley, D. (2009): The global biogeochemical silicon cycle. Silicon, 1, 207–213.

Struyf, E., Mörth, C.-M., Humborg, C., Conley, D. J. (2010): An enormous amorphous silica stock in boreal wetlands. J. Geophys. Res., Biogeosci., 115, G04008.

Sun, J., Zhao, H., Wang, Y. (1994): Study of the contents of trace rare earth elements and their distribution in wheat and rice samples. J. Radioanal. Nucl. Chem., 179, 377–383.

Sun, L., Wu, L. H., Ding, T. P., Tian, S. H. (2008): Silicon isotope fractionation in rice plants, a experimental study on rice growth under hydroponic conditions. Plant Soil, 304(1–2), 291–300.

EBSCOhost - printed on 2/10/2023 8:05 PM via . All use subject to https://www.ebsco.com/terms-of-use

Sun, X., Andersson, P. S., Humborg, C., Pastuszak, M., Mörth, C.-M. (2013): Silicon isotope enrichment in diatoms during nutrient-limited blooms in a eutrophied river system. J. Geochem. Explor., 132, 173–180.

Sun, X., Olofsson, M., Andersson, P. S., Fry, B., Legrand, C., Humborg, C., Mörth, C.-M. (2014): Effects of growth and dissolution on the fractionation of silicon isotopes by estuarine diatoms. Geochim. Cosmochim. Acta, 130, 156–166.

Sun, Y., Wu, L., Li, X., Sun, L., Gao, J., Ding, T. (2016): Silicon isotope fractionation in rice and cucumber plants over a life cycle: Laboratory studies at different external silicon concentrations. J. Geophys. Res., Biogeosci., 121(11), 2829–2841.

Sutton, J. N., Varela, D. E., Brzezinski, M. A., Beucher, C. P. (2013): Species-dependent silicon isotope fractionation by marine diatoms. Geochim. Cosmochim. Acta, 104, 300–309.

Swann, G. E. A., Leng, M. J., Juschus, O., Melles, M., Brigham-Grette, J., Sloane, H. J. (2010): A combined oxygen and silicon diatom isotope record of Late Quaternary change in Lake El'gygytgyn, North East Siberia. Quat. Sci. Rev., 29, 774–786.

Syvitski, J. P. M., Vorosmarty, C. J., Kettner, A. J., Green, P. (2005): Impact of humans on the flux of terrestrial sediment to the global coastal ocean. Science, 308, 376–380.

Takahashi, E., Okuda, A. (1962): The characteristics of silicic acid uptake in paddy rice. J. Sci. Soil Manure Japan, 33, 217–221.

Takahashi, E., Tanaka, T., Miyake, Y. (1981): Distribution of silicicolous plants in plant kingdom. J. Sci. Soil Manure, 52(5), 503–510 (in Japanese).

Tamai, K., Ma, J. F. (2003): Characterization of silicon uptake by rice roots. New Phytol., 158(3), 431–436.

Tanaka, T., Masuda, A. (1973): Rare-earth elements in matrix, inclusions, and chondrules of the Allende meteorite. Icarus, 19(4), 523–530.

Tang, M., Anders, E., Zinner, E. (1988): Noble gases, C, N, and SI isotopes in interstellar SiC form the Murchison carbonaceous chondrite. Lunar and Planetary XIX (pp. 1177–1178). Houston: Lunar and Planetary Institute.

Taniguchi, M., Burnett, W. C., Cable, J. E., Turner, J. V. (2002): Investigation of submarine groundwater discharge. Hydrol. Process., 16, 2115–2129.

Tatzel, M., von Blanckenburg, F., Oelze, M., Schuessler, J. A., Bohrmann, G. (2015): The silicon isotope record of early silica diagenesis. Earth Planet. Sci. Lett., 428, 293–303.

Taylor, H. P., Epstein, S. (1962): Relationship between O^{18}/O^{16} ratios in coexisting minerals of igneous and metamorphic rocks: part 1: principles and experimental results. Geol. Soc. Am. Bull., 73(4), 461–480.

Taylor, H. P. J., Epstein, S. (1973a): O^{18}/O^{16} and Si^{30}/Si^{28} studies of some Apollo 15, 16, and 17 samples. In Proceedings of the 4th lunar science conference.

Taylor, H. P. Jr., Epstein, S. (1973b): Oxygen and silicon isotope ratios of the Luna 20 soil. Geochim. Cosmochim. Acta, 37(4): 1107–1109.

Taylor, B. E., Slack, J. F. (1984): Tourmalines from Appalachian-Caledonian massive sulfide deposits; textural, chemical, and isotopic relationships. Econ. Geol., 79(7), 1703–1726.

Tegen, I., Kohfeld, K. E. (2006): Atmospheric transport of silicon. In V. Ittekkot, D. Unger, C. Humborg, N. T. An (Eds), The Silicon Cycle: Human Perturbations and Impacts on Aquatic Systems. Island Press, SCOPE, 66, 81.

Tranter, M. (2005): Geochemical weathering in glacial and proglacial environments. In J. I. Drever (Ed.) Surface and ground water, weathering, and soils (pp. 189–205). London: Elsevier.

Tréguer, P. J. de La Rocha, C. L. (2013): The world ocean silica cycle. Annu. Rev. Mar. Sci., 5, 477–501.

Tréguer, P., Nelson, D. M., Van Bennkom, A. J., DeMaster, D. J., Leynaert, A., Queguiner, B. (1995): The silica balance in the world ocean: a reestimate. Science, 268, 375–379.

EBSCOhost - printed on 2/10/2023 8:05 PM via . All use subject to https://www.ebsco.com/terms-of-use

Travaglio, C., Gallino, R., Amari, S., Zinner, E., Woosley, S., Lewis, R. S. (1999): Low-Density Graphite Grains and Mixing in Type II Supernovae. Astrophys. J., 510(1), 325–354.

Trendall, A. F. (2002): The significance of iron-formation in the Precambrian stratigraphic record. Spec. Publ. Int. Assoc. Sedimentol., 33, 33–66.

Turner, R. J. W., Leitch, C. H. B. (1992): Relationship of albitic and chloritic alteration to gabbro dykes and sills at the Sullivan deposit and nearby area, southeastern British Columbia. Canada Geol. Survey Paper, 92-1E, 95–105.

Tsuchiyama, A. (1990): Fo-En-Gas equilibrium and Mg/Si ratios of chondritic meteorites. In Antarctic meteorites XV.

Ueda, K., Ueda, S. (1961): Effect of silicic acid on bamboo-growth. Bull. Kyoto Univ. Forests, 33, 79–99 (in Japanese).

Uyeda, C., Tsuchiyama, A. (1990): Mass fractions of minerals produced from gas-condensation process. In: 15th Symposium on Antarctic Meteorites, (pp. 173–175) Tokyo: NIPR.

Uyeda, C., Tsuchiyama, A., Okano, J. (1990): Isotopic abundances of silicates produced in gas-condensation furnace. In A. Benninghoven (Ed.) Secondary ion mass spectrometry, SIMS VII (pp. 381–384). Berlin: Springer.

Uyeda, C., Tsuchiyama, A., Okano, J. (1991): Magnesium isotopic fractionation of silicates produced in condensation experiments. Earth Planet. Sci. Lett., 107(1), 138–147.

Valkiers, S., Ding, T., Inkret, M., Rußе, K., Taylor, P. (2005): Silicon isotope amount ratios and molar masses for two silicon isotope reference materials: IRMM-018a and NBS28. Int. J. Mass Spectrom., 242(2–3), 319–321.

Valkiers, S., Mana, G., Fujii, K., Becker, P. (2011): Si primary standards for the calibration of ion-current ratios in the molar-mass measurement of natural Si single crystals. Metrologia, 48(2), S26–S31.

Van den Boorn, S. H. J. M., Vroon, P. Z., Belle, C. C. V., Wagt, B. V. D., Schwieters, J., Bergen, M. J. V. (2006): Determination of silicon isotope ratios in silicate materials by high-resolution MC-ICP-MS using a sodium hydroxide sample digestion method. J. Anal. At. Spectrom., 21(8), 734–742.

Van den Boorn, S. H. J. M., van Bergen, M. J., Nijman, W., Vroon, P. Z. (2007): Dual role of seawater and hydrothermal fluids in Early Archean chert formation: evidence from silicon isotopes. Geology, 35, 939–942.

van den Boorn, S. H. J. M., van Bergen, M. J., Vroon, P. Z., de Vries, S. T., Nijman, W. (2010): Silicon isotope and trace element constraints on the origin of ~3.5 Ga cherts: implications for Early Archaean marine environments. Geochim. Cosmochim. Acta, 74, 1077–1103.

Vance, D., Teagle, D. A. H., Foster, G. L. (2009): Variable quaternary chemical weathering fluxes and imbalances in marine geochemical budgets. Nature, 458, 493–496.

Varela, D. E., Pride, C. J., Brzezinski, M. A. (2004): Biological fractionation of silicon isotopes in Southern Ocean surface waters. Glob. Biogeochem. Cycles, 18(1), GB104.

Viers, J., Dupre, B., Gaillardet, J. (2009): Chemical composition of suspended sediments in world rivers: new insights from a new database. Sci. Total Environ., 407, 853–868.

Wade, J., Wood, B. J. (2005): Core formation and the oxidation state of the Earth. Earth Planet. Sci. Lett., 236(1), 78–95.

Wadham, J. L., Tranter, M., Skidmore, M., Hodson, A. J., Priscu, J., Lyons, W. B., Sharp, M., Wynn, P., Jackson, M. (2010): Biogeochemical weathering under ice: size matters. Glob. Biogeochem. Cycles, 24, GB3025.

Walker, J. C. G., Lohmann, K. C. (1989): Why the oxygen isotopic composition of seawater changes with time. Geophys. Res. Lett., 16, 323–326.

Wan, D. F., Li, Y. H., Song, H. B., Liu, Z. J. (1997): Preparation and calibration of reference material for silicon isotope. Acta Geos. Sin., 18(3), 330–335 (in Chinese with English abstract).

EBSCOhost - printed on 2/10/2023 8:05 PM via . All use subject to https://www.ebsco.com/terms-of-use

Wang, D. A., Chen, R. J. (1996): Discussion on silicon isotope of bedded siliceous rocks of different ages in Yangtze Platform. Acta Sendimentologica Sinica, 14, 82–88 (in Chinese with English abstract).

Wang, J. H., Davis, A. M., Clayton, R. N., Mayeda, T. K. (1994): Kinetic isotopic fractionation during the evaporation of the iron oxide from liquid state. Lunar Planet. Sci., 25, 1459–1460.

Wang, C., Udatsu, T., Tang, L., Zhou, J., Zheng, Y., Sasaki, K., Yanagisawa, K., Fujiwara, H. (1998): Cultivar group of rice cultivated in Caoxishan Site (B. P. 6000~present) determined by the morphology of plant opals and its historical change. Breed. Sci., 48, 387–394.

Wang, J. H., Davis, A. M., Clayton, R. N., Hashimoto, A. (1999): Evaporation of single crystal forsterite: evaporation kinetics, magnesium isotope fractionation, and implications of mass-dependent isotopic fractionation of a diffusion-controlled reservoir. Geochim. Cosmochim. Acta, 63(6), 953–966.

Wang, J. H., Davis, A. M., Clayton, R. N., Mayeda, T. K., Hashimoto, A. (2001): Chemical and isotopic fractionation during the evaporation of the FeO–MgO–SiO_2–CaO–Al_2O_3–TiO_2 rare earth element melt system. Geochim. Cosmochim. Acta, 65(3), 479–494.

Wang, Y.-H., Xue, C.-J., Zhang, F.-F., Liu, J.-J., Gao, J.-B., Qi, T.-J. (2015): SHRIMP zircon U–Pb geochronology, geochemistry and H–O–Si–S–Pb isotope systematics of the Kanggur gold deposit in Eastern Tianshan, NW China: Implication for ore genesis. Ore Geol. Rev., 68, 1–13.

Wedepohl, K. H. (1995): The composition of the continental crust. Geochim. Cosmochim. Acta, 59(7), 1217–1232.

Weinstein, Y., Yechieli, Y., Shalem, Y., Burnett, W. C., Swarzenski, P. W., Herut, B. (2011): What is the role of fresh groundwater and recirculated seawater in conveying nutrients to the Coastal Ocean? Environ. Sci. Technol., 45, 5195–5200.

Weiss, A., De La Rocha, C., Amann, T., Hartmann, J. (2015): Silicon isotope composition of dissolved silica in surface waters of the Elbe Estuary and its tidal marshes. Biogeochemistry, 1–19.

Wen, Q., Diao, G., Pan, J., Wu, M. (1996): Comparison of average chemical composition of loess in loess plateau with clark values of crust. Acta Pedologica Sinica, 33(3), 225–231.

West, A. J., Galy, A., Bickle, M. (2005): Tectonic and climatic controls on silicate weathering. Earth Planet. Sci. Lett., 235, 211–228.

Wetzel, F., de Souza, G. F., Reynolds, B. C. (2014): What controls silicon isotope fractionation during dissolution of diatom opal? Geochim. Cosmochim. Acta, 131, 128–137.

Weyer, S., Schwieters, J. B. (2003): High precision Fe isotope measurements with high mass resolution MC-ICPMS. Int. J. Mass Spectrom., 226(3), 355–368.

Wheat, C. G., McManus, J. (2005): The potential role of ridge-flank hydrothermal systems on oceanic germanium and silicon balances. Geochim. Cosmochim. Acta, 69(8), 2021–2029.

White, A. F., Vivit, D. V., Schulz, M. S., Bullen, T. D., Evett, R. R., Aagarwal, J. (2012): Biogenic and pedogenic controls on Si distributions and cycling in grasslands of the Santa Cruz soil chronosequence, California. Geochim. Cosmochim. Acta, 94, 72–94.

Whitehouse, M. J., Kamber, B. S., Fedo, C. M., Lepland, A. (2005): Integrated Pb- and S-isotope investigation of sulphide minerals from the early Archaean of southwest Greenland. Chem. Geol., 222(1–2), 112–131.

Wickbold, R. (1959): Die Anreicherung sehr kleiner Mengen Kieselsäure durch Ionenaustausch. Fresenius J. Anal. Chem., 171(2), 81–87.

Wickramasinghe, D. B., Rowell, D. L. (2006): The release of silicon from amorphous silica and rice straw in Sri Lankan soils. Biol. Fertil. Soils, 42, 231–240.

Wille, M., Sutton, J., Ellwood, M. J., Sambridge, M., Maher, W., Eggins, S., Kelly, M. (2010): Silicon isotopic fractionation in marine sponges: a new model for understanding silicon isotopic variations in sponges. Earth Planet. Sci. Lett., 292(3–4), 281–289.

EBSCOhost - printed on 2/10/2023 8:05 PM via . All use subject to https://www.ebsco.com/terms-of-use

Williams, C. D., Ushikubo, T., Bullock, E. S., Janney, P. E., Hines, R. R., Kita, N. T., Hervig, R. L., MacPherson, G. J., Mendybaev, R. A., Richter, F. M., Wadhwa, M. (2017): Thermal and chemical evolution in the early solar system as recorded by FUN CAIs: Part I – Petrology, mineral chemistry, and isotopic composition of Allende FUN CAI CMS-1. Geochim. Cosmochim. Acta, 201(Supplement C), 25–48.

Wilson, J. P., Fischer, W. W., Johnston, D. T., Knoll, A. H., Grotzinger, J. P., Walter, M. R., McNaughton, N. J., Simon, M., Abelson, J., Schrag, D. P., Summons, R., Allwood, A., Andres, M., Gammon, C., Garvin, J., Rashby, S., Schweizer, M., Watters, W. A. (2010): Geobiology of the late Paleoproterozoic Duck Creek Formation, Western Australia. Precambrian Res., 179(1), 135–149.

Wu, S., Ding, T., Meng, X., Bai, L. (1997): Determination and geological implication of O-Si isotope of the sediment core in the CC area, the Pacific Ocean. Chin. Sci. Bull., 42, 1462–1465.

Wu, S., Zhang, D., Wang, K., Chen, C., Bai, L. (2000): Geochemical characteristics of stable isotopes from hydrothermal chimneys in the mariana trough, West Pacific Ocean. Chin. J. Oceanol. Limnol., 0(4), 378–384.

Wu, Z. Q., Huang, F., Huang, S. C. (2015a): Isotope fractionation induced by phase transformation: first-principles investigation for Mg_2SiO_4. Earth Planet. Sci. Lett., 409, 339–347.

Wu, F., Qin, T., Li, X. F., Liu, Y., Huang, J. H., Wu, Z. Q., Huang, F. (2015b): First-principles investigation of vanadium isotope fractionation in solution and during adsorption. Earth Planet. Sci. Lett., 426, 216–224.

Xiong, Z., Li, T., Algeo, T., Doering, K., Frank, M., Brzezinski, M. A., Chang, F., Opfergelt, S., Crosta, X., Jiang, F., Wan, S., Zhai, B. (2015): The silicon isotope composition of Ethmodiscus Rex laminated diatom mats from the tropical West Pacific: implications for silicate cycling during the Last Glacial Maximum. Paleoceanography, 30(7), 803–823 (2015PA002793).

Xu, B., Huang, J. (1996): Isotopic composition and genesis of various types of bentonite ores in zhejiang province. Geochim. Cosmochim. Acta.

Xu, J., Wang, L. S. (1987): Radiolaria discovered in Devonian strata of Nandan-Dachang area, Guangxi. Monogr. Ser. Miner. Depos., 1, 22.

Xu, Y. T., Hu, W., Xu, K., Hu, S. (1997): The geochemical characteristics of the Carboniferous bedded siliconites in West Zhejiang and their sedimentary environment. J. Stratigr., 21(1), 47–54 (in Chinese with English abstract).

Xu, Y. T. (1998): The geochemical characteristics of cherts in the carboniferous period and their sedimentary environment implications in Xinjiang basin. Sci. Geol. Sin., 33(1), 39–49 (in Chinese with English abstract).

Xue, C. (1991): A study on the seafloor hydrothermal sedimentary nature of jasperoid rocks in Yindongzi. Journal of Mineralogy & Petrology, 11, 31–40 (in Chinese).

Xue, C. J., Jiang, S. Y., Li, Y. H. (1998): A study on silicon and oxygen isotopic geochemistry of the Devonian silica rock in Qinling Range. Journal of Earth Sciences and Environment, 20(1), 10–13 (in Chinese).

Yang, R. D., Wei, H. R., Bao, M., Wang, W., Wang, Q., Zhang, X. D., Liu, L. (2008): Discovery of hydrothermal venting community at the base of Cambrian barite in Guizhou Province Western China: implication for the Cambrian biological explosion. Prog. Nat. Sci., 18, 65–70.

Yang, X. Y., Sun, W. D., Zhang, Y. X., Zheng, Y. F. (2009): Geochemical constraints on the genesis of the Bayan Obo Fe–Nb–REE deposit in Inner Mongolia, China. Geochim. Cosmochim. Acta, 73, 1417e143.

Yao, X. M., Ding, T. P. (1994): Silicon and oxygen stable isotope studies on the siliceous rocks and stratiform ore bodies of the Dachang tin polymetallic deposit, Guangxi. Acta Geoscientia Sinica, 1–2, 124–130.

Yeh, H. W., Epstein, S. (1978): $^{29}Si/^{28}Si$ and $^{30}Si/^{28}Si$ of meteorites and Allende inclusions. 9, 1289–1291.

EBSCOhost - printed on 2/10/2023 8:05 PM via . All use subject to https://www.ebsco.com/terms-of-use

Yool, A., Tyrrell, T. (2003): Role of diatoms in regulating the ocean's silicon cycle. Glob. Biogeochem. Cycles, 17.

Young, E. D., Manning, C. E., Schauble, E. A., Shahar, A., Macris, C. A., Lazar, C., Jordan, M. (2015): High-temperature equilibrium isotope fractionation of non-traditional stable isotopes: experiments, theory, and applications. Chem. Geol., 395, 176–195.

YRCC (2007): Bulletin on water resource of the Yellow River, Zhengzhou, China: YRCC (in Chinese).

Yuan, Z., Bai, G., Wu, C., Zhang, Z., Ye, X. (1992): Geological features and genesis of the Bayan Obo REE ore deposit, Inner Mongolia, China. Appl. Geochem., 7, 429–442.

Yund, R. A., Anderson, T. F. (1974): Oxygen isotope exchange between potassium feldspar and KCl solution. In A. W. Hofmann, B. J. Giletti, H. S. Yoder Jr., R. A. Yund (Eds.) Geochemical transport and kinetics (Vol. 634, pp. 99–105). Carnegie Inst Wash Publ.

Zachariasen, W. H. (1932): The atomic arrangement in glass. J. Am. Chem. Soc., 44(10), 3841–3851.

Zambardi, T., Poitrasson, F. (2011): Precise determination of silicon isotopes in silicate rock reference materials by MC-ICP-MS. Geostand. Geoanal. Res., 35, 89–99.

Zambardi, T., Poitrasson, F., Corgne, A., Méheut, M., Quitté, G., Anand, M. (2013): Silicon isotope variations in the inner solar system: implications for planetary formation, differentiation and composition. Geochim. Cosmochim. Acta, 121, 67–83.

Zambardi, T., Lundstrom, C. C., Li, X. X., McCurry, M. (2014): Fe and Si isotope variations at Cedar Butte volcano; insight into magmatic differentiation. Earth Planet. Sci. Lett., 405, 169–179.

Zeebe, R. E. (2005): Stable boron isotope fractionation between dissolved $B(OH)_3$ and $B(OH)_4^-$. Geochim. Cosmochim. Acta, 69(11), 2753–2766.

Zhang, B. Y., Chen, D. X., Li, Z. J., Gu, X. M. (1988): The Regional Geochemistry of the Zhashui-Shanyang Sulfide Mineralization Zone, Shaanxi, China. Beijing: China University of Geosciences Publishing House. (249 pp.) (in Chinese).

Zhang, F. (1991): Exhalites associated with Pb-Zn mineralization in Devonian System and their prospecting implications, Qinling, China. Chin. J. Geochem., 10(4), 348–356.

Zhang, Q. D., Song, T. R., He, Z. J., Ding, X. Z. (2002): Pb-Pb age determination of Meso-to Neoproterozoic carbonates in the Mingtoms district, Beijing. Geol. Rev., 48(4), 416–423 (in Chinese with English abstract).

Zhang, Y. N., et al. (2014): The isotopic characteristics of silicon and oxygen and the genesis of the dengying siliceous rock series in the North Verge of the Upper Yangtze Block. Bull. Miner. Petrol. Geoch., 33(4), 452–456 (in Chinese with English abstract).

Zhao, H., Zeng, Z., Yin, X., Chen, S. (2014): Silicon and oxygen isotopic composition of igneous rocks from the eastern Manus Basin. J. Ocean Univ. China, 13(3), 421–427.

Zheng, X. Y., Beard, B. L., Reddy, T. R., Roden, E. E., Johnson, C. M. (2016): Abiologic silicon isotope fractionation between aqueous Si and Fe(III)–Si gel in simulated Archean seawater: implications for Si isotope records in Precambrian sedimentary rocks. Geochim. Cosmochim. Acta, 187(15), 102–122.

Zhou, T., Yuan, F., Yue, S., Liu, X., Zhang, X., Fan, Y. (2007): Geochemistry and evolution of ore-forming fluids of the Yueshan Cu–Au skarn- and vein-type deposits, Anhui Province, South China. Ore Geol. Rev., 31(1), 279–303.

Zhu, S., Zhu, M., Knoll, A. H., Yin, Z., Zhao, F., Sun, S., Qu, Y., Shi, M., Liu, H. (2016): Decimetre-scale multicellular eukaryotes from the 1.56-billion-year-old Gaoyuzhuang Formation in North China. Nat. Commun., 7, 11500. doi:10.1038/ncomms11500.

Ziegler, K., Chadwick, O. A., Brzezinski, M. A., Kelly, E. F. (2005a): Natural variations of δ^{30}Si ratios during progressive basalt weathering, Hawaiian Islands. Geochim. Cosmochim. Acta, 69(19), 4597–4610.

Ziegler, K., Chadwick, O. A., White, A. F., Brzezinski, M. A. (2005b): δ^{30}Si systematics in a granitic saprolite, Puerto Rico. Geology, 33, 817–820.

EBSCOhost - printed on 2/10/2023 8:05 PM via . All use subject to https://www.ebsco.com/terms-of-use

Ziegler, K., Young, E. D., Schauble, E. A., Wasson, J. T. (2010): Metal–silicate silicon isotope fractionation in enstatite meteorites and constraints on Earth's core formation. Earth Planet. Sci. Lett., 295(3–4), 487–496.

Zinner, E., Amari, S., Travaglio, C., Gallino, R., Busso, M., Woosley, S. (1995): The isotopic composition of interstellar graphite from the Murchison meteorite: Evidence for supernova mixing. In: Lunar and Planetary Science Conference.

Zinner, E., Ming, T., Anders, E. (1987): Large isotopic anomalies of Si, C, N and noble gases in interstellar silicon carbide from the Murray meteorite. Nature, 330, 730–732.

Zinner, E., Ming, T., Anders, E. (1989): Interstellar SiC in the Murchison and Murray meteorites: isotopic composition of Ne, Xe, Si, C and N. Geochim. Cosmochim. Acta, 53(12), 3273–3290.

EBSCOhost - printed on 2/10/2023 8:05 PM via . All use subject to https://www.ebsco.com/terms-of-use

Index

EBSCOhost - printed on 2/10/2023 8:05 PM via . All use subject to https://www.ebsco.com/terms-of-use

EBSCOhost - printed on 2/10/2023 8:05 PM via . All use subject to https://www.ebsco.com/terms-of-use

EBSCOhost - printed on 2/10/2023 8:05 PM via . All use subject to https://www.ebsco.com/terms-of-use

EBSCOhost - printed on 2/10/2023 8:05 PM via . All use subject to https://www.ebsco.com/terms-of-use

EBSCOhost - printed on 2/10/2023 8:05 PM via . All use subject to https://www.ebsco.com/terms-of-use

EBSCOhost - printed on 2/10/2023 8:05 PM via . All use subject to https://www.ebsco.com/terms-of-use